NASA Technical Memorandum 84273

(NASA-TM-84273) SIXTEENTH ANNUAL CONFERENCE ON MANUAL CONTROL (NASA) 647 p
HC A99/MF A01 CSCL 05H
N82-34037
THRU
N82-34075
Unclas
G3/54 35306

Sixteenth Annual Conference on Manual Control

May 5-7, 1980
Massachusetts Institute of Technology
Cambridge, Massachusetts
and
Ames Research Center
Moffett Field, California

SEP 1982
RECEIVED
NASA STI FACILITY
ACCESS DEPT.

NASA
National Aeronautics and
Space Administration

NASA Technical Memorandum 84273

Sixteenth Annual Conference on Manual Control

May 5-7, 1980
Massachusetts Institute of Technology, Cambridge, Massachusetts
Ames Research Center, Moffett Field, California

National Aeronautics and
Space Administration

Ames Research Center
Moffett Field, California 94035

CONFERENCE CO-CHAIRMEN

Sheldon Baron

Bolt, Beranek and Newman, Inc.

Thomas B. Sheridan

Massachusetts Institute of Technology

PUBLICATIONS COMMITTEE

Thomas Wempe

NASA-Ames Research Center

FOREWORD

This volume contains the proceedings of the Sixteenth Annual Conference on Manual Control held at the Massachusetts Institute of Technology at Cambridge, Massachusetts, May 5-7, 1980. It contains complete manuscripts of most of the papers presented at the meeting and abstracts of the others. The papers and abstracts are ordered as presented, with session titles indicated in the table of contents.

This was the sixteenth in a series of conferences dating back to December 1964. These earlier meetings and their proceedings are listed below:

1. The University of Michigan, December 1964. (Proceedings not printed.)
2. M.I.T., February 28 to March 2, 1966, NASA SP-128.
3. University of Southern California, March 1-3, 1967, NASA SP-144.
4. The University of Michigan, March 21-23, 1968, NASA SP-192.
5. M.I.T., March 27-29, 1969, NASA SP-215.
6. Wright-Patterson AFB, April 7-9, 1970.
7. University of Southern California, June 2-4, 1971, NASA SP-281.
8. University of Michigan, Ann Arbor, Michigan, May 17-19, 1972.
9. M.I.T., May 23-25, 1973.
10. Wright-Patterson AFB, April 9-11, 1974.
11. NASA-Ames Research Center, May 21-23, 1975, NASA TM X-62,464.
12. University of Illinois, May 25-27, 1976, NASA TM X-73,170.
13. M.I.T., June 15-17, 1977.
14. University of Southern California, April 25-27, 1978.
15. Wright-Patterson AFB, March 20-22, 1979.

TABLE OF CONTENTS

Page

Operator Modeling

MODELING OF HUMAN OPERATOR DYNAMICS IN SIMPLE MANUAL CONTROL UTILIZING TIME SERIES ANALYSIS 1
Gyan C. Agarwal, Frank Osafo-Charles, William D. O'Neill and Gerald L. Gottleib

A GUNNER MODEL FOR AN AAA TRACKING TASK WITH INTERRUPTED OBSERVATIONS 29
C. F. Yu, K. C. Wei and M. M. Vikmanis

MODELING HUMAN TARGET ACQUISITION IN GROUND-TO-AIR WEAPON SYSTEMS 40
A. V. Phatak, R. L. Mohr, M. Vikmanis and K. C. Wei

THE EFFECT OF VISUAL INFORMATION ON THE MANUAL APPROACH AND LANDING 49
P. H. Wewerinke

PILOT/VEHICLE MODEL ANALYSIS OF VISUAL AND MOTION CUE REQUIREMENTS IN FLIGHT SIMULATION 68
R. Lancraft, G. Zacharias, S. Baron

PURSUIT TRACKING AND HIGHER LEVELS OF SKILL DEVELOPMENT IN THE HUMAN PILOT 92
Ronald A. Hess

MULTI-AXIS TRACKING VIA AN OPTIMAL-CONTROL PILOT MODEL 106
S. N. Prasad and David K. Schmidt

THE EFFECTS OF MULTIPLICATIVE MOTOR NOISE ON THE OPTIMAL HUMAN OPERATOR MODEL 107
Alper K. Caglayan and William H. Levison

MODELLING OF AIRCRAFT IN-TRAIL FOLLOWING 118a
Ahmet Buhareli

TRAINING AIRCRAFT DESIGN CONSIDERATIONS BASED ON THE SUCCESSIVE ORGANIZATION OF PERCEPTION IN MANUAL CONTROL 119
Robert K. Heffley, Warren F. Clement and Samuel J. Craig

Measurement of Human Response

AN EXPERIMENTAL STUDY OF HUMAN PILOT'S SCANNING BEHAVIOR 128
Kyuichro Washizu, Keiji Tanaka and Tatsuo Osawa

INVESTIGATION OF A SUM OF SINUSOIDS REPRESENTATION OF GAUSS-MARKOV RANDOM PROCESSES - IMPLICATIONS FOR MANUAL CONTROL RESEARCH 135
R. L. Mohr, A. V. Phatak and R. A. Hess

PARAMETRIC IDENTIFICATION OF HUMAN OPERATOR MODELS 137
Norbert R. Ninz

TABLE OF CONTENTS

A COMPUTER SIMULATION APPROACH TO MEASUREMENT OF HUMAN CONTROL STRATEGY 146
Joanne Green, Esther Lee Davenport, Harold F. Engler, William E. Sears

PILOT MODEL HYPOTHESIS TESTING 152
John R. Broussard and Paul W. Berry

Mental Workload

SUBJECTIVE SCALING OF MENTAL WORKLOAD IN A MULTI-TASK ENVIRONMENT 172
Bahman Daryanian

EFFECT OF COUNTING AND TRACKING ON VERBAL AND PRODUCTION METHODS OF TIME ESTIMATION 189
Kathleen L. Bird and Sandra Hart

EFFECT OF ESTIMATION TECHNIQUE AND TASK CONDITION ON TIME ESTIMATION METHODS 212
Kathleen L. Bird and Sandra G. Hart

PILOT WORKLOAD IN THE AIR TRANSPORT ENVIRONMENT: THEORY, MEASUREMENT AND THE INFLUENCE OF AIR TRAFFIC CONTROL 213
Jeff Katz and Robert Simpson

WORKLOAD AND PILOT EYE SCANNING BEHAVIOR 214
J. R. Tole, A. Ephrath, A. T. Stephens and L. R. Young

THE LOCUS OF PROCESSING DEMANDS OF HIGHER-ORDER CONTROL: AN ELECTRO-PHYSIOLOGICAL APPROACH 215
Christopher Wickens and Richard Gill

Pilot/Operator Opinion

A MODEL-BASED TECHNIQUE FOR PREDICTING PILOT OPINION RATINGS FOR LARGE COMMERCIAL TRANSPORTS 216
William H. Levison

AN ANALYTICAL PREDICTION OF PILOT RATINGS UTILIZING HUMAN PILOT MODEL 243
Keiji Tanaka and Kyuichiro Washizu

EFFECTS OF HIGHER ORDER CONTROL SYSTEMS ON AIRCRAFT APPROACH AND LANDING LONGITUDINAL HANDLING QUALITIES 254
Muhammad A. Pasha, John J. D'Azzo and James T. Silverthorn

PILOT OPINIONS OF SAMPLING EFFECTS IN LATERAL-DIRECTIONAL CONTROL 265
Robert F. Stengel and Geoorge E. Miller

A MODEL OF SUBJECTIVE PROBABILITIES FROM SMALL GROUPS 271
William R. Ferrell and Kelly Rehm

TABLE OF CONTENTS

Effects of Motion

VISUAL/MOTION CUE MISMATCH DURING A COORDINATED ROLL MANEUVER 285
D. K. Shirachi

COMBINED EFFECT OF THE OCULOGYRAL ILLUSION AND OF A FIXED PERIPHERAL FIELD ON SENSATIONS OF YAW MOTION 286
J. K. Huang and L. R. Young

A PERFORMANCE ANALYSIS STUDY OF A COMPLEX G FIELD EXPERIMENT 292
Daniel W. Repperger

A LINEARIZED MODEL FOR VIBRATION EFFECTS ON THE EYE CONTROL SYSTEM 316
Raymond E. Magdaleno and Henry R. Jex

DESCRIPTION/DEMONSTRATION OF "BIODYN-80": A SOFTWARE PACKAGE FOR EVALUATING THE TRANSMISSIBILITY BETWEEN VEHICLE VIBRATION AND MOTIONS OF HANDS (IN CONTROLS), LIMBS, HEAD AND EYES 317
Systems Technology, Inc.

MODELING LATERAL ACCELERATION EFFECTS ON PILOT PERFORMANCE 340
Jonathan Korn and David L. Kleinman

A COMPREHENSIVE SYSTEM MODEL FOR MOTION/SPACE SICKNESS - PRELIMINARY RESULTS 349
Susan A. Riedel

Aircraft Displays

EVALUATION OF A TRAJECTORY COMMAND CONCEPT FOR MANUAL CONTROL OF CARRIER APPROACHES AND LANDINGS 370
Walter E. McNeill, G. Allen Smith, Jr., Ronald M. Gerdes

WIND SHEAR SIMULATION EXPERIMENTS
COMBINED USE OF AIRBORNE TRAFFIC SITUATION DISPLAYS 393
Mark Connelly

APPLICATION OF A PILOT CONTROL STRATEGY IDENTIFICATION TECHNIQUE TO A JOINT FAA/NASA GROUND-BASED SIMULATION OF HEAD-UP DISPLAYS FOR CTOL AIRCRAFT 395
Wayne F. Jewell

PILOT REACTION TO ATTITUDE GYRO FAILURE 410
Richard L. Newman and David L. Quam

PILOT INDUCED LONG PERIOD OSCILLATIONS CREATED BY CERTAIN DISPLAYS CONFIGURATIONS 423
James J. Adams

DESIGN, SIMULATION AND EVALUATION OF ADVANCED DISPLAY CONCEPTS FOR THE F-16 CONTROL CONFIGURED VEHICLE 424
Robert W. Klein and Walter M. Hollister

SEPARATION MONITORING WITH FOUR TYPES OF PREDICTORS ON A COCKPIT DISPLAY OF TRAFFIC INFORMATION 439
Sharon Jago and Everett Palmer

TABLE OF CONTENTS

Supervisory Control

COMBINED DISCRETE NETWORK - CONTINUOUS CONTROL MODELING OF OPERATOR BEHAVIOR 448
R. A. Miller and Deborah J. Seifert

A MODEL OF HUMAN DECISION MAKING IN MULTIPLE PROCESS MONITORING SITUATIONS 465
Joel S.Greenstein and William B. Rouse

PROCRU: A MODEL FOR ANALYZING FLIGHT CREW PROCEDURES IN APPROACH TO LANDING 488
S. Baron, G. Zacharias, R. Muraldiharan, R. Lancraft

A MODEL FOR REAL-TIME HUMAN DECISION-MAKING IN A MULTI-TASK ENVIRONMENT 521
P. Krishna-Rao, Arye R. Ephrath, David L. Kleinman

APPLICATION OF OPTIMAL CONTROL PRINCIPLES TO DESCRIBE THE SUPERVISORY CONTROL BEHAVIOR OF AAA CREW MEMBERS 523
Chris Hale and George J. Valentino

DOES MAN ALWAYS CLOSE THE LOOP IN TRYING TO PILOT A LARGE SHIP? 533
Douglas R. Arnett and T. Govindaraj

SUPERVISION OF DYNAMIC SYSTEMS: MONITORING, DECISION-MAKING AND CONTROL 540
Ted N. White

EFFECT OF INFERENTIAL MONITORING AND VIGILANCE 548
Janice J. Wrye and Renwick E. Curry

Automobile Driving

EFFECTS OF MOTIVATION ON CAR-FOLLOWING 549
Tom Bösser

LEVELS OF STEERING CONTROL: REPRODUCTION OF STEERING-WHEEL MOVEMENTS 557
Hans Godthelp

Remote Manipulation

THE ROLE OF ANTAGONIST COACTIVATION IN THE CONTROL OF NATURAL MOVEMENT 571
Neville Hogan

A COMPARISON OF CONTROL MODES FOR TIME-DELAYED REMOTE MANIPULATION 584
Gregory P. Starr

EXPERIMENTAL EVALUATION OF THE CONCEPT OF SUPERVISORY MANIPULATION 593
Thurston L. Brooks and Thomas B. Sheridan

TABLE OF CONTENTS

EVALUATION OF "SMART" SENSOR DISPLAYS FOR MULTIDIMENSIONAL PRECISION CONTROL OF SPACE SHUTTLE REMOTE MANIPULATOR 607
A. K. Bejczy, R. W. Brown and J. L. Lewis

A NEW FEEDBACK INSTRUMENT FOR ROBOTS AND MANIPULATORS, AND ITS USE IN ROBOT TEACHING, SELF CORRECTION AND LEARNING 628
D. S. Seltzer and D. E. Whitney

THE NOSC/MIT SUBMERSIBLE-MANIPULATOR: AN EXPERIMENT IN REMOTE SUPERVISORY CONTROL OF A MICROPROCESSOR BASED ROBOT 629
Dana Yoerger and Thomas B. Sheridan

ANALYSIS OF DRIVER PERFORMANCE UNDER REDUCED VISIBILITY 630
Wolf-Dieter Kaeppler

N82 34038

MODELING OF HUMAN OPERATOR DYNAMICS IN SIMPLE MANUAL CONTROL UTILIZING TIME SERIES ANALYSIS

Gyan C. Agarwal, Frank Osafo-Charles, William D. O'Neill, and Gerald L. Gottlieb

College of Engineering, University of Illinois at Chicago Circle, Chicago, 60680, and Department of Physiology, Rush-Presbyterian-St. Luke's Medical Center, Chicago, 60612.

ABSTRACT

Time series analysis is applied to model human operator dynamics in pursuit and compensatory tracking modes. The normalized residual criterion is used as a one-step analytical tool to encompass the processes of identification, estimation, and diagnostic checking. A parameter constraining technique is introduced to develop more reliable models of human operator dynamics. The human operator is adquately modeled by a second order dynamic system both in pursuit and compensatory tracking modes. In comparing the data sampling rates, 100 msec between samples is adequate and is shown to provide better results than 200 msec sampling. The residual power spectrum and eigenvalue analysis show that the human operator is not a generator of periodic characteristics.

I. INTRODUCTION

Equipment designers have traditionally called upon man to act as part of control systems. The value of having a human link was recognized long before it became possible to describe systems in mathematical terms. The human operator could be asked to furnish that particular information transduction needed to overcome unexpected environmental situations and compensate for deficiences of the equipment. The advent of costly and increasingly complex equipment has focused attention upon the need for detailed knowledge of the human transfer characteristics within its normal operating range. This would reduce the great expense and delay attendant upon modification or redesign of hardware during the development process. The determination of models describing human dynamics in an operating system is a complex and an important problem.

The human controller has several unique characteristics. His input - output relationships cannot be described as being purely linear, non-linear, time-variable, random, or discrete. They are complex combinations of all of these characteristics [1]. The problem of identification is further compounded by the fact that the human operator is an adaptive controller who learns from experience.

Presented at the Sixteenth Annual Conference on Manual Control, M.I.T, May, 1980. This work was supported in part by National Science Foundation Grant ENG-7608754 and grants from the National Institutes of Health NS-00196 and NS-12877.

Earlier approaches to representing the mathematical characteristics of the human operator using classical control theory (frequency domain analysis, describing functions, and spectral analysis) as well as modern control theory approaches (state variable and optimal estimation - Kalman filtering) have been extensively reviewed in the literature [2]-[12].

For a simple compensatory tracking task with a controlled element of unity gain, Elkind and Forgie [13] obtained the transfer function of the human operator of the form.

$$G_H(s) = \frac{K\,e^{-\tau s}}{(T_1 s+1)\,(T_N s+1)} \tag{1}$$

where K = Operator static gain, T_1 = Lag time constant, T_N = Neuromuscular lag time constant, τ = Effective time delay.

The parameters were found to be dependent on the frequency characteristic of the input spectrum. In the model development, the net phase lag can be approximated by an effective time delay which is the sum of transport delays and central nervous system latencies, a time varying component of delay and high frequency lead equalization. Thus the effective time delay has a measurable mean value over a particular run, but instantaneous values may vary about this mean [27]. In a study similar to [13], Young, et.al. [14] obtained the following parameter values for a rectangular input spectrum: $K = 40$, $\tau = 0.1$ sec, $1/T_1 = 0.3\ \text{sec}^{-1}$, $1/T_N = 6.2\ \text{sec}^{-1}$.

In a variety of experimental situations and controlled elements, McRuer and his colleagues have shown that the human operator follows a Cross-over model [4] and has a transfer function of the form [12]:

$$G_H(s) = \frac{K(T_L s+1)\ \ e^{-\tau s}}{(T_1 s+1)\ T_N s+1)} \tag{2}$$

where T_L = lead time constant and the other terms are same as in equation (1).

In recent studies, Shinners [1] and Tanaka, Goto, and Washizu [15] have pioneered the application of stochastic time series analysis in the modeling of human operator dynamics. Shinners basically uses the methods of Box and Jenkins [16,17]. In estimating the order and the parameters of an autoregressive/moving average (ARMA) model, a three-stage iterative procedure is used for: a) identification of the order of the model, b) estimation of its parameters, and c) diagnostic checking with the aim of revealing model inadequacies. In compensatory tracking with a controlled element of unity gain, Shinners [1] has obtained the following transfer function for the human operator (his subject C):

$$G_H(z) = \frac{-0.65(1-0.803\ z^{-1})z^{-1}}{(1-0.386\ z^{-1})\ (1-0.97\ z^{-1})} \tag{3}$$

where $z^{-1}\,x(k) = x(k-1)$ and the data sampling interval was 0.2 seconds.

Tanaka, et.al. [15] have used Akaike's Minimum Final Prediction Error [MFPE] method to obtain the order of the system [18,19]. Akaike's information criterion

(AIC) which is an alternative method to obtain the order of the system is based on the maximum likelihood principle.

Recently, Suen and Liu [20] have proposed a Normalized Residual Criterion (NRC) which seems to offer several advantages over other least square type identification methods. In comparing against Akaike's AIC method, Suen and Liu [20] have shown that their method consistently gives as good or better estimates; Akaike's criterion sometimes gives a system order higher by one or two (cf.[28] [29]). O'Neill [21] has successfully applied the NRC method of Suen and Liu to model suspended particulate pollution as an autoregressive process.

Suen and Liu's NRC method has the advantage that it is a one-step analytical tool that encompasses the processes of identification, estimation, and diagnostic checking. Pre-whitening of the input is not necessary (cf. Shinners' [1]). Also no presumption of stationarity of the data time series is required for effective characterization of the system. A review of identification methods is given by Astrom and Eykhoff [30]. They also discuss the relative merits of parametric (such as time series) versus nonparametric (such as impulse response, transfer function) modeling techniques.

The significant difference between this work and previous works, is the introduction of a theory which deals with the constraining of the parameters of the estimated time series models. By re-estimating the constrained models, more reliable and significant models for describing human dynamics are obtained. Since Shinners and Tanaka et.al., applied time series analysis to the human subject only in a compensatory tracking mode, this also represents the first time the technique has been extended to investigate the human characteristics in both compensatory and pursuit tracking modes.

II. EXPERIMENTAL DESIGN AND DATA ANALYSIS

Two subjects were used for these experiments. They will be referred to as subjects FOC and BXK. Prior to collection of data, both subjects were run through a scaled down set of experimental practice blocks to allow them to approach asymptotic performance levels.

The experimental set up is shown schematically in Figure 1. The human operator sat before an oscilloscope and manipulated a one degree of freedom joystick. The joystick moved freely with no springs or dashpots. The plant dynamics consisted of a simple unity gain. Two vertically driven horizontal lines were displayed on the oscilloscope. The first line served as the target in the pursuit case and as a zero-error reference line in the compensatory case. The other line displayed system output in the pursuit case and system error in the compensatory case. The lines were adjusted in focus and intensity which made it easy for subjects to discriminate between the two. The display configuration could be changed between pursuit and compensatory by means of a switch. Error was computed by a simple analog circuit. The entire experiment was under the control of a real-time digital computer (General Automation SPC-16/65) with D/A and A/D channels. The computer sampled at 20 msec intervals generating the appropriate system input and recording the system output. The entire observation period of 66.56 seconds, 3328 data point arrays both for input and output time series were simultaneously recorded on magnetic tape.

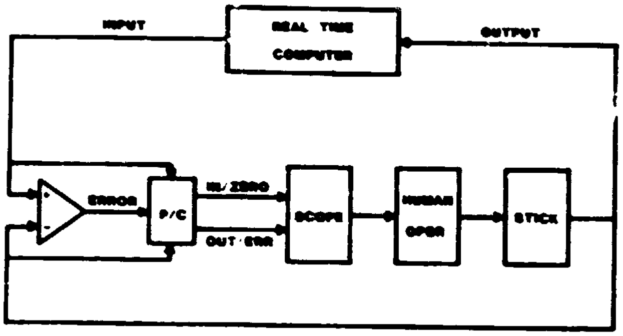
INPUT
REAL TIME COMPUTER
OUTPUT
+
-
ERROR
P/C
IN/ZERO
OUT/ERR
SCOPE
HUMAN OPER
STICK

SCHEMATIC OF EXPERIMENT

Figure 1: Schematic of the experimental set up. The scope is dual beam; one channel is used to display input in pursuit mode and zero reference in compensatory mode; the second channel is used for output in pursuit and system error in compensatory mode. The error is computed by a simple analog circuit using an EAI-TR-20 analog computer. The switch P/C allowed the display to be changed from pursuit to compensatory or vice-versa.

Two inputs consisting of summed sinusoids were used with each display configuration. The first was a low frequency range (0.0488; 0.1465; 0.2604; 0.4557; 0.8138 Hz) and the second was a high frequency range (0.0813; 0.1465; 0.2604; 0.4557; 1.4811 Hz). The sum of amplitudes of individual sinusoids in the input signal was always equal to ten and the component sinusoids were equal in amplitude. These summed sinusoids generated a wave form which was unpredictable by the subjects. Each operator was tested with four experimental variables: pursuit versus compensatory display mode; low frequency versus high frequency summed sine waves.

Most of the statisitical analysis was done using the Minitab 2 statistical software package on an IBM 370 computer. Graphics and detailed computations were accomplished with the Speakeasy computer language. Due to size considerations of Minitab 2 and the ability of the time series technique to use fewer samples to model a process that is stationary, we could use fewer observations than would be necessary in Fourier series analysis. Although the experiments were done with 20 ms sampling, the time series analysis was done first using a sampling interval of 0.2 sec. To check the adequacy of the 0.2 sec sampling interval, the procedure was repeated using an interval of 0.1 sec. Shinners [1] had found that the faster sampling rate of 0.1 sec did not add any additional useful information to the human transfer function models. This point will be discussed later on. The first 5 seconds of data were discarded in both cases to exclude the operators start-up transient. Figure 2 shows the last 20 sec of the original data series of the two subjects in compensatory and pursuit tracking.

III TIME SERIES THEORY

Transfer Functions Models (TF)

The time series analysis can be extended to obtain discrete linear transfer functions of systems having an input x(t) and output y(t). By x(t) and y(t) we mean pairs of observations that are available at equispaced intervals of time. The behavior of the dynamic system can be adequately represented by the present and past responses and the current and past inputs of the system. We denote This process as TF (n,m) and write its equation as

$$y(t) = \alpha_0 + \alpha_1 y(t-1) + \ldots + \alpha_n y(t-n) + \beta_0 x(t) + \ldots + \beta_m x(t-m) + v(t) \quad (4)$$

In equation (4) the parameters to be estimated are: $\alpha_0, \ldots, \alpha_n, \beta_0, \ldots \beta_m$, n and m The time series v(t) is a random term measuring the difference between the response y(t) and the variables used to explain the time series data. The parameter α_0 measures the mean output or the response of the process when there are no inputs, i.e., $y(t) = \alpha_0$, for $t \leq 0$.

In precognitive or single sine-wave pursuit tracking mode, the human operator is known to be non-causal (possesses ability to anticipate or predict future input [3]). In these experiments, however, where mixed sinusoids are used, the human controller behaves as a causal system. Therefore, we can assume $y(t) \equiv 0$ prior to the applied input. Consequently, the coefficient α_0 can be eliminated from the model to be estimated and equation (4) becomes:

$$y(t) = \sum_{i=1}^{n} \alpha_i y(t-i) + \sum_{j=0}^{m} \beta_j x(t-j) + v(t), \; (m \leq n) \quad (5)$$

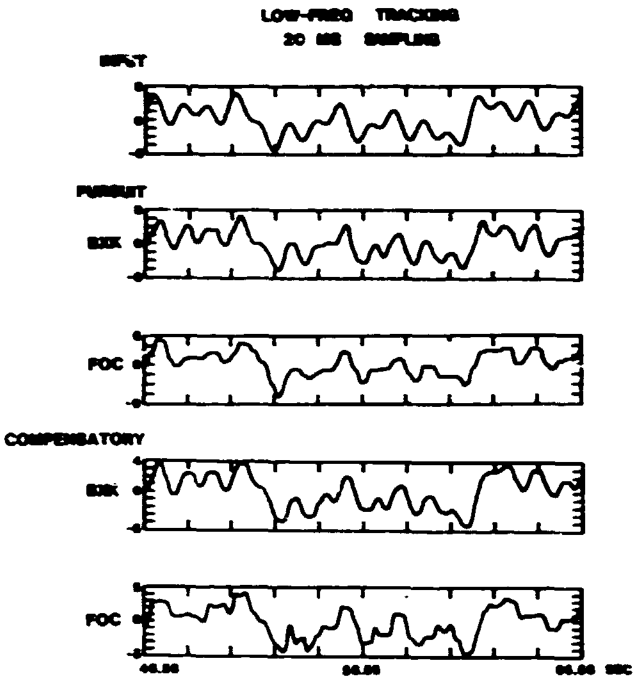

Figure 2: Last 20 seconds of the original data series at 20 ms sampling with low frequency summed sine-wave input. In both pursuit and compensatory, BXK is slightly better than FOC in their tracking ability.

The autocorrelation and the autocovariance functions suggested by Box and Jenkins [10] as tools for model estimation will not be considered here because these methods require much trial and error in the estimation procedures. Instead a technique proposed by Suen and Liu [20] and O'Neill [21] which is simple and very reliable will be introduced to estimate the desired model. This technique which is a derivation of ordinary least squares regression analysis is called the Normalized Residual Criterion (NRC) and is briefly described below.

Theory of Normalized Residual Criterion

Equation (5) reduces to an autoregressive model AR(n) if $x(t)$ is omitted from the model, and reduces to a moving average model MA(m) if lags of y are omitted. The following assumptions will be made concernig $v(t)$ for a given output time sequence $y(t)$, $t = [0, T]$,

(i) $E[v(t)] = 0$

(ii) $E[v(i)v(j)] = \sigma_v^2 \, \delta_{ij}$ (6)

where $\delta_{ij} = \begin{cases} 1 \text{ for } i = j \\ 0 \text{ for } i \neq j \end{cases}$

(iii) $T \gg n$.

The last assumption in equation (6) is commonly made in such analysis [32].

From equation (5)

$$v(t) = y(t) - \sum_{i=1}^{n} \alpha_i \, y(t-i) - \sum_{j=0}^{m} \beta_j \, x(t-j), \; t = 1, 2, \ldots T-n \tag{7}$$

Define

$$\sum_{t=1}^{T-n} v^2(t) = ||\underline{V}||^2 \text{ and } \sum_{t=1}^{T-n} y^2(t) = ||\underline{Y}||^2 \tag{8}$$

Note that in the discussion below $\underline{V}$ and $\underline{Y}$ are vectors such that

$$\underline{V} = \begin{bmatrix} v(1) \\ v(2) \\ \vdots \\ v(T-n) \end{bmatrix}, \text{ and } \quad \underline{Y} = \begin{bmatrix} y(1) \\ y(2) \\ \vdots \\ y(T-n) \end{bmatrix} \tag{9}$$

Squaring eq (7) and normalizing by the total sum of squares, we have

$$\frac{||\underline{V}||^2}{||\underline{Y}||^2} = \frac{||y - \Sigma\alpha_i y - \Sigma\beta_j x||^2}{||\underline{Y}||^2} = \varepsilon\,(n,m,T) \tag{10}$$

and therefore

$$E\,[||\underline{V}||^2] = E[||\underline{Y}||^2 \; \varepsilon(n,m,T)] \tag{11}$$

Since y(t), the data series, is deterministic, eq (11) can be rewritten as:

$$E[\ ||\underline{V}||^2\ ] = ||\underline{Y}||^2\ E[\epsilon(n,m,T)] \tag{12}$$

From eq (9) we have

$$E[\ ||\underline{V}||^2] = E[v^2(1) + v^2(2) + \dots + v^2(T-n)], \tag{13}$$

which by assuption (ii) in eq (6) reduces to

$$E[\ ||\underline{V}||^2\ ] = [T - n]\sigma_v^{\ 2} \tag{14}$$

Substituting eq (14) in eq (12) we have,

$$E[\epsilon(n,m,T)] = \frac{(T-n)\sigma_v^{\ 2}}{||\underline{Y}||^2} \tag{15}$$

and by assumption (iii) eq (15) becomes

$$E[\epsilon(n,m,T)] = \frac{T\sigma_v^{\ 2}}{||\underline{Y}||^2} \tag{16}$$

The quantity $\epsilon(n,m,T)$ depends on n,m, and T and is proportional to the normalized variance of the regression for a given n and m. If this ratio is minimized over n and m, then the data fit as measured by the correlation coefficient ρ will be maximized.

Note that

$$\rho = \left[1 - \frac{||\underline{V}||^2}{||Y||^2}\right]^{\frac{1}{2}} \tag{17}$$

or

$$\hat{\rho} = [1 - \hat{\epsilon}(n,m)]^{\frac{1}{2}} \tag{18}$$

where T, being a constant for the data, is omitted in the optimization procedure, and $\hat{\epsilon}(n,m)$ is the minimum value for $\epsilon(n,m)$. This optimization technique is the so called Normalized Residual Criterion (NRC).

Values of $\epsilon(n,m)$ were computed for the various tracking situations and then plotted against different values of n in Figs. 3 and 4. A typical graph (Fig. 3A) consists of the AR curve (m = 0), and a family of TF curves. In Fig. 3B the MA curve, though a function of m, is superimposed on the AR and TF curves to assist in comparison among all three models. The ordinate measures the normalized residual, $\epsilon(n,m)$, and this value is desired to be as small as possible. The analysis of various tracking data showed that the MA curve was the worst. The AR curve, though lower than the MA curve was still much higher than the family of TF curves. Clearly then the TF model is to be prefered and the question to ask is which TF model is optimal.

The percentage drop in $\epsilon(n,m)$ between the TF curves is negligible - the exception being the graphs for the high-freq. input, Figure 4, where the drop for m = 0, is considerable compared to m = 1, 2, ..., 6. Thus the selected TF model will have at most m = 1 since there is no apparent explanatory difference contributed by m = 2, ..., 6. To add statistical significance to our selection of model order note that the critical test is whether for $n \geq 1$, one can justify going from $n_1 = 1$ to $n_2 = 2$.

ORIGI... OF POOR QUALITY

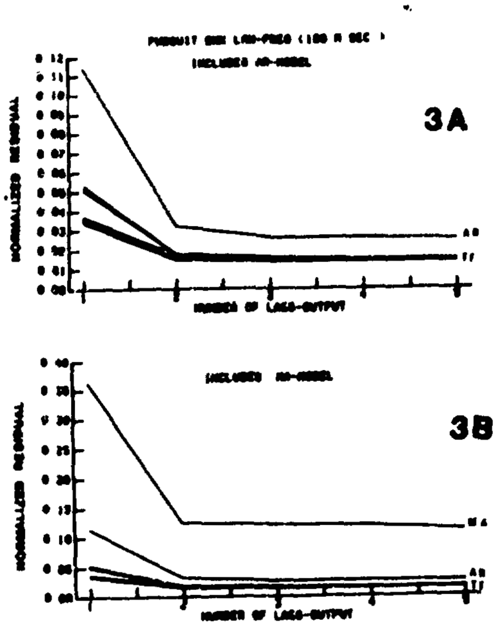

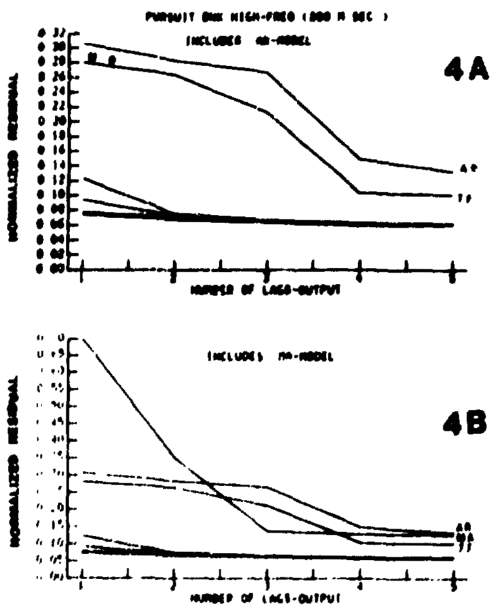

Figure 3: Normalized residuals $\epsilon(n)$ as a function of the order of the system, n. AR(n) is autoregressive model, MA(m) is moving average model, and TF(n,m) is transfer function model; $m = 0,1,2,\ldots\ldots, 6$ are in descending order. The optimal order of the system $n=2$.

Figure 4: Normalized residuals $\epsilon(n)$. (See Figure 3).

Since [26],

$$\Delta = \left[\frac{||\underline{v}||^2 n_2 - ||\underline{v}||^2 n_1}{||\underline{v}||^2 n_2} \right] \left[\frac{T - n_2}{n_2 - n_1} \right] \tag{19}$$

is $F(n_2 - n_1, T - n_2)$ distributed for large T, we tested this difference in going from $n_1 = 1$ to $n_2 = 2$. For example in Fig. 4A, for m = 1 in TF model, using T = 330, $n_1 = 1$, and $n_2 = 2$, we get $\Delta = 297.1$. Since the F - distribution table gives $F_{0.1}(1,120) = 6.85$, it is clear that the data decisively rejects the hypothesis of no significant difference in normalized residual for n = 1 and n = 2. (cf. Astrom and Eykhoff [30]).

We, therefore, find that for both input forms, for both sampling intervals, and for both subjects in pursuit as well as compensatory tracking modes, the optimal lag structure $\hat{n}$ is always equal to 2. Enstrom and Rouse (33) using discriminant analysis noted that considering the tradeoffs between accuracy and feasibility for using a human operator model in real-time applications a second-order model was most appropriate. Beyond n = 2, the $\varepsilon(n,m)$ curves do not add any explanatory power to the model selected. The resulting estimated models of the operator are of the form:

$$y(t) = \hat{\alpha}_1 y(t-1) + \hat{\alpha}_2 y(t-2) + \hat{\beta}_0 x(t) + \hat{v}(t) \tag{20}$$

for the low-frequency range, and

$$y(t) = \hat{\alpha}_1 y(t-1) + \hat{\alpha}_2 y(t-2) + \hat{\beta}_0 x(t) + \hat{\beta}_1 x(t-1) + \hat{v}(t) \tag{21}$$

for the high-frequency range.

The parameter values are listed in Tables 1 and 2 under the column unconstrained models for FCC at 100 ms sampling and BXK at 200 ms sampling.

These tables show, as Shinners [1] had observed, that the faster sampling rate of 100 msec did not add any additional information to the human transfer function models. In both cases, the model is of second-order. However, the value of the correlation coefficient of regression for pooled data from both subjects (equation 18) are significantly different at the two sampling intervals: $\hat{\rho}(100 \text{ ms}) = 0.988$ and $\hat{\rho}(200 \text{ ms}) = 0.958$. Although the t-test would show this difference to be significant at $P<0.0005$, the standard t-test is not valid for models with endogenous lags [26]. The estimated standard deviation of regression value of the pooled data are also significantly different at 100 and 200 msec sampling intervals: $\hat{\sigma}(100 \text{ msec}) = 0.394$ and $\hat{\sigma}(200 \text{ msec}) = 0.751$. Here again, although the t-test would indicate a significant difference at $P<0.0005$, it is not a valid test. The mean variance of the residuals v(t) are also significantly different at the two sampling intervals: $\sigma_v^2(100 \text{ ms}) = 0.495$ and $\sigma_v^2(200 \text{ ms}) = 1.988$. Based on the average values of the correlation coefficients, the estimated standard deviation of regression and the variance of the residuals, the 100 msec sampling is certainly preferable to 200 msec sampling.

Constrained Parameter Modeling

In general, information is transduced to guide a physical system through a

ORIGINAL PAGE IS
OF POOR QUALITY

TABLE 1

HUMAN OPERATOR MODELS							POC 100 MSEC	
Tracking Mode	Frequency Range	Estimate of Parameter (Unconstrained)	t Value of Parameter	Explained Sum of Squares	Correlation Coefficient of Regression	Estimated Stan. Deviation of Regression	Estimated Constrained Parameter	Estimated Stan. Deviation of Regression
Pursuit	Low	$\alpha_1 = 1.379$	45.68	3521	0.985	0.426	$\alpha_1 = 1.366$	0.429
		$\alpha_2 = -0.512$	-18.34	162			$\alpha_2 = -0.483$	
		$\beta_0 = 0.108$	14.82	40			$\beta_0 = 0.118$	
	High	$\alpha_1 = 1.168$	35.34	3014	0.989	0.345	$\alpha_1 = 1.170$	0.346
		$\alpha_2 = -0.308$	-10.11	76			$\alpha_2 = -0.299$	
		$\beta_0 = -0.046$	- 3.84	38			$\beta_0 = -0.041$	
		$\beta_1 = 0.171$	12.19	18			$\beta_1 = 0.170$	
Compensatory	Low	$\alpha_1 = 1.228$	37.30	4000	0.987	0.420	$\alpha_1 = 1.230$	0.420
		$\alpha_2 = -0.359$	-11.87	116			$\alpha_2 = -0.361$	
		$\beta_0 = 0.132$	17.27	53			$\beta_0 = 0.132$	
	High	$\alpha_1 = 1.248$	39.93	4387	0.986	0.476	$\alpha_1 = 1.247$	0.470
		$\alpha_2 = -0.404$	-14.18	132			$\alpha_2 = -0.400$	
		$\beta_0 = -0.019$	- 1.28	55			$\beta_0 = -0.017$	
		$\beta_1 = 0.170$	9.88	22			$\beta_1 = 0.170$	

TABLE 2

HUMAN OPERATOR MODELS BXK 200 MSEC

Tracking Mode	Frequency Range	Estimate of Parameter (Unconstrained)	t Value of Paramuter	Explained Sum of Squares	Correlation Coefficient of Regression	Estimated Stan. Deviation of Regression	Estimated Constrained Parameter	Estimated Stan. Deviation of Regression
Pursuit	Low	$\alpha_1 = 0.894$	27.24	1635	0.955	0.878	$\alpha_1 = 0.888$	0.902
		$\alpha_2 = -0.409$	-13.09	378			$\alpha_2 = -0.355$	
		$\beta_0 = 0.424$	22.18	379			$\beta_0 = 0.467$	
	High	$\alpha_1 = 0.937$	30.23	1238	0.963	0.[illegible]59	$\alpha_1 = 0.969$	0.742
		$\alpha_2 = -0.422$	-14.40	44			$\alpha_2 = -0.340$	
		$\beta_0 = -0.175$	-10.03	34			$\beta_0 = -0.136$	
		$\beta_1 = 0.504$	27.90	338			$\beta_1 = 0.507$	
Compensatory	Low	$\alpha_1 = 0.955$	29.03	1182	0.969	0.572	$\alpha_1 = 0.950$	0.593
		$\alpha_2 = -0.324$	-10.79	164			$\alpha_2 = -0.267$	
		$\beta_0 = 0.291$	22.86	171			$\beta_0 = 0.317$	
	High	$\alpha_1 = 0.629$	18.41	1438	0.932	1.040	$\alpha_1 = 0.654$	1.070
		$\alpha_2 = -0.251$	- 7.82	35			$\alpha_2 = -0.214$	
		$\beta_0 = -0.123$	- 4.64	132			$\beta_0 = -0.095$	
		$\beta_1 = 0.639$	22.70	561			$\beta_1 = 0.655$	

predefined course of action or sequence of states. This is accomplished through a series of decisions, each intended to minimize or otherwise constrain some function of the perceived error [22]. Consequently, a desirable property of any model for the human operator should be the ability, in the steady state, to track constant inputs with zero or negligible error.

Such a model can be obtained from the estimated model under conditions of equilibrium. That is, for sufficiently large t

$$y(t) \equiv y(t-1) \equiv y(t-2) \equiv y_e, \text{ and} \qquad (22)$$

$$x(t) \equiv x(t-1) \equiv x_e$$

where y_e and x_e are the steady state response and input, respectively.

For the estimated models eq. (20) and (21), at physical and statistical equilibrium the hypothesized form of eq (20) with $y(t) \equiv y_e$, $x(t) \equiv x_e$ and $E[v(t)] \equiv 0$ become,

$$y_e = \alpha_1 y_e + \alpha_2 y_e + \beta_0 x_e$$

and for $y_e = x_e$ to be true we must have

$$\beta_0 = 1 - \alpha_1 - \alpha_2 \qquad (23)$$

Substituting eq (23) in the hypothesized form of eq (20), we get

$$y(t) - x(t) = \alpha_1 [y(t-1) - x(t)] + \alpha_2 [y(t-2) - x(t)] + v(t) \qquad (24)$$

Similarly the hypothesized form of eq (21) becomes,

$$y(t) - x(t) = \alpha_1 [y(t-1) - x(t)] + \alpha_2 [y(t-2) - x(t)] + \beta_1 [x(t-1) - x(t)] + v(t) \qquad (25)$$

using the constraint,

$$\beta_0 = 1 - \alpha_1 - \alpha_2 - \beta_1 \qquad (26)$$

Again regression analysis is used to estimate the parameters α_1, α_2 and β_1. The parameter β_0 is then obtained from eqs (23) or (26). The resulting parameters are also listed in Tables 1 and 2 under the column constrained models. The differences in the estimated unconstrained and constrained parameters are small as is the change in the estimated standard deviation of regression.

Model Unit Step Response

To judge the accuracy and performance of the constrained - parameter models and the unconstrained - parameter models, they are each tested with a unit step input.

Figures (5) and (6) show the step responses of both the constrained and unconstrained models plotted against time in seconds. The resultant curves are revealing and the following remarks can be made concerning them:

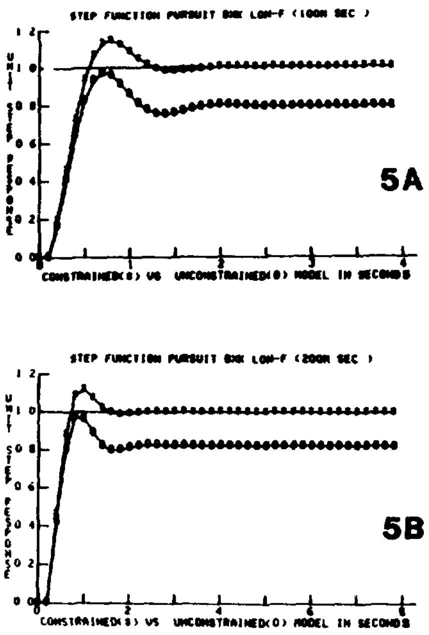

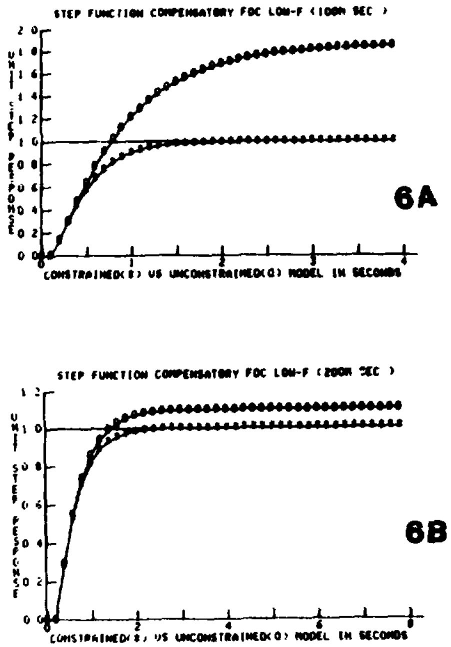

Figure 5: Model responses to unit step input. Constrained models have zero steady state error while the unconstrained models show an error of 20%.

Figure 6: Model responses to unit step input. The uncosntrained models show steady state errors of 80% and 10%.

a) Both models have time delays of about 0.2 seconds to 0.5 seconds, which is the time required for the response to reach 50% of the final value of unity.

b) The rise times of the constrained models are shorter than that of the unconstrained models.

c) The constrained models have settling times (the time to reach the 95% of the desired final valve) between 1 and 2 seconds. The unconstrained models have indeterminate settling times since some never reach within 5% of the required value of unity due to steady state errors.

d) The uncosntrained models have varying degrees of steady state errors, making them inconsistent in their steady state responses. For example, the steady state error is about 20% in both samples of Fig. 5 and about 80% in the top sample of Fig. 6.

The importance of constraining the operator models is obvious. Since the unconstrained model is inaccurate in transmitting the known response of the unit step signal, it cannot be relied upon to predict the system response to unknown inputs to which the human may be subjected to in practice. This makes these models undesirable in describing the dynamics of the human controller.

Shinners [1] did not constrain his operator models and his model for operator C (equation (3)) with unity feedback gives an error of 15.8% for a step input function.

In figures (7) and (8), the pursuit and compensatory responses are compared. These graphs also reveal interesting dynamics. For the low-frequency range, the pursuit models all have shorter rise time and shorter time delay than the corresponding compensatory models. On the other hand, for the high-frequency range, the situation is reversed, i.e., the rise time and the time delay are shorter for the compensatory models. It is important to observe that the difference between the pursuit and the compensatory tracking modes lies only in the transient stage.

Residual Analysis

To determine whether the probability assumptions of ordinary least squares have been met and also to statistically justify the selection of $\hat{n} = 2$, several statistical tests were performed on the estimated residuals $\hat{v}(t)$. Basically we require the $\hat{v}(t)$ to have a normal distribution and to be statistically independent. Since we are estimating a lag model, a Durbin-Watson test is inappropriate [21]. While the histograms of residuals appeared to be bell shaped and normal, we need to support this assessment quantitatively. The sampling distribution of this statistic is approximately the Chi-square distribution with K-1 degrees of freedom, where K is the number of intervals for a given histogram. For example, for the pursuit FOC low-freq at 100 msec, $\chi^2 = 0.0503$. Since this is much less than 24.9958, the value of $\chi^2_{0.05}$ for 16-1 = 15 degrees of freedom, the hypothesis that the residuals come from a normal population cannot be rejected at the 5% level of significance. From this test we conclude that the residuals are almost certainly from a normal distribution.

Although the $\hat{v}(t)$ values pass the normality test well, (our χ^2 tables only go down to significance levels of 0.005 and the measured χ^2 is still orders below that entry), they might be autocorrelated. Such autocorrelation would indicate that more lags should be used in the models of the human operator. In this

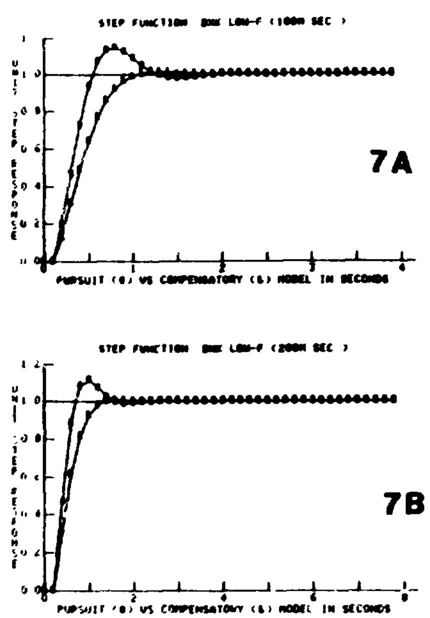

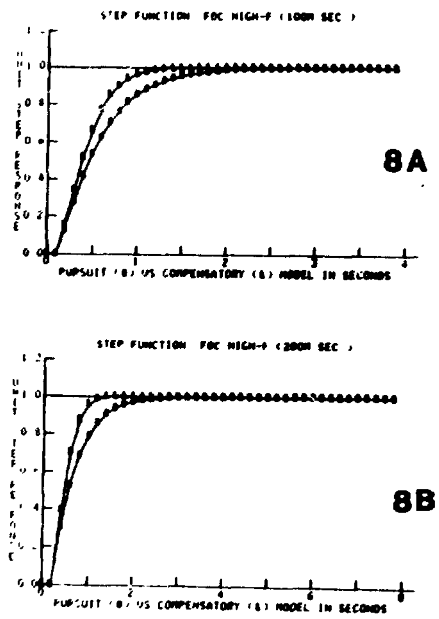

Figure 7: Constrained model responses to unit step inputs in pursuit and compensatory modes for subject BXK.

Figure 8: Constrained model responses to unit step inputs in pursuit and compensatory modes for subject FOC.

sense an autocorrelation test is more important than a normality test. We applied an autocorrelation test to the residuals. This test was the standard 'runs' randomness test applied to a sequence [23]. In this case, since the $\hat{v}(t)$ have zero mean, if s_1 is the number of times the $\hat{v}(t)$ are less than 0 and s_2 the number of times the $\hat{v}(t)$ are greater than 0, then the number of runs q of successive (+) signs and (-) signs in the $v(t)$ sequence should be normally distributed with mean and variance depending on s_1 and s_2 . If autocorrelation exists in the $\hat{v}(t)$ then s_1 and s_2 will make q deviate significantly from its expected value. We applied the standardized test statistic.

$$\bar{q} = \frac{[q - E(q)]}{\sigma_q} \tag{27}$$

t all of the residuals.

For example, for the compensatory BXK high-freq at 200 msec, the expected number of runs is 153 and the observed number of runs is $s_1 = 141$, $s_2 = 165$. This test was found to be statistically significant at level 0.0000 (within the resolution and accuracy limits of Minitab 2) indicating a measured 100% confidence that the residuals are certainly uncorrelated. (Details of all of the statistical test applied in this section can be found in [23]).

IV SPECTRAL ANALYSIS

A stationary stochastic process is simply described by its autocovariance function. An equivalent description is provided by its power spectrum, which is the Fourier transform of the autocovariance function [17].

Residual Spectra

In the anlysis of the residuals, Shinners [1] observed that the human operator is a generator of seasonality characteristcs. He defined seasonality as the periodicity in the observations, i.e., an observation at a particular time is related to observations from previous times in a periodic manner. The seasonality periods in his residual analysis were calculated to be 0.4, 1.6, and 3.4 sec for a unity feedback system. The origin of this seasonality effect was not clear.

In the residual spectra in Figure 9, for the low-frequency input signal, the peaks occur at 0 and 0.7 Hz for both subjects in pursuit and compensatory modes using 100 msec sampling. The nearest input frequencies were 0.4557 and 0.8138 Hz. For the high-frequency input, these peaks occur at 0.2 and 1.5 Hz in three out of four cases and at 0.5 and 1.7 Hz for BXK in pursuit mode. The highest input frequency was 1.48 Hz.

The peaks in residual spectra using 200 msec sampling analysis with low-frequency input occur at 1.25 Hz in two cases, at 1.35 Hz and at 2.2 Hz in one case each. These are outside the input frequency range. With the high-frequency input, the power spectra show peaks at 0.7 and 2 Hz and in some cases remain high even at the end interval. Thus the error spectra for 200 msec sampling suggests that this rate is not as capable and effective as the 100 msec rate in reproducing the information content of the data series.

Shinners [1] had used a noise generator with a bandwidth of 1.5 Hz (our highest frequency sinusoid input was at 1.48 Hz). His 200 msec sampling analysis was probably inadequate as we have observed in our analysis. He we find that the

ERROR SPECTRA

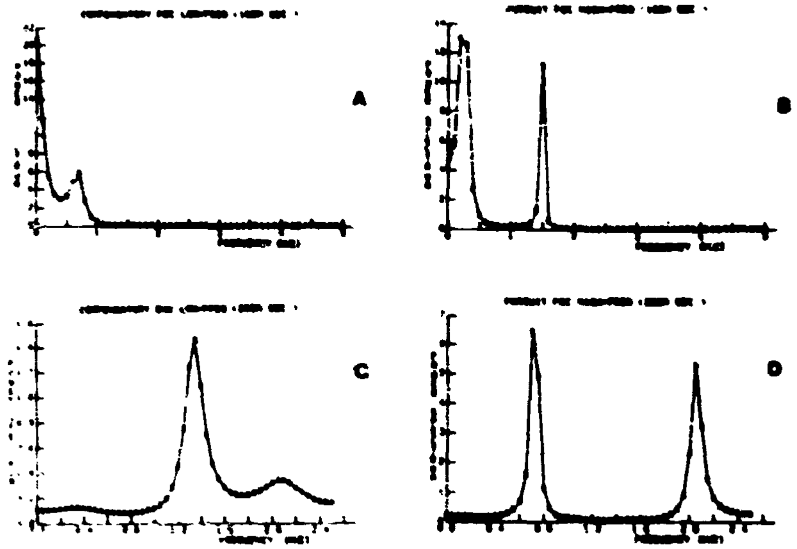

Figure 9: Power spectra of the residuals.

dominant peak in residuals is at zero frequency for the low-frequency input and at about 0.2 Hz for the high-frequency input. This does not seem to represent operator's generated seasonality.

Model Spectra

In any analysis of a time series model one is tempted to retain only the most significant lags and external variables [21]. Since our primary use of the model is for description of the operator dynamics and to some extent for prediction, we must also weigh the sum of squares explained by each lag and external variable. As indicated in Tables 1 and 2 some apparently statistically significant lag coefficients (high t values), explain little of the total variation in the operator responses. Conversely, some less significant coefficients (low t values) are associated with lags that explain a large amount of variation in the data and therefore would be strong predictors. Rather than arbitrarily eliminate lags from the model, all the lags were kept regardless of the t values of their coefficients and their explained sum of squares. (The name "sum of squares" refers to the individual contribution to the sum of squares of regression).

The estimated models (24) and (25) have deterministic expected value of the form:

$$\bar{y}(t) = \hat{\alpha}_1 \bar{y}(t-1) + \hat{\alpha}_2 \bar{y}(t-2) + \hat{\beta}_0 \bar{x}(t) \tag{28}$$

$$\bar{y}(t) = \hat{\alpha}_1 \bar{y}(t-1) + \hat{\alpha}_2 \bar{y}(t-2) + \hat{\beta}_0 \bar{x}(t) + \hat{\beta}_1 \bar{x}(t-1) \tag{29}$$

where $\bar{y}(t) = E[y(t)]$; $E[v(t)] = 0$ by virtue of the linear regression assumptions and $\hat{\alpha}_1$, $\hat{\alpha}_2$, $\hat{\beta}_0$, $\hat{\beta}_1$ are the estimated parameters from Tables 1 and 2.

Since (28) and (29) are linear, autonomous, difference equations, the stability of their equilibrium determines whether the predicted operator responses will be bounded in magnitude as t becomes large. The eigenvalues of the models, λ_1 and λ_2 satisfy the characteristic polynomial:

$$\lambda^2 - \alpha_1 \lambda - \alpha_2 = 0 \tag{30}$$

The equilibrium $\bar{y}(t) \equiv 0$ is asymptotically stable if and only if $|\lambda_i| < 1$, $i = 1,2$. The eigenvalues are listed in Tables 3 and 4 for 100 msec sampling models. If λ_i is complex the term containing $\lambda_i{}^t$ in the solution of $\bar{y}(t)$ can be written as:

$$\lambda_i{}^t = |\lambda_i|^t [\mathrm{Cos}(2\pi t/T_i) + j\ \mathrm{Sin}(2\pi t/T_i)] \tag{31}$$

where T_i is the characteristic period associated with λ_i and is given by

$$T_i = 2\pi [\tan^{-1} \mathrm{Im}(\lambda_i)/\mathrm{Re}(\lambda_i)]^{-1} \tag{32}$$

where $\mathrm{Im}(\lambda_i)$ and $\mathrm{Re}(\lambda_i)$ are the imaginary and real parts of λ_i, respectively. The T_i is the period of oscillation of the components of $\bar{y}(t)$. The values of T_i are also tabulated in Tables 3 and 4.

TABLE 3

EIGENVALUE ANALYSIS OF MODELS BKX 100 MSEC						
TRACKING MODE	FREQUENCY RANGE	i	EIGENVALUE λ_i	$\lvert\lambda_i\rvert$	Period T_i of λ_i in seconds	Frequency, f_i $(1/T_i)$ of λ_i in HERTZ
PURSUIT	LOW	1	0.696 + 0.32j	0.766	14.56	0.07
		2	0.696 - 0.32j	0.766	14.56	0.07
	HIGH	1	0.737 + 0.263j	0.783	18.18	0.06
		2	0.737 - 0.263j	0.783	18.18	0.06
COMPEN-SATORY	LOW	1	0.679 + 0.173j	0.701	25.21	0.04
		2	0.679 - 0.173j	0.701	25.21	0.04
	HIGH	1	0.657 + 0.323j	0.732	13.74	0.07
		2	0.657 - 0.323j	0.732	13.74	0.07

TABLE 4

EIGENVALUE ANALYSIS OF MODELS						FOC 100 MSEC
TRACKING MODE	FREQUENCY RANGE	i	EIGENVALUE λ_i	$\lvert\lambda_i\rvert$	Period T_i of λ_i in seconds	Frequency, $f_i\,(1/T_i)$ of λ_i in HERTZ
PURSUIT	LOW	1	0.683 + 0.13 j	0.695	33.39	0.03
		2	0.683 - 0.13 j	0.695	33.39	0.03
	HIGH	1	0.377	0.377	∞	0
		2	0.793	0.793	∞	0
COMPEN-SATORY	LOW	1	0.615 + 0.325j	0.695	12.91	0.08
		2	0.615 - 0.325j	0.695	12.91	0.08
	HIGH	1	0.623 + 0.107j	0.632	36.91	0.03
		2	0.623 - 0.107j	0.632	36.91	0.03

It is important to observe that the operator models for the pursuit and compensatory tracking modes in all categories produce system eigenvalues which have very large periods and the system is absolutely stable.

Discrete Time Series models can be Fourier transformed into the frequency domain [17]. That is,

$$Y(f) = H(f)\ X(f) \tag{33}$$

where

$$H(f) = \frac{\beta_0 + \beta_1 e^{-j2\pi f\Delta} + \ldots + \beta_m e^{-j2\pi fm\Delta}}{1 - \alpha_1 e^{-j2\pi f\Delta} - \ldots - \alpha_n e^{-j2\pi fn\Delta}} \tag{34}$$

is the frequency response function of the system. $Y(f)$ and $X(f)$ are the Fourier transforms of the response of and input to the system, respectively. The frequency response function $H(f)$ is of interest because it contains both the amplitude and the phase - shift information. Thus,

$$H(f) = G(f)e^{j\phi(f)} \tag{35}$$

where

$$G(f) = |H(f)|,$$

and $\phi(f) = \tan^{-1}\{\mathrm{Im}[H(f)] / \mathrm{Re}[H(f)]\}$

The frequency response functions, gain and phase of the closed loop system incorporating a human operator, are depicted in the Bode plots in Figure 10. The Bode plots reveal interesting and physically plausible dynamics of the human controller. The gain and phase characteristics of both pursuit and compensatory tracking are quite similar. The human operator behaves as a low-pass filter. The phase drops steadily from low to high frequency, i.e., the output lags behind the input.

V. HUMAN OPERATOR TRANSFER FUNCTION

The analysis so far has been concerned with the human operator in the forward path of a closed-loop unity feedback system. Equation (33) defines the closed-loop transfer function with the parameter values given in Tables 1 and 2. Thus, for FOC in the pursuit mode with low frequency input and 100 msec sampling,

$$H(z) = \frac{0.188}{1-1.366z^{-1} + 0.483z^{-2}} = \frac{G_H(z)}{1 + G_H(z)} \tag{36}$$

where $G_H(z)$ is the human operator transfer function (as in equation (3)). Therefore,

$$G_H(z) = \frac{0.134}{(1-z^{-1})\ (1-0.548z^{-1})} \tag{37}$$

The Z- transform may be converted into a Laplace transform function using the following relation:

$$\mathcal{L}\{e^{-at}\} = \frac{1}{s+a} \quad \text{and} \quad \mathcal{Z}\{e^{-akT}\} = \frac{z}{z - e^{-aT}} \tag{38}$$

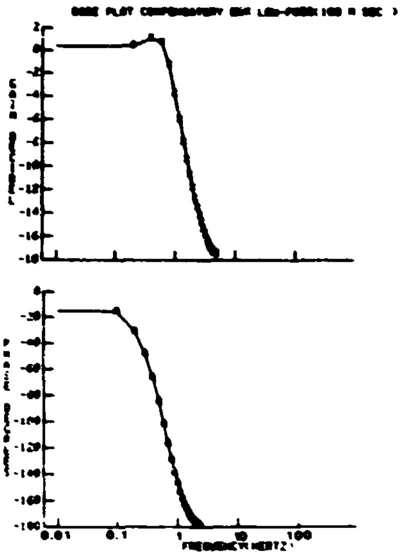

Figure 10: Frequency response functions of the closed-loop model with unity feedback, subject BXK in compensatory mode.

where T is the sampling interval.

From equations (37) and (38) (T=0.1 sec),

$$G_H(s) = \frac{0.134(s+13.3)}{s(s+6.02)} \tag{39}$$

The human operator transfer functions in Z - transform and Laplace transform equivalents are given in Table 5 for both subjects using 100 msec sampling analysis. These transfer functions are not in the normal forms given in equation (2) where an effective time delay is included. The phase lag observed can be accounted for by a second order transfer function and with a zero located in the left half plane for low-frequency inputs and in the right-half plane for high-frequency inputs. The effective time delay is not a measure of the human operator reaction time to unpredictable inputs but a quantity which models the phase lag over the range of experimental input frequencies.

Shinners [1] found the human operator in compensatory tracking to be adequately represented by

$$G_H(z) = \frac{K(1-T_1 z^{-1}) \quad z^{-1}}{(1-T_2 z^{-1}) \quad (1+T_3 z^{-1})} \tag{40}$$

Fot the sampling interval of 0.2 sec, his time constants had the following limits: $0<T_1<0.83$, $0.39<T_2<0.99$, $-0.97<T_3<0.54$, and $0.48<K<0.65$.

In our analysis, (Table 5), T_2 is always equal to one because the model is constrained to have zero steady state error for a step input. T_3 ranges between 0.287 and 0.728 with 100 msec sampling. Our numerator polynomials are different from Shinners and require at most one lag term.

VI CONCLUSIONS

Time-series modeling is a powerful and versatile technique in modeling human operator dynamics. Its versatility lies in the fact that it can very effectively model the operator in both the time and the frequency domain. In the former case, which lies in the realm of parametric modeling, the method is very parsimonious in the use of parameters to represent the model structure.

Fourier series analysis, which finds its greatest utility in spectral analysis (or frequency domain), does not outperform the time-series methods. Time-series analysis incorporating the stochastic properties of the data is a more useful device for prediction. Time-series analysis does not require any special type of input and can be used in a normal operating environment.

A remarkable feature of the time series technique is its ability to use fewer observations than Fourier analysis in capturing the necessary dynamics of the system.

In a recent study, Jaeger, Agarwal, and Gottlieb [24] suggested that the predictor operator performs essentially the same in both pursuit and compensatory tracking modes. Our findings here are consistent with those results.

TABLE 5 : HUMAN OPERATOR TRANSFER FUNCTIONS (100 ms sampling)

		B X K		P O C	
		Low-frequency	High-frequency	Low-frequency	High-frequency
Pursuit	$G_H(z)$	$\frac{0..12}{(1-z^{-1})(1-0.728z^{-1})}$	$\frac{-0.12(1-2.017z^{-1})}{(1-z^{-1})(1-0.538z^{-1})}$	$\frac{0.134}{(1-z^{-1})(1-0.548z^{-1})}$	$\frac{-0.039(1-4.146z^{-1})}{(1-z^{-1})(1-0.287z^{-1})}$
	$G_H(s)$	$\frac{0.242(S+11.69)}{s(s+3.18)}$	$\frac{-0.12(s-13.64)}{s(s+6.2)}$	$\frac{0.134(s+13.3)}{s(s+6.02)}$	$\frac{-0.039(s-55.1)}{s(s+12.48)}$
Compensatory	$G_H(z)$	$\frac{0.153}{(1-z^{-1})(1-0.566z^{-1})}$	$\frac{-0.106(1-2.877z^{-1})}{(1-z^{-1})(1-0.479z^{-1})}$	$\frac{0.152}{(1-z^{-1})(1-0.416z^{-1})}$	$\frac{-0.017(1-9.824z^{-1})}{(1-z^{-1})(1-0.393z^{-1})}$
	$G_H(s)$	$\frac{0.153(s+13.15)}{s(s+5.7)}$	$\frac{-0.106(s-26.52)}{s(s+7.36)}$	$\frac{0.152(s+15.0)}{s(s+8.77)}$	$\frac{-0.017(s-135.8)}{s(s+9.35)}$

The method of sampling at 100 msec is found to be adequate and effective in capturing the information from the total observations. The 200 msec interval is less accurate, especially in sampling with high-frequency inputs, and is not recommended, although the overall dynamics after modeling are similar for the two sampling rates.

The Normalized Residual Criterion is a reliable tool for estimation of the model structure; it eliminates the use of the auto-correlation functions (ACF), Autocovariance function (ACVF) and the partial correlation function (PCF) [16] and it combines the trial and error procedures of identification, estimation and diagnostic cheking used by Shinners [1] into a one step process.

The importance of constraining the parameters of the estimated time series models are stressed in this study. This is necessary if the models are to be accurate in describing the human dynamics.

The model spectra and the eigenvalue analysis clearly show that the human operator is not a generator of periodic characteristics. The human controller's response eventually reaches a steady state if there is an input or decays asymptotically if the input is removed.

VII REFERENCES

1. Shinners, S.M., "Modeling of Human Operator Performance Utilizing Time Series Analysis", IEEE Transactions on Systems, Man and Cybernetics, Vol. SMC-4, No 5, pp. 446 - 458, September, 1974.

2. Sheridan, T.B., and Ferrell, W.R., Man-Machine Systems: Information, Control, and Decision Models of Human Performance, M.I.T. Press, Cambridge, Mass., 1974.

3. Stark, L., Neurological Control Systems; Studies in Bioengineering, Plenum Press, New York, 1968.

4. McRuer, D.T., and Jex, H.R., "A Review of Quasi-Linear Pilot Models", IEEE Trans. on Human Factors in Electronics, Vol. HFE - 8, No. 3, pp. 231 - 249, September, 1967.

5. Stark, L., Iida, M., and Willis, P.A., "Dynamic Characteristics of the Motor Coordination System in Man", Biophysical Journal, Vol. 1, pp. 279 - 300, 1961.

6. Navas, F., and Stark, L., "Sampling or Intermittency in Hand Control System Dynamics", Biophysical Journal, Vol. 8, pp. 252 - 302, 1968.

7. Taylor, Jr., L.W., "A comparison of Human Response Model in the Time and Frequency Domains", Third Annual NASA - University Conference on Manual Control, NASA SP-133, pp. 137 - 153, 1967.

8. Shirley, R.S., "A Comparison of Techniques for Measuring Human Operator Frequency Response", Sixth Annual Conference on Manual Control, AFFDL, pp. 803-869, April, 1970.

9. Kleinman, D.L. Baron, S., and Levinson, W.H., "An Optimal Control Model of Human Response - I: Theory and Validation", Automatica, Vol. 6, pp. 357 - 370, 1970.

10. Baron, S., Kleinman, D.L., and Levinson, W.H., "An Optimal Control Model of Human Response - II: Prediction of Human Performance in a Complex Task", Automatica, Vol. 6, pp. 371 - 384, 1970.

11. Young, L.R., "On Adaptive Manual Control", IEEE Transactions on Man-Machine Systems, Vol. 10, No. 4, pp. 292 - 331, December, 1969.

12. Bekey, G.A., "Description of the Human Operator in Control Systems", in Modern Control Systems Theory, C.T. Leondes, Editor, pp. 431 - 462, McGraw and Hill Book Comp., N.Y., 1965.

13. Elkind, J.I., and Forgie, C.D., "Characteristic of the Human Operator in Simple Manual Control Systems", IRE Transactions on Automatic Control. Vol. AC-4, No. 1, pp. 44 - 55, May, 1959.

14. Young, L.R., Green, D.M., Elkind, J.I., and Kelly, J.A., "Adaptive Dynamic Response Characteristics of the Human Operator in Simple Manual Control", IEEE Transactions on Human Factors in Electronics, Vol. HFE - 5, pp. 6 - 13, 1964.

15. Tanaka, K., Goto, K., and Washizu, K., "A comparison of Techniques for Identifying Human Operator Dynamics Utilizing Time Series Analysis", Proceedings of the Twelfth Annual Conference on Manual Control, NASA TM X - 73170, pp. 673 - 693, 1976.

16. Box, G.E.P., and Jenkins, G.M., Time Series Analysis: Forecasting and Control, Holden-Day Inc., San Francisco, Revised edition, 1976.

17. Jenkins, G.M. and Watts, D.G., Spectral Analysis and Its Applications, Holden-Day, Inc., San Francisco, 1968.

18. Akaike, H., "Autoregressive Model Fitting for Control", Ann. Inst. Statistics Math., Vol. 23, pp. 163 - 180, 1971.

19. Akaike, H., "A New Look at the Statistical Model Identification", IEEE Transactions on Automatic Control, Vol. AC - 19, No. 6, pp. 716 - 723, December, 1974.

20. Suen, L.C., and Liu, R., "A Normalized Residual Criterion for the Determination of Structure of Linear Systems", Policy Analysis and Information Systems, Vol. 1, pp. 1 - 22, July, 1977.

21. O'Neill, W.D., "Time Series Modeling of Chicago Particulates", ASCE Journal of Environmental Engineering, Vol. 105, EE5, pp. 855 - 866, October, 1979.

22. Fogel, J.L. Human Information Processing, Prentice - Hall, Inc., Englewood Cliffs, N.J., pp. 219 - 271, 1967.

23. Miller, I. and Freund, J.E., Probability and Statistics for Engineering, 2nd edition. Prentice-Hall, Inc., Englewood Cliffs, N.J., 1977.

24. Jaeger, R.J., Agarwal, G.C., and Gottlieb, G.L., "Predictor Operator in Pursuit and Compensatory Tracking", Fifteenth Annual Conference on Manual Control, Wright State University., AFFDL-TR-79-3134, pp. 311 - 330, 1979.

25. McRuer, D.T. and Krendel, Ed. S., "The Human Operator as a Servo System Element" *Journal Franklin Inst.*, Vol. 267, pp. 381 - 403 and pp. 511 - 536, 1959.

26. Johnston, J., *Econometric Methods*, 2nd Edition, McGraw-Hill Co., New York, 1972.

27. Jex, H.R., McDonnell, J.D., and Phatak, A.V., "A Critical Tracking Task for Manual Control Research", *IEEE Trans. Human Factors in Electronics*, Vol. HFE-7, pp. 138 - 145, 1966.

28. Maklad, M.S. and Nichols, S.T., "A New Approach to Model Structure Discrimination", *IEEE Trans. Systems, Man, and Cybernetics*, SMC-10, pp. 78 - 84, 1980.

29. Fine, T.L. and Hwang, W.G., "Consistent Estimation of System Order", *IEEE Trans. on Automatic Control*, Vol. AC-24, pp. 387 - 402, 1979.

30. Astrom, K.J. and Eykhoff, P., "System Identification - A Survey", *Automatica* Vol. 7, pp. 123 - 162, 1971.

31. Jex, H.R. and Allen, R.W., "Research on a New Human Dynamic Response Test Battery", Proceedings of the Sixth Annual Conference on Manual Control. AFFDL, WPAFB, pp. 743 - 777, 1970.

32. Mehra, R.K., "On the Identification of Variances and Adaptive Kalman Filtering", *IEEE Trans. on Automatic Control*, Vol. AC-15, pp. 175 - 184, 1970.

33. Enstrom, K.D. and Rouse, W.B., "Real - Time Determination of How a Human has Allocated his Attention Between Control and Monitoring Tasks", *IEEE Transactions on Systems, Man, and Cybernetics*, Vol. SMC-7, pp. 153 - 161, 1977.

N82 34039 D2

A GUNNER MODEL FOR AN AAA TRACKING TASK WITH INTERRUPTED OBSERVATIONS

C. F. YU

K. C. WEI

Systems Research Laboratories, Inc. Dayton, OH 45440

M. M. VIKMANIS

Aerospace Medical Research Laboratory, Wright-Patterson AFB
OH 45433

ABSTRACT

This paper deals with the problem of modeling a trained human operators' tracking performance in an anti-aircraft system under various display blanking conditions. The input to the gunner is the observable tracking error subjected to repeated interruptions (blanking). A simple and effective gunner model was developed by extending Kou's observer model [1], which dealt with the case of no blanking. Our approach is to model the effect of blanking on the gunner's tracking performance via modeling the observer and controller gains.

I. INTRODUCTION

One of the fundamental goals of the Air Force in its Manned Threat Qualification Program is to evaluate and predict the effectiveness of a manned anti-aircraft artillery system. The main problem associated with it is to develop a mathematical model(s) for the gunner so that analysis and computer simulations of the closed loop man-machine system become possible. The fact that a trained human operator performing simple control tasks has consistent response is crucial for the effort of human operator modeling.

The mathematical modeling of a human operator in a simulated AAA system has been studied by many investigators during the past twenty years. Basically, the human operator was treated as a feedback controller or compensator in the closed loop system. McRuer [2], using frequency domain analysis, described the human operator with a linear transfer function and a remnant element. Kleinman [3], using an optimal stochastic control formulation, quantified the human operator as an optimal estimator and controller w.r.t. a lost functional and constraints. Kou [1], using a reduced order observer, characterized the human operator as a linear state feedback controller and Luenberger state reconstructor, with all system noises lumped into one remnant. All these models were able to explain their laboratory data under certain specified tracking conditions. For a discussion of model validation and the PID model (simplified optimal control model), see Phatak [4], [5].

This paper develops a blanking model (interrupted observations) for a human operator performing a two-axis tracking task in a simulated AAA system. As in the previous studies, the human operator perceives his tracking error as a displayed feedback signal. However, in this case, the display error signal is subjected to repeated interruptions which occur at pseudo-random times. The interruptions are, in the real world, due to electronic/optical countermeasures, or weather conditions like fog and visibility, etc. Using the optimal control model, Kleinman [6] has done an initial study of this condition (one second blanking without repetition). In [6], the effects of blanking on tracking performance were modelled via increasing the observation noises. We apply the observer formulation, and model the effects of blanking via degrading the observer and controller gains.

II. THE EXPERIMENTS AND THE TRACKING DATA

The general configuration of the manned AAA system is shown in Figure 1. For a detailed description of the AAA simulator, see Rolek [7].

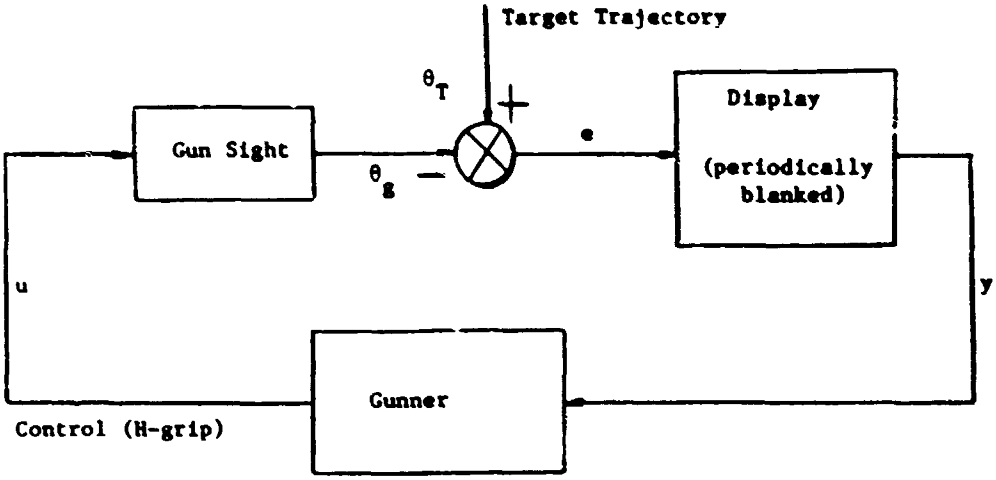

Figure A. General Configuration of the Blanking Experiments Conducted at AMRL

Three trained subjects were asked to track a moving target (simulated aircraft) on the display screen during an entire run of approximately 40 seconds. The subject used a rate control to direct the gunsight (pedestal) to follow the target. The screen was blanked periodically according to one of the following five blanking conditions.

(1) blanking duration 1.5 seconds, percentage of time blanked 25%
(2) blanking duration 3 seconds, percentage of time blanked 25%
(3) blanking duration 6 seconds, percentage of time blanked 25%
(4) blanking duration 3 seconds, percentage of time blanked 25%
(5) no blanking during the entire run (base line)

There were four pre-programmed, deterministic, input target trajectories, namely, the 2x2 flyby, the 4x5 flyby, the recon, and the weapon delivery. At each run, the subject had no information about (a) which of the four trajectories was used as the driving input, and (b) which of the five blanking conditions was being applied. With that experimental design, the subject was considered as tracking unknown target motion under pseudo-random interruptions. Each of the twenty tracking situations were run 40 times each and the time history of the tracking errors recorded. The means and standard deviations were then computed from the 40 replications. The whole experiment generated twenty sets of ensembled tracking data per subject. One subject's tracking data were selected for the modeling and simulation study.

Some observations on the tracking data

(1) The three subjects had reasonably consistent tracking responses. The "patterns" of the mean tracking errors and the standard deviations were very similar. In some situations, the magnitudes of the tracking data differed

slightly. The differences could be explained as due to a subject's tracking skill or his individual psychophysical parameters.

(2) The degration of tracking performance due to blanking was very significant. The "induced errors" (relative to no blanking data) depended on blanking duration, percentage of time blanked, and local characteristics of target motion. For example, if the target acceleration reversed its direction within a long blanking, the peak tracking errors were significantly much larger than that of the no blanking case.

III. OBSERVER MODEL WITH TIME VARYING GAINS

A close examination of the gunner's tracking performance indicates that the gunner can be regarded as a feedback controller. The feedback available to him consists of the displayed signal (observation) and the non-visual feedback generated through his control interaction with the dynamics of the system (perception). With this understanding, we assume that the gunner has an internal model of the closed loop system driven by his observation and his perception. It is natural to further assume that the gunner's control output is completely based on that internal model. Also, with the rate control in mind, it is not difficult to realize that the gunner's whole tracking efforts are basically designed to generate a key internal state variable - the target velocity. The gunner's internal model of target velocity was considered as the key variable in his feedback strategy. To quantify the gunner's internal target velocity, we assume that the internal velocity is actually generated via a Luenberger observer or state reconstructor. The associated observation or reconstruction gains are, in general, time varying. The gains depend on tracking conditions (information feedback), task difficulties (local trajectory characteristics), tracking skill, and the gunner's psychophysical parameters. Finally we assume that the gunner's feedback control law is linear in his observation and his perception. The closed loop model structure is shown in Figure B. Items (1) to (6) summarize the modeling assumptions.

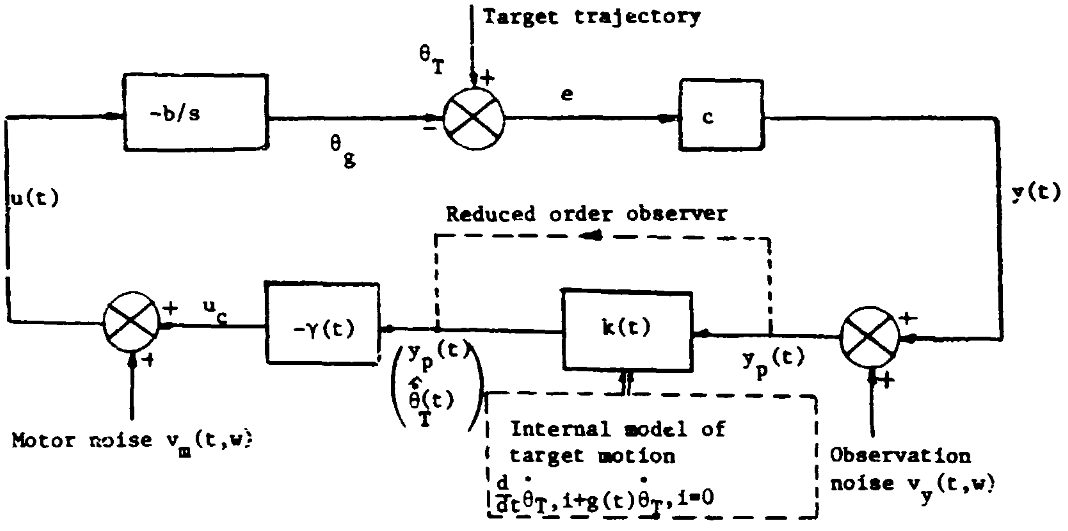
Target trajectory
θ_T
+
$-b/s$
θ_g
−
e
c
$y(t)$
$u(t)$
Reduced order observer
+
u_c
$-\gamma(t)$
$k(t)$
$\begin{pmatrix} y_p(t) \\ \hat{\theta}_T(t) \end{pmatrix}$
$y_p(t)$
+
+
+
Motor noise $v_m(t,w)$
Internal model of target motion
$\frac{d}{dt}\dot{\theta}_{T,i}+g(t)\dot{\theta}_{T,i}=0$
Observation noise $v_y(t,w)$

Figure B. Observer Model with Time-Varying Gains

ORIGINAL PAGE IS
OF P[illegible] QUALITY

The modeling assumptions:

(1) Human operator's internal model of target motion (adaptive)	$g(t)$
(2) Gun dynamics and visual observation factor (learned by H.O.)	$-b/s$, c
(3) Feedback control law (linear)	$-\gamma(t)$
(4) Estimation error dynamics (reduced-order observer)	$k(t)$
(5) Time delay (neglected)	0
(6) Noise structures (white, with suitable covariances)	$Vm(t)$, $Vy(t)$

Define the state variables of the closed loop system as
$X(t) = (x_1(t), x_2(t), x_3(t))^T$, where

$x_1(t) = y(t) = c\ e(t) = c\ (\theta_T - \theta_g)$ -- displayed tracking error

$x_2(t) = \dot{\theta}_T(t)$ ------------------------ true target velocity

$x_3(t) = \delta(t) = \dot{\theta}_T(t) - \hat{\dot{\theta}}_T(t)$ --------- velocity estimation error

In lieu of the assumptions (1) to (6), we have

$$\dot{\theta}_g(t) = -b\ u(t)$$

$$u_c(t) = -\gamma_1(t)\ y_p(t) - \gamma_2(t)\ \hat{\dot{\theta}}\ (t)$$

$$\dot{\beta}(t) = -(k(t)+g(t))\ \beta(t) + \ddot{\theta}_T(t) + g(t)\ \dot{\theta}_T(t) - kbcv_m(t,w)$$

$$y_p(t) = y(t) + v_y(t,\omega)$$

$$u(t) = u_c(t) + v_m(t,\omega)$$

The above equations can be written in matrix form as

$$\dot{X}(t) = A(t)\ X(t) + F\ \ddot{\theta}_T(t) + \text{noise terms}$$

where

$$A(t) = \begin{bmatrix} \frac{\dot{c}}{c} - bc\gamma_1 & c(1-b\gamma_2) & bc\gamma_2 \\ 0 & 0 & 0 \\ 0 & g(t) & -(k(t)^c+g(t)) \end{bmatrix} \qquad F = \begin{bmatrix} 0 \\ 1 \\ 1 \end{bmatrix}$$

$$\text{Noise terms} = \begin{bmatrix} bcv_m(t,w) - bc\gamma_1 v_y(t,w) \\ 0 \\ -kbcv_m(t,w) \end{bmatrix}$$

IV THE BLANKING MODEL AND THE SIMULATION STUDIES

Only the elevation case is considered here, the azimuth case is similar and will be reported elsewhere. Note that $c = 1$ and $b = -1.34$ for the elevation case. For simplicity, we assume that the observation noise can be lumped into the motor noise (or simply assume that there is no observation noise). The covariance of the motor noise is assumed to be of the form

$$E\ [v_m(t,w)\ v_m(t',w)] = \left(\alpha_1 + \alpha_2 [\hat{\dot{\theta}}_t(t)]^2 + \alpha_3\ [\hat{\ddot{\theta}}_t(t)]^2\right) \cdot \delta\ (t-t')$$

The control gains $\gamma(t)$ and the observation gains $k(t)$ are modelled as expontentially decreasing as the blanking proceeds, and exponentially increasing as the blanking stops. Both theoretic arguments and actual identification lead to the relation $b \cdot \gamma_2 \approx 1$, we assume that $\gamma_2(t)$ is a constant. Also, $g(t) = 0$, i.e., no target acceleration is perceived by the gunner.

Parameters identified

(PO) The base line parameters were identified from the 2x2 flyby - no blanking data:

$k = 0.48,\ \gamma_1 = -2.9,\ \gamma_2 = -0.77$

$\alpha_1 = 0.0003,\ \alpha_2 = 0.009,\ \alpha_3 = 1.3$

(PB) The time constants were identified from the 2x2 flyby - blanking condition 2 data:

$\tau\ (\gamma_1$, blanking$) = 2.32$ secs $\quad \tau\ (\gamma_1$, recovery$) = 1.92$ secs

τ (k, blanking) = 13.0 secs $\quad \tau$(k, recovery) = 4.0 secs

The above identified parameters were used in the simulation studies. Since the 4x5 flyby is considered to be similar to the 2x2 flyby, we only illustrate simulation results for the 2x2 flyby, the recon, and the weapon delivery. The results under various blanking conditions are shown in Figure 1 through Figure 8. Figure 9 is included for the discussion of an adaptive observer in the next section ($k = 1.2$ instead of 0.48).

V. CONCLUDING REMARKS AND FURTHER RESEARCH

Modelled as a linear feedback controller and a state reconstructor, the gunner was parameterized by the control gains and the estimation gains. These time varying gains together with the noise covariances characterized the gunner's tracking performance. The time varying gains directly reflect the gunner's tracking skill, tracking conditions, and his own psychophysical parameters. Hence, the gains were modelled and identified from the experimental data.

It is worth noting that the time varying estimation gains in this paper are not completely equivalent to the time-varying gains in Kalman filter. (Note that in both cases, the estimators have the same form of dynamics:

$$\dot{\hat{X}} = (A - K(t))\,\hat{X} + \text{obs. data}).$$

The Ricatti equations in the Kalman filter describe the propagation of error covariances for given noise statistics. The time varying nature of the filter gains is due to a finite time of observation. The noise covariances always affect the filter gains in a fixed manner. If one treats a human operator as a Kalman filter in his estimation process, the human operator's estimation gains are optimal w.r.t. mean-square criterion. However, a constrained Kalman type estimator can be designed, see Aoki [8] for an example of limited number of memory elements. On the other hand, a Luenberger observer can be extended to a stochastic estimator, see Tse [9] for a unifying approach. For relevant work on the implicit adaptive observer, see Nuyan [10].

The simulation results show very good model vs data matches. However, as indicated from Figure (1) to (8), some peak tracking errors predicted by the model tend to either overshoot or undershoot. This is due to the non-adaptive internal model of target motion in the current simulation ($g(t) = 0$). In the observer formulation, the "local bandwidth" g(t) of the internal velocity directly enters the observation gain as $(k(t) + g(t))$. The adaptive nature of the gunner's perception of target motion can be modelled by continuously "updating" the gain.

In other words, by modeling the gain according to the gunner's perception of target acceleration, the overshoots can be eliminated. Figure 9 shows a typical simulation result based on the idea of an adaptive observer.

ACKNOWLEDGEMENTS

This work was supported by the 6570th Aerospace Medical Research Laboratory, Wright-Patterson AFB, Dayton, Ohio, under Contract F33615-79-C-0500. The authors wish to thank Mr. Walt Summers, Dr. D. W. Repperger, and Dr. C. N. Day, Capt. A. Dickson for their valuable suggestion and support.

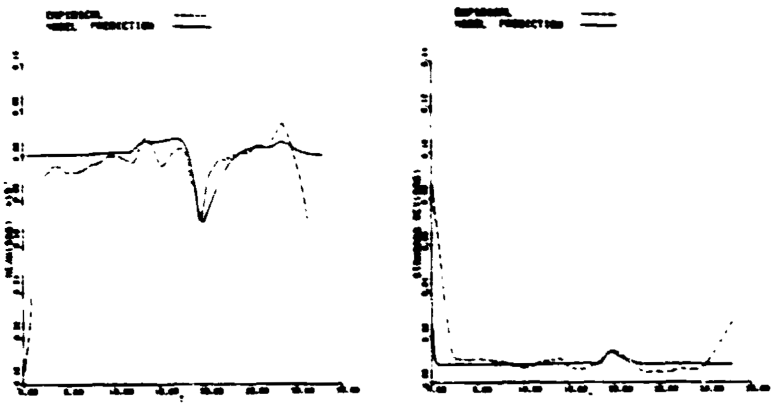

Figure 7, Weapon delivery, no blanking.

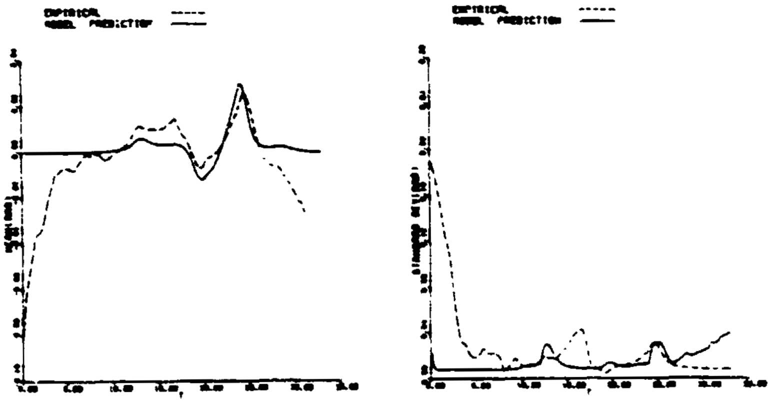

Figure 8, Weapon delivery, blanking duration 3 seconds, 25%.

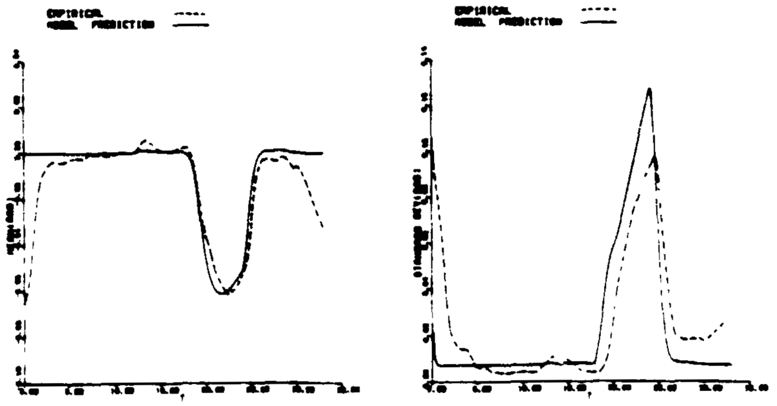

Figure 9, Weapon delivery, blanking duration 6 seconds.

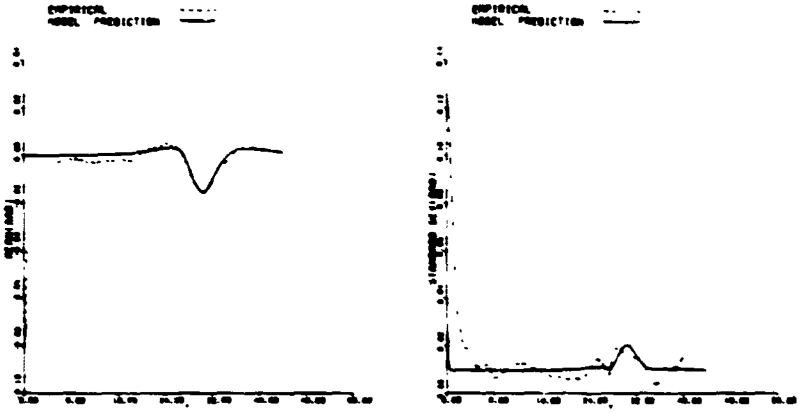

Figure 1, 2x2 flyby, no blanking.

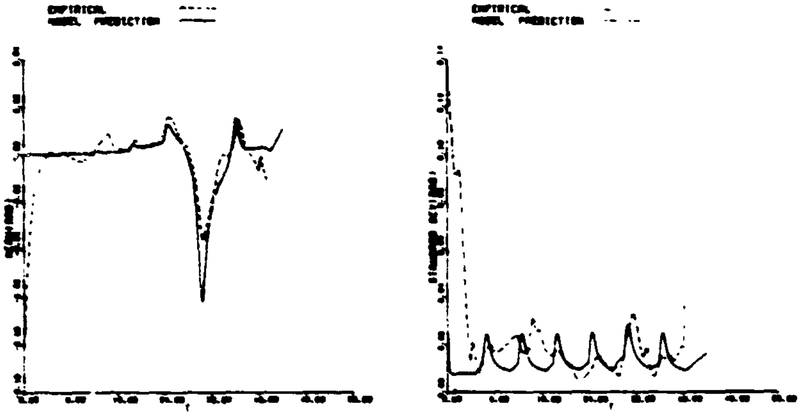

Figure 2, 2x2 flyby, blanking duration 1.5 seconds.

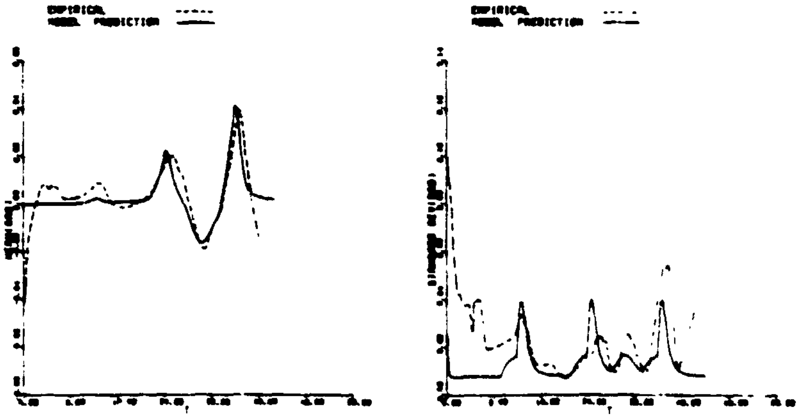

Figure 3, 2x2 flyby, blanking duration 3 seconds, 25%.

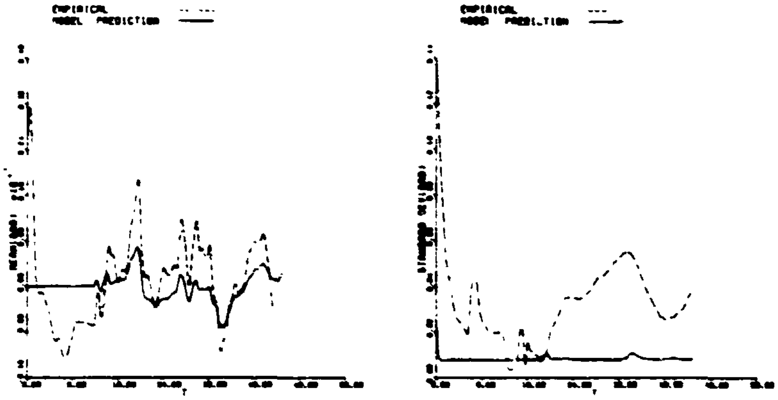

Figure 4, Recon, no blanking.

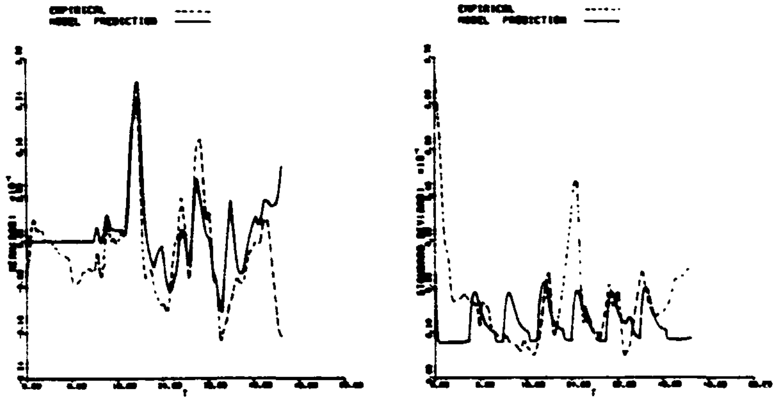

Figure 5, Recon, blanking duration 1.5 seconds.

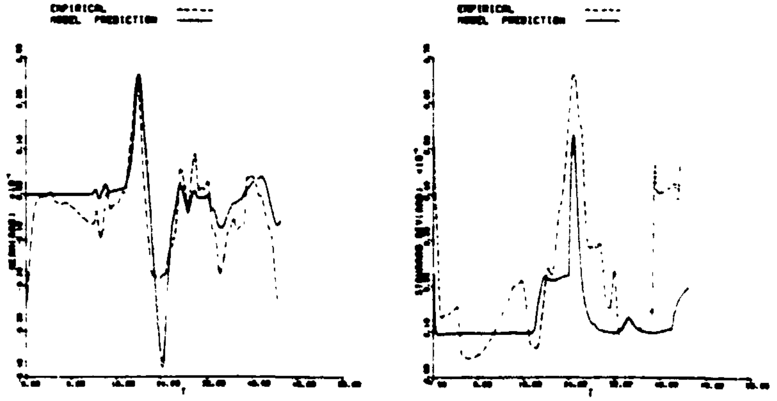

Figure 6, Recon, blanking duration 6 seconds.

REFERENCES

1. Kou, R. S., B. C. Glass, C. N. Day and M. M. Vikmanis, "Development of an AAA Gunner Model Based on Reduced-Order Observer Theory", Proc. 1979 Conference on Decision and Control, San Diego, CA.
2. McRuer, D. T. and E. S. Krendel, "Mathematical Models of Human Pilot Behavior", AGARD-AG-188, 1974
3. Kleinman, D. L. and B. Glass, "Modeling AAA Tracking Data Using the Optimal Control Model", 13th Annual Conference on Manual Control, MIT, June 1977.
4. Phatak, A. V., "Investigation of Alternate Human Operator Optimal Control Model Structures", Proc. of the 15th Annual Conference on Manual Control, 1979.
5. Phatak, A. V., "Modeling the Human Gunner in an Anti-Aircraft Artillery (AAA) Tracking Tasks" Human Factors, 1977, 19(5).
6. Kleinman, D. L., A. R. Ephrath and P. Krishna Rao, "A Model for the Target Tracking Ability of a Human Operator in an AAA System", Technical Report EECS TR 79-3, January, 1979.
7. Rolek, E. P., "MTQ AZ EL ONE STUDY", MTQ Experimentation Report No. 5, Systems Research Laboratories, Inc., Dayton, OH, 1977.
8. Tse, E. and M. Athans, "Optimal Minimal-Order Observer-Estimators for Discrete Linear Time Varying Systems", IEEE Trans. on Automatic Control, August, 1970.
9. Aoki, M. and J. R. Huddle, "Estimation of the State Vector of a Linear Stochastic System with Constrained Estimator", IEEE Trans. on Automatic Control, August, 1967.
10. Nuyan, S. and R. L. Carroll, "Minimal Order Arbitrary Fast Adaptive Observers and Identifiers", IEEE Trans. on Automatic Control, April, 1979.

N82 34040

D3

MODELING HUMAN TARGET ACQUISITION IN GROUND-TO-AIR WEAPON SYSTEMS

A.V. Phatak and R.L. Mohr
Analytical Mechanics Associates
Mountain View, California

M. Vikmanis
AMRL/HEC
WPAFB, Ohio

and

K.C. Wei
Systems Research Laboratories
Dayton, Ohio

SUMMARY

Several models have been developed for describing human operator input-output behavior in ground-to-air target tracking tasks. These models are intended to be used for predicting human gunner performance and hence manned weapon systems effectiveness. However, a complete evaluation of a given system must include a quantitative understanding of human target acquisition control strategies and resulting performance.

This paper considers the problems associated with formulating and validating mathematical models for describing and predicting human target acquisition response. In particular, the extension of the human observer model to include the acquisition phase as well as the tracking segment is presented. Relationship of the Observer model structure to the more complex Standard Optimal Control model formulation and to the simpler Transfer Function/Noise representation is discussed. Problems pertinent to structural identifiability and the form of the parameterization are elucidated. A systematic approach towards the identification of the observer acquisition model parameters from ensemble tracking error data is presented.

PRECEDING PAGE BLANK NOT FILMED

INTRODUCTION

The purpose of this paper is to discuss the problems associated with identification of an observer model structure[1] for the human gunner in an anti-aircraft artillery (AAA) target-acquisition task. Figure 1 shows the block diagram for the AAA tracking task. The visual display has a 30° field-of-view (FOV) and provides the gunner with azimuth (traverse plane) and elevation pointing errors with respect to the moving target. Experimental data for the acquisition and tracking of target trajectories were obtained at the Aerospace Medical Research Laboratories (AMRL) for a variety of initial conditions. Ensemble tracking error data for the azimuth and elevation axes were obtained for subsequent use in identifying the observer model parameters.

EXPERIMENTAL DATA

Two trajectories, a standard 2x2 flyby and a high-speed flyby called 2x2++ were simulated. Figure 2 describes the two target profiles relative to the gunsight position. The target aircraft begin at the nominal xyz coordinates of (610, 10058, 610) meters and end at (610, -2743, 610) meters. At the start of each run, the gunsight display cross-hair is slewed to the nominal initial target position. This corresponds to the initial condition (0.0, 0.0) on the visual display shown in Figure 3. Ten other target trajectories corresponding to the initial conditions shown in Figure 3 were simulated. The azimuth and elevation angles for the flyby trajectory may be computed using

$$\text{Target Azimuth} \quad \theta_T = \tan^{-1} \frac{y}{x} \tag{1}$$

$$\text{Target Elevation} \quad \phi_T = \tan^{-1} \frac{z}{\sqrt{x^2 + y^2}} \tag{2}$$

$$\text{where:} \quad y = 10058 - \frac{12801t}{D} \tag{3}$$

D being the duration of flight in seconds. Note that D = 70 s for the standard 2x2 flyby and 40 s for the 2x2++ flyby trajectory. The different display initial conditions are simulated by offsetting the x_o and z_o coordinates of the target initial position while keeping y_o fixed at -10058 m. Eight runs per initial condition were obtained and the individual tracking errors in the azimuth and elevation axes were processed to give ensemble error statistics (mean and standard deviation). These data are to be used for identifying the parameters of the observer model structure for the target acquisition phase and subsequently for the tracking segment. The ensemble data consists of the following variables:

t — time

$\bar{e}_\theta$ — mean azimuth error

σ_θ — standard deviation of azimuth error

$\bar{e}_\phi$ — mean elevation error

σ_ϕ — standard deviation of elevation error

ORIGINAL PAGE IS
OF POOR QUALITY

sampled at intervals of 0.03 seconds. Trajectory data for the 11 target profiles in the form of

t: time

$\theta_T, \dot{\theta}_T, \ddot{\theta}_T$: Target azimuth angle, velocity and acceleration

$\phi_T, \dot{\phi}_T, \ddot{\phi}_T$: Target elevation angle, velocity and acceleration

was also recorded every 0.03 seconds.

Figure 3 also shows the relative apparent initial velocity vector on the display for the 11 trajectories. Targets to the left of the vertical line BB require a counterclockwise slew rate while those to the right demand clockwise sight motion.

OBSERVER MODEL

Figure 4 shows a block diagram of the observer theory model for the human gunner. The input to the model is the displayed error y

$$y = e_T = c(\theta_T - \theta_g) \tag{3}$$

where:
$$\begin{aligned} c &= 1 \quad \text{for the elevation axis} \\ &= \cos(\theta_g)_{E\ell} \quad \text{for the azimuth axis.} \end{aligned} \tag{4}$$

The observer estimates the target rate $\hat{\dot{\theta}}_T$ according to the equations

$$\hat{\dot{\theta}}_T = z + ky \tag{5}$$

$$\dot{z} = -k\,c\,z - (kc + \dot{c}/c)ky - k\,b\,c\,u_c \tag{6}$$

where:
$$u_c = -\gamma_1 y - \gamma_2 \hat{\dot{\theta}}_T \tag{7}$$

$$\dot{\theta}_g = -b\,u \tag{8}$$

$$\begin{pmatrix} b_{Az} = -1.28 \\ b_{E\ell} = -1.34 \end{pmatrix} \tag{9}$$

an
$$u = u_c + v \tag{10}$$

where:
$$v \triangleq N(0, Q) \tag{11}$$

$$Q = \text{cov}(v) \triangleq \alpha_1 + \alpha_2\, \hat{\dot{\theta}}_T^2 + \dot{\hat{\dot{\theta}}}_T^2 \,. \tag{12}$$

In this model, k is the observer gain, γ_1 and γ_2 are the control law feedback gains, and α_1, α_2 and α_3 are the noise model parameters. The resulting quasi-stationary (frozen point) closed-loop system including the gunsight and the human gunner is shown in Figure 5. The equivalent human gunner describing function model assuming quasi-stationary conditions is given as

ORIGINAL PAGE IS
OF POOR QUALITY

$$\frac{u_c}{y}(s) = -\frac{(\gamma_1 + k\gamma_2)s + k(c\gamma_1 - \frac{\dot{c}}{c}\gamma_2)}{s + kc(1 - b\gamma_2)} . \tag{13}$$

Note that $\gamma_2 = \frac{1}{b}$ would result in a "type" 1 system guaranteeing zero steady-state track errors for constant target angular velocity (i.e., $\dot{\theta}_T$ = constant) inputs.

The resulting closed-loop system is described by the equations

$$\dot{x} = Fx + G\theta_T + \Gamma v , \tag{14}$$

where: $x = (\theta_g, z)^T$

$$F_{11} = -bc(\gamma_1 + k\gamma_2)$$

$$F_{12} = b\gamma_2 \tag{15}$$

$$F_{21} = ck\left[\frac{\dot{c}}{c} + ck - bc(\gamma_1 + k\gamma_2)\right]$$

$$F_{22} = ck(b\gamma_2 - 1)$$

$$G = (-F_{11}, F_{12})^T \tag{16}$$

$$\Gamma = (-b, 0)^T \tag{17}$$

and b, c, and v are described earlier.

Then the ensemble statistics can be computed using

$$\dot{\bar{x}} = F\bar{x} + G\theta_T: \quad \text{Ensemble Mean} \tag{18}$$

and

$$\dot{P} = FP + PF^T + GQG^T: \quad \text{Ensemble Standard Deviation.} \tag{19}$$

Then

$$\begin{aligned} \bar{y} &= \theta_T - \bar{\theta}_g \\ &= \theta_T - (1,0)\bar{x} \end{aligned} \tag{20}$$

gives the ensemble tracking error, and

$$\sigma_y^2 = c^2 P_{11} \tag{21}$$

provides the ensemble error standard deviation. The observer model parameters must be identified so that the model predictions of ensemble error mean and standard deviation match experimental data according to some criterion.

STRUCTURAL IDENTIFIABILITY

Note that the closed-loop transfer function

$$\frac{Y}{\theta_T}(s) = \frac{s[s+ck(1-b\gamma_2)]}{s^2+(k+b\gamma_1)cs+bk(c^2\gamma_1-\dot{c}\gamma_2)} \tag{22}$$

$$\equiv \frac{s(s+\beta_3)}{s^2+\beta_1 s+\beta_2} \tag{23}$$

where: $\beta_1 = c(k+b\gamma_1)$

$$\beta_2 = bc(c^2\gamma_1-\dot{c}\gamma_2) \tag{24}$$

$\beta_3 = ck(1-b\gamma_2)$.

For elevation channel, $c = 1$ and $\dot{c} = 0$. Thus,

$$\frac{Y}{\theta_T}(s) = \frac{s[s+k(1-b\gamma_2)]}{s^2+(k+b\gamma_1)s+bk\gamma_1} . \tag{25}$$

For such a system, only the zero and two poles of the transfer function can be uniquely identified from tracking error data. The two poles that can be identified are the roots of the characteristic equation:

$$s^2+(k+b\gamma_1)s+bk\gamma_1 = 0 . \tag{26}$$

This implies two solutions for k and γ_1 given that we have identified two roots $-a_1$ and $-a_2$ for the characteristic equation. They are

$$\begin{pmatrix} k = a_1 \\ \gamma_1 = \frac{a_2}{b} \end{pmatrix} \quad \text{or} \quad \begin{pmatrix} k = a_2 \\ \gamma_1 = \frac{a_1}{b} \end{pmatrix} . \tag{27}$$

γ_2 can be obtained from the single zero at $-k(1-b\gamma_2)$ using k identified in Eq. (27), thus giving rise to two possible solutions for γ_2. However, for the AAA task, it is reasonable to assume

$$\gamma_2 = \frac{1}{b} \tag{28}$$

in order to assure "type" 1 system response.

OPTIMAL CONTROL ALTERNATIVE

Finally, the feedback gains (γ_1, γ_2) need not be free but could be constrained to being optimal with respect to some standard quadratic cost functional. Thus, given the gunsight dynamics, the operator's internal model for the target may be assumed to be

$$\ddot{\theta}_T = w \tag{29}$$

giving a state-space model for the gunsight/target trajectory of the form

$$\begin{aligned} \dot{x}_1 &= \dot{\theta}_T - \dot{\theta}_g = x_2 + bu \\ \dot{x}_2 &= \ddot{\theta}_T = w \ . \end{aligned} \tag{30}$$

The operator may be assumed to be minimizing a quadratic cost

$$J_{oc} = \int_o^{t_f} (c^2 x_1^2 + g u_c^2) dt \ . \tag{31}$$

The optimal control law[2] may be obtained by solving the corresponding Riccati equation for $t_f \rightarrow \infty$ as

$$\gamma_1 = \frac{1}{\sqrt{g}} \ ; \qquad \gamma_2 = \frac{1}{b} \ . \tag{32}$$

Thus with $\gamma_2 = \frac{1}{b}$ a type 1 system is guaranteed by the optimal feedback controller as would be expected.

PARAMETER IDENTIFICATION APPROACH

The above discussion elucidates the problems associated with model structure identifiability. The problem involves the determination of the parameters

k = observer gain

γ_1, γ_2 = control gains

$\bar{\theta}_g(0), \bar{z}(0)$ = mean state initial conditions

$\alpha_1, \alpha_2, \alpha_3$ = noise covariance parameters

$P_{11}(0), P_{12}(0), P_{22}(0)$ = state covariance initial conditions.

These are to be chosen so as to minimize a cost function

$$J = \int_0^{t_f} [(y^* - \bar{y})^2 + \lambda(\sigma_y^* - \sigma_y)^2] dt \ , \qquad (33)$$

where y^* and σ_y^* are ensemble tracking error mean and standard deviation data and $\bar{y}$ and σ_y are the corresponding observer model outputs.

Thus, there are 11 observer model parameters that must be identified according to the fit-error criterion of Eq. (33). This can lead to serious numerical problems in the application of the identification algorithm (e.g., modified Gauss-Newton). Therefore, a systematic iterative approach to the determination of these 11 parameters is proposed using the complete tracking data including the acquisition phase, as follows:

(1) Identify (k,γ_1) using mean tracking error data with $\gamma_2 = \frac{1}{b}$.

(2) Identify $\bar{z}(0)$ from mean acquisition error data using $\{k,\gamma_1,\gamma_2\}$ from step 1, and $\bar{\theta}_g(0)$ from data.

(3) Identify $\{\alpha_1,\alpha_2,\alpha_3\}$ from standard deviation tracking data using $\{k,\gamma_1,\gamma_2\}$ from step 1.

(4) Identify $\{P_{12}(0),P_{22}(0)\}$ from standard deviation acquisition data Using $P_{11}(0) = \sigma_{\theta_g}^2$ from data.

(5) Repeat steps 1-4 for various values of λ in J of Eq. (33).

(6) Determine functional model (if it exists) relating acquisition model parameters to trajectory parameters.

CONCLUDING REMARKS

The above outline provides a framework for systematic identification of the observer model parameters. It is understood that the search over $\{k,\gamma_1\}$ would be restricted in parameter space to converge to one of the two possible solutions given in Eq. (27). Finally, the assumption of the adequacy of the observer model for the acquisition phase is implicitly assumed in this paper. This may not be justified if the sample time histories for the gunner input-output variables indicate nonlinear or mode switching behavior.

REFERENCES

1. D.G. Luenberger, "An Introduction to Observers," IEEE Trans. on Auto. Cont., Vol. AC-16, pp. 596-602, Dec. 1971.

2. A.E. Bryson, Jr. and Y.C. Ho, Applied Optimal Control, Gunn-Blaisdell, 1969.

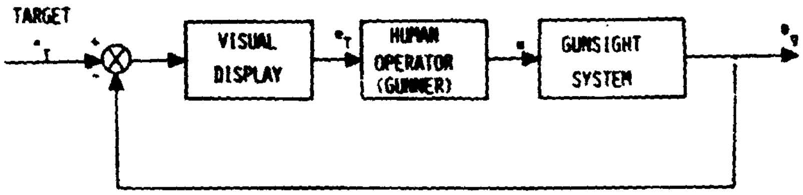
TARGET
θ_T
+
-
VISUAL DISPLAY
e_T
HUMAN OPERATOR (GUNNER)
u
GUNSIGHT SYSTEM
θ_g

Figure 1. Block Diagram of an AAA tracking System

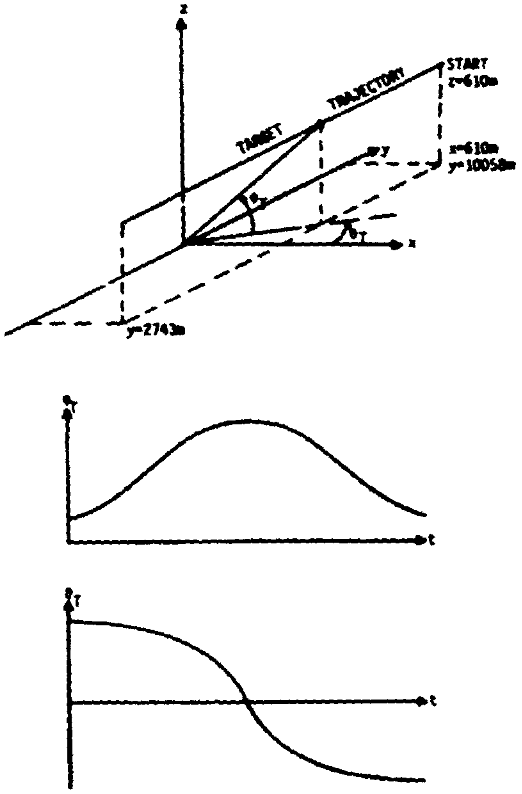
z
START
z=610m
TARGET
TRAJECTORY
y
x=610m
y=10058m
ϵ_T
θ_T
x
y=2743m
ϵ_T
t
θ_T
t

Figure 2. Flyby Trajectory

[illegible]
OF POOR QUALITY

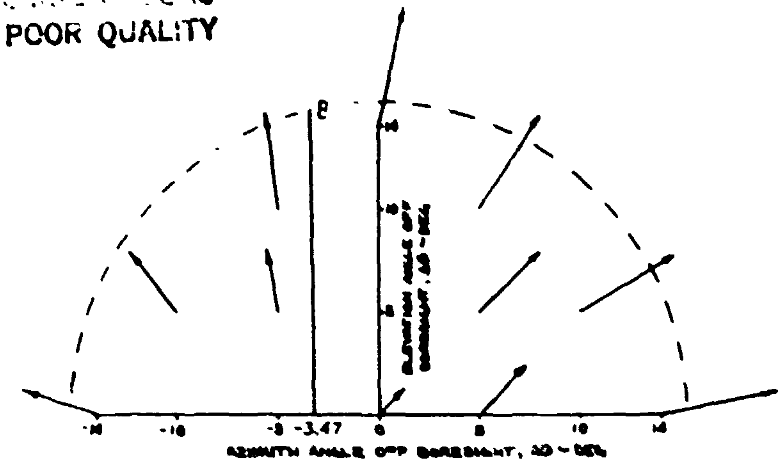
-15
-10
-5
-3.47
0
5
10
15
AZIMUTH ANGLE OFF BORESIGHT, AO ~ DEG
ELEVATION ANGLE OFF BORESIGHT, EO ~ DEG
5
10
15

Figure 3. Gunsight Display

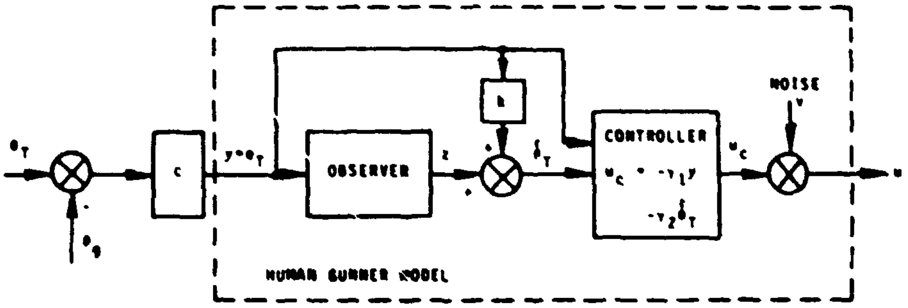
θ_T
θ_g
c
y=e_T
OBSERVER
z
h
+
ê_T
CONTROLLER
u_c = -γ_1 y
-γ_2 ê_T
NOISE
v
u_c
u
HUMAN GUNNER MODEL

Figure 4. Observer Model Structure

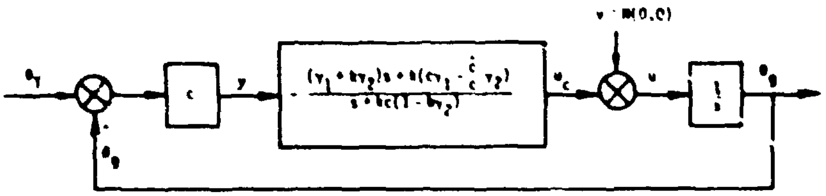
θ_T
θ_g
c
y
(γ_1 + hγ_2)s + h(cγ_1 - ċ/c γ_2) / s + hc(1 - hγ_2)
u_c
v ~ N(0,Q)
u
1/s
θ_g

Figure 5. Equivalent Quasi-stationary diagram of the
AAA Closed-Loop System

N82 34041 D4

THE EFFECT OF VISUAL INFORMATION ON THE MANUAL APPROACH AND LANDING

by P.H. Weverinke
National Aerospace Laboratory NLR
The Netherlands

ABSTRACT

The visual scene is an important source of information for the manual approach and landing task. This paper deals with the effect of this information in combination with basic display information on the approach performance. In this context, a pre-experimental model analysis has been performed in terms of the optimal control model.
The resulting aircraft approach performance predictions were compared with the results of a moving base simulator program.

The results illustrate that the model provides a meaningful description of the visual (scene) perception process involved in the complex (multivariable, time varying) manual approach task with a useful predictive capability. The theoretical framework has been shown to allow a straightforward investigation of the complex interaction of a variety of task variables.

INTRODUCTION

The manual approach and landing is a complex manual control task. The process is time (range) varying and involves multivariable task objectives, visual scene and display information and a complex pilot's control strategy. Although many studies have dealt with a variety of aspects of this approach and landing task, accident statistics indicate that there are still important unanswered questions.

This paper summarizes the results of a theoretical and experimental program addressing the effect of visual information on the manual approach and landing. Specifically, this concerned visual scene information which was the subject of a previous study (Refs. 1 and 2) and basic (head-up) display information. From that study it could be concluded that the visual scene perception process can be modelled (described) on the basis of linear perspective geometry and relative motion cues.

In the present study the effect of visual scene information was investigated by considering three (good, poor and night) visibility conditions. These three conditions were combined with three basic head-up

PRECEDING PAGE BLANK NOT FILMED

display (HUD) configurations representing a variety of visual cues. This is discussed in the following.

A pre-experimental model analysis has been performed resulting in a variety of aircraft approach performance predictions. These predictions will be compared with the results of an experimental program on a moving base simulator in order to investigate the predictive capability of the model.

VISUAL INFORMATION IN THE MANUAL APPROACH

Visual approach scene

The visual scene provides a variety of perspective geometrical and relative motion cues. A previous study (Ref. 2) has demontrated that these characteristics can be considered as separate cues among which the human operator must divide his attention. A schematic version of the visual approach scene is shown in figure 1. The cues which are assumed to be derived from this scene are indicated.

The most important cue for lateral guidance is derived from the inclination of the runway sides and/or the runway centerline. The lateral deviation is zero if the inclination of both runway sides is the same ($\omega_r = \omega_\ell$) and the inclination of the centerline is zero ($\omega_c = 0$).

Vertical guidance must be based on the (average) inclination of the runway sides when no runway end and no horizon is visible. In that case, the observer must know the nominal inclination (which is range varying). However, a better indication of the vertical position can be obtained when the depression of the runway threshold with respect to the horizon is visible. Also in that case, the observer must know the nominal depression angle, which is, however, constant during a standard approach (i.e. 3 deg). The final approach and landing requires also the estimation of the distance to touchdown. This can be based on the apparent size of ground objects, the most important one probably being the runway width.

Aircraft attitude providing "inner loop" information for aircraft control can be derived from the relative position and inclination of (e.g.) the horizon and any aircraft reference. In the figure the three attitude angles are indicated.

In this paper the effect of two visual scene conditions is considered: a good visibility condition (GV) implying that the complete visual scene including the horizon is visible and a poor visibility condition (PV) such that no runway end and no horizon can be discerned. These visual scene conditions were combined with three display configurations resulting in six task configurations considered in the following theoretical and experimental analysis.

Display information

In a visual approach the pilot is provided with not only the visual scene but also display information. Typical aircraft variables of interest are the rate of descent, airspeed, or groundspeed, aircraft position, etc.. In the study described in this paper three display configurations were involved so as to investigate the effect of various aircraft variables on the manual approach performance and their interaction with the visual scene information.

Figure 2 contains the visual information involved in the three head-up display (HUD) configurations. The "no HUD" configuration (NH) involves only an aircraft reference allowing a rough estimation of the aircraft attitude. The "simple HUD" configuration (SH) is included to investigate the effect of accurate, aircraft attitude information. This configuration involves a fixed reference line which nominally coincides with the touchdown line. This reference provides primarily accurate aircraft attitude information and, to some extent, approach position information. The "advanced HUD" configuration (AH) contains, in addition, the aircraft velocity vector (earth-related), the runway contours including the centerline and touchdown line and the horizon line. This configuration was intended to investigate the effect of precise movement information and synthetic perspective runway information which was hypothesized to become useful in reduced visibility situations.

The six task configurations are summarized in table 1.

MODEL ANALYSIS

Once the visual scene characteristics are linearly related to the aircraft variables of interest (system states) the visual cues of both the visual scene and the HUD can be described in terms of the perception and information processing model (Refs. 1 and 2) which is part of the optimal control model (Ref. 3).

The approach task considered consisted of the control of a medium weight twin engine jet in the presence of moderate turbulence (details are given in reference 4). A steady-state model analysis was performed assuming that the aircraft was "frozen" at a fixed point of the approach path corresponding with a nominal altitude of 200 ft for a 3° approach. In addition, a time varying model analysis was performed accounting for the time varying turbulence characteristics during a descent and the time varying (range varying) visual cues.

Model parameters

Model parameters can be divided in parameters which are constant for all configurations and parameters which were considered as the remaining model variables.

It was assumed that the pilot adopts a control strategy that minimizes a performance index consisting of a weighted sum of mean-squared path, attitude and control variables. The weightings were selected by first determining maximum allowable values ("limits") of each variable and then setting the weighting equal to the square of the reciprocal of the corresponding limit. For details the reader is refered to reference 4.

The selection of the visual perception parameters is based on the results of previous studies (Ref. 2). The key model parameters are the perceptual thresholds summarized in table 2. Herein, ε is the approach angle (deviation), δ is the velocity vector deviation from the touchdown point; the subscript o means: with respect to touchdown and the subscripts g and ℓ refer to the vertical (glideslope) and lateral (localizer) direction, respectively. Only those variables are given among which the pilot divides his attention (optimally, i.e. minimizing the afore-mentioned performance index). An equal attention was assumed between the vertical and lateral task.

Typical values were used for the remaining model parameters which have been found to be relatively constant or insensitive (task independent): a perceptual time delay of 0.2 s, an overall level of attention of -18 dB and a motor noise ratio of -25 dB.

Steady-state model analysis

Based on the model assumptions and parameter values discussed before model predictions could be made for the six task configurations of table 1. The results consist of standard deviations of system variables (path errors d and y, forward velocity u, aircraft attitude angles θ, ϕ and ψ and control deflections δ_e and δ_a) and pilot workload. The latter can be predicted using the workload model discussed in reference 5.

System performance is summarized in table 3 for tasks C1 to C4. The model predicts that approach performance is clearly improved when the simple HUD is provided. A substantial improvement is obtained for the advanced HUD. This demonstrates clearly the favourable effect of HUD information on the manual approach performance, both vertically and laterally, especially in terms of path deviations.

The effect of visibility can be appreciated by comparing configuration C1 with C4. The model predicts that reduced visibility results in a minor performance deterioration laterally. The vertical performance remains the same. This somewhat surprisingly result is explained by the predicted pilot's shift in attention allocation among the visual cues (Ref. 4). For the simple and advanced HUD configurations the effect of visibility is negligible. Because of the favourable HUD information almost (in case of simple HUD) all (in case of the advanced HUD) attention is devoted to the HUD cues. Consequently, a reduction in visibility has no effect as long as the touchdown point is visible (or indicated).

Pilot workload predictions (W) are also given in table 3 containing also the overall performance index J. Workload is relatively constant for the four vertical control configurations. Significantly more effect is predicted for the lateral tasks. The workload results for the combined tasks indicate that pilot's workload is the same for the good and poor visibility condition. Furthermore, the effect of the simple HUD is favourable with respect to not only the approach performance but also the corresponding workload. The model predicts that the superior performance of the advanced HUD corresponds to a somewhat higher level of pilot workload than corresponding to the simple HUD configuration.

Time varying analysis

A time varying analysis was performed to account for possibly range dependent effects of the approach task involved in the simulation program. Apart from the height dependent turbulence (only a varying turbulence bandwidth was considered) the range varying viewing characteristics were included in the analysis. The latter implied range varying visual cues and pilot's control strategy. For further details the reader is referred to reference 4.

It was assumed that the pilot's allocation of attention among the visual cues was constant during the approach. This "average" allocation of attention was identical to the optimal allocation of attention (yielding the best approach performance) computed in the steady-state model analysis. Also the same (equal) division of attention between the vertical and lateral task was assumed.

The experimental approach task which will be discussed in the next chapter began at a range of 5813 m from the touchdown point (corresponding with a nominal altitude of 1000 ft) with zero intial deviations. The same initial condition was adopted in the following model analysis.

The model results of configuration C1 are given in terms of the standard deviation of the path errors (in figure 3a) and of the aircraft attitude angles and control deflections (in figure 3b) as function of the range. It will be clear from the figure that (linear) path deviations (d and y) are strongly range dependent.

Pitch attitude and elevator activity increase during the approach. This result orginates partly from the model assumption that the pilot's control strategy is determined by the angular glidepath deviation. This implies that during the approach relatively more weight is placed upon (linear) glidepath error than upon pitch attitude and elevator deflection.

The roll angle and aileron activity increase somewhat during the approach. Heading is slightly decreasing. Analogous to the vertical task this results from the range varying control strategy.

It is interesting to compare the results of the time varying analysis with the steady-state results. Therefore, steady-state results are indicated in figure 3 corresponding with a nominal altitude of 200 ft and a nominal altitude of 600 ft. Both the path errors and the attitude and control scores closely agree for the steady-state analysis and the time varying analysis (with the exception of the low range height error and pitch attitude angle). Thus , range varying effects can be investigated by a steady-state model analysis at different approach positions. Tedious time varying analysis is necessary, however, when dealing with deterministic processes such as windshears (Ref. 6).

EXPERIMENTAL PROGRAM

Th objective of the experimental program was to test the foregoing model results. In addition, the experimental results might allow model refinements thereby extending the predictive capability of the pilot-aircraft model.

Description of the experiment

The experiment was conducted on the NLR moving base simulator. Details about the apparatus, experimental and data analysis procedures are given in reference 4. The flight simulator was configured to represent the linear equations of motion of a medium weight twin engine jet transport having a weight of 29,000 kgf.

The task was to track a 3° flight path to touchdown under VFR conditions beginning at a range of 5813 m from the touchdown point. Each run lasted approximately 90 s. The subjects were instructed to conceive the task as a realistic approach task (given the simplified circumstances) using exclusively the outside world information. Apart from the aforementioned good and poor visibility conditions also a night condition was included. These visual scene conditions were combined with the aforementioned three HUD configurations yielding 9 experimental conditions.

Three experienced pilots participated in the experiment. In each session the 9 configurations were presented to the pilots in a random order. On the first two days and at the beginning of the third day each pilot was trained such that a relatively stable performance level was reached for each condition. All together, 225 training trials were performed. On the third and fourth day the subjects "flew" 6 formal sessions containing the 9 configurations in a random order for data collection. Thus, 6 replications per experimental condition per pilot were obtained. No performance was fed back during the formal sessions. Data were collected in terms of a variety of system variables and subjective ratings concerning pilot workload and visual informational aspects.

Comparison of model and experimental results

For an extensive presentation of all experimental results the reader is referred to reference 4. In this paper, only the principal experimental results of the same configurations as involved in the model analysis will be considered.

The model performance predictions reflect the stochastic nature of the approach task. The statistical measures are given in terms of standard deviations of path errors and aircraft attitude and control angles. These random deviations result from the system disturbances (turbulence) and pilot's randomness in perceiving and processing information and executing control deflections. The corresponding experimental measures for the vertical approach task are the standard deviations of the ensemble (six replications times three subjects). The ensemble means of some configurations clearly reflect specific control strategy. This is discussed in reference 4. For the lateral approach task no systematic ensemble mean has been found. So for this task the best overall experimental measure of random pilot control behavior is the root-mean-squared value (RMS).

The resulting approach performance of configuration 1 (good visibility, no HUD) is shown in figure 4 as a function of the range The agreement between the model predictions and experimental height errors is excellent. The lateral deviations do not match as well. The model predicts somewhat larger errors than the experimental scores. A close match, however, can easily be obtained when assuming that somewhat more attention is devoted to the lateral task (corresponding with a reduced observation noise ratio of 2 dB). This is indicated in the figure by the dashed line.

The aircraft attitude and control scores are summarized in table 4 as averages over four range intervals. The agreement for the pitch attitude and elevator deflection is quite good. The model predicts an increase in pitch angle with decreasing range. This effect is only partly reflected by the experimental pitch angles for this configuration 1. However, the experimental pitch attitude results of almost all other configurations did confirm this model prediction (Ref. 5).

The roll angle scores agree closely. Both the model and experimental results exhibit an increase in roll angle with decreasing range. The model predicts a heading angle and aileron activity which are clearly larger than the corresponding experimental scores. This could be the result of a somewhat different pilot's control strategy.

The effect of visual scene information can be appreciated by comparing configuration 1 and 4. The model predicts that reduced visibility does not result in a deterioration of the vertical approach performance. This is confirmed by the experimental results showing no significant difference between both configurations. Laterally, however, the model predicts that reduced visibility results in a (15 %) larger lateral deviation. This trend is in accordance with the experimental results: the lateral deviation of configuration 4 is, on the average (30 %) larger than the one of configuration 1.

As predicted by the model no significant effect of visual scene information was found experimentally for the simple and advanced HUD configurations.

The effect of HUD information is illustrated in figure 5 for the good visibility condition. The model predicts that the simple HUD yields an improvement in vertical approach performance. The experimental results show the same (statistically significant) trend although the effect is larger than predicted. The model predicts a substantial improvement in vertical performance when the advanced HUD is provided. This corresponds rather well with the experimental results showing approximately the same fractional (statistically significant) improvement.

Laterally, the model predicts that the simple HUD, providing the pilot with more accurate attitude information, results in reduced lateral deviations. This result is not obtained experimentally. Figure 5 shows that the simple HUD results in substantial larger lateral deviations.

One explanation might be that the pilot spent, during the first part of the approach, less attention to the lateral task than assumed in the model analysis. This is illustrated in figure 6 showing the lateral model results of the simple HUD configuration for both the orginally assumed level of attention and for half of this level. During the first part of the approach the data closely match the model results assuming half of the original level of attention. In the course of the approach (below a range of 3 km) the level of attention is increased resulting in lateral approach performance as approximately predicted by the model.

Pilot workload results in terms of normalized subjective ratings and the model predictions (larger values signify higher pilot workload) are summarized in table 5. The experimental differences are not statistically significant (at the 0.05 level) partly because of the subject variability. Nevertheless, the model prediction that the simple HUD (C2) corresponds with a lower workload level than the no HUD configuration (C1) seems to be supported experimentally. Furthermore, the model prediction that the advanced display (C3) corresponds to a lower workload level than the no HUD configuration is not supported experimentally. The model predicts that visibility has hardly any effect on pilot workload (c.f. C1 and C4). On the average this seems to be supported by the subjective ratings.

CONCLUDING REMARKS

A detailed comparison of model predictions and experimental results of the "good visibility, no HUD" condition has demonstrated that the predictive capability of the pilot-aircraft model describing the complex, time-varying approach task is substantial.

The model predicts that reduced visibility has no effect on the vertical approach performance and some negative effect on the lateral approach performance. This is supported by the experimental results. Furthermore, as predicted by the model, no significant effect of visual scene information was found experimentally for the simple and advanced HUD configuration.

Th model predicts that the simple HUD yields an improvement in vertical approach performance. The experimental results show the same trend although the effect is larger than predicted. The model predicts a substantial improvement in vertical performance when the advanced HUD is provided. This agrees well with the experimental results. Laterally, the model predicts that the simple HUD results in a better approach performance. The experimental results, however, show larger lateral deviations. This can be closely matched by the model when assuming that for this configuration less attention is dedicated to the lateral task during the first part of the approach. The same applies to the advanced HUD.

REFERENCES

1. Weverinke, P.H.: A theoretical and experimental analysis of the outside world perception process. Paper presented at the 14th Annual Conference on Manual Control, Los Angeles, April 1978 (Also NLR MP 78020 U).

2. Weverinke, P.H.: Visual scene perception process involved in the manual approach. NLR TR 78130 U, October 1978.

3. Baron, and Levison, W.H.: Display analysis with the optimal control model of the human operator. Human Factors, 1977, 19(5).

4. Weverinke, P.H.: The effect of visual information on the manual approach and landing. NLR TR 80 U (forthcoming).

5. Weverinke, P.H.: Performance and workload analysis of in-flight helicopter missions. NLR MP 77013 U, June 1977.

6. Levison, W.H.: Analysis and in-simulator evaluation of display and control concepts for a terminal configured vehicle in final approach in a windshear environment. NASA CR 3034, August 1978.

CONF.	DISPLAY	VISIBILITY
C 1	NO HUD	GOOD
C 2	SIMPLE HUD	
C 3	ADVANCED HUD	
C 4	NO HUD	POOR
C 5	SIMPLE HUD	
C 6	ADVANCED HUD	

Table 1 Task configurations

PARAMETER	DISPLAY		
	NH	SH	AH
ρ_o	1	0.1	0.1
$\dot{\theta}_o$	1	0.2	0.2
ϕ	1 (2)	0.2	0.2
ψ	1 (2)	-	-
$\dot{\psi}_o$	1	0.1	0.1
ε_g	0.5 (2)	0.5 (2)	0.2 (2)
ω_c	2	2	2
δ_g	-	-	0.1
δ_ℓ	-	-	0.1

(·): poor visibility condition; all variables in units of degrees visual arc

Table 2 Visual thresholds used for the model analysis

TASK	PARAMETER	CONFIGURATION			
		C1	C2	C3	C4
VERTICAL	σ_d (m)	7.1	5.8	4.1	7.2
	σ_θ (deg)	1.5	1.3	1.1	1.5
	σ_u (m/s)	1.4	1.2	1.3	1.3
	σ_{δ_e} (deg)	1.1	1.0	1.1	1.1
	J (-)	0.14	0.09	0.06	0.14
	W (dB)	10.1	9.7	10.4	9.9
LATERAL	σ_y (m)	9.4	7.1	6.0	10.6
	σ_ϕ (deg)	3.6	[illegible] 0	3.1	4.1
	σ_ψ (deg)	3.5	3.4	3.4	3.6
	σ_{δ_a} (deg)	2.6	2.4	2.7	2.8
	J (-)	0.48	0.35	0.35	0.54
	W (dB)	14.0	13.0	13.4	13.8
total	J_t (-)	0.62	0.44	0.41	0.69
	W_t (dB)	16.4	15.5	15.8	16.2

Table 3 System performance and workload predictions

PAR.	RANGE INTERVAL	R1	R2	R3	R4
θ	measured	1.1	1.1	1.5	1.2
	model	0.9	1.0	1.4	2.0
δ_e	measured	0.52	0.72	0.77	1.1
	model	0.43	0.51	0.74	1.2
ϕ	measured	3.3	2.9	2.9	4.4
	model	3.1	3.4	3.5	3.8
ψ	measured	2.1	2.3	2.1	2.3
	model	3.8	3.9	3.8	3.6
δ_a	measured	1.6	1.5	2.3	1.7
	model	2.5	2.6	2.6	2.7

Table 4 A comparison of model and experimental attitude and control scores - Configuration 1

Workload measure	CONFIGURATION			
	C1	C2	C3	C4
model prediction	16.4	15.5	15.8	16.2
demand rating	-.17	-.58	-.25	.03
effort rating	-.16	-.39	-.07	-.24

Table 5 Model and experimental workload measures

ORIGINAL PAGE IS
OF POOR QUALITY

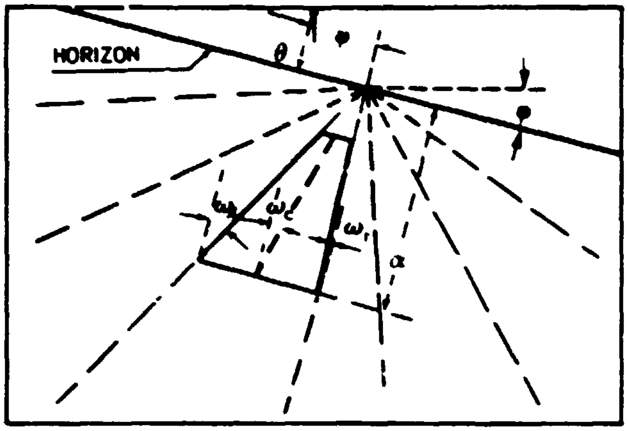

Fig. 1 Cues derived from the visual approach scene

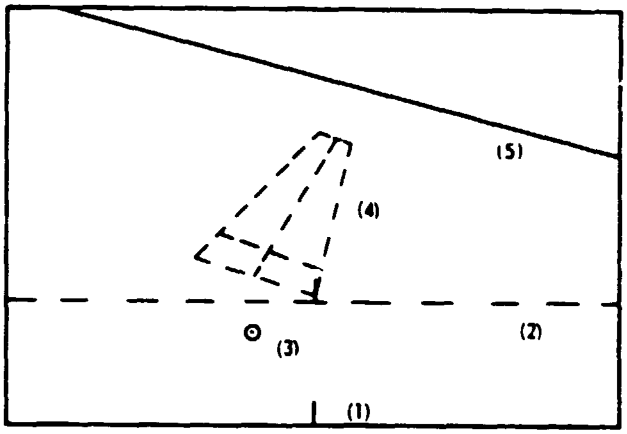

CONF.	CUES
NO HUD, NH	(1)
SIMPLE H., SH	(2)
ADVANCED H., AH	(2), (3), (4), (5)

(1) AIRCRAFT REFERENCE
(2) REFERENCE TO TOUCHDOWN POINT
(3) VELOCITY VECTOR
(4) RUNWAY CONTOURS
(5) ARTIFICIAL HORIZON

Fig. 2 Head-up display information

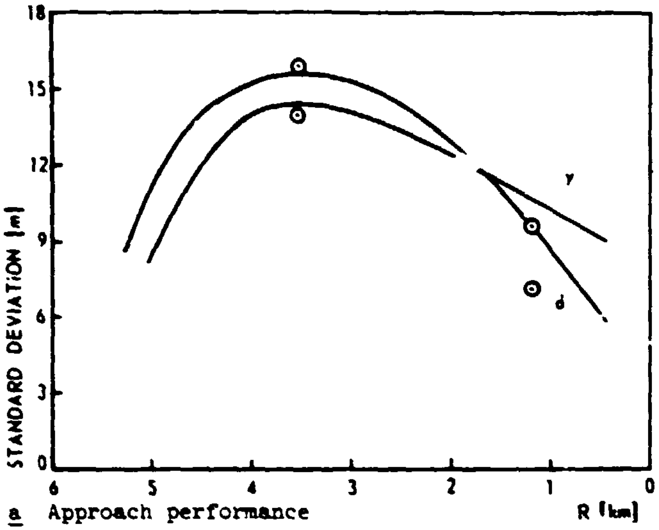

a Approach performance

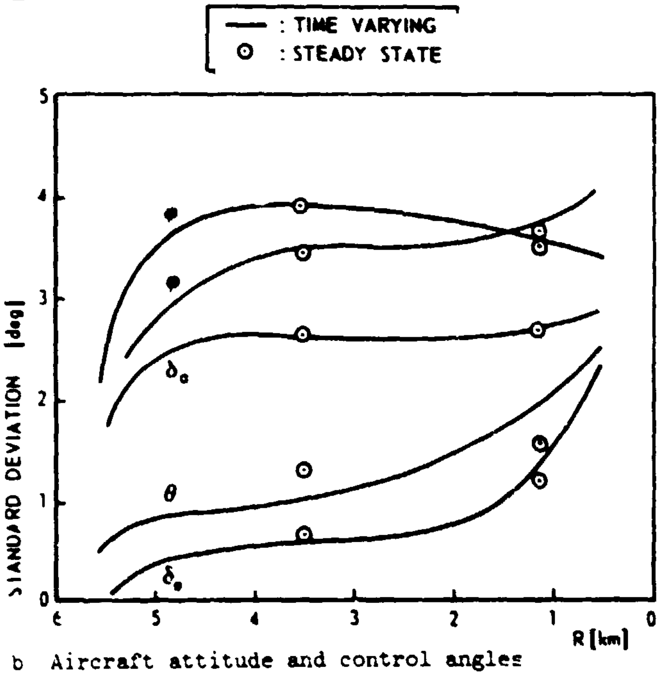

b Aircraft attitude and control angles

Fig. 3 Approach performance predictions as a function of range - Configuration C1

OF POOR QUALITY

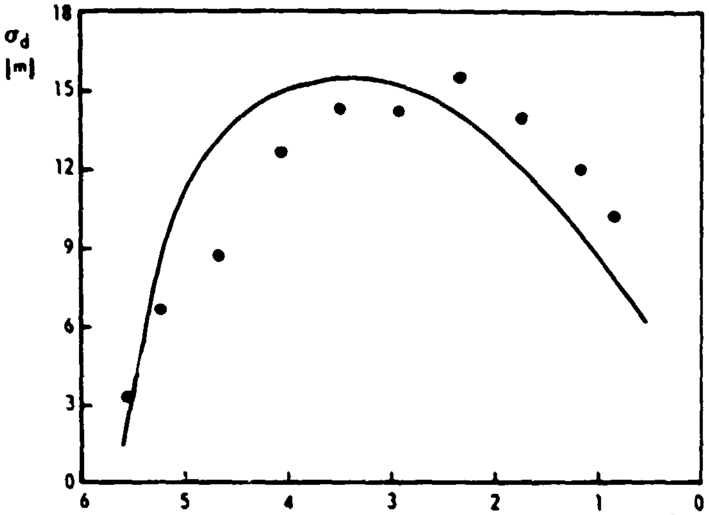

a Height error

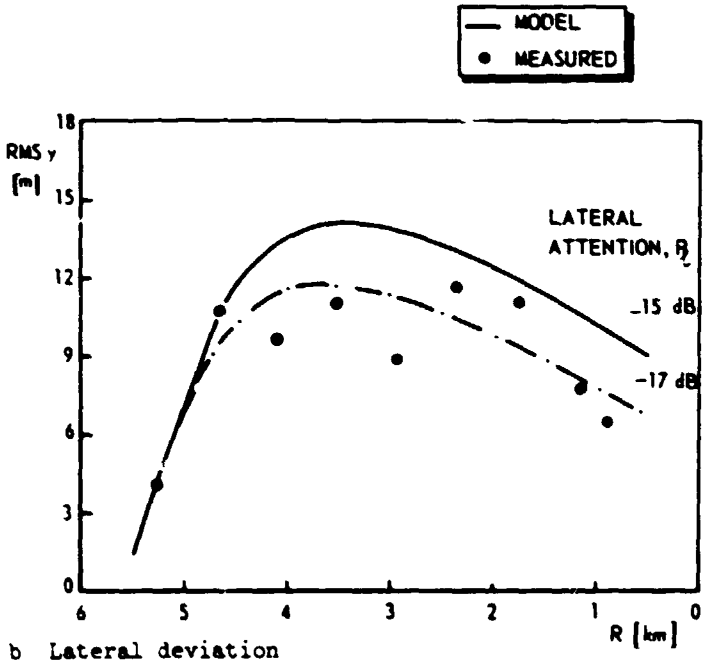

b Lateral deviation

Fig. 4 Comparison of model and experimental approach performance - Configuration C1

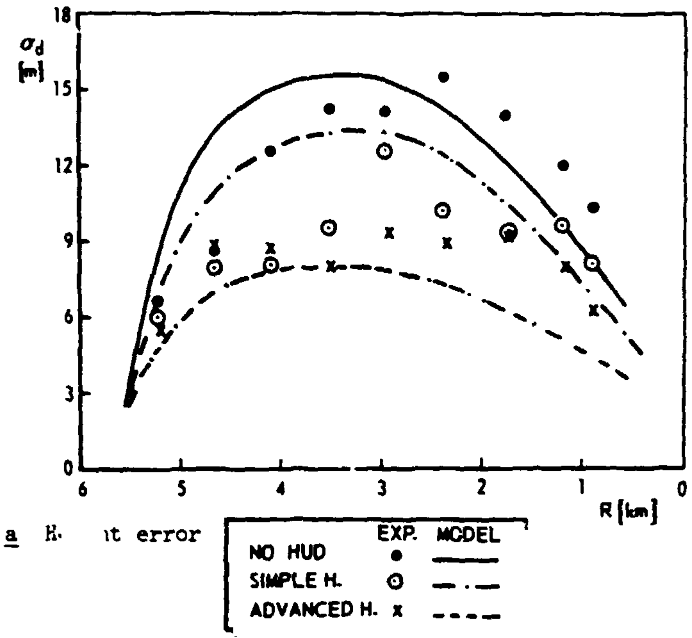

a Height error

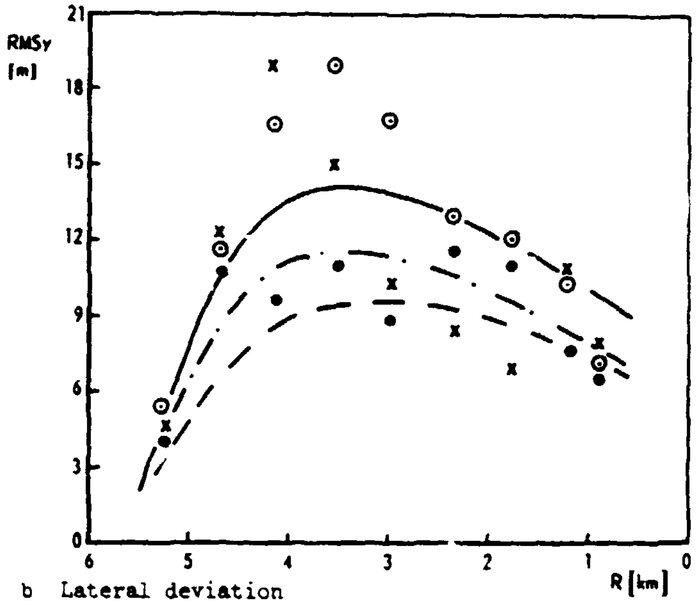

b Lateral deviation

Fig. 5 Comparison of model and experimental approach performance-The effect of HUD information for the good visibility condition

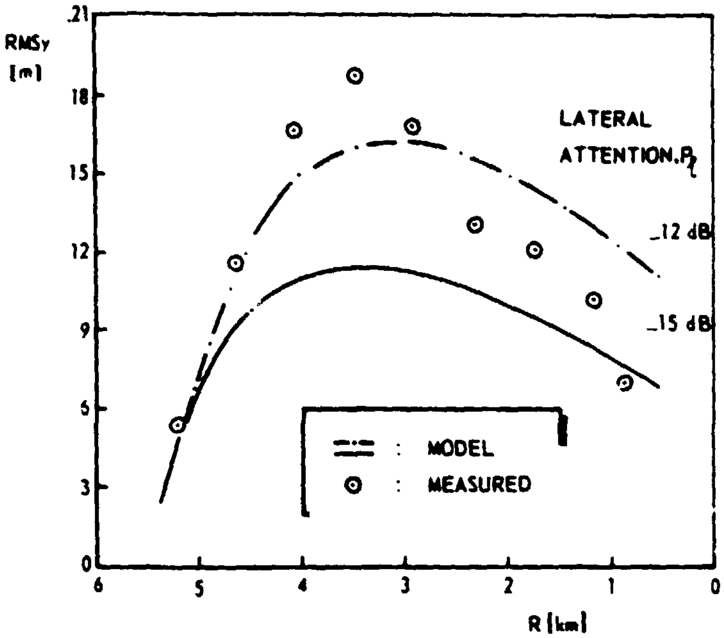

Fig. 6 Comparison of model and experimental lateral approach performance - Configuration C2

OMIT
Accessioned AS
81A 36561

Pilot/Vehicle Model Analysis of Visual and Motion Cue Requirements in Flight Simulation

R. Lancraft, G. Zacharias, S. Baron

ACKNOWLEDGEMENT

The work reported here was performed under NASA Ames Research Center Contract Number NAS2-10145. The authors wish to thank Mr. Frank Crane, technical monitor for NASA, for his assistance throughout the course of the program.

ABSTRACT

The optimal control model for pilot/vehicle analysis is used to explore the effects of a CGI visual system and motion system dynamics on helicopter hover simulation fidelity. This is accomplished by expanding the perceptual aspects of the model to include motion sensing and by relating CGI parameters to information processing parameters of the model. Simulator fidelity is examined by comparing predicted performance and workload for flight with that predicted for various simulator configuration.

The results of the analysis suggest that simulator deficiencies or a reasonable nature (by current standards) can result in substantial performance and/or workload infidelity. Both CGI and motin system effects are significant for this task. There is also a distinct interaction between the two sources of pilot cues. In particular, the presence of motion reduces the sensitivity to CGI limitations.

With respect to the CGI system, the most important parameter in terms of its effect on performance was display delay. This was followed in order of importance by display resolution and field-of-view. The main effect associated with motion system bandwidth was introduced by going to a fixed-base only configuration.

INTRODUCTION

As flight control and management tasks become more complex so, too, do the simulators used to investigate these tasks. The designers of simulations are confronted with difficult choices between requirements for simulation fidelity and the needs for cost-effective methods of simulation. The latter demands have resulted in a trend toward the use of digital equipment in simulation both in modeling the vehicle and in generating visual

PRECEDING PAGE BLANK NOT FILMED

cues (CGI systems) for the pilot of the simulator. These digital simulations can have characteristics that are significantly different from those desired. In particular, unwanted delays frequently result in such a simulation. When motion cues are also needed, the problems can be aggravated further both by delays in generating motion cues (even with analog hardware) and by the potential lack of correlation between visual and motion cues. The significance of these problems has been amply demonstrated in recent studies (Gum and Albery (1977), Queijo and Riley (1975)).

In this paper, the optimal control model for pilot/vehicle analysis is used to investigate the closed-loop consequences of the performance limitations associated with a computer generated image (CGI) visual system and a six degree-of-freedom motion simulator (VMS) in a helicopter hover task. The specific problem addressed in this study was to determine the potential effects of CGI and VMS system characteristics on closed-loop hover performance and pilot workload, and to evaluate these effects in lignt of performance/workload levels we might expect to see in the actual flight situation. To accomplish this, the basic OCM is elaborated to include sensory perception of both CGI-generated visual cues and VMS-generated motion cues.

MODEL IMPLEMENTATION

Our objective in this section is to describe how this task is modelled in the context of the Optimal Control Model (OCM) of the pilot. Inasmuch as the model has been documented extensively, the discussion will be brief, with emphasis on those aspects of the model that are of special relevance to this study.

Figure 1 presents in block diagramatical form the structure of the OCM as envisioned for this study. Notice that the basic OCM is immediately distinguished as the lower portion of the dashed block labelled pilot model. The upper portion of the pilot model displays the form of the expanded perceptual model. Observe that output signals from the simulator pass through dynamical blocks representing the visual and vestibular sensory systems of the human (such as inner ear dynamics) to form two display vectors, one from each modality. The displayed signals are then combined via a monitor. The monitor allocates attention to the individual elements, to form the usual display vector. The other blocks in Figure 1 represent the simulator hardware in a straightforward and conventional fashion. The main frame digital computer is assumed to generate the vehicle dynamics and its characteristics are a part of that block. Likewise the display computer characteristics are included in the simulator drive logic block. In our study, stick

ORIGINAL PAGE IS
OF POOR QUALITY

dynamics and stick transducer dynamics (such as computer generated force loading) were not considered. Also, flight instruments were not displayed to the pilot and can be ignored.

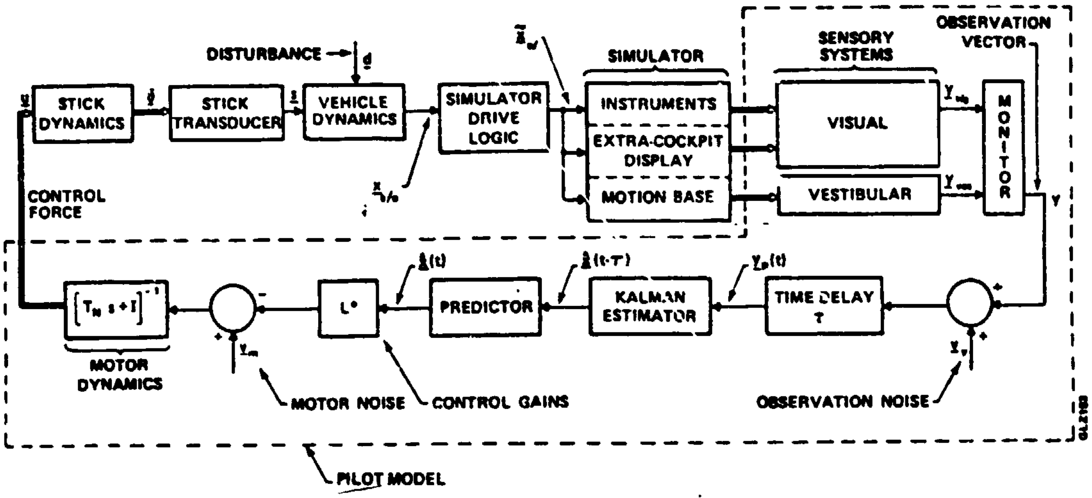
DISTURBANCE
STICK DYNAMICS
STICK TRANSDUCER
VEHICLE DYNAMICS
SIMULATOR DRIVE LOGIC
SIMULATOR
INSTRUMENTS
EXTRA-COCKPIT DISPLAY
MOTION BASE
SENSORY SYSTEMS
VISUAL
VESTIBULAR
OBSERVATION VECTOR
MONITOR
CONTROL FORCE
MOTOR DYNAMICS
L*
PREDICTOR
KALMAN ESTIMATOR
TIME DELAY
MOTOR NOISE
CONTROL GAINS
OBSERVATION NOISE
PILOT MODEL

Figure 1: Overall Pilot/Vehicle System

Our basic modelling approach will be to define simulator hardware and human sensor dynamics, where appropriate, and to form a mapping between simulator and HO perceptual limitaitons and established OCM parameters. To this end, we will begin with a brief description of the task/vehicle, followed by a statement of the basic simulator (main frame computer, VMS, and CGI) characteristics and how they were modelled. A simple model for the perception of the visual scene will then be discussed along with the vestibular models. Finally, a summary of model parameters and assumptions will be presented.

Task/Vehicle Description

The pilot's tas is to hover over a fixed point at a fixed altitude, in the presence of disturbances generated by air turbulence. Control is to be maintained by relying on extra-cockpit visual cues obtained from an out-the-window view and by motion cues associated with helicopter rotation and translation. Where visual cueing is provided by a computer generated image (CGI) system, and motion cueing is provided by a vertical motion simulator (VMS).*

---

* In spite of its name, the VMS is not restricted to vertical motion cues; it is a six degree-of-freedom cueing system.

The specific helicopter chosen for this study was the CH-47 tandem rotor transport helicopter. The linearized and decoupled equations of motion for the helicopter, as well as the Drygen gust models for the air turbulence, were obtained from Hoffman et al (1976). The reader is referred to this report for specific details concerning the basic airframe equations.

The hovering task is modelled as a disturbance regulation task. As is standard procedure for application of the OCM, it is assumed that the objective of the task may be characterized as minimization of the following cost functional (see Kleinman (1976)):

$$J= E\ [(y_i/y_{i_{max}})^2 + r_j u_j^2] \qquad (1)$$

where $y_{i_{max}}$ is a performance tolerance on the corresponding variable. The values for $y_{i_{max}}$ were chosen to be 5 ft and 1 ft/sec for position (x,y,z) and velocity $(\dot{x},\dot{y},\dot{z})$ variables and 1 deg and .05 deg/sec for attitude (ψ, θ, ϕ) and attitude rate (ψ, θ, ϕ) variables; these values were taken from Hoffman et al (1976). The weightings on control rate activity, r_i, were chosen by means of an error-control tradeoff analysis. This resulted in a value of approximately .1 for the diagonal elements of the T_N matrix.

It should be noted that hover control of the unaugmented CH-47 is not an easy task. The results of the reference cited above suggest that the task cannot be performed to within acceptable tolerances under IFR conditions.

Main-Frame Computer

The vehicle equations of motion were implemented on a digital computer, operating at a nominal update rate of 30 Hz. Based on results from the analytic study by Baron et al (1978), we assumed for simplicity that the integration routine introduced no "distortion" in the continuous vehicle dynamics being modelled, and that the only effect of digitization was the introduction of a sample and hold delay associated with the base cycle time of the main-frame computer.

CGI Characteristics

Table 1 summarizes the characteristics used to define the nominal CGI configuration. The nominal field-of-view specification is illustrated in figure 2 as screen configuration B. Notice from the table that no dynamics were associated with the CGI system.

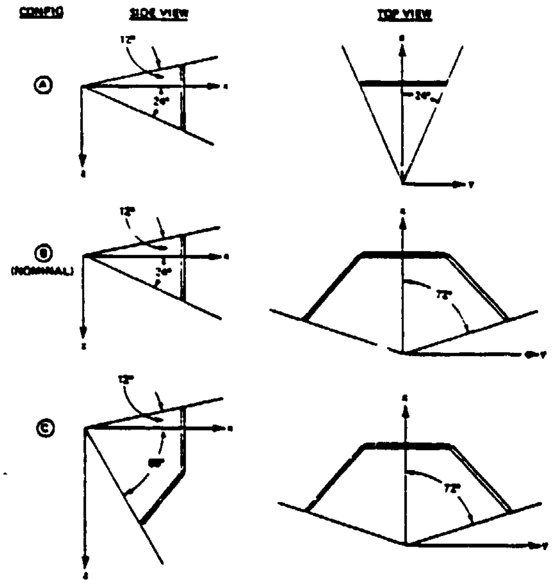
CONFIG
SIDE VIEW
TOP VIEW
Ⓐ
Ⓑ
(NOMINAL)
Ⓒ
12°
24°
72°
60°
x
y
z

Figure 2: CGI Screen Configuration

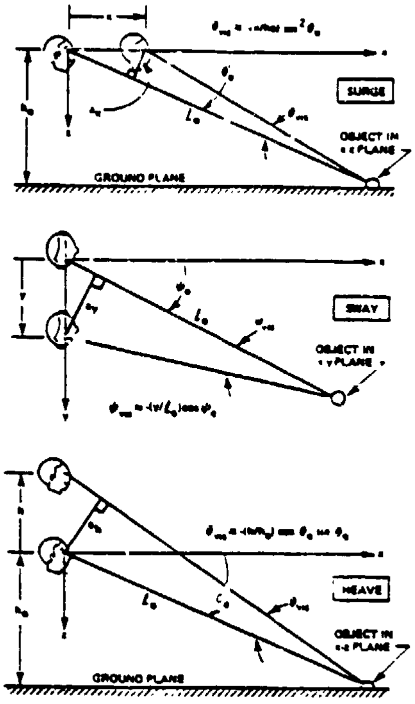
SURGE
OBJECT IN x-z PLANE
GROUND PLANE
SWAY
OBJECT IN x-y PLANE
HEAVE
OBJECT IN x-z PLANE
GROUND PLANE

Figure 3: LOS Changes Due to Translation

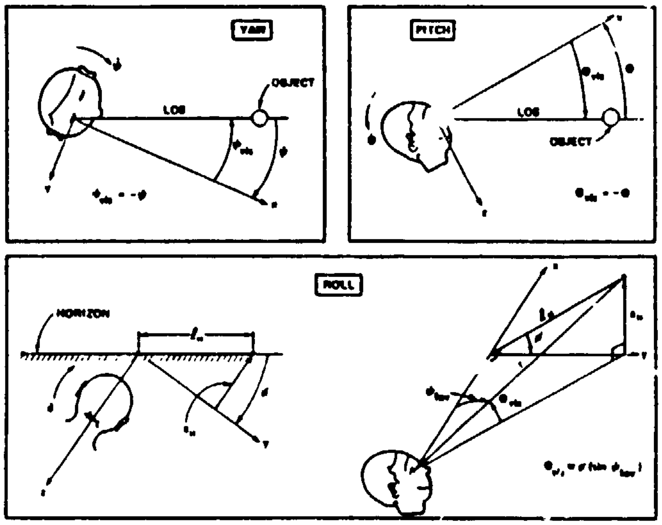
YAW
OBJECT
LOS
PITCH
LOS
OBJECT
ROLL
HORIZON

Figure 4: LOS Changes Due to Rotation

Table 1: Nominal CGI Characteristics

Picture Refresh Rate	30 frames/s
Display Compute Time	66 msec
Effective Sample Rate/Delay	15 Hz/99 msec
Scene Content	6000 edges/frame
Field-of-View	3 screens across (144° horiz,36° vert)
Display Resolution	1024 lines/frame x 1024 pixels/line

The graphics computer was modelled in the same fashion as the main frame computer; as a sample and hold delay based based on the refresh rate and a compute delay. Because the display computer is in series with the main frame computer the total visual delay must include the main frame delay. The effective sample rate is simply the slowest component in this path (i.e., the fastest rate at which information can change). This determines the effective visual hold time for information so that the total visual delay can simply be written as:

$$T_{vis} = T_c + T_d + 1/(2f_{eff}) \qquad (2)$$

where f_c is the reciprocal of the base cycle time of the main frame computer, T_d is the display compute time, and f_{eff} is the effective sample rate. $T_{vis} - 3T_c/2$ seconds of the total delay was modelled as a Pade' delay in the visual path, while the rest of the delay was lumped into the human's time delay. (Since the main frame delay is common to both the VMS and the CGI)

Scene content was not modelled except insofar as it was needed in the assumptions for our visual perception model. Field of view serves to limit the utility of the displayed information and its effect will be seen when we discuss the pilot's perception of the visual scene. Screen resolution limits the fineness of detail the CGI system is able to present. Therefore, we have modelled it as a threshold equal in value to the average vertical and horizontal angular resolution level. This threshold is, of course, in addition to any H.O. imposed threshold, and will be described shortly.

ORIGINAL PAGE IS
OF POOR QUALITY

VMS Characteristics

The nominal VMS was modelled in all axes as a second-order dynamic model with appropriate position/rate/acceleration servo limits. Table 2 defines the nominal parameter values associated with each motion axis. The nominal motion system did not include washout filters as all predicted motions except the surge (x) motion were well within their respective simulator limits. In addition to dynamical models for the VMS servo system, there is an effective motion system delay due to the main frame computer.

Table 2: VMS Model Parameters

LINEARIZED TRANSFER FUNCTION: $\frac{\lambda}{\lambda_c} = \frac{\omega_n^2}{s^2 + 2\zeta_n\omega_n s + \omega_n^2}$

PARAMETERS:

Axis		ω_n^*	ζ_n	$\ddot{\lambda}^{max}$	$\dot{\lambda}^{max}$	λ^{min}	λ^{max}
ROLL	(ϕ)	9.4	0.7	50°/s²	15°/s	-22°	22°
PITCH	(θ)	9.4	0.7	50°/s²	15°/s	-24°	26°
YAW	(ψ)	9.4	0.7	50°/s²	15°/s	-29°	29°
SURGE	(x)	9.4	0.7	16FT/s²	2FT/s	-2.5FT	2.5FT
SWAY	(y)	18.8	0.7	24FT/s²	10FT/s	-20FT	20FT
HEAVE	(z)	18.8	0.7	32FT/s²	20FT/s	-30FT	30FT

* RAD/S

Visual Perception Model

In contrast to the relatively well-defined set of visual cues provided by within-cockpit instrumentation, the extra-cockpit visual scene can provide the pilot with an exceptionally rich stimulus environment, even for a relatively simple display. Attempting to describe and quantify this stimulus environment has been the object of many studies and is well beyond the scope of this paper. The reader is refered to Brown (1973), Staples (1970), and Gibson (1950).

Our initial approach to modeling the visual scene was to follow the perspective geometric arguments of Wewerinke (1978).

Consequently, each object of importance would be modeled as a series of line segments, and incorporated into the display matrix C. As a result, each object can yield many cues. In his study of the approach and landing of a conventional aircraft there were a limited number of well-defined line elements comprising the visual scene, and thus the construction of the display matrix C was a relatively straightforward exercise. However because of the nature of the hover task, no single object is important. Instead, a pilot can use various portions of his visual field, and any number of objects or parts of objects to maintain hover position and attitude. Furthermore, in our study no specific scene was available. As a consequence, we have assumed that a relatively "realistic" visual scene is made available to the pilot. Since such a scene is typically comprised of thousands (or perhaps tens of thousands) of discriminable line elements (and hence cues), the display analysis used by Wewerinke was not employed.

Our approach, instead, was to take a much simplified view of visual cue processing, based on the following notion. Information from cues involve changes in the location, and/or orientation of the various line elements comprising the visual scene. These changes, in turn, can be expressed in terms of changes to the angular coordinates associated with the line element, two coordinates per point For our study, we have taken these two coordinates to be the azimuth and elevation angles associated with the line-of-sight (LOS) to a particular line element endpoint. This is illustrated in figures 3 and 4, which show how specific vehicle rotations and translations result in changes in the azimuth and elevation angles associated with the line-of-sight to specific points in the visual scene.

Changes in the LOS angles are due to changes in vehicle state (position and attitude). Assuming small changes, we can use linearized relations, so that

$$\psi_{vis} = \underline{c}'_{\psi}\underline{x} \tag{3a}$$

$$\theta_{vis} = \underline{c}'_{\theta}\underline{x} \tag{3b}$$

where ψ_{vis} and θ_{vis} are the azimuth and elevation LOS angles, $\underline{c}_{\psi}$ and $\underline{c}_{\theta}$ are the display "gains", and it is understood that the above relation holds (with different gains) for each specific point in the visual scene. We then assumed, for each vehicle state the pilot was trying to estimate, that he would chose one particular point in the visual scene to provide the most appropriate visual cue, and then share his attention among these now competing cues. Thus, if the vehicle state is comprised of three rotational coordinates and three translational coordinates, then, in general, there would be six specific points in the visual scene the pilot would use for inferring changes in vehicle states. Notice there is a many on one mapping between the vehicle state and each point in the scene, however, rather than postulating a cue decoupling model it was assumed the pilot was able to perform the inverse transformation needed to infer correct vehicle motion (via many observations).

It is now appropriate to consider the fact that the pilot will be limited in his ability to detect changes in the LOS angle cues available to him. This limitation will be due either to his own inherent sensory/perceptual limitations, or, in the simulator situation, possibly due to CGI-imposed resolution limits. The effective visual cue threshold will be the greater of the two thresholds associated with the pilot and the display hardware, and will ultimately limit the pilot's ability to infer vehicular state changes from changes in the visual scene. Naturally, if display hardware is not involved (as in the actual helicopter environment), then the effective threshold will be determined solely by the pilot's visual limitations.

Turning first to the pilot's visual limitations, we make a distinction between angular resolution threshold (α_R) and angular discrimination threshold (α_D). The former refers to his visual acuity, and his ability to resolve small angular differences in the LOS angle, when given a visual reference which, in angular distance, is very close to the object being sighted. The latter refers to the pilot's ability to discriminate between two large visual angles, and thus his ability to identify a small angular difference in the LOS angle, when given a visual reference which, in angular distance, is relatively far from the object being sighted.

The angular resolution threshold (α_R) might be chosen on the basis of measured human visual acuity, which appears to be on the order of one minute of arc (Riggs (1965)). However, we chose to set it at a slightly higher level, based on an earlier analysis of the data obtained from dynamic tracking experiments (Levison (1971)):

$$\alpha_R = 0.05 \text{ deg}$$

The angular discrimination threshold (α_D) was chosen in accordance with the Weber-Flechner law (Luce and Galanter (1963)), and set at a fixed fraction of the total angle being viewed:

$$\alpha_D = \alpha_o/30$$

where α_o is the total angle being viewed.

We now define the pilot-associated visual threshold as the maximum of the resolution and discrimination thresholds:

$$\alpha = \mathrm{MAX}(\alpha_R, \alpha_D) \qquad (4)$$

The overall pilot/simulator visual threshold will be given by

$$\gamma = \max(\alpha, \beta) \qquad (5)$$

where α is the effective pilot threshold obtained previously, and the overall simulator threshold is:

$\beta = (\beta_H + \beta_V)/2$
β_H = horizontal CGI resolution threshold
β_V = vertical CGI resolution threshold.

The discussion to this point has concentrated on static "position" thresholds. To determine dynamic "velocity" thresholds associated with visual cueing, one might attempt to assign a value on the basis of past psychophysical motion detection/discrimination experiments. However, a review of the subject by Graham (1965) shows that a wide range of values can be assigned, depending on the particular experimental situation and empirical measures used. We again chose to assign a value on the basis of earlier dynamic tracking experiments.

In a study of tracking, with a quantized visual display (Levison et al (1972)), a good OCM model match was obtained by setting $\dot{\gamma}_{TH}$ equal to the display quantization level, and adjusting γ_{TH} to provide the best fit to the data. This resulted in

$$\gamma_{TH} = 0.25 \text{ deg}$$

$$\dot{\gamma}_{TH} = 1.1 \text{ deg/sec}$$

yielding a $\dot{\gamma}_{TH}/\gamma_{TH}$ ratio of approximately 4.4. Other studies have shown similar ratios between velocity and position thresholds, and thus we chose for this study to specify the visual velocity threshold according to:

$$\dot{\gamma} = 4\gamma$$

where, if γ is given in degrees, $\dot{\gamma}$ is given in d
Hence, we tie the rate threshold to the position thresh
in turn, depends on the pilot-associated and display·
resolution limitations. These ideas are summarized bel

RESOLUTION, DISCRIMINATION, & RATE THRESHOLDS

- PILOT ANGULAR RESOLUTION THRESHOLD
  $\alpha_R = 0.05°$ (TRACKING EXPERTS)
- PILOT ANGULAR DISCRIMINATION THRESHOLD
  $\alpha_D = \alpha_R/30$ (WEBER-FLECHNER)
- CGI-IMPOSED ANGULAR RESOLUTION THRESHOLD
  RESOLUTION: N LINES/FRAME, M PIXELS/LINE
  FRAME SIZE: 48° HORIZONTAL, 36° VERTICAL
  H,V THRESHOLDS: $\beta_H = 48°/M$, $\beta_V = 36°/N$
  CGI THRESHOLD: $\beta_R = (\beta_H+\beta_V)/2$
- EFFECTIVE RESOLUTION THRESHOLD
  $\gamma = \mathrm{MAX}(\alpha_R, \beta_R)$
- EFFECTIVE RATE THRESHOLD
  $\dot{\gamma} = 4\gamma$ (TRACKING EXPERTS)

We are now in a position to define the effective "informational" thresholds, associated with the visual cues available to the pilot. As we noted earlier, we assume the pilot can "invert" the appropriate display equations to obtain an estimate of the vehicular attitude/position change from the visual cues available to him. If we assume that the effective visual threshold applies equally to the azimuth (ψ_{vis}) and elevation (θ_{vis}) LOS changes, we can use figures 3 and 4 to generate informational threshold functions as shown in table 3.

This table relates visual scene thresholds to (displayed) vehicle state thresholds. To determine the specific values for these informational thresholds, first assume a nominal hover altitude (h_o) of 10 ft, and a nearest eye level visual target at a distance (l_o) of 50 ft. Note that the maximum lateral field of view (ψ_{FOV}) and LOS depression angle (θ_o) are both set by the screen configuration. Then, minimizing the threshold functions of Table 3 and solving for θ and ψ, for each screen configuration and display resolution considered, determines the "best" viewing locations along with the values for the informational thresholds. The resulting thresholds are summarized in Table 4.

Table 3: Visual Scene Informational Function

AXIS	POSITION	VELOCITY
YAW	$\psi_{TW} = \gamma$	$\dot{\psi}_{TW} = \dot{\gamma}$
PITCH	$\theta_{TW} = \gamma$	$\dot{\theta}_{TW} = \dot{\gamma}$
ROLL(1)	$\phi_{TW} = \left(\frac{1}{2\sin\psi_{TW}}\right)\gamma$	$\dot{\phi}_{TW} = \left(\frac{1}{2\sin\psi_{TW}}\right)\dot{\gamma}$
SURGE(2)	$x_{TW} = \left(\frac{h_0}{\sin^2\theta_0}\right)\left(\frac{\theta_0}{30}\right)$	$\dot{x}_{TW} = \left(\frac{h_0}{\sin^2\theta_0}\right)\dot{\gamma}$
SWAY(3)	$y_{TW} = \ell_0\gamma$	$\dot{y}_{TW} = \ell_0\dot{\gamma}$
HEAVE(2)	$z_{TW} = \left(\frac{h_0}{\sin\theta_0\cos\theta_0}\right)\left(\frac{\theta_0}{30}\right)$	$\dot{z}_{TW} = \left(\frac{h_0}{\sin\theta_0\cos\theta_0}\right)\dot{\gamma}$

(1) FACTOR OF 2 ACCOUNTS FOR TWO END-POINT HORIZON

(2) POSITION THRESHOLD IS DISCRIMINATION LIMITED

(3) ASSUMES VISUAL TARGET STRAIGHT AHEAD ($\psi_0 = 0$)

Table 4: Visual Scene Informational Threshold Values

THRESHOLD*	RESOLUTION 500 LINES/FRAME			1000/2000 LINES/FRAME		
CONFIG	A	B	C	A	B**	C
ROTATION						
θ_w	.38	.38	.08	.05	.05	.25
$\dot{\theta}_w$	.34	.34	–	.20	.20	.20
ψ_w	.38	.38	.38	.05	.05	.05
$\dot{\psi}_w$	.34	.34	.34	.20	.20	.20
ϕ_w	.10	.04	.04	.06	.02	.02
$\dot{\phi}_w$	.42	.16	.16	.25	[illegible]	[illegible]
TRANSLATION						
x_w	[illegible]	[illegible]	[illegible]	[illegible]	[illegible]	[illegible]
$\dot{x}_w$	.56	.56	.02	.21	.21	.35
z_w	.57	.57	.57	.57	.57	.57
$\dot{z}_w$	.17	.17	.17	.10	.10	.10
y_w	.37	.37	.37	.34	.08	.08
$\dot{y}_w$	.30	.30	.30	.17	.17	.17

* ROTATION THRESHOLD VALUES IN DEG & DEG/SEC
TRANSLATION THRESHOLD VALUES IN FT & FT/SEC

** NOMINAL CONFIGURATION

In summary, since the perceptual dynamics of the human visual system are relatively wide-band with respect to the system dynamics we are modelling, we chose not to include any dynamic visual effects. This allowed us to implement our visual perception model by simply thresholding the appropriate system state variables: the linear/angular positions and velocities of the (simulated) vehicle.

Vestibular Perception Model

Models of vestibular motion perception have been the subject of study for a number of years, and we will not attempt to summarize this work. Instead, we refer the reader to a relatively recent review of motion cue models by Zacharias (1978), in which a number of these models are described and critically reviewed.

Figure 5 shows the vestibular model in block diagram form. The upper portion models the semi-circular canals as transducers of angular velocity, while the lower portion models the otoliths as transducers of specific force. Table 5 sumarizes the parameter values used in each of the vestibular models.

Figure 5: Vestibular Model

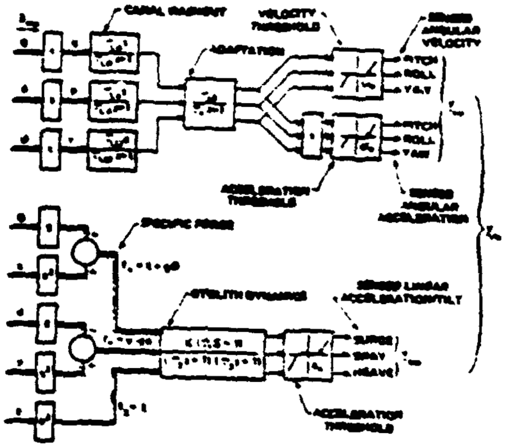
VELOCITY THRESHOLD
SENSED ANGULAR VELOCITY
ADAPTATION
PITCH
ROLL
YAW
PITCH
ROLL
YAW
ACCELERATION THRESHOLD
SENSED ANGULAR ACCELERATION
SPECIFIC FORCE
OTOLITH DYNAMICS
SENSED LINEAR ACCELERATION/TILT
SURGE
SWAY
HEAVE
ACCELERATION THRESHOLD

CANAL PARAMETERS

AXIS	τ_L (DEG/S)	ω_0 (DEG/S)	α_0 (DEG/S^2)	
PITCH (θ)	5.3	3.6	0.67	$\tau_a = 30s$
ROLL (ϕ)	6.1	2.5	0.41	
YAW (ψ)	10.2	4.2	0.41	

OTOLITH PARAMETERS

$\tau_1 = 13.2s$, $\tau_2 = 5.33s$, $\tau_3 = 0.66s$ } ALL AXES
$K = 0.4$, $a_0 = 0.053\text{FT}/s^2$

Table 5: Parameter Values for Vestibular Model

To reduce computational requirements imposed by the vestibular model, we performed an analysis of the power spectrum of the vestibular signals. By comparing the power spectra of incoming vestibular signals to that of their filtered outputs, pass-bands were identified which accounted for the majority of the correlated power. Utilizing this information allowed the elimination of any lead or lag elements having break frequencies not in the pass-bands. Table [illegible] outlines the resulting simplifications. Although many of the vestibular dynamics were simplified or eliminated, the vestibular thresholds given in table 5 were still implemented.

Table 6: Simplifications to the Vestibular Model

Axis	Simplification
Pitch (θ)	Eliminate canal washout and adaptation filters
Roll (ϕ)	Eliminate adaptation filter
Yaw (ψ)	Eliminate canal washout and adaptation filters
Surge (f_x)	No simplification
Heave (f_z)	Set $\tau_1 = \tau_2 = 0$
Sway (f_z)	No simplification

Attention-Sharing Model

The general features and method of implementation of the attention-sharing model are well known (see, for example, Kleinman (1976)). Here, we wish to describe features of the model which are specific to the particular helicopter hover task under consideration.

In our modelling of the hover task, we assumed that "full attention" corresponds to an overall noise/signal ratio of -20 dB, a level which is consistent with the finding of many earlier manual control studies (see, Kleinman et al (1971)). Further there would be an optimum allocation of attention among the displayed variables subject to several constraints. These constraints are summarized in Table 7.

Table 7: Monitor Constraints

1. $f_{LAT} = f_{LONG} = .5$
2. $f_s = f_s$; ie equal attention to a signal and its rate of change.
3. $f_{vest} = f_{vis}$ = total axis attention
4. $f_{TOT} = 1.0$

Notice, although the lateral axis control task is more demanding than the longitudinal axis (see Hoffman (1976)), for the purpose of this study we assumed an equal split of attention between the two axis. In addition no interference is allowed between modalities (ie. visual and vestibular signals are processed in parrallel). This requires that within an axis the total visual attention equal the total vestibular attention. This last assumption will clearly favor the use of motion cues, provided they are useful for control, since the pilots total attention to the task is effectively doubled.

Sumary of Model Implimentation Characteristics

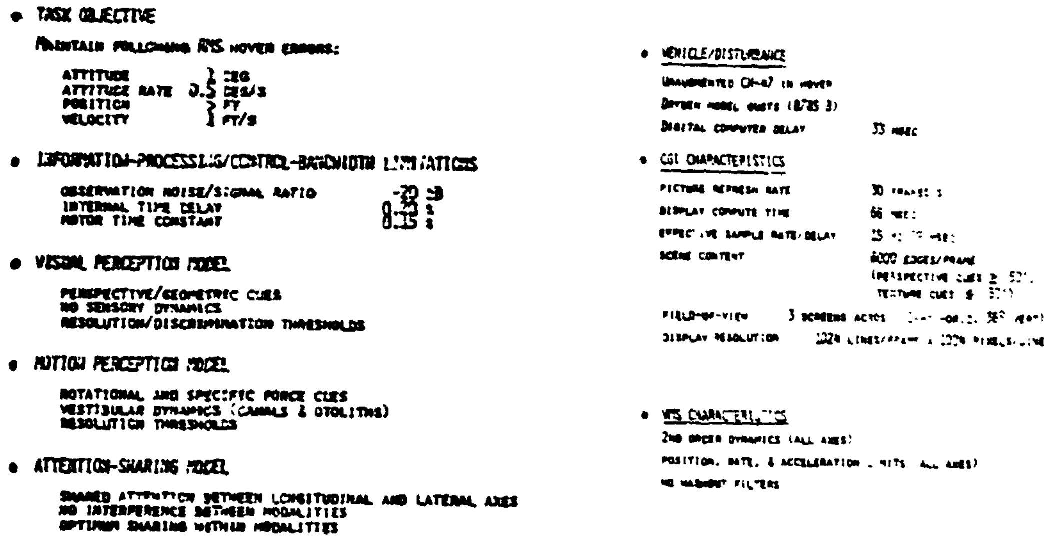

- TASK OBJECTIVE

  MAINTAIN FOLLOWING RMS HOVER ERRORS:

  ATTITUDE } DEG
  ATTITUDE RATE 0.5 DEG/S
  POSITION } FT
  VELOCITY } FT/S

- INFORMATION-PROCESSING/CONTROL-BANDWIDTH LIMITATIONS

  OBSERVATION NOISE/SIGNAL RATIO -20 dB
  INTERNAL TIME DELAY 0.[illegible] s
  MOTOR TIME CONSTANT 0.15 s

- VISUAL PERCEPTION MODEL

  PERSPECTIVE/GEOMETRIC CUES
  NO SENSORY DYNAMICS
  RESOLUTION/DISCRIMINATION THRESHOLDS

- MOTION PERCEPTION MODEL

  ROTATIONAL AND SPECIFIC FORCE CUES
  VESTIBULAR DYNAMICS (CANALS & OTOLITHS)
  RESOLUTION THRESHOLDS

- ATTENTION-SHARING MODEL

  SHARED ATTENTION BETWEEN LONGITUDINAL AND LATERAL AXES
  NO INTERFERENCE BETWEEN MODALITIES
  OPTIMUM SHARING WITHIN MODALITIES

- VEHICLE/DISTURBANCE

  UNAUGMENTED CH-47 IN HOVER
  DRYDEN MODEL GUSTS ([illegible])
  DIGITAL COMPUTER DELAY 33 MSEC

- CGI CHARACTERISTICS

  PICTURE REFRESH RATE 30 FRAMES/S
  DISPLAY COMPUTE TIME 66 MSEC
  EFFECTIVE SAMPLE RATE/DELAY 15 Hz/[illegible] MSEC
  SCENE CONTENT 6000 EDGES/FRAME (PERSPECTIVE CUES ≥ 50%, TEXTURE CUES ≤ 50%)
  FIELD-OF-VIEW 3 SCREENS ACROSS ([illegible] HORIZ., 38° VERT)
  DISPLAY RESOLUTION 1024 LINES/FRAME x 1024 PIXELS/LINE

- VMS CHARACTERISTICS

  2ND ORDER DYNAMICS (ALL AXES)
  POSITION, RATE, & ACCELERATION LIMITS (ALL AXES)
  NO WASHOUT FILTERS

CLOSED-LOOP ANALYSIS OF CGI AND VMS EFFECTS

In this section, the optimal control model with the expanded perceptual model is used to analyze the effects of CGI and VMS limitations on closed-loop hover performance. The goal of this analysis is to determine the effects of CGI and VMS characteristics on simulator fidelity (more precisely, performance and workload). To this end, a "perfect" or ideal simulator is defined in which there are no simulation time delays, no motion system dynamics, and an infinite resolution imagery system. This simulator configuration corresponds essentially to flight* and provides a benchmark against which to measure simulator deficiencies. In addition to the nominal and perfect motion conditions, results were also obtained for a "no-motion" or fixed-base simulator configuration.

---

* Through an oversight, the assumptions for the perfect configuration included a field-of-view constraint relevant to the nominal CGI configuration. This degraded performance only slightly from what would have been obtained without the constraint.

Thus, there were six basic simulator configurations to be analyzed so as to evaluate the effects of the visual and motion systems, separately and together. These configurations are listed in Table 8.

Table 8: Simulator Configurations

CONFIGURATION	DESCRIPTION
Perfect (Flight)	**No simulator delays, nominal field of view, human operator thresholds, no VMS dynamics**
Perfect CGI- Realistic VMS	**Includes main frame computer delays and VMS platform dynamics**
Realistic CGI- Perfect VMS	**Includes main frame and display computer delays, CGI imposed visual thresholds, no platform dynamics**
Realistic CGI- Realistic VMS	**Includes all simulator nominal characteristics (see Table 5.1)**
Perfect CGI- Fixed Base	**Includes main frame computer delays in visual cues, no motion cues**
Realistic CGI- Fixed Base	**Includes CGI limitations, no motion cues**

Results and Discussion

The effects of CGI and motion system characteristics will be examined largely in terms of relative performance in the hovering task. For each axis, relative performance is defined as

$$\text{Performance (in \%)} = 100 \times (J-J_{FLT})/J_{FLT} \qquad (6)$$

where J is the value of the cost functional of Eq. 1 and J_{FLT} corresponds to the value of J obtained for flight or the "perfect" simulator. Thus, relative performance is a normalized metric of performance that measures the percent deviation from "flight" performance introduced by the simulator characteristics. In this sense, relative performance is a measure of simulator fidelity.

The results will be presented in terms of J (rather than individual error and control scores) because this quantity is a scalar metric of overall performance and, therefore, provides a concise description of the simulator effects. In addition, Hess (1977) has shown that the value of J may be correlated with vehicle flying qualities, so increases in J owing to simulator deficiencies may be related to degraded flying qualities for the simulator. Nonetheless, individual error and control scores may also be of interest and these are presented later in table 9 for the six simulator configurations.

ORIGINAL PAGE IS
OF POOR QUALITY

Table 10 summarizes the optimal attention split found for the nominal fixed and moving base simulator configurations. As discussed in Kleinman (1976), the attention paid to a variable indicates its relative importance to the task. Table 10 shows that pitch and pitch rate information is the single most important visually obtained variable for the longitudinal axis, while roll and roll rate are most useful for lateral control. Of the vestibular cues, pitch, pitch rate, and z-axis specific force are all important for longitudinal control, while y-axis specific force is the most useful cue for lateral control.

		Unaugmented CH-47 Dynamics						Augmented CH-47 Dynamics		
		Simulator Configuration								
Variable	Units	P Sim	R VMS P CGI	P VMS R CGI	R VMS R CGI	F B P CGI	F B R CGI	P Sim *	R VMS R CGI	F B R CGI
σ_x	ft	4.85	5.14	5.72	5.93	5.49	6.87	2.76	3.05	3.32
$\sigma_{\dot{x}}$	ft/sec	0.92	0.80	1.09	1.13	1.04	1.30	0.55	0.60	0.65
σ_z	ft	1.77	1.91	2.06	2.11	2.11	2.47	0.99	1.12	1.31
$\sigma_{\dot{z}}$	ft/sec	0.60	0.66	0.67	0.70	0.78	0.87	0.39	0.42	0.56
σ_θ	deg	0.82	0.87	0.96	1.00	0.92	1.13	0.5	0.54	0.56
$\sigma_{\dot{\theta}}$	deg/sec	0.85	0.92	0.99	1.03	0.97	1.17	0.43	0.46	0.45
σ_y	ft	6.50	6.91	7.46	7.52	8.37	9.72	4.31	4.56	5.63
$\sigma_{\dot{y}}$	ft/sec	1.27	1.35	1.44	1.46	1.65	1.91	0.88	0.93	1.15
σ_ϕ	deg	1.72	1.76	1.81	1.82	1.90	2.06	1.53	1.54	1.62
$\sigma_{\dot{\phi}}$	deg/sec	1.05	1.1	1.18	1.20	1.27	1.46	0.65	0.67	0.73
σ_ψ	deg	0.42	0.44	0.37	0.47	0.46	0.62	0.06	0.06	0.07
$\sigma_{\dot{\psi}}$	deg/sec	0.15	0.16	0.15	0.17	0.20	0.24	0.04	0.05	0.05
σ_{δ_e}	inches	0.23	0.23	0.23	0.24	0.23	0.24	0.24	0.24	0.24
σ_{δ_c}	inches	0.14	0.1:	0.15	0.15	0.15	0.16	0.12	0.12	0.13
σ_{δ_a}	inches	0.16	0.16	0.17	0.17	0.17	0.19	0.27	0.27	0.28
σ_{δ_r}	inches	0.03	0.03	0.03	0.03	0.03	0.04	0.04	0.04	0.04

*P Perfect
R Realistic
F B Fixed Base

Table 9: RMS Performance Scores

Table 10: Attention Allocation Nominal Configurations

		VARIABLE	MOVING BASE	FIXED BASE
LONGITUDINAL AXIS	VISUAL	$x,\dot{x}$	0.047	0.045
		$z,\dot{z}$	0.087	0.053
		$\theta,\dot{\theta}$	0.366	0.402
			0.500	0.500
	VESTIBULAR	f_x	0.021	
		f_z	0.187	
		$\theta,\dot{\theta}$	0.291	
			0.500	
LATERAL AXIS	VISUAL	$v,\dot{v}$	0.105	0.088
		$\phi,\dot{\phi}$	0.366	0.336
		$\psi,\dot{\psi}$	0.029	[illegible]
			0.500	0.500
	VESTIBULAR	f_y	0.339	
		$\dot{\phi},\ddot{\phi}$	0.141	
		$\dot{\psi},\ddot{\psi}$	0.020	
			0.500	

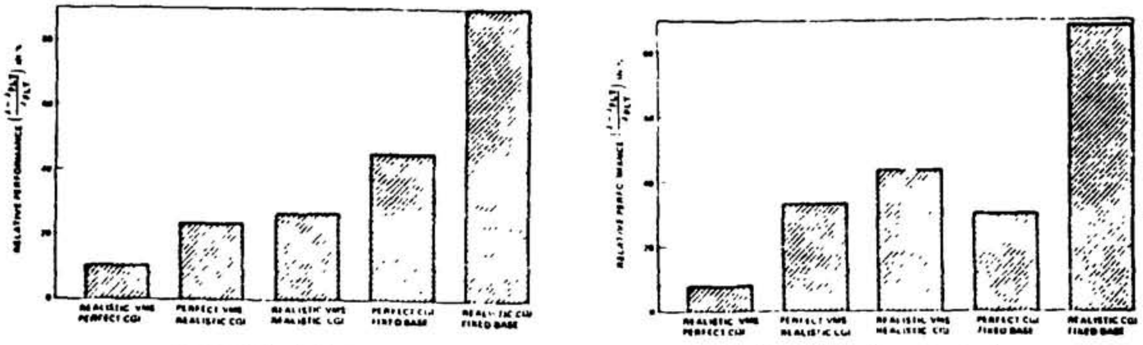

Lateral Axis

Longitudinal Axis

Figure 6: Relative Performance vs. Simulator Configurations

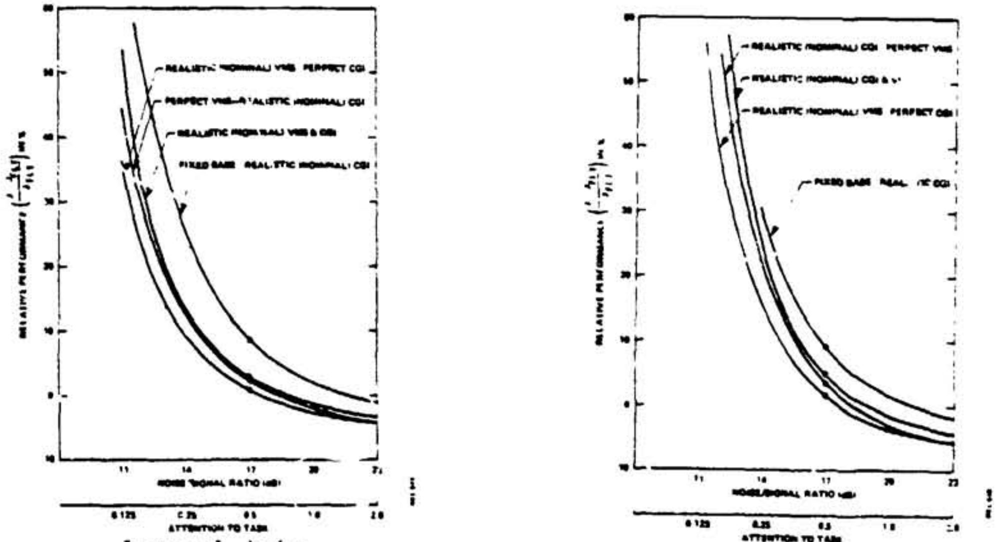

Lateral Axis

Longitudinal Axis

Figure 7: Relative Performance Vs. Workload

Overall CGI and Motion System Effects

Figure 6 presents the model performance predictions for the five simulator configurations, relative to that expected from the "perfect" simulator (which, by definition, has a relative performance of zero). With respect to longitudinal performance, it can be seen that the effect of the CGI is much more significant (35%) than that of the motion system (10%). Indeed, performance is better with a perfect CGI and no motion than with perfect motion and a realistic CGI. However, motion is still important particularly if the realistic CGI deficiencies are accounted for. This is shown by the prediction of approximately twice the relative performance for the realistic CGI-fixed base configuration as for the realistic CGI-realistic VMS configuration.

The results for the lateral control task are similar to those for the longitudinal task, but motion is even more important. In this case, having a perfect CGI does not compensate for lack of motion, since the fixed base configurations are worse than any other motion configuration. Compared to the longitudinal task, going from perfect to realistic motion introduces less performance degradation. Also, motion ameliorates the consequences of any visual deficiencies.

For either longitudinal or lateral control, the performance change (10-15%) due to introducing the realistic motion system alone is probably within the inter- and intra-pilot variations that might be expected. However, once realistic CGI effects are considered, or motion is removed entirely, this is no longer likely to be true for skilled pilots inasmuch as the deviations predicted can be substantially greater than 20%.

Table 9 gives the effects of simulator configurations on individual rms error scores. These scores generally tend to parallel the effects shown for relative performance, as would be expected. However, it is interesting to note that predicted control scores are less affected by simulator changes than are output variables. Indeed, the control scores remain fairly constant over the various conditions.*

The above model predictions are based on the assumption that the pilot will maintain a fixed level of attention for the longitudinal and lateral control tasks regardless of simulator configuration. However, in actuality, the pilot may choose to devote more (or less) attention to the control tasks, based on simulator configuration. To explore the effects of such a change in strategy, model predictions were obtained for various attention levels. The results are presented in figure 7. Note that the solid dots on the curves indicate the nominal level of attention for that simulator configuration. It can be seen that the relative ordering of simulator configurations is maintained at all levels of attention. At high levels of attention, the performance with the realistic CGI-perfect VMS configuration approaches that for the realistic VMS-perfect CGI configuration. Apparently, if the noise/signal ratio is lowered sufficiently on the motion cues, it can offset some of the visual deficiencies associated with the nominal CGI.

---

* As a result, inner loop variables (θ and ϕ) are somewhat less affected than outer loop quantities (x, y, z and ψ).

If it is assumed that the pilot adapts his behavior and increases attention levels to achieve performance equivalent to that in flight, then the incremental attention required may be considered a workload penalty associated with the simulator. The curves of figure 7 can be used to determine this workload penalty for maintaining flight level performance in the simulator; one simply determines the intersection of the particular sensitivity curve with the line of zero relative performance. The computed attention or workload penalties for the various configurations analyzed in Figure 7 are given in table 11. For the nominal CGI and motion system, the pilot would have to increase attention by 50% over that needed in flight in order to achieve the same performance, whereas almost three times as much attention is required for a fixed base simulation.

Effects of CGI Parameters

The results of the previous section suggest that the visual processing limitations introduced by a nominal CGI configuration could result in significant deteriorations of closed-loop hover performance. Here, we examine the effects of variations in individual, design-related CGI parameters. In these analyses, a single parameter is varied while all other CGI parameters are kept at their nominal or realistic values. Results will be presented for both realistic motion base and fixed base configurations.

Figures 8 and 9 show the effect of incremental delays on relative performance for motion-base and fixed-base simulators, respectively. Results are presented as a function of CGI display computer delay, for three values of main-frame computer delay (T_C). Recall, the nominal display delay is 99 msec. For the range of delays considered. relative performance appears to degrade linearly as a function of either display delay or main-frame delay, when motion is present. Comparison of figures 8 and 9 (note the difference in scale) reveals that the absence of motion cues will accentuate the deterioration of performance for a given delay. Moreover, for a fixed base configuration, performance degrades more rapidly than linearly. It can also be seen from these figures that the longitudinal control task is more sensitive to increases in delay than is the lateral task, particularly to increases in display delays.

In general, the magnitude of the effects of display delay are quite significant. Increasing display delay from zero to the nominal, but reasonably conservative, value of 99 msec, causes an increase in relative performance of approximately 20-30% for the motion-base simulation and about 40-50% for the fixed-base case.

C-2

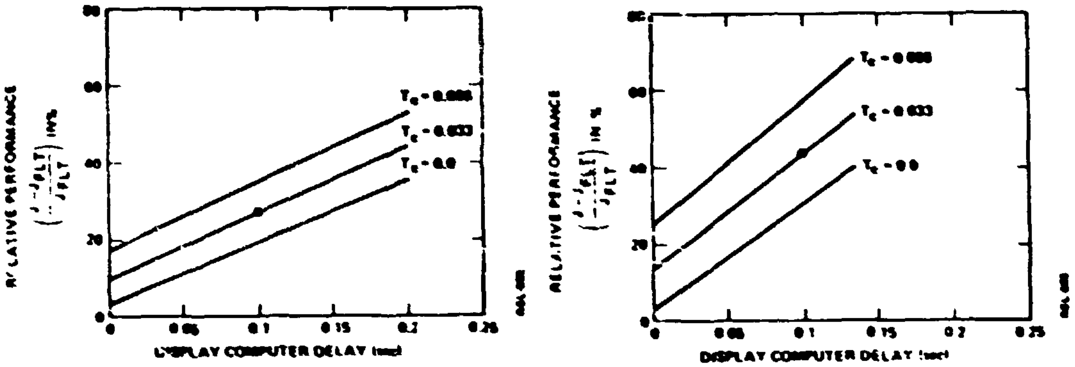

Lateral Axis

Longitudinal Axis

Figure 8: Relative Performance vs. Time Delay (moving base simulator)

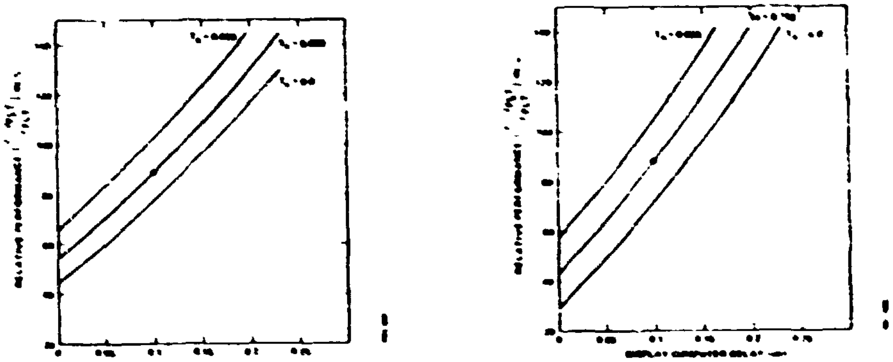

Lateral Axis

Longitudinal Axis

Figure 9: Relative Performance vs. Time Delay (fixed base simulator)

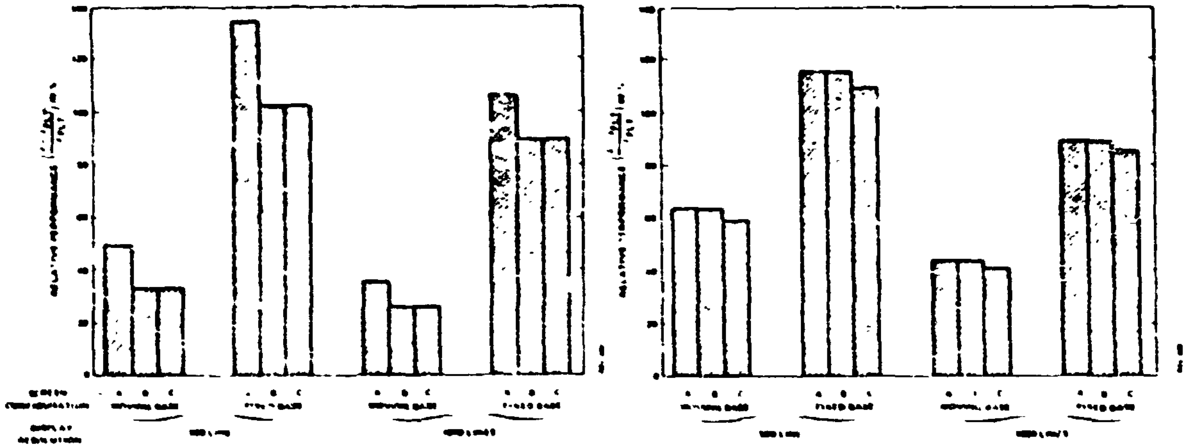

Lateral Axis

Longitudinal Axis

Figure 10: Relative Performance vs. Field of View and Display Resolution

An examination of the relative performance values for zero display and computer delay shows that the effects of other CGI or motion system limitations are much less significant (at nominal values) than are the effects due to delays.

The effects of field-of-view and display resolution are presented in figure 10. Recall that screen configuration B is the nominal configuration corresponding to a 144° horizontal, 36° vertical field of view. Configurations A and C provide 48° by 36° and 144° by 72° fields of view, respectively. The nominal display resolution is 1024 lines. Both field of view and display resolution are assumed to affect observational thresholds as discussed previously.

It can be seen from figure 10 that decreasing the horizontal field of view (configuration A) does not affect longitudinal performance and increasing the vertical field-of-view has no effect on lateral performance. This is expected because of the assumed decoupling between longitudinal and lateral control tasks.* Figure 10 also suggests that increasing vertical field-of-view has very little performance payoff and probably would not be justified on the basis of these results. On the other hand, the improvement in performance with increased lateral field-of-view appears to be significant, especially if the cue presentation is degraded in other ways, such as poorer resolution or no motion. For the 500 line display, fixed base configuration, reduction of the horizontal field-of-view from 144° to 48° degrades relative performance by more than 30%.

The effects of display resolution are somewhat different than for field-of-view in that a greater effect is observed for the longitudinal task than the lateral task. With motion, longitudinal performance is about 20% poorer for the 500 line display as compared to about a 5% degradation in the lateral case; for the fixed-base configurations, these effects are increased to about 25-30% and 10%, respectively.

Before leaving this discussion of the effects of individual CGI parameters, it should be noted, as a caution, that the assumption of a one-to-one correspondence with model parameters is made for simplicity. In reality, design changes can alter several factors related to information processing and tradeoffs are often

---

* The possible effects of increased field of view providing useful peripheral information on vehicle rates have not been examined here.

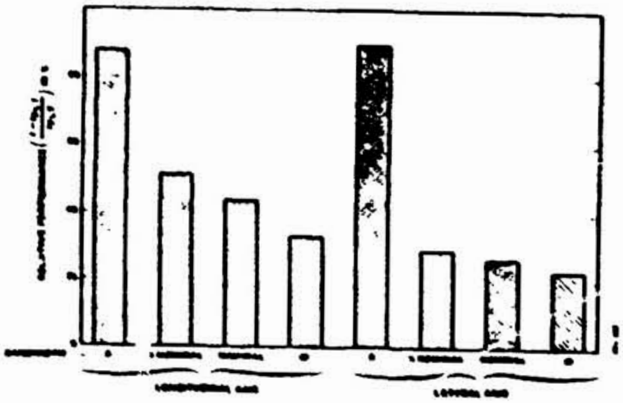

Figure 11: Relative Performance vs. VMS Platform Bandwidth

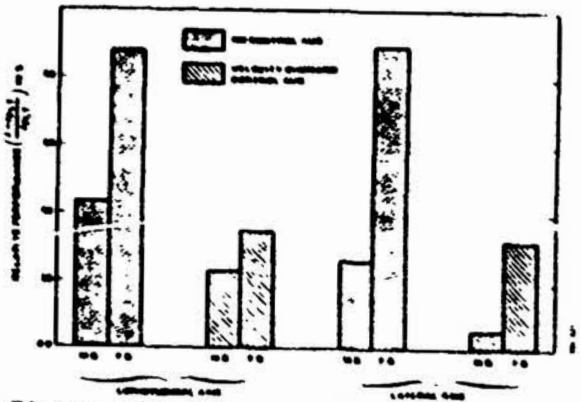

Figure 12: Relative Performance vs. Control Augmentation

Table 11: Simulator Workload Penalties

CONDITION	- ATTENTION -		
	LONG.	LAT	TOTAL
	.5	.5	
R. VMS, P. CGI	.55	.58	1.0
P. VMS. R. CGI	.66	.69	1.35
R. VMS, R. CGI	.76	.76	1.52
R. CGI - F. B.	1.25	1.5	2.75

the result. For example, improved scene content may lower noise/signal ratios but may require more computation and, hence, increase delay.

Effects of VMS Parameters

Relative performance is plotted as a function of platform bandwidth and control task in figure 11. A bandwidth of zero corresponds to a fixed base configuration and an infinite bandwidth corresponds to flight motion. It can be seen that changing the bandwidth does not have an appreciable effect on relative performance, so long as a reasonable degree of motion fidelity is maintained. The effects of bandwidth are somewhat more pronounced for the longitudinal control task than for the lateral.

Effects of Vehicle Dynamics

The effects of simulator parameters will depend on the specifics of the task, including the vehicle dynamics. This has already been illustrated in differences between predicted longitudinal and lateral performance. To explore further the effects of vehicle dynamics, results were obtained for the CH-47 with a velocity command control augmentation system, as specified in Hoffman et al (1976) as system F. The augmented vehicle presents a significantly less difficult control task. Figure 12 gives relative performance as a function of control augmentation for the nominal simulator configuration (and for the nominal fixed-base configuration). The effect of simulator characteristics is substantially less for the augmented vehicle. However, the effect is still significant for longitudinal control and for fixed-base simulation of lateral (augmented) control.

SUMMARY AND CONCLUSIONS

The optimal control model for pilot/vehicle analysis has been used to explore the effects of a CGI visual system and motion system dynamics on helicopter hover simulation fidelity. This was accomplished by expanding the perceptual aspects of the model to include motion sensing and by relating CGI parameters to information processing parameters of the model. Simulator fidelity was examined by comparing predicted performance and workload for flight with that predicted for various simulator configurations.

The results of the analysis suggest that simulator deficiencies of a reasonable nature (by current standards) can result in substantial performance and/or workload infidelity. Both CGI and motion system effects are significant for this task. There is an interaction between the two sources of pilot cues. In particular, the presence of motion reduces the sensitivity to CGI limitations.

With respect to the CGI system, the most important parameter in terms of its effect on performance was display delay. This was followed in order of importance by display resolution and field-of-view.

The main effect associated with motion system bandwidth was introduced by going to a fixed-base configuration. Halving the VMS platform bandwidth or going to full flight motion made only a marginal change in the performance predicted for the nominal VMS bandwidths.

The trends of the results are fairly consistent although there were some differences between lateral and longitudinal control tasks. The magnitude of the effects and relative importance of various parameters are clearly dependent on the task as exemplified here by longitudinal vs. lateral and unaugmented vs. augmented vehicle dynamics. It is, of course, for this reason that models of the pilot/vehicle system are needed to evaluate the importance of simulator parameters for a given situation.

REFERENCES

1. Baron, S. and Levison, W. H., "A Manual Control Theory Analysis of Vertical Situation Displays for STOL Aircraft," NASA CR-114620, April 1973.

2. Baron, S., Muralidharan R. and Kleinman, D. L., "Closed Loop Models for Analyzing the Effects of Simulator Characteristics", *AIAA Flight Simulation Tech. Conf.*, Arlington, TX, September 1978.

3. Brown, J. L., "Visual Elements in Flight Simulation", University of Rochester, TR-73-2, December 1973.

4. Gibson, J. J., *The Perception of the Visual World*, Riverside Press, Cambridge, Mass., 1950.

5. Graham, C. H., "Perception of Movement", in *Vision and Visual Perception*, C. H. Graham (editor), John Wiley and Sons, N.Y., 1965.

6. Gum, D. R. and Albery, W. B., "Time Delay Problems Encountered in Integrating the Advanced Simulator for Undergraduate Pilot Training", *J. of Aircraft*, *4*, 1977.

7. Hess, R., "Prediction of Pilot Opinion Ratings Using an Optimal Pilot Model", *Human Factors*, *19*, 1977.

8. Hoffman, W. C., Kleinman, D., and Young, L., "Display/Control Requirements for Automated VTOL Aircraft", ASI-TR-76-39, October 1976.

9. Kleinman, D. L., "Solving the Optimal Attention Allocation Problem in Manual Control", *IEEE Trans. on Automatic Control*, *AC-21*, 1976.

10. Kleinman, D. L., Baron, S. and Levison, W. H., "A Control Theoretic Approach to Manned-Vehicle Systems Analysis", *IEEE Trans. on Auto. Control*, *AC-16*, 1971.

11. Levison, W. H., "The Effects of Display Gain and Signal Bandwidth on Human Controller Remnant", AMRL-TR-70-93, Wright-Patterson Air Force Base, Ohio, March 1971.

12. Levison, W. H., Elkind, J. I., and Ward, J. L., "Studies of Multivariable Manual Control Systems: A Model for Task Interference", NASA-Ames Research Center, NASA CR-1746, May 1971.

13. Quiejo, M. J. and Riley, D. R., "Fixed-Base Simulator Study of the Effect of Time Delays in Visual Cues on Pilot Tracking Performance", NASA TN D-8001, October 1975.

14. Riggs, L. A., "Visual Acuity", in Vision and Visual Perception, C. H. Graham (editor), John Wiley and Sons, NY, 1965.

15. Staples, K. J., "Motion, Visual, and Aural Cues in Piloted Flight Simulation", AGARD Conference Proceedings No. 79 on Simulation, AGARD CP-79-70, March 1970.

16. Wewerinke, P. H., "A Theoretical and Experimental Analysis of the Outside World Perception Process", Proceedings of the Fourteenth Annual Conference on Manual Control, NASA conf. Pub. 2060, November 1978.

17. Zacharias, G. L., "Motion Cue Models for Pilot-Vehicle Analysis", AMRL-TR-78-2, Wright-Patterson Air Force Base, Ohio, May 1978.

Omit.
accessioned as
81A 37258

PURSUIT TRACKING AND HIGHER LEVELS OF SKILL DEVELOPMENT IN THE HUMAN PILOT

Ronald A. Hess
NASA Ames Research Center, Moffett Field, CA 94035

ABSTRACT

This paper serves as a synoptic of the research reported in Ref. 1. In Ref. 1, a model of the human pilot is offered for pursuit tracking tasks; the model encompasses an existing model for compensatory tracking. The central hypothesis in the development of this model states that those primary structural elements in the compensatory model responsible for the pilot's equalization capabilities remain intact in the pursuit model. In this latter case, effective low-frequency inversion of the controlled-element dynamics occurs by feeding-forward derived input-rate through the equalization dynamics, with low-frequency phase "droop" minimized. The sharp reduction in low-frequency phase lag beyond that associated with the disappearance of phase droop is seen to accompany relatively low-gain feedback of vehicle output. The results of some recent motion cue research are discussed and interpreted in terms of the compensatory-pursuit display dichotomy. Tracking with input preview is discussed in a qualitively way. In terms of the model, preview is shown to demand no fundamental changes in structure or equalization, and to allow the pilot to eliminate the effective time delays that accrue in the inversion of the controlled-element dynamics. Precognitive behavior is discussed and a model that encompasses all the levels of skill development outlined in the successive organizations of perception (SOP) theory is finally proposed.

INTRODUCTION

Nearly all the manual control displays used in continuous tracking tasks can be classified as either "compensatory" or "pursuit" in nature, depending upon the amount of information presented to the operator. Consider the functional block diagrams of Fig. 1, which represent a pair of single-axis tracking tasks (scalar system input and output). In Fig. 1a , the operator is presented with a display of system error alone. This display, shown in Fig. 2a , is referred to as compensatory. The visually displayed effects of the operator's responses are not distinguishable from the system input. In Fig. 1b, the operator is presented with both system input and output. The corresponding display, shown in Fig. 2b, is referred to as pursuit. Here the operator's corrective responses can be distinguished from his input. Note that system error can be easily inferred from the spatial separation of the "target" and "follower" dymbols.

It is the purpose of the research described in Ref. 1 to provide a structural model for pursuit tracking that is similar to the compensatory model introduced in Ref. 2 and refined in Ref. 3. As in Ref. 3, it is hoped that such a model can provide 1) a theoretical framework within which a variety of empirical pilot-vehicle response phenomena can be interpreted, and 2) some insight into the mechanisms of skill developement.

THE COMPENSATORY AND PURSUIT MODELS

Fig. 3 is a block diagram of a structural model of the human pilot for compensatory behavior. The model was discussed in detail in Ref. 3 and shown capable of matching human pilot-describing functions and remnant for a wide variety of controlled-element dynamics. The central hypothesis in the development of a pursuit model of the human pilot is that the primary structural elements in the compensatory behavior model also serve as the primary structural elements of the pursuit model. Fig. 4 shows the proposed pilot model for pursuit behavior. The primary difference between Figs. 3 and 4 lies in the physical definition of the variable u_s. In the compensatory model, u_s is proportional to error (switch position 0) or to error-rate (position 1). In the pursuit model, u_s is postulated to be proportional to a weighted difference of error and output (position 0), to error-rate alone (position 1), or to input-rate alone (position 2). As was the case in the compensatory model, input-rate is assumed to be a derived quantity with a time delay τ_1 associated with the rate calculation. In the model of Fig. 4, the operation of the switch will be parameterized by P_1 and P_2, the respective probabilities of the switch being in position 1 or 2 at any instant. The probability of its being in position 0 is, of course, simply $1 - P_1 - P_2$. Note that by allowing $Y_{d_m} = Y_{d_c} = P_2 = 0$, the pursuit model is identical to the compensatory model.

It is shown in Ref. 1, that the feed-forward of input-rate through the dynamics $u_\delta(j\omega)/u_s(j\omega)$ can effectively invert the controlled-element dynamics at low frequencies.

Fig. 5 shows a comparison of the compensatory and pursuit display describing functions from Ref. 4 with the describing functions obtained from the compensatory and pursuit models of Figs. 3 and 4 using the parameter values shown in Table I. The model describing functions were obtained by using an approximation procedure discussed in some detail in Ref. 3. Note the model's ability to capture the large low-frequency phase differences.

SOME RESULTS FROM MOTION-CUE RESEARCH

Reference 5 summarizes some recent research involving a single-axis piloted tracking task that was performed on a motion simulator constrained to rotate about the longitudinal or roll axis. In an air-to-air tracking scenario, the task consisted of following the target's roll angle while suppressing gust disturbances. Figs. 6a and 6b show, respectivley, a block diagram of the tracking task and the pilot's compensatory visual display. The experiments were performed with (1) no motion, (2) with full motion and the roll axis horizontal (pilot nominally erect), (3) with full motion and the roll axis vertical (pilot nominally supine), (4) with washed-out motion, and (5) with attenuated motion. The latter two conditions were studied with the roll-axis horizontal. The first and third of the these experiments, and to some extent, the fourth, were designed to suppress the so-called "tilt cue" which the pilot receives when tracking with full motion and the roll-axis horizontal.

Figure 7 summarizes the describing functions for experiments (1-3) just described. Two distinct describing functions were measured for each of the experimental conditions, one corresponding to the Y_δ of Fig. 5 (ϕ_e/ϕ in Fig. 6), and a second corresponding to δ_1/δ in Fig. 6. Only the first of these will be discussed here since these tie in with the measurements of Ref. 4.

If we extend our concept of "display" to include vestibular cues, the experimental conditions of Ref. 5 are quite similar to the compensatory and pursuit tracking displays discussed previously. In the static case (ST), of course, the only display is visual and compensatory in nature: that is, ϕ_e alone is displayed. In the full-motion-erect case (FO), the vestibular "tilt cue" is availabe as an additional display element, effectively giving the pilot information about the controlled-element output ϕ in addition to the displayed error ϕ_e, thus yielding a pursuit display. In addition, the FO case may allow higher derivatives of ϕ to be sensed , but the effect of this feedback will be beyond the frequency range of interest here ($\omega < 4$ rad/sec)[5]. When the cab is rotated 90° (F90), the tilt cue is no longer available to the pilot, leading to a compensatory display.

Fig. 8 illustrates the model-generated describing functions corresponding to the controlled-element dynamics of Ref. 5 and the models of Figs. 3 and 4. The corresponding model parameters are listed in the last two rows of Table I. Model parameters were selected using the technique discussed in Ref. 3. Strictly speaking, only the static case (ST of Fig. 7) should be subject to comparison because the models of Figs. 3 and 4 are not specifically formulated for motion cues involving higher derivatives of the vehicle output. If we restrict out attention to the lower frequencies ($\omega < 4$ rad/sec), however, a qualitative, if not quantitative, comparison of modeling results with the experimental motion data is reasonable. As Fig. 8 indicates, the model can capture the salient differences in the experimental data in terms of the compensatory-pursuit dichotomy just suggested.

This limited discussion of motion-cue research has emphasized the concept that in tracking tasks the human pilot can be viewed as a data-organizing device. This organization tends to be independent of the physical nature of the display and proceeds along lines suggested by the model of Fig. 4. That is. sensory stimuli tend to be utilized in a manner that allows the pilot ot progress from compensatory to pursuit behavior.

TRACKING WITH PREVIEW AND PRECOGNITIVE BEHAVIOR

Reference 1 suggests that, in terms of the model that has been discussed here (Fig. 4), tracking with preview would result in improved performance. primarily by allowing reduction of the "open-loop" time delay $\tau_1 + \tau_e$, which occurs in feeding-forward input-rate. Theoretically, this delay can be reduced or completely eliminated through preview by allowing the subject to estimate $\dot{c}(t)$ at $t = t_o + \tau_1 + \tau_e$. If one generalizes the concept of a preview display to include an input wave form or stimulus internally generated by the pilot in the higher levels of the central nervous system, then the structure of Fig. 9 can serve as a paradigm for manual control behavior not considered as tracking activity per se; that is, the "precognitive" mode viewed by Krendel and McRuer[6] as the highest form of skill development. Fig. 9, a slight modification of Fig. 4, now includes the possibility of the pilot internally generating a $c(t_o + \tau_1 + \tau_e)$ signal. Note that Fig. 9 encompasses all the models that describe lower levels of skill development or display utilization.

CONCLUDING REMARKS

A model of the human pilot has been offered for pursuit tracking tasks; the model encompasses the model for compensatory tasks introduced in Ref. 2

and refined in Ref. 3. The central hypothesis in the development of this model is that the structural elements in the compensatory model that are responsible for the pilot's equalization capabilities remain intact in the pursuit model. The utility of the model propsed in Ref. 1 and described briefly here does not lie in its "predictive"capability in the sense of generating performance estimates, nor in its ability to offer a structure involving the minimum number of parameters necessary to simulate measured pilot frequency domain characteristics in a particular task. Rather, its value lies in its ability to serve as a tool for unifying the entire base of single-axis tracking data and to provide a structure for understanding aspects of motor skill development.

REFERENCES

[1] Hess, R. A., "Pursuit Tracking and Higher Levels of Skill Development in the Human Pilot," submitted to *IEEE Transactions on Systems, Man, and Cybernetics*.

[2] Hess, R. A., "A Dual-Loop Model of the Human Controller," *Journal of Guidance and Control*, Vol. 1, No. 4, pp. 254-260, July-Aug. 1978.

[3] Hess, R. A., "A Structural Model of the Adaptive Human Pilot," to appear in *Journal of Guidance and Control*, Sept.-Oct. 1980.

[4] Wasicko, R. J., McRuer, D. T., and Magdaleno, R. E., "Human Pilot Dynamic Response in Single-Loop Systems With Compensatory and Pursuit Displays," Air Force Flight Dynamics Laboratory, AFFDL-TR-66-137, 1966.

[5] Jex, H. R., Magdaleno, R. E., and Junker, A. M., "Roll Tracking Effects of G-Vector Tile and Various Types of Motion Washout," *Proceedings of the 14th Annual Conference on Manual Control*, April, 1978, pp. 463-502.

[6] Krendel, E. S., and McRuer, D. T., "A Servomechanisms Approach to Skill Development," *Journal of the Franklin Institute*, Vol. 269, No. 1, pp. 24-42, Jan. 1960.

TABLE I

PILOT MODEL PARAMETER VALUES USED TO GENERATE DESCRIBING FUNCTIONS

Controlled-element dynamics	Display	k	K_e	$K_{\dot{e}}$	K_m	$K_{\dot{c}}$	K_2	P_1	P_2	T_1	T_2	K_1	τ_0	τ_1	ζ_n	ω_n
K/s^2	Comp.	2	65.0	10.5	—	—	10	0.2	—	2.5	2.5	1.0	0.14	0.20	0.707	10
K/s^2	Pursuit	2	65.0	—	2.5	16.2	10	0.0	0.1	100	100	1.0	0.14	0.20	0.707	10
$Y_c(s)$*	Comp.	2	1.5	0.7	—	—	20	0.2	—	0.5	25	1.0	0.14	0.20	0.707	10
$Y_c(s)$*	Pursuit	2	1.5	—	0.25	1.1	20	0.0	0.1	0.5	25	1.0	0.14	0.20	0.707	10

$$^*Y_c(s) = 17 \frac{(-s/25 + 1)}{s(s/1.6 + 1)(s/5 + 1)(s^2/121 + 6.6s + 1)} .$$

ORIGINAL PAGE IS
OF POOR QUALITY

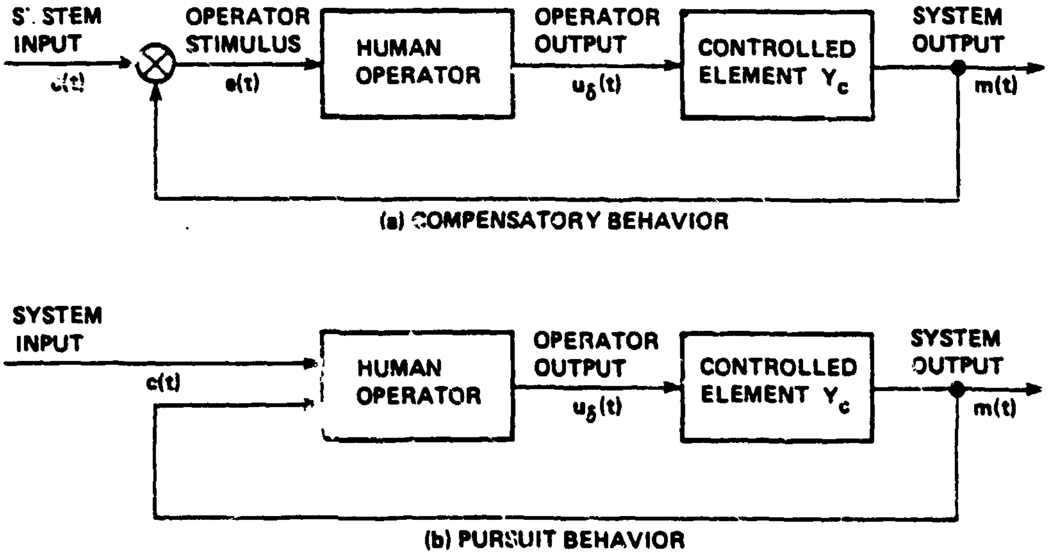
SYSTEM INPUT
c(t)
OPERATOR STIMULUS
e(t)
HUMAN OPERATOR
OPERATOR OUTPUT
$u_\delta(t)$
CONTROLLED ELEMENT Y_c
SYSTEM OUTPUT
m(t)
(a) COMPENSATORY BEHAVIOR
SYSTEM INPUT
c(t)
HUMAN OPERATOR
OPERATOR OUTPUT
$u_\delta(t)$
CONTROLLED ELEMENT Y_c
SYSTEM OUTPUT
m(t)
(b) PURSUIT BEHAVIOR

Figure 1. Compensatory and Pursuit Manual Control Systems.

(a) COMPENSATORY DISPLAY

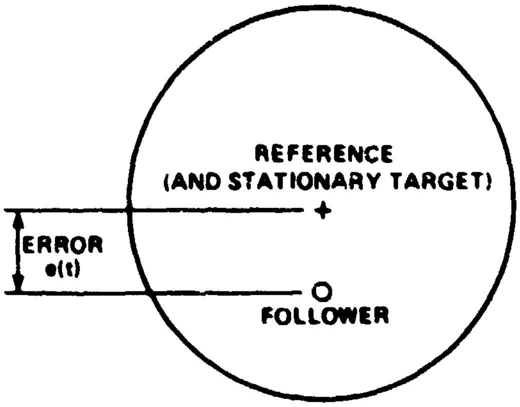
REFERENCE
(AND STATIONARY TARGET)
ERROR
e(t)
FOLLOWER

(b) PURSUIT DISPLAY

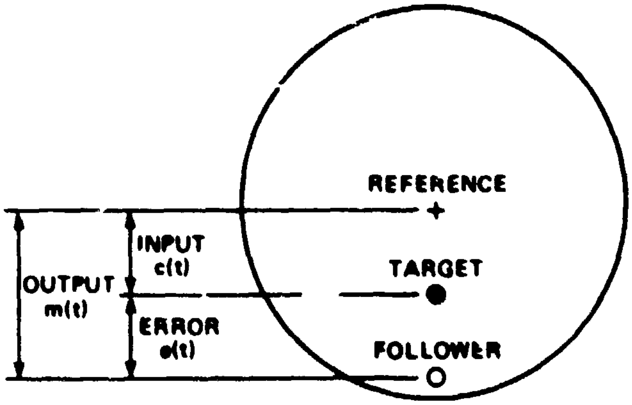
REFERENCE
INPUT
c(t)
TARGET
OUTPUT
m(t)
ERROR
e(t)
FOLLOWER

Figure 2. Compensatory and Pursuit Displays.

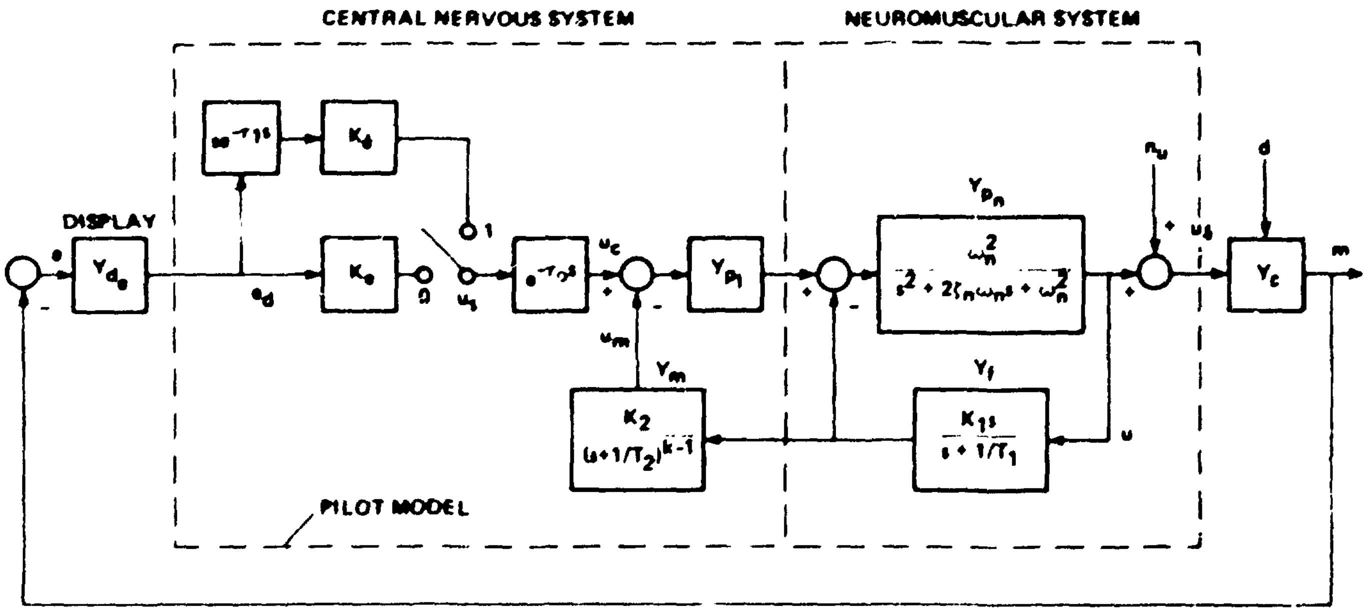
CENTRAL NERVOUS SYSTEM
NEUROMUSCULAR SYSTEM
DISPLAY
e
-
Y_{d_e}
e_d
$e^{-\tau_1 s}$
$K_{\dot{e}}$
K_e
1
0
u_s
$e^{-\tau_0 s}$
u_c
+
-
u_m
Y_m
$\frac{K_2}{(s+1/T_2)^{k-1}}$
Y_{p_1}
+
-
Y_{p_n}
$\frac{\omega_n^2}{s^2+2\zeta_n\omega_n s+\omega_n^2}$
Y_f
$\frac{K_1 s}{s+1/T_1}$
u
n_u
+
+
u_δ
d
Y_c
m
PILOT MODEL

Figure 3. Structural Model of the Adaptive Human Pilot for Compensatory Behavior.

OR[illegible]
OF POOR QUALITY

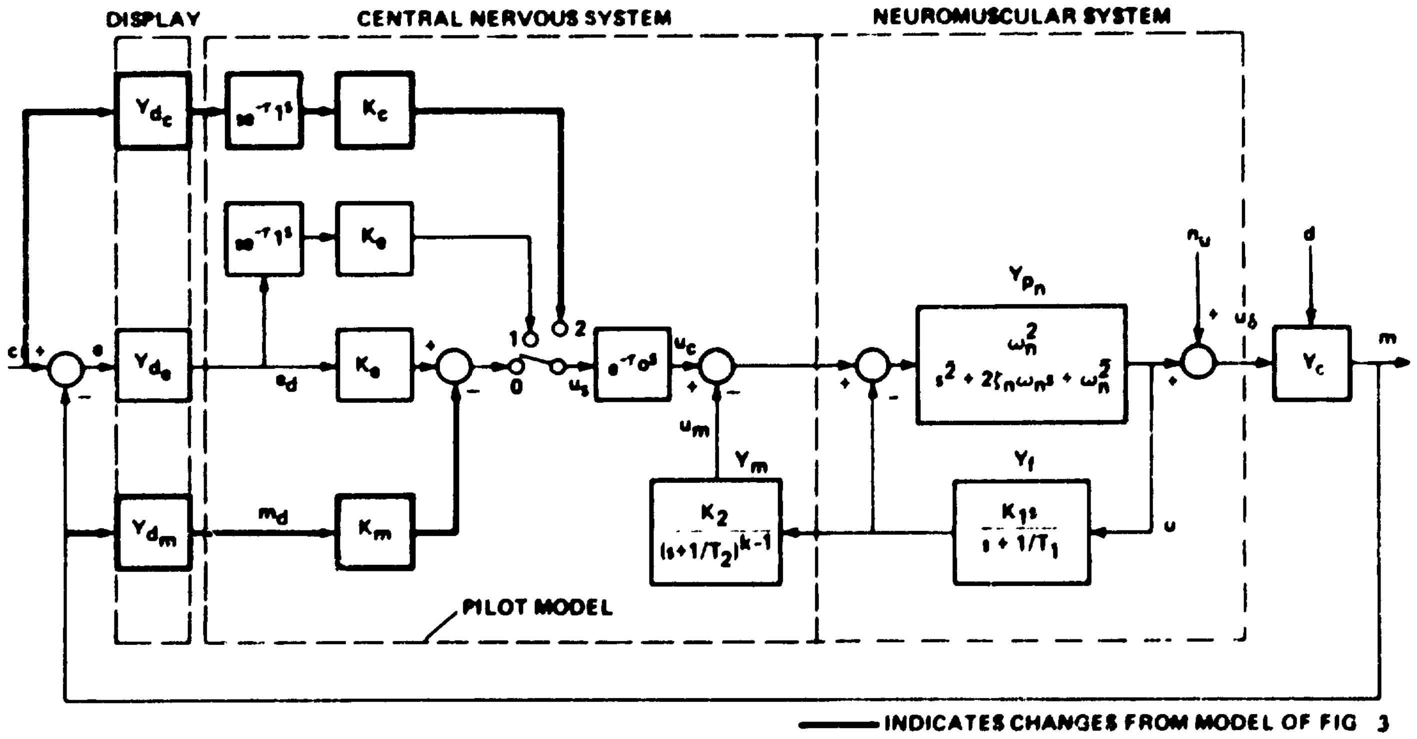
DISPLAY
CENTRAL NERVOUS SYSTEM
NEUROMUSCULAR SYSTEM
c
+
-
e
Y_{d_c}
Y_{d_e}
Y_{d_m}
$se^{-\tau_1 s}$
$se^{-\tau_1 s}$
K_c
K_e
K_e
K_m
e_d
m_d
+
-
0
1
2
u_s
$e^{-\tau_0 s}$
u_c
+
-
u_m
Y_m
$\frac{K_2}{(s+1/T_2)^{k-1}}$
+
-
Y_{p_n}
$\frac{\omega_n^2}{s^2 + 2\zeta_n\omega_n s + \omega_n^2}$
Y_f
$\frac{K_1 s}{s + 1/T_1}$
u
n_u
+
+
u_δ
d
Y_c
m
PILOT MODEL
INDICATES CHANGES FROM MODEL OF FIG 3

Figure 4. Structural Model of the Adaptive Human Pilot for Compensatory-Pursuit Behavior.

ORIGINAL PAGE IS
OF POOR QUALITY

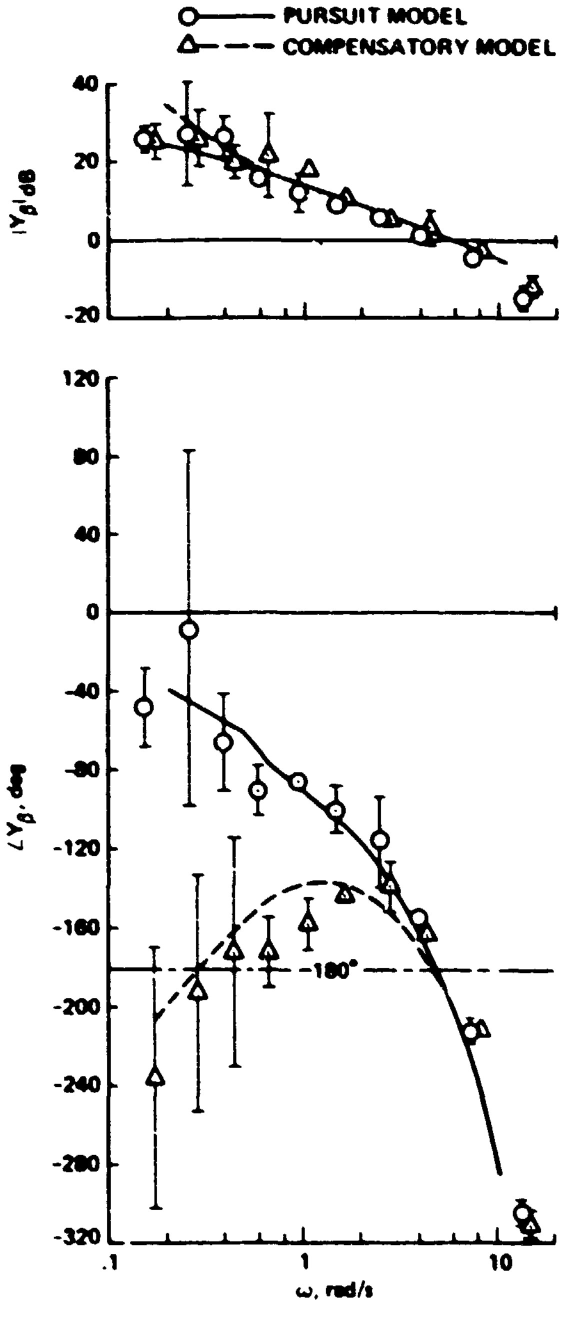

Figure 5. Comparison of Pursuit and Compensatory Display Describing Functions from Ref. 4 with Model Describing Functions.

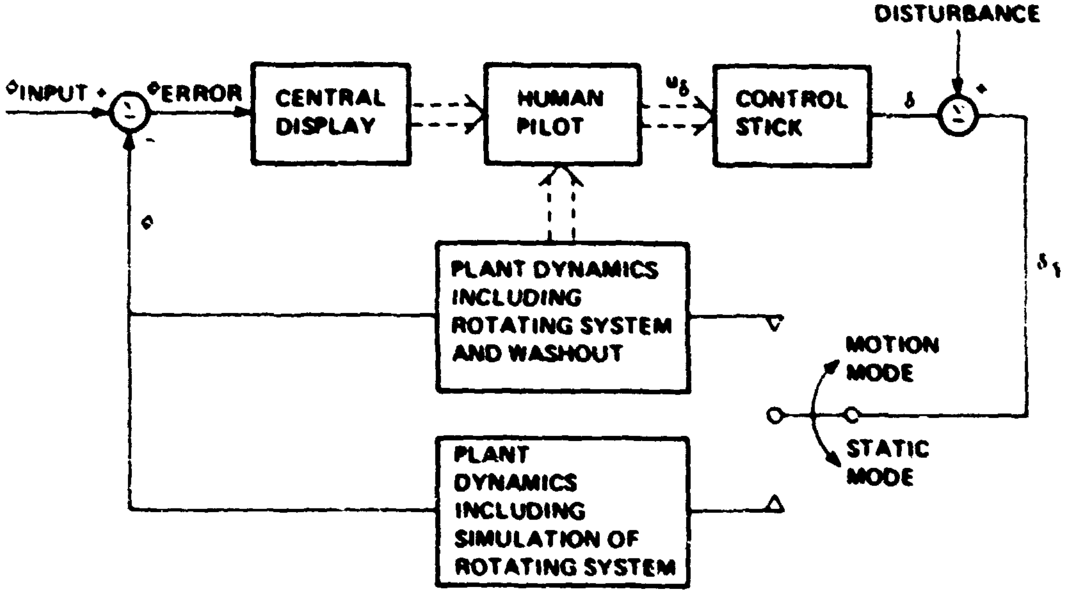
ϕINPUT
+
Σ
ϕERROR
-
ϕ
CENTRAL DISPLAY
HUMAN PILOT
u_δ
CONTROL STICK
δ
DISTURBANCE
+
Σ
δ_t
PLANT DYNAMICS INCLUDING ROTATING SYSTEM AND WASHOUT
MOTION MODE
STATIC MODE
PLANT DYNAMICS INCLUDING SIMULATION OF ROTATING SYSTEM

(a) BLOCK DIAGRAM

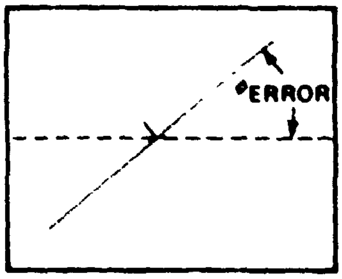

(b) DISPLAY

Figure 6. Experimental Tracking Task of Ref. 5.

ORIGINAL PAGE IS
OF POOR QUALITY

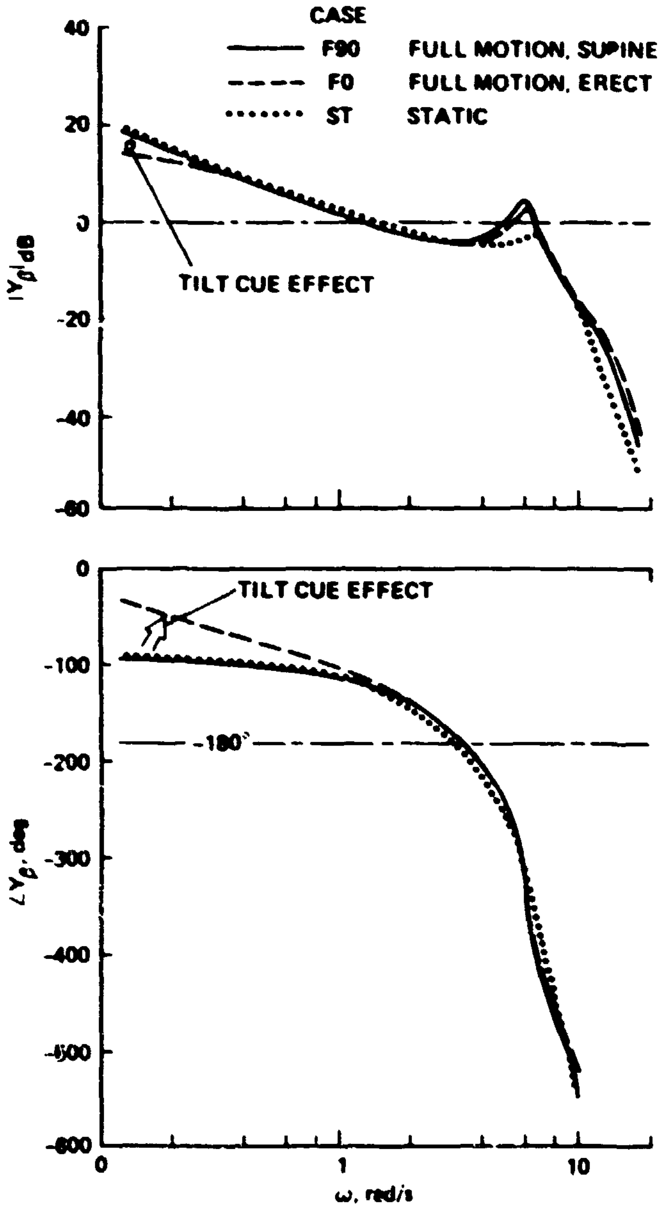

Figure 7. Comparison of Experimental Describing Functions from Ref. 5.

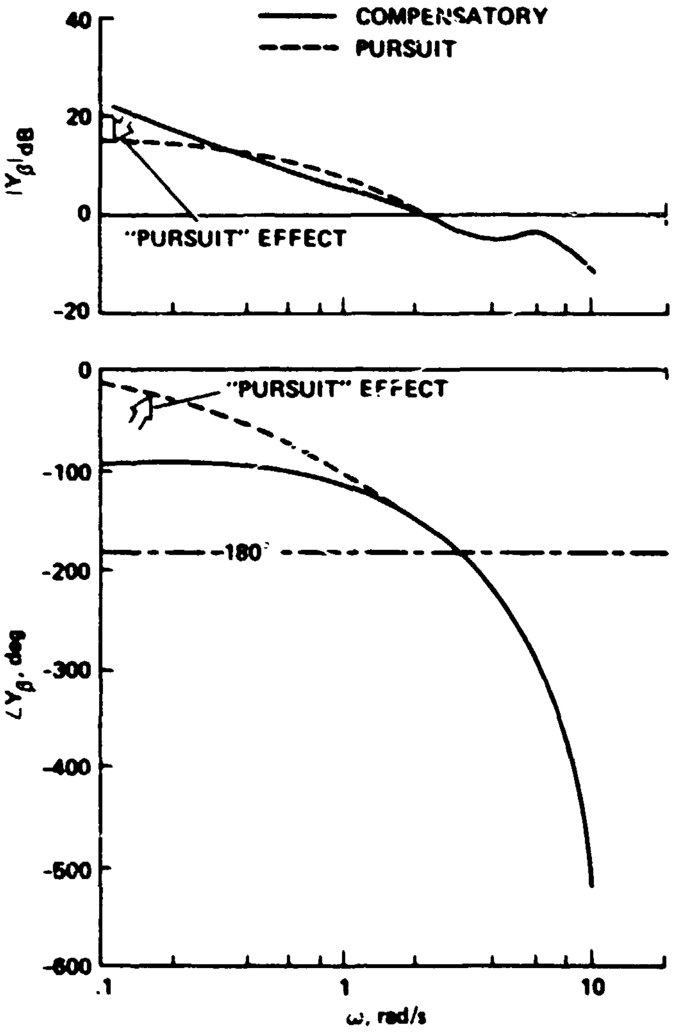

Figure 8. Comparison of Pursuit and Compensatory Model Describing Functions.

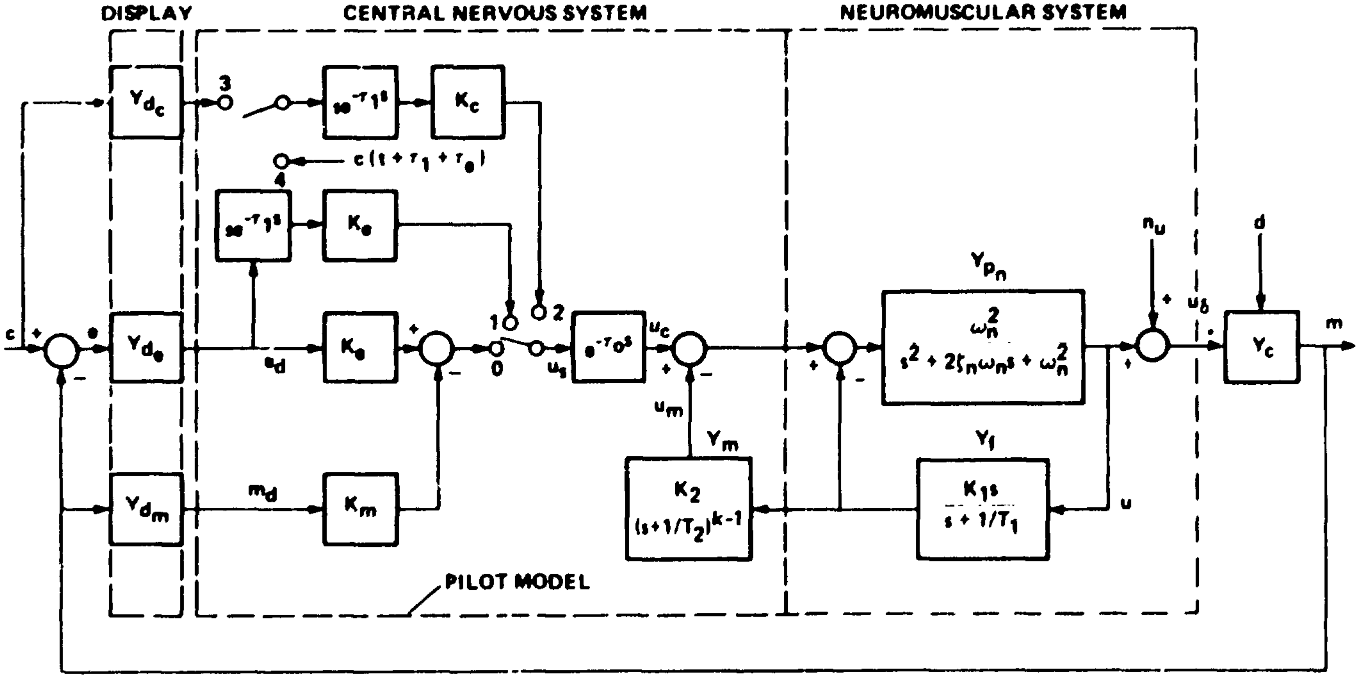
DISPLAY
CENTRAL NERVOUS SYSTEM
NEUROMUSCULAR SYSTEM
PILOT MODEL
c
e
Y_{d_c}
Y_{d_e}
Y_{d_m}
3
4
$se^{-\tau_1 s}$
K_c
$c(t+\tau_1+\tau_e)$
K_e
e_d
m_d
K_m
0
1
2
u_s
$e^{-\tau_0 s}$
u_c
u_m
Y_m
$\frac{K_2}{(s+1/T_2)^{k-1}}$
Y_{p_n}
$\frac{\omega_n^2}{s^2+2\zeta_n\omega_n s+\omega_n^2}$
Y_f
$\frac{K_1 s}{s+1/T_1}$
u
n_u
u_δ
d
Y_c
m

Figure 9. Structural Model of the Adaptive Human Pilot for Compensatory-Pursuit-Precognitive Behavior.

N82 34042

MULTI-AXIS TRACKING VIA AN OPTIMAL-CONTROL PILOT MODEL

by

S.N. Prasad and David K. Schmidt

School of Aeronautics and Astronautics
Purdue University
West Lafayette, IN 47907

The well known optimal control model (OCM) of the human operator has been applied numerous times to the piloting task, with air-to-air tracking or landing approach tasks comprising typical operational situations. However, almost all investigations consider essentially single-axis tasks, the longitudinal and lateral-directional axes evaluated independently. This approach is preferred to limit the order of the dynamic model, and in wings-level flight, the equations of motion yield uncoupled vehicle dynamics.

In contrast to this situation, the problem addressed here is the application of an optimal control model (OCM) to investigate tracking in a highly banked turning flight condition. The analytical (model) results are compared to experimental data obtained in the large amplitude motion simulator (LAMARS) at the Air Force Flight Dynamics Laboratory, Wright-Patterson AFB.

It will be shown that significantly increased observation noise resulting from reduced available attention and possibly threshold effects, as well as high motor noise are required to match the experimental results.

THE EFFECTS OF MULTIPLICATIVE MOTOR NOISE ON THE OPTIMAL HUMAN OPERATOR MODEL

by

Alper K. Caglayan and William H. Levison
Bolt Beranek and Newman Inc.
50 Moulton Street
Cambridge, MA

ABSTRACT

The effects of a multiplicative motor noise model on the optimal-control human operator model have been analyzed. A study of the interaction between multiplicative motor noise variance, plant dynamics, and predicted operator response behavior shows that, in general, an increase in motor noise variance produces a decrease in operator gain and a decrease in high-frequency remnant. An increase in multiplicative motor noise variance is also reflected by an increase in the effective motor time constant; in the absence of a cost penalty on commanded control, the motor time constant equals the motor noise variance.

INTRODUCTION

A substantial body of manual control data, obtained in a variety of laboratory tracking tasks, has been analyzed with the "optimal-control" pilot/vehicle model. For many of these studies, pilot response behavior has been reflected in terms of a relatively invariant set of values for pilot-related parameters; specifically, a "motor time constant" of between 0.08 and 0.1 seconds, a "time delay" of between 0.15 and 0.2 seconds, and an "observation noise/signal ratio" of about -20 dB [1-3]. These tasks have largely involved wide-band dynamics with minimal delays.

Consistent deviations from these "nominal" values have been noted for certain kinds of tasks. Of particular interest here are the larger values for motor time constant (implying reduced operator bandwidth) that have been found for tasks involving control of slowly-responding systems [4-6].

The predictive capability of the optimal-control model will be enhanced if we can find either an alternate set of pilot-related parameters that are more nearly invariant, or a consistent rule for adjusting the current parameter set according to the characteristics of the task. The apparently consistent trend of the motor time constant with respect to the response characteristics of the controlled element suggests that this goal is achievable.

In this paper we explore the possibility that changes in motor time constant reflect, in part, a multiplicative motor noise process underlying human controller response behavior. The notion of a multiplicative noise process is consistent with the empirical finding that, in idealized control situations, both motor noise and observation noise appear to scale with the variances of corresponding control and display variables. In previous studies, these processes have been considered to affect only the estimator (Kalman filter) portion of the pilot model; in this paper, however, we consider the multiplicative motor noise process to influence the control gains.

OPTIMAL HUMAN OPERATOR MODEL WITH MULTIPLICATIVE MOTOR NOISE

The following linearized description of the vehicle dynamics will be assumed:

$$\dot{x}(t) = Ax(t) + Bu_p(t) + Ew_g(t) \tag{2.1}$$

where x is the n-dimensional state vector including the variables corresponding to the gust states, u_p is the r-dimensional operator input, and w_g is the white Gaussian process noise with covariance $W_g\delta(t-s)$. We will assume the following multiplicative motor noise model for the human operator's input dynamics:

$$\dot{u}_{p_i}(t) = u_{c_i}(t) + u_{c_i}(t)w_{m_i}(t) \tag{2.2}$$

where u_{c_i} is the i'th component of the commanded control rate in the absence of motor noise and w_{m_i} is the i'th component of the r-dimensional motor noise which is a white Gaussian process with covariance $W_m\,\delta(t-s)$. The effective additive noise, $u_{c_i}w_{m_i}$, in equation 2.2 will have the following properties for the stationary case:

$$Eu_{c_i}w_{m_i} = 0 \tag{2.3}$$

$$E[u_{c_i}(t)w_{m_i}(t)][u_{c_i}(s)w_{m_i}(s)] = (Eu^2_{c_i})W_{m_{ii}}\delta(t-s) \tag{2.4}$$

Comparison of the covariance of the effective additive noise with that of the empirical relationship in 1 reveals that the variance of the multiplicative motor noise in the model above corresponds to the motor noise ratio in 1 with a scale factor of π . The multiplicative motor noise model specified by equation 2.2 would also allow correlation between the noise components w_{m_i} for the multi-input case through the off-diagonal elements in the motor noise covariance W_m. The task requirements for the human operator will be expressed by the standard quadratic cost functional:

$$J = \frac{1}{2} E \int_0^{\infty} (x_o(t) Q x_o(t) + u_c(t) G u_c(t) dt \qquad (2.5)$$

where x_o is the state vector augmented with the operator input u_p.

It can be shown [8-10] that under suitable regularity conditions the optimal human operator control in the space of linear controls with full state feedback will be given by:

$$u_c{}^*(t) = -F x_o(t) \qquad 6)$$

where the feedback gain F is defined by

$$F = (G+P(K))^{-1} B_o' K \qquad (2.7)$$

with the positive-semidefinite matrix P(K) defined by

$$P(K)_{ij} = K_{n+i,n+j} W_{m_{ji}} \quad i,j=1,2,\ldots,r \qquad (2.8)$$

where K is the positive definite solution of the algebraic Riccati equation

$$K A_o + A_o' K + Q - K B_o (G+P(K))^{-1} B_o' K = 0 \qquad (2.9)$$

with the augmented system matrices A_o and B_o (of dimension n+rxn+r and n+rxr, respectively) given by

$$A_o = \begin{bmatrix} A & B \\ 0 & 0 \end{bmatrix} \qquad B_o = \begin{bmatrix} 0 \\ I \end{bmatrix} \qquad (2.10)$$

The comparison of the Riccati equation above with that given in reference 1 shows that the control dependent noise effectively increases the control weighting G further by the term P(K) relative to the case with additive motor noise. For a fixed set of control weightings Q and G, the effect of the multiplicative motor noise is to reduce the control gains of the human operator from their values corresponding to the additive motor noise case. This effect of the multiplicative motor noise model is expected since the control effort has some destabilizing effect on the system through the control dependent noise. This relationship between the motor noise and the control gains should be useful in modelling the learning behavior of inexperienced human operators [11].

The term G+P(K) in the Riccati equation 2.9 can be considered as an effective control weighting matrix. If the multiplicative motor noise covariance W_m is chosen to be positive definite, then P(K) will be positive definite even when the commanded control is not penalized in the human operator's cost function (i.e. G=0). This result is intuitively pleasing in that the multiplicative motor noise models the human operator's inherent constrained control capability. That is, even if no explicit or subjective penalty is associated with control activity, the predicted control gains will remain finite.

While it is possible to find an equivalent commanded control rate weighting, G_e, for any solution of the Riccati equation (2.9) corresponding to a certain Q,G combination ($G_e = G + P(K)$), the multiplicative motor noise model brings new interpretations to the motor time constant and control gains and provides a link between the human operator's control gains and the motor noise ratio. These issues will be discussed in the later sections. In the multi-input case, the equivalent control rate weighting G_e would have off-diagonal terms when the control dependent noise components are correlated. Therefore, trial and error search for an equivalent control rate weighting G_e would be more complicated for the multi-input case.

The effect of the multiplicative motor noise on the human operator model characteristics has been studied using several plant dynamics. A lower order Riccati equation (2.9) excluding the gust state variables is first solved using an algorithm similar to that in [10] and then the the gains on gust variables are obtained by solving a linear algebraic equation similar to the deterministic case. For these studies, the filtering part of the human operator model has been taken from the pseudo motor noise model in [4]. In order to differentiate between the different motor noise ratios, we will call the one used for the control computations as the control motor noise ratio, the one used for the estimator computations as the filter motor noise ratio (called pseudo motor noise ratio in [4]), and the real driving motor noise as the actual motor noise ratio. In the sequel, "motor noise ratio" without an explicit reference will imply control motor noise ratio.

EFFECTS ON THE MOTOR TIME CONSTANT

In the single input case, with G and W_m scalars in (2.8) and (2.9), ($G = g$, $W_m = v$), the motor time constant, T_N, defined as the inverse of the gain on pilot input u_p, will be given by

$$T_N = \frac{g}{p} + v \qquad (3.1)$$

where p is the lower right element $K_{n+1,n+1}$ of the solution of the Riccati equation (2.9). As can be seen from equation (3.1), the motor time consant is composed of two terms: The first one, g/p, is directly proportional to the control rate weighting in the human operator's objective function. The second term, v, is equal the variance of the multiplicative motor noise and corresponds to the motor noise ratio defined in [4], scaled by a factor of π.

The effects of multiplicative motor noise on the optimal human operator model has been studied using the following set of vehicle dynamics:

Rate Dynamics:

$$\dot{x} = \begin{bmatrix} -2. & 0 \\ 1. & 0. \end{bmatrix} x + \begin{bmatrix} 0. \\ 1. \end{bmatrix} u + \begin{bmatrix} 1. \\ 0 \end{bmatrix} w \qquad 3.2$$

$$y = \begin{bmatrix} 0. & 1. \\ 1. & 0. \end{bmatrix} x + \begin{bmatrix} 0. \\ 1. \end{bmatrix} u \qquad 3.3$$

Yaw Dynamics:

$$\dot{x} = \begin{bmatrix} -1. & 0. & 0. & 0. & 0. \\ 533. & 0. & 0. & 0. & 0. \\ -16. & 1. & -33.3 & 0. & 0. \\ 0. & 0. & 19. & -19. & 0. \\ 0. & 0. & 0. & 1. & 0. \end{bmatrix} x + \begin{bmatrix} 0. \\ 533. \\ -16. \\ 0. \\ 0. \end{bmatrix} u + \begin{bmatrix} 1.41 \\ 0. \\ 0. \\ 0. \\ 0. \end{bmatrix} w \qquad 3.4$$

$$y = \begin{bmatrix} 0. & 0. & 0. & 0. & 1. \\ 0. & 0. & 0. & 1. & 0. \\ 0. & 0. & 0. & 1. & 0. \\ 0. & 0. & 19. & -19. & 0. \end{bmatrix} x \qquad 3.5$$

Filtered Rate Dynamics:

$$\dot{x} = \begin{bmatrix} -2. & 0. & 0. & 0. \\ 0. & 0. & 1. & 0. \\ 0. & -1. & -1.414 & 1. \\ 1. & 0. & 0. & 0. \end{bmatrix} x + \begin{bmatrix} 0. \\ 0. \\ 0. \\ 1. \end{bmatrix} u + \begin{bmatrix} 1. \\ 0. \\ 0. \\ 0. \end{bmatrix} w \qquad 3.6$$

$$y = \begin{bmatrix} 0. & 1. & 0. & 0. \\ 0. & 0. & 1. & 0. \end{bmatrix} x \qquad 3.7$$

In each case, $\tau = .2$ sec. for the human operator time delay, -90 dB for the actual motor noise ratio, -40 dB for the filter motor noise ratio, -20 dB for the observation noise ratio were used for the model parameter values. The plant with the rate dynamics represent a velocity control task under a velocity disturbance created by a first order noise spectrum with a break frequency 2 rad/sec. The filtered rate dynamics is the same plant as the rate dynamics with a two-pole Butterworth filter of cutoff frequency 1 rad/sec. Yaw dynamics represent k/s^2 dynamics with approximately 60 msec. time delay.

The effects of different multiplicative motor noise levels on the motor time constant have been analyzed using the dynamics above. The control rate weighting, g, was chosen to obtain a nominal value of .1 sec. for T_N at the -40 dB motor noise level. In general, an increase in the motor noise level produced a higher motor time constant T_N. The results are tabulated in Table I. Bringing up the motor noise ratio to the -20 dB level resulted in a 10% increase in the motor time constant T_N compared to the negligible motor noise case (-40 dB) in all of the three dynamics tested.

As predicted by equation (3.1), the motor noise ratio starts effecting the motor time constant T_N when its value is around -20 dB. This level corresponds to a motor noise ratio of $v=.0314$.

ORIG
OF POO

Since the term p in (3.1) is a function of both g and v and since increasing v results in a higher p, the term g/p decreases as the motor noise ratio is increased to -20 dB level. However, in all of the three cases tested, the decrease due to the g/p term was more than compensated by the increase in the motor noise ratio v.

When the commanded control is not weighted (i.e. g=0), a motor noise ratio of -15 dB, as predicted by equation 3.1, resulted in a motor time constant T_N=.1 sec for all the dynamics tested. In this case with no penalty on commanded control rate, the motor time constant T_N is equal to the variance of the multiplicative motor noise (0.1). That is, the motor noise ratio value completely specifies T_N independent of the plant dynamics. In this case, the human operator's cost function (2.5) would only consist of mean-squared error which is the real objective in a compensatory tracking task.

EFFECTS ON THE HUMAN OPERATOR TRANSFER FUNCTION

The effects of varying the multiplicative motor noise variance on the human operator's equivalent describing function have been analyzed by using the plant dynamics in the previous section. Figure 1 shows the results for the filtered rate dynamics.

In general, for increasing motor noise ratio, the human operator's equivalent describing function gain decreases as expected with greatest variation occurring for frequencies $\omega<1$ rad/sec and $\omega>8$ rad/sec. Motor noise ratio variation has a small effect on the phase of human operator's transfer function. The greatest change is around the 8-10 rad/sec range since increasing the motor noise ratio to -17 dB from the -40 dB level results in the shift of pole due to the motor time constant from 10 rad/sec to 8.5 rad/sec. "Remnant" (control activity not correlated with the tracking input [7]) decreases at high frequencies ($\omega\geq8$ rad/sec) as the motor noise ratio is increased to -17 dB level. This result is to be expected since the bandwidth of the controller is decreased due to the increase in the control dependent noise. These results indicate the conservative nature of the feedback controller based on a multiplicative motor noise model. In summary, an increase in the multiplicative motor noise variance causes a decrease in the gain and, at high frequencies, a decrease in the remnant for the human operator's equivalent describing function.

VARIATION IN T_N WITH BANDWIDTH

In this section, we will discuss how the multiplicative motor noise model can be used in explaining the inverse variation of the motor time constant T_N with plant bandwidth. For this analysis, the following set of dynamics are used:

KSG Dynamics

$$\dot{x} = \begin{bmatrix} -2. & 0. \\ 15. & 0. \end{bmatrix} x + \begin{bmatrix} 0 \\ 20. \end{bmatrix} u_p + \begin{bmatrix} 2. \\ 0 \end{bmatrix} w \tag{4.1}$$

$$y = \begin{bmatrix} 0. & .1 \\ 1.5 & 0. \end{bmatrix} x + \begin{bmatrix} 0. \\ 2 \end{bmatrix} u_p \tag{4.2}$$

BW1 Dynamics

$$\dot{x} = \begin{bmatrix} -2. & 0. & 0. & 0. \\ 10. & 0. & 0. & 0. \\ 0. & 1. & -1.414 & -1. \\ 0. & 0. & 1. & 0. \end{bmatrix} x + \begin{bmatrix} 0. \\ 20. \\ 0. \\ 0. \end{bmatrix} u_p + \begin{bmatrix} 2. \\ 0. \\ 0. \\ 0. \end{bmatrix} w \tag{4.3}$$

$$y = \begin{bmatrix} 0. & 0. & 0. & .02 \\ 0. & 0. & .02 & 0. \\ 0. & .02 & -.028 & -.02 \end{bmatrix} x \tag{4.4}$$

BW2 Dynamics

$$\dot{x} = \begin{bmatrix} -2. & 0. & 0. & 0. \\ 10. & 0. & 0. & 0. \\ 0. & 4. & -2.82 & -4. \\ 0. & 0. & 1. & 0 \end{bmatrix} x + \begin{bmatrix} 0. \\ 20. \\ 0. \\ 0. \end{bmatrix} u_p + \begin{bmatrix} 2. \\ 0. \\ 0. \\ 0. \end{bmatrix} w \tag{4.5}$$

$$y = \begin{bmatrix} 0. & 0. & 0. & .02 \\ 0. & 0. & 0.02 & 0. \\ 0. & .08 & -0.056 & -.08 \end{bmatrix} x \tag{4.6}$$

These dynamics correspond to three laboratory tracking experiments. The plant with the KSG dynamics represents velocity control task under disturbance. BW1 and BW2 dynamics represent the same plant with a two-pole Butterworth filter of cutoff frequency 1 and 2 rad/sec, respectively. Model matching analysis of the actual data has shown that an increase in the value of T_N from .06 sec to .15 sec is needed as the bandwidth is decreased (change from KSG to BW1 dynamics). With the standard human operator model, these different values of T_N are obtained by selecting a different control rate weighting, g, value for each case. As Table II shows, with the multiplicative motor noise based model, it is possible to match the variation in T_N with only one value for the control rate weighting g and the motor noise ratio v.

CONCLUSIONS

The effects of a multiplicative motor noise model on the optimal-control human operator model have been analyzed. A study of the interaction between multiplicative motor noise variance, plant dynamics, and predicted operator response behavior shows that, in general, an increase in motor noise variance produces a decrease in operator gain and a decrease in high-frequency remnant. An increase in multiplicative motor noise variance is also reflected by an increase in the effective motor time constant; in the absence of a cost penalty on commanded control, the motor time constant equals the motor noise variance.

For the cases explored in this analysis, variations in the motor time constant were accounted for by fixed values assigned to motor noise ratio and cost of control. Thus, even though a new parameter was added to the optimal control model, the number of degrees of freedom required to account for variations in controlled-element dynamics was actually reduced! Further work is required to determine the extent to which a fixed set of cost and noise parameters can explain human operator behavior across a variety of task conditions, including the differences observed between inexperienced and trained human operators [11].

REFERENCES

1. Kleinman, D. L., S. Baron and W. H. Levison, "An Optimal Control Model of Human Response, Part I: Theory and Validation", Automatica, Vol. 6, pp. 357-369, 1970.

2. Kleinman, D. L., S. Baron and W. H. Levison, "A Control Theoretic Approach to Manned-Vehicle systems Analysis", IEEE Trans. on Auto. Control, Vol. AC-16, No. 6, December 1971.

3. Levison, W. H., J. I. Elkind and J. L. Ward, "Studies of Multivariable Manual Control Systems: A Model for Task Interference", NASA CR-1746, May 1971.

4. Levison, W. H., S. Baron and A. M. Junker, "Modeling the Effects of Environmental FActors on Human Control and Information Processing", Wright-Patterson Air Force Base, Ohio, AMRL-TR-76-74, August 1976.

5. Levison, W. H., "A Model for the Pilot's Use of Roll-Axis Motion Cues in Steady-State Tracking Tasks", Report No. 3808, Bolt Beranek and Newman Inc., Cambridge, MA, May 1978.

6. Levison, W. H., "The EFfects of Display Gain and Signal Bandwidth on Human Controller Remnant", AMRL-TR-70-93, Wright-Patterson Air Force Base, Ohio, March 1971.

7. Levison, W. H., S. Baron and D. L. Kleinman, "A Model for Human Controller Remnant", IEEE Trans. on Man-Machine Syst., Vol. MMS-10, No. 4, Dec. 1969.

8. McLane, P. J., "Optimal Stochastic Control of Linear Systems with State and Control Dependent Disturbances", IEEE Trans. on Auto. Contr., Vol. AC-16, No. 6, pp. 793-798, Dec. 1971.

9. Wonham, W. M., "Random Differential Equations in Control Theory", Probabilistic Methods in App. Math., A. T. Bharucha-Reid, Ed., New York, Academic Press, 1970.

10. Kleinman, D. L., "Optimal Stationary Control of Linear Systems with Control Dependent Noise", IEEE Trans. on Auto. Contr., Vol. AC-14, pp. 673-677, Dec. 1969.

11. Levison, W. H., R. E. Lancraft and A. M. Junker, "Effects of Simulator Delays on Performance and Learning in a Roll-Axis Tracking Task", Proc. of the Fifteenth Annual Conf. on Manual Control, Dayton, Ohio, March 1979.

Dynamics	Motor Noise Ratio dB	g	T_N
rate	-40	4×10^{-4}	0.100
rate	-30	4×10^{-4}	0.101
rate	-20	4×10^{-4}	0.110
yaw	-40	1.58×10^{-2}	0.100
yaw	-20	1.58×10^{-2}	0.106
filtered rate	-40	8×10^{-6}	0.100
filtered rate	-20	8×10^{-6}	0.107
filtered rate	-17	8×10^{-6}	0.113

TABLE I. Variation of T_N with Respect to Motor Noise Ratio

Dynamics	Motor Noise Ratio, dB	g	T_N
KSG	-17	8×10^{-6}	.0645
BW2	-17	8×10^{-6}	.114
BW1	-17	8×10^{-6}	.143

TABLE II. Variation of T_N with Bandwidth Using Multiplicative Motor Noise Model

ORIGINAL PAGE IS OF POOR QUALITY

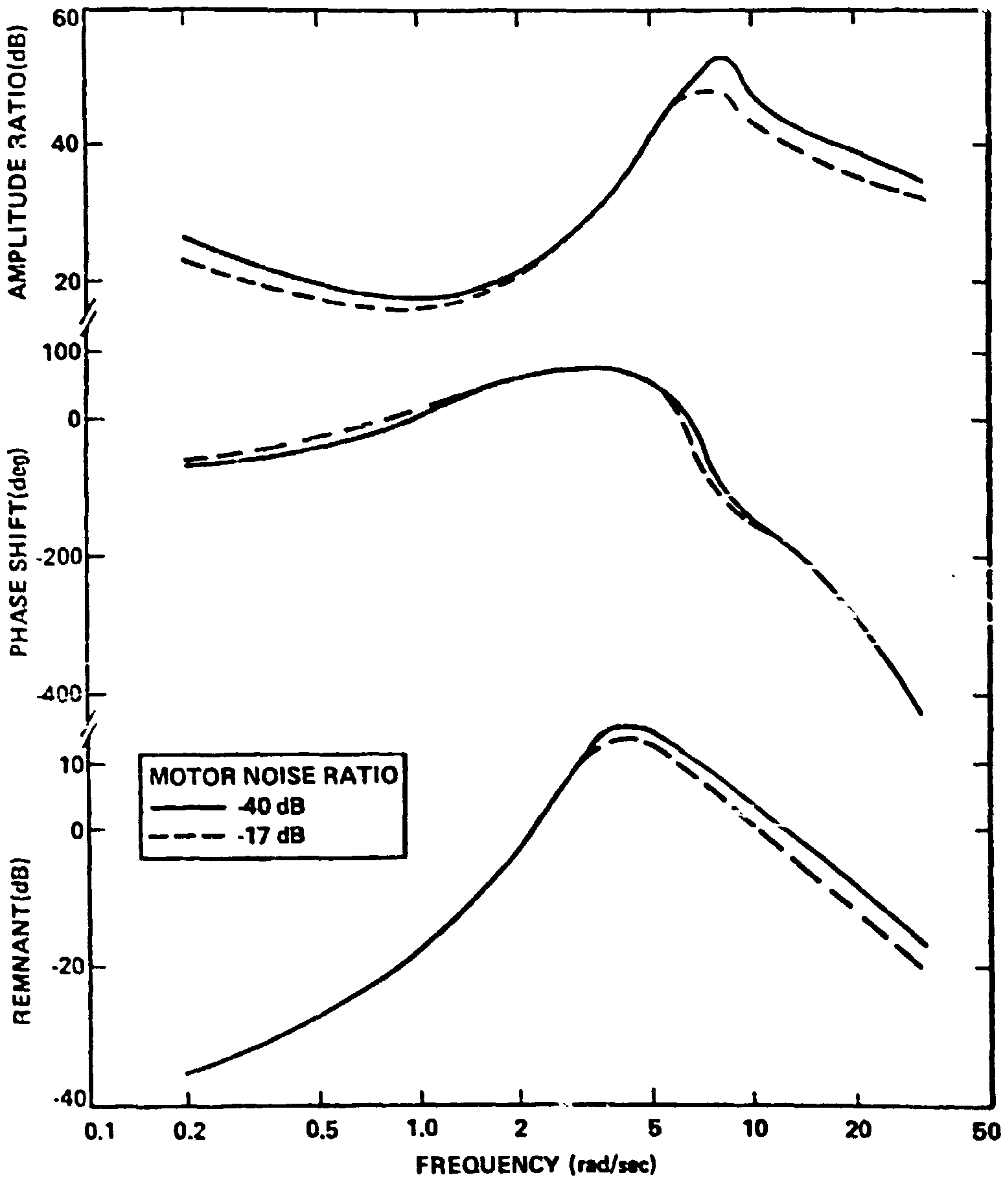

Figure 1. Human Operator Transfer Functions Variations Due to Motor Noise Ratio (filtered rate dynamics)

MODELLING OF AIRCRAFT IN-TRAIL FOLLOWING

Ahmet Buharali, Man-Machine Systems Laboratory, M.I.T., Cambridge, MA

This project is mainly concerned with the investigation of airplanes following each other in a string as often occurs during the landing process, where the string has an average velocity, which may be constant, piecewise-constant or continuously decreasing.

The basic differential equations for the string are derived and modern control theory is used to describe the characteristics of the feedback control by the pilots. Two different kinds of performance indices are used and a comparison between them is made.

To obtain the elements of the cost matrices and because such data was not available, some data analyses were derived using a basic model for one aircraft. This was then applied to the complete string of airplanes by means of some simulations to adjust the coefficients until some reasonable trajectories were obtained.

The pilot's goal was to eliminate collision with the leading airplane and to avoid excessive acceleration. It was assumed that the following pilot could not see more than two leading airplanes. The main weighting on the feedback was based on velocity and distance error.

Some other factors and use of some former researchers concerning car-following models are discussed. These suggest less error sensitivity when the spacing is increasing and more error sensitivity with decreasing spacing. Variable feedback coefficients which are inversely proportional to both velocity and spacing error are also taken into consideration. Even though the major portion of the work consists of simulation done with constant average velocity, some models dealing with continuously decreasing average velocity are also studied.

The effect of some thresholds and different sampling intervals are also discussed.

All these different factors were supported with simulations which showed the response of the system to various kinds of disturbances by means of some numerical and graphical output.

N82 34043 -6

TRAINING AIRCRAFT DESIGN CONSIDERATIONS BASED ON THE SUCCESSIVE ORGANIZATION OF PERCEPTION IN MANUAL CONTROL

Robert K. Heffley and Warren F. Clement
Systems Technology, Inc.
Mountain View, California 94043

and

Samuel J. Craig
Vought Corporation
Hawthorne, California 90250

ABSTRACT

The thesis of this work is that pilot skill development in the Navy approach and landing task is very strongly tied to the aircraft closure rate and, therefore, that pilot training for this task should be based on an appropriate progression closure rate. This, in turn, leads to a rational and explicit determination of design point approach speeds as well as other important aerodynamic features for training aircraft. One key is to recognize the significance of transitioning from a purely compensatory control loop technique to one involving a pursuit crossfeed between throttle and pitch attitude. Such transitioning requires significant skill development, yet reduces pilot workload while enhancing flight path and airspeed performance. The second key is to address the terminal flight path adjustment in terms of range-to-go. This establishes a bridge between the visual field and the combination of manual control technique and vehicle flight dynamics. A design summary plot is thus created in terms of: 1) performance (flight path bandwidth), 2) critical range-to-go (for terminal path correction), and 3) closure rate. This performance-range-closure rate space serves to map the training progression in light of the various critical aircraft and control technique constraints. A specific advanced trainer design point can thus be established for any combination of primary trainer and operational fleet aircraft.

OVERVIEW

Command of an aircraft consists of two types of tasks:

1) Psychomotor tasks requiring the pilot to be active in closed-loop regulation of the aircraft flight path; control commends are imposed and effects of disturbances are suppressed.

2) Discrete, normally open-loop, tasks wherein the pilot communicates, navigates, operates systems, etc.; these tasks usually are not required to be performed at an exact time but during a specific time period.

ORIGINAL PAGE IS
OF POOR QUALITY

During a maneuver, the portion of available time required for performing the psychomotor flying tasks is called "attentional workload" in the literature (e.g., Refs. 1 and 2).

The methodology and rationale for psychomotor skill development applied here follows the Successive Organization of Perception (SOP) theory of manual control derived from Krendel and McRuer (Ref. 3). This hypothesis of psychomotor skill development is based on the concept that a supervisory control system of the human dominates the learning process. It is the limitation of the supervisory system that sets the pilot workload margin; as skill is developed in a given sensory-motor task , supervisory involvement and, hence, perceptual-motor loading (i.e., workload) become less. Furthermore, it is theorized that skill development involves a progression from an instant-by-instant conscious perceptual-motor action to execution of programmed responses. The three stages of development are described by this theory of manual control skill development to be:

- Compensatory; the pilots acts mainly in response to an error signal (he is "behind the aircraft").
- Pursuit; most of the pilot's actions are learned responses to discrete perceptual cues or sets of perceptual cues.
- Precognitive; most of the pilot's actions are executions of learned control routines and strategies.

These three stages of skill development represent levels of the pilot's workload capacity.

In actual flight situations, the pilot attempts to cope with each control task by use of strategies which reduce his workload and improve his performance. Pilots reach their maximum performance capacity when they gain the ability to primarily use precognitive skills for aircraft control.

METHODOLOGY AND APPROACH

The thesis of this specific application is that the pilot's skill development in the Navy approach and landing task is very strongly tied to the aircraft closure rate and, therefore, that pilot training for this task should be based on an appropriate progression in closure rate. This, in turn, leads to a rational determination of design approach speeds as well as other key aerodynamic features for training aircraft.

The following summarizes the analysis approach for choosing, in particular, the design point for an advanced jet trainer in the context of the night carrier approach task. This context includes a variety of important factors, i.e.,

- Prescribed longitudinal piloting technique.
- Overall multiaxis control task.

- Desired manual control performance, i.e., minimum path errors and system stability.
- Aircraft flight dynamics (flight path, speed or AOA).
- Outside visual perception.
- Need for excess time to communicate [with LSO, instructor pilot (IP), etc.].

Most important, we are able to view these factors in terms of the progression of training from introduction to the primary trainer, through an advanced trainer, to the fleet aircraft.

The analysis approach that covers the above is illustrated in Fig. 1. It begins with a statement of the task and a prospectus of the control loop structure needed to accomplish that task. A control loop analysis is then performed to identify the important features of the vehicle, of the displays (outside visual and cockpit instruments), and of the piloting technique. Following that, we estimate the pilot's discrete task duty cycle and compare that to his multiloop excess control capacity in order to assess his partition of workload between continuous and discrete tasks. Pilot/vehicle performance

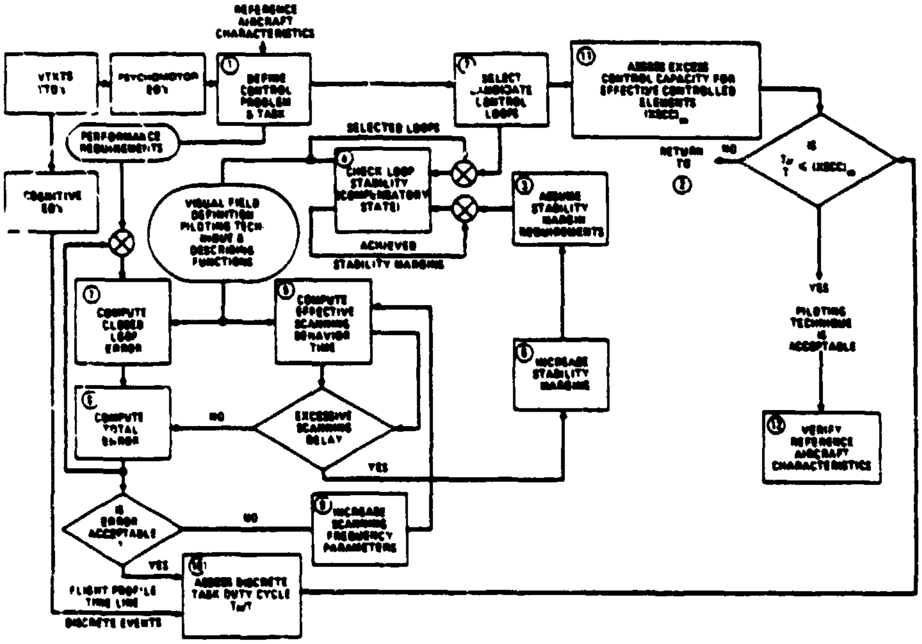
REFERENCE AIRCRAFT CHARACTERISTICS
PSYCHOMOTOR
COGNITIVE
1 DEFINE CONTROL PROBLEM & TASK
PERFORMANCE REQUIREMENTS
SELECTED LOOPS
CHECK LOOP STABILITY (COMPENSATORY STATE)
ACHIEVED STABILITY MARGINS
VISUAL FIELD DEFINITION PILOTING TECHNIQUE & DESCRIBING FUNCTIONS
COMPUTE CLOSED LOOP ERROR
COMPUTE EFFECTIVE SCANNING BEHAVIOR TIME
COMPUTE TOTAL ERROR
NO
EXCESSIVE SCANNING DELAY
YES
IS ERROR ACCEPTABLE ?
NO
INCREASE SCANNING FREQUENCY PARAMETERS
YES
ASSESS DISCRETE TASK DUTY CYCLE
FLIGHT PROFILE TIME LINE
DISCRETE EVENTS
SELECT CANDIDATE CONTROL LOOPS
11 ASSESS EXCESS CONTROL CAPACITY FOR EFFECTIVE CONTROLLED ELEMENTS
ASSESS STABILITY MARGIN REQUIREMENTS
INCREASE STABILITY MARGINS
RETURN TO
NO
YES
PILOTING TECHNIQUE IS ACCEPTABLE
VERIFY REFERENCE AIRCRAFT CHARACTERISTICS

Figure 1. Flow diagram of process for selection of flight media requirements based on imposed workload

is brought into the analysis along with visual motion efffects, and this finally permits us to formulate a manageable quantification of all factors in common terms. The resulting overall system parameters consist of aircraft speed (airspeed and closure rate), aerodynamic flight path sensitivity (n_{z_α}), range-to-go, and piloting technique (regarding flight path and speed). A bridge common to each of these parameters is the height regulation bandwidth (expressed as crossover frequency, (ω_{c_h}).

The problem, briefly stated, is to accomplish a manual approach and landing in the fleet night CV environment and to consider the training progression required to build up to this. The Navy's prescribed piloting technique specifically calls for height corrections with throttle and speed (or AOA) corrections with pitch attitude. Taken literally, this corresponds to our concept of a parallel compensatory loop structure (with an inner series loop of pitch attitude controlled by elevator).

A key point of the analysis is that a purely compensatory structure will not permit satisfactory execution of the approach and landing task, especially in adverse conditions. Rather, the pilot must ultimately develop a pursuit crossfeed of throttle-to-attitude in order to enable full realization of the aircraft's flight path regulation potential (see Fig. 2). This pursuit crossfeed satisfies the prescribed Navy technique, but it brings about a quantum decrease in pilot workload (increase in excess control capacity) with a commensurate improvement in flight path performance. We see, in fact, that the crossfeed becomes essential to success in the CV environment as approach speed increases to that typically encountered in fleet aircraft (i.e., flighter/attack).

Two key parameters describe the relevant airplane dynamics, i.e., total airspeed, V, and normal acceleration sensitivity, n_{z_α} ($= C_{L_\alpha}/C_L$ or $-Z_c'/g$). These parameters, for example, provide accurate estimates of attitude-constrained speed and heave modes, $1/T_{\theta_1}$ and $1/T_{\theta_2}$, respectively. , $1/T_{\theta_1} \doteq (2/n_{z_\alpha})(g/V)$ and $1/T_{\theta_2} \doteq n_{z_\alpha}(g/V)$. The above parameters establish limits on path and speed regulation for given piloting technique variations, especially compensatory versus pursuit crossfeeds.

- Comfortable compensatory bandwidth $\doteq 1/T_{\theta_1}$ [$\doteq (2/n_{z_\alpha})(g/V)$].
- Limit compensatory bandwidth ($\doteq \sqrt{2}$ (g/V).
- Limit pursuit crossfeed bandwidth ($\doteq 1/T_{\theta_2}$ [$\doteq n_{z_\alpha}(g/V)$].

The above constraints are mapped in the performance-range-closure rate space in Fig. 3. The piloting technique and aircraft-dependent determined limits are shown as normalized performance measures, and are characterized by the normalized flight path bandwidth and range-to-go. The normalization of the scales relates the differences in approach speed between the advanced trainer and fleet aircraft to the skill level that the student acquires at the end of his primary training. Unity, on the range-to-go scale, at end of primary training is 200 feet distance and the corresponding flight path performance is a bandwidth frequency of 0.5 radians per second. Range-to-go is defined as the pilot's final path correction distance. These normalized metrics provide standards relative to student skill. The illustration in

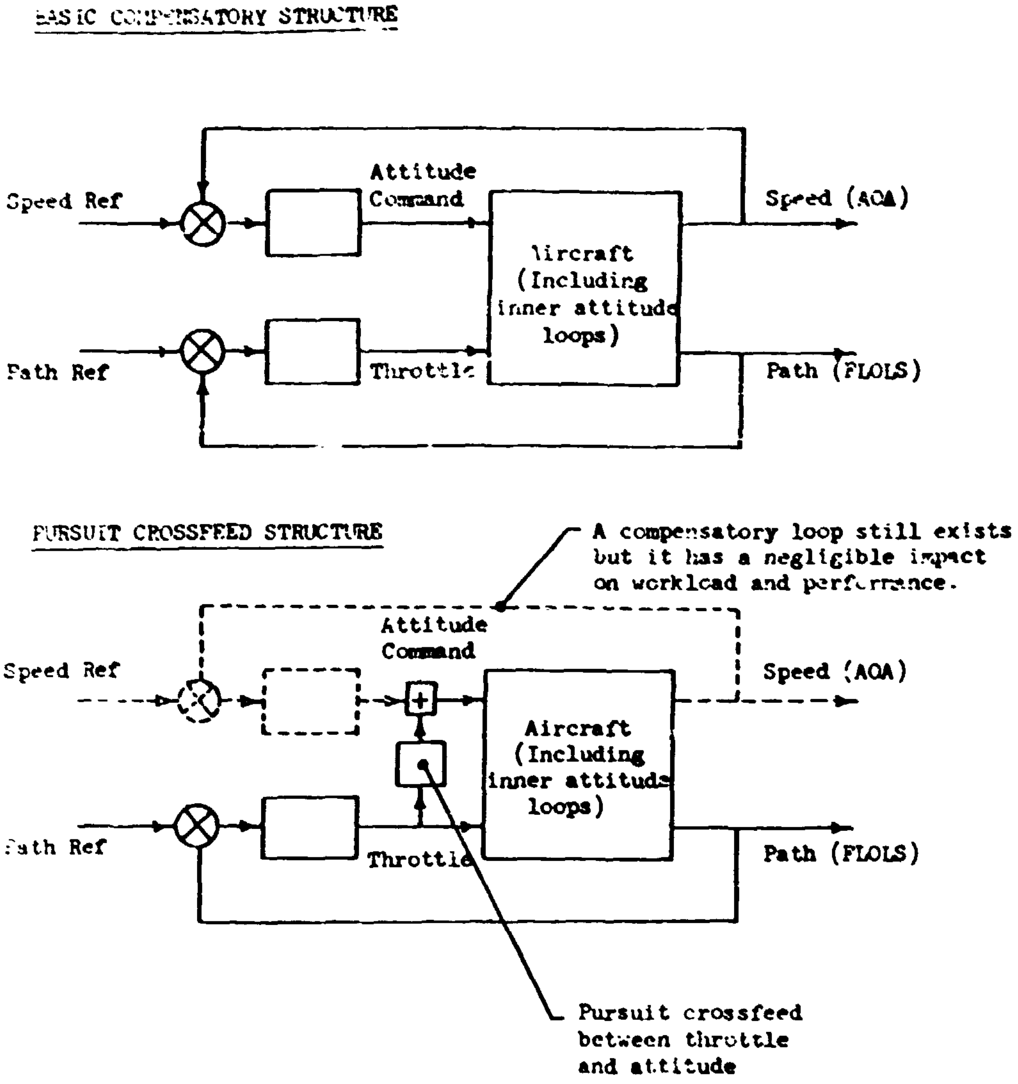
BASIC COMPENSATORY STRUCTURE
Speed Ref
Attitude Command
Aircraft (Including inner attitude loops)
Speed (AOA)
Path Ref
Throttle
Path (FLOLS)
PURSUIT CROSSFEED STRUCTURE
A compensatory loop still exists but it has a negligible impact on workload and performance.
Speed Ref
Attitude Command
Speed (AOA)
Aircraft (Including inner attitude loops)
Path Ref
Throttle
Path (FLOLS)
Pursuit crossfeed between throttle and attitude

Figure 2. Comparison of pilot loop structure forms (in terms of Successive Organization of Perception)

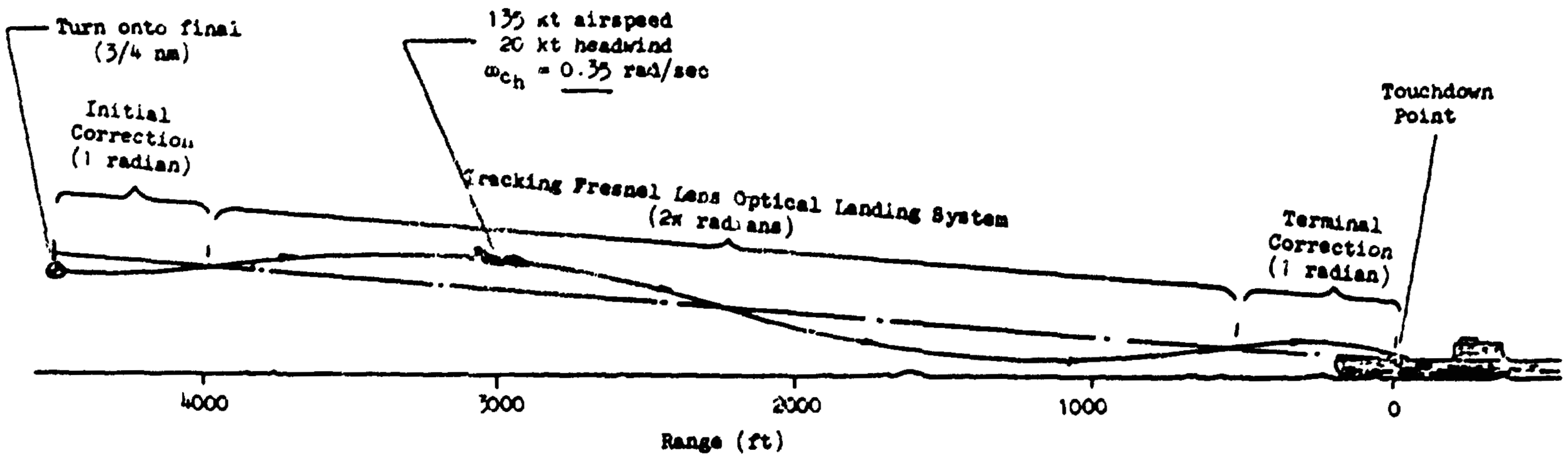

Figure 3. Sample CV approach showing an initial correction, FLOLS tracking, and a terminal correction

Fig. 4 indicates that for a night carrier approach, the design point is 105 knots airspeed for a 20 knot headwind with path response (n_{z_α}) approximately equal to 3.0 This level of n_{z_α} is established by the need to insure that the student reaches his response limit for the pursuit control technique. By achieving this level of skill he will be capable of operating to the airframe-dependent limit for the fleet aircraft. The governing factors are the pilot's perspective view of the Fresnel lens sensitivity and landing area.

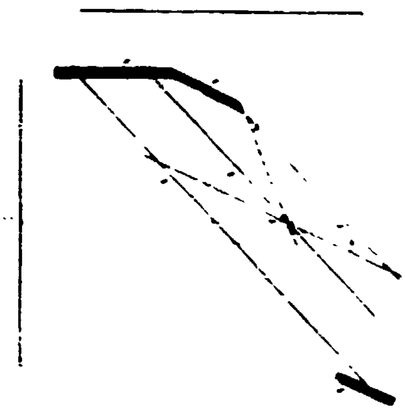

Figure 4. Approach performance design constraints of aircraft for night qualification

TRAINING IMPLICATIONS

A training scenario can be derived from the analysis. As shown in Fig. 5, the student's skill development begins with the primary trainer at Point A. For clarity, the small arrows are used to trace the student's skill development while the "bolder" arrows indicate points for advancement in training. In his "naive" state, the student applies the prescribed Navy flight path control technique in the compensatory manner. At this level of proficiency, the governing aircraft parameter is the attitude-constrained speed mode, $1/T_{\theta_1} = (2/n_{z_\alpha})(g/V)$, where n_{z_α} is the normal load factor sensitivity to change in angle of attack, V is true airspeed, and g is the gravitational constant.

As his proficiency increases from the compensatory level, his performance improves until he reaches an intermediate performance constraint (i.e., Point B) imposed by the aircraft phugoid response characteristics (ω_p) in radians per second.

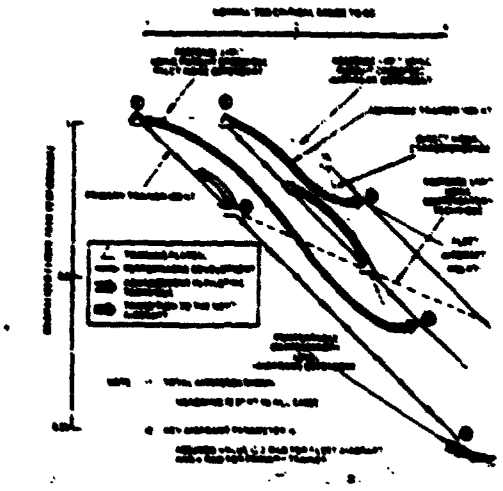

Figure 5. Training scenario suggested for night qualification

The student cannot improve his performance beyond this point unless he learns a more efficient control strategy. This occurs through the TP prompting and self-organizing (i.e., SOP). The strategy required is a control phasing technique (i.e., crossfeed) between throttle and attitude. This so-called "pursuit control" technique imposes no additional workload, and increases his excess control capacity. Upon adoption of the pursuit control, his performance can potentially be extended to the aircraft's heave mode limit given by $1/T_{\theta_2} = n_{z_\alpha}(g/V)$, which is Point C. Because of this "timesharing" between control axes, the student reaches a "plateau" of proficiency. This "training plateau" is a "soft limit" which stems from the human's inherent time delays in processing and execution, and visual scanning frequency limit. In a practical sense, this limit varies between subjects. At Point C, the student's repertoire of skills has improved sufficiently to go to an advanced trainer.

In this advanced trainer, depending upon the increment approach speed and degree loss in visual correspondence, the student will regress to a highly skilled compensatory state as indicated by the "bold" arrow at Point D. Due to the change in approach speeds, his visual cues at the critical range for decisions of the advanced trainer do not correspond to those learned in the primary trainer. He must learn the new preview perspective, and, in so doing, he regresses to the compensatory techniques until the visual cues and timing strategy necessary for advancing to the pursuit technique have been re-established at the higher approach speed of the advanced trainer (Point E).

The final progression in the learning cycle is the transition to the fleet aircraft, and is considered the major hurdle (Point F). Consequently, an aircraft-to-aircraft visual correspondence is necessary between the advanced trainer and the fleet aircraft. Some regression in proficiency occurs, but the student need only fall back to the cues learned in the advanced trainer. The pursuit technique applies to this condition, and the student is fully capable of progressing in skill to the limits of the fleet aircraft.

CONCLUSIONS

The following points may be inferred from the above:

1) The flight path performance metric (i.e., closed-loop bandwidth) in the critical range-to-go region provides a unique measure which is sensitive to pilot control technique and pilot proficiency level. This metric could logically be used to determine when a student should advance in training.

2) For the student, transition from the primary trainer environment to the advanced trainer is more challenging than from the advanced trainer to the fleet aircraft, in terms of imposed workload. Initial regression of technique is to be expected at the primary to advanced transition, but very little regression in proficiency is permissible in transitioning to the fleet aircraft. Therefore, visual correspondence between these aircraft is maintained.

3) Increased training time may be required if a high approach speed increment occurs between the primary and advanced trainer.

4) Aircraft characteristics which enhance training progression are explicitly determined.

REFERENCES

1. Roscoe, Stanley N., "Man as a Precious Resource: The Enhancement of Human Effectiveness in Flight Operations," AIAA Paper 74-1296, presented at AIAA Life Sciences and Systems Conference, Arlington, Texas, 6-8 November 1974.

2. Jex, Henry R., and Warren F. Clement, "Defining and Measuring Perceptual-Motor Workload in Manual Control Tasks," in N. Moray, ed., Mental Workload, New York, Plenum Press, 1979.

3. Krendel, Ezra S., and Duane T. McRuer, "A Psychological and Physiological Skill Development A Control Engineering Model," in Fourth Annual NASA-University Conference on Manual Control, NASA SP-192, 1968, pp. 275-286.

N82 34044 D7

AN EXPERIMENTAL STUDY OF HUMAN PILOT'S SCANNING BEHAVIOR

by

Kyuichiro Washizu*, Keiji Tanaka** and Tatsuo Osawa*

*Department of Aeronautics, University of Tokyo, Tokyo,
**Instrumentation and Control Division, National Aerospace
Laboratory, Tokyo

INTRODUCTION

In order to disclose the characteristics of the human pilot who controls the multi-variable system, we have to investigate both the control behavior and the scanning behavior. Researches on pilot's scanning behavior during the actual operation of airplanes have been conducted previously, from which the data concerning the scanning properties among various instruments have been already obtained[1]. Furthermore, various models of pilot's dynamics based upon multi-variable manual control experiments have been constructed[2-4]. There are, however, very few which summarize these scanning properties taking account of the various control situations where the pilot is actually placed.

The aim of this paper is to investigate the scanning behavior and the control behavior of the pilot who manually controls the two-variable system, which is the most basic one of multi-variable systems. In our experiment, we set up two control tasks, which simulate the actual airplane attitude and airspeed control. In order to simulate the change of the situation where the pilot is placed, such as changes of flight phase, mission and others, the subject was requested to vary the weightings, as his control strategy, upon each task. Changes of human control dynamics and his scanning properties caused by the modification of the situation have been investigated.

By making use of the experimental results, the optimal model of the control behavior and the scanning behavior of the pilot in the two-variable system is proposed from the standpoint of making the performance index minimal. This model enables us to predict both the optimal human control dynamics and the optimal scanning properties. The model validation is done by comparing the model predictions with the experimental results.

EXPERIMENT

The previous works have already pointed out that the pilot's scanning behavior varies according to the instruments he attends to; namely, the dwell time on the flight director is relatively long and spreads widely, whereas, the dwell time on other instruments, such as the airspeed indicator, is short and remains almost constant[1]. Referring to this fact, the subject is assigned to two tasks, the main task and the side task, each having different characteristics in this experiment. As shown in Fig.1, each error between the forcing-function and the output of the controlled element is displayed on each CRT. The subject actuates the respective controller by making use of the displayed information. Thus, each control loop forms a compensatory tracking task. As we postulate the situations similar to the actual operation, we chose as the main task the stable controlled element to which the random-appearing forcing-function is added, and as the side task the unstable first-order controlled element to which no forcing function is added. The following three kinds of controlled elements are employed for the main task:

$$G_{cm1}(s) = 5/(s^2 + \sqrt{5}s + 5) \quad , \qquad (1)$$

$$G_{cm2}(s) = 1/s \quad , \qquad (2)$$

$$G_{cm3}(s) = 1 \quad ; \qquad (3)$$

while the controlled element for the side task has a first-order divergent dynamics:

$$G_{cs}(s) = 0.3/(s - 0.3) \quad . \qquad (4)$$

On the other hand, in order to evaluate the total control performance, the performances of both the main task and the side task must be considered. In this paper,

$$J = K_m \overline{e_m(t)^2} + K_s \overline{e_s(t)^2} \quad (K_m + K_s = 1) \quad (5)$$

was postulated as the total performance index, where $\overline{e_m(t)^2}$ and $\overline{e_s(t)^2}$ are the mean-squared error of the main task and the side task respectively. K_m and K_s are weighting coefficients, and these are considered to be variable according to the change of situation, such as flight phase or mission, in case of the actual operation. Referring to Eq.(5), we change the experimental mode by directing the weightings verbally. The experimental mode are as follows:

mode WM ; put more weighting on the main task ($K_m > K_s$)
mode WE ; almost equalize the weightings ($K_m = K_s$)
mode WS ; put more weighting to the side task ($K_m < K_s$).

The results of the experiment are summarized as follows·

1) As seen in the time history indicated in Fig.2, the control of the main task is done almost continuously, whereas, the control of the side task has the tendency to be interrupted during the period between fixations.

2) The dwell time on the main-task display is relatively long and spreads widely, whereas, the dwell time on the side-task display is short and almost constant.

3) The control performance of each task varies according to the weightings.

4) As indicated in Fig.3, the dwell time on the display of each task varies according to the weightings. This change is observed mainly in the dwell time on the main-task display. The dwell time on the side-task display remains almost constant.

The mean value of the sum of the both dwell times is defined as a scanning period. The scanning period varies according to the dwell time on the main-task display, since the dwell time on the side-task display is almost constant.

5) Figs.5 and 7 indicate that, when the scanning period T increases, the main-task control performance becomes better, while the side-task control performance becomes worse.

As the main-task control can be considered to be continuous, we can apply the time series analysis using Multiple Final Prediction Error method to the data of the main task[5].

6) Using the results of the time series analysis, the describing functions of the pilot are obtained. These show the tendency for the gain to deteriorate as the scanning period becomes shorter.
On the other hand, the control of the side task, which seems to be interrupted between fixations, indicate that the pilot perceives both the error and its rate of change during a short dwell time.
7) As shown in Fig.6, there is a proportional relationship between the magnitude of error and the pilot's control, when pilot's eyes are fixed on the side-task display. The pilot's gain for the side task has a tendency to decrease when the scanning period becomes longer.

MODELING

We propose here a model of the scanning behavior based upon the results of the experiment. This model consists of the optimal control models for both tasks and the optimal scanning model.

Since the control of the main task appears to be continuous, the pilot's optimal transfer function, which minimizes the performance index,

$$J_m = \overline{e_m(t)^2} + k^2\overline{c_m(t)^2} \quad , \qquad (6)$$

is derived from Wiener's optimum filtering theory. Here, e_m and c_m denote the error and the control of the main task respectively. The effects of the scanning are dealt by adding the relevant observation noise to the system. In Ref.2, there is an example of assuming the power spectrum density of the observation noise Φ_{vv} by:

$$\Phi_{vv} = T_s \overline{e^2} / \pi \quad , \qquad (7)$$

where T_s is the sampling period of the display and $\overline{e^2}$ is the mean squared error. Referring to Eq.(7), we assume that the ratio of the amplitudes of the observation noise up to π[rad/sec] and of the error corresponds to the square of the ratio of the dwell time on the side-task display T_{ds} and the scanning period T, namely the power spectrum density of the relevant observation niose Φ_{vv} is assumed to be obtained by the following equation:

$$\Phi_{vv} = (T_{ds} / T)^2 \overline{e_m(t)^2} \quad . \qquad (8)$$

The dwell time on the side-task display T_{ds} remains almost constant in all the cases. For the model, we fixed as:

$$T_{ds} = 0.4 \ [\text{sec}] \quad . \qquad (9)$$

Thus, the pilot's optimal transfer function and the main-task performance can be obtained as the function of T. Fig.4 shows a comparison of the frequency response of the optimal model obtained above and the pilot's describing function obtained from the experiment. Fig.5 shows the experimental results of the control performance and the prediction by the optimal model. It seems possible for the model to predict the average of the experimental values if T is given.

The modeling of the control of the side task is based upon the descrete-time optimal regulator. Here, we replaced the sampling period with the scanning period, assuming that one piece of information is perceived at one fixation and that the pilot controls in such a way that he interrupts his control during the period between fixations. When the controlled element of the side task is the first-order unstable system as Eq.(4), the pilot's optimal control model has proportional characteristics; the gain of the model changes according to the scanning period T. As shown in Fig.6, there is a proportional relationship between the error (i.e. pilot's input) and the pilot's output, and it indicates a good accord with the gain of the optimal control model. Moreover, as seen in Fig.7, the control performance of the side task for each T can be predicted by using this model.

As stated above, the control performance of each task is predicted by employing the optimal models for both tasks as the function of the scanning period T. According to Eq.(5), the total task performance is also obtained as the function of T. The optimal scanning period T satisfies the equation:

$$dJ / dT = 0 \quad . \qquad (10)$$

Comparisons between the model prediction and the experimental values of the dwell time on the main-task display are shown in Fig.8, under assumptions that the dwell time on the side-task display is held constant and that the following weightings can be applied to the experiment: $K_m = 0.6\text{–}0.8$ with mode WM, $K_m = 0.4\text{–}0.6$ with mode WE, $K_m = 0.2\text{–}0.4$ with mode WS. Note that in Fig.8, the average of the display dwell time is expressed. These results indicate that we can predict the scanning behavior by using the proposed model.

CONCLUSION

By setting up an experimental condition similar to the actual operation of airplanes, the data of two-variable manual control system were successfully obtained. It was confirmed that the pilot's control dynamics and his scanning properties change with the weightings put on the two assigned task. The proposed pilot model in the two-variable manual control system can predict both the pilot's dynamics and the average tendencies of the scanning properties.

REFERENCES

1. Spady,A.A.Jr.: Airline Pilot Scan Patterns During Simulated ILS Approaches, NASA TP-1250, 1978.
2. Allen,R.W.; Clement,W.F.; and Jex,H.R.: Research on Display Scanning, Sampling, and Reconstruction Using Separate Main and Secondary Tracking Tasks, NASA CR-1569, 1970.
3. Levison,W.H.; Elkind,J.I.; and Ward,L.L.: Studies of Multivariable Manual Control Systems: A Model for Task Interference, NASA CR-1746, 1971.
4. Kleinman,D.L.; and Baron,S.: Manned Vehicle Systems Analysis by Means of Modern Control Theory, NASA CR-1753, 1971.
5. Tanaka,K.; Goto,N.; and Washizu,K.: A Comparison of Techniques for Identifying Human Operator Dynamics Utilizing Time Series Analysis, Proc. of 12th Annual Conf. on Manual Control, NASA TM X-73,170, 1976, pp.673-693.

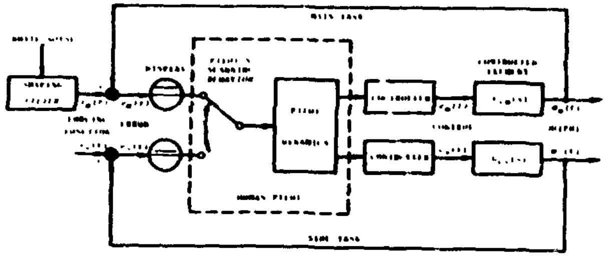

Figure 1. Block Diagram of the Experiment

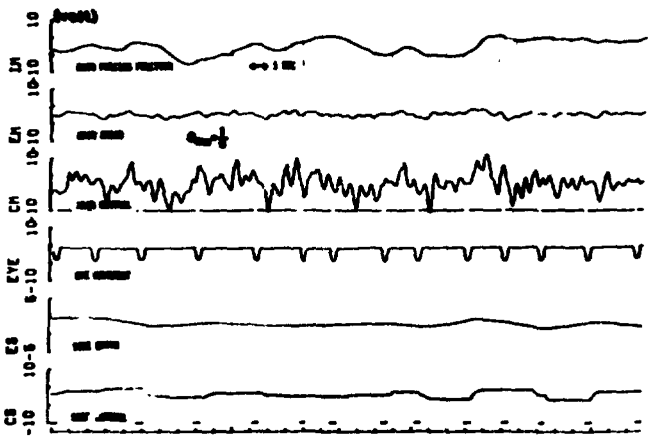

Figure 2. An Example of the Time Histories of the Recorded Data

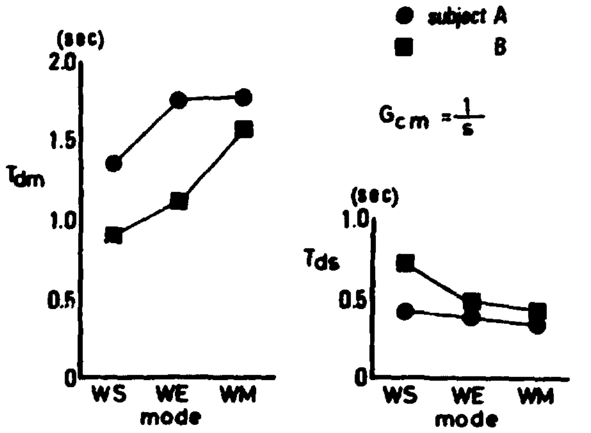

Figure 3. Changes of the Dwell Time on the Main-Task Display T_{dm} and of the Side-Task Display T_{ds} According to the Weightings

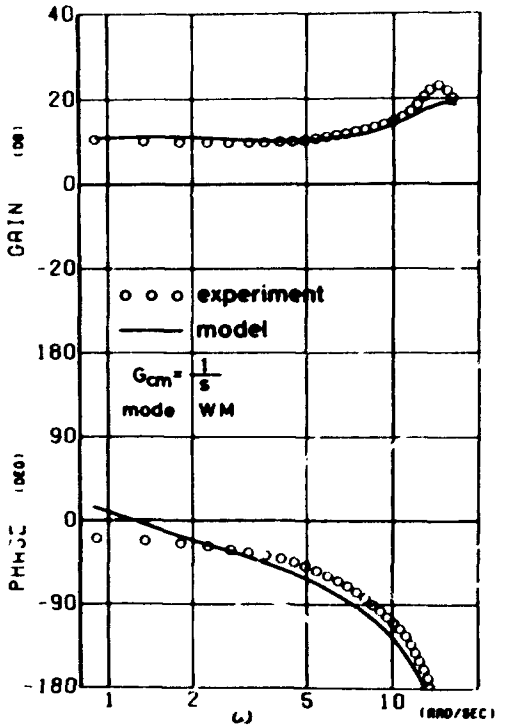

Figure 4. An Example of the Pilot's Describing Function and the Frequency Response of the Optimal Model

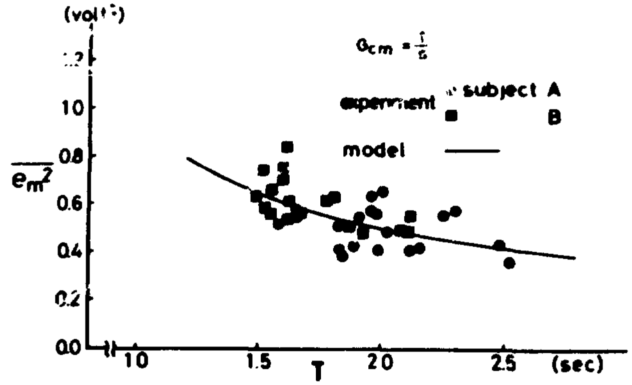

Figure 5. Main-Task Performance as a Function of the Scanning Period T

ORIGINAL PAGE IS
OF POOR QUALITY

ORIGINAL PAGE IS
OF POOR QUALITY

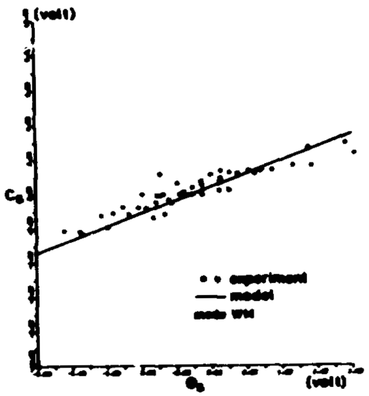

Figure 6. Relationship between the Error and the Control of the Side-Task

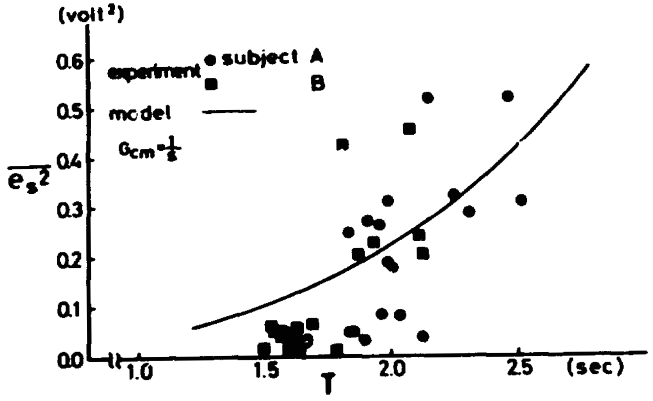

Figure 7. Side-Task Performance as a Function of the Scanning Period T

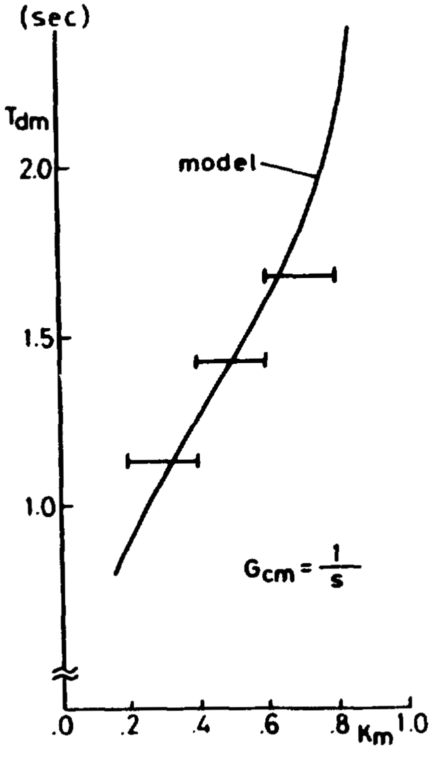

Figure 8. Comparison of the Experimental Results and the Model Prediction of the Dwell Time on the Main-Task Display T_{dm}

INVESTIGATION OF A SUM OF SINUSOIDS REPRESENTATION OF GAUSS-MARKOV RANDOM PROCESSES - IMPLICATIONS FOR MANUAL CONTROL RESEARCH

R.L. Mohr and A.V. Phatak
Analytical Mechanics Associates, Inc.
Mountain View, CA

R.A. Hess
NASA/Ames Research Center
Moffett Field, CA

Abstract

An important problem in the design of piloted simulation experiments is the selection of appropriate mathematical models for the external wind gust disturbance inputs. Wind gust turbulence spectra are typically represented as gauss-markov random processes, such as the "Dryden" or "Preyss-Meadows" models. Assuming that turbulence spectra are rational, these models provide an efficient and adequate approach towards simulating the effects of external gust disturbances. However, such gauss-markov gust models are not necessarily the best representation to use if the objectives of the manned simulation experiments are not merely empirical experimental analysis but include the identification of a dynamic input-output pilot model. The drawbacks of using gauss-markov disturbance models relate to the statistical properties of the pilot model parameter and spectral estimation procedures when finite data segments are used for identification. These problems do not arise if a sum of sinusoids is used to model the gust turbulence spectra. At present, the number, relative amplitudes, frequencies and phase angles of the sinusoids are selected to match the characteristics of the desired spectrum according to some qualitative or quantitative criterion. Furthermore, these representations are used interchangeably in the formulation of optimal control theoretic models for the human operator, which require the assumption of state-space "internal models" for the plant/disturbance dynamics.

Recent work has shown the impact of varying internal models for the random disturbances on the optimal control model describing function and remnant outputs. Therefore, a better understanding of the relationship between random signals and sum of sinusoids representation should provide valuable insight into plausible internal models for the plant/disturbance dynamics adopted by the trained human operator.

This paper presents results of a preliminary investigation into the mathematical relationship between a state-space model for external disturbances to a pilot-vehicle system and an "equivalent" deterministic sum of sinusoids representation of that disturbance. Systematic model structure determination and maximum likelihood parameter identification are applied to sum of sinusoids data and variables (as in standard k, k/s and k/s^2 laboratory tracking tasks) excited by sum of sinusoids data . The purpose was to study the effects of various parameters, such as run length, sampling rate, and sum of sinusoids variables (number, relative amplitudes, frequencies and phase angles) on the identified state space model structure and parameter estimates.

The results are compared to state-space models assumed by previous investigators, and the implications to man-vehicle simulation and human operator modeling are discussed.

N82 34045 DB

PARAMETRIC IDENTIFICATION OF HUMAN OPERATOR MODELS

Norbert R. Ninz
Department of Human Factors Engineering
and Simulation

VFW-Company Bremen
Federal Republic of Germany

SUMMARY

The accurate and efficient identification of the human operator is still a need in human factors engineering especially concerning multivariable control. Control theoretic identification methods need to be tested with human operator models under realistic boundary conditions. The requirements and criteria for the use of parametric methods, selected models as well as the Maximum Likelihood Method and the Extended Kalman Filter are displayed. The experiments and results are comparativly discussed from the point of practical engineering.

INTRODUCTION

The multivariable control of man-maschine-systems by the human operator will remain even in highly complex systems like present and future aircraft generations. For example, questions concerning crewconcepts must also be answered in the field of continuous manual control not only in categories of decision theory. In the optimization of manual controlled systems the identification of the human operator is a supposition to solve this task on analytical methods. For this purpose some models for the manual control of single and multivariable control have been developed an tested /1, 2, 3/. The use of even efficient models as a tool for design engineers is normally restricted by the capacity of identification methods and generates the need for powerful identification approaches.

In the past non-parametric methods were preferred which produced an operator description in graphical form like the Bode-plot. This curve had to be approximated by those of a model to achieve an analytical form. Generally the weighting function or transfer-function via correlation methods were computed. The expense in computing time and effort were high and normally only capable in research experiments and in single variable control tasks. The identification of model-parameters and information about the human operator remnant were not available in the same identification run.

In the last years in identification, parametric methods based on estimation theory became available and were tested on technical systems /4/. These results cannot be transferred on man-machine-systems without further investigations for the boundary conditions are not comparable. In the human factors field parametric methods were often used with restrictions in the operator model (no remnant) or in special control situations were parts of the model were neglectable (time delay) or unusual forms appeared (all elements of the state vector measurable).

The aim of this work is to test parametric methods without specific restrictive assumptions to gain experience on their versatility as an engineering tool for a broader scope of control tasks.

Starting with requirements for modelling questions of the identifiability of the Quasi-linear Model and the Optimal Control Model have to be answered and also attention has tc be payed on the convergence criteria of the identification methods under test. These are the Maximum Likelihood Method and the Extended Kalman Filter. Both were used in identifying the computer-simulated man-machine-systems including the human operator. Also experiments with manual control tasks performed by testpersons were achieved. The accuracy and convergence in regard to the software, hardware and computing time expense will be valuated.

REQUIREMENTS AND CRITERIA FOR THE USE OF PARAMETRIC METHODS

Identification methods are characterized by their convergence. This includes that they evaluate the true parameters with a minimum of measured data and minimum error. A very desirable quality is an asymptotic unbiased estimate with minimum variance. The achievability of this performance depends on the identification method itself and on the structure of the man-machine-system-model.

The Maximum-Likelihood Method provides this quality if a canonical form of the man-machine-system-model is found and some other conditions concerning the data acquisitions are fulfilled /6/.

The Extended Kalman Filter will only reach suboptimal estimates in the described sense for the linearisation of the system-model and the variances will always be greater than that of a minimum-variance-estimator /5/. Nevertheless the use of canonical forms supports convergence.

For single-variable control canonical forms have unique solutions which is not true for multivariable control models and in addition the effort to acnieve a canonical form is extremly higher /8/.

Normally the human operator models do not have a canonical form in their orgin so that the model parameters and the "canonical" parameters are not identical. The identification method will estimate the "canonical" parameters which have to be transformed back into model parameters to work with. This requires the deterministic identifiability of the model parameters out of the canonical form /7/. These requirements do not only concern that a human operator model can be employed for identifying parameters from real data and is not only able to describe human behaviour. Besides the performance in convergence the usefulness of an identification method as an engineering tool in human factors has also be taken into account by the on/off-line capability, needed computer-size and computing time.

MODELS AND IDENTIFICATION METHODS UNDER INVESTIGATION

For the testing of parameter estimation methods under human factors conditions validated human operator models were used. The discussion of the models in a general sense was not the subject of the research. To reduce the effort in computer and program handling a single controlled variable task was chosen with a first order vehicle dynamic (fig. 1). This does not restrict the validity of the results in respect to multivariable control for the structure of the man-machine-system-models and the identification methods cover both cases.

Some versions of the Quasi-linear Model and the Optimal Control Model were checked if the man-machine-system-model including them could fulfil the requirements for a structure which can provide minimum-variance estimates.

The system with the Quasi-linear-Model is lcoal identifyable for the models MOD 3 and MOD 5 (fig. 2) and only for some very restricted parameter spaces for MOD 6. This last statement is also valid for the version of the Optimal Control Model proposed as identifyable in /2/. All model versions are designed for single-variable control that a canonical or minimal form can be found with a unique solution. The presentation of the man-machine-system-model is written in the state-space description

$$\begin{bmatrix}\dot{x}_1\\ \vdots\\ \vdots\\ \dot{x}_n\end{bmatrix}\begin{bmatrix}0 & 0\ldots 0 & 1\\ -b_0 & 0\ldots 0 & -a_0\\ -b_1 & 1\ldots 0 & -a_1\\ -b_m & 0\ldots 1 & -a_m\end{bmatrix}\cdot\begin{bmatrix}x_1\\ \vdots\\ \vdots\\ x_n\end{bmatrix} + \begin{bmatrix}1\\ \\ \underline{0}\\ \end{bmatrix} w + \begin{bmatrix}1\\ \\ \underline{0}\\ \end{bmatrix} r$$

It is an extended equation of a standard canonical form of the operator model and contains one additional non-zero element for the vehicle dynamic. With the assumption that this dynamic is known this element is no parameter to be estimated so that this minimal form fulfils the criteria for convergence of the identification methods in use.

The main problem arises when the origin parameters have to be computed from the elements of the estimated parameter vector in return. In the cases of MOD 6 and MOD B this leads to extensive analytical expressions with higher order terms depending on the selected padé-approximation of the time delay. In the frame of testing identification methods the effort to obtain a solution was not bearable for the Optimal Control Model and all experiments were performed with the Quasi-linear Model (MOD 3 - MOD 6).

The Maximum-Likelihood identification as an acknowledged and powerful method in control engineering was chosen and the Extended Kalman Filter for its principal on-line capability. With the implementation of the Maximum-Likelihood Method on the man-machine-system under investigation arises the problem, that the covariance-matrix of the measurement noise is singular, for the vehicle output contains no noise with the assumption that under laboratory conditions measurement noise can be neglected. The remnant on the other hand must be interpreted as measurement noise. The singularity of the covariance-matrix prevents a steady-state solution of the Riccati-equation in the Likelihood-computer. The following directions have been tried to by-pass this difficulty:

- Open-loop-Likelihoodcomputer

Likelihoodcomputer with:

- reduced order
- virtual measurement noise
- measurement of one state variable (human operator output).

The last way proved to be the efficient one in achievable accuracy and effort /9/.

These problems do not arise in implementing the Extended Kalman Filter for a steady-state-solution is not aspired. The Maximum Likelihood method uses discrete state equations but continuous parameters are estimated by the Gauss-Newton algorithm. This division into discrete state equations and continuous parameter estimation is not possible with the Extended Kalman Filter. The continuous filter was chosen to prevent a transform from the Laplace-domain into z-domain and in reverse for the latter would induce analytical difficulties.

In the experiments the main attention was payed to the following items concerning convergence:

- Noise-to-signal ratio of remnant/human operator output
- Order of human operator models
- Number of measured data sets
- Selected starting values.

Both parametric methods were compared with the results of a cross-correlation-analysis on the same data. This acknowledged method in human factors was performed via FFT and a Direct Search to obtain an analytical expression out of the Bode-plot.

EXPERIMENTS AND RESULTS

All mentioned identification methods were tested on acquisitioned data from a man-machine-system computersimulation and on data measured with testpersons. In the computersimulation the human operator model was implemented with an exact time delay. The remnant and the disturbance were introduced as filtered white noise into the control loop. During the identification with the simulation derived data the identification method used the same model as the simulation except the padé-approximation of the time-delay. All model versions were tried out on the testpersons data.

The results are summarized in fig. 3 and 5. The label of the identification program is referred to the model's label of fig. 2. All times in the table are based on the described computer type and on 2043 data sets which were measured with 20 cps.
Beginning with the Maximum-Likelihood Method, a asymptotical convergence is achievable with all versions of the used operator model if the starting values are selected properly. The number of values leading to convergence reduces with the model's order. Increasing noise-to-signal ratio of the remnant gains the estimation error and the number of iterations necessary to reach the maximum of the likelihoodfunction. Increasing the number of data increases the accuracy but levels out at 1500 data sets. The accuracy is within good acceptance for all model versions and also for remnant levels well above that of typical human operators. The identification of the testpersons data gives results which could be expected for a first order dynamic of the controlled element. The Maximum-Likelihood Method could be validated also for these real world data for the parametersets of all models applied, generate an equivalent transfer function.

The Extended Kalman Filter requires more comutation time per cycle than available on a 20 cps data acquisition basis. So an on-line use is not possible. This time cannot be reduced significantly due to the chosen continuous filter and the Runge-Kutta-algorithm.
The filter is very sensitive to the selection of starting values which influences the speed and the accuracy of convergence considerably. Another disadvantage is that the covariance-matrix including the remnant must be known à priori. The estimation of the remnant covariance influences also the convergence of the filter. For there is no possibility except a faster computer to accelerate the filter algorithm into a region where on-line computation can be performed. The filter was not used with higher order models which would increase computation time again.
Comparing the parametric identification methods the superiority of the Maximum-Likelihood Method is shown (fig. 3). If the cross-correlation analysis in the here implemented sophisticated form is taken into account this is not that clear for it takes a

12-fold computation time. The cross-correlation analysis can be applied very easily on a spectrum of models. The programming of the Maximum-Likelihood Method is always special for each of the model version and needs more algebraic effort. Nevertheless for higher order models the Maximum-Likelihood Method is the most accurate (fig. 4).

CONCLUSIONS

The Extended Kalman Filter could not fulfil on-line requirements. In comparison with the Filter and a sophisticated cross-correlation analysis the Maximum-Likelihood Method proved to be the most accurate, but the analysis with FFT and Direct Scarch is faster and needs not to be programmed for every model version. Identification of real human operators and the simulation showed that the Maximum-Likelihood Method and still the cross-correlation analysis are powerful instruments for engineering in human factors even without restrictive models or conditions. More attention should be payed to identifyable multivariable models for the human controller.

REFERENCES

1. Baron, S., Elkind, J. I., Levison, W. H.: "Application of Optimal Control Theory to the Prediction of Human Performance in a Complex Task", Bolt, Beranek and Newman Inc. AFFDL-TR-81 1970
2. Kirchhoff, U.: "Beitrag zur Identifizierbarkeit des BBN-Modells und die Bedeutung des Modells als Beschreibungsform der Arbeitsweise des Menschen in teilautomatischen Flugführungssystemen" Dissertation, Technische Universtität Berlin 1978
3. McRuer, D., Jex, H. R.: "A Review of Quasi-Linear Pilot Model" IEEE Transaction onf Human Factors in Electronics Vol HFE-8 No. 3, 1967
4. Isermann, R.: "Prozessidentifikation", Springer-Verlag Berlin, Heidelberg, New York 1974
5. Schrick, K. W.: "Anwendung der Kalman-Filter-Technik" Oldenburg Verlag 1977
6. Stepner, D. E., Mehra, R.: "Maximum-Likelihood Identification and Optimal Input Design for Identifying Aircraft Stability and Control Derivatives", System Control Inc. NASA CR 2200 1973
7. Glover, K., Willems, J. C.: "Parametrizations of Linear Dynamical Systems" Canonical Forms and Identifyability", IEEE Transactions on Automatic Control Vol. AC-19, No. 6,1974
8. Denham, M. J.: "Canonical Forms for the Identification of Multivariable Linear Systems", IEEE Transactions on Automatic Control Vo. AC-19, No. 6, 1974
9. Ninz, N. R.: "Vergleichende Untersuchung von Identifikationsverfahren für Regler-Mensch-Modelle", Institut für Luft- und Raumfahrt, Technische Universität Berlin, ILR-Bericht Nr. 48, 1980

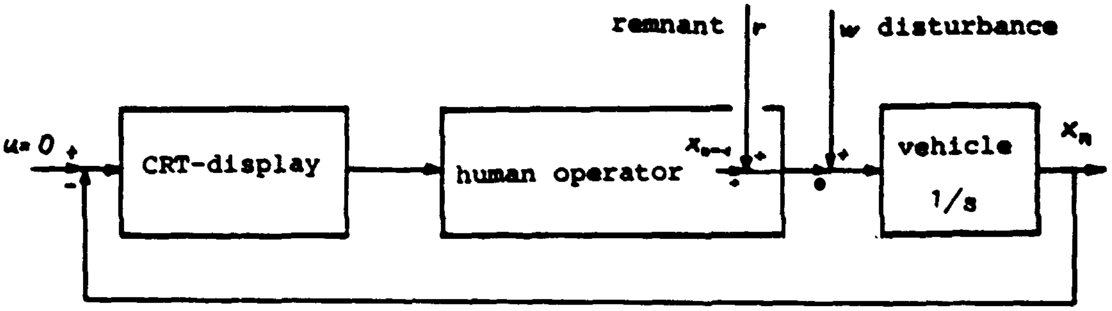
remnant
r
w
disturbance
u = 0
+
-
CRT-display
human operator
+
-
+
vehicle
1/s
x_n

Figure 1: Simulated man-machine-system

Label	frequency domain
MOD3	$\frac{K}{T_N j\omega + 1} \quad \frac{2 - \tau j\omega}{2 + \tau j\omega}$
MOD5	$\frac{K\ (2 - \tau j\omega)}{\frac{1}{\omega_n^2}(j\omega)^2 + \frac{2\ \zeta}{\omega_n} j\omega + 1)(2 + \tau j\omega)}$
MOD6	$\frac{K}{T_N\ j\omega + 1} \quad \frac{T_L\ j\omega + 1}{T_I\ j\omega + 1} \quad \frac{2 - \tau\ j\omega}{2 + \tau\ j\omega}$
MOD 8	$\frac{\{(L_1 M_1 + L_2 M_2) j\omega + L_2 (M_1 + 2M_2)\} (2 - \tau j\omega)}{\{[(j\omega + M_2)(T_N\ j\omega + 1) + L_2] + [M_1\ T_N\ j\omega + M_1 - M_1 L_1]\} (2 + \tau j\omega)}$

Fig. 2: Examinated versions of human operator models

ORIGINAL PAGE IS
OF POOR QUALITY

		EKF3	MAX3
Mean estimation error	$\lambda_r = 0\,\%$	7,5 %	4,6
	$\lambda_r = 5\,\%$	24 %	---
	$\lambda_r = 10\,\%$	21 %	---
	$\lambda_r = 20\,\%$	29 %	3,7
	$\lambda_r = 47\,\%$	---	5,1
Computing time on CD 6600		7h 20 min	200 sec for 10 Iterations
core-requirements (k-words)		12	16
parameter for remnant		no	covariance
required Starting values		9	4

Fig. 3 : Comparison of the Extended Kalman Filter with Maximum-Likelihood-Method

λ_r = Noise-to-Signal ratio of remnant to controlled variable

ORIGINAL PAGE IS
OF POOR QUALITY

		CCA 6 with FFT	MAX 6
Mean estimation error	$\lambda_r = 0\,\%$	13 %	12 %
	$\lambda_r = 5\,\%$	27 %	
	$\lambda_r = 10\,\%$	33 %	16 %
	$\lambda_r = 20\,\%$	67 %	10 %
Computing time on PDP 11/20		25 min	5h for 15 Iterations
core-requirements (k-words)		max 22 +)	20
parameter for remnant		Power-Density-Spectrum	covariance
required Starting values		5	6

Fig. 4: Comparison of cross-correlation analysis via FFT and Direct Search approximation with Maximum Likelihood-method

*) Several programms are initialized in sequence

Program	$\hat{K}$	$\hat{T}_N$	$\hat{T}_I$	$\hat{T}_L$	$\hat{\xi}$	$\hat{\omega}_n$	$\hat{\tau}$
MAX3	2,4	0,23					0,11
MAX5	2,5				1.	16,6	0,18
MAX6	2,5	0,23	0,21	0,19			0,1

Fig. 5: Results of the identification runs on human operator data with Maximum-Likelihood-method

N82 34046

A COMPUTER SIMULATION APPROACH TO MEASUREMENT OF HUMAN CONTROL STRATEGY

Joanne Green, Esther Lee Davenport,
Harold F. Engler, William E. Sears, III

Systems Engineering Laboratory
Engineering Experiment Station
Georgia Institute of Technology

This research has involved the development and testing of a psychologically-based computer simulation designed for measurement of strategy changes during the learning of continuous control behavior. Strategy in task performance is believed by many to be an important determinant of the quality of performance.[1,2,3] What comprises an individual's control strategy? First, as defined in this research, it includes criteria for behaviorial output in various aspects of the task. These criteria include subjective performance standards and criteria associated with the style of motor movements. Second, an individual's control strategy guides criteria for perceptual input. This includes selective attention to certain environmental cues. Finally, control strategy dictates how attention is allocated to mental processes. This includes a sequence for those mental processes which make high demands on mental resources, and hence cannot be performed in parallel. In summary, control strategy has been defined for this research as the set of parameters determining the functioning of mental processes important in manual control.

It has been suggested that variation in control strategy is the means by which the individual tailors his behavior to the demands of a specific task.[2] Thus, measurement of control strategy could permit identification of important individual differences among trainees. Control strategy is sensitive to the nature of environmental cues, and its measurement will allow better identification of the effects of these cues. This is especially important for the design of training simulators where the inclusion of a minimal set of critical cues can greatly increase cost-effectiveness.

The aim of the research is to measure human control strategy through use of a psychologically-based computer simulation which reflects a broader theory of control behavior. The simulation is called the human operator performance emulator, or HOPE. HOPE was designed to emulate control learning in a one-dimensional preview tracking task and to measure control strategy in that setting. When given a numerical representation of a track and information about current position in relation to that track, HOPE generates positions for a stick controlling the cursor to be moved along the track. In other words, HOPE generates control stick behavior corresponding to that which might be used by a person learning preview tracking.

The basic organization of HOPE is depicted in Figure 1. HOPE was designed to be consistent with the psychological literature on mental processes in continuous control. For example, in HOPE there is a distinction made between mental processes which demand considerable mental resources, such as performance monitoring and evaluation, and those pro-

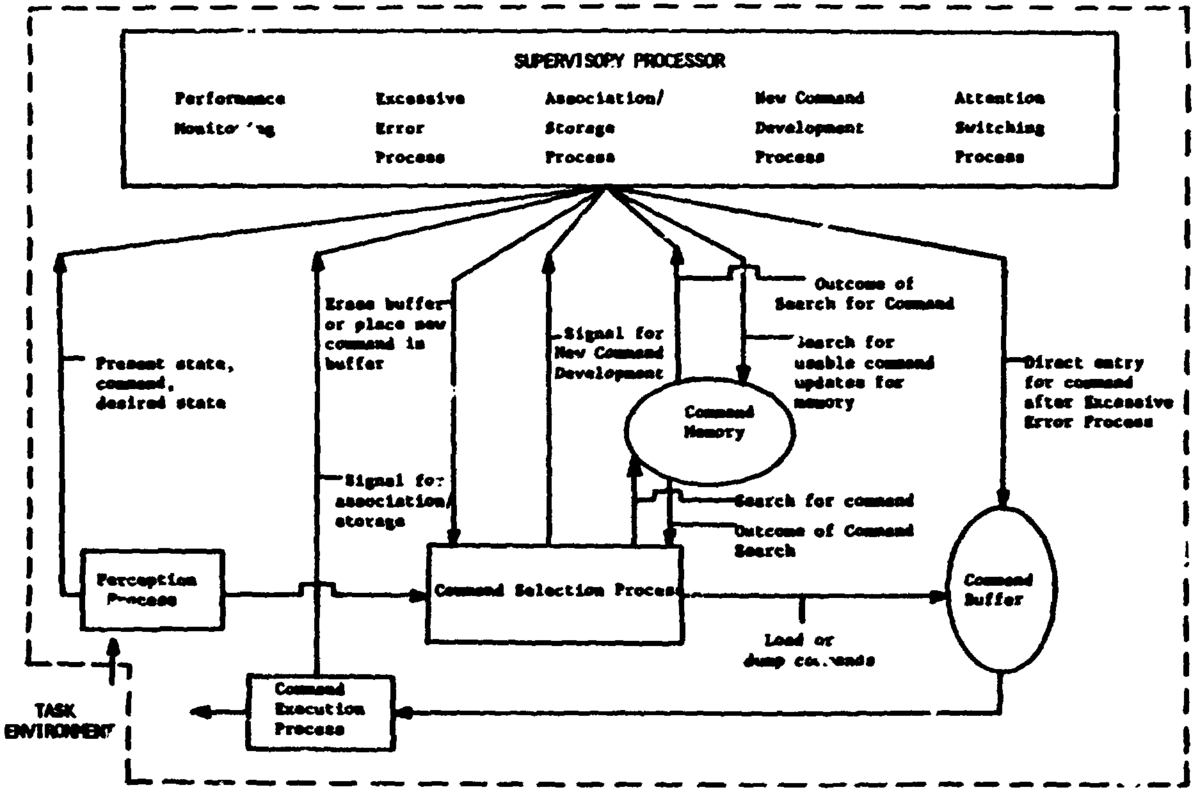
SUPERVISORY PROCESSOR
Performance Monitoring
Excessive Error Process
Association/ Storage Process
New Command Development Process
Attention Switching Process
Present state, command, desired state
Erase buffer or place new command in buffer
Signal for association/ storage
Signal for New Command Development
Outcome of Search for Command
Search for usable command updates for memory
Command Memory
Search for command
Outcome of Command Search
Direct entry for command after Excessive Error Process
Perception Process
Command Selection Process
Command Buffer
Load or dump commands
Command Execution Process
TASK ENVIRONMENT

Figure 1. Organization of the Human Operator Performance Emulator (HOPE)

cesses which demand minimal resources, such as execution of an already selected motor command.[4] In HOPE, processes believed to be mentally demanding are performed by the Supervisory Processor in a serial fashion. Less demanding processes, such as command execution or command selection, the accessing of a stored motor command, are done in a more parallel fashion. HOPE improves its performance by building a Command Memory describing control stick positions appropriate for moving between specific pairs of cursor positions. This feature allows HOPE to model learning and to model control of both linear and non-linear control dynamics.

Control strategy is represented in HOPE's operation by control strategy parameters which dictate how certain processes function. The current HOPE includes three control strategy parameters: Command Operative Time, ERRLIM, and ADJUST. Command Operative Time, or COT, is an upper limit on the frequency with which new control stick positions are selected, and affects, for example, Command Execution. It is sensitive to cues such as track frequency. Shorter Command Operative Times are more appropriate for more quickly varying tracks, where position must be changed more frequently. ERRLIM, a subjective performance standard, dictates the amount of cursor position error allowed before drastic action is taken to reduce position error. ERRLIM's value, either large or small, dictates whether the performance monitor in HOPE judges performance as acceptable. As ERRLIM grows larger, a larger position error is tolerated before major corrective action is taken. ADJUST, the third control strategy parameter, helps determine the magnitude of the corrective adjustment taken in response to excessive error. A large ADJUST represents more aggressive corrective action.

These control strategy parameters, Command Operative Time, ERRLIM, and ADJUST, represent aspects of human control strategy in the learning of a one-dimensional preview tracking task. How is HOPE used to measure human control strategy? Subjects are asked to perform a one-dimensional preview tracking task. Subjects are asked to use a control stick to keep a cursor on the center line of an apparently randomly curving track, scrolling down from the top of a screen. The cursor can be controlled only in the horizontal dimension, moving left and right. The plant dynamics are non-linear, and allow first order, position control of the cursor. As the subject performs this task, his control stick position is recorded every 40 msec.

HOPE operates on a numerical representation of the same track as that followed by the subjects. HOPE is run multiple times, each time using a different set of control strategy parameter values and generating a different pattern of control stick positions. Each run generates a HOPE model of human behavior and learning guided by a particular control strategy. Current testing involves generation of 100 models of behavior using all of the possible combinations of five values of COT, five values of ERRLIM and four values of ADJUST (see Figure 2).

FIGURE 2. HOPE GENERATION OF MODELS OF STRATEGY-CONTROLLED BEHAVIOR

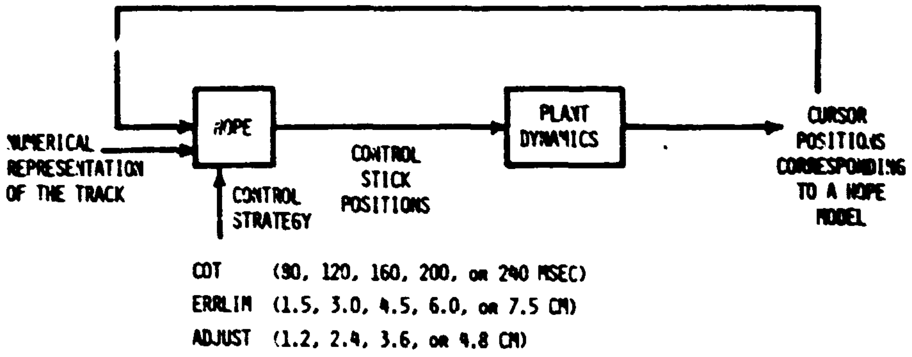
NUMERICAL REPRESENTATION OF THE TRACK
HOPE
CONTROL STRATEGY
CONTROL STICK POSITIONS
PLANT DYNAMICS
CURSOR POSITIONS CORRESPONDING TO A HOPE MODEL
COT (90, 120, 160, 200, OR 240 MSEC)
ERRLIM (1.5, 3.0, 4.5, 6.0, OR 7.5 CM)
ADJUST (1.2, 2.4, 3.6, OR 4.8 CM)

Human control stick positions in a given time interval are matched against each HOPE model's control stick positions for that same interval. The root mean square difference score is used to pick the HOPE model which best matches human behavior during that time interval. The values of the control strategy parameters modulating the HOPE model that best matches human behavior are identified as the human control strategy for that interval.

This approach to measurement using HOPE has received some validation testing, the results of which are quite encouraging. HOPE models are able to match human control stick behavior remarkably well. In preliminary and ongoing validation tests, HOPE models have succeeded in matching over 90% of the subject control stick behavior generated within 10% of the control stick's range of motion. Figure 3 illustrates the similarity of human and HOPE control behaviors, as well as the improvement in matching, when the control strategy in HOPE is permitted to vary. In addition to HOPE's ability to match human behavior, the human control strategies identified by HOPE have intuitive appeal in view of tracking requirements. For example, Figure 4 depicts the averages of the Command Operative Times measured for four subjects. These subjects had five, three-minute trials tracking a random track with a ½ Hz cut-off frequency. Then they tracked five trials of a random ¼ Hz cut-off frequency track, followed by five trials on the same ½ Hz track as they experienced earlier. Their measured Command Operative Times are longer on trials with the ¼ Hz track and shorter on trials with the ½ Hz track. These changes make sense in view of the more rapidly varying nature of the ½ Hz track.

Figure 3. Sample of control stick positions used by a subject during ten time bins of tracking and those used by (a) the HOPE model which best-matches human behavior during each 2 sec time bin, (b) those generated by a single HOPE model for the time frame tracked by the subject. The subject had experienced about 9.2 minutes of tracking a 1/4 Hz cut-off frequency track when this sample was taken.

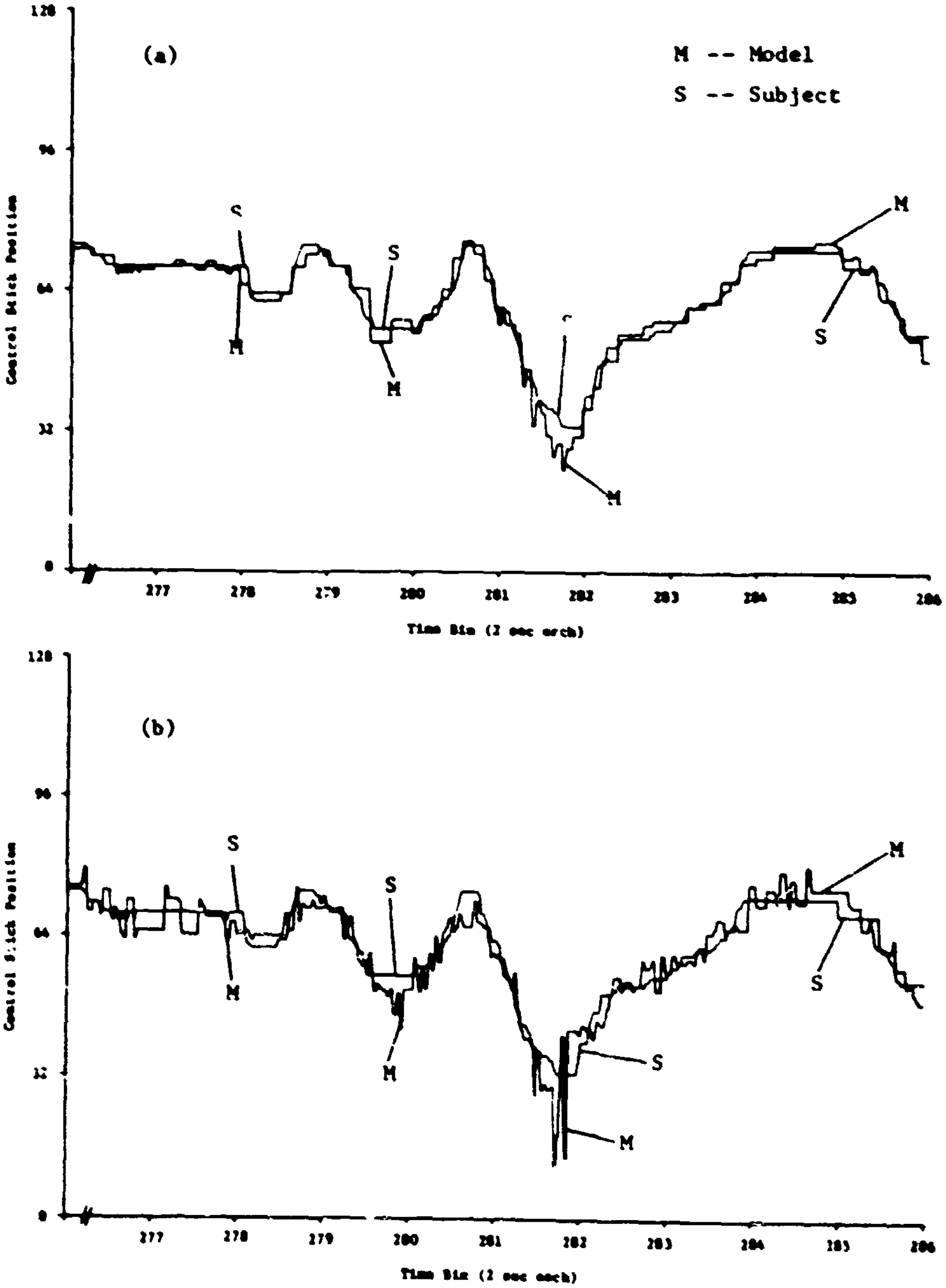

FIGURE 4. HOPE ESTIMATES OF HUMAN COMMAND OPERATIVE TIME FOR TWO TRACK CONDITIONS -- MEANS FOR A SAMPLE OF FOUR SUBJECTS ARE INDICATED & BRACKETED BY ONE STANDARD DEVIATION OF SUBJECT ESTIMATES AROUND THE MEAN.

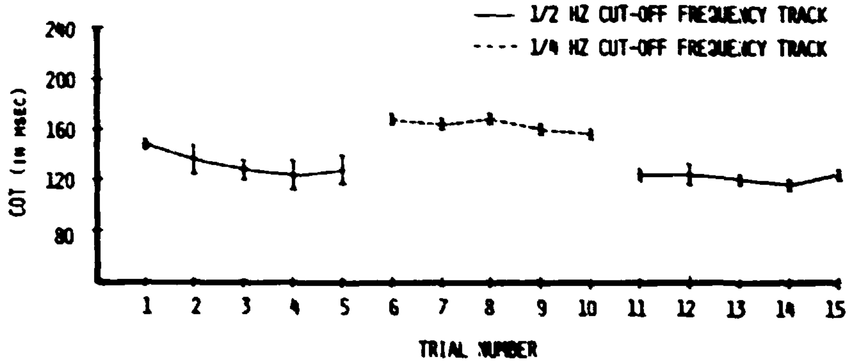

These results are encouraging and suggest that HOPE can provide a useful supplement to current measures of manual control behavior. HOPE has particular potential because it can measure behavior in a variety of conditions for which current models were not originally designed. In a new tracking environment, HOPE begins with no data on the form of plant dynamics or on the external forcing function, but builds up a representation of this knowledge from experience in the task in a way that is representative of human learning. Since HOPE models the learning of control dynamics, it can be used to measure the control strategy of both trained and untrained operators. HOPE models preview tracking behavior, an important instance of control behavior largely unaddressed by other current models. Finally, and most importantly, HOPE can model and measure a rich, psychologically meaningful representation of human control strategy. Measurement of control strategy through use of HOPE has great potential for improving our understanding of the changes in behavior that occur during training, for allowing us to describe individual differences in behavior, and for aiding the design of effective training of control behavior, and for providing insight into how unobservable mental processes and structures are operating.

References

1. Welford, A. T. Fundamentals of Skill. London: Methuen & Company, Ltd., 1968.
2. Moray, N. The strategic control of information processing. In G. Underwood (Ed.), Strategies of Information Processing. New York: Academic Press, 1978.
3. Poulton, E. C. Tracking Skill and Manual Control. New York: Academic Press, 1974.
4. Kerr, B. Processing demands during mental operations. Memory and Cognition, 1973, 1, 401-412.

N82 34047

ORIGINAL PAGE IS
OF POOR QUALITY

PILOT MODEL HYPOTHESIS TESTING

John R. Broussard
Information & Control Systems, Inc.
28 Research Drive
Hampton, Virginia 23666

Paul W. Berry
The Analytic Sciences Corporation
Six Jacob Way
Reading, Massachusetts 01867

ABSTRACT

The optimal control model of a human pilot has been used in previous studies in an attempt to model and understand a pilot's discretionary behavior in departure-prone maneuvering tasks for a fighter aircraft. When the pilot model's internal model of the aircraft's dynamic response is different from the actual aircraft dynamics, pilot-aircraft instabilities can be pedicted that are very similar to observed piloting difficulties. This paper attempts to verify the predictions and conclusions of the previous studies by rigorous analysis of the aircraft control time history predicted by the optimal control pilot model and actual pilot tracking data obtained from NASA Langley's Differential Maneuvering Simulator (DMS). The analysis is performed using a hypothesis testing scheme modified to allow for changes in the true hypothesis. A finite number of pilot models, each with different hypothesized internal model representations of the aircraft dynamics, are constructed. The hypothesis testing scheme determines the relative probability that each pilot model best matches the DMS data. By observing the changes in probabilities, it is possible to determine when the pilot changes control strategy and which hypothesized pilot model best represent's the pilot's control behavior.

INTRODUCTION

When a pilot controls and monitors an aircraft, it is recognized ([1], [2]) that the pilot uses an internal model of the system to determine a control strategy. The assumption of a perfect internal model appears to be satisfactory in many instances where the pilot has mastered the skills necessary to execute maneuvers with precision. There are situations, however, in which the pilot's internal model can differ significantly from the aircraft's dynamics. Examples of these situations include rapid maneuvering, which causes significant changes in the aircraft's angle of attack, and component failures.

The optimal control pilot model is a complex optimal control system which has been shown to capture fundamental aspects of human operator control behavior ([3], [4]) and is constructed using a perfect internal model of the system being controlled. Previous studies ([5], [6]) have investigated the use of the optimal control pilot model to investigate the effects of an internal model mismatch by the pilot in an effort to predict piloting difficulty. In [5] and [6], the effect of internal model variation was studied along a wind-up turn maneuver. The angle of attack of the piloted aircraft increases significantly along the wind-up turn maneuver. Six results about pilot-aircraft stability were obtained in the study: (1) The pilot model easily stabilized the aircraft throughout the maneuver using a perfect internal model of the aircraft dynamics; (2) If the pilot model is controlling the bare frame* using only lateral and longitudinal stick, the pilot-aircraft system has a divergence instability (unstable sprial mode) if the pilot model keeps a low α_0 (below 12 deg α_0) flight condition internal model of the aircraft while the aircraft's actual flight condition exceeds 16 deg α_0; (3) The pilot model can compensate for control difficulties beyond 16 deg α_0 without changing the low α_0 internal model by using lateral stick and pedals; (4) Difficulties can still occur beyond 25 deg α_0 using stick and pedals if the pilot model keeps a low α_0 control strategy; (5) If only pedals are used, no difficulties are encountered up to 30 deg α_0 when the pilot model keeps a low α_0 internal model of the aircraft; (6) If a particular aileron-rudder interconnect system is activated, the pilot-aircraft divergence instability is eliminated, but the Dutch roll mode can become unstable. These results tend to agree with observed behavior of a human pilot flying the aircraft with the SAS off.

The research reported in this paper attempts to validate the approach used to investigate the above problem. Additionally, the use of the optimal control pilot model to determine when changes in the internal model of the pilot occur is investigated. The method used to perform the analysis is a hypothesis testing scheme developed in [7] and [8] and outlined in the paper. For a finite number of pilot models, each with a different hypothesized internal model of the aircraft, the hypothesis testing scheme determines the relative probability that each pilot model best matches recorded pilot data. The changes in probability give an indication of the pilot's actual adaptive control procedure.

The pilot data used in the hypothesis testing scheme is obtained from one NASA Langley pursuit-tracking simulation using their Differential Maneuvering Simulator (DMS). The DMS consists of an enclosed hemispherical screen within which a pilot sits in a cockpit mock-up. The pilot views a computer-controlled display of a tracking situation on the screen. The pilot generates control commands which drive the nonlinear computer model of the aircraft. The computer portrays the resulting aircraft motions on the screen as viewed by the pilot.

The pilot model hypothesis testing scheme discussed in the paper is very general and is not restricted to investigating situations where the pilot model's internal model varies. Any situation in which there is more than one choice for a pilot model parameter can be tested to determine which pilot model best matches the data. This capability is also demonstrated in this paper using different choices for the optimal control pilot model's cost function quadratic weights.

---

*The stability augmentation system (SAS) is off and an aileron-rudder interconnect system (ARI) is not operating.

OPTIMAL CONTROL PILOT MODEL

This section briefly reviews the elements of the optimal control pilot model to be used in hypothesis testing. The optimal control pilot model for which detailed mathematical development can be found in [5] is based on the premise that a motivated, well-trained human controls a system optimally. To construct the pilot model, the assumptions needed to specify an optimal controller are formulated, then modified to reflect basic human characteristics and limitations. The hypothesis testing scheme requires an analytic pilot model, hence, the pure time delay in the optimal control model representing the human's lumped time delay is replaced by its Padé approximation. The straightforward solution for the optimal control pilot model with the Padé approximation is given in [9]. A block diagram is shown in Fig. 1. The mathematical representation is

$$\begin{bmatrix} \Delta\dot{\underline{u}} \\ \Delta\dot{\hat{\underline{x}}}_E \\ \Delta\dot{\underline{z}} \end{bmatrix} = \begin{bmatrix} -R_L & (C00) & 0 \\ & F_E-KH_E & \frac{4}{\tau}K \\ 0 & 0 & -\frac{2}{\tau}I \end{bmatrix} \begin{bmatrix} \Delta\underline{u} \\ \Delta\hat{\underline{x}}_E \\ \Delta\underline{z} \end{bmatrix} + \begin{bmatrix} 0 \\ -K \\ I \end{bmatrix} \Delta\underline{y} + \begin{bmatrix} \Delta\underline{v}_u \\ -K\Delta\underline{v}_y \\ \Delta\underline{v}_y \end{bmatrix} \qquad (1)$$

The n-vector, $\Delta\underline{x}(t)$ in Fig. 1, represents the perturbation aircraft dynamics, aircraft sas states, tracking error states, and target states for which a more detailed discussion is given later. The aircraft's stick inputs are represented by the m-vector $\Delta\underline{u}(t)$; $\underline{w}(t)$ represents white Gaussian noise disturbances affecting the aircraft model dynamics as perceived by the pilot. The pilot's observations, $\Delta\underline{y}(t)$, are degraded by zero mean white Gaussian noise, $\Delta\underline{v}_y(t)$, then processed by a lead-lag network which is a Padé approximation to the pilot time delay. The resulting signal is the measurement vector for the pilot model's Kalman filter which generates a best estimate ($\Delta\hat{\underline{x}}_E$ in (1)) of the states controls, and lagged observation states. The state estimate component of $\Delta\hat{\underline{x}}_E$ is multiplied by the pilot model's state feedback matrix, C, to form the pilot model's internal control command, $\Delta\underline{u}_C(t)$. A special quadratic cost functional is used to find the linear-optimal regulator gain C. The command is corrupted with additive, zero-mean white, Gaussian noise, $\Delta\underline{v}_u(t)$ which together form the input to the neuromuscular dynamics model which represents the human's neuromotor bandwidth limitation. The output is the pilot model's aircraft control, $\Delta\underline{u}(t)$ which drives the aircraft model's control actuators. The matrix, K in (1), is the pilot model's Kalman filter gain. The filter gain, K, depends upon input signal levels, neuromotor noise levels, and observation noise levels; the latter are related to the former by constant noise-to-signal ratios. The matrices K and C are determined by solving Riccati equations which depend on the pilot's internal description of the aircraft. The pilot model is unadapted when the internal model description of the aircraft used to determine the pilot model is not the same as the mathematical model of the aircraft at the flight condition under investigation.

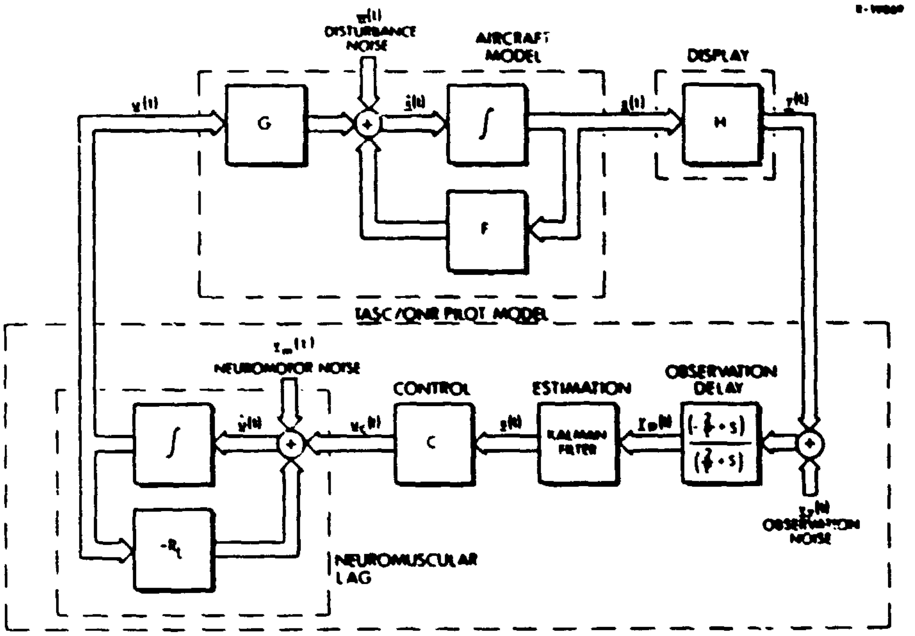
DISTURBANCE NOISE
$\underline{w}(t)$
AIRCRAFT MODEL
DISPLAY
$\underline{u}(t)$
G
$\dot{\underline{x}}(t)$
$\int$
$\underline{x}(t)$
H
$\underline{y}(t)$
F
IASC/ONR PILOT MODEL
$\underline{v}_m(t)$
NEUROMOTOR NOISE
CONTROL
ESTIMATION
OBSERVATION DELAY
$\int$
$\dot{\underline{u}}(t)$
$\underline{u}_c(t)$
C
$\hat{\underline{x}}(t)$
KALMAN FILTER
$\underline{y}_p(t)$
$\frac{(-\frac{2}{\tau}+s)}{(\frac{2}{\tau}+s)}$
$-R_L$
$\underline{v}_y(t)$
OBSERVATION NOISE
NEUROMUSCULAR LAG

Figure 1 Block Diagram of the Pilot Model Containing the Padé Approximation to Pure Time Delay

In order to use (1) in hypothesis testing, a discrete time representation is required. Assuming that a sampling interval, Δt, is chosen small enough so that Δy is essentially constant over the interval, the discrete representation of the pilot model is

$$\Delta\underline{x}_{k+1} = \Phi_{PM}\,\Delta\underline{x}_k + \Gamma_{PM}\,\Delta\underline{y}_k + \Delta\underline{w}_k \qquad (2)$$

where

$$\Phi_{PM} = e^{F_{PM}\Delta t} \;;\; \Gamma_{PM} = \int_0^{\Delta t} e^{F_{PM}t}\,dt\,K_{PM} \qquad (3)$$

$$\Delta\underline{x}^T = [\Delta\underline{u}^T,\ \Delta\hat{\underline{x}}_E^T,\ \Delta\underline{z}^T] \quad ; \quad K_{PM}^T = [0 \quad -K^T \quad I] \qquad (4)$$

$$E\{\Delta\underline{w}_k\Delta\underline{w}_k^T\} = W_{PM} = \int_0^t e^{F_{PM}t}\,Q_{PM}\,e^{F_{PM}^Tt}\,dt \qquad (5)$$

The matrix F_{PM} is the system matrix in (1) while Q_{PM} is the covariance of the noise vector driving the dynamics in (1).

HYPOTHESIS TESTING

The hypothesis testing philosophy for investigating pilot control adaptation in flight is to construct a number of pilot models, each using different internal models, and then determine which pilot model best represents the actual pilot control behavior. The hypothesis testing procedure, illustrated in Fig. 2, is based on a model structure identification algorithm (see [7] and [8]) modified to allow for changes in the true hypothesis.

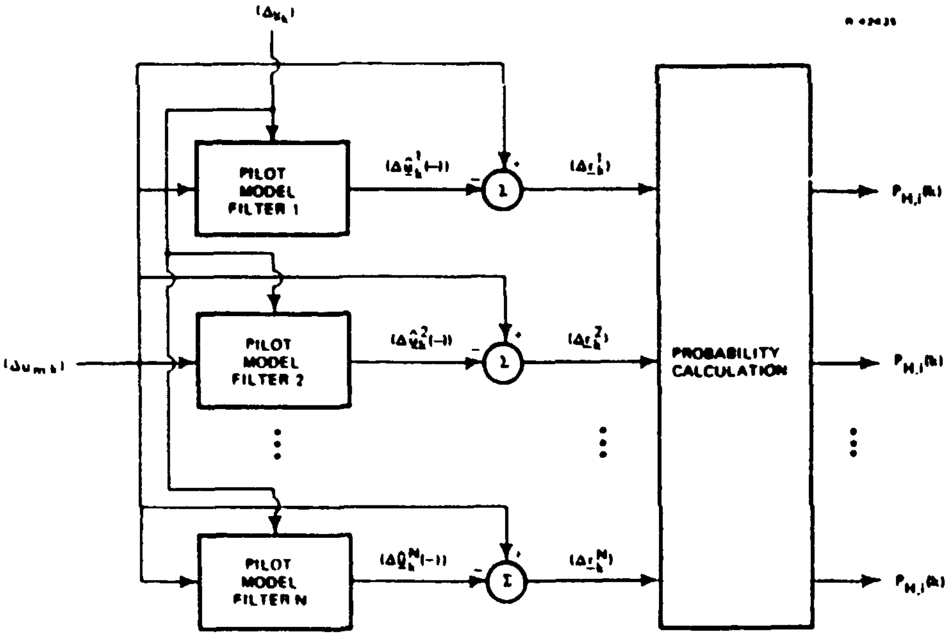
{Δy_k}
{Δu_m,k}
PILOT MODEL FILTER 1
PILOT MODEL FILTER 2
PILOT MODEL FILTER N
{Δŷ_k^1(-)}
{Δŷ_k^2(-)}
{Δŷ_k^N(-)}
Σ
{Δr_k^1}
{Δr_k^2}
{Δr_k^N}
PROBABILITY CALCULATION
P_H,i(k)
P_H,i(k)
P_H,i(k)

Figure 2 Kalman Filter Approach to Pilot Control Strategy Hypothesis Testing

The notation used in the figure is as follows:

$\Delta \underline{u}_{m,k}$: measured value of pilot perturbation control at t_k

$\Delta \underline{y}_k$: measured values of perturbation states assumed observed by the pilot

$\Delta\hat{\underline{u}}^i_k(-)$: one-step predicted value of $\Delta\underline{u}_{m,k}$ based upon $\{\Delta\underline{u}_{m,1},\ldots,\Delta\underline{u}_{m,k-1}\}$ and $\{\Delta\underline{y}_1,\ldots,\Delta\underline{y}_{k-1}\}$ for the ith pilot model Kalman filter

$\Delta\underline{r}^i_k$: one-step predicted residual at the kth step for the ith pilot model Kalman filter

$P_{H,i}^{(k)}$: probability that the ith pilot model is best, based upon knowledge of $\{\Delta\underline{u}_{m,1},\ldots,\Delta\underline{u}_{m,k-1}\}$ and $\{\Delta\underline{y}_1,\ldots,\Delta\underline{y}_{k-1}\}$

Mathematically, the hypothesis testing scheme is implemented by viewing each pilot model represented in (2) as a dynamic system whose input is the pilot observation vector, $\Delta\underline{y}_k$, with process noise, $\Delta\underline{w}_k$, and whose measurement output vector is the actual measured pilot control (m×1) vector,

$$\Delta\underline{u}_{m,k} = [I \quad 0 \quad 0] \quad \Delta\underline{x}_k + \underline{v}_k \tag{6}$$

$\underline{v}_k$ is a zero-mean gaussian measurement noise with covariance V. The ith pilot model Kalman filter shown in Fig. 2 using the ith pilot model as the plant and the control measurements as the observation vector is constructed as

$$\Delta\hat{\underline{x}}^i_k(+) = \Delta\hat{\underline{x}}^i_k(-) + K^i_H\left[\Delta\underline{u}_{m_k} - \Delta\hat{\underline{u}}^i_k(-)\right] \tag{7}$$

$$\Delta\hat{\underline{x}}^i_{k+1}(-) = \Phi^i_{PM}\,\Delta\hat{\underline{x}}^i_k + \Gamma^i_{PM}\,\Delta\underline{y}_k \tag{8}$$

$$K^i_H = P^i(-)\begin{bmatrix} I \\ 0 \\ 0 \end{bmatrix}\left\{[I \quad 0 \quad 0]\; P(-)\begin{bmatrix} I \\ 0 \\ 0 \end{bmatrix} + V\right\}^{-1} \tag{9}$$

$$P^i(-) = \Phi^i_{PM} P^i(+) \Phi^{iT}_{PM} + W^i_{PM} \tag{10}$$

$$P^i(+) = [I - K^i_H\,[I \quad 0 \quad 0]]\; P^i(-) \tag{11}$$

In this application, the above Kalman filter is assumed to be in steady state. If the ith pilot model is correct, the filter residuals

$$\Delta\underline{r}^i_k = \Delta\underline{u}_{m,k} - \Delta\hat{\underline{u}}^i_k(-) \tag{12}$$

are a zero-mean white gaussian noise sequence with covariance

$$E\{\Delta \underline{r}_k^i \Delta \underline{r}_k^{iT}\} = [I \quad 0 \quad 0] \quad P^i(-) \begin{bmatrix} I \\ 0 \\ 0 \end{bmatrix} + V = S^i \tag{13}$$

If the pilot model is not correct, then $\Delta\underline{r}_k^i$ may not be a white gaussian noise sequence and does not satisfy (13). The pilot model Kalman filter just described is not to be confused with the internal Kalman filter in the pilot model.

For notational purposes, let

$$U_k = \{\Delta\underline{u}_{m,1}, \ldots, \Delta\underline{u}_{m,k}\} \tag{14}$$

Applying Bayes' rule, it is shown in [8] and [9] that one can write:

$$P_{H,i}(k) = \frac{P(\Delta\underline{u}_{m,k} | H,i,U_{k-1}) P_{H,i}(k-1)}{\sum_{i=1}^{N} P(\Delta\underline{u}_{m,k} | H,i,U_{k-1}) P_{H,i}(k-1)} \tag{15}$$

Using the fact that $\Delta\underline{w}_k$ is assumed to be a zero-mean gaussian sequence, along with the assumption that the Kalman filter state vector $[\Delta\underline{u}^T(-), \Delta\hat{\underline{x}}_E^{iT}(-), \Delta\underline{z}^T(-)]^T$ is also gaussian, it follows that

$$P(\Delta\underline{u}_{m,k} \; H,i,U_{k-1}) \simeq \frac{1}{(2\pi)^{m/2} |\det S^i|^{1/2}} e^{-\frac{1}{2}(\Delta\underline{r}_k^i)^T (S^i)^{-1} (\Delta\underline{r}_k^i)} \tag{16}$$

At each time interval, the measured pilot control is used to compute the residual in (12). The residual and (13) are used to compute the probability in (16). The probability is used in (15) to recursively update the probability that pilot model i best matches the data. The residual and measured values of states assumed observed by the pilot are used to update the Kalman filter in (7) and (8) and the process is repeated with the next control measurement.

The solution to the problem of computing the $P_{H,i}(k)$ when the true hypothesis changes with time is given in [10]. Under certain simplifying assumptions it can be shown that the solution requires N^2 parallel filters to discriminate between the N possible hypothesis at any given time. Since this may impose an excessive computational burden, an efficient suboptimal approach to the problem is developed in [8]. The suboptimal approach is nearly optimal in situations where the probability of switching hypotheses at any given time is low. The suboptimal approach is derived by noting that if the ith pilot model is true then the recursive calculation in (15) causes $P_{H,i}$ to approach 1. If $P_{H,i}$ should equal one, it will remain "trapped" at one regardless of changes in the pilot's control strategy. To prevent this, each probability is checked at each time instant to determine if it has fallen below some minimum value ε. If any probabilities are smaller than ε, they are reset to ε and the other probabilities are suitably modified so that they all sum to one. This procedure can be implemented with only N parallel filters. Results presented later in this paper, using $\varepsilon=0.05$, indicate that this suboptimal procedure is effective in detecting changes in the true hypothesis.

FLIGHT TEST SELECTION

The simulated flight test selected for study in a wind-up turn tracking task implemented on the NASA-Langley Differential Maneuvering Simulator (DMS). The pilot is instructed to track a target aircraft which is displayed on a large hemi-spherical screen, within which the cockpit is mounted. A sky-earth representation is also displayed. The target aircraft's trajectory is prestored. There are no intentional disturbances affecting either the target aircraft or the piloted aircraft, although the prestored target trajectory exhibits rapid and continuous maneuvering. The pilot is flying a complete nonlinear computer model of a high performance fighter.

The pilot is instructed not to use rudder pedals. Lateral-directional control by the pilot is accomplished using only lateral stick. The simulation is performed with the pitch and yaw SAS operational, although the roll Command Augmentation System (CAS) is off. The yas SAS improves the lateral-directional stability of the aircraft at high angles of attack. This means that the stability boundaries of the bare-aircraft determined in [5] and [6] cannot be used directly to evaluate pilot performance and the performance of the hypothesis testing scheme. The SAS states also have to be included in the aircraft model increasing the dimension of the problem.

The view through the cockpit which is useful in constructing the tracking error equations is shown in Fig. 3. The vertical and lateral components of tracking error are ε_n and ε_v, respectively, which the pilot can directly perceive. The difference between the pilot's fixed pipper and the aircraft's velocity vector are the angle of attack, α, and sideslip angle, β, which the pilot cannot directly perceive. The difference between the aircraft's stability-axis roll angle, ϕ_v, and the stability-axis roll angle of the target, ϕ_{vT}, is $\delta\phi_v$ and is directly perceived by the pilot. The pilot does not have any motion cues. Any computational time delay in the DMS between the pilot's stick movement and changes on the screen is assumed to be small and is not modeled in the analysis. A complete record of the aircraft state and control histories is recorded at 32 samples per second. Additionally, the tracking angles and range to the target are recorded, and target motion is inferred from these measurements. The aircraft measurements are computer generated and together with the pilot's control movements have virtually no measurement noise. This implies that V in (6) is zero and the process noise in (1) contains no contribution from possible measurement noise errors in $\Delta \underline{y}$.

The wind-up turn tracking task lasted 90 sec. At 50 sec into the run, the pilot is forced to saturate lateral stick almost continuously in order to continue tracking. Because of this, only the first 40 sec of the

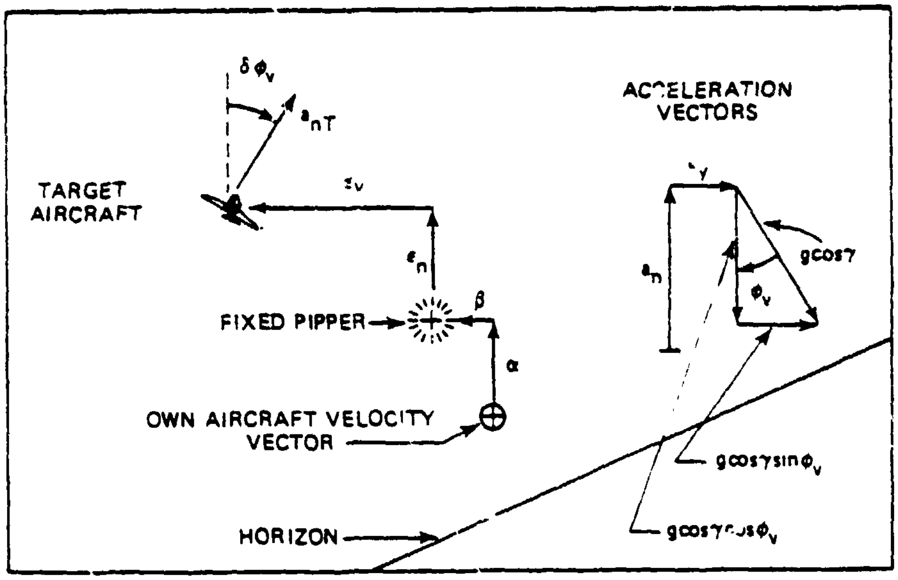
$\delta\phi_v$
a_{nT}
TARGET AIRCRAFT
ϵ_v
ϵ_n
FIXED PIPPER
β
α
OWN AIRCRAFT VELOCITY VECTOR
HORIZON
ACCELERATION VECTORS
a_y
a_n
$g\cos\gamma$
ϕ_v
$g\cos\gamma\sin\phi_v$
$g\cos\gamma\cos\phi_v$

Figure 3 Pursuit-Tracking Task View Through the Cockpit

run are analyzed. Only the lateral-directional dynamics are investigated with the pilot model.

Variations of angle of attack are shown in Fig. 4 for the 40 sec interval. The aircraft remains at a low angle of attack flight condition for the first 10 seconds. then the aircraft angle of attack increases to a maximum of 21 deg as the aircraft enters the wind-up turn. Using the aircraft time histories shown in Fig. 4, the pilot model hypothesis test can be well posed: when the angle of attack of the aircraft increases beyond 5 deg, significantly changing the aircraft's dynamics, does the pilot's control behavior remain fixed to a 5 deg α_o strategy or does the pilot change his strategy to match the aircraft's changing dynamics? To begin answering this question, the model of the aircraft-target dynamics and the pilot model parameters are presented in the next two sections, respectively.

TRACKING TASK MODEL

The tracking task model is composed of four components at the adaptation point; the linearized dynamics of the subject aircraft, the SAS dynamics, the linearized tracking error dynamics, and the linearized target model. A derivation of the models is presented in [9]. A summary of all the linearized models is given in Table 1.

The tracking task model is typical of air-to-air combat models discussed in [11] and [12]. In both references the aircraft models are simplified linear time-invariant longitudinal dynamics implemented on simulators. Simple target dynamics are used both in the simulation and the model. In

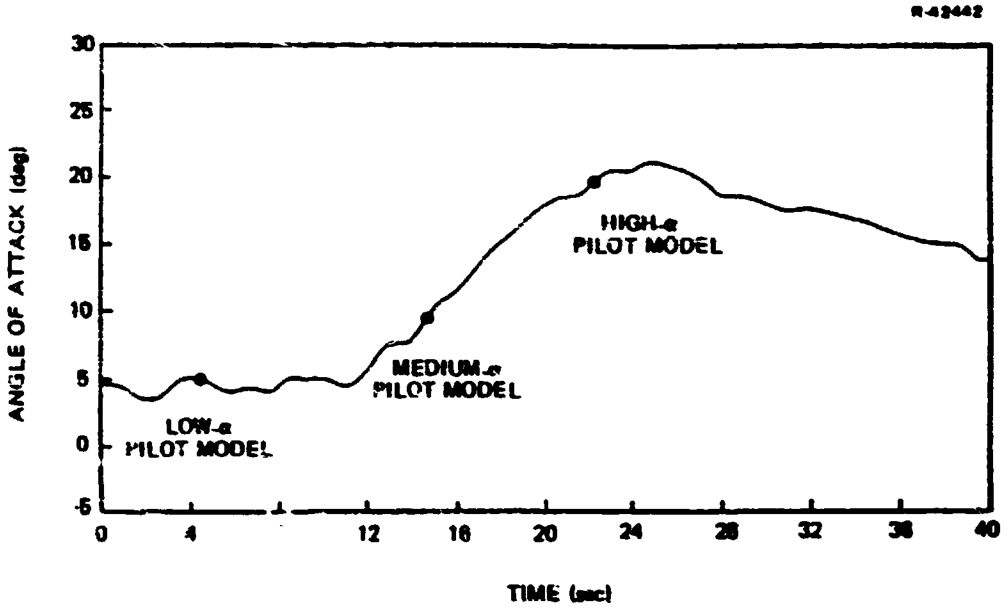

Figure 4 Angle of Attack Time History

this case, the use of the complete target aircraft model (another fighter aircraft) in the tracking task model is infeasible. An approximation whereby only the target aircraft states Δp_{wT} and $\Delta\phi_{vT}$ are modeled in the tracking task model is made. Unmodeled target dynamics are lumped into a zero mean gaussian noise term Δw_T which drives Δp_{wT}, as shown in 4, Table 1. The implication is that the human has no explicit information about the dynamics driving Δp_{wT} and also regards the effect as white noise. The parameters in the simplified target model in Table 1 are determined by identification based on measured values of ϕ_{vT} as discussed in [9]. The values used are $a_1=-4.4$, $a_2=1.6$ and $E\{w_T^2\}=4.0$ (deg^2/sec^2).

PURSUIT TRACKING PILOT MODEL PARAMETERS

The parameters yet to be specified at this point are the pilot observations, the flight conditions, a choice of the pilot model's quadratic state weighting matrix and the standard parameters of the pilot model. The flight conditions are a priori specifications of aircraft-target dynamics along the maneuver under investigation at which the pilot may formulate a control strategy.

From Fig. 3, the pilot observations are the lateral error, $\Delta\epsilon_y$, and the stability-axis roll angle error, $\Delta\hat{\phi}_v$. As is customary in the optimal control model, the rates of these states are also assumed observed. From

TABLE 1
LINEARIZED TRACKING MODEL DYNAMICS

1. Bare Aircraft Dynamics $\Delta\dot{\underline{x}}_a = F_a \Delta\underline{x}_a + G_a \Delta\underline{u}_a$ $\Delta\underline{u}_a = K_1 \Delta\underline{u}_p + \Delta\underline{u}_{SAS}$	F_a, G_a Linearized aircraft matrices $\Delta\underline{x}_a$ Aircraft states Δv, lateral body-axis velocity, Δr, body-axis yaw rate, Δp, body-axis roll rate and $\Delta\phi_v$ stability-axis roll angle $\Delta\underline{u}_a$ Aircraft controls $\Delta\delta_{sp}$, spoilers, $\Delta\delta_{ds}$, differential stabilators and $\Delta\delta r$, rudder $\Delta\underline{u}_p$ Pilot's lateral stick control
2. SAS Dynamics $\Delta\underline{u}_{SAS} = K_2\Delta\underline{x}_a + K_3 \Delta\underline{u}_a + K_4 \Delta\underline{x}_{SAS}$ $\Delta\dot{\underline{x}}_{SAS} = F_{SAS} \Delta\underline{x}_{SAS} + G_{SAS}\Delta\underline{x}_a$	$\Delta\underline{u}_{SAS}$ Stabilization commands from SAS to aircraft controls F_{SAS}, G_{SAS} Dynamical representation of the SAS yaw rate wash-out filter given by $\Delta\delta_{r,SAS} = k_1\Delta a_y - \Delta r - \Delta x_{SAS}$ $\Delta\dot{x}_{SAS} = -\frac{1}{\tau}\Delta x_{SAS} + \frac{1}{\tau}\Delta r$ τ Wash-out filter time constant
3. Tracking Error Dynamics $\Delta\dot{\epsilon}_y = K_5\Delta\underline{x}_a + K_6\Delta\underline{u}_a + K_7 \Delta\underline{x}_T$	Represents the equation $\Delta\dot{\epsilon} = -\frac{a_{nT_0}}{V_0}(\Delta\phi_{vT} - \Delta\phi_v) + \frac{\Delta a_y}{V_0} - \Delta\beta$ a_{nT_0} Target's nominal normal acceleration V_0 Aircraft's nominal velocity a_y Inertial lateral acceleration expressed in body axis
4. Target Model $\Delta\dot{\underline{x}}_T = F_T \Delta\underline{x}_T + G_T\Delta\underline{w}_T$	Represents the equation $\begin{bmatrix}\Delta\dot{p}_{vT}\\ \Delta\dot{\phi}_{vT}\end{bmatrix} = \begin{bmatrix}a_1 & a_2\\ 1 & 0\end{bmatrix}\begin{bmatrix}\Delta p_{vT}\\ \Delta\phi_{vT}\end{bmatrix} + \begin{bmatrix}\Delta w_T\\ 0\end{bmatrix}$ $\Delta\phi_{vT}$ target stability-axis roll angle Δp_{vT} target stability-axis roll rate

Fig. 4, three flight conditions which primarily differ in angle of attack are chosen to form the pilot's internal model: low (α_0=5.2 deg), medium, (α_0=9.3 deg) and high (α_0=19.2 deg).

The quadratic cost function weights used to construct the pilot model quantify the pilot's tradeoff of tracking error and control effort. High weights imply that the pilot expends significant control effort in order to minimize tracking error. He can be said to be a "high-gain" or "tight" pilot. On the other hand, low quadratic weights typify a "low-gain" or "loose" piloting technique. The specific values for the state quadratic weights used in the tests reported here are given in Table 2. The tracking error rate weight in the pilot model's cost function is chosen to be one-fourth of the tracking error weight, as suggested in Ref 11. Based on plots

ORIG
OF POO

of these states during the maneuver, lateral velocity is weighted and $\Delta\phi_v$ variations rather than $\Delta\delta\phi_v$ variations are weighted in the cost function. At the low α_0 and medium α_0 flight conditions in Table 2, a high weight, cost function (2), and a low weight, cost function (1), are specified. The rest of the pilot model parameters are standard (human perceptual time delay of 0.2 sec, neuromuscular time constant of 0.1 sec, observation noise to signal ratio of -20 db and a neuromotor noise to signal ratio of -30 db).

TABLE 2
SQUARE ROOT OF PILOT MODEL COST FUNCTION WEIGHTS

AIRCRAFT ANGLE OF ATTACK	COST FUNCTION	LATERAL VELOCITY	ROLL ANGLE	TRACKING ERROR	TRACKING ERROR RATE
5.2	1	0.25	0.50	5.0	1.25
5.2	2	0.50	1.00	10.0	2.5
9.3	1	0.25	0.25	5.0	1.25
9.3	2	0.25	0.25	10.0	2.5
19.5	1	0.25	0.25	5.0	1.25

The resulting pilot model feedback gain elements are shown in Table 3. The gains exhibit little change when the cost function changes between 1 and 2. The pilot model control gains at α_0=5.2 deg and α_0=9.3 deg are somewhat different, while the high α_0 versus low α_0 pilot model gain are significantly different. These differences indicate the hypothesis testing scheme should be able to make a clear decision between the high and low α_0 strategies.

HYPOTHESIS TESTING RESULTS

This section presents the results from the hypothesis testing scheme in two formats. In the first format, the one-step predicted pilot model control time history is overlaid on the actual pilot's lateral stick control time history. The closer these two trajectories match, the better the indication is that the assumed pilot model is correct. The second format is composed of plots of the probabilities that each pilot model is the best of those tested. The first format gives an absolute indicate of pilot model performance while the second format gives a relative indication of performance between the pilot models.

Hypothesis testing procedure and the accompanying Kalman filter require perturbation variables, $\Delta\underline{u}_{m,k}$ and $\Delta\underline{y}_k$, but only total values, $\underline{u}_{m,k}$

TABLE 3
PILOT MODEL LATERAL STICK GAINS

T-3124

AIRCRAFT ANGLE OF ATTACK	COST FUNCTION	SIDE VELOCITY $\partial\delta/\partial v$	YAW RATE $\partial\delta/\partial r$	ROLL RATE $\partial\delta/\partial p$	ROLL ANGLE $\partial\delta/\partial\phi$	TRACKING ERROR $\partial\delta/\partial\epsilon$	TARGET ROLL RATE $\partial\delta/\partial P$	TARGET ROLL ANGLE $\partial\delta/\partial\phi_{wT}$	SAS $\partial\delta/\partial\delta_{SAR}$
5.2	1	-1.69	-9.51	2.44	4.98	51.9	-1.22	-5.60	7.38
5.2	2	-1.72	-9.64	2.47	5.05	52.8	-1.24	-5.70	7.53
9.3	1	-1.45	-10.63	3.59	5.08	44.7	-0.787	-4.68	-1.25
9.3	2	-1.38	-14.85	3.77	4.18	48.5	-0.587	-4.01	-3.96
19.2	1	14.05	-77.2	5.34	-30.2	-43.4	4.14	19.06	-98.6

and, $\underline{v}_k$, are available from the flight tests. A high-pass filter (wash-out filter) was initially tested with the procedure. It was determined that the pilot manages to keep ϵ_y, $\delta\phi_v$, and δ_a near the zero axis and the high pass filter proved to be unnecessary. A high-pass filter would be necessary for investigating the longitudinal axis with the hypothesis testing procedure.

Initial trials of the hypothesis testing calculation procedure with the piloted data indicated a severe mismatch occurs between the Kalman filter's estimate of its output error covariance, S in (13), and the actual output error covariance, which is calculated as

$$S_k = \frac{1}{k} \sum_{i=1}^{k} (\underline{u}_{m,i} - \hat{\underline{u}}_i(-))\,(\underline{u}_{m,i} - \hat{\underline{u}}_i(-))^T \tag{17}$$

For a large number of data points (k is large in (17)), the matrix S_k should approach S for a linear, time-invariant system. The mismatch occurs because the pilot's internal model of the target driving covariance, $E\{\delta_T^2\}$, appears to differ continuously from the actual constant value discussed previously. The mismatch also arises due to the existence of unmodeled dynamics, nonlinearities, and due to the time-varying nature of the actual piloted simulation.

To resolve this mismatch, a simple approach is used whereby an estimate of S, based on (17), is used in the hypothesis testing scheme. The usefulness of this modification is confirmed by the agreement observed in the next paragraphs between the hypothesis testing results and the pilot control trajectory comparisons.

Comparisons of the actual pilot control time history to the pilot model predictions are illustrated in Fig. 5. The low α_0 pilot mode with normal piloting technique shown in Fig 5a matches the actual pilot's responses quite well, except perhaps in the regions circled. The low α_0 pilot model with especially "tight" piloting technique (Fig. 5b) exhibits no discernable difference from the low α_0 nominal pilot model. The medium α_0 pilot model (Fig. 5c) does not match the pilot control inputs as well as the low α_0 pilot model except perhaps within the circled regions. The high α_0 pilot model does a poor job of predicting pilot behavior even in high α_0 flight. This pilot does not significantly adapt his control strategy to match the changes in aircraft dynamics. Note that no conlusion regarding quadratic weight ("tight" or "normal" control effort-tracking error trade-off) can be made based on visual inspection of these figures. The reasonable match in Fig. 5a tends to justify the modeling simplifications used in the analysis and the attempt to capture human control behavior using the optimal control model. The fact that different assumptions in the construction of the model produce a poor match as shown in Fig. 5d adds further credence to these conclusions.

The hypothesis testing pilot model probabilities are shown in Fig. 6. Recall that the results take the form of a probability for each of the hypothesized pilot models; the sum of the probabilities of all hypotheses in a given test is equal to one. The hypothesis testing algorithm is allowed to choose between the low α_0, medium α_0 and high α_0 pilot models with nominal quadratic weight. The low α_0 model best matches the pilot's responses except in the circled regions. The medium α_0 pilot model best matches the pilot's response in the circled regions. At no time does the high α_0 model predict the actual pilot's behavior, even when the aircraft really is in a high α_0 flight condition. The hypothesis testing result confirms the qualitative analysis of the control time histories.

Choice of pilot tracking error control effort trade-off (quadratic weight level) could not be made from a visual examination of the control responses, but the hypothesis testing algorithm clearly indicates in Fig. 7 that the "normal" weights give a much better fit to the data than the "high" weights. This indicates that the "high-gain" or "tight" pilot model is not as good a representation of what the pilot actually did in this test as is the normal or "low-gain" pilot model values.

SUMMARY

This paper presents a method for comparing actual pilot control actions in the time domain with pilot model predictions. A modified hypothesis testing scheme combined with the linear optimal control pilot model is developed that can be used to analyze nonlinear piloted aircraft data. Actual data from the NASA Differential Maneuvering Simulator of a pilot in pursuit-tracking of an aircraft target is analyzed with the hypothesis testing scheme The primary result is that for the lateral directional control channel, the pilot, throughout most of the simulation, did not change his internal model of the aircraft's dynamics from a low angle of attack flight condition to another model better representative of the aircraft dynamics. This observation validates the approach used in [5] and [6] where a priori predictions of pilot-aircraft instabilities are made using a nonadapting pilot model It is suggested that the reason the pilot may not choose to continually adapt is as given in [6]: the minimum control effort strategy. To adapt to high α_0, the pilot would have to increase his control effort by

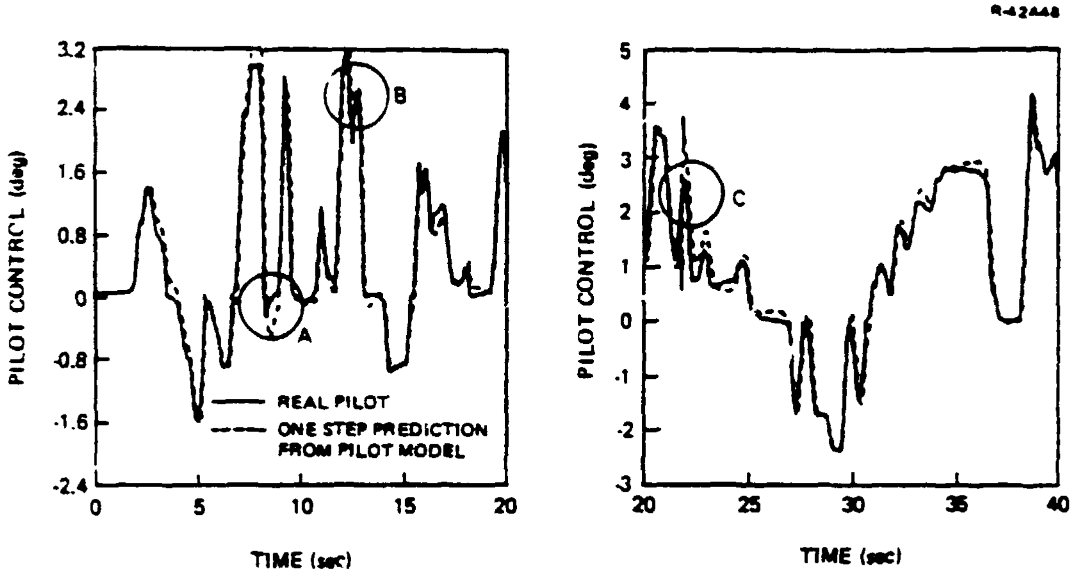

a) Low α_0 Pilot Model With Nominal Quadratic Cost Weights

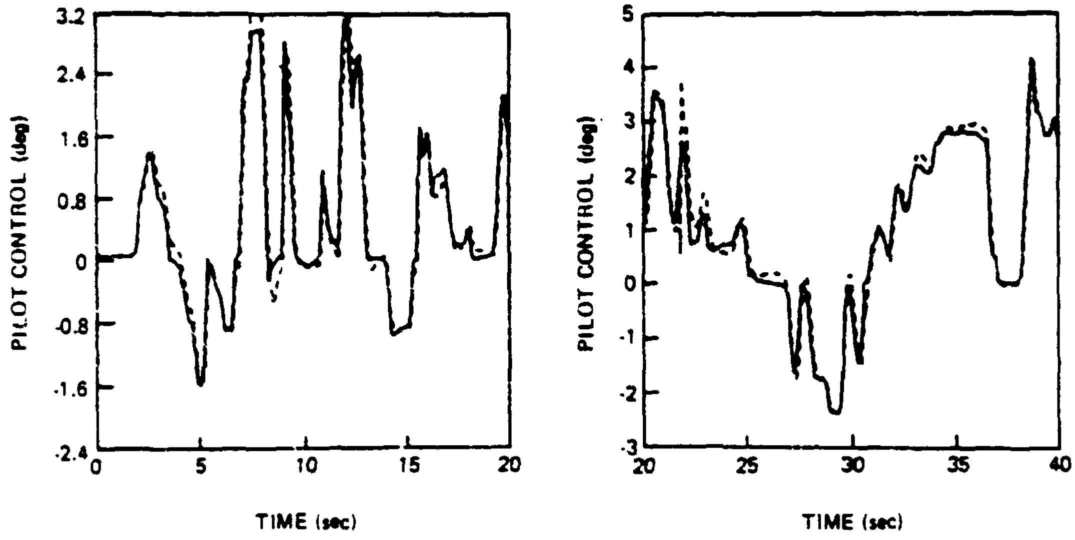

b) Low α_0 Pilot Model With High Quadratic Cost Weights

Figure 5 Comparison of Actual and Predicted Pilot Controls

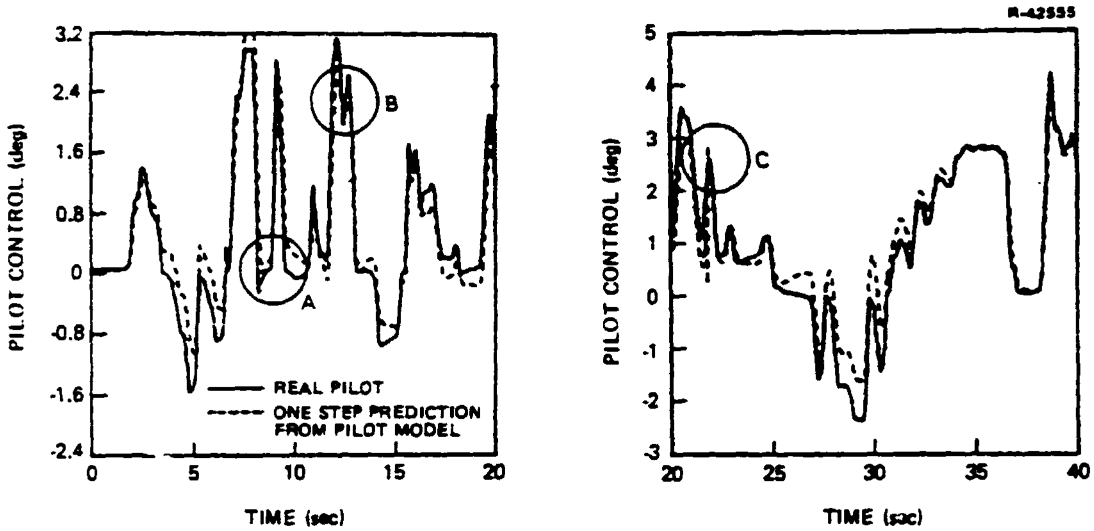

c) Medium α_0 Pilot Model With Nominal Quadratic Weights

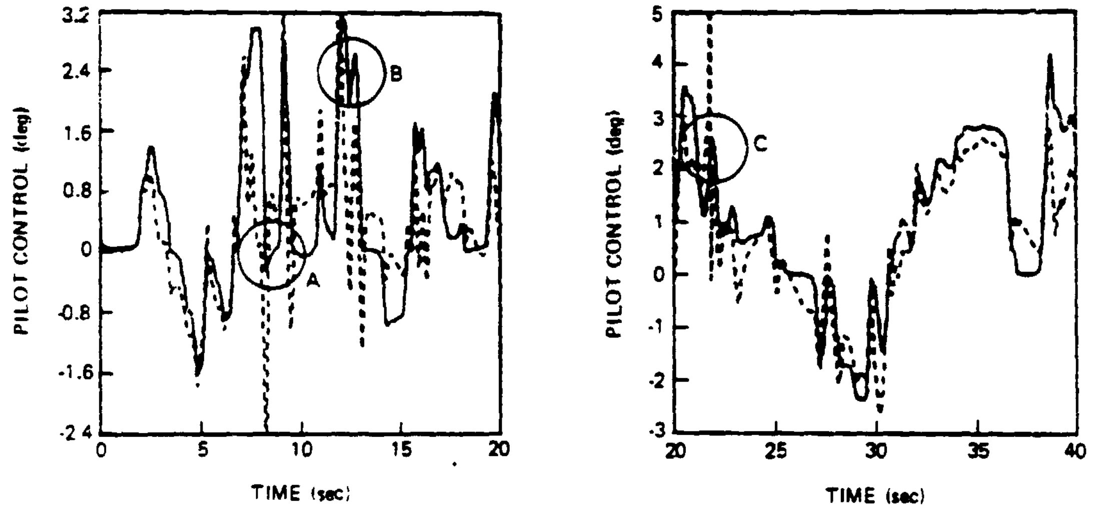

d) High α_0 Pilot Model

Figure 5 Comparison of Actual and Predicted Pilot Controls (Continued)

PRECEDING PAGE BLANK NOT FILMED

ORIGINAL PAGE IS
OF POOR QUALITY

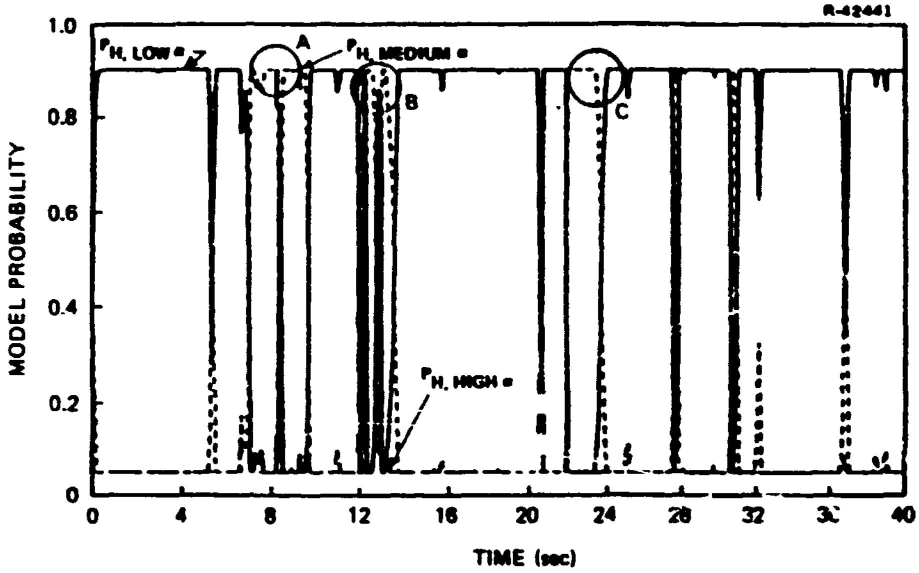

Figure 6 Pilot Model Probabilities

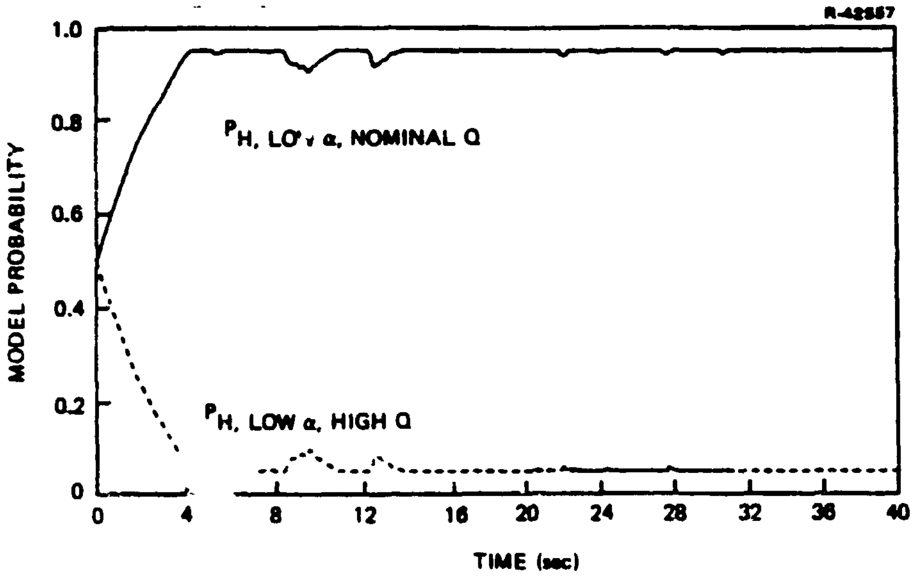

Figure 7 Pilot Model Probabilities for Two Pilot Models at α_0 = 5 deg with Different Quadratic Weights

subjectively increasing his feedback gain as shown in Table 3. Even when the internal aircraft model in the pilot model remains at the one preferred by the pilot, the hypothesis testing scheme shows in Fig. 7 that the pilot does not, at any time, modestly increase his feedback gain for the flight condition to which he is adapted.

These results demonstrate the feasibility and usefulness of the hypothesis testing approach using one piloted trajectory. It is apparent that analysis of many trajectories, with an improved target dynamics modeling effort, as in [13], is necessary before more general conclusions can be made.

ACKNOWLEDGEMENT

The authors wish to thank Prof. R.F. Stengel, now at Princeton University, for suggesting the hypothesis testing approach to the problem. The authors are grateful to L.T. Nguyen for providing the NASA DMS data. This work was performed at The Analytic Sciences Corporation and sponsored by the Office of Naval Research under Contract No. N00014-75-C-0432.

REFERENCES

1. Baron, S., and Berliner, J., "The Effects of Deviate Internal Representations In the Optimal Model of The Human Operator," 15 IEEE Conference on Decision and Control, Clearwater, Florida, December 1976.

2. Jagacinski, R.J., and Miller, R.A., "Describing the Human Operator's Internal Model of a Dynamic System," Human Factors, Vol. 20 No. 4, 1978.

3. Kleinman, D.L. and Baron, S., "Manned Vehicle Systems Analysis by Means of Modern Control Theory," Bolt Beranek and Newman, Inc., Cambridge Mass., BBN Rep. 1967, June 1970.

4. Kleinman, D.L., Baron, S., and Levison, W.H., "A Control Theoretic Approach to Manned-Vehicle Systems Analysis," IEEE Trans. on Automatic Control, Vol. AC-16, No. 6, December 1971.

5. Stengel, R.F., Broussard, J.R., Berry, P.W., and Taylor, J.H., "Modern Methods of Aircrft Stability and Control Analysis," ONR-CR215-237-2, May 1977. Pilot model results reported in "Prediction of Pilot-Aircraft Stability Boundaries and Performance Contours," IEEE Trans. on Systems, Man, and Cybernetics, Vol. SMC-8, No. 5, May 1978.

6. Stengel, R.F., Taylor, J.H., Broussard, J.R., and Berry, P.W., "High Angle of Attack Stability and Control," ONR-CR215-237-1, April 1976. Pilot model results reported in "Stability of the Pilot-Aircraft System in Maneuvering Flight," J. of Aircraft, Vol. 14, No. 10, pp. 959-965, October 1977.

7. Fiske, P.H., and Price, C.F., "A New Approach to Model Structure Identification," AIAA Atmospheric Flight Mechanics Conference, Paper No. 77-1171, Hollywood, Florida, August 1977.

8. Fiske, P.H., "Advanced Estimation and Control Concepts for Air-to-Air Missile Guidance," The Analytic Sciences Corporation, Report No. TR-1353-1, February 1979.

9. Berry, P.W., Broussard, J.R., and Gully, S.W., "Validation of High Angle of Attack Methods," ONR-CR215-237-3, September 1979.

10. Chang, C.B., and Athans, M., "State Estimation for Discrete Systems with Switching Parameters," IEEE Transactions on Aerospace and Electronic Systems, Vol. AES-14, No. 3, May 1978.

11 Harvey, T.R. and Dillow, J.D., "Fly and Fight: Predicting Piloted Performance in Air-to-Air Combat," Proceedings of the 10th Annual Conference on Manual Control, Wright-Patterson AFB, April 9-11, 1974.

12. Korn, J., Boal, H.S., and Vikmanis, M., "Modeling Human Tracking Performance in a High g-Stress Environment," 17th IEEE Conference on Decision and Control, San Diego, California, January 1979.

13. Rao, P.K., Kleinman, D.L., and Ephrath, A.R., "Adaptive Estimation Schemes for Minimizing Uncertainty in Manual Control Tasks," 17th IEEE Conference on Decision and Control, San Diego, California, January 1979.

N82 34048

SUBJECTIVE SCALING OF MENTAL WORKLOAD IN A MULTI-TASK ENVIRONMENT

Bahman Daryanian

M.I.T.

INTRODUCTION

This paper reports and examines the results of a mental workload (MWL) experiment which was carried out in a simulated multi-task environment. The objective of the experiment was to develope and examine a method that would qualitatively and quantitatively identify those factors in a multi-task environment that contribute to the operators' "sense" of mental workload. In the experiment the subjective judgment as conscious experience of mental effort was decided to be the appropriate method of measurement.

Thurstone's law of comparative judgment was employed in order to construct interval scales of subjective mental workload from paired comparisons data.

An experimental paradigm (Simulated Multi-Task Decision-Making Environment) developed by Tulga (1), was employed in this work to represent the ideal experimentally controlled environment in which subjects (human operators) were asked to "attend" to different cases of Tulga's decision-making tasks.

Through various statistical analyses it was found that, in general, a lower number of tasks-to-be-processed per unit time (a condition associated with longer interarrival times), results in a lower mental workload, a higher consistency of judgments within a subject, a higher degree of agreement among the subjects, and larger distances between the cases on the Thurstone scale of subjective mental workload.

The overall method employed in this experiment brings into notice the effects of various control variables and their interactions, and the different characteristics of the subjects on the variation of subjective mental workload.

THE EXPERIMENT

A multi-task decision-making situation in Tulga's experimental paradigm is characterized by a number of blocks (tasks) of differing dimensions simultaneously displayed on the CRT (Figure 1), randomly appearing and moving to the right

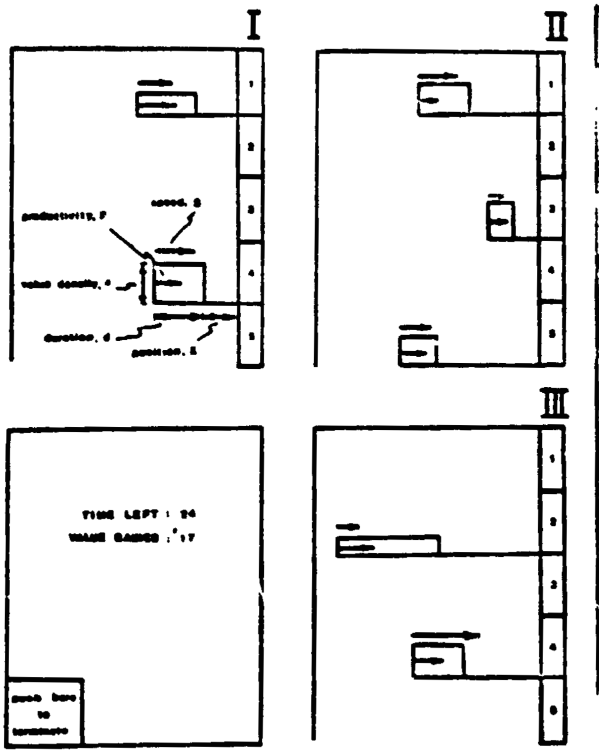
I
II
III
1
2
3
4
5
productivity, P
speed, S
value density, ν
duration, d
position, x
TIME LEFT : 24
VALUE GAINED : 17
push here to terminate

Figure 1.1 Paradigm of Dynamic Task Demands with Multiple (3) Queues.

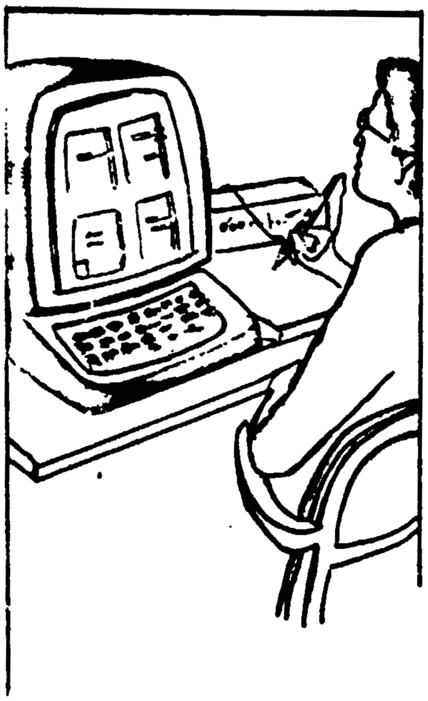

Figure 2

What the Subject Sees and Does.

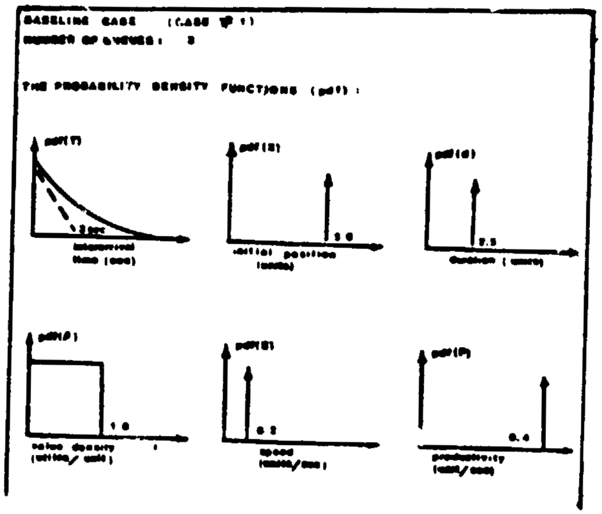

Figure 1.2 Properties of the Baseline Case.

towards a deadline, after which they disappear. Each block is characterized by its "importance" (indicated by the height of each block), and the operator's "productivity" (the rate at which the width of a block is decreased through the action of the operator).

The subject "attends" to these tasks one at a time by holding the cursor of a data-tablet to the right of the block (Figure 2), when thus attended the width of a block decreases at a constant rate. The subject is asked to maximize his/her total value gained, which is the sum of the reduction in areas of all blocks attended to by him/her, i.e. the total area diminished.

Blocks appear randomly with Poisson arrival and move at differing speeds towards the deadline. Height or "importance" of a block can be thought of as the "value density" of the task which indicates the benefit accrued per unit time the operator acts on it. Value can then be earned as the time integral of value densities of tasks acted upon. The value density for each case has a rectangular probability density distribution of 1.0 unit/time.

The explicit parameters that differ for each case (trial) are speed "S", productivity "P", and interarrival time "T" of the blocks (tasks). For three levels of each, a factorial experiment requires 27 cases where,

Task Speeds S_1=0.2, S_2=0.4, S_3=0.8 units/sec

Operator Productivities : P_1=0.4, P_2=0.8, P_3=1.6 units/sec

Interarrival times T_1=3.0, T_2=6.0, T_3=12 seconds.

In short, the operator monitors the arrival of different tasks, evaluates the tasks, chooses one, and acts on it before it hits the deadline.

One female subject (operator 1), and two male subjects (operators 2 and 3), were invited to participate in the experiment. After initial stages of training each subject was asked to "attend" to multi-task decision-making cases for 100 seconds each; and then compare the cases on a pair-wise basis in order to give a subjective assessment of the relative mental workload induced by the pair.

Cases were presented in a random fashion. Care was taken to avoid any noticable order in the presentation of the cases. Most of the pairs were presented more than once. For each subject the experiment was carried out in a period of two to three weeks for a total of 35-45 hours.

The paired comparisons judgments of a subject resulted in one of the three categories of responses:

A- The subject was certain that the mental workload induced by one of the cases was greater than the other.

B- The subject thought that probably the mental workload induced by one of the cases was greater than the other.

C- The subject was unable to make a relative judgment between the cases.

THE SCALING METHOD

The "law of comparative judgment", which is based on Thurstone's judgment scaling model, provides the necessary simplifying assumptions and the set of equations that transform the paired comparison data into the scale values of mental workload (refn's 2,3,4).

Thurstone's model assumes that the psychological distance between two stimuli is proportional to the normal deviate transform of the proportion of times a difference between the stimuli is noticed. The distance between a pair of stimuli is highest if one is always judged to be greater than the other, and zero if they are judged to be equal. Therefore, the subjective scale of Thurstone is based upon the degree of confusion of the subject in the judgment of relative intensity of the psychological attribute in a pair of stimuli.

Thurstone's Judgment Scaling Model

Thurstone postulated that for any given attribute (e.g., mental workload) of a series of stimuli (e.g., decision tasks) there exist a "psychological continuum" associated with that attribute. A subject presented with a series of stimuli would react "discriminally" with respect to the given attribute (e.g., the subject would discriminate between the different levels of mental workload associated with a series of decision tasks). The process by which the subject identifies the attribute and reacts discriminally to it is called a "discriminal process"; and each of the "discriminal responses" associated with a discriminal process has a value on the psychological continuum associated with that attribute. It is assumed that due to the stochastic nature (noise generation, momentary fluctuation) of the organs of the human mind (sensation and cognition), i.e. of the discriminal processes, the discriminal response associated with a given attribute of a stimulus could be thought of as having a frequency distribution on the psychological continuum. Furthermore, it is postulated that the frequencies with which the discriminal responses are associated have the form of a normal distribution.

In a normal frequency distribution the modal, mean, and the mode coincide. A possible choice for the "scale value" of the attribute on psychological continuum is the "modal discriminal response ".

Figure 3 provides examples of discriminal responses on a psychological continuum for four stimuli. Note that the modal

C - 3

O[illegible] IS
OF [illegible] Q[illegible]ITY

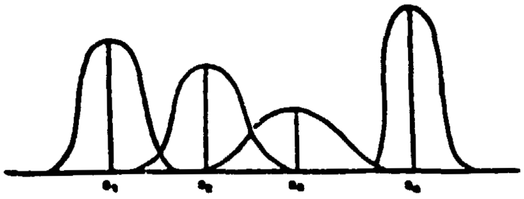

Figure 3 Distribution of Discriminal Responses Associated with Four Stimuli on the Psychological Continuum.

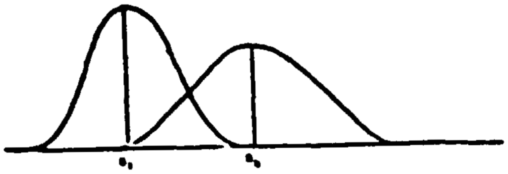

Figure 4.1 Distribution of Discriminal Responses Associated with Stimuli j and k on the Psychological Continuum.

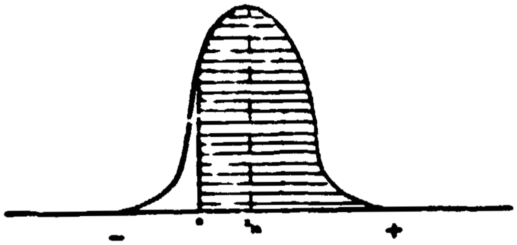

Figure 4.2 Distribution of Discriminal Differences on the Psychological Continuum. The Quantity x_{jk} is the difference in Scale Values measured in σ_{dk-dj} units.

discriminal responses S_1, S_2, S_3, and S_4 and the respective discriminal dispertions vary for each stimulus.

It is assumed that the subject can not directly report the modal values of the discriminal responses or their dispersions on the psychological continuum. However, presumably he can judge and report relations among stimuli (e.g., judgment of relative orders).

The Law of Comparative Judgment

The law of comparative judgment is a set of equations relating the scale values and discriminal dispersions of a set of stimuli on the psychological continuum to the proportion of times any stimulus is judged greater than the others for a given attribute.

When a pair of stimuli is presented to a subject the difference between two discriminal responses (discriminal differences, $d_j - d_k$), should also form a normal distribution. The mean of this distribution is equal to the difference in scale values of the two stimuli. The standard deviation of differences is computed from

$$\sigma_{d_j - d_k} = (\sigma_j^2 + \sigma_k^2 - 2\, r_{jk}\, \sigma_j\, \sigma_k)^{1/2}, \qquad \text{(Eq.1)}$$

where r_{jk} is the correlation between momentary values of discriminal responses associated with stimuli j and k.

As a result of Thurstone's judgment model the following relation holds for the difference in scale values of the two stimuli:

$$S_k - S_j = X_{jk}\, \sigma_{d_j - d_k}, \qquad \text{(Eq.2)}$$

where X_{jk} (see Figure 4), is evaluated from the table of areas under the unit normal curve, and it is in units of the standard deviation of discriminal differences.

Combining Equations 1 and 2, the fundamental equation of the law of comparative judgment results:

$$S_k - S_j = X_{jk}(\sigma_j^2 + \sigma_k^2 - 2\, r_{jk}\, \sigma_j\, \sigma_k)^{1/2}. \qquad \text{(Eq.3)}$$

In general, for n stimuli, there are n scale values, n discriminal dispersions, and n(n-1)/2 independent correlations which are unknown. Against these, there are only n(n-1)/2 observable equations corresponding to the independently observable proportions. In order to decrease the number of unknowns some simplifying assumptions are necessary. It should be noted that X_{jk} is related to the proportion of the times stimulus j is judged greater than stimulus k.

A Workable Set of Equations

Assuming that the standard deviation of discriminal differences is constant and the same for all pairs of stimuli, a "least square" solution results in the following equation for detemining the estimated scale values of stimuli:

$$S_k = \frac{1}{n} \sum_{j=1}^{n} X_{jk} \qquad (k=1, 2, \ldots\ldots n) . \qquad (Eq.4)$$

In derivation of this equation it was assumed that the origin of the scale is set at the mean of the estimated scale values.

REDUCTION OF THE DATA

As mentioned before, the subjects judged the relative greatness of mental workload for a pair of multi-task decision-making cases, and the verbal responses resulted in one of the three categories of A, B, or C.

By accumulation of these paired comparisions data verbal response matrices "R", were constructed whose elements were one of the five possibilities (certainly greater, probably greater, equal, probably less, certainly less) for "relative" mental workload induced by each pair of cases. Due to replication, as shown in the example of Figure 5, some elements contained more than one response. The diagonal matrices were left blank, assuming that the response of any subject when a case is compaired to itself would be "C". In addition, in order to indicate wether a case represented by a row induced more mental workload or the one represented by the column, the verbal responses were added a "+" or "-" prefix. Hence, the response matrix of the Figure 5 is skew symmetric matrix. These verbal responses were transformed into the frequency response form by the criteria shown below :

Category	Verbal Response	element ij i: row j: column	element ji j: row i: column
I: +aij	i certainly greater than j	4	0
II: +bij	i probably greater than j	3	1
III: cij	i equal to j	2	2
IV: bij	i probably less than j	1	3
V: -aij	i certainly less than j	0	4

Verbal to Frequency
Transformation Criteria

ORIGINAL PAGE IS
OF POOR QUALITY

The above criteria translates into the following:

I : Is equivalent to judging stimulus i to be greater than stimulus j four times in four trials.

II : Is equivalent to judging stimulus i to be greater than stimulus j three times in four trials.

III : Is equivalent to judging stimulus i to be greater than stimulus j twice in four trials.

IV : Is opposite of II.

V : Is opposite of I.

According to this criteria the verbal response matrix of Figure 5 is transformed into the frequency response matrix "F" of Figure 6. In turn, matrix "F" is transformed into the proportion matrix "P" of Figure 7 by deviding each element of f_{jk} by the sum of $f_{jk}+f_{kj}$. From matrix "P", matrix "X" of Figure 8 is constructed whose elements are equal to the unit normal deviate corresponding to the element p_{jk}. Finally, by substituting the values of x_{jk} in Equation 4 the scale of Figure 9 is constructed.

Figure 10 presents the resulting Thurstonian scales of subjective mental workload for each of the subjects.

ANALYSIS OF DATA, RESULTS, AND CONCLUSIONS

For the purpose of the study of the experimental data three independent techniques of analysis were employed:

i) Analysis of variance, which tests the significance of the effects of different variables of decision-task environment (T: interarrival time; S: task speeds; P: productivity; O: operators) on the variation of subjective mental workload.

ii) Analysis of agreement among the subjects, which tests how well subjects agree among themselves in their judgments.

iii) Analysis of transitivity, which provides a basis upon which the consistencies of the judgments of subjects are compared.

It was found that the interrarival time "T" of the tasks has the most significant effect (among all the control variables) on the variation of mental workload (see Table 1). As could be seen in Figure 10, the 27 cases are clustered into 3 seperate groups corresponding to 3 levels of interarrival time "T". Based on this finding, analyses of variance was performed for each level of "T". Results are shown in Tables 2 to 4.

Analysis of agreement is based on computing the Spearman's Rank Correlation Coefficients for pairs of subjects and testing their significance for the final rank ordered results. Also included in the analysis was the computation and testing of the

ORIGINAL PAGE IS OF POOR QUALITY

Cases	1	2	3	4	5	6
1		+a+a-b+a -b+a +a+a	+a +a +a	+a-a -a +b	+a+a -ac +b+a	+ac -b+a +a
2	-a-a+b +b-a -a-a		+a+a-a +a+a +b-b	+a-a -b-a c	+b+a -a -a	+ac +a-a +a
3	-a -a -a	-a-a+a -a-a -b+b		-b-b -a-a -a	+a+b c -a -a	+a+a -a +a
4	-a+a +a -b	-a+a +b+a c	-b+b +a+a +a		+a c -a-a -a-a	-b+a -a +a
5	-a-a +a c -b-a	-b-a +a +a	-a-b c +a +a	-a c +a+a -a+a		+a+a +a+a -a
6	-a c +b-a -a	-a c -a+a -a	-a-a +a -a	+b-a +a -a	-a-a -a-a -a	

Figure 5 : An Example of Verbal Response Matrix

CASES	1	2	3	4	5	6
1		22	12	7	17	15
2	6		20	7	7	14
3	0	8		4	9	12
4	9	12	16		10	9
5	7	9	11	11		16
6	5	6	4	7	4	

Figure 6 : Frequency Response Matrix F

CASES	1	2	3	4	5	6
1		0.782	1.00	.437	.708	.750
2	.214		.714	.350	.437	.700
3	0.00	.286		.200	.450	.750
4	.563	.650	.810		.417	.563
5	.242	.563	.55[illegible]	.583		.800
6	.250	.300	.250	.437	.200	

Note: $p'_{jk} + p'_{jk} = 1.00$

Figure 7 : Proportion Matrix P

CASES	1	2	3	4	5	6	
1	0.00	.79	5.00	-.16	.55	.67	
2	-.79	0.00	0.57	-.39	-.16	-5.	
3	-5.00	-.57	0.00	-.84	-.13	-67	
4	.16	.39	.84	0.00	-.21	.16	
5	-.55	.16	.13	.21	0.00	.84	
6	-.67	-.52	-.67	-.16	-.84	0.00	
$\sum_{j}^{n} x'_{jk} =$	-6.05	.25	5.87	-1.34	-.79	2.86	= 0.00
$\frac{1}{n} \sum_{j}^{n} x'_{jk} = S'_k$	-1.14	.04	.97	-.22	-.23	.48	= 0.00

Note 1: $x'_{jk} + x'_{jk} = 0$

2: x'_{jk} is equal to the unit normal deviate corresponding to element P'_{jk}

Figure 8: Distance Matrix X

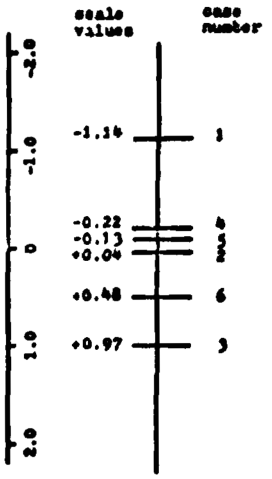

Figure 9: An Example of the Scale of Subjective Mental Workload

ORIGINAL PAGE IS OF POOR QUALITY

ORIGINAL PAGE IS
OF POOR QUALITY

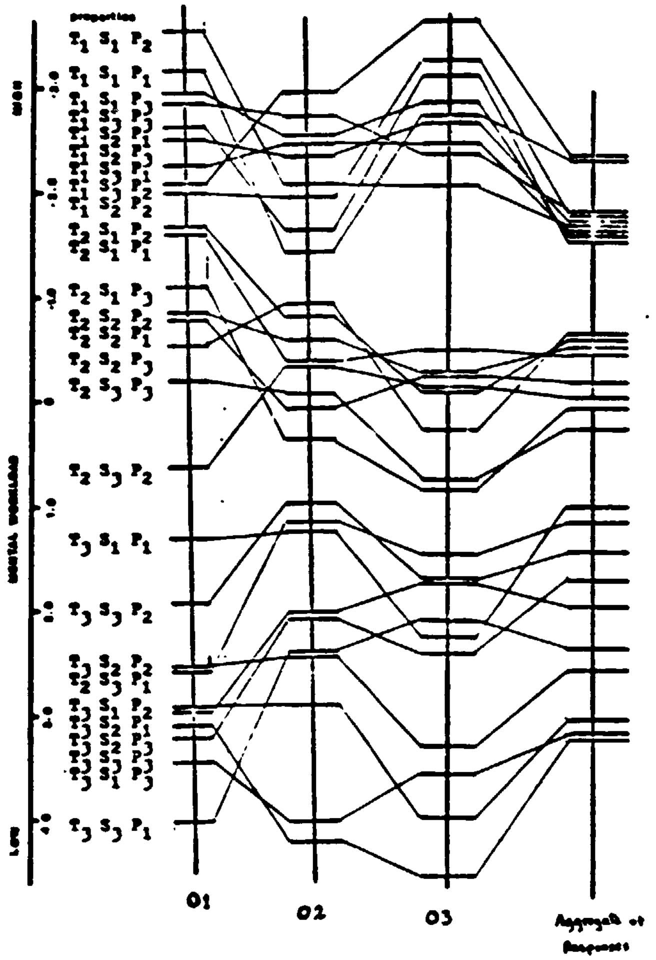

Figure 10 : Scale of subjective mental workload for three subjects, and for the aggregate of responses.

Coefficient of Concordance. Results are shown in Table 5.

Analysis of transitivity is based on the computation of the number of the inconsistent triads for the subjects' responses. The diagram below illustrates the meaning of the transitivity (consistency of responses). Results are shown in Table 6.

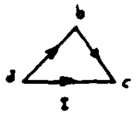

I: Transitivity resulting from Consistency in choice.

II Intransitivity resulting from inconsistency in choice.

(Arrow indicates the direction of choice or Preference)

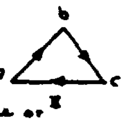

The following is an overview of the results of the analyses. For a more detailed exposition of the results the reader should refer to Ref. 6.

The experimental environment and the results of the subjective judgments provide support for a conceptual model of subjective mental workload with the following general properties:

- Subjective mental workload is stochastic in nature.
- Subjective mental workload is a property of the environment-operator interface, and it depends on both environment and operator characteristics.
- Subjective mental workload can be quantified on a unidimensional scale, as demonstrated by this work.
- There exists a substantial degree of agreement among subjects in their judgments of mental workload.

The following more specific conclusions can be drawn from the study:

1- Among the experimentally controlled variables the interarrival time between tasks "T", has the most significance effect on the variation of subjective mental workload. A longer interarrival time, which is associated with a lower number of tasks-to-be-processed per unit of time, results in a lower subjective mental workload.

2- In general, a lower number of tasks-to-be-processed per unit time (a condition associated with longer interarrival times) is associated with the following:
- lower subjective mental workload.
- higher degree of consistency (more transitive responses) within subjects.
- better agreement among subjects on rank ordering of cases with respect to their associated mental workloads.
- larger intervals between adjacent cases on the aggregate scale of subjective mental workload (see Figure 10).

3- Analysis of consistency indicates a high degree of transitivity of responses for the aggregate data except for short

Table 1

Results of Analysis of Variance for all Levels of Interarrival Time

Nature of effect	Source	Sums of squares	d.f.	Variance Estimate	Significance Level %
Main factors	T *	4303.19	2	2151.60	1
	S	9.85	2	4.93	-
	P *	32.67	2	16.34	15
	O	0	2	0.00	-
Interaction between Pair of factors	TS *	84.74	4	21.19	1
	TP *	55.92	4	13.98	5
	TO	1.03	4	0.26	-
	SP *	93.26	4	23.32	1
	SO	93.71	4	23.43	1
	PO	24.44	4	6.11	-
Interaction between Triples of factors	SPO	36.07	8	4.51	-
	TPO	38.08	8	4.76	-
	TSO	32.31	8	4.10	-
	TSP *	51.04	8	6.38	17†
Interaction of all factors	TSPO	57.19	16	3.57	
	Residual	0	0	0	
TOTAL		4914	80		

*: Significant effects
†: Computed by linear interpolation

Table 2

Results of Analysis of Variance at Short Interarrival Time (T = 3 seconds)

Name of Effect	Source	Sum of Squares	d.f.	Variance Estimate	Signif. Level
Main factor	S	6.00	2	3.00	-
	P	4.67	2	2.34	-
	O	0	2	0	-
Interaction between Pairs of Factors	SP	14.66	4	3.67	-
	SO *	76.00	4	19.00	17 +
	PO	12.89	4	3.22	-
Interaction of all Factors	SPO	65.78	8	8.22	-
	Residual	0	0	0	-
	Total	180.0	26		

* Significant effects
+ By linear interpolation

Table 3

Results of Analysis of Variance at Medium
Interarrival Time (T = 6.0 seconds)

Name of Effect	Source	Sum of Square	d.f.	Variance Estimate	Signif. Level
Main Factor	S •	60.67	2	30.34	1
	P •	17.56	2	8.78	21 ♦
	O	0	2	0	
Interaction between Pairs of Factors	SP •	32.44	4	8.11	18 •
	SO	18.44	4	4.61	-
	PO	21.33	4	5.33	-
Interaction of all Factors	SPO	29.56	8	3.70	-
	Residual	0	0	0	-
	Total	180.0	26		

• Significant effects

♦ Computed by linear interpolation

Table 4

Results of Analysis of Variance at Long
Interarrival Times (T = 12.0 seconds)

Name of Effect	Source	Sum of Square	d.f.	Variance Estimate	Signif. Level
Main Factor	S	8.22	2	4.11	-
	P •	54.89	2	27.45	5
	O	0	2	0	-
Interaction between Pairs of Factors	SP •	64.65	4	17.41	1
	SO •	21.78	4	5.45	10
	PO •	13.78	4	3.45	16 ♦
Interaction of all Factors	SPO	11.68	8	1.46	-
	Residual	0	0	0	-
	Total	180.0	26		

• Significant effects

♦ Computed by linear interpolation

ORIGINAL PAGE IS
OF POOR QUALITY

Table 5

	Coeff. of Concordance	rank-diff. correl.	Spearman's rank Corr. Coeff.(R) Pair of Subjects (operators)		
	W	$\bar{r}$	O_1O_2	O_1O_3	O_2O_3
Overall Ranked Data	0.94	0.91	0.91	0.89	0.94
Level of Sig.	%0.5		%0.5	%0.5	%0.5
T_1 Level	0.14	0.033	−0.01	−0.29	0.18
Level of Signif.	•		•	%30−%20	•
T_2 Level	0.61	0.69	0.31	0.54	0.58
Level of Signif.	%10−%5		%20−%10	%10−%5	%5−%2.5
T_3 Level	0.74	0.83	0.61	0.47	0.96
Level of Signif.	%2.5−%1		%5−%2.5	%10−%5	%0.5

Degrees of Agreement Among Subjects

	For all 27 Cases	Short inter-arrival time T_1	Medium inter-arrival time T_2	Long inter-arrival time T_2	
Operator 1	100	15.5	5	12.4	d
	.87	.48	.83	.58	k
Operator 2	93.7	22.0	14.8	7	d
	.88	.25	.5	.76	k
Operator 3	134.2	19.2	19.1	12.2	d
	.83	.35	.36	.59	k
Aggregate Responses	44	26.2	7.5	5.25	d
	.94	.11	.75	.82	k

d: number of inconsistent triads

k: coefficient of consistency

Transivity and Consistency of Responses

Table 6

interarrival times of tasks, which supports the hypothesis of the existence of a unidimensional psychological continuum associated with the attribute of subjective mental workload for medium and low levels of mental workload.

4- Absence of agreement among the subjects with respect to the ordering of the experimental cases according to their mental workload, and a very low degree of consistency (low transitivity of responses) at the shortest interarrival time indicate that either,

i) mental workload is a multidimensional psychological attribute at high levels of mental workload; or,

ii) the difference between scale values of mental workload for cases become less noticeable (i.e., differentiable) at higher levels of mental workload, thus indicating the approach of an upper threshold of mental workload. The author accepts the second interpretation.

5- Analysis of consistency resulted in a higher degree of transitivity of responses for the aggregate data than that of each indivitual subjects' data except for the short interarrival time; thus indicating that the aggregate scale of subjective mental workload is a more reliable scale than the individual scales of the subjects.

6- Short and medium interarrival times are associated with cases which demand some degree of monitoring and decision making, whereas the long interarrival time is associated with cases that require little monitoring and decision making and may even provide free times between the appearances of tasks. Therefore, the nature of the decision-making environment is fundamentally different for different levels of interarrival times. At different levels of interarrival time, experimentally controlled task variables and their interactions have different effects on the variation of subjective mental workload, as discussed in detail in reference 5.

7- The study supports the notion that subjects form internal models of environment based on their own abilities, dispositions, and tendencies which result in their dissimilar perceptions of mental workload. In the analysis, the underlying characteristics of the subjects was inferred from their judgment patterns. The differences of opinion among subjects with respect to mental workload occures when the subjects' personal characteristics result in adaptation of different strategies of action. It is postulated that for environments, where only one optimal strategy of action exists, trained subjects would be in better agreement.

REFERENCES

1. Tulga, M.K., "*Dynamic Decision Making in Multi-Task Supervisory Control: Comparison of an Optimal Algorithm with Human Behavior*", Sc.D. Thesis, MIT, September 1978.
2. Thorndike, E.L., "Handwriting", *Teach. Coll. Rec.*, *11*, no. 2, 1910.
3. Thurstone, L.L., "A Law of Comparative Judgment", *Psychol. Rev.* 1927, *34*, 273-286.
4. Torgerson, W.S., "*Theory and Methods of Scaling*", John Wiley and Sons, Inc., 1958.
5. Daryanian, B. "*Subjective Scaling of Mental Workload in a Multi-Task Environment*", M.S. Thesis, MIT, February 1980.

N82 34049 -12

EFFECT OF COUNTING AND TRACKING ON VERBAL AND PRODUCTION METHODS OF TIME ESTIMATION

Kathleen L. Bird[*]
San Jose State University

Sandra Hart[**]
Tufts University

ABSTRACT

This study investigated the effects of time estimation technique and task condition on the production and verbal estimation of time intervals ranging from 5 to 14 sec. Sixteen male college students were randomly assigned to two groups, each of which utilized a different estimation method: (a) production; or (b) verbal estimation. The subjects were instructed either to produce or to give a verbal estimate of the duration of these time intervals during each task condition: (a) pretracking, (b) tracking (subject performed a one-axis tracking task), and (c) posttracking. Each subject used each of the two estimation techniques: (a) vocal counting and (b) no counting. The ratio of the subject's time estimate to actual interval length was computed for each trial.

Productions were typically longer than verbal estimates of the same duration and produced durations were typically too long whereas verbal estimates were too short relative to the correct duration. These effects were evident in both the counting and no-counting conditions, with and without a concurrent tracking task.

A significant interaction was found between counting technique and tracking condition for both estimation methods. When subjects were instructed to count out loud they were able to perform an additional tracking task while maintaining consistent and accurate performance on the time estimation task. In contrast, when subjects were instructed not to count out loud, their ability to keep track of time while performing a tracking task was reduced.

A significant effect could be attributed to the addition of a tracking task: produced durations increased in length, whereas verbal estimates decreased in length. The durations produced without counting were significantly less accurate and consistent with the addition of a tracking task. Verbal estimation mean accuracy, but not consistency, was adversely affected by the addition of a tracking task when the subjects were instructed not to count.

---

[*] This research was conducted at NASA-Ames Research Center and was sponsored by NASA grant NCC-2-34 to San Jose State University.

[**] This research was conducted at NASA-Ames Research Center and was sponsored by NASA grant NSG-2156 to Tufts University.

INTRODUCTION

Performance on a secondary task is often used as an index of primary task workload. Many secondary tasks are designed to increase the overall workload in order to measure residual capacity for work still available during performance on the main task. The assumption is that processing resources are limited and that performance will deteriorate when several activities compete for the same resources (Norman & Bobrow, 1975). A secondary task may interfere with performance on the main task if it employs the same sensory-motor pathways or interferes functionally with it (Michon, 1966). A secondary task may employ the same sensory-motor pathway if, for instance, an operator watches a complicated display and calls out the information obtained, while at the same time performing a secondary task that consists of calling out random sequences of letters presented visually. Less obvious, however, is the possibility that a secondary task may interfere functionally with the main task without making use of the same peripheral pathways. For instance, if one of the tasks used to investigate workload was the selection of a changing number in a series of eight digit numbers and the main task consisted of deciphering numerical codes, the performance of one task would interfere functionally with performance on the other task even if one task was presented auditorially and the other visually because they require the same processing resources.

An alternative type of secondary task is one which does not interfere with the main task but does require some attention. As attention required by the primary task increases, secondary task performance deteriorates, thus providing an indirect measure of primary task demands.

Time estimation tasks which measure the individual's ability to judge the passage of time under different circumstances have been used as secondary measures of primary task workload (Goldstone, Boardman, & Lhamon, 1958; Hart, McPherson, & Loomis, 1978). As primary task demands increase and attention is drawn away from time estimation, estimates typically become less accurate and more variable, reflecting the level of concurrent primary task demands. However, this occurs without degrading performance on the primary task.

There are three experimental methods commonly used to obtain time estimates: (a) verbal estimation, in which subjects verbally report judgments of elapsed time between presentation of stimuli, (b) production, in which subjects physically generate a time interval specified by the experimenter, and (c) reproduction, in which subjects physically generate a time interval previously demonstrated by the experimenter.

It has been suggested that individuals use two basic modes of estimation: active (prospective) and retrospective. Active estimation involves a conscious attempt to keep track of time continuously during the designated interval. Various timekeeping techniques may be tried such as counting, mentally replaying a musical passage of appropriate duration, and counting heart beats or breaths. In retrospective estimation subjects cannot or do not attend to the passage of time during an interval. Instead, they may recall events that occurred during the interval, compare them temporally with experiences of known duration, and arrive at an estimate of the amount of time that elapsed during the interval at its conclusion.

Hicks, Miller, and Kinsbourne (1976) have suggested that the apparent inconsistencies found among different time estimation studies may be attributed to a failure to distinguish between modes (active and retrospective) employed. Bindra and Waksberg (1956) further suggest these inconsistencies may be explained in terms of the experimental method (e.g., production, verbal estimation, reproduction) employed. For example, a common finding is that the lengths of produced and verbally estimated durations are inversely related. With the production method, subjects are required to perform a task, e.g., depress a key for a specified period of time. If they attempt to employ an active mode of estimation such as counting "one thousand one, one thousand two," and are distracted during the interval, they will generally resume counting where they left off. Their performance will, therefore, consume more time than they estimate, resulting in underestimation of elapsed time and a produced duration that is too long. If distracted from active timekeeping during the presentation of an interval whose length must be verbally estimated, subjects will again underestimate the elapsed time since they tend to overlook the period of distraction in resuming their counting, and the verbal estimate duration will be too short. Thus the lengths of actively made verbal estimates and productions, under similarly distracting conditions, will be inversely related although both occur as a consequence of underestimation of elapsed time.

Techniques such as counting or tapping that focus the subject's attention on the time estimation task and segment the interval into concrete, standardized units, result in produced durations that are less variable and less subject to the distracting effects of concurrent activity (Hart, McPherson, & Loomis, 1978). Less concrete production techniques, such as mentally replaying an experience of known duration, result in productions that are more variable and more subject to distraction from concurrent tasks. The accuracy and consistency of actively made verbal estimates should also be affected by the estimation technique employed. Techniques such as counting and tapping that focus attention on the passage of time should result in verbal estimates that are less subject to the distracting effects of concurrent activities. The interactive effects of estimation technique and concurrent activity on verbally estimated and produced durations has not been studied in such a manner as to allow direct comparison between the results obtained with the two methods.

The proposed study examined the effects of a concurrent manual control task on time estimates made by the verbal estimation and production methods. Specifically, it attempted to answer these questions: (a) Does the presence of a concurrent task result in verbally estimated durations that are inversely related to productions obtained under similiar circumstances? (b) Does a vocal-counting technique result in more stable verbal estimates than a no-counting technique with no concurrent activity? (c) Are verbal time estimates that use continuous vocal counting affected by the introduction of a concurrent task? (d) Are verbal time estimates based on no systematic estimation technique affected by the introduction of a concurrent task?

METHOD

Subjects

Sixteen male college students ranging in age from 18 to 35 served as paid volunteers. They were alternately assigned by order of appearance to the verbal estimation method group or production method group. None of the subjects had participated in previous time estimation research.

Apparatus

This study was conducted in a small, enclosed experimental chamber. The subjects were seated alone in a comfortable chair in front of a cathode-ray tube (CRT). A control stick with a response button was located directly in front of the subject's chair. The response button, used to initiate and terminate productions and to begin the verbal estimation trials had an audible click upon both depression and release. An intercom transmitter/receiver was located on the wall next to the subject to allow the subject and experimenter to communicate verbally.

Visual display. The experimental tracking task was displayed on a 38 cm x 28 cm CRT which was located approximately at the subject's eye level. The subject was able to adjust the distance from the chair to the CRT between the range of 48.90 and 57.15 cm to allow for individual differences in visual acuity.

Experimenter's station. Data acquisition and presentation of experimental conditions were controlled by a Digital Equipment Corporation PDP-12 computer. The experimenter was seated outside of the experimental chamber near the PDP-12 computer. A second intercom transmitter and receiver was located next to the experimenter.

Procedure

Subjects were familiarized with the experimental chamber and asked to put their watches (if any) in their pockets. Instructions appropriate for each experimental condition were read aloud and subjects were given three practice trials to familiarize them with the procedure. Each subject was required to use each of the two time-keeping techniques (vocal counting and no-counting) and one of two estimation methods (production or verbal estimation). The subjects estimated or produced time intervals with and without a concurrent task. All subjects received the following sequence of conditions for counting and no-counting: (a) no tracking, (b) tracking, and (c) no tracking. The order of presentation of the experimental conditions was the same for both the production and verbal estimation methods however, half of the subjects received the no-counting trials first and half received the counting trials first. Thus, each subject experienced a total of six conditions (Table 1). Ten durations, each presented twice, were presented in a different random order for the six conditions experienced by each subject. The 10 intervals ranged in length from 5 to 14 sec in 1-sec steps.

Verbal Estimation. The interval to be verbally estimated was demonstrated by different messages on the CRT. The messages "BEGIN INTERVAL" and "END OF INTERVAL" provided the interval boundaries. The message "INTERVAL" was displayed continuously during the interval. Subjects were required to acknowledge that they had noticed the beginning and end of the interval presentation by pressing the response button. After each interval a message "ESTIMATE" appeared on the screen indicating that the subjects should verbally report their judgment of the duration of the interval (to the nearest second) over the intercom system. The experimenter then recorded each estimate. The length of the interval between presentation of trials was 5 sec.

Production. The message "BEGIN PROD.[N SEC]" was displayed on the CRT (where N equals the number of seconds). The subject depressed the response button to initiate the production. The message on the screen changed to "PROD.[N SEC]" to remind subjects of the task called for. The subject depressed the response button again when he felt that the specified amount of time had elapsed, and the message, "END OF PROD.," appeared on the screen. The subject produced the 10 different time intervals twice. The intertrial interval length was 5 sec.

Counting/no counting. In the no-counting condition, subjects were asked not to count (vocally or subvocally) or perform any rhythmic activities while producing an interval or during presentation of the interval whose duration was to be verbally estimated. They were instructed that if they should find themselves counting or tapping, to try to think of something else and report it to the experimenter. For the counting condition, subjects were asked to count aloud using the method "thousand one, thousand two, etc."

Tracking task. The tracking task consisted of a CRT display upon which was displayed a moving 5.56 cm vertical line (the cursor). The subjects were instructed to keep this cursor centered between two stationary 2.11 cm vertical lines by maneuvering the control stick right and left. Maximum displacement of the cursor was 12.07 cm subtending a visual angle of .32 rads (16 deg of arc). Maximum rate of travel was 63.50 cm/sec.

The movement of the cursor was generated by the filtered output of a random number generator. The random number generator provided a rectangular distribution of frequencies with a bandwidth of 60 rad/sec. These values were passed through a first order filter with a natural frequency of 1 rad/sec. The standard deviation of the forcing function was 1.18 cm (see Figure 1).

RESULTS

Effect due to length of interval

Each subject gave two verbal estimates or made two productions for each of the 10 different interval lengths under each of the six experimental conditions he experienced. The mean duration of the two estimates was obtained and a ratio was formed with the length of the interval to be judged. Values greater than 1.0 signified verbal estimates or productions that were too long and values less than 1.0 signified verbal estimates or productions that were too short. These ratios were compared within each time estimation condition using twelve one-way analyses of variance for repeated measures to determine whether the length of the interval estimated resulted in relative differences in subjective judgments of duration. Only one of these F values exceeded the critical value of 1.74 for 9 and 63 degrees of freedom (Dixon & Massey, 1957). Using the 10% significance level, it is expected that 1 in 10 F tests will be falsely significant thus, the appearance of one significant F value ($F(9,63) = 1.75$, $p < .10$) is not unreasonable. Since no significant differences were found for verbal estimates or productions attributable to the length of the time interval judged, the mean ratios were combined for subsequent analyses.

Comparison of pretracking and posttracking (average duration)

A 2 (counting-no counting) x 2 (pre- vs. posttracking) analysis of variance with repeated measures on both factors was computed individually on verbal estimates and productions. These analyses were performed to determine the relationship between estimates obtained prior to and following the tracking task. With the production method, no significant effect attributable to counting technique was found, $F < 1$; however, pretracking estimates were significantly shorter than posttracking estimates, $F(1,7) = 7.86$, $p < .05$. There was no significant interaction between counting technique and pre- and posttracking estimates, $F(1,7) = 4.11$, $p > .05$.

With the verbal estimation method there was no significant effect attributable to counting technique alone, $F < 1$; however, pretracking estimates were significantly longer than posttracking estimates, $F(1,7) = 6.29$, $p < .05$. No significant interaction between counting technique and pre- and posttracking estimates was found, F (1,7) = 3.14, $p >.05$ (see Figure 2).

Although pretracking productions were significantly shorter than posttracking, their average length was still shorter (1.14) than the mean of the tracking productions (1.32), as would be expected. Pretracking verbal estimates were longer than posttracking estimates, however their average length (.91) was still longer than all tracking estimates (.80). In effect, the subjects underestimated elapsed time more at the end of the experiment than the beginning for both the production and verbal estimation methods. As predicted, the length of verbally estimated and produced durations were inversely related.

Comparison of pretracking and posttracking (variability)

A 2 (counting technique) x 2 (pre- vs. posttracking condition) analysis of variance with repeated measures on both factors was performed on the within-subjects standard deviations for the verbal estimation and production methods individually to compare estimates obtained before and after performing the tracking task. For the production method, there was no significant difference between pre- and posttracking estimates, F (1,7) = 1.38, $p >.05$, nor was there any significant interaction between counting technique and tracking condition, F (1,7) = 4.55, $p >.05$. Estimates made without counting were significantly more variable than those made with counting for both pre- and posttracking conditions, F (1,7) = 19.26, $p <.01$.

For the verbal estimation method there was no significant difference between pretracking and posttracking , F (1,7) = 4.12, $p >.05$, nor was there a significant interaction between counting technique and the pretracking and posttracking conditions, F (1,7) = 3.06, $p >.05$. There was a significant effect due to the counting technique, F (1,7) = 18.10, $p <.01$ (see Figure 3).

Effect of counting technique and tracking condition on production method (average duration)

The effect of counting technique (counting and no-counting) and tracking condition (pretracking and tracking) on production method was evaluated using a 2 (counting technique) x 2 (tracking condition) analysis of variance with repeated measures on both factors. There was no significant difference attributable to counting technique alone, F (1,7) = 1.34, $p >.05$. There was a significant difference attributable to tracking condition, F (1,7) = 17.68, $p <.01$, and a significant interaction between counting technique and tracking condition, F (1,7) = 12.19, $p <.05$. During the pretracking condition, productions obtained with and without the counting technique were not significantly different (Table 2). However, when subjects were required to perform a concurrent tracking task, productions made without counting increased in length by nearly 50 % (from 1.08 to 1.51) whereas the productions made with counting increased only slightly (from 1.04 to 1.12). See Figure 4.

Effect of counting technique and tracking condition on production method (variability)

A 2 (counting technique) x 2 (pretracking vs. tracking condition) analysis of variance with repeated measures on both factors was performed on the within-subjects standard deviations of the ratios of produced duration to the specified duration. Durations produced with no counting were significantly more variable than those made with counting, $F(1,7) = 18.87$, $p < .01$. Although there was no significant overall difference in production variability attributable to the tracking condition, $F(1,7) = 4.77$, $p > .05$, there was a significant interaction between counting technique and tracking condition, $F(1,7) = 12.16$, $p < .05$. The mean standard deviations ranged from .04 to .37 with no counting and from .01 to .17 with counting. With counting, mean standard deviations were .05 both with and without tracking. When subjects were not allowed to count, however, mean standard deviations increased to .11 with no concurrent tracking task and to .22 for the tracking condition (see Figure 5).

Effect of counting technique and tracking condition on verbal estimation method (average duration)

The effect of counting technique and tracking (pretracking vs. tracking) condition on verbal estimates was evaluated in a 2 (counting technique) x 2 (tracking condition) analysis of variance with repeated measures on both factors. There was no significant difference attributable to counting technique alone, $F < 1$ and no significant interaction between counting technique and tracking condition, $F(1,7) = 5.33$, $p > .05$. Pretracking estimates were significantly longer, $F(1,7) = 15.62$, $p < .01$, than estimates obtained during tracking (.96 versus .79) although both were shorter than the standard. Although there was no significant interaction between counting technique and tracking condition, the difference between the mean ratios of the no counting condition for pretracking and tracking conditions was .28, while the difference was only .04 in the counting condition (see Figure 6).

Effect of counting technique and tracking condition on verbal estimation (variability)

A 2 (counting technique) x 2 (pretracking vs. tracking) analysis of variance with repeated measures on both factors was performed on the within-subject standard deviations of the ratios of verbally estimated to standard durations. Estimates made without counting were significantly more variable, $F(1,7) = 12.47$, $p < .01$, than those made with counting, but no main effect due to tracking condition was found. $F(1,7) = 2.85$, $p > .05$. The interaction between counting technique and tracking condition was significant, $F(1,7) = 7.10$, $p < .05$. Pretracking estimates were more variable (.17) than estimates obtained in the tracking condition (.11) for the no counting technique, a decrease rather than the expected increase. With counting, standard deviations of verbal estimates were nearly identical with and without tracking (.05

and .05, respectively). See Figure 7.

Comparison of the verbal estimation and production methods (average duration)

The effect of estimation method was examined in a 2 (estimation method) x 2 (counting technique) x 2 (pretracking vs. tracking condition) mixed analysis of variance with repeated measures on counting technique and tracking condition . There was a significant difference attributable to estimation method, F (1,14) = 6.91, p <.05. Produced durations were typically longer than the standard whereas verbal estimates of duration were typically shorter. There was no significant difference due to counting technique alone, F (1,14) = 1.83, p >.05, or tracking condition alone (pretracking and tracking), F (1,14) = 1.65, p >.05. A significant interaction was found between estimation method and tracking condition, F (1,14) = 32.36, p <.001 among estimation method, counting technique, and tracking condition, F (1,14) = 17.30, p <.001.

The length of the subject's productions increased with the tracking task (with and without counting) however, there was less increase when subjects were permitted to count. The length of the subjects' verbal estimates decreased during the tracking task condition, with and without counting. Again, the magnitude of the change was less when the subjects were permitted to count. During pretracking, mean produced durations were virtually the same with and without counting (1.08 and 1.04), however the verbal estimates made with counting (.87) were significantly shorter than those made without (1.05).

Comparison of verbal estimation and production methods (variability)

A 2 (estimation method) x 2 (counting technique) x 2 (pretracking vs. tracking condition) mixed analysis of variance with repeated measures on the counting technique and tracking condition was performed on the standard deviations of the ratios. No significant differences attributable to variability were found for estimation method, F <1, or tracking condition (pretracking vs. tracking), F (1,14) = 1.17, p >.05. Variability was significantly greater, F (1,14) = 31.29, p <.001, for the no counting technique (range .04 to .37) than the counting technique (range .01 to .17). There was a significant interaction between estimation method and tracking condition, F (1,14) = 7.46, p <.05 and among estimation method, counting technique, and tracking condition, F (1,14) = 18.89, p <.001. With the counting technique, there was a slight increase in mean variability of verbal estimates with the addition of the tracking task (from .05 to .06); however, there was no change for the production method (.050 versus .050). Without counting, however, verbal estimation variability decreased between the pretracking (.17) and tracking (.11) conditions. There was a substantial increase in mean variability between the pretracking (.11) and tracking (.22) conditions for the production method. The decrease in variability for the no-counting verbal estimations may have occurred if the subjects became very distracted by the tracking task and responded by repeatedly reporting the same estimate, therefore decreasing the variability among estimates for the tracking condition.

DISCUSSION

Each subject consistently overestimated or underestimated the different intervals by a relatively consistent percentage independent of the interval length. For this reason the ratios of estimated to actual durations within each experimental condition were pooled for subsequent analyses.

A consistent difference was found between the lengths of produced and verbally estimated durations: productions were consistently longer than verbal estimates of the same intervals (Figure 2). In addition, produced durations were typically too long whereas verbal estimates were too short relative to the correct duration. These effects were evident in both the counting and no-counting conditions, with and without a concurrent tracking task.

As hypothesized, an inverse relationship between the length of time productions and verbal estimations was found. The addition of a tracking task made the relationship clearly evident: produced durations increased in length, whereas verbal estimates decreased in length for both estimation techniques. The greatest difference between production and verbal estimation occurred if the subjects did not count as predicted. Produced durations were twice as long as verbal estimates with no counting whereas they were only half again as long with counting during the tracking condition. There was also an interesting inverse relationship between the standard durations of produced and verbally estimated durations: production variability increased with the addition of a tracking task whereas verbal estimation variability decreased. Again the differences between the two methods were particularly great when subjects did not count.

Although there was no significant difference in productions or verbal estimates due to counting technique alone, a significant interaction was found between counting technique and tracking condition for both estimation methods. When subjects were permitted to use an overt form of timekeeping, they were able to perform an additional tracking task while maintaining consistent and accurate performance on a production or verbal estimation task. There was only a slight decrease in the length of verbal estimations and a slight increase in the length of productions when the subjects performed a tracking task while vocally counting.

In contrast, when the subjects were instructed not to count out loud, their ability to keep track of time while performing a tracking task was reduced. The durations produced without counting were significantly less accurate and consistent with the addition of a tracking task. Verbal estimation accuracy, but not consistency, was adversely affected by the addition of a tracking task if the subjects were instructed not to count.

Because performance on the tracking task was the same h both production and verbal estimation techniques, it appears the subject's shift of attention away from time estimation with the no counting technique was not because subjects could perform both tasks but merely that they did not. When attention was focused on the time estimation task by the counting technique, production and verbal estimation accuracy was not degraded and there was no concomitant degradation of tracking task performance.

These results support the findings of Hart (1975) who asked subjects to estimate and produce 10-, 20-, and 30-sec intervals while performing six different compensatory tracking tasks. Production lengths and variability increased and verbal estimate lengths decreased as concurrent task difficulty increased.

The overall difference between the counting and no-counting technique on the ratio of estimated to required time was greater for the production method (1.26 vs. 1.13) than for the verbal estimation method (.88 vs. .86) as was the difference in average within-subject standard deviation (.16 vs. .05 for productions and .13 vs. .05 for verbal estimates). In addition, the magnitude of the interaction between counting technique and presence or absence of concurrent activity was greater for productions than verbal estimates. Whether or not the subject was permitted to vocally count did not seem to have as large an effect on the length of the subjects verbal estimates as it did on his produced durations.

These experimental results support the findings of Hart, McPherson and Loomis (1978) who report that techniques such as counting or tapping that focus the subject's attention on the time estimation task segment the interval into concrete, standardized units, resulting in produced durations that are less variable and less subject to the distracting effects of concurrent activity. Presumably, counting should have a simillar effect on the verbal estimation method and result in estimates that are less subject to the distracting effects of concurrent activities, when in fact the subjects' estimates of the duration of the intervals were quite simillar for both the counting and the no-counting conditions when the subjects performed the tracking task.

The nature of the two estimation methods are somewhat different. The production method is an active process in that the subject plays a role in actually producing the time interval. The verbal estimation method is a more passive process in that the subject must verbally estimate the duration of the interval but plays no role in delimiting the actual interval length. Because of the passive nature of the verbal estimation method the possibility exists that the subjects judged the interval duration relative to the preceding interval or used some form of categorization to judge which interval had been presented rather that viewing the time intervals as a whole series of independent estimates. It is difficult to determine if, in fact, these methodological differences contributed to the different experimental results, however the possibility must be considered.

A significant difference was found between the pretracking and posttracking baseline conditions for the production and verbal estimation methods. The length of the productions increased from pretracking to posttracking for both counting and no counting techniques, although the increase was greater without counting than with counting. Conversely, verbal estimates decreased in length for both the counting and the no-counting conditions, and again the difference was greater with the no-counting technique than for the counting technique. These results are similiar to those reported by Carlson and Feinberg (1970) who found that counting rate decreased from the beginning to the end of each session for the production method. With a decreased counting rate, the length of the productions would be expected to increase. They further reported an increase in counting rate with the verbal estimation method which would results in a decrease in the length of verbal estimations over trials.

No significant interaction was found between counting technique and pre- and posttracking conditions for either estimation method despite the fact that the no-counting and counting conditions were affected somewhat differently by the tracking condition (pre or post tracking). These contradictory results may have occurred due to the large within-subject variability encountered in the no-counting condition.

These results would seem to support Hogan's (1978) premise that boring time intervals are experienced as longer than nonboring intervals. When subjects performed a tracking task while verbally estimating the lengths of time intervals, the estimates decreased in length. When they performed a tracking task while producing time intervals, the productions increased in length. It is conceivable that the subjects perceived the tracking task intervals as more stimulating or interesting than the non-tracking intervals, thus shorter. When the tracking task was removed and the time intervals were less stimulating or interesting for the subjects, verbal estimate lengths increased and production lengths decreased, indicating that the subjects may have experienced boredom.

The lengths of the posttracking productions and verbal estimations may have also been influenced by a fatigue factor. The subjects were required to adjust to the posttracking condition after they had experienced the more stimulating tracking task condition. The decrease in the cognitive/motor stimulation may have resulted in less vigilant attention to the time estimation task.

These experimental results demonstrate: (a) The relative accuracy of both verbal estimates and produced durations appears to be roughly equivalent for standard intervals ranging from 5 to 14 sec, indicating some consistency in individual estimation ability or style. (b) As the difficulty of concurrent activity is increased, the length of time productions increased and the length of verbal estimations decreased. (c) If subjects count while producing or verbally estimating the length of an interval, the resulting estimates will be more consistent. (d) Counting techniques (vocal counting vs. no counting) differentially affect the lengths of time productions and verbal estimations both in the presence or absence of additional tasks. (e) The length of productions increased and the length of verbal estimations decreased from before tracking to after tracking. (f) The effect of concurrent activity on time estimations was less pronounced when subjects were permitted to use the vocal counting technique and (g) Verbal estimates obtained with both counting techniques were less affected by a concurrent task than were productions.

REFERENCES

Bindra, D., & Waksberg, H. Methods and terminology in studies of time estimation. Psychological Bulletin, 1956, 53 (2), 155-159.

Carlson, V.R., & Feinberg, I. Time judgment as a function of method, practice, and sex. Journal of Experimental Psychology, 1970, 85 (2), 171-180.

Dixon, W.J., & Massey, F.J. Introduction to statistical analysis. New York: McGraw-Hill, 1957.

Hart, S.G. Time estimation as a secondary task to measure workload. (Proceedings of the 11th Annual Conference on manual control. NASA TM X-62, 464). Washington, D.C.: U.S. Government Printing Office, 1975.

Hart, S. G., McPherson, D., & Loomis, L. L. Paper presented at the 49th Annual Meeting of the Aerospace Medical Association, Los Angeles, California, 1978.

Goldstone, S., Boardman, W. K., & Lhamon, W. T. Kinesthetic cues in the development of time concepts. Journal of Genetic Psychology, 1955, 93, 185-190

Hicks, R. E., Miller, G. W., & Kinsbourne, M. Prospective and retrospective judgements of time as a function of amount of information processed. *American Journal of Psychology*, *89*, 719-730.

Hogan, H.W. A theoretical reconciliation of competing views of time perception. *American Journal of Psychology*, 1978, *91* (3), 417-428.

Michon, J. A. Tapping regularity as a measure of perceptual motor load, *Ergonomics*, 1966, *9* (5), 401-412.

Norman, D.A., & Bobrow, D.G. On data-limited and resource-limited processes. *Cognitive Psychology*, 1975, *7*

Table 1

Diagrammatic Representation of Experimental Design

Production Method
(N = 8)

	Pretrack	Track	Posttrack
Counting			
No Counting			

Verbal Estimation Method
(N = 8)

	Pretrack	Track	Posttrack
Counting			
No Counting			

Table 2

Summary Table of Means and Within-Subject Standard Deviations
(1) Production and (2) Verbal
Estimation Methods

Production Method

Counting Condition	Tracking Condition		
	Pretracking	Tracking	Mean
No-counting	1.04 (.11)	1.51 (.22)	1.27
Counting	1.08 (.05)	1.12 (.05)	1.10
Mean	1.06	1.32	

Verbal Estimation Method

Counting Condition	Tracking Condition		
	Pretracking	Tracking	Mean
No-counting	1.05 (.17)	.76 (.11)	.90
Counting	.87 (.05)	.83 (.06)	.85
Mean	.96	.80	

Note: Standard deviations are in parentheses, directly below mean scores.

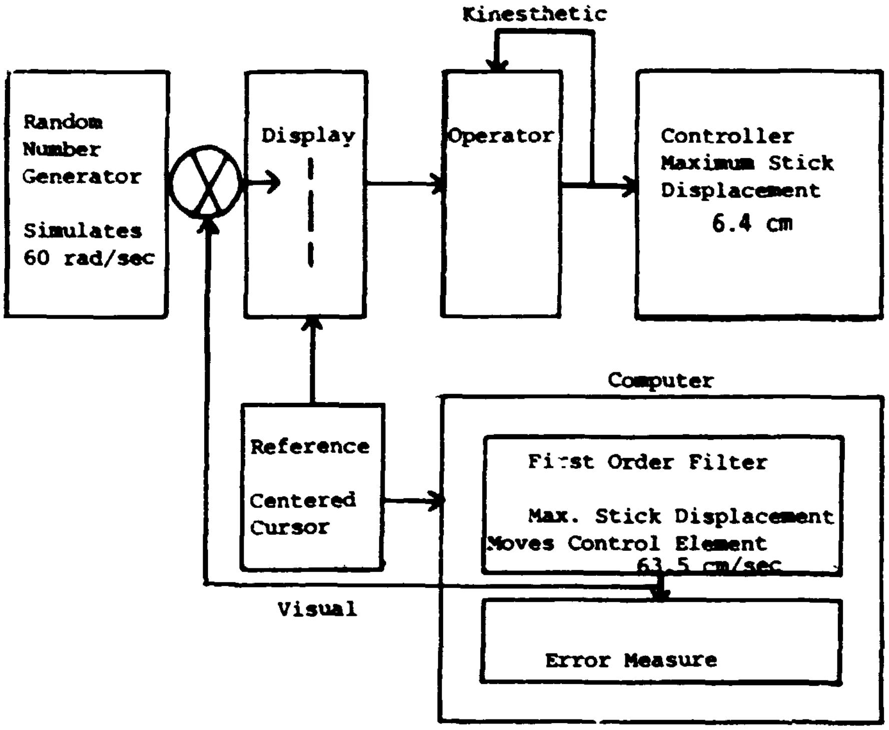
Kinesthetic
Random Number Generator
Simulates 60 rad/sec
Display
Operator
Controller Maximum Stick Displacement 6.4 cm
Computer
Reference
Centered Cursor
First Order Filter
Max. Stick Displacement Moves Control Element 63.5 cm/sec
Visual
Error Measure

Figure 1. Diagrammatic Representation of Tracking Task

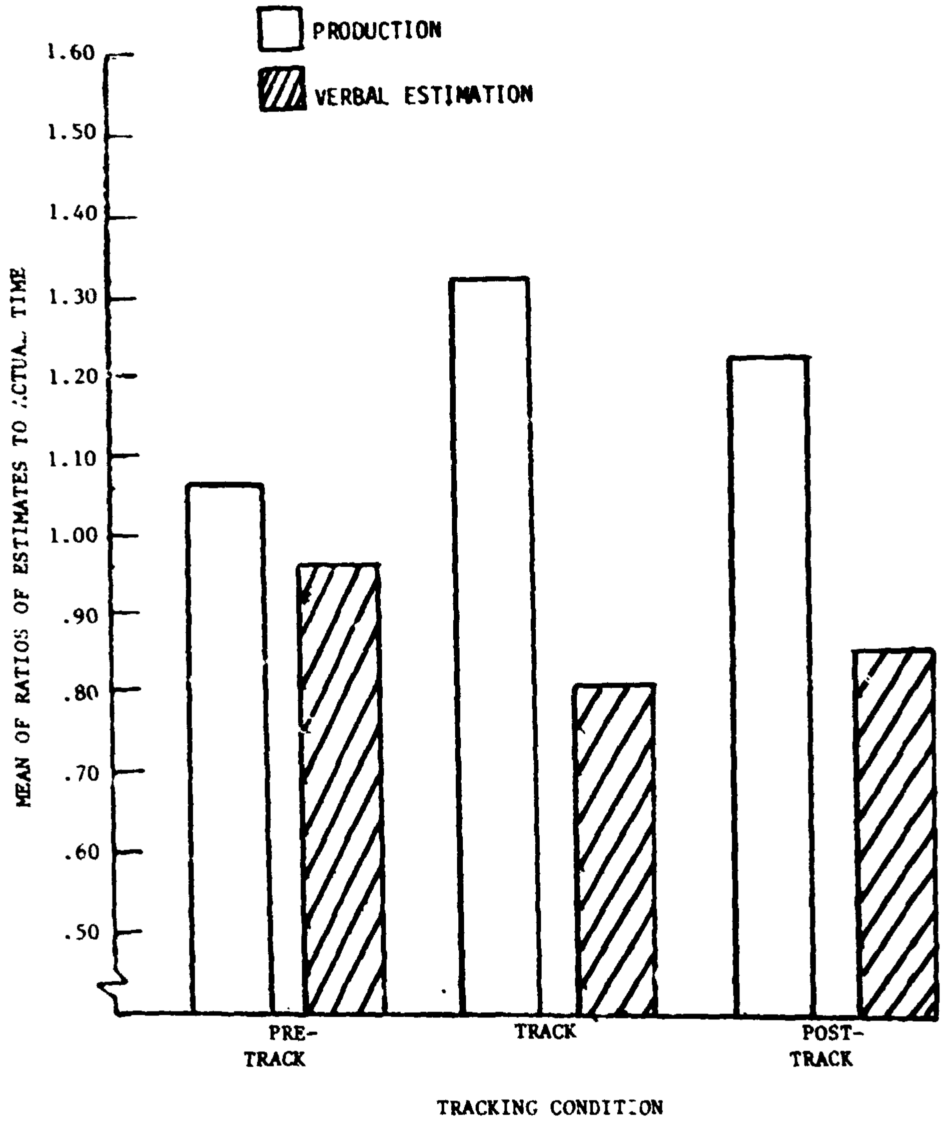

Figure 2. Mean of Ratios of Estimates to Actual Time for Production and Verbal Estimation Methods (N = 8)

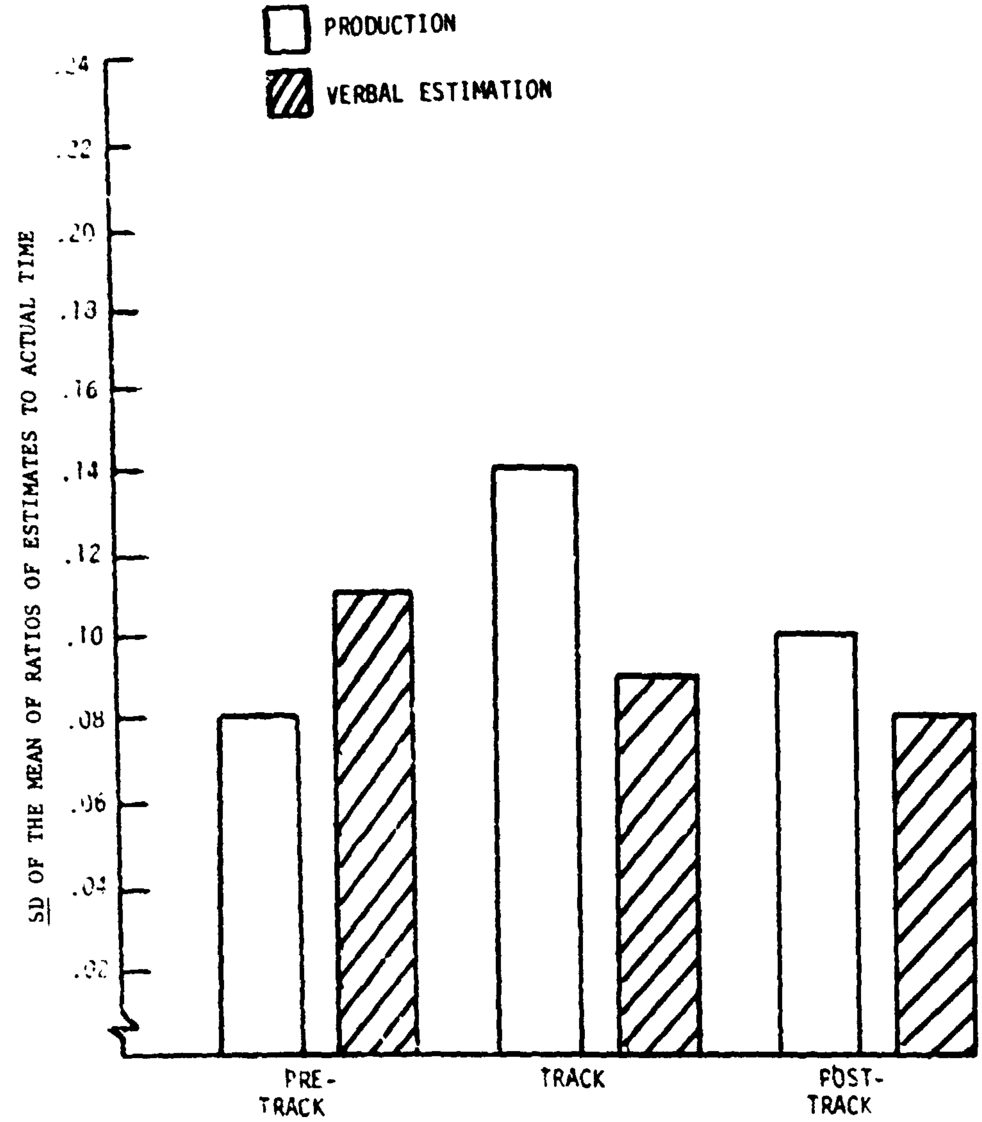

Figure 3. Standard Deviation of the Mean of Ratios of Estimates to Actual Time for Production and Verbal Estimation Methods (N = 16)

ORIG... OF POO...

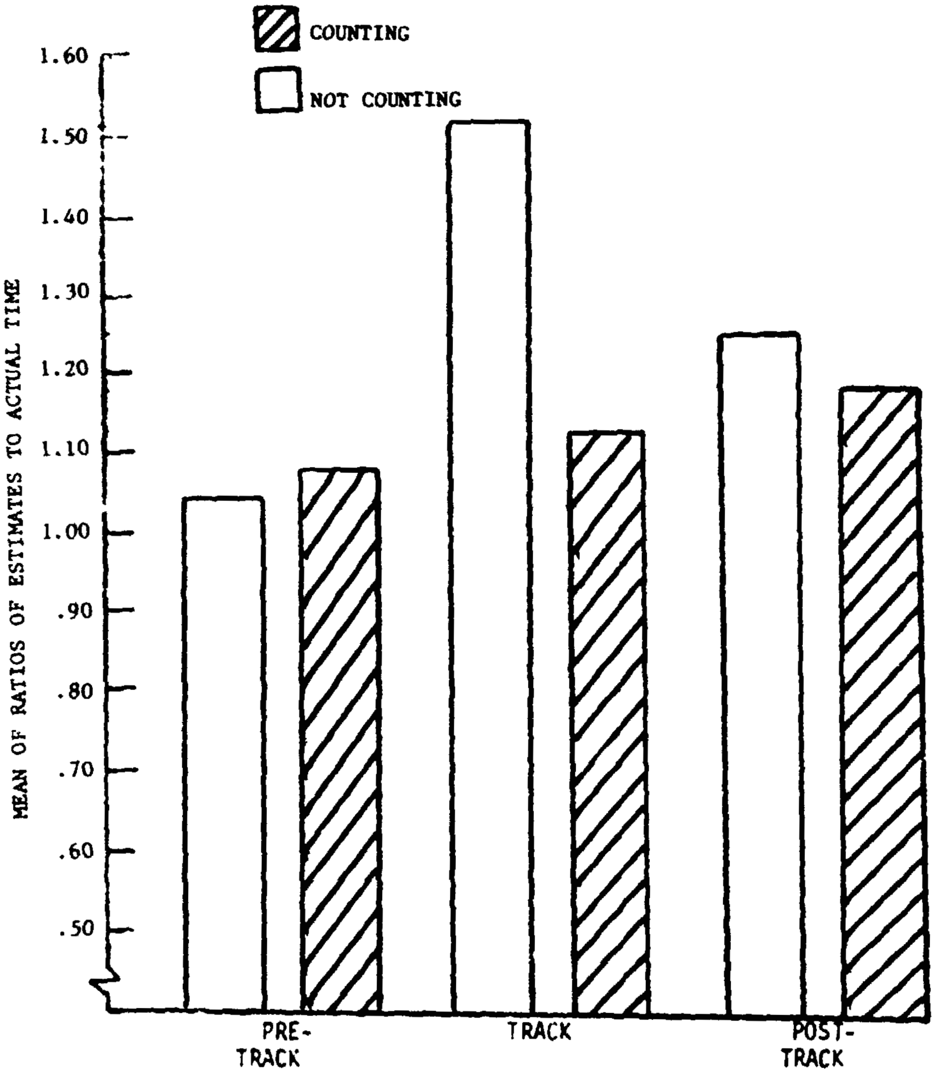

TRACKING CONDITION

Figure 4. Mean of Ratios of Estimates to Actual Time (No Counting - Counting) for Production Method (N = 8)

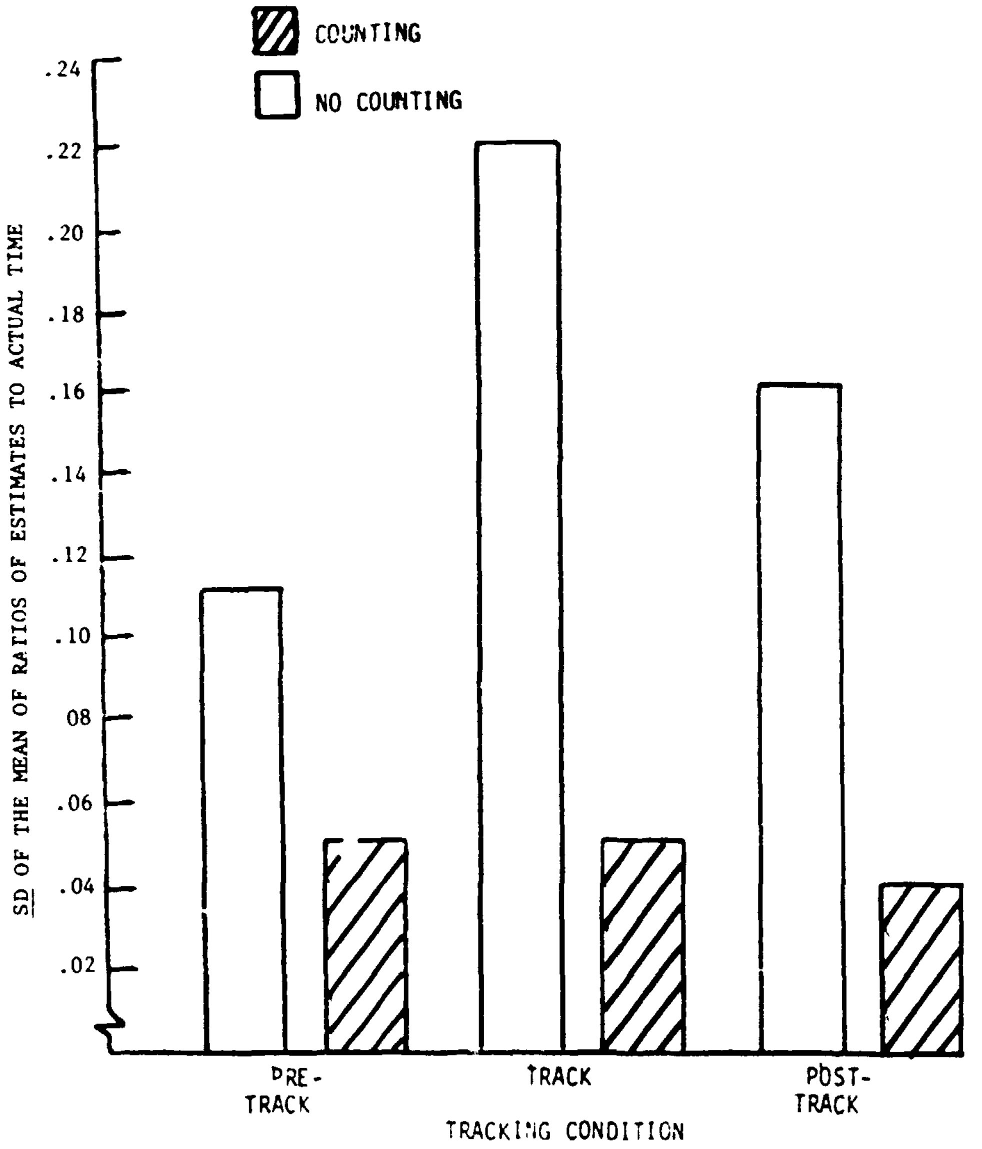

Figure 5. Standard Deviation of the Mean of Ratios of Estimates to Actual Time (No Counting - Counting) for Production Method (N = 8)

ORIGINAL PAGE IS
OF POOR QUALITY

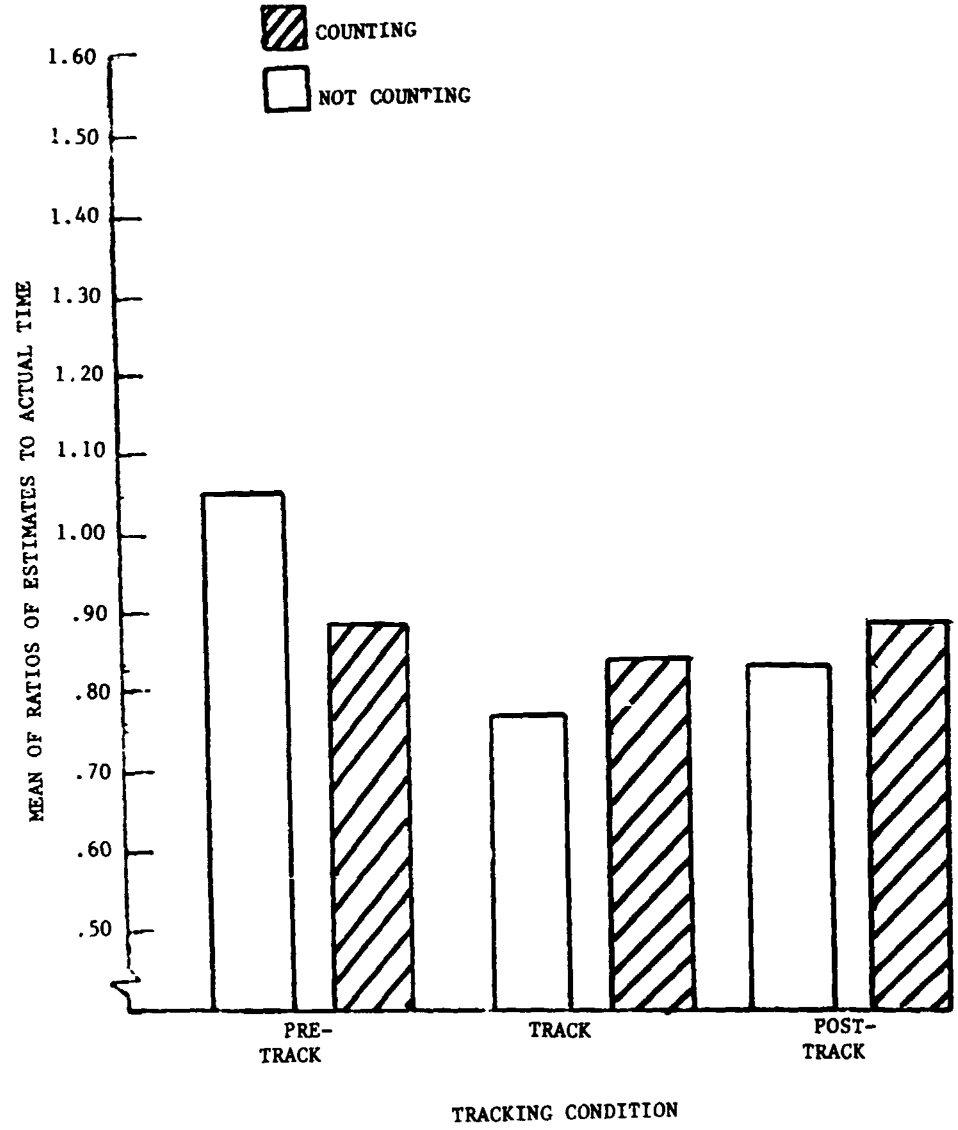

Figure 6. Mean of Ratios of Estimates to Actual Time (No Counting - Counting) for Verbal Estimation Method (N = 8)

C[illegible]
OF [illegible]

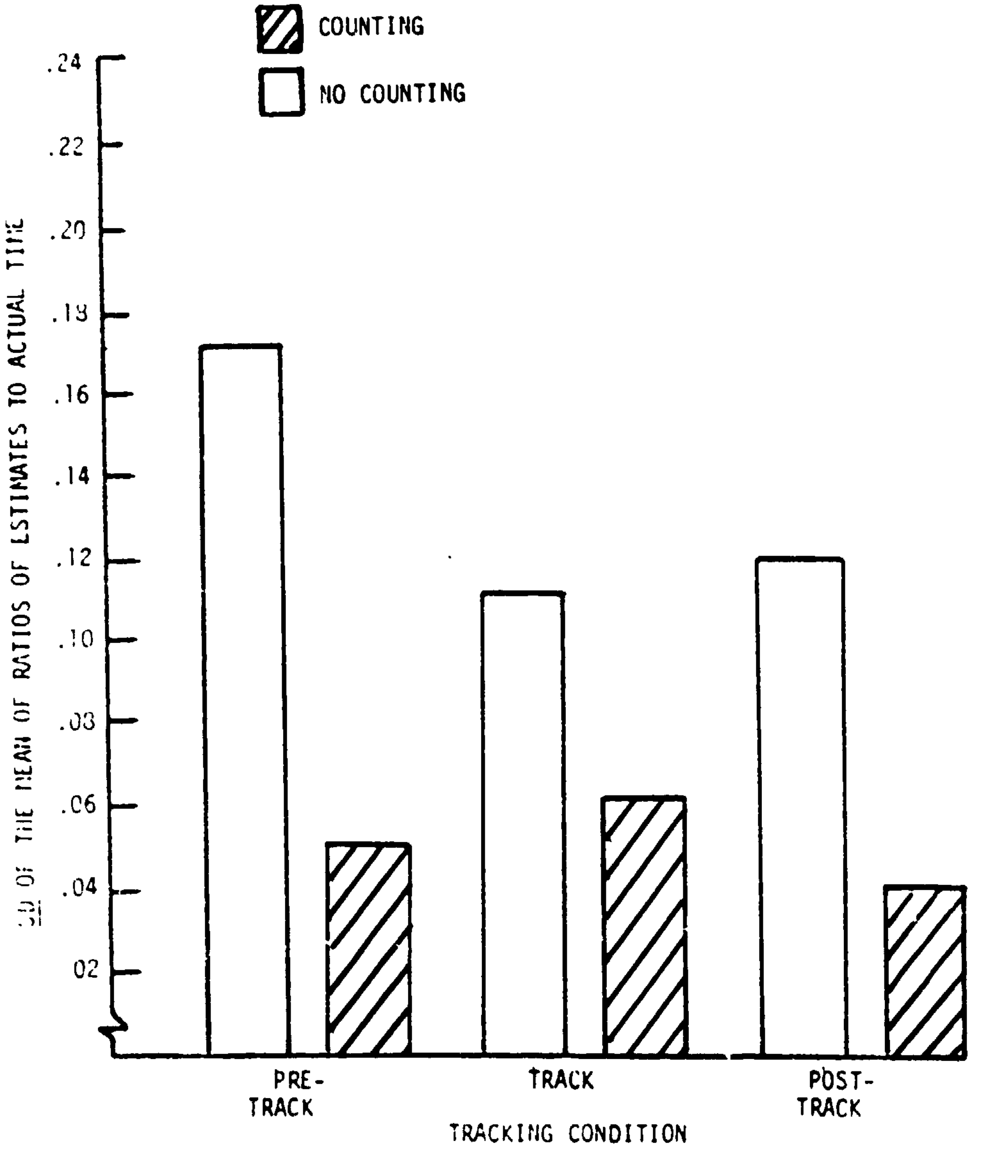

Figure 7. Standard Deviation of the Mean of Ratios of Estimates to Actual Time (No Counting - Counting) for Verbal Estimation Method (N = 8)

EFFECT OF ESTIMATION TECHNIQUE AND TASK CONDITION ON TIME ESTIMATION METHODS (F)

Kathleen L. Bird, San Jose State Univ. and Sandra G. Hart, Tufts Univ.

This study investigated the effects of time estimation technique and task condition on the production and verbal estimation of time intervals ranging from 5 to 14 sec. Sixteen male college students were randomly assigned to two groups, each of which experienced a different estimation method: (a) production; or (b) verbal estimation. The subjects were instructed to either produce or give a verbal estimate of the duration of these time intervals during each task condition: (a) baseline 1 (pre-tracking baseline); (b) tracking (subject performed a one-axis tracking task); and (c) baseline 2 (posttracking baseline). All subjects performed the time estimation task with each condition using both estimation techniques: (a) vocal counting and (b) no counting. The ratio of subjects time estimate to actual interval length was computed for each trial.

A consistent difference was found between the lengths of produced and verbally estimated durations of the 10 time intervals. The subjects productions were typically longer than the verbal estimates of the same duration. Produced durations were typically too long and verbal estimates were too short relative to the actual interval duration. These effects were evident in both the counting and no-counting conditions, with and without a concurrent tracking task.

Estimation technique alone did not produce a significant effect for either time estimation method possibly due to the large within-subject variability for the no-counting condition. A significant interaction was found between estimation technique and task condition for both estimation methods. When subjects were instructed to count out loud they were able to perform an additional tracking task while maintaining consistent and accurate performance on the time estimation task. In contrast, when subjects were instructed not to count out loud, their ability to keep track of time while performing a tracking task was reduced.

A significant effect could be attributed to the addition of a tracking task: produced durations increased in length, whereas verbal estimates decreased in length with and without counting. The durations produced without counting were significantly less accurate and consistent with the addition of a tracking task. Verbal estimation accuracy, but not consistency, was adversely affected by the addition of a tracking task, if the subjects were instructed not to count.

These findings indicate that there is an inverse relationship between the length of subject's productions and the length of verbal estimates. When the subject is instructed to vocally count, the within-subject variability decreases and the subject's ability to estimate time interval durations is less affected by performance of a concurrent tracking task. In contrast, when the subject's were instructed not to count, the accuracy of time productions and verbal estimates was hindered by the addition of a concurrent tracking task.

Performance on a secondary task, e.g., estimating time intervals, is often used as an index of primary task workload, in this case, a compensatory tracking task. The assumption is that processing resources are limited and that performance will deteriorate when several activities compete for the same resources. The results indicate that both time estimation methods were similiarly affected by the addition of a tracking task. The increase in production lengths and decrease in verbal estimate lengths both resulted from underestimation of elapsed time. When subjects were instructed to count, and were distracted by a task, they generally resumed counting where they left off. The interval, therefore, consumed more time than the subject estimated resulting in produced durations that were too long and verbal estimates that were too short.

Jeff Katz and Robert Simpson
Flight Transportaion Laboratory, Dept. of Aeronautics and Astronautics, M.I.T., Cambridge, MA

Title: Pilot Workload in the Air Transport Environment: Theory, Measurement, and the Influence of Air Traffic Control

ABSTRACT

The operating environment of an air transport crew is characterized by multiple interrupting tasks, these tasks being composed of a mixture of purely physical control and purely mental planning processes. Measurement of crew workload is thus a difficult undertaking due to the necessity to resolve workload contributions imposed by several sources. These sources include physical efforts, mental efforts, random task interruptions, and emotional disturbances.

A subjective opinion rating scale is presented for use as an effective workload measure for this air transport cockpit environment. Flight simulator experiments will be run to evaluate the degree of pilot acceptance and the consistency and sensitivity of the rating scale. During these experiments other candidate workload measures (sinus arrythmia, task performance, flight control activity) will be recorded for comparison with the ratings from the subjective scale.

Finally, an analysis is presented which indicates that a major component of workload is induced by the federal air traffic control system. Mechanizations of this loading include speed and altitude restrictions imposed by regulation, confinement and restraint imposed by the structure of the National Airspace System, and loads induced by a stochastic interruption process associated with voice communications. Flight simulator experiments will be run that attempt to measure loading effects due to the presence of air traffic control voice communications during the approach phase of a flight mission.

Workload and Pilot Eye Scanning Behavior

Tole,* J.R., Ephrath, A., Stephens, A.T., and Young, L.R.

Biomedical Engineering Center for Clinical Instrumentation and
Department of Aeronautics and Astronautics, M.I.T.

A number of schemes have been advanced over the years to measure the pilot's mental workload. These schemes include side tasks, physiological measures, and subjective questionaires. While these methods work reasonably well in the laboratory and in ground based simulators, generally they are not well suited to the production of continuous, real time quantitative data in flight. In an effort to develop a technique suitable for implementation in the field, we have investigated the pilot's instrument scanning behavior under various levels of mental loading.

In the current work, experiments were conducted in the Terminal Configured Vehicle (TCV) ground based flight simulator at NASA Langley Research Center. Three NASA test pilots were presented with a piloting task, an arithmetic task designed to vary mental loading, and a side task for calibration of the mental loading task. The pilot lookpoint was obtained using a highly modified Honeywell oculometer system. Pilot eye scan of instruments was recorded in all cases as discussed below. The piloting task involved flying a curved Microwave Landing System (MLS) approach from a specified waypoint to touchdown. To aid in data analysis the approach was divided into six segments: downwind, turn to base, base, turn to approach, approach, and flare. The pilots were aided by a new generation of flight instruments based on CRT displays which were installed in the simulator

The mental loading task was chosen so as not to interfere with the visual scanning of the pilot while providing constant loading during the approach. A series of evenly spaced three-number sequences which were presented verbally. The pilots were asked to verbally indicate the relative ordering of a series. he was instructed to give these responses a priority equal to the primary piloting task. The difficulty of the task was controlled by varying the interval between number sequences.

The workload measuring side task employed two lights, one mounted above the other placed just outside the pilot's peripheral view just above the instrument panel. This was done only when the pilot had time left from performing the primary task of flying the airplane. Thus the number of correct responses on the lights gave a measure of the residual capacity of the pilot from which workload can be calculated.

The conditions were the presence or absence of traffic (other airplanes in the same approach pattern) on the pilot's CRT display, presence or absence of the side task lights, and mental loading task (no numbers, three-number sequences at 20 sec and 10 sec intervals). Two replications were obtained for each pilot.

Visual inspection of X-Y plots of pilot scan over each approach segment show large qualitative differences between different levels of loading. First-order, discrete-state, discrete-transition Markov models are used as a first step in the data analysis. It is assumed that workload is constant along each of the six approach segments since the workload and piloting tasks are essentially constant over each segment. This allows comparison of the instrument transition matricies for each segment with those obtained under different loading conditions. The relationship between visual scanning and workload is given by the change in the elements of these matrices as loading varies.

This work was supported by NASA cooperative agreement #NCCI-23

*Address : Dr. J.R. Tole, 20A-113, MIT, Cambridge, Mass.

The Locus of Processing Demands of Higher-order Control: An Electrophysiological Approach

Christopher D. Wickens and Richard Gill

University of Illinois

Research has well established that the demands imposed upon the operator's limited processing resources are greater in the control of second, as opposed to first, order dynamics. However, within the framework of more sophisticated, multidimensional models of processing resources, the locus of such demands is not well established. Second order control may impose load on perceptual encoding, through the requirement to extract higher derivatives from the display; upon central processing, through the increased complexity of updating an internal model of the dynamic system; and upon response processes, through the requirement to generate alternative "bong-bong" response programs.

In the data reported, the evoked cortical potential is employed to provide a selective index of the perceptual/encoding load imposed in manual control of first and second order systems. This index of the degree of load furthermore is correlated on a trial by trial basis with variations in parameters of the describing function, in order to index its sensitivity to the extent of load generation and perceptual or motor noise.

N82 34050

A Model-Based Technique for Predicting Pilot Opinion Ratings for Large commercial Transports

William H. Levison
Bolt Beranek and Newman Inc.
50 Moulton Street
Cambridge, MA

ABSTRACT

A model-based technique for predicting pilot opinion ratings is described. Features of this procedure, which is based on the optimal-control model for pilot/vehicle systems, include (1) capability to treat "unconventional" aircraft dynamics, (2) a relatively free-form pilot model, (3) a simple scalar metric for attentional workload, and (4) a straightforward manner of proceeding from descriptions of the flight task environment and requirements to a prediction of pilot opinion rating. The method was able to provide a good match to a set of pilot opinion ratings obtained in a manned simulation study of large commercial aircraft in landing approach.

INTRODUCTION

Manufacturers of commercial aircraft require more general and more reliable methods of predicting aircraft handling qualities than currently exist. Existing criteria have been developed primarily for military aircraft and have been validated largely for high-performance aircraft such as fighters. At present, reliable techniques for extending existing criteria to large commercial transports are not available.

This paper summarizes the results of a study performed by Bolt Beranek and Newman Inc. (BBN), with the aid of Douglas Aircraft Company (Douglas), to develop and test a model-based technique for predicting the influence of aircraft response parameters and other relevant factors on pilot opinion ratings. While the procedure is intended to have general application, the focus in this paper is on large transports. Frequent reference is made to a manned simulation study performed by Douglas in 1975.** To facilitate discussion, the analytic study that is the subject of this paper will be referred to as the "BBN study", whereas the preceding simulation program will be referred to as the "Douglas study". Further documentation of the BBN study is provided in reference 1.

---

* The research described in this paper was supported by NASA Langley Research Center under Contract No. NAS1-15529.

** This effort included a subcontract to Douglas Company to provide a data base extracted from the 1975 Douglas simulation study and to provide other consulting services. Mr. William W. Rickard was project engineer for the Douglas effort.

Vehicle-Centered Handling Qualities Criteria

Handling qualities specifications are based almost exclusively on open-loop vehicle response characteristics[2]. Criteria are specified for both transient response and frequency response characteristics. Requirements of this sort allow the aircraft manufacturer to evaluate aircraft performance through a series of relatively straightforward in-flight tests.

Despite the relative convenience with regard to compliance testing, application of vehicle-centered handling qualities specifications to large commercial transports is limited in a number of ways. For example (1) existing handling qualities criteria have been developed primarily for high-performance military aircraft; (2) most existing criteria are based on simple models of aircraft dynamics in which phugoid and short-period response characteristics can be distinguished -- a condition not necessarily met by aircraft having relaxed static stability and substantial control augmentation; (3) turbulence effects are largely ignored; (4) effects of displays (such as flight directors), which may influence overall mission suitability, are not considered; and (5) present methods do not consider effects of dynamic aeroelasticity.

Model-Based Schemes for Predicting Handling Qualities

Pilot/vehicle analysis can allow considerably greater insight into the handling qualities of an aircraft control system than can be obtained by analysis of open-loop response, and the demands made on the pilot can be explored. The effects of external disturbances and control/display parameters, as well as inherent pilot limitations, can be considered. Furthermore, predictive schemes based on pilot/vehicle analysis are not constrained to deal with "conventional" dynamics and are thus potentially more general than techniques based solely on open-loop vehicle characteristics.

Until recently, application of pilot/vehicle analysis to studies of vehicle handling qualities has been based primarily on servo or "classical" control techniques. Perhaps the most comprehensive effort of this type has been conducted by R. O. Anderson and his associates in the development of the "Paper Pilot" analysis scheme[3]. This scheme relates pilot rating to metrics of both closed-loop system performance and pilot workload, and it introduces the concept that the pilot operates so as to minimize his rating score.

Pilot rating is assumed to be an explicit function of system performance and pilot lead requirements (lead compensation being the index of pilot workload in this scheme). A frequency response pilot model is used in this scheme, and pilot parameters are adjusted to minimize pilot rating. Good matches to experimental data have been obtained for a variety of control tasks through appropriate formulation of the rating expression and adjustment of the relative weighting coefficients associated with performance and workload (i.e., pilot lead).[3-6]

While the "Paper Pilot" scheme realizes many of the advantages of a model-based approach, its applicability is limited by lack of general rules for choosing the form of the rating expression and for quantifying the various weighting coefficients. Other factors limiting the generality of this and other procedures based on servo-theory models include: (a) use of a relatively constrained fixed-form pilot model; (b) the need to assume specific loop closures prior to analysis; (c) a cumbersome treatment of pilot workload, especially when multiple loops are closed; and (d) the inability to account directly for factors related to the perceptual environment (e.g., perceptual resolution limitations, whole-body motion cues).

More recently, Hess[7] has described a scheme for predicting pilot ratings based on optimal (or "modern") control theory. He suggests an index of performance that consists of a weighted sum of integral- (or mean-) squared error and control terms. "Error" is a vector quantity that consists of the system variables that the pilot wishes to maintain within acceptable limits. The pilot is assumed to adopt control and estimation strategies that minimize this performance index.

Hess tested his scheme against 19 different configurations covering a range of pilot ratings. "Cost" coefficients of the quadratic performance index were chosen to match experimental scores, and pilot-related model parameters were chosen partly on the basis of previous results and partly to match observed performance. Pilot ratings could be matched to within ±1 rating unit by a linear relationship between pilot rating and the logarithm of the performance index. More recently, Schmidt has used this prediction scheme as the basis for a model-based control design procedure[8].

Although not validated as a reliable predictive tool, Hess' procedure lays the foundation for a scheme that seems › overcome some of the limitations inherent in techniques based on classical servo analysis. The basic form of the performance index is consistent across tasks, the form of the pilot model and nature of loop closures are determined by the optimal pilot model and need not be specified by the user, a scalar metric of workload is provided, and factors related to perceptual environment are considered.

Perhaps the most severe limitation of the optimal-model-based approach, as developed so far, is the requirement to specify numerous task- and pilot-related model parameters. To some extent, the "artistry" in specifying pilot model forms and loop closures for servo-theory models is replaced by the artistry in specifying parameters (especially weighting matrices) of the optimal-control model.

Another limitation, in the opinion of this author, is the lack of a suitable metric for information-processing workload. The metric proposed by Hess (the number of system variables to be regulated) does not appear to add to the rating scheme beyond what is encompassed by the performance index. That is, if workload is to be realted to controlled variables that are of concern to the pilot, then only those variables contributing significantly to the performance index will increase pilot workload. Such effects are accounted for by the numeric value of the index itself.

The methodology described in this paper builds upon the work of Hess and encompasses a pilot rating prediction scheme based on the optimal-control model for pilot/vehicle performance. Emphasis is placed on the predictive aspects of the procedure, and a rationale is offered for selecting model parameters on the basis of an adequate description of the task and in the absence of experimental data. In addition, a well-defined model parameter is suggested as a potential scalar workload metric for the purposes of predicting pilot opinion ratings.

Because pilot opinion is assumed to reflect both pilot workload requirements as well as system performance capabilities, methods for predicting pilot ratings should include consistent and straightforward treatments of workload.

The term "workload" is intended to refer to information-processing -- rather than physical -- activity of the pilot. Specifically, workload is considered synonymous with "attention" in the remainder of this paper. Although attention is not defined here in a way that lends itself to direct physical measurement, the pilot model used in the rating prediction scheme does include a parameter that can be related to attention on both theoretical and empirical grounds. Thus, for the purposes of obtaining rating predictions, attention (workload) is an unambiguous and workable concept.

METHODOLOGY

Basic Approach

The prediction scheme described in this report is based on the following assumptions: (a) pilot rating is a function of the flight task; (B) for a given flight task there exist one or more critical subtasks which serve as the primary determinants of pilot rating; (c) performance requirements are well defined for each critical subtask; (d) pilot opinion is based partly on the degree to which desired performance is achieved and partly on the information-processing workload associated with the task; and (e) a reliable model exists for predicting performance/workload tradeoffs for relevant flight tasks.

These assumptions lead to the procedure diagrammed in Figure 1. The following steps are required for predicting an average pilot rating for a specific situation.

1. Task Definition. Pilot opinion ratings are task dependent. For example, the rating associated with a specific vehicle, relative to other vehicles or other configurations of the same basic airframe, may not be the same in final approach as, say, in high-altitude cruise. Therefore, separate assessments must be made for each flight task of interest.

2. Subtask Definition. Use of the methodology requires a quantitative description of the specific task or subtask for which predictions are to be obtained. For example, if ratings are desired for landing approach, a critical aspect of that task (say, ILS tracking) must be quantified. Task specification requires a linearized description of vehicle dynamics plus a quantitative description of the external environment (e.g., spectral characteristics of the wind gusts if the subtask is path regulation in the presence of zero-mean random turbulence).

3. Define Performance Criteria. Performance criteria must be defined in precise quantitative terms. In order to obtain performance/workload predictions with the pilot/vehicle model used in this procedure, a quadratic performance index containing error- and control-related terms must be specified. The user must specify both the terms to be included in the performance index as well as

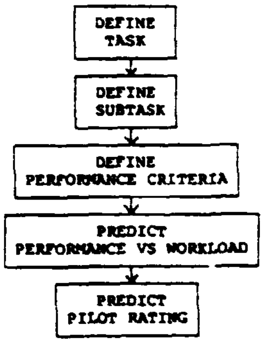
DEFINE TASK
DEFINE SUBTASK
DEFINE PERFORMANCE CRITERIA
PREDICT PERFORMANCE VS WORKLOAD
PREDICT PILOT RATING

Figure 1. Procedure for Predicting Pilot Rating

values for the cost weighting coefficients. Cost weighting coefficients based on assumed maximum allowable values are suggested. As illustrated below, these coefficients are determined partly from the physical constraints of the flight control system, partly from objective performance requirements of the closed-loop system, and partly from pilot preference. The performance criterion used in the rating expression should be a monotonic function of this quadratic performance index.

4. Predict Performance/Workload Tradeoff. The "optimal-control" pilot/vehicle model is used to predict performance as a function of information-processing workload. "Workload"--considered synonymous with "attention" in the context of the model--is defined in terms of a model parameter relating to signal/noise characteristics of the human operator.

5. Predict Pilot Rating. The results of the preceding step are used in a rating expression to predict the pilot rating. If

experimental data are available for the flight task/subtask of interest, a regression analysis is performed to "calibrate" the independent parameters of the rating expression; in this case, absolute rating predictions are obtained. In the absence of such calibration data, rating parameters are adjusted on the basis of previous results, and rating predictions are interpreted on a relative basis with regard to predictions obtained for other vehicle configurations.

Pilot/Vehicle Model

The prediction technique described in this paper is built around the so-called "optimal-control" model for pilot/vehicle systems. The theoretical foundation for this model has been described in the literature, and the model has been validated for both simple laboratory tracking tasks as well as for more complex control situations. As discussed above, this model has also been shown to yield good handling qualities predictions[7].

Only key features of the model are summarized here. Readers unfamiliar with the optimal-control model are directed to the references cited in Reference 1.

The human operator is assumed to adopt strategies of state estimation and control that minimize a scalar quadratic performance index. For airplane piloting tasks, this performance index consists of "error" terms relating to path, attitude, speed, and control variables. Pilot-related limitations reflected in the model include information-processing delay, response bandwidth limitations, and limitations associated with attention-sharing and perceptual resolution.

Attentional and perceptual limitations are accounted for by a set of "observation noise" parameters. Each perceptual variable utilized by the pilot is assumed to be perturbed by a Gaussian white noise process linearly independent of other such noises and of external inputs to the system. In the case of an idealized single-variable tracking task, the variance of each observation appears to scale with the variance of the associated perceptual variable. In this case, response randomness is accounted for by a noise/signal ratio. A more complex definition of the observation noise variance has been derived for situations in which perceptual resolution limitations are important[9].

The model is able to reproduce pilot response behavior in a number of simple laboratory tracking tasks with a nearly constant value of noise/signal ratio of about 0.01 (i.e., -20 dB). The consistency of this parameter across tasks and across subject populations suggests that it reflects a basic central-processing (rather than perceptual or motor) limitation, and these results have led to the following model for central attention sharing:

$$P_i = \frac{P_o}{f_i} \cdot \frac{1}{f_t} \qquad (1)$$

where f_t is the fraction of attention devoted to the tracking task as a whole, f_i is the subfraction of such attention devoted to display variable y_i, and P_o is the baseline noise/signal ratio associated with a high-workload single-variable tracking task (typically, -20 dB).

The attention-sharing model of Eq. (1) has a theoretical base[10] and has been validated in a study of multi-axis tracking by Levison, Elkind, and Ward[11], who found that this model yielded accurate predictions of multi-axis system performance. Wewerinke[12] has also obtained generally good agreement between subjective workload assessments and a "workload index" based partly on this model.

The model parameter, f_t, representing attention to the control task as a whole, serves as the metric for workload in the proposed handling qualities prediction scheme. Because it is a scalar quantity, it may be used in a straightforward manner to predict handling qualities for multi-variable, multi-axis flight control tasks. Unlike workload metrics used in alternative model-based prediction schemes, the attention parameter defined here has a theoretical as well as empirical basis.

Because the predicted "cost" for a given task increases monotonically with increasing noise/signal ratio, and because noise/signal ratio is related inversely to the attention parameter f_t, cost is a monotonically decreasing function of "workload" as we have defined it here. Thus, if other independent model parameters are kept fixed, tradeoff curves of performance versus workload can be predicted for configurations of interest. As described below, these curves can be further processed to yield predictions of pilot rating.

Prediction of Pilot Rating

In keeping with Anderson's philosophy[3], pilot rating is predicted by means of a mathematical expression that includes both performance and workload effects. In general, "performance" is defined in terms of a scalar function of the signal deviations predicted by model analysis. As described above, "workload" is synonymous with the total attention to the task, f_t, which affects performance through the noise/signal ratio.

Best results in this study were obtained through use of a performance metric defined as the joint probability of one or more system variables being outside their respective "limits" (i.e., maximum desirable values). The following alternative philosophies were tested and found to yield good replications of experimentally obtained pilot ratings: (1) pilot rating is determined by the performance achievable at some particular level of workload; (2) pilot rating is determined by the workload required to achieve some criterion level of performance; and (3) pilot rating is a continuous function of both performance and workload, and the pilot operates at a workload so as to minimize the numeric value of his rating (i.e., achieve the best rating).

These philosophies were implemented, respectively, by the following rating expressions:

$$R = 1 + 9 \frac{S}{S+S_o} \Big|_{A=A_o} \tag{2}$$

$$R = 1 + 9 \frac{A}{A+A_o} \Big|_{S=S_o} \tag{3}$$

$$R = 10 \left[\frac{S}{S+S_o} + \frac{A}{A+A_o}\right] \tag{4}$$

$$1 \leq R \leq 10$$

where R is the predicted pilot rating on the Cooper-Harper Scale[13]; S is predicted performance in terms of a probability as defined above, A is the attention model parameter (equivalent to f_T of Eq. (1)), and S_o and A_o are constants of the rating expressions.* For convenience, we shall refer to these rating expressions as the "performance model", the "attention model", and the "minimum-rating model".

The first two expressions are intended as predictors of rating only, not as predictors of the specific point on the performance-workload tradeoff curve at which the pilot will operate. The minimum-rating expression of Eq. (4), on the other hand, embodies the notion expressed by Anderson that the pilot trades between performance and workload in such a way as to minimize the rating score. In principle, use of the minimum-rating expression should allow one to predict pilot workload and overall system performance as well as the pilot rating.

---

* Numerical values for A_o and S_o may vary from one expression to the next.

DATA BASE

The data base used for developing and testing the handling qualities prediction scheme was obtained from two sources: (1) an experimental study performed by Douglas Aircraft Company in 1975[14], and (2) the results of a questionnaire, submitted during the course of this study, to the test pilots who participated in the Douglas study.

Description of Experiments

A manned simulation study was conducted by Douglas to explore the applicability of various handling qualities criteria to longitudinal flying qualities of large transport aircraft in the landing approach. Criteria that were evaluated included several vehicle-centered criteria from MIL-F-8785B[1], vehicle-centered criteria from other sources[14], and a pitch tracking criterion involving a closed-loop pilot model[2]. This study is described in detail by Rickard[14]; a summary of the experiments is given below.

The Douglas study explored a total of 42 vehicle configurations. The first group of 26 configurations were obtained by selecting stability derivatives typical of wide-body aircraft and either varying the simulated cg location from far forward to far aft of the neutral point, or by varying a single stability derivative. Configurations of the second group were obtained by specifying vehicle frequency-response characteristics and then solving for the stability derivatives. All handling-qualities variations were confined to the longitudinal control axis; lateral-directional aircraft parameters were kept fixed throughout the experiment to provide response characteristics typical of a wide body transport.

Five Douglas test pilots performed evaluations of these configurations on a six-degree-of-freedom moving-base simulator. Each evaluation typically consisted of two ILS approaches: the first performed in the absence of simulated atmospheric disturbances, the second in the presence of simulated zero-mean turbulence. Approach was initiated at a range of 7.4 n. mi. from runway threshold at an altitude of 1500 feet on the extended runway center line. The 3-degree glide slope was intercepted at a range of about 4.7 n. mi.; the pilot flew down the glide slope relying on ILS instrumentation for path information to an altitude of about 700 feet, at which point the pilot transitioned to a visual display for flare and touchdown.

The test pilots were encouraged, in general, to perform maneuvers that would aid in their evaluations (e.g., intentionally impose and then eliminate a path or attitude error), but no specific set of maneuvers was required. A single Cooper-Harper rating was given by each pilot for the pair of still-air and turbulent-air approaches for each configuration. Some configurations were evaluated more than once by some of the test pilots. Evaluations were performed on the basis of approach performance only; flare and touchdown characteristics were not considered.

Configurations Explored in the BBN Study

The rating expression described in Eq. (2) - (4) were tested against eight configurations selected from the first group used in the Douglas study. Three configurations were chosen to span a range of pilot ratings as well as a range of handling qualities problems. Modal characteristics for the configurations explored in the BBN study are given in Table 1.

The test pilots were assumed to utilize the ILS instrument, attitude indicator, and airspeed indicator as their primary displays during the instrument-flight portion of the simulated approach.

Zero-mean turbulence was simulated in the three linear and three rotational degrees of freedom in the Douglas study. Turbulence models (based on models suggested in the flying qualities specifications[1]) were used to provide disturbances to longitudinal-axis variables. RMS u- and w- gust levels were fixed at 7.8 ft/sec and 6.5 ft/sec, respectively. Further details on these gust models are given in reference 1.

Performance Requirements

Application of the prediction scheme described above requires that one or more specific subtasks be selected for analysis and that performance requirements be specified for each subtask. To obtain this information, a questionnaire was prepared by BBN and administered by Douglas personnel to 4 of the 5 test pilots that had participated in the 1975 manned simulation study. Through this questionnaire the pilots were requested to (1) state whether or not pilot ratings were determined primarily by longitudinal handling characteristics; (2) specify whether ratings were based mainly on the instrument-flight portions of the approach; (3) specify in order of priority, the subtasks that were important determinants of pilot rating; and (4) specify in as quantitative manner as possible the "desired" and "acceptable" levels of performance for each subtask. A sample of the questionnaire is provided in reference 1.

TABLE 1

Configuration Characteristics

$V = 140$ kts $\gamma = -3^{\circ}$ wt = 350,000 lbs

Config.* Number	ω_{sp}	ξ_{sp}	ω_{ph}	ξ_{ph}	n/α	dγ/dV	$1/T_{\theta 1}$ or [ω	$1/T_{\theta 2}$ or [ξ]
1	0.846	0.628	0.186	0.072	3.80	-0.043	-0.084	-0.506
3	(-0.633)	(-0.307)	0.086	0.318	4.14	-0.049	-0.082	-0.556
4	(-0.811)	(+0.090)	0.200	0.363	4.20	-0.051	-0.082	-0.564
5	(-0.909)	(+0.158)	0.184	0.210	4.24	-0.053	-0.082	-0.568
8	0.811	0.662	0.194	0.041	3.80	-0.324	+0.041	-0.631
15	(-0.991)	(+0.225)	0.211	0.388	4.29	-0.055	-0.082	-0 575
16	(-1.061)	(+0.291)	0.210	0.331	4.35	-0.057	-0.082	-0.583
21	0.441	0.665	0.170	0.042	1.05	-0.285	[0.149]	[0.676]

ω_{sp} = short-period natural frequency, rad/sec

ξ_{sp} = short-period damping ratio

ω_{ph} = phugoid natural frequency, rad/sec

ξ_{ph} = phugoid damping ratio

n/α = normal acceleration per unit angle of attack, g/rad

dγ/dV = path angle change per speed change, deg/kt

T_{θ} = numerator time constant, sec

( ) signifies first-order factor

* Configuration number of the Douglas Study [25].

All four pilots agreed that lateral-directional handling qualities were quite satisfactory and that pilot ratings were influenced primarily by longitudinal handling characteristics. They all stated that the instrument-flight phase was more important in determining ratings.

All subjects indicated at least three subtasks as important determinants of pilot rating. Relative importance of these subtasks for the subject population as a whole was determined from "priority score", computed by assigning 5 "points" to an item receiving highest priority, 4 points to the next priority, and so on to 1 point for tasks ranked fifth or more in the list. Priority scores for each task are shown in Table 2, along with the total score obtained by summing across pilots.

Table 2

Priority Scores for Important Subtasks

	Priority Score				
Subtask	LB	BM	JM	AT	Total
Glide-Slope Capture	5	5	4	4	18
Glide-Slope Tracking	4	-	2	5	11
Recover from Glide Slope Mistrim	3	3	1	4	11
Altitude Station-Keeping	-	4	5	-	9
Open-loop Response	-	2	3	3	8
Recover from Airspeed Mistrim	2	-	1	-	3
Recover from Pitch Mistrim	-	-	1	-	1

Table 2 shows that ratings were largely determined by the ability of the pilot to regulate path error. Highest priority was given to tasks involving transient maneuvering (glide-slope capture, correcting self-induced height error). Next in importance were tasks requiring continuous regulation of height error (altitude station-keeping prior to glide slope acquisition, post-acquisition glide-slope tracking). Open loop response and correction of pitch and airspeed mistrim were of substantially less importance overall in terms of influencing pilot opinion.

Obtaining quantitative comments related to performance requirements was considerably more difficult than anticipated. Only two of the four pilots provided quantitative responses, and only one of these (Subject JM) differentiated between "desired" and "acceptable" performance.* Performance requirements indicated by these two subjects for tasks requiring continuous regulation are given in Table 3.

---

* To aid the pilot in making this distinction, "adequate" performance was defined in the questionnaire as corresponding to the boundary between a rating of 6 and 7, whereas "desired" performance was to be associated with a rating of 1.

Table 3

Subjective Performance Requirements

	JM				BBN
	Alt. Regulation		G-S Tracking		G-S
	Desired	Acceptable	Desired	Acceptable	Tracking
Height Error	± 30 ft.	± 100 ft.	± 1/4 dot	± 1/4 dot at 200' ± 1 dot at 1100'	± 1/4 dot
Sinkrate Error (ft/sec)	± 200	± 500	± 200	± 500	-
Airspeed Error (knots)	± 5	± 10	± 2	± 5	- 5, + 10

Pilot Ratings

Mean and standard deviations of the pilot ratings obtained in the Douglas study are given in Table 4, along with handling qualities levels as determined from two of the vehicle-centered criteria considered by Rickard. Rating statistics were derived by first averaging multiple ratings (where such existed) for each pilot for each configuration, and then using these averages to compute a mean and standard deviation across subjects for each configuration.* Table 4 shows both a wide spread of average pilot ratings across the configurations explored in the BBN study as well as a variety of handling qualities problems. The short-period response criterion predicts adverse handling qualities for five of the configurations -- four of which exhibit static instability. Two of the remaining configurations, on the other hand, exhibit adverse flight path stability ($d\gamma/dV$).

TEST OF METHODOLOGY

The prediction scheme described above and diagrammed in Figure 1 was applied to the data base obtained in the 1975 Douglas study. In order to apply this scheme, twenty independent model parameters had to be specified. As the following discussion demonstrates, eighteen of these parameters were defined largely on the basis of task analysis, tempered by some engineering judgement. Once selected, three parameter values were held fixed throughout the analysis; only the two parameters of the rating expression were adjusted to match experimental data.

---

* Ratings shown for configurations 4 and 5 differ slightly from those presented by Rickard, who computed the mean of all ratings pertaining to a given configuration regardless of the number of evaluations per pilot.

Table 4

Pilot Opinion Ratings

Config.	Pilot Rating Mean	SD	$d\gamma/dV$ Level	ω_{sp} vs. n/α Level	Static Stability
1	2.5	1.5	1	1	Yes
3	4.3	2.3	1	4	Yes
4	4.2	2.1	1	4	No
5	5.3	1.6	1	4	No
8	8.3	2.1	4	1	Yes
15	6.7	1.5	1	4	No
16	7.7	2.5	1	4	No
21	6.2	3.5	4	2	Yes

Mean rating for 5 pilots, configurations 1,2,4,5

Mean rating for 3 pilots, configurations 8,15,16,21

Problem Definition

The methodology described in this paper was applied to the general flight task of final approach, exclusive of landing. On the basis of the questionnaire submitted to the Douglas test pilots, two specific subtasks were initially selected for study: continuous glide-slope tracking in turbulence, and recovery from intentional glide-slope offset. Preliminary exploration of the latter (transient) task was performed, but resources permitted a complete analysis of only the continuous tracking task. Therefore, discussion is confined to tests based on the continuous tracking task.

Although continuous in nature, glide-slope tracking following capture is not, strictly speaking, a steady-state task because of time variations in various task parameters. For example (a) turbulence bandwidth changes with altitude; (b) path control becomes more important as the touchdown point is approached; and (c) since the ILS instrument displays path error in terms of angular deviation, the effective display gain (inches of indicator deflection per foot of height error) also varies with range. Nevertheless, because these time variations are slow compared to the time constants of important system variables, piecewise-steady-state analysis can yield meaningful predictions of pilot/vehicle performance at various points along the glide path.

A "frozen-point" analysis was performed at a simulated altitude of 1000 feet. Parameters of the turbulence model appropriate to this altitude (see reference 1) were chosen for this analysis.

Weighting coefficients for the quadratic performance index given in Eq. (1) were selected as the reciprocals of the maximum allowable deviations (or "limits") on important system variables -- a procedure that has been followed with apparent success in previous applications of the optimal-control pilot model.[9,15] Limits of 117 ft. height error (corresponding to 1 dot glide-slope deviation at an altitude of 1000 ft.) and 10 kts (16.9 ft/sec) airspeed error were chosen on the basis of pilot commentary summarized in Table 3. Limits of 40 pounds stick force (10 degrees elevator deflection), 60 pounds/sec force rate, and 21,500 pounds thrust were chosen, in part, on the basis of physical constraints of the control system. A limit of 10,750 pounds/sec rate of change of thrust was chosen to induce a control-related lag time constant of about 2 sec; this selection was based on the assumption that the pilot would not make continuous wide-band throttle movements during approach.

No limits (i.e., no terms in the quadratic performance index) were associated with either sinkrate error or attitude variables. Penalties on attitude variables were omitted because no limitations on such variables were specified by the test pilot; sinkrate error was omitted from the performance index to prevent overemphasis on height-related variables. Despite the lack of explicit performance penalties on attitude variables, the penalties on control-related variables constrained the model to predict a reasonable "mix" of height, attitude, and control deviations.

The pilots were assumed to make longitudinal-axis flight-control inputs primarily on the basis of perceptual information obtained from the ILS, attitude, and airspeed instruments. Rate information was also assumed to be obtained from the ILS and attitude indicators. Thus, the "display vector" assumed for model analysis consisted of height, sinkrate, pitch, pitch rate, and airspeed errors.

Attention was assumed to be divided equally between the ILS, attitude, and airspeed instruments; no attention-sharing penalties were considered between displacement and rate information from the same physical display. On the basis of analysis performed in a previous analytic study of landing approach,[14] 34% of the pilot's attention was assumed to be "lost" because of large eye movements required to scan the flight-control instruments. Thus, fractional attentions of 0.22 were associated with the ILS, attitude, and airspeed displays.

Effective perceptual thresholds were computed from the display gains (i.e., inches of display deflection per unit change in problem variable), the eye-to-display distance, and assumed values of perceptual resolution limitations based on previous laboratory experiments as described by Levison.[1] A residual noise was also

ORIGINAL PAGE IS
OF POOR QUALITY

associated with perception of pitch attitude change. Display and performance-related model parameters are given in Table 5.

Table 5

Display- and Performance-Related Model Parameters

Variable	Limit	Cost Coefficient	Threshold	Residual Noise	Relative Attention
h	117	7.31 E-05	9.3	0	.22
$\dot{h}$	-	-	37.	0	.22
θ	-	-	.43	0.5	.22
q	-	-	1.72	0	.22
u_1	16.9	3.5 E-03	1.9	0	.22
δ_e	40	6.25 E-04	-	-	-
$\dot{\delta}_e$	60	2.78 E-04	-	-	-
δ_t	21,500	2.16 E-09	-	-	-
$\dot{\delta}_t$	10,750	8.65 E-09	-	-	-

h = altitude error, feet

θ = pitch change, degrees

q = pitch rate, degrees/second

u_1 = airspeed relative to moving air mass, feet/second

δ_e = force on the control column, pounds

δ_t = thrust deviation from trim, pounds

Additional pilot-related model parameters -- not shown in the table -- were (a) an observation noise/signal ratio of -20 dB associated with a relative attention of unity, (b) a motor noise/signal ratio of -60 dB, and (c) a time delay of 0.2 seconds.

Prediction of Performance/Workload Tradeoffs

Performance/workload tradeoffs were predicted for each of the eight configurations defined in Table 1. For purposes of predicting handling qualities, "performance" was defined as the probability of one or more system variables exceeding maximum allowable values. To obtain an approximation to this joint probability, system variables were treated as independent Gaussian variables,

(5)

where Pr_i is the probability that the ith variables of interest will lie outside its prescribed boundary, and Pr is the probability that at least one such variable is out of bounds. The probability Pr_i was readily computed from the predicted variance of the ith system variable. (Since we considered steady-state conditions, all variables were assumed to be zero-mean Gaussian processes.) "Workload" was represented in the analysis by the attentional variable f_t; the f_i were adjusted to reflect attention-sharing as shown in Table 5. A noise/signal ratio $P = 0.01$ was associated with a relative attention of unity. Thus, variations in attentional workload were reflected by changed in the noise/signal ratios according to Eq. (1).

Predictions of performance versus attentional workload are shown in Figure 2 for the eight configurations explored in the BBN study. Values of attention shown on the abscissa are relative to that inferred from data obtained in a standardized laboratory tracking task. That is, unity attention is intended as a benchmark level of workload and does not necessarily relate to maximum effort of capability. Thus, for configurations in which predicted performance is especially sensitive to attention, predictions are shown for relative attentions greater than unity.

The trends shown in Figure 2 are consistent with the pilot ratings given in Table 4. Except for configuration 8, the ordering of the performance/workload curves is consistent with the ordering of the pilot ratings. For attentions of 0.5 and greater, predicted performance for the remaining seven configurations follows the trend of the ratings. Operation on these results to yield predicted pilot ratings is discussed below.

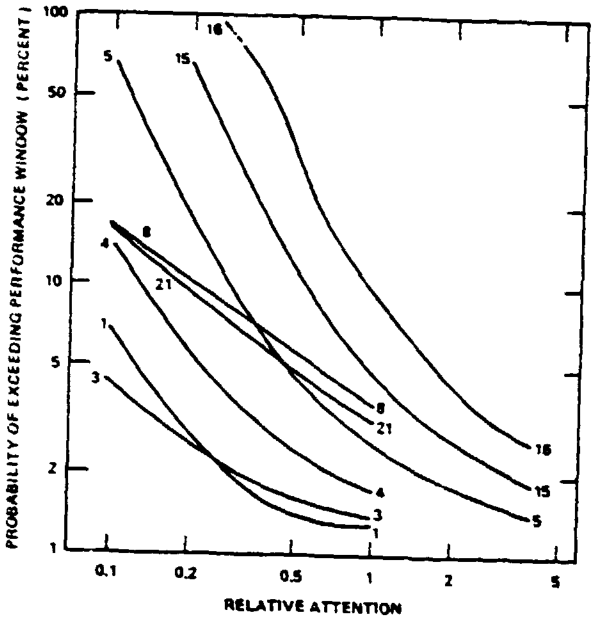

Figure 2. Prediction of Performance versus Workload

Predicted Ratings

The three rating expressions presented in Eqns. (2-4) were applied to the performance/workload tradeoff curves to provide a test of the proposed methodology. Values were assigned to the independent parameters of each expression as shown below in Table 6.

The value of A_0 of the performance model was chosen to represent a moderate-to-high workload level, and the corresponding value for S_0 was found through a regression procedure that minimized the mean-squared difference between predicted and experimental pilot ratings, normalized with respect to the variance of each experimental rating. The value for S_0 of the attention model was selected to represent a moderate-to-stringent performance requirement, and the value for A_0 was found through a similar regression analysis.

Table 6

Independent Parameters for the Rating Expression

Expression	σ_o	A
Performance Model	5.3%	0.50
Attention Model	5.0%	0.47
Minimum-rating Model	10.0%	2.0

Because of the lack of a tractable analytic expression relating performance to workload, the parameters S_0 and A_0 of the minimum-rating model were not found through a computerized regression analysis. Rather, pairs of integers were explored on a trial-and-error basis to provide a good match to experimental pilot ratings. The predicted (minimum) rating for a given configuration was obtained by superimposing the predicted performance/workload tradeoff curve (Figure 2) on the curves of constant rating, shown in Figure 3.

Because of the difficulty in matching the predicted pilot ratings of Configuration 8, ratings for this configuration were omitted from all three regression analyses.

Figure 4 provides a graphical comparison of predicted versus experimental pilot ratings for the three rating expressions. Dashed lines indicate boundaries of 1 rating unit. The three rating schemes performed about equally well on the average and were able to match 6 of the 8 experimental ratings to within one rating unit. The configuration matched least well was Configuration 8, which was omitted from the regression analysis.

Prediction errors may be compared against the variability of the experimental data in Figure 5. Experimental ratings are indicated by filled circles, with brackets to indicate 1 standard deviation; open symbols indicate predictions obtained with the three rating expressions.

Except for Configuration 8, predicted ratings are within one standard deviation of the experimental mean. Even for the worst case, the prediction error is well within two standard deviations of the mean. Thus, the reliability of the predicted ratings is commensurate with the reliability of the experimental data.

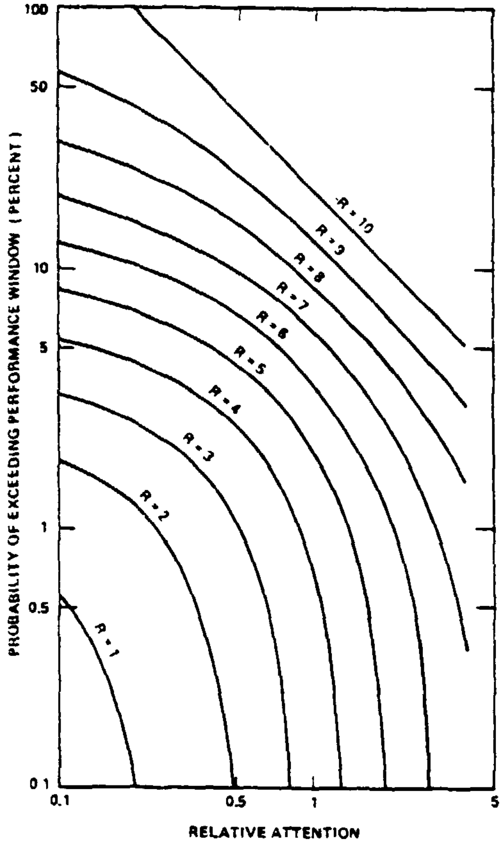

Figure 3. Curves of Constant Rating for the "Minimum Rating" Model

T_o = .04 A_o = 2

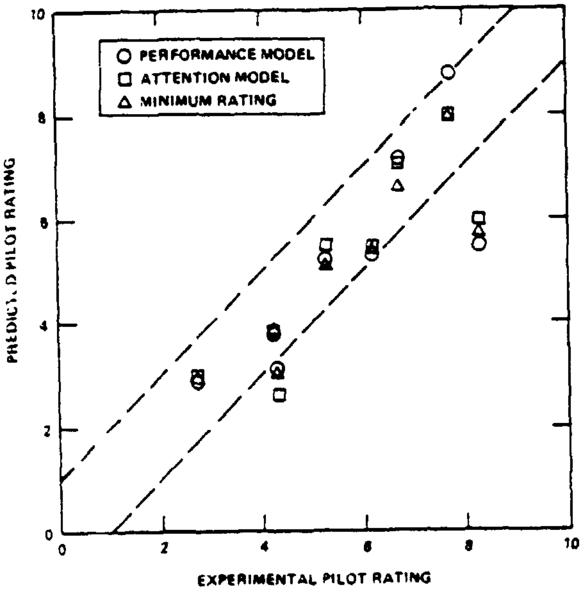

Figure 4. Predicted versus Experimental Pilot Ratings

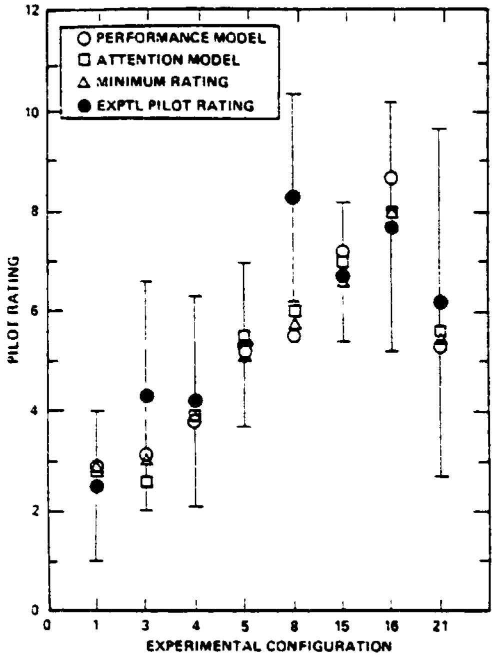

Figure 5. Comparison of Predicted and Experimental Ratings

Discussion of Results

The generally good match between "predicted" and experimental pilot opinion ratings demonstrates the validity of the model-based approach described in this paper. The technique is shown to replicate experimental results reasonably well across a set of conditions that spans a range of handling qualities levels and problems. Because the procedure is based on a pilot/vehicle model of considerable generality and demonstrated validity, this scheme ought to be valid for other aircraft configurations and , with appropriate definitions of performance requirements, other flight tasks as well. Further study is required to compare the BBN techniques against other model-based procedures and to further compare the usefulness of the three rating expressions tested in this study.

Resources did not permit a detailed study of the inability to obtain a good match to the experimental rating for Configuration 8. The differences between the average ratings for Configurations 8 and 21 (which our prediction scheme predicts to be negligible) were apparently not due to training effects; these two configurations were presented to the test pilots in a balanced order.

It should be noted that all tests of the proposed methodology have been based on steady-state analysis appropriate to conditions at a single altitude. Although steady-state-like tasks were important determinants of pilot opinion, transient-response behavior was also important. There may have been some aspects of glide-slope capture and other transient maneuvers that were especially adverse for Configuration 8. Additionally, it is possible that a different choice of steady-state parameters (e.g., turbulence appropriate to a lower altitude, different "limits" on throttle response) may have differentiated between Configuration 8 and 21.

Data from the Douglas experiments were used in the BBN study because of their applicability to large transports. Because the experimental study was performed well before the BBN analytical study, the Douglas effort was not designed to allow a thorough test of the model-based prediction to scheme. Hindsight reveals the following methodological deficiencies:

1. Sparcity of Performance Measurements. Pilot opinion ratings were the only data published relating to closed-loop pilot/vehicle performance. Objective performance measures such as rms errors, pilot describing functions, spectra, or time histories are not available. Thus, we cannot determine the pilot's "operating point" in terms pilot-related model parameters, and we cannot verify the ability of the model to predict objective performance measures.

2. Large Rating Variability. Standard deviations for pilot ratings, as determined across subjects, were relatively large, reaching a maximum of 3.5. Clearly, large variability in the data hinders a rigorous test of the prediction scheme. To some extent, the large standard deviations resulted from a small subject population (only 3 subjects provided ratings for 4 of the configurations explored in the BBN study). As described below, a more significant factor may have been an insufficiently specific evaluation procedure.

3. Insufficiently Specific Evaluation Procedure. Typically, each pilot was allowed two "flights" per configuration: an initial flight without turbulence, and a follow-up flight with moderate turbulence. The pilots were encouraged to perform maneuvers that would aid in developing their rating, and they were asked for a single overall rating of the configuration of the end of the two slights. While all subjects appeared to consider the same basic maneuvers and subtasks (glide-slope capture, glide-slope tracking, recover from mistrim, open-loop vehicle response), we do not know the extent to which each pilot weighted the various response categories. Different weightings might have led to different ratings for the same configuration -- a possible explanation for the large pilot-to-pilot variability observed in this study. Differences in the pilot's expectations of system performance are another potential source of rating variability.

Consideration of these methodological shortcomings suggests alternative approaches in future studies, as outlined below.

CONCLUSIONS AND RECOMMENDATIONS

A technique based on the optimal-control model for pilot/vehicle systems has been developed for predicting pilot opinion ratings. Three variations of this technique provide a good match to opinion ratings obtained in a manned simulation study of large commercial transports in landing approach.

The model-based technique developed in this study has a number of features which should enhance its applicability to other aircraft configurations and other flight tasks and should allow wider application than alternative handling qualities prediction schemes:

1. One is able to proceed in a straightforward manner from a description of the task environment and of task requirements to a prediction of pilot opinion ratings. The general form of the

rating expression and of the underlying pilot model is invariant across applications.

2. No constraints are placed on the nature of the vehicle response and the pilot model is relatively free form. Thus, "unconventional" aircraft dynamics may be considered.

3. A scalar metric for attentional workload is expressed in terms of a model parameter related to the signal/noise properties of the pilot's response. Thus, the treatment of workload is independent of the details of the flight task.

4. The effects of display parameters, turbulence, and other environmental factors on pilot opinion rating are readily considered.

Encouraging results obtained with the model-based technique tested in this study warrant further research to provide a more rigorous test of the procedure and to determine its range of validity. Such a study should be subjected to the following guidelines:

1. *Flight Test Standardization.* The flight tests performed for the purpose of obtaining pilot opinion ratings should be standardized so that all pilots perform the same maneuvers on the aircraft. Either separate ratings should be obtained for individual maneuvers, or care should be taken to assure that all pilots weight the various maneuvers in the same manner when assigning an overall rating to the aircraft.

2. *Define Performance Criteria.* Through a carefully prepared and administered questionnaire, subjective performance criteria should be determined for the various test maneuvers. If practical, test pilots should be encouraged to adopt a common set of criteria to minimize rating variability.

3. *Performance Measurement.* Objective measures of system performance and pilot response behavior should be obtained, in addition to pilot opinion ratings, to provide a more rigorous test of the method.

REFERENCES

1. Levison, W. H., "A Model-Based Technique for Predicting Pilot Opinion Ratings for Large Commercial Transports", NASA Contractor Report No. 3257, April 1980.

2. "Flying Qualities of Piloted Airplanes", Military Specification, MIL-F-8785B (ASG),1969.

3. Anderson, R. O., "A New Approach to the Specification and Evaluation of Flying Qualities", Wright-Patterson Air Force Base, AFFDL-TR-69-120, 1970.

4. Arnold, J. D., R. B. Johnson, and J. D. Dillow, "Pitch Paper Pilot Revisited", *Proceedings of the Ninth Annual Conference on Manual Control*, Massachusetts Institute of Technology, Cambridge, Massachusetts, 1973.

5. Naylor, F. R., J. D. Dillow, and R. A. Hannen, "Roll Paper Pilot", *Proceedings of the Ninth Annual Conference on Manual Control*, Massachusetts Institute of Technology, Cambridge, Massachusetts, 1973.

6. Stone, J. R., "Paper Pilot Ponders Supersonic Transports", *Proceedings of the Ninth Annual Conference on Manual Control*, Massachusetts Institute of Technology, Cambridge, Massachusetts, 1973.

7. Hess, R. A., "Prediction of Pilot Opinion Ratings Using an Optimal Pilot Model", HUMAN FACTORS, 1977, 19(5), 459-475.

8. Schmidt, D. K., "Optimal Flight Control Synthesis via Pilot Modeling", *Journal of Guidance and Control*, Vol. 2, No. 4, Jul.-Aug. 1979.

9. Baron, S. and W. H. Levison, "Display Analysis with the Optimal Control Model of the Human Operator", HUMAN FACTORS, 1977, 19(5) 437-457.

10. Levison, W. H., "A Model for Mental Workload in Tasks Requiring Continuous Information Processing", *Mental Workload Its Theory and Measurement*, Plenum Press, New York and London, 1979.

11. Levison, W. H., J. I. Elkind and J. L. Ward, "Studies of Multi-Variable Manual Control Systems: A Model for Task Interference", NASA CR-1746, May 1971.

12. Wewerinke, P. H., "Human Operator Workload for Various Control Situations", *Tenth Annual Conference on Manual Control*, Wright-Patterson Air Force Base, Ohio, 1974.

13. Cooper, G. E., "The Use of Pilot Rating in the Evaluation of Aircraft Handling Qualities", NASA TN D-5153, April 1969.

14. Rickard, W. W., "Longitudinal Flying Qualities in the Landing Approach", *Proceedings from the Twelfth Annual Conference on Manual Control*, NASA TMX-73,170, May 1976.

15. Levison, W. H., "Analysis and In-Simulator Evaluation of Display and Control Concepts for a Terminal Configured Vehicle in Final Approach in a Windshear Environment", NASA Contractor Report 3034, August 1978.

N82 34051 -14

AN ANALYTICAL PREDICTION OF PILOT RATINGS UTILIZING HUMAN PILOT MODEL

by

Keiji Tanaka* and Kyuichiro Washizu**

*Instrumentation and Control Division, National Aerospace Laboratory, Tokyo, **Department of Aeronautics, University of Tokyo, Tokyo

ABSTRACT

In order to analytically predict pilot ratings an evaluation method of a manual control system which consists of an aircraft and a human pilot, is proposed and examined. The method is constructed upon the assumptions that the control mission determines the critical frequency the pilot should bring to his focus, and that the degree of closed-loop stability and the human compensation necessary to attain the stability determine the human subjective evaluation of the system. As a result, a simple evaluation chart is introduced. The chart enables us to predict the subjective evaluation, if the controlled element dynamics and the mission are given. The chart is in good accord with almost all of the existing results of pilot ratings. This method has the following four advantages: (i) Simplicity, in a sense that the method needs to evaluate only two typical controlled element parameters, namely, the gain slope and the phase at the critical control frequency; (ii) Applicability to unstable controlled elements; (iii) Predictability of controllability limits of manual control; (iv) Possibility of estimating human compensatory dynamics.

INTRODUCTION

In recent years, handling quality criteria of aircraft have been influenced by rapid development of the automatic flight control system. Newly developed flight control system enables aircraft to be designed with any handling characteristics. Aircraft with those flight control systems are sometimes called higher order system (HOS), the response of which doesn't indicate significant short period mode any more. Urged by thus obtained increase of degrees of freedom in designing aircraft handling characteristics, revisions to the handling quality criteria have been proposed[1-3]. These revisions, however, have the following common problems: (1) There is no direct relationship between the criteria and the human pilot models; (2) To measure gain or phase characteristics, careful attention is needed. If measured frequencies differ, the result becomes quite different.

The objective of this paper is to propose and examine an improved method to perdict pilot ratings, which fully utilizes human pilot models and their limitations, and which aims at overcoming the above problems. In this paper, we treat a typical single-loop manual control system keeping in mind the application of this method to determining the short-period pitch maneuver response requirements for aircraft design.

FORMULATION OF AN IMPROVED METHOD

Evaluation Process of Manual Control System by Human Pilot

In this paper, we treat a typical single-loop manual control system shown in Fig.1. Evaluation by a human pilot is considered as follows: when he is assigned a control mission, his evaluation is due to the amount of his workload and the extent of fulfilment of the mission. To make the above notion clear, let's define the following terms:

(1) *Control Mission* This is the objective of manual control set up by external factors of the human pilot. To be concrete, the external factors are the features of the forcing-function and the controlled element, etc.. We assume that the mission is represented by the gain-crossover frequency ω_c, which we hereafter treat as the critical control frequency. If the mission is a severe one, the system should be tightly closed; then the larger ω_c becomes appropriate.

(2) *Pilot Workload* This may be divided broadly into mental workload and physical workload. The mental workload corresponds to the human compensatory characteristics, which means the pilot's self-adjustment of his control dynamics according to the controlled element dynamics in order to accomplish the control mission. The mental workload imposed by pilot compensation can be measured by using an identification technique of human describing functions. On the other hand, the physical workload corresponds to the amount of physical work done by the pilot. Measures of the physical workload can be the magnitude of control column deflection c, or physiological responses. As modern aircraft are equipped with power-boosted control, it is possible to adjust the control column gain at the designer's option. Under this trend, we had better distinguish the problem of designing the control column gain from man-machine closed-loop analysis. Hence, we hereafter choose the mental workload, or in another word, pilot compensation, as the index of the pilot workload.

(3) *Control Performance* This is expressed by the variance of the error. In general, manual control systems sometimes have insufficient stability among various representative closed-loop characteristics. For such cases control performance is mainly determined by the closed-loop resonance.

(4) *Pilot Rating* This is a rated mark put to a given system by the human pilot. He subjectively evaluates the system putting his workload and the control performance together.

(5) *Pilot Compensation* This is the most influential factor upon the mental workload and the control performance. The human pilot compensates the controlled element so that the total closed-loop response shows satisfactory

characteristics.

Analysis of Manual Control System

In order to obtain the closed-loop characteristics, it is convenient to employ the amplitude-phase plots of the open-loop transfer function $Y_pY_c(s)$ in Fig.1. As typical examples of Y_pY_c plots, Fig.2 is quoted from Ref.1; in the figure we arranged the plots so that the preselected bandwidth (BW) becomes ω_c. It can be seen that in most cases the plots are approximated by an essentially straight lines near ω_c in amplitude-phase plane, and the slopes of the plots are relatively shallow so that the closed-loop resonance is directly estimated by the gain margin GM, rather than the phase margin ΦM. For such a case, GM can be approximated by using the slope of the plots and ΦM as:

$$GM = \{d|Y_pY_c|/d\angle Y_pY_c\}_{\omega=\omega_c}\cdot \Phi M \quad [dB], \tag{1}$$

where ΦM is defined as follows:

$$\Phi M = \angle Y_c(j\omega_c) + \angle Y_p(j\omega_c) + \pi \quad [rad]. \tag{2}$$

It is worth noting here that the above GM and ΦM can be defined even though the controlled element has one or two unstable poles. When the controlled element has unstable poles, there exists a permitted range of gain variability which can make the system stable. In those cases, there are two phase-crossover frequencies. If we choose the larger frequency, the plots similar to Fig.2 are obtained.

Consider the human compensation which is necessary for closed-loop stability. We rewrite Eq.(1) by using Eq.(2) as:

$$\{d|Y_c|/d(\log\omega)\}_{\omega=\omega_c} = \frac{GM\{d\angle Y_pY_c/d(\log\omega)\}_{\omega=\omega_c}}{\angle Y_c(j\omega_c) + \angle Y_p(j\omega_c) + \pi} - \{d|Y_p|/d(\log\omega)\}_{\omega=\omega_c} \tag{3}$$

In Eq.(3), pilot dynamics is expressed by; $\angle Y_p(j\omega_c)$, $\{d|Y_p|/d(\log\omega)\}_{\omega=\omega_c}$ and $\{d\angle Y_pY_c/d(\log\omega)\}_{\omega=\omega_c}$. Among these, the first and the second have direct relationship with human compensation. On the other hand, it is difficult to find a simple relationship between $\{d\angle Y_pY_c/d(\log\omega)\}_{\omega=\omega_c}$ and human compensation, for human pilot dynamics contains the reaction time delay which appears only in phase characteristics. For simplicity of the analysis, $\{d\angle Y_pY_c/d(\log\omega)\}_{\omega=\omega_c}$ is tentatively held constant. Referring to Eq.(3), the actual fluctuation of $\{d\angle Y_pY_c/d(\log\omega)\}_{\omega=\omega_c}$ can be considered to be the error of the assumed GM.

Now, we estimate the degree of compensation which the pilot can produce by employing human pilot models as follows[4,5]:

$$Y_p(s) = k_pe^{-\tau s}(\ 1 + T_Ls\ )\quad , \tag{4}$$

$$Y_p(s) = K_pe^{-\tau s}(\ 1 + T_Ls + T_L's^2\ )\ , \tag{5}$$

and

$$Y_p(s) = K_pe^{-\tau s}\frac{1}{1 + T_Is}\quad , \tag{6}$$

where s denotes the Laplace variable, and the human reaction time delay, denoted by τ, contains the neuro-muscular lag time constant and is fixed here as:

$$\tau = 0.3 \quad [\mathrm{sec}] \tag{7}$$

Then, the relations between $\{d|Y_p|/d(\log\omega)\}_{\omega=\omega_c}$ and $\angle Y_p(j\omega_c)$ are obtained as follows: for Eq.(4),

$$\{d|Y_p|/d(\log\omega)\}_{\omega=\omega_c} = 10(\ 1 - \cos 2\phi\ ) \quad [\mathrm{dB/decade}]; \tag{8}$$

for Eq.(5),

$$\{d|Y_p|/d(\log\omega)\}_{\omega=\omega_c} = 20 + 10\sqrt{1 + 4\alpha\tan^2\phi}(\ 1 + \cos 2\phi\ ), \quad [\mathrm{dB/decade}] \tag{9}$$

where $\alpha = T_L'/T_L^2$; and for Eq.(6),

$$\{d|Y_p|/d(\log\omega)\}_{\omega=\omega_c} = -10(\ 1 - \cos 2\phi\ ) \quad [\mathrm{dB/decade}]. \tag{10}$$

In the above equations, ϕ denotes the amount of human phase compensation at $\omega=\omega_c$ as:

$$\phi = \angle Y_p(j\omega_c) + \tau\omega_c \quad . \tag{11}$$

There are sufficient amount of human describing functions for confirming the human compensatory dynamics, which have been obtained through various experiments so far. We can sample the human compensatory dynamics in the form of $\{d|Y_p|/d(\log\omega)\}_{\omega=\omega_c}$ and $\angle Y_p(j\omega_c)$. Comparison of these data with Eqs. (8),(9) and (10) are shown in Figs.3 and 4, which indicate distinct features of human compensatory dynamics and their limitations. It should be noted that for simplicity, we employ an approximation: $\omega_c = \sqrt{2}\omega_n$ for the cases of second-order controlled element; that is due to the fact that the most effective factor in determining the crossover frequency for those cases seems to be the natural frequency of the controlled element. In summary, for cases where human phase lead ϕ is negative, we can approximate Y_p with Eq.(6); for cases where ϕ is positive and within $\pi/2$[rad], we can use Eq.(4); for the cases where ϕ is greater than $\pi/2$[rad] and within π[rad], we can use Eq.(5). Using these human pilot models and their limitations, we now introduce an analytical method for estimating pilot ratings.

Derivation of Evaluation Chart

Let's make an evaluation chart which shows the distinct relationship between the controlled element characteristics at ω_c and the closed-loop performance determined by human compensation.

Firstly, we derive conditions of the controlled element in which closed-loop stability holds for a given human pilot model.

(i) *stability conditions of the closed-loop system without any pilot compensation*

The closed-loop system is stable when

$$GM > 0 \quad [dB] \qquad (12)$$

and

$$\Phi M > 0 \quad [rad]. \qquad (13)$$

Substituting the above conditions into Eqs.(1) and (2), we obtain:

$$\left\{\frac{d|Y_pY_c|}{d(\log\omega)} \Big/ \frac{d\angle Y_pY_c}{d(\log\omega)}\right\}_{\omega=\omega_c} > 0 \quad [dB/rad] \qquad (14)$$

and

$$\angle Y_c(j\omega_c) - \tau\omega_c > -\pi - \phi \quad [rad]. \qquad (15)$$

In general,

$$\{d\angle Y_pY_c/d(\log\omega)\}_{\omega=\omega_c} < 0 \quad [rad/decade], \qquad (16)$$

thus, from Eq.(14):

$$\{d|Y_c|/d(\log\omega)\}_{\omega=\omega_c} < -\{d|Y_p|/d(\log\omega)\}_{\omega=\omega_c} \quad [dB/decade]. \qquad (17)$$

As the pilot employs no compensation:

$$\{d|Y_p|/d(\log\omega)\}_{\omega=\omega_c} = 0 \quad [dB/decade] \qquad (18)$$

and

$$\phi = 0 \quad [rad]. \qquad (19)$$

Substituting the above equations into Eqs.(15) and (17), we finally obtain the following stability conditions:

$$\{d|Y_c|/d(\log\omega)\}_{\omega=\omega_c} < 0 \quad [dB/decade] \qquad (20)$$

and

$$\angle Y_c(j\omega_c) - \tau\omega_c > -\pi \quad [rad]. \qquad (21)$$

The human pilot can stabilize the controlled elements in the region satisfying Eqs.(20) and (21) without any compensation: the region is shown in the chart of Fig.5, where the abscissa is $\angle Y_c(j\omega_c)-\tau\omega_c$, and the ordinate is $\{d|Y_c|/d(\log\omega)\}_{\omega=\omega_c}$. Hereafter, we explain the following regions by using the same chart.

(ii) *stability conditions with first-order pilot lead*

Stability conditions are the same as Eqs.(15) and (17). Employing Eq.(8), we can rearrange Eq.(17) as:

$$\{d|Y_c|/d(\log\omega)\}_{\omega=\omega_c} < -10(\ 1 - \cos 2\phi\ ) \qquad (22)$$

The human pilot can stabilize the controlled elements in the region satisfying the above conditions with first-order lead. Noting that Eq.(8) holds when

$0 \leq \phi \leq \pi/2$[rad], the region in the chart is obtained by moving the region satisfying conditions (i) in parallel along:

$$\{d|Y_c|/d(\log\omega)\}_{\omega=\omega_c} = -10(\ 1 - \cos 2\phi\ )\ (\ 0 \leq \phi \leq \pi/2[\mathrm{rad}]\ ).(23)$$

(iii) *stability conditions with second-order pilot lead*
Substituting Eq.(9) into Eq.(17), we obtain the conditions:

$$\{d|Y_c|/d(\log\omega)\}_{\omega=\omega_c} < -20 - 10\sqrt{1 + 4\alpha\tan^2\phi}(\ 1 + \cos 2\phi\ ) \qquad (24)$$

and Eq.(15). The widest region is obtained when $\alpha=0$ in Eq.(24) as:

$$\{d|Y_c|/d(\log\omega)\}_{\omega=\omega_c} < -10(\ 3 + \cos 2\phi\ ). \qquad (25)$$

Noting that Eq.(9) holds when $\pi/2<\phi\leq\pi$[rad], the region in the chart is obtained by moving the region satisfying conditions (i) in parallel along:

$$\{d|Y_c|/d(\log\omega)\}_{\omega=\omega_c} = -10(\ 3 + \cos 2\phi\ )\ (\ \pi/2 < \phi \leq \pi[\mathrm{rad}]\ ).(26)$$

(iv) *stability conditions with first-order pilot lag*
Similarly, the region in the chart is obtained by moving the region satisfying conditions (i) in parallel along:

$$\{d|Y_c|/d(\log\omega)\}_{\omega=\omega_c} = 10(\ 1 - \cos 2\phi\ )\ \ (\ -\pi/2 \leq \phi < 0[\mathrm{rad}]\ ).(27)$$

(v) *stability conditions with first-order pilot lead and lag*
This region is obtained by moving the region satisfying conditions (ii) in parallel along Eq.(27), just as the region satisfying conditions (iv) is obtained from the region satisfying condiitons (i).

Secondly, we derive conditions of the controlled element in which GM is kept greater than a certain value. As an example, the following condition is examined:

$$GM > 1.5 \quad [\mathrm{dB}]. \qquad (28)$$

It seems proper as condition of the phase slope to choose:

$$\{d\angle Y_pY_c/d(\log\omega)\}_{\omega=\omega_c} = -4 \quad [\mathrm{rad/decade}]. \qquad (29)$$

Using Eqs.(28) and (29), the conditions are:

$$\{d|Y_c|/d(\log\omega)\}_{\omega=\omega_c} < \frac{-6}{\angle Y_c(j\omega_c) - \tau\omega_c + \phi + \pi} - \{d|Y_p|/d(\log\omega)\}_{\omega=\omega_c} \qquad (30)$$

and Eq.(15).
(vi) *GM > 1.5 [dB] without any pilot compensation*
The conditions are directly obtained from Eqs.(30) and (15) as:

$$\{d|Y_c|/d(\log\omega)\}_{\omega=\omega_c} < \frac{-6}{Y_c(j\omega_c) - \tau\omega_c + \pi} \qquad (31)$$

and

$$\angle Y_c(j\omega_c) - \tau\omega_c > -\pi \qquad (32)$$

In the same way, the following conditions are obtained:
(vii) *GM > 1.5 [dB] with first-order pilot lead*
(viii) *GM > 1.5 [dB] with first-order pilot lag*
(ix) *GM > 1.5 [dB] with first-order pilot lead and lag*

COMPARISON OF THE EVALUATION METHOD WITH PREVIOUS DATA

The data $\{d|Y_c|/d(\log\omega)\}_{\omega=\omega_c}$, $\angle Y_c(j\omega_c)$ and corresponding pilot rating are obtained from previous experiments. Firstly, comparison with the data from Ref.1 is shown in Fig.6, where we tentatively set ω_c as equal to BW. Fig.6 indicates: (1) If the human pilot can keep GM>1.5[dB] without any compensation, pilot rating is acquired as $PR \leq 3.5$; (2) If the human pilot can keep GM>1.5[dB] with first-order compensation, pilot rating is acquired as $3.5 < PR \leq 6.5$; (3) Otherwise, $6.5 < PR$.

Now, we examine the method in the extreme cases near human controllability limits. The controllability limits are reported in various papers[9-12]. $\angle Y_c(j\omega_c)$ and $\{d|Y_c|/d(\log\omega)\}_{\omega=\omega_c}$ of the second-order controlled elements in the region of human controllability limits are shown in Fig.7, where we set ω_c as equal to $\sqrt{2}\omega_n$. Note that for these cases the human reaction time delay is modified as τ=0.2[sec]. It can be seen from Fig.7 that near the controllability limits the human pilot employs second-order lead. Finally, it is noted that the controllability limits of the first-order divergent elements are also explained by this chart. It should be added here that experimental results of these cases are somewhat greater than the analytical results; this implies that controllability limits are not determined by GM=0 but that GM should be greater than a some positive value.

DISCUSSION ON ADVANTAGES AND DISADVANTAGES OF THE EVALUATION METHOD

The precedent comparisons indicate that the proposed evaluation method can generally predict the ratings by human pilots. Advantages of this evaluation method compared with existing ones are as follows: (1) Easiness of evaluation; (2) Applicability to any controlled element irrespective of its stability; (3) Predictability of controllability limits of manual control; (4) Possibility of estimating human pilot dynamics simultaneously with control difficulty or pilot control efforts.

Items to be discussed concerning this evaluation method are as follows: (1) The method gives no definite ω_c. In general, ω_c depends on the control mission. It seems proper that ω_c should be classified according to the flight phases just as Ref.2. Nevertheless, the proposed method has another advantage: the results of the method is insensitive to the change of ω_c. Referring to Bode's theorem, $\angle Y_c(j\omega_c)$ has correlation with $\{d|Y_c|/d(\log\omega)\}_{\omega=\omega_c}$ when the controlled element is of minimum phase system; thus the results move almost in parallel along to the borders and then slightly laterally due to the difference of ω_c; (2) In the cases to which the assumptions of this method cannot be applied, the results may have large error. Possible origins of such error may be: assumptions that closed-loop stability is most effective in the determination of pilot ratings, that τ and $\{d\angle Y_pY_c/d(\log\omega)\}_{\omega=\omega_c}$ are set to be constants.

CONCLUSION

By fully making use of human pilot models and their limitations, an analytical evaluation method of predicting pilot ratings is proposed and examined. The evaluation chart can generally explain the pilot ratings and human controllability limits. The method can be widely applied to problems of single-loop manual control.

REFERENCES

1. Neal,T.P.; and Smith,R.E.: An In-Flight Investigation to Develop Control System Design Criteria for Fighter Airplanes, AFFDL-TR-70-74, 1970.
2. Chalk,C.R.; DiFranco,D.A.; Lebacqz,J.V.; and Neal,T.P.: Revisions to MIL-F-8785B(ASG) Proposed by Cornell Aeronautical Laboratory, AFFDL-TR-72-41, 1972.
3. Ashkenas,I.L.; Hoh,R.H.; and Craig,S.J.: Recommended Revisions to Selected Portions of MIL-F-8785B(ASG) and Background Data, AFFDL-TR-73-76, 1973.
4. Tanaka,K.; Goto,N.; and Washizu,K.: A Comparison of Techniques for Identifying Human Operator Dynamics Utilizing Time Series Analysis, Proc. of 12th Annual Conf. on Manual Control, NASA TM X-73,170, 1976, pp.673-693.
5. McRuer,D.T.; Graham,D.; Krendel,E.S.; and Reisner,W.Jr.: Human Pilot Dynamics in Compensatory Systems, AFFDL-TR-65-15, 1966.
6. Tanaka,K.; Morihisa,H.; and Noguchi,K.: On the Relationship between Pilot Rating and Pilot Dynamics, Part I. An Experimental Approach, Trans. of the Japan Society for Aeronautical and Space Sciences, Vol.21, No.53, 1978, pp.128-138.
7. Goto,N.: ———, Part II. An Analytical Approach,———, pp.139-152.
8. Washizu,K.; Tanaka,K.; and Osawa,T.: A Study of the Effect of Forcing Function Characteristics on Human Operator Dynamics in Manual Control, Proc. of 14th Annual Conf. on Manual Control, NASA CP-2060, 1978, pp.19-32.
9. Washizu,K.; Tanaka,K.; Endo,S.; and Itoko,T.: Motion Cue Effects on Human Pilot Dynamics in Manual Control, Proc. of 13th Annual Conf. on Manual Control, 1977, pp.403-413.
10. Jex,H.R.; Cornwell,C.H.; and Siskind,R.K.: Correlation of Experimental and Theoretical Limits for Pilot Control of Unstable Second Order Systems, WADD TM-56, 1960.
11. Washizu,K.; and Miyajima,K.: Controllability Limits of a Human Pilot, AIAA J., Vol.3, No.5, 1965, pp.941-947.
12. Smith,R.H.: On the Limits of Manual Control, IEEE Trans., Vol.HFE-4, 1963, pp.56-59.

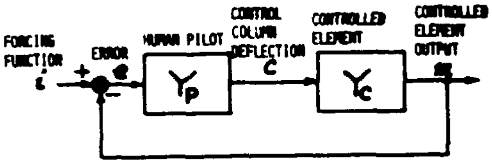
FORCING FUNCTION
i
+
−
ERROR
e
HUMAN PILOT
Y_p
CONTROL COLUMN DEFLECTION
c
CONTROLLED ELEMENT
Y_c
CONTROLLED ELEMENT OUTPUT
m

Figure 1. Single-Loop Manual Control System

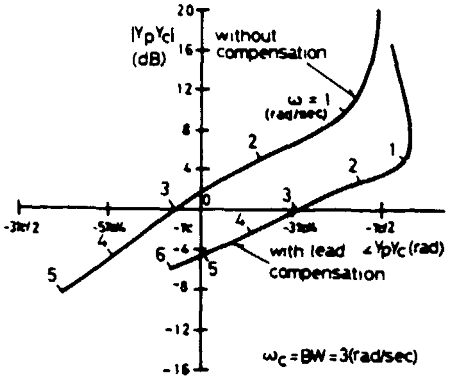

Figure 2. Example of Amplitude-Phase Plots from Ref.1

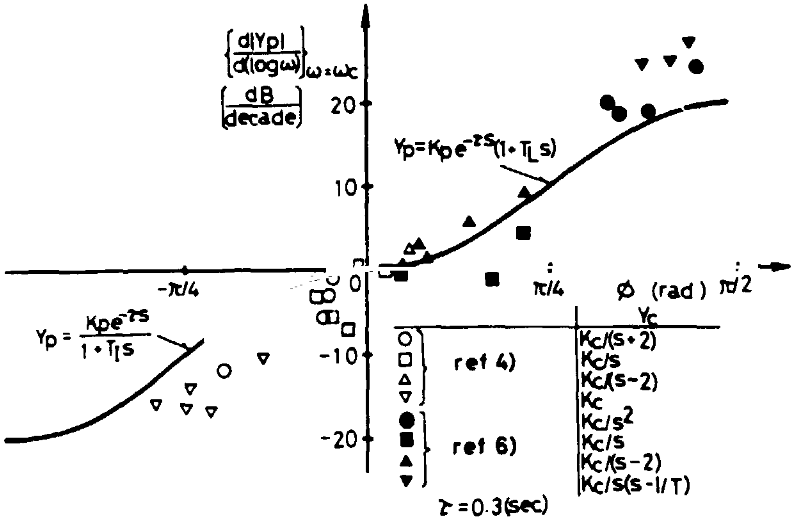

Figure 3. Comparison between Human Pilot Models and Experimental Results

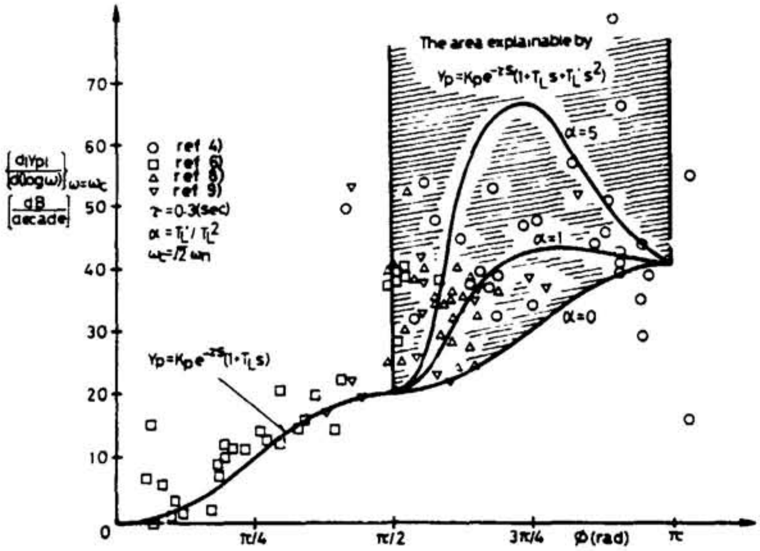

Figure 4. Comparison between Human Pilot Models and Experimental Results when $Y_c = \omega_n^2/(s^2 + 2\zeta\omega_n s + \omega_n^2)$

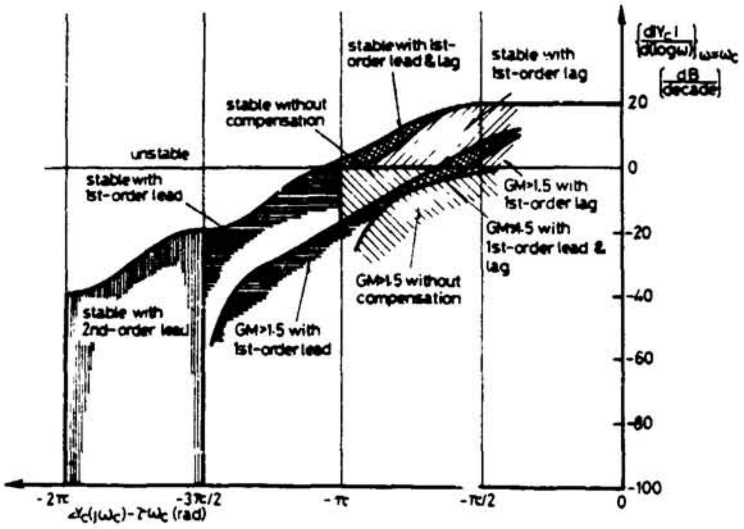

Figure 5. Chart for Evaluating Manual Control System

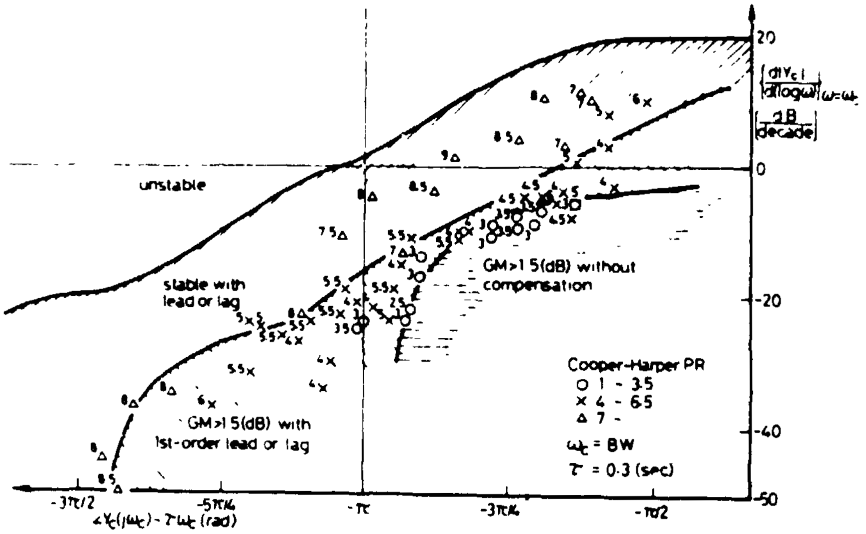

Figure 6. Proposed Evaluation Method Plotted Against Experimental Results from Ref.1

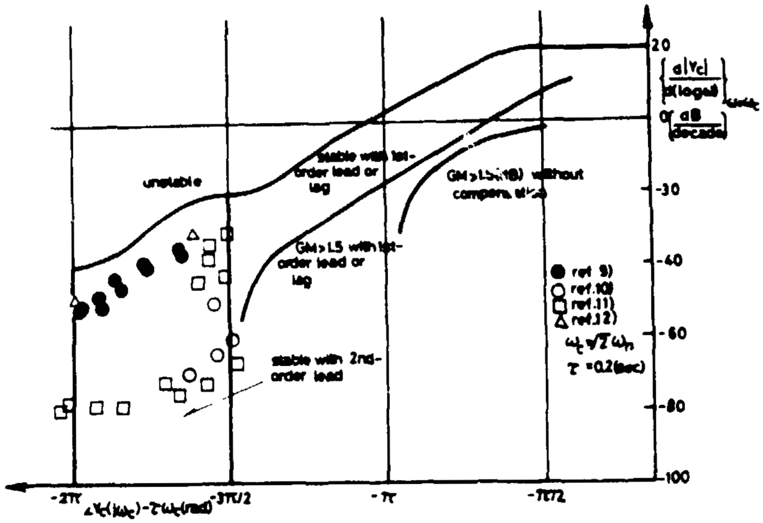

Figure 7. Proposed Evaluation Method Plotted Against Experimental Controllability Limits when $Y_c = \omega_n^2/(s^2 + 2\zeta\omega_n^2 s + \omega_n^2)$

N82 34052 -15

EFFECTS OF HIGHER ORDER CONTROL SYSTEMS ON AIRCRAFT APPROACH AND LANDING LONGITUDINAL HANDLING QUALITIES

Sqd. Ldr. Muhammad A Pasha
Pakistan Air Force

DR. JOHN J. D'AZZO
Professor of Electrical Engineering
Air Force Institute of Technology

CAPT JAMES T. SILVERTHORN
Assistant Professor
of Aeronautical Engineering
Air Force Institute of Technology

ABSTRACT

This report presents a study of approach and landing longitudinal flying qualities, based on data generated by Calspan using a variable stability NT-33 aircraft combined with significant control system dynamics. An optimum pilot lead time for pitch tracking, flight path angle tracking, and combined pitch and flight path angle tracking tasks is determined from a closed-loop simulation using integral squared error (ISE) as a performance measure. Pilot gain and lead time were varied in the closed-loop simulation of the pilot and aircraft to obtain the best performance for different control system configurations. The results lead to the selection of an optimum lead time using ISE as a performance criterion. Using this value of optimum lead time, a correlation is then found between pilot rating and performance with changes in the control system and in the aircraft dynamics. It is also shown that pilot rating is closely related to pilot workload which, in turn, is related to the amount of lead which the pilot must generate to obtain satisfactory response. The results also indicate that the pilot may use pitch angle tracking for the approach task and then adds flight path angle tracking for the flare and touchdown.

INTRODUCTION

Aircraft handling qualities and pilot behavior during the glide slope, flare, and landing phases of the flight regime are considered in this paper. The results are extracted from the study performed by Pasha[1], and complete details may be obtained from that report. This study is based on data generated by Calspan[2] which investigated the effects of control system dynamics on approach and landing longitudinal flying qualities by using an NT-33A variable stability aircraft. A large number of aircraft/control system configurations were flown by Calspan and pilot comments and ratings are contained in Ref. 2. Anderson has postulated[3] that pilot rating is closely related to pilot workload and that this is determined by the amount of lead which the pilot must generate to maintain reasonable response. Using these postulates, the direction of this study was to investigate: (1) the relationship between pilot workload and aircraft control system dynamics, (2) the output variables of primary interest to the pilot. This was accomplished by simulating the combined pilot model, aircraft dynamics, and control system as a closed-loop pitch angle and flight path angle tracking task with the objective of finding a correlation between the closed-loop performance and the pilot ratings. The closed-loop pitch response to a step pitch command was studied. Pilot gain and pilot generated lead were varied in order to obtain the "best" performance for different control system configurations. This was repeated for closed-loop flight path angle response (both with and without pitch feedback). The closed-loop pitch and flight path angle responses were studied for different aircraft dynamics. Again the pilot gain and pilot generated lead were varied to obtain the best response. The integral of error squared (ISE) was used throughout as a measure of performance.

Aircraft Equations

The linearized longitudinal aircraft equations are well known [4,6] and are not repeated here. The coefficients used in these equations for the different aircraft dynamics are included in the original reports [1,2]. The aircraft forward speed was considered constant. The phugoid mode is easily controlled by the pilot and, since the time frame in which the landing task is completed is relatively small, only the short period aircraft dynamics were used in this study.

The Landing Task As Seen By A Pilot

During the approach-to-landing phase of flight the aircraft is initially on the glide slope and the pilot must decide on the minimum height to flare. At this time the pitch attitude θ and the flight path angle γ appear to be of considerable importance to the pilot. The minimum height to flare is an imaginary window on the glide slope which the pilot selects relative to the runway threshold or touchdown point. The selection of the imaginary window in space depends on the aircraft forward speed, aircraft dynamic characteristics, and the experience of the pilot in handling the aircraft. During the flare maneuver the sink rate $\dot{h}$ (vertical velocity) and the slant range rate $\dot{R}$ (the rate at which the runway threshold or touchdown point appears to be approaching) are visual motion cues for the pilot. The pilot pitches up and establishes a desired $\dot{h}$ and/or $\dot{R}$ until touch down, where h, $\dot{h}$ and R go to zero. All three output variables, h, $\dot{h}$, and R, are mathematically related to the flight path angle γ as shown below.

For small angles the flight path angle γ is given by [4]

$$\gamma = \theta - \alpha \tag{1}$$

The sink rate $\dot{h}$ is given by:

$$\dot{h} = U_0 \sin\gamma \approx U_0\gamma \tag{2}$$

The slant range rate $\dot{R}$ is the vector sum of U_0 and $\dot{h}$. Since U_0 is assumed constant, $\dot{R}$ is directly proportional to $\dot{h}$ or γ. Therefore, all the motion cues are direct functions of flight path angle γ. Hence the dynamic behavior of θ and γ for elevator commands (δ_e) is representative of the overall landing task.

Pilot Describing Function

The basic McRuer pilot model[5] used in this study is represented by

$$Y_p(s) = K_p e^{-\tau s}(T_L s+1) \tag{3}$$

By adjusting K_p, T_L, and τ the pilot achieves the level of closed-loop system performance which he considers desirable or necessary. This is accomplished at the expense of pilot activity and workload. One way to optimize performance is to adjust the model parameters to minimize the integral of squared error (ISE). The "lead only" form of pilot model was used because pilot lag may be neglected when higher-order control system lags are present. A value of $\tau = 0.3$ was used.

Pilot Rating Concepts

Pilot Ratings are based on numerical rating scales, such as the Cooper-Harper scale, which represent an attempt to relate pilot comments about the ease of difficulty with which airplanes can be controlled in certain flight situations. The ratings are ordinal scales subjectively applied and hence are difficult to quantify. Predictions of pilot ratings require mathematical relations between the numerical rating scale and "how hard a pilot must work" to achieve "desired closed-loop performance". Developing mathematical relation appears to be extremely complex, though certain trends have been identified. For example a pilot objects if he has to generate "leads" (T_L) of more than 0.5 to 1.0 seconds [6]. The factors which may be taken into account by a skilled test pilot in providing an opinion or rating are [5]: Measure of task performance, Pilot workload, and System sensitivity. These factors are obviously affected by the particular aircraft dynamics, including any additional control systems. As a mathematical function, pilot ratings (PR) can be expressed as:

$$PR = f(\text{Performance, workload, sensitivity,}\ldots) \tag{4}$$

Pilot Workload

The pilot workload can be divided into pilot activity and pilot equalization. Pilot activity is dependent on the pilot gain K_p and is an important component of Pilot Ratings in the presence of gust disturbances and remnant. Pilot gain is also determined by the mechanical arrangement of the controls placed between the pilot and the elevator. The data generated by Calspan[2] allowed the pilot to select the gearing ratio for each flight evaluation[2]. The pilot equalization can be represented[5] by the pilot's "lead" time constant and is used in this study to represent workload.

Analog Computer Simulation

An analog computer simulation was used to find an optimum pilot lead time which yields the best system performance for the aircraft-control system. The objective was two fold: (1) To see if a correlation exists between performance and Pilot Rating, (2) To see if the pilot could improve the system performance by choosing different forms of pitch angle and flight path angle feedback. The pilot gain K_p and lead, T_L were adjusted to minimize ISE (the performance criterion) when the pilot performed a tracking task for a step command. The effects of adding control systems on the performance were first studied for an aircraft characterized by a short period natural frequency and damping ratio of 1.02 rad/sec and 0.74 respectively, here after referred to as A/C 1. See Ref 2 for the stability and control derivatives of this aircraft. The tracking task was analyzed in three phases: 1) Inner-loop pitch attitude (θ) tracking for a step pitch command; 2) outer-loop flight path angle (γ) tracking for a step γ-command; and 3) combined pitch and flight path angle tracking (inner and outer loop) to minimize the error in the flight path angle for a step γ-command. These three phases were repeated for four additional aircraft using the baseline control system (control system = 1) to observe the performance variations between the five aircraft configurations. The objective of the analog simulation study was to find optimum pilot parameters K_p and T_L which would minimize the ISE for a particular tracking task.

Pitch Attitude Tracking Task

The block diagram used for the simulation is shown in Fig. 1. The aircraft with no control system dynamics was analyzed first. The control systems which were flown[2] with this aircraft were then simulated.

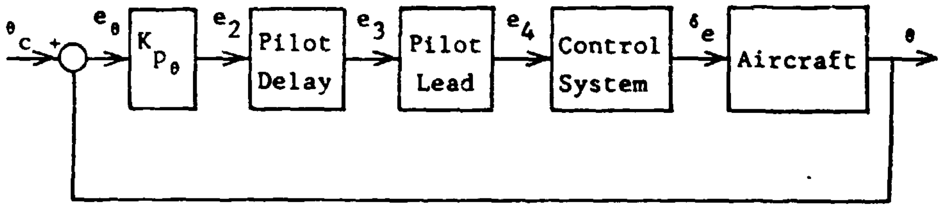

Figure 1. Block Diagram of Pitch Tracking Task

The pilot lead time T_L was varied from 0 to 1.25 sec in steps of 0.25 sec. For each value of T_L, the pilot gain K_p was varied and the value of ISE was recorded for a step pitch command (θ_c). Representative graphs showing the data thus generated are shown in Figs 2 thru 5. While pilot lead times greater than 0.5 or 0.75 sec produce a slight improvement in the system performance, they do so at the expense of greater pilot workload. Also, the curves for 1.0 and 1.25 sec. lead time show much larger variations in the value of ISE about the minimum, thus indicating higher system sensitivity to pilot gain variations. Therefore, a value of 0.5 or 0.75 sec. pilot lead seems to be the optimum choice. Fig. 4 shows the performance curve with control system dynamics $2/(s+2)$. Since this control system introduces a significant amount of lag near the short period natural frequency of the aircraft (1 rad/sec), the aircraft dynamics response is very sensitive to gain change. In other words, for good performance the pilot must hold the gain very steady to maintain good performance. This amounts to an additional workload in terms of pilot concentration and hence a degraded pilot opinion of the task. The value of minimum ISE and the corresponding pilot ratings are plotted in Figs. 6 and 7 for a 0.5 and 0.75 sec. pilot lead, respectively. The plots show an increase in pilot rating as the performance degrades for control systems which introduce lag. The reverse trend for control systems which introduce lead is a puzzle which could not be explained.

Flight Path Angle Tracking Task

During the flare maneuver, the sink rate information is one of the visual cues the pilot uses in performing the landing task. Since flight path angle γ is directly related to the sink rate, it is logical to analyze the pilot in the γ-loop. This was done by first assuming no pitch angle feedback. The block diagram used for this simulation is shown in Fig. 8.

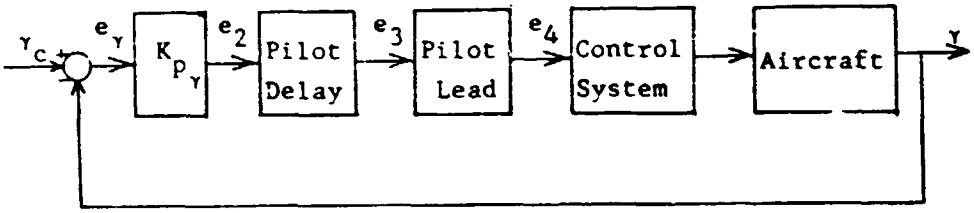

Figure 8. Block Diagram of γ Tracking Task

The ISE (e_γ^2) was measured for a step γ-command. The pilot parameters K_{p_γ} and T_L were varied and the procedure used for the analysis of pitch loop was repeated, vis-a-vis, measuring the value of ISE until a minimum is reached, as K_{p_γ} and T_L were varied. Similar performance was obtained as for the pitch angle control and the results are contained in Ref. 1. The optimum pilot lead was 0.75. However, the minimum values of ISE achieved were much greater than for pitch angle tracking. Therefore it was concluded that the pilot is more inclined to use pitch angle tracking while on the glide slope.

Combined Pitch and Flight Path Angle Tracking

The next step was to study the effect of feeding both pitch and flight path angle as a multi-output system for a single input step γ-command. Figure 9 shows a block diagram of the system used for simulation.

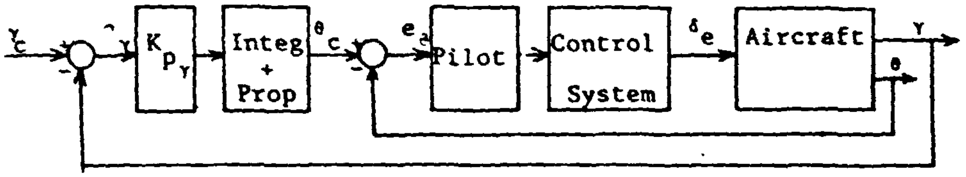

Figure 9. Both θ and γ Tracking Task For A Step γ-Command

The analysis was restricted to aircraft 1 and the lag control systems flown with aricraft 1. The 'lead only' form of pilot dynamics was used for the pilot in the pitch loop. Two values of T_L, 0.5 and 0.75 seconds, were used, and the corresponding gains K_{p_θ} which minimized the ISE in the pitch tracking task were obtained. Since the closed-loop pitch transfer function forms a type zero system, using only pilot gain K_{p_γ} in the outer loop would result in a steady-state error e_γ for a step γ-command input[7]. Therefore an, integral plus proportional control system was used, as shown in Figure 9, to represent the pilot in the outer loop. Pilot reaction time delay was not included in the outer loop. The transfer function used for integral and proportional control has the form;

$$G(s) = 1 + \frac{a}{s} \tag{5}$$

Determining the appropriate value of 'a' to be used for the task was the next step. Therefore, K_{p_γ} was varied and the ISE $\int e_\gamma^2$ was measured for a step γ-command, while the value of "a" was varied from 0.1 to 0.4 in steps of 0.05. This proceedure was used with both a T_L of 0.5 and 0.75 seconds for pilot lead in the pitch loop. The data thus generated showed that a value a = 0.2 minimized the ISE, and this value was used for subsequent analysis.

The lag control systems flown with aircraft 1 were simulated to study the effect of performance degradation on pilot rating. The outer loop pilot gain K_{p_γ} was varied and the ISE $\int e_\gamma^2$ was recorded for a step γ-command.

Figure 10 shows a plot of ISE $\int e_\gamma^2$ versus the K_{p_γ} for various lag control systems. The pilot rating (PR) is also shown. The effect of performance degradation on pilot rating can be clearly seen from these plots. Figure 11 shows the plot of minimum ISE $\int e_\gamma^2$ versus the PR for aircraft 1 without the control system and with the lag control systems. These figures indicate a direct relationship between PR and performance for a fixed pilot workload.

In this control system an outer loop gain and integral plus proportional control is required from the pilot. The task of integrating an error essentially means remembering the past errors and thus represents an increase in the pilot workload. Whether the pilot likes this kind of additional workload or if the additional workload is worth the improvement in the performance needs to be determined. Also, for a multi-output tracking task, how the pilot would time share his control of the two outputs θ and γ needs to be investigated. It may be possible that during the glide slope the pilot is flying the aircraft by tracking only the pitch angle θ up to a certain altitude where the sink rate $\dot{h}$ becomes important. This altitude may be about 100 feet, where the pilot may begin tracking both pitch angle and flight path angle until the flare maneuver. During flare, especially the last 50 feet, the pilot may switch over to tracking only the altitude, assuming that he has done his best to stabilize the θ-loop. A plot of ISE versus K_p is shown in Figure 12 for a pitch loop T_L of 0.5 and 0.75 seconds for the three tracking tasks using aircraft 1 without the control systems.

The above hypothesis, i.e., during approach the pilot is essentially tracking the pitch attitude and during flare and landing phase the pilot is tracking the flight path angle while holding a fixed optimum pitch loop performance may be verified by the following proceedure. In a large number of flight configurations flown, the pilot evaluated the approach task and the overall landing task separately and provided two different ratings. An optimum pilot workload and performance evaluation can be performed on an analog computer. The proceedure described in this paper and those flight configurations for which both ratings were provided may be used; first as a pitch tracking task, and then as a γ-loop tracking task with the pitch loop optimized as per the first analysis. The results thus obtained can be correlated with the corresponding approach and overall pilot ratings to validate the hypotheses. This analysis was not carried out due to lack of time. The data generated in this study indicates a possible correlation with pilot ratings but is insufficient to draw positive conclusions about this hypothesis.

Pitch Attitude Tracking for Different Aircraft

The previous analysis was extended to other aircraft. Similar results were obtained for all aircraft as shown in Fig. 13.

Summary of Results of Closed-Loop Analog Simulation

The following are the results of the study:

1) A lead time of 0.5 to 0.75 seconds seems to be the optimum pilot lead for most of the aircraft-control system combinations.

2) Control systems generating significant lag at the short period natural frequency tend to make the system very sensitive to gain changes.

3) Performance, measured in terms of ISE, has a direct correlation with PR for aircraft with control systems which introduce lag.

4) Closing both the pitch and flight path angle loops for a γ-command, improves the performance but at the cost of increased pilot compensation.

BIBLIOGRAPHY

1. Pasha, M.A.: Analysis of the Effects of Higher Order Control Systems on Aircraft Approach and Landing Longitudinal Handling Qualities, M.S. Thesis, Air Force Institute of Technology, AFIT/GE/EE/79-27, 1979. DDC No. ADA-080519.

2. Smith, R. E. Effects of Control System Dynamics On Fighter Approach and Landing Longitudinal Flying Qualities, Vol I. AFFDL-TR-78-122. WPAFB, Ohio: Air Force Flight Dynamics Laboratory, March 1978.

3. Anderson, R. O., A. J. Conners, and J. D. Dillow. Paper Pilot Ponders Pitch. AFFDL/FGC-TM-70-1. WPAFB, Ohio: Flight Control Division, Air Force Flight Dynamics Laboratory, November 1970 (Revised January 1971)

4. Blakelock, John H. Automatic Control of Aircraft and Missiles. New York: John Wiley and Sons, Inc., 1965.

5. McRuer, D. T. and E. S. Krendel. Mathematical Models of Human Pilot Behavior. AGARD-AG-188: North Atlantic Treaty Organization, January 1976.

6. Roskam, Jan. Flight Dynamics of Rigid and Elastic Airplanes. Lawrence, Kansas: Roskam Aviation and Engineering Corporation, 1972.

7. D'Azzo, John J. and Constantine H. Houpis. Linear Control System Analysis and Design: Conventional and Modern. New York: McGraw-Hill Book Company, 1975.

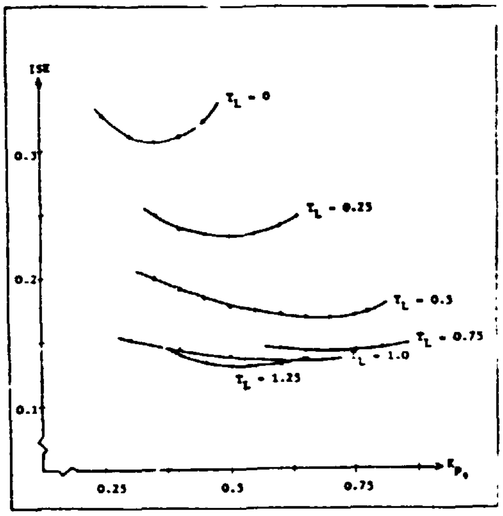

Fig. 2 ISE Vs. K_{p_e} For Different T_L - Aircraft 1 C/S = 1

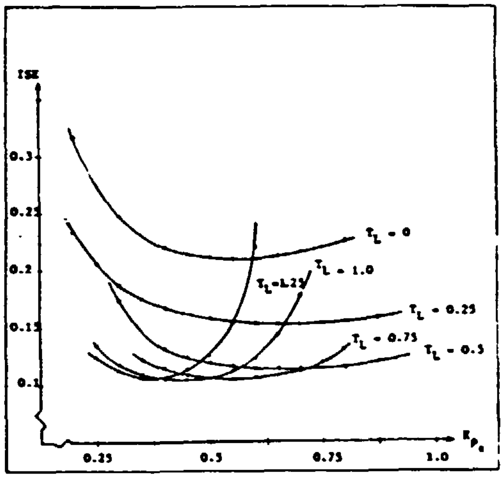

Fig. 3 ISE Vs. K_{p_e} For Different T_L - Aircraft 1 C/S 1

$$G_c(s) = \frac{4(s+2.5)}{s+10}$$

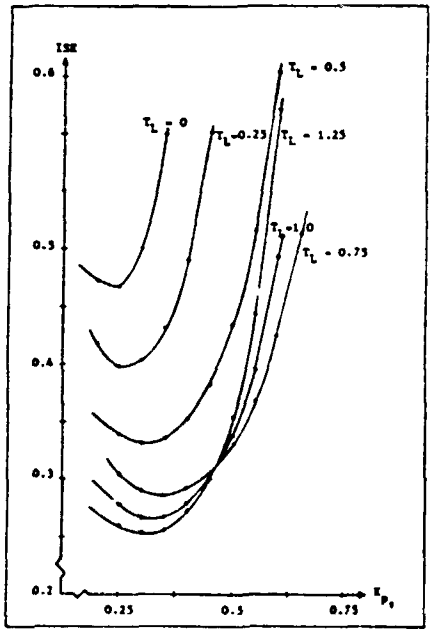

Fig. 4 ISE Vs K_{p_e} For Different T_L - Aircraft 1 C/S 6

$$G_c(s) = \frac{2}{s+2}$$

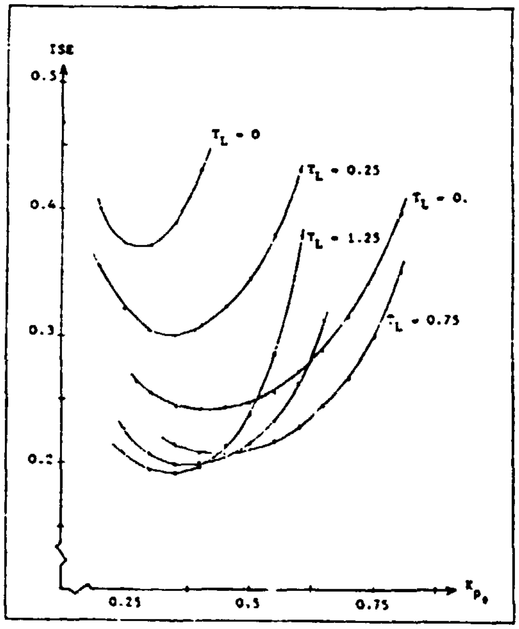

Fig. 5 ISE Vs. K_{p_e} For Different T_L - Aircraft 1 C/S 10

$$G_c(s) = \frac{81}{s^2+12.6s+81}$$

ORIGINAL PAGE IS
OF POOR QUALITY

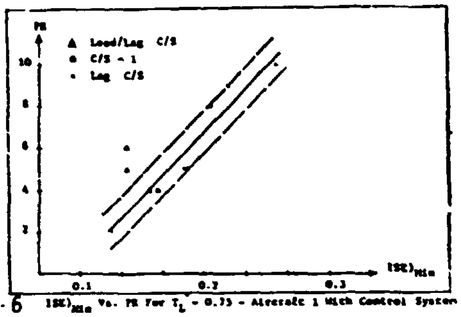

Fig. 6 ISE)$_{Min}$ Vs. PR For T_L = 0.75 - Aircraft 1 With Control System

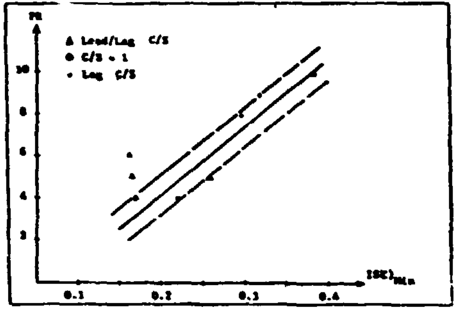

Fig. 7 ISE)$_{Min}$ Vs. PR For T_L = 0.5 - Aircraft 1 With Control Systems

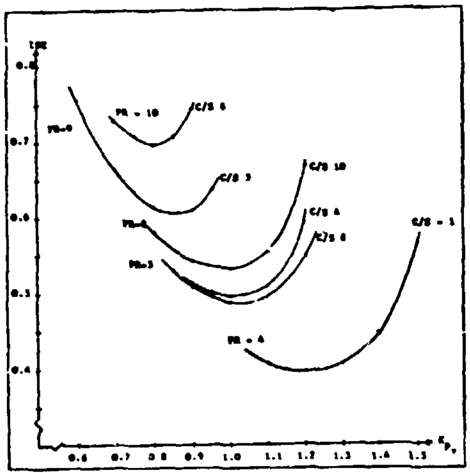

Fig. 10 ISE Vs. K_{p_γ} For T_L = 0.5 Aircraft 1 With Lag C/S -
θ and γ tracking task

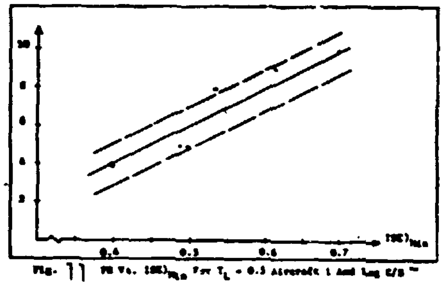

Fig. 11 PR Vs. ISE)$_{Min}$ For T_L = 0.5 Aircraft 1 And Lag C/S —
Combined θ and γ Tracking Tasks

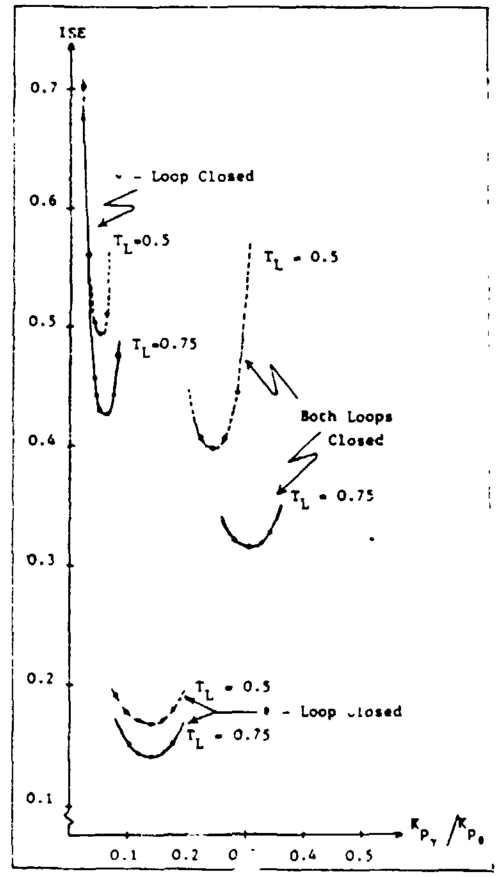

Fig. 12 ISE Vs. $K_{p_\gamma}/K_{p_\theta}$ Aircraft 1 C/S = 1

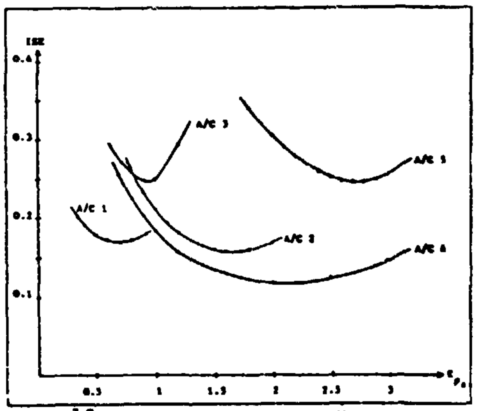

Fig. 13 ISE Vs. K_{p_θ} Pitch Tracking Task – Different Aircraft And C/S = 1 For T_L = 0.5

N82 34053 -16

PILOT OPINIONS OF SAMPLING EFFECTS IN LATERAL-DIRECTIONAL CONTROL

Robert F. Stengel* and George E. Miller**
Flight Research Laboratory
Princeton University
Princeton, N. J. 08544

Flight experiments with a microprocessor control system have been conducted to determine the effects of variations in sampling parameters on several pilots' opinions of lateral-directional flying qualities.+ Princeton's Variable-Response Research Aircraft (VRA), which is equipped with a microprocessor-based digital flight control system (Micro-DFCS), was the test vehicle. Two U.S. Navy pilots evaluated the effects of sampling rate, quantization, and pure time delay during tracking, approach, and landing. Aircraft carrier approach tasks were conducted using a Navy approach mirror. Acquisition and tracking of fixed objects on the ground provided additional information related to the Navy mission.

This research is an extension of the longitudinal investigation reported in Ref. 1. In the present case, the longitudinal controls were implemented with analog electronics, while the lateral-directional pilot inputs (stick and rudder) were fed to the Micro-DFCS, which commanded the ailerons and rudder. Full details of the systems and experimental procedures can be found in Refs. 1 to 3. Figure 1 illustrates the conceptual relationship between the evaluation pilot's lateral-directional inputs, the flight computer, and the aircraft.

---

* Associate Professor of Mechanical and Aerospace Engineering.

** Member of the Technical Staff.

+ This work was conducted under Contract No. N00014-78-C-0257 for the Office of Naval Research.

Presented at the 16th Annual Conference on Manual Control, Cambridge, Mass., May, 1980.

The flight test results are summarized in Figs. 2 to 4. For simulated carrier landing approaches, the two naval aviators found sampling rates of 10 per sec or higher acceptable, with computational time delay fixed at 10 msec, as indicated by pilot opinion ratings[4] of 3.5 or less (Fig. 2). Holding sampling rate at 20 per sec, equivalent time delays of about 100 msec or less were acceptable, and the degradation in pilot rating was found to be linear in the delay. (The equivalent delay is defined to be the computational delay plus half the sampling interval). With sampling rate and pure delay fixed at 20 per sec and 10 msec, respectively, control word lengths of 10 bits were found to be acceptable, while the allowable value dropped to 8 bits for tracking at altitude (Fig. 3). Figure 4 illustrates that somewhat lower values of sampling rate were found acceptable when tracking at altitude, but the tolerance to equivalent time delays was greatly reduced.

The present results are applicable to the VRA with unaugmented dynamics; the effects of dynamic variations, which can be provided by the VRA's variable-stability system, remain to be defined.

REFERENCES

1. Stengel, R. F., and Miller, G. E., "Flight Tests of a Microprocessor Control System", AIAA Paper No. 79-1962 Los Angeles, Oct 1979 (to appear in the AIAA Journal of Guidance and Control).

2. Seat, J. C., Miller, G. E., and Stengel, R. F., "A Microprocessor System for Flight Control Research", Proceedings of the 1979 National Aerospace & Electronics Conference, Dayton, May 1979, pp. 319-326.

3. Stengel, R. F., "Digital Flight Control Research Using Microprocessor Technology", IEEE Transactions on Aerospace and Electronic Systems, Vol. AES-15, No.3, May 1979, pp.397-404.

4. Cooper, G. E., and Harper, R. P., Jr., "The Use of Pilot Rating in the Evaluation of Aircraft Handling Qualities", NASA TN D-[illegible]53, April 1969.

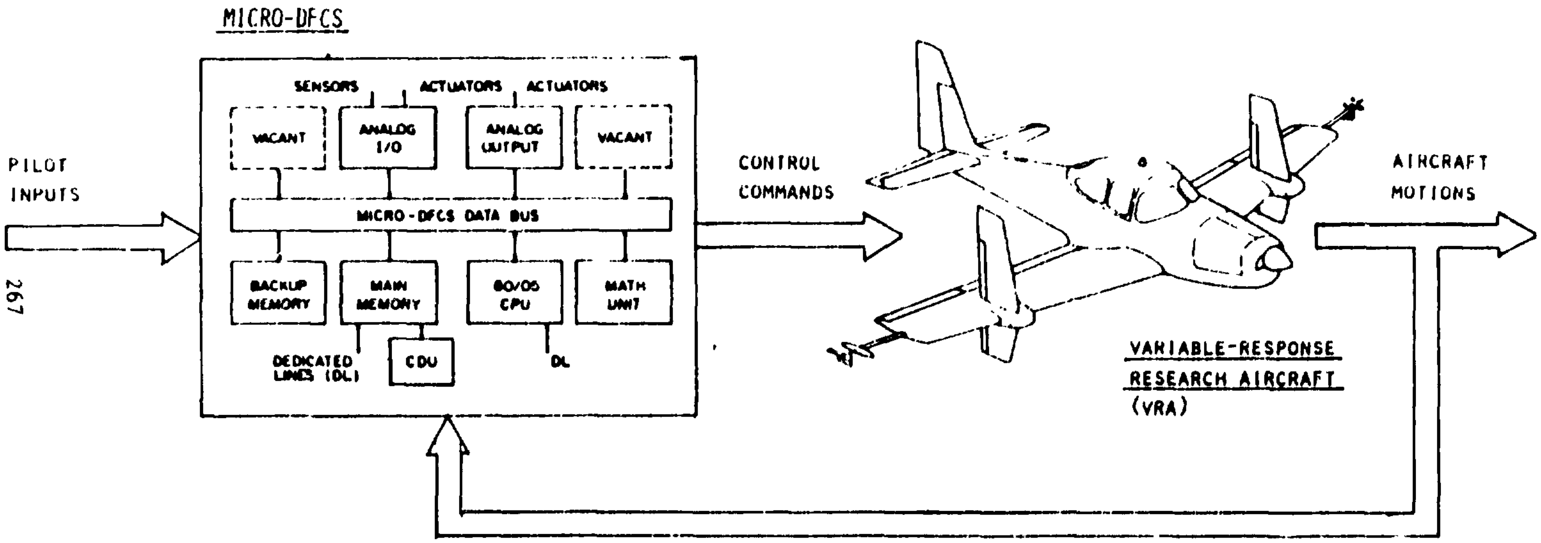
MICRO-DFCS
SENSORS
ACTUATORS
ACTUATORS
VACANT
ANALOG I/O
ANALOG OUTPUT
VACANT
MICRO-DFCS DATA BUS
BACKUP MEMORY
MAIN MEMORY
80/05 CPU
MATH UNIT
DEDICATED LINES (DL)
CDU
DL
PILOT INPUTS
CONTROL COMMANDS
AIRCRAFT MOTIONS
VARIABLE-RESPONSE RESEARCH AIRCRAFT (VRA)

FIGURE 1. SCHEMATIC DIAGRAM OF THE MICRO-DFCS AND THE VRA.

C-4

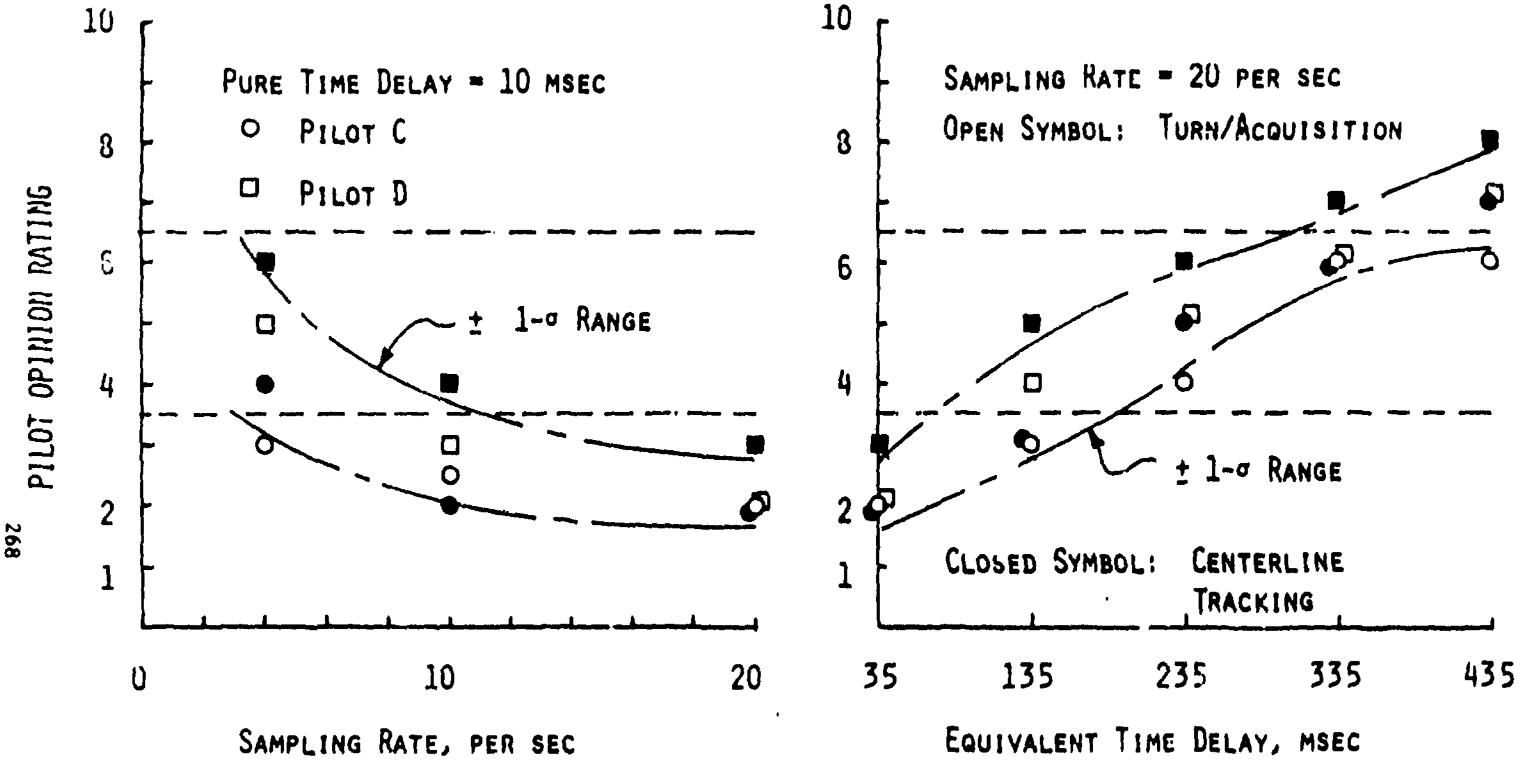

FIGURE 2. PILOT OPINION RATINGS FOR FIELD CARRIER LANDING PRACTICE, V=86 KIAS.

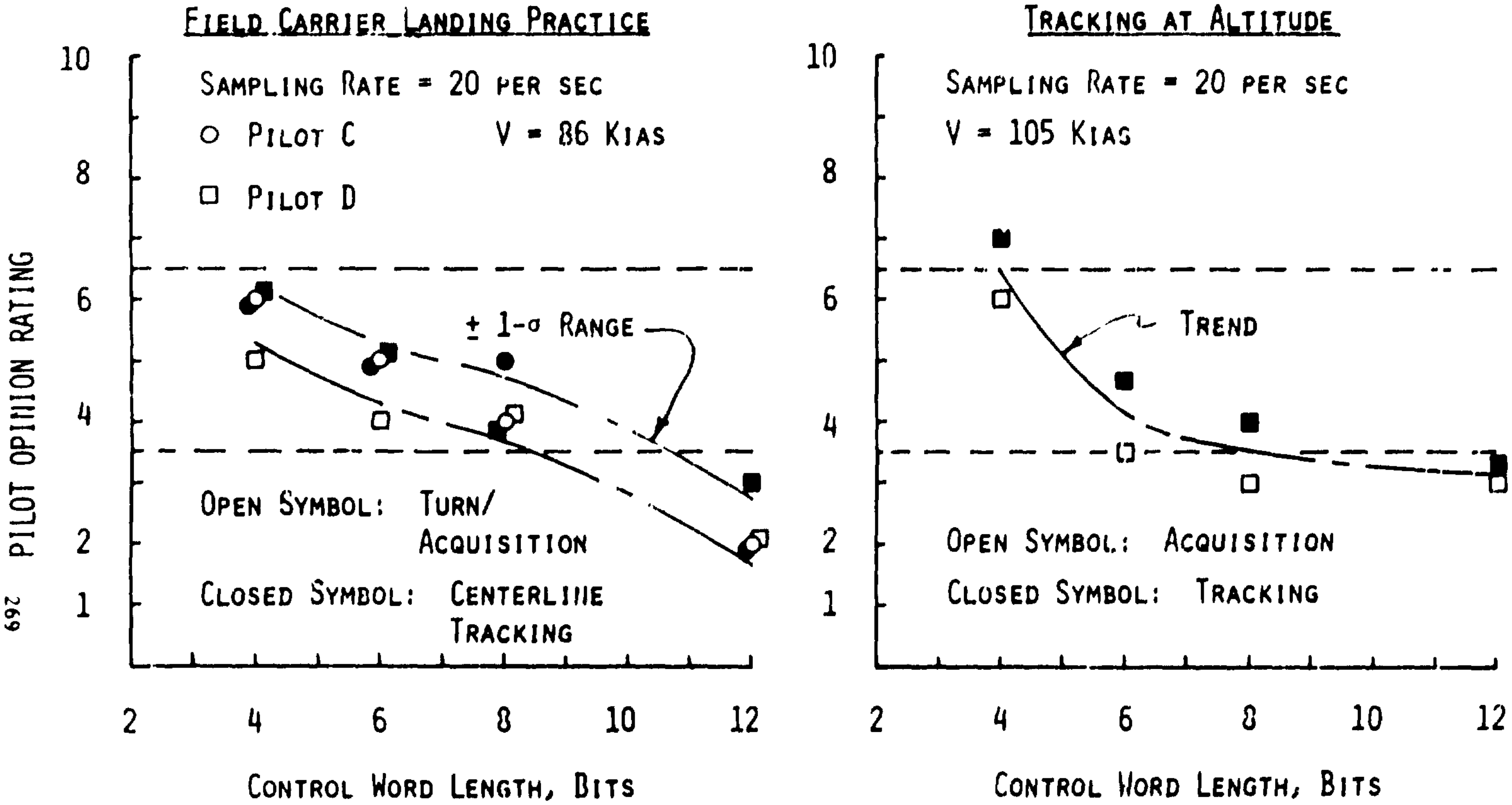

FIGURE 3. EFFECTS OF CONTROL RESOLUTION ON PILOT OPINION RATINGS.

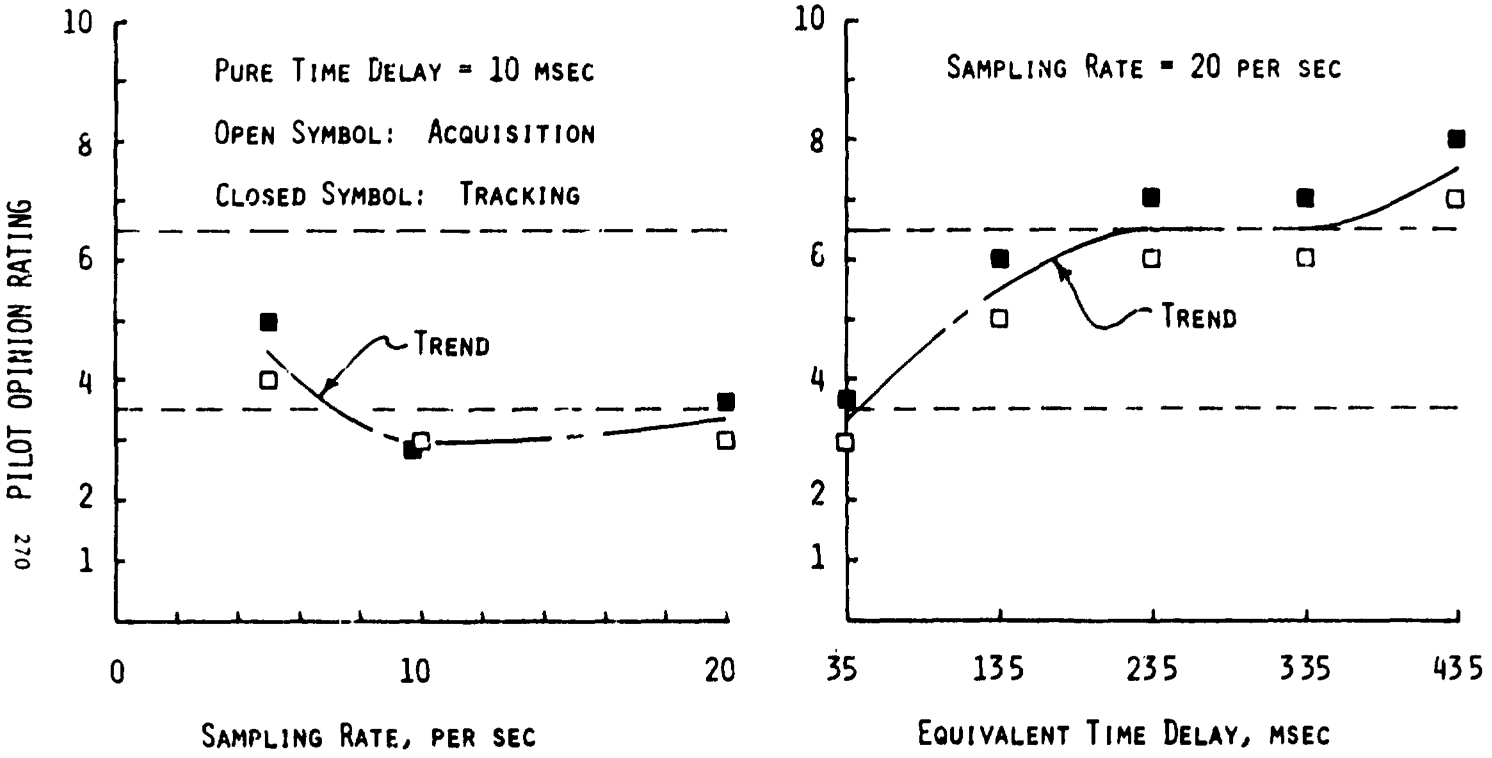

FIGURE 4. PILOT OPINION RATINGS FOR TRACKING AT ALTITUDE, V=105 KIAS.

N82 34054

A MODEL OF SUBJECTIVE PROBABILITIES FROM SMALL GROUPS*

William R. Ferrell
and
Kelly Rehm

Human Factors/Man-Machine Systems Laboratory
Department of Systems and Industrial Engineering
The University of Arizona
Tucson, Arizona 85721

INTRODUCTION

There is good evidence that the quality of probabilistic forecasts, and meteorological forecasts in particular, is improved by aggregating the opinions of individual forecasters.[8,9,10,12] The question of how best to do the aggregation has raised a number of important issues. How large should the group be? Should it be a nominal group or one in which members interact, and if the latter, what sort of interaction? By what mathematical rule should individual judgments be combined to form the group judgment, or, alternatively, should the group produce a consensus forecast? How should individual judgments be weighted mathematically?

A major step toward an experimental answer to these questions, excepting that of group size, has been made by Seaver[6,7] in his study of probability judgments by groups of 4 people. The research reported here used the decision variable partition model of subjective probability[2] and a simple model of the effects of interaction on judgments to simulate the group judgment of discrete probabilities investigated by Seaver. The initial results of the simulation are very promising in that (1) they show the principal effects Seaver observed and (2) these effects can, for the most part, be traced to specific characteristics of the models. This work may thus provide a basis for further investigation of how best to aggregate individual forecasts.

SEAVER'S EXPERIMENT

Seaver[7] investigated the performance of groups of 4 people, acquainted with each other, at making probability judgments about discrete events and about continuous random variables. Only discrete events will be considered here, since the decision variable partition model used in the simulation does not, in its present form, accommodate continuous distributions. Seaver posed general knowledge questions of the sort: "Absinthe is: a) a liqueur or (b) a precious stone." Group members individually chose an answer and recorded a subjective probability r, on the half-range .5 to 1.0, of being correct. They then interacted according to a prescribed method and then again chose an answer and recorded probability judgments. In addition, they rated themselves and the other group members on expertise. Finally, group judgments were created by different mathematical methods of weighting and combining the individual judgments.

---

*This work was supported by the National Science Foundation, Division of Engineering under Grant ENG-7809365, "Bayesian Methodology for Rainflood Forecasting and Reservoir Control."

The experimental conditions for which Seaver obtained results, from eleven groups with 20 questions per group, are set out in Table 1. The conditions simulated by the model are also indicated. The differences among the types of interaction are given in Table 2. Since Seaver found no reliable differences among the interaction methods, all of which allowed individuals to consider the judgments of others, the methods were lumped together as interaction for modeling purposes.

The aggregation methods produce a group probability p_G for the correct hypothesis from individual probabilities p_i, $i = 1,2,3,4$. The value of p_i is the individual's half-range response r_i if he chose correctly and $(1 - r_i)$ if he did not. Similarly, the group response r_G is $p_G \geq .5$ and $(1 - p_G)$ if $p_G < .5$. The equations for p_G under the different aggregation methods are set out below, where w_i is the weight assigned to the ith individual's judgment, and the weights sum to one over the group.

1) Linear combination

$$p_G = \sum_{i=1}^{4} w_i \, p_i \tag{1}$$

2) Weighted geometric mean

$$p_G = \frac{\prod_{i=1}^{4} p_i^{w_i}}{\prod_{i=1}^{4} p_i^{w_i} + \prod_{i=1}^{4} (1 - p_i)^{w_i}} \tag{2}$$

3) Likelihood ratios

$$\frac{p_G}{(1 - p_G)} = \prod_{i=1}^{4} \frac{p_i}{(1 - p_i)} \tag{3}$$

The latter relation (3) reduces to (2) when all w_i are equal to one.

Seaver used three weighting methods: equal, normalized self ratings, and DeGroot[1] weights which are determined for an individual from others' ratings of his expertise. Since there is no model to predict the assignment of weights, only the equal weight case could be simulated, i.e. $w_i = 1/4$.

SEAVER'S RESULTS

Seaver summarized his results in terms of 1) a quadratic scoring rule score, 2) the average probability assigned to the correct answer, and 3) calibration curves, the plot of the proportion correct $p(C|r)$ as a function of response r. The actual proportions of correct response were not reported. Although interaction on the whole had a significant effect, the several methods of interaction could not be shown to differ significantly. In addition, the differences among the weighting methods were slight, in keeping with the results of previous research.[11] But it seems likely that differential weighting would be advantageous if certain questions were to require different specialized knowledge and the groups were composed of people with diverse expertise.

Figure 1 shows the observed effects of aggregation and interaction on calibration. The frequent finding of over-confidence for individuals is evident.[4]

		none	linear			geometric mean				
		individuals	equal weights	self weights	De Groot weights	equal weights	self weights	De Groot weights	likelihood ratio	actual consensus
before	none	▨	▧			▧			▧	
after	Delphi	▧	▨			▨			▨	
	MIX	▧	▨			▨			▨	
	NGT	▧	▨			▨			▨	
	CON	▧	▨			▨			▨	

Table 1. The conditions for Seaver's experiments. Each cell represents a condition for which judgments were obtained. Each shaded region indicates a separate condition represented by the model and for which simulation results were obtained. In the model no distinction is made among interaction types.

Type of Interaction	Reconsider with Information about Other Judgments	Knowledge of Judgment Source	Verbal Information Exchange	Uncontrolled Discussion	Consensus Necessary
None					
Delphi	Yes				
MIX	Yes	Yes	Yes		
NGT	Yes	Yes	Yes	Yes	
CON	Yes	Yes	Yes	Yes	Yes

Table 2. Differences among the several types of interaction examined by Seaver. These differences did not produce significant differences in performance.

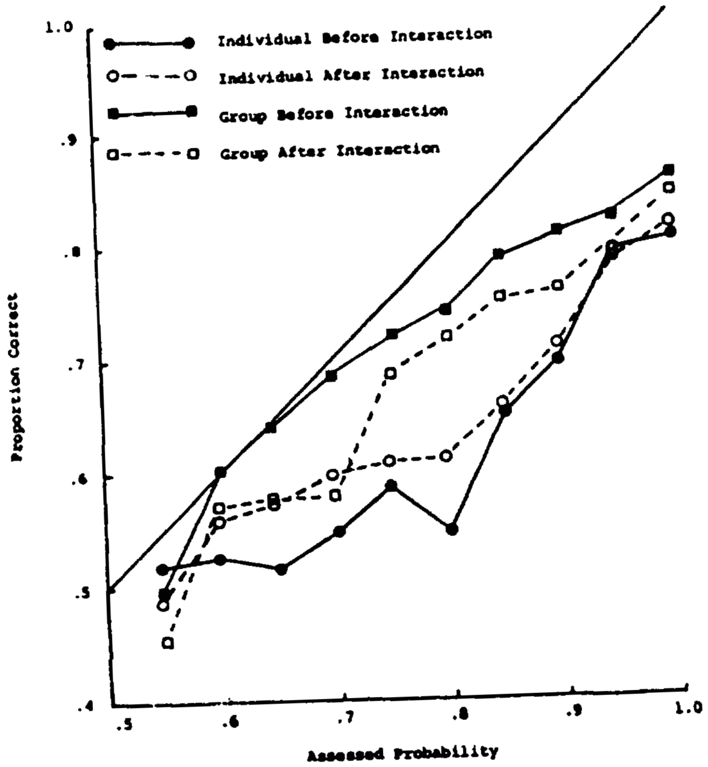

Figure 1. Seaver's results for calibration of discrete probability judgments pooled over type of aggregation, weighting method and type of interaction.

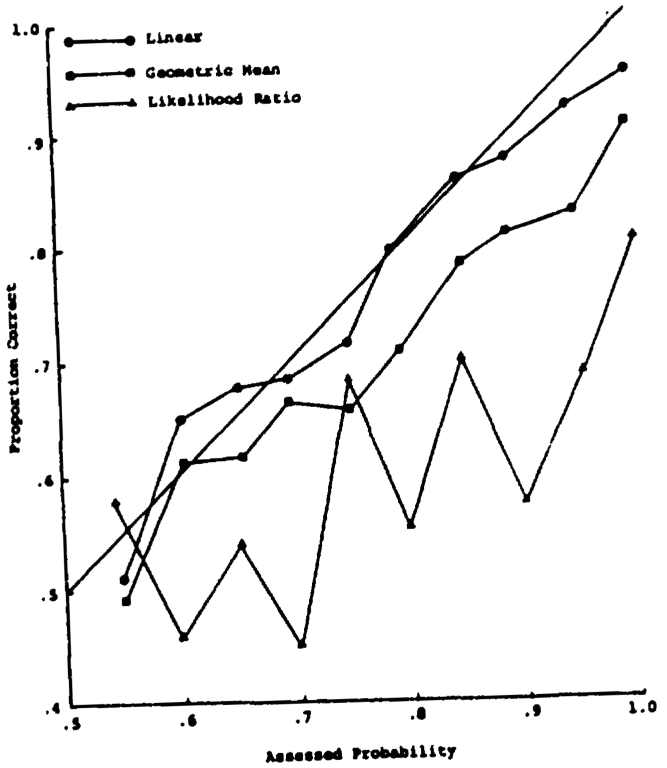

Figure 2. Seaver's results for discrete probability judgments by aggregation method pooled over weighting methods.

The results are pooled over interaction methods and aggregation methods. It appears, and Seaver concluded, that over-confidence is reduced by aggregation, and that interaction increases over-confidence for groups but decreases it for individuals. Figure 2 shows the differential effects of aggregation method, pooled over weighting methods. Linear combination gives the least and likelihood ratios the most over-confidence. For each aggregation method interaction produced greater overconfidence.

THE MODEL FOR GROUP JUDGMENTS

Structure of the Model

The model of subjective probability judgments by groups assumes that individuals initially make judgments in a manner described by the decision variable partition model of Ferrell and McGoey[2] However, it is assumed that individual judgments p_i are then aggregated according to the appropriate mathematical scheme. When there is interaction, a deterministic model of the effects of the group on individual opinion is applied to modify the p_i values before aggregating them into a group opinion. The model of interaction attempts to take account of two phenomena frequently observed in small groups, conformity[3] and polarization.[5]

The Decision Variable Partition Model

The decision variable partition model of calibration[2], applied to two alternative forced choice questions of the sort used in Seaver's study, assumes that consideration of each answer by each individual generates a scalar random variable Y which is differently distributed for correct answers C than for incorrect ones $\bar{C}$. For simplicity, normal distributions are assumed: $f(y|C) = \phi(y - d'/2)$ and $f(y|\bar{C}) = \phi(y + d'/2)$, where ϕ is the probability density function of the standard normal and d' is a parameter of the model. The individual chooses as correct the answer that gives the larger value of Y, y(1), and bases his judgment of confidence on the difference between the values of the two variables y(1) - y(2). Let $X = Y(1) - Y(2)$, $X \geq 0$. The individual partitions the range of X into m intervals by the set of cutoff values $\{x^i\}$, associating with each interval a member of the allowed set of m probability responses $\{r_i\}$. The partition is selected, within the limits of the individual's knowledge, to achieve good calibration. The expected values of the resulting calibration can be determined from $\{x^i\}$ and the distributions of X conditional on correct and incorrect choice.

When the Y distributions are assumed normal, as above, the distributions of X are readily found to be: $f(x|C) = \phi(\frac{x - d'}{\sqrt{2}})$ truncated below at x = 0, and $f(x|\bar{C}) = \phi(\frac{x + d'}{\sqrt{2}})$ also truncated below at x = 0. The expected values of the calibration proportions, $p(C|r_i)$ are found in general by

$$p(C|r_i) = \frac{p(C)[F(x^i|C) - F(x^{i-1}|C)]}{p(C)[F(x^i|C) - F(x^{i-1}|C)] + [1 - p(C)][F(x^i|\bar{C}) - F(x^{i-1}|\bar{C})]} \tag{4}$$

where p(C) is the proportion of correct choices and F is the cumulative distribution function. For the present case, the values of p(C) and [1 - p(C)] that weight the truncated normals cancel with those in (4) to give

$$p(C|r_i) = \frac{\Phi\left[\frac{x^i - d'}{\sqrt{2}}\right] - \Phi\left[\frac{x^{i-1} - d'}{\sqrt{2}}\right]}{\Phi\left[\frac{x^i - d'}{\sqrt{2}}\right] - \Phi\left[\frac{x^{i-1} - d'}{\sqrt{2}}\right] + \Phi\left[\frac{x^i + d'}{\sqrt{2}}\right] - \Phi\left[\frac{x^{i-1} + d'}{\sqrt{2}}\right]} \qquad (5)$$

where Φ is the cumulative distribution function of the standard normal. The parameter d' is related to the proportion of correct choices by

$$p(C) = \Phi(d'/\sqrt{2}). \qquad (6)$$

Figure 3 shows a partition that gives approximately perfect calibration for $d' = 1$ ($p(C) = .76$). Perfect calibration is not always possible. Figure 4 shows the calibration curves that result from holding a partition constant and varying p(C).

It was concluded by Ferrell and McGoey[2] that people tend, unless given feedback about calibration, to use a partition suited to a value of p(C) around .75 regardless of the difficulty of the questions. An example of the model, with constant $\{x^i\}$, fitted to calibration results from Lichtenstein and Fischhoff[4] is shown in Figure 5. The effect of P(C) is clearly evident.

The Interaction Model

Knowledge of other group members' views is assumed to affect each member's confidence which is represented in the model by the decision variable X. For computational convenience, the range of the decision variable X is taken to be the entire real line, with negative values indicating choice of the incorrect alternative and positive ones choice of the correct one. The partition $\{x^i\}$ is symmetric about $x = 0$, with intervals on the negative range producing the same subjective probability responses r as those in the corresponding interval on the positive range, but being associated with the incorrect answer.

Interaction, in the model, operates thusly: an individual's initial value of x is influenced by the average $\bar{x}_3$ of the x values of the other three members to give a new individual value x' according to

$$x' = x + k_1 (\bar{x}_3 - x) + k_2 \bar{x}_3, \qquad \begin{array}{l} 0 < k_1 < 1, \\ 0 < k_2 < 1. \end{array} \qquad (7)$$

The first term mimics conformity in that the value of x (confidence in the right answer) moves toward the mean of the other members' confidence. The second term mimics extremity shift in that the value of x moves in the positive or negative direction depending on whether the mean of the other members' feelings is positive or negative. The individual member's new confidence x' is transformed into a response r in the same way as the original value. And, in all cases, aggregation to give a group judgment is performed only upon the responses (or one minus them if the individual chose wrongly) not upon the x values, which are assumed not to be explicitly available in numerical form.

The Simulation

The simulation program (available from the authors) computes four pseudo random numbers x_i, with intercorrelation ρ, distributed normally with mean

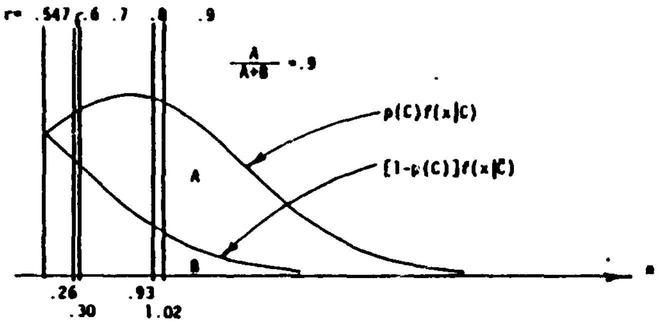

Figure 3. An example of the conditional distributions and a partition on the decision variable for the model for two alternative forced choice questions. The response set is {.5, .6, .7, .8, .9, ∞ }. The partition gives perfect calibration for all but r = .5. Completely perfect calibration is not possible for this case for which d'=1.

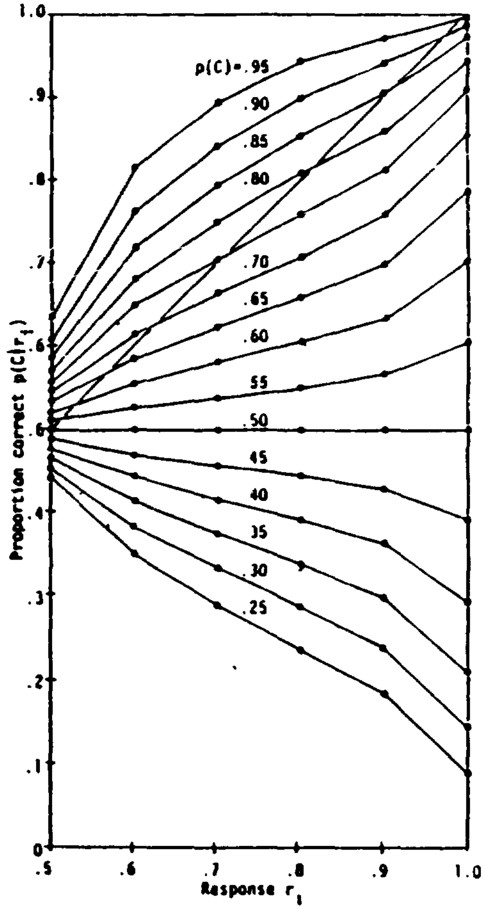

Figure 4. An illustration of the effect on calibration of varying d', and thus p(C), when the partition is kept fixed. The partition is the same as in Figure 5

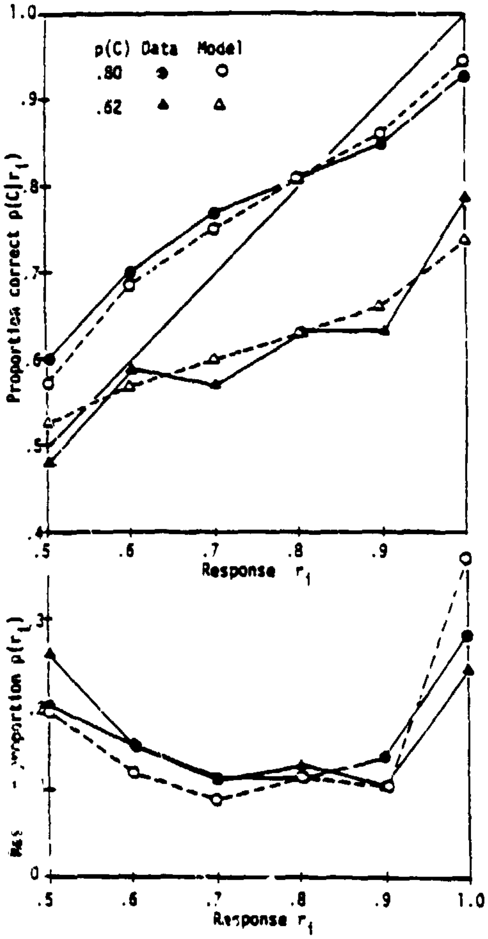

Figure 5. Model and data from Lichtenstein and Fischhoff's experiment 5. $\{x^1\} = \{0, .347, .570, .744, .982, 1.219, \infty\}$. Response proportions for p(C) = .62 were fitted exactly.

$d'/\sqrt{2}$ and variance 1.0. These are the group members' initial confidence estimates. Negative values indicate preference for the incorrect alternative. All individuals are assumed exactly alike in their proportion of correct responses (see equation 6) and in their partitions $\{x^i\}$. These are only approximations, and would still be so even if the model of individual behavior were exact. The intercorrelation reflects the commonality of shared information. Each group member does not have entirely independent information about the correct answer.

The initial values of x for the group members are transformed into response values r by the partition and the results contribute to the simulation of individuals before interaction. The response values are then aggregated according to equations (1), (2) and (3) to contribute to calibration proportions for groups before interaction. The x values are then transformed by equation (7) and responses r_i calculated according to the partition and these contribute to calibration statistics for individuals and groups after interaction. Simulation of 25,000 groups (100,000 individuals) gives stable calibration proportions.

SIMULATION RESULTS

Model Parameters

The decision variable partition model was fitted to the experimental calibration curve for individuals before interaction shown in Figure 1. The degree of over-confidence suggested a proportion correct $p(C) = .65$ and thus a value of $d' = 545$. With an interactive computer program an approximate fit to the data was obtained with

$$\{x^i\} = \{0, .2, .36, .53, 1.045, \infty\}.$$

The other parameters were chosen unsystematically, but with a view toward producing calibration curves that resembled those obtained by Seaver. If his data were available, it might be possible to estimate the parameters from it. However, obtaining suitable values was not difficult, i.e., the effects are not dependent on critical parameter values, and the values chosen also seem plausible a priori. Parameters used were: $\rho=.4$, the member's intercorrelation; $k_1=.1$ the conformity parameter; and $k_2=.2$ the polarization parameter.

Model Results

Figure 6 shows calibration curves from Seaver[7] which allow comparison between individuals and the equally weighted linear combination (i.e., the average)of group members' judgments. Figure 7 shows the results of the model for the same conditions. The effects found by Seaver are clearly evident in the model's output. Over-confidence is markedly reduced by taking the group average, and interaction has the opposite effect on groups that it has on individuals. With individual judgments, the conformity effect makes them slightly resemble group judgments, and thus less over-confident, and the polarization effect makes them somewhat larger, thus more over-confident. The net result is slightly less over-confident after interaction for individual judgments. With groups, on the other hand, the conformity effect is already at a maximum, because of the explicit averaging, so polarization due to interaction makes the judgments more extreme and increases over-confidence. Note that, in the model, the fact that grou judgments are better calibrated than the individual judgments is simply a consequence of the fact that the individuals are over-confident to begin with. Averaging their responses improves the proportion correct $p(C)$ (from .64 to .71 in this case) and with fixed partition $\{x^i\}$ this causes a reduction in over-confidence. Had the individual group members been well calibrated, the groups would have proved to be under-confident, and interaction would reduce the

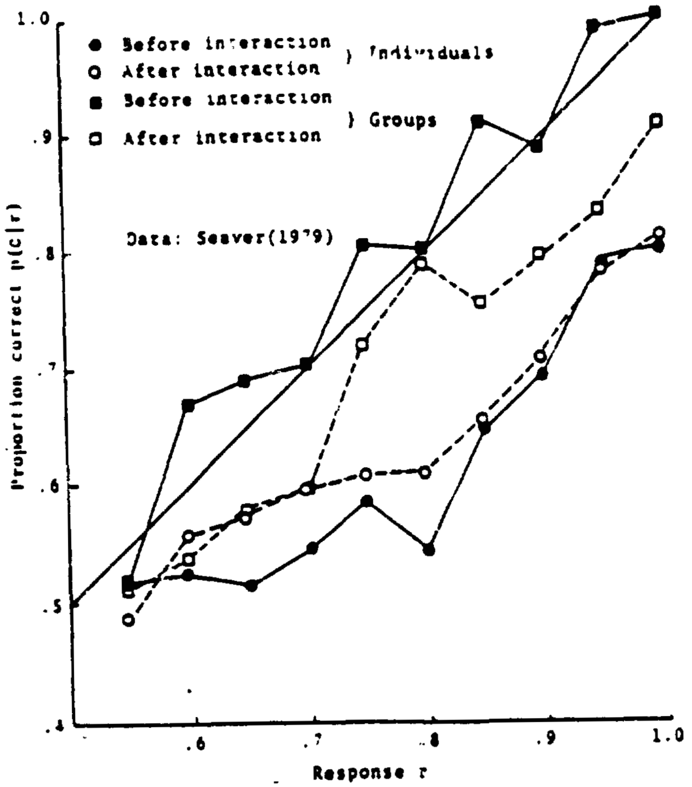

Figure 6. Seaver's calibration results pooled over interaction type, as in Figure 1, but not over aggregation method. Only the linear, equal weights aggregation method is represented.

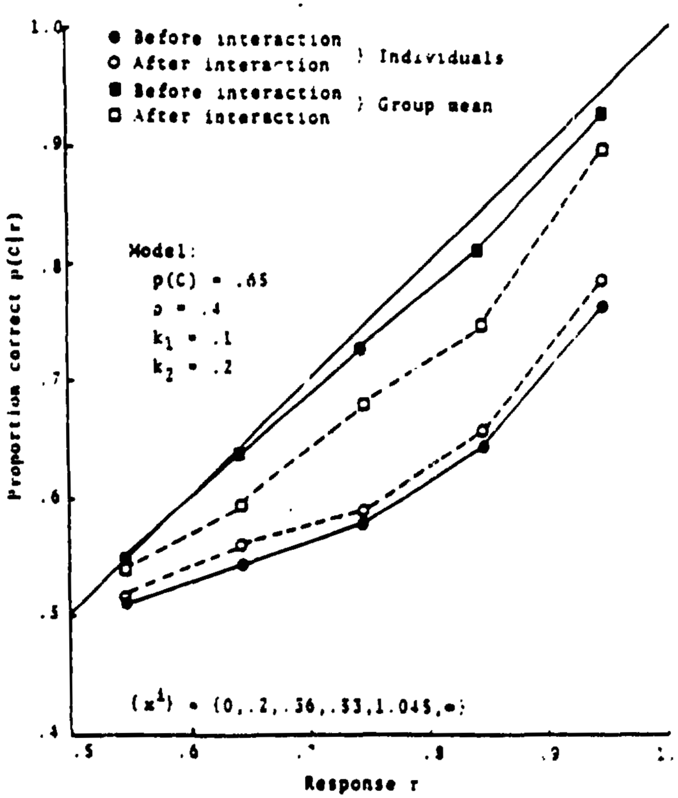

Figure 7. Results from the model corresponding to the conditions of Figure 6, showing the same effects of aggregation and interaction as in the data.

under-confidence for groups and increase it for individuals. This predicted effect is shown in Figure 8, in which the group calibration is the worst, but still least over-confident. It would be interesting to test this prediction empirically.

The effects of the different aggregation methods (equations 1, 2, 3) as found by Seaver are shown in Figure 9, to be compared with output from the model in Figure 10. Again the model reflects Seaver's findings in that the geometric mean and the likelihood ratio methods of aggregation compensate less well for the over-confidence of individual members. Each of these methods gives more extreme values (and thus more over-confidence) than the simple average, at least when the component values tend to agree, the likelihood ratio giving much more extreme values. The model does not give results for the likelihood ratio method as close to Seaver's as it does for the other methods, and this may be due to its extremeness interacting with the rather coarse partition (m = 5 response categories).

The model results in terms of quadratic score and average response probability for each condition have been computed. The model scores are much higher than those Seaver found and this may be due to the assumed proportion of correct response being too high. The average response probabilities from the model are somewhat too high but they follow the same pattern over conditions as Seaver reports. Since the model was not fitted in any precise way and has been used only to demonstrate that it reproduces the structure of the experimental results, the numerical values are not included here. If model parameters could be estimated from data, however, it would be important to look for consistency at such a level. But the data is not yet available.

CONCLUSIONS

Seaver's basic findings about calibration of group and individual discrete probability judgments can be accounted for in a consistent and intuitively satisfying way by the decision variable partition model of individual subjective probability judgment coupled with a simple linear model of the effects of group interaction on individual certainty. The effects Seaver reports are then due to two competing influences. The first is grouping, whereby combining judgments leads to a greater proportion of correct responses and thereby to reduced over-confidence or even under-confidence. The effect is the same as that of an increase in p(C) on individual calibration. The second influence is extremeness whereby the judgments are made larger and thereby increase over-confidence.

Aggregation methods all manifest grouping to some extent, but of those considered only linear averaging avoids introducing extremeness effects which tend to counteract the effect of grouping on reduction of over-confidence. Intercorrelation of individual judgments also counters the effects of grouping. Group interaction also combines grouping, as a manifestation of conformity, and extremeness as a manifestation of polarization. These psychological characteristics of interaction are widely observed and reported.

The practical implications of these findings for aggregating group judgments are substantial.

1. The quality of calibration of aggregated judgments depends, in a complex but predictable way, on the quality of individual calibration. If individuals are quite over-confident groups will be less so, but if individuals are well calibrated, groups will be under-confident. This result has not been reported but is predicted.

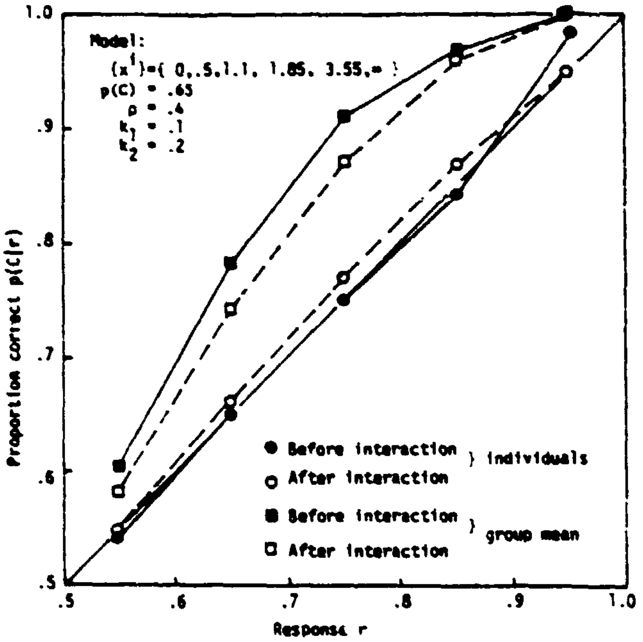

Figure 8. The effect on group calibration predicted by the model when individuals are well calibrated; groups are then under-confident.

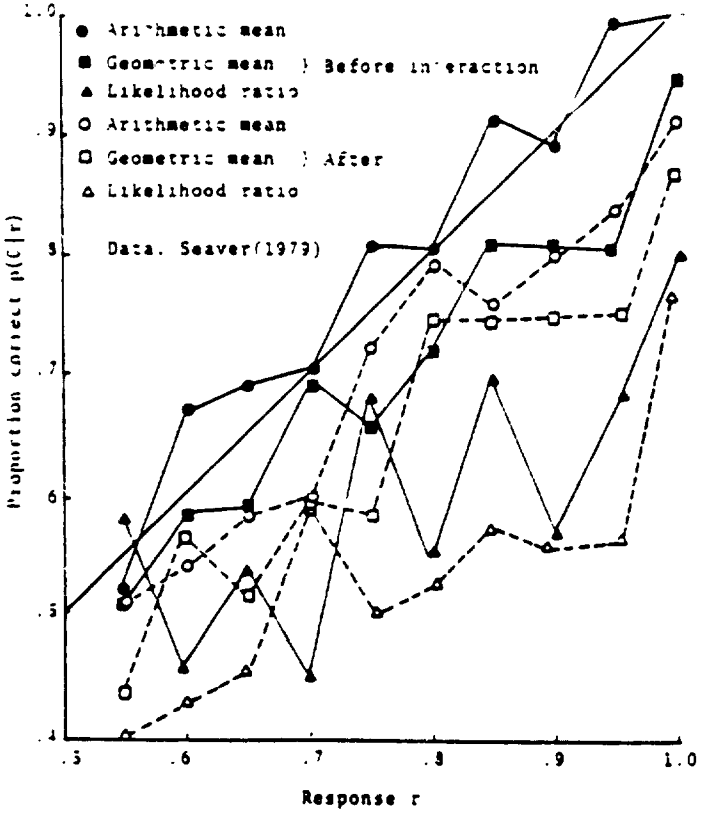

Figure 9. Seaver's results for the effects of type of aggregation on calibration. Only the case of equal weights is included.

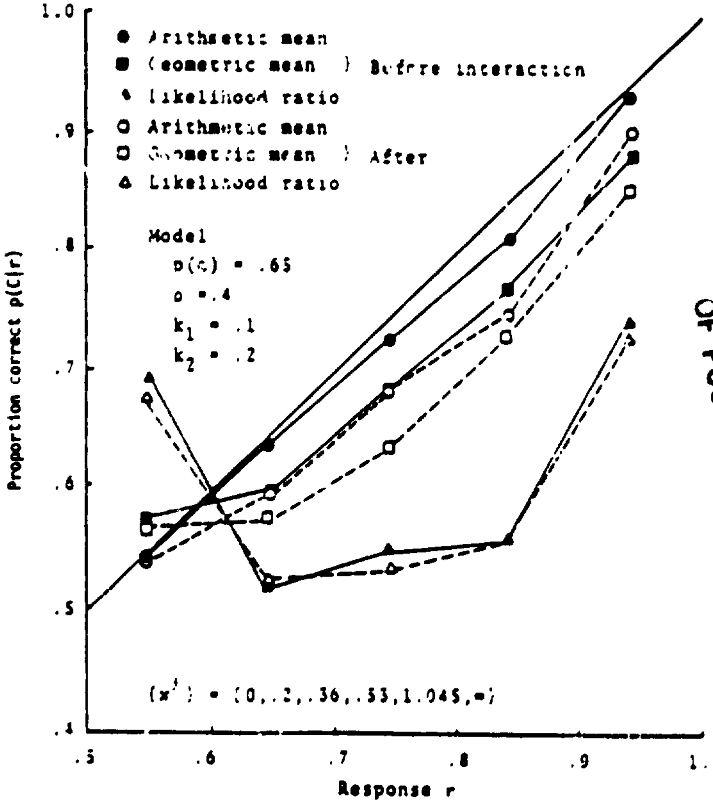

Figure 10. Results from the model corresponding to the conditions of Figure 9, showing similar effects of interaction type.

ORIGINAL PAGE IS OF POOR QUALITY

2. Aggregation methods can be tested beforehand for their influences on calibration.
3. Interaction, for questions of the sort studied by Seaver, is of no practical value since its beneficial effects of grouping can be obtained by averaging.
4. If individual calibrations were known, the effects of aggregation could be predicted and the aggregation method adjusted to give perfectly calibrated group judgments.

REFERENCES

1. DeGroot, M., Reaching a Consensus, *Journal of the American Statistical Association*, 69, 118-121, 1974.
2. Ferrell, W.R. and McGoev, P.J., A Model of Calibration for Subjective Probabilities, *Organizational Behavior and Human Performance*, 1980 (in press).
3. Kiesler, C.A. and Kiesler, S.B., *Conformity*, Reading, MA: Addison-Wesley, 1969.
4. Lichtenstein, S. and Fischhoff, B., Do Those who Know More Know More About How Much They Know? *Organizational Behavior and Human Performance*, 20, 159-183, 1977.
5. Myers, D.G. and Lamm, H., The Polarizing Effect of Group Discussion, *American Scientist*, 63, 297-304, 1975.
6. Seaver, D.A. How groups can assess uncertainty; Human interaction vs. mathematical models, *Proceedings: International Conference on Cybernetics and Society*, 185-189, 1977.
7. Seaver, D.A. *Assessing Probability with Multiple Individuals: Group Interaction versus Mathematical Aggregation*. Unpublished doctoral dissertation, University of Michigan, 1979.
8. Sanders, F., On Subjective Probability Forecasting, *Journal of Applied Meteorology*, 2, 191-201, 1963.
9. Stael von Holstein, C.A., An Experiment in Probabilistic Weather Forecasting, *Journal of Applied Meteorology*, 10, 635-1971.
10. Winkler, R.L., The Consensus of Subjective Probability Distributions, *Management Science*, 15, 61-75, 1968.
11. Winkler, R.L. Probabilistic prediction: Some experimental results, *Journal of the American Statistical Association*, 66, 675-685, 1971.
12. Winkler, R.L., Murphy, A.H. and Katz, R.W., The Consensus of Subjective Probability Forecasts: Are Two, Three... Heads Better than One? *Fifth Conference on Probability and Statistics in Atmospheric Sciences*, Boston, MA: American Meteorological Society, 1977.

N82 34055

VISUAL/MOTION CUE MISMATCH DURING A COORDINATED ROLL MANEUVER

D. K. Shirachi

Computer Sciences Corporation
Mountain View, California

ABSTRACT

Two major factors involved in creating realistic simulations are the visual and motion systems which provide important cues of vehicular attitude. velocities and accelerations to the pilot for purposes of stable control and simulation realism. However, it is difficult to match the dynamic response characteristics of these two display systems to each other because of the inherently higher inertia, limited available power and constrained positioning for the motion system. Furthermore, as a means of dynamically compensating for simulator dimensional constraints, washout filters are used which in turn modify the frequency characteristics of the motion simulator.

The purposes of this experiment were to determine the following:
(1) the effect of a performance mismatch between the simulator visual and motion display systems on pilot performance while engaged in a compensatory tracking task, and
(2) the effect of a reduction in simulator motion scaling, maintaining constant visual scaling, on pilot performance for this same task.

A jet transport aircraft with motion in the roll and lateral simulator axes was used as a test vehicle for this computer simulation investigation. The aircraft was disturbed by moderate levels of turbulence which resulted in flight path deviations in the roll and lateral axes. The pilot's task was to maintain flight formation behind the aircraft in front of him as displayed by a video monitor located in the simulator cockpit.

Experimental data consisting of pilot describing functions and pilot performance scores are presented and discussed as they relate to previously published experimental evidence.

COMBINED EFFECT OF THE OCULOGYRAL ILLUSION AND OF A FIXED PERIPHERAL FIELD ON SENSATIONS OF YAW MOTION

J.K. HUANG AND L.R. YOUNG
Man Vehicle Laboratory, M.I.T.

INTRODUCTION

It is well known that visual and vestibular information interact in perception of spatial orientation and in pilot control tasks. The perception of self-rotation while viewing an isolated visual target rotating with the subject is several times more sensitive than without the target.[4] This is the oculogyral illusion[6] (OGI) and thresholds for OGI are significantly lower than thresholds in the dark. In contrast, measurements of vestibular nucleus unit activity in rotating alert monkeys show that the firing rate with a conflicting visual field is significantly lower than the firing rate in the dark,[15] indicating that the threshold for perception of self-rotation could be lower in the latter case. The purpose of this work was to study the combined effect of the oculogyral illusion and of a fixed peripheral visual field on sensations of rotation about a vertical axis.

METHODS

Subjects were seated in a rotatable trainer with four possible visual fields: DK (dark); DM (a dim peripheral field fixed with respect to the subject - 60 fc illumination near the bulb); LT (the same as DM, but with 80 fc); and OGI (only a fixed spot can be seen). For DK, DM and LT, the subjects particpated in three sub-experiments: Threshold measurement, closed-loop velocity nulling, and open-loop magnitude estimation. A total of 13 male subjects participated, aged 22 to 29, in normal health.

A modified Link GAT-1 trainer, driven as a velocity dependent servo, rotates about the vertical axis.[16] During LT and DM, a projector presents a vertical stripe pattern to the subject via two translucent side windows. A 1" diameter white spot is fixed 30" in front of the subject. For DK, the subject is blindfoled with eyes open. For the closed-loop velocity nulling method, a featureless control wheel in the horizontal plane in front of the subject is used to null the trainer velocity. For the open loop magnitude estimation method, a pen was affixed at the edge of the wheel and the subject asked to use it as a pointer to a laboratory fixed location.

Threshold measurement: Six subjects were instructed to use the wheel to indicate the direction of rotation as soon as possible. All had six randomized sessions. In each, six accelerations were used with periods of 15 s and with 30 s between stimuli. Closed-loop velocity nulling method: The trainer was driven by a disturbance signal d which is a pseudo-random, zero-mean, velocity command signal with a period of 409.6 s, consisting of a sum of 12 sinusoids spanning the range from 0.007 to 0.715 Hz. Four subjects were instructed to use the wheel to keep the trainer as motionless as possible by concentrating on their sensed angular velocity. The wheel deflection was added to the disturbance to drive the trainer with a net velocity ω. The subject was trained to null the velocity as best he could and was given the same six sessions as before with four minute intervals between runs. A separate experiment compared conditions in DK and OGI with four runs for each subject (two each for DK and OGI). Open loop magnitude estimation method: The subject was required to estimate his rotational displacement relative to a fixed laboratory frame for two types of stimuli - triangular (TRI) and trapezoidal (TRZ) waveforms. TRI waveforms were selected as they approximate stimuli experienced in natural motion

ORIGINAL PAGE IS
OF POOR QUALITY

and avoid difficulties with unnatural stimulation.[8] Six subjects were instructed to move the pointer in a compensatory direction so that it maintained a fixed (compass) heading as the trainer was rotated. After practice, the same six sessions were given. In each, seven TRI stimulations with four types of acceleration were used with 30 s between stimuli. To investigate open loop magnitude estimates during sudden decelerations, two stimuli were constructed as follows: $5°/s^2$ acceleration to a constant velocity of 30°/s for 20 to 26 s, followed by a deceleration of $15°/s^2$ or $20°/s^2$ to zero. Because of the long and different durations of constant peak velocity, the subject senses both himself and the trainer in a stationary state until the onset of the upredictable deceleration causes an after-rotation effect in the opposite direction. The subject was asked to ignore the first acceleration, but to perform the same pointing task as before to show the after-rotation effect. There were again six sessions, each using two types of deceleration, with one minute between each. Subjects were instructed to look at the white spot during LT and DM.

RESULTS

Threshold measurement: The latency time for perception of angular rotation was measured. All the data were averaged and are plotted in Fig. 1, along with other results[2,11] corresponding to DK stimuli. The 'Mulder Product', $\alpha\tau$ (acceleration x latency) = K, is plotted to fit the data for each visual presentation. A t-test shows no significant difference between the DM and LT. However, the threshold for the DM and LT stimuli is significantly lower than the threshold in the DK.

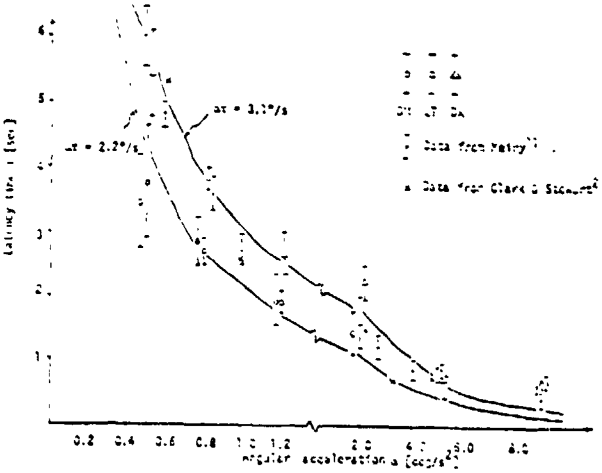

Figure 1. Threshold for perception of angular acceleration about the vertical axis with DM, LT, and DK visual input.

Closed-loop velocity nulling method: Using the same analysis techniques established by Zacharias[16] the describing function can be evaluated after Fast Fourier Transformation of the wheel input and trainer output signals in the frequency domain. The amplitude ratio data were obtained by pooling the subject data across the test population. The parameter values of a lag lead transfer function were obtained from a nonlinear regression program providing a least-squares parameter fit to the data.[5] A dead time is added to the phase data to obtain a better fit. The AR asymptotes and the values of all parameters are shown in Fig. 2.

The gains for the LT (or DM) and DK, at the low frequency, are significantly different, as is τ_2. The changes in τ_1 and τ_d are not significantly different. Although the gain for the LT is slightly higher than that for DM, the difference is not significant nor is that in τ_2 for the LT and DM. Furthermore, the highest gain was in OGI and all subjects stated that there was a clear oculogyral illusion which they could use to detect the direction of self-rotation or to estimate the magnitude of velocity. This was especially true at low frequency and acceleration.

Open loop magnitude estimation method: The mean and standard deviation magnitude estimates of the actual motion with the TRI stimuli are shown in Fig. 3. For $\alpha = 5°/s^2$, the subjective displacement is quite near the actual displacement and the subjects tended to underestimate more when the duration of the waveform increases. This is to be expected on the basis of cupula displacement, relative to velocity, during constant acceleration.[8] Although the means are slightly higher in the DK, analysis of the raw data shows that this is not significant.

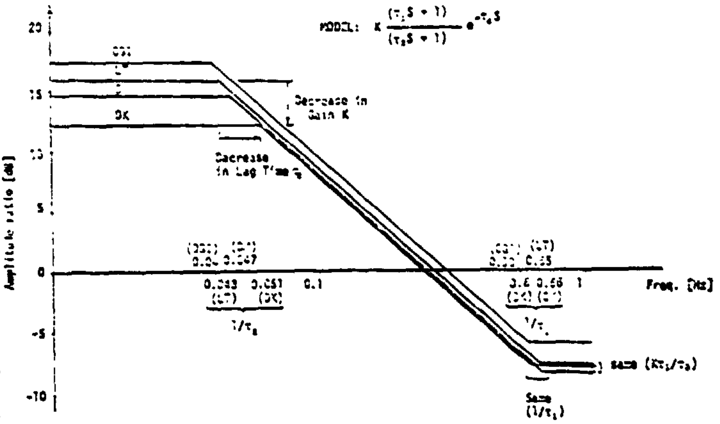

Figure 2a: Amplitude ratio asymptotes for four visual fields.

For TRZ stimulation, the subjective velocity was calculated from the disk position after the beginning of deceleration and the means are plotted in Fig. 4 for $20°/s^2$. From the raw data, we find that each subject showed smaller subjective velocity in the DK for both decelerations, although the difference is not significant. In the DK, the subjective velocity rises more slowly and reaches a smaller peak than it does in the DM or LT. For $15°/s^2$, the result is similar.

DISCUSSION

Threshold measurement: Several investigators have measured the threshold for perception of acceleration about the vertical, however, one should be aware that there is a limited region of applicability of the Mulder product.[1,2,11] τ_d was found as 0.4 s at $\alpha^{-1} = 0$, by plotting α^{-1} vs τ. By using $\tau' = \tau - \tau_d$ in Fig. 5, the data were fitted with the whole region of $\alpha(\tau - \tau_d)^x = K$, a revised form of $\alpha\tau = K$. The parameter values were obtained from a nonlinear regression program.[5] In Fig. 1, the data show a shorter latency time in DM or LT compared to DK for all subjects. We propose that since the subject first senses the motion of the white spot and later his self-rotation in the same direction, he "learns" to sense the self-rotation at the onset of the oculogyral illusion and achieves a lower threshold. Marshall[10] found the same effect. Another possible explanation of the longer latency in the dark is that, because of dizziness or disorientation, the signal from the vestibular nucleus is processed with a higher

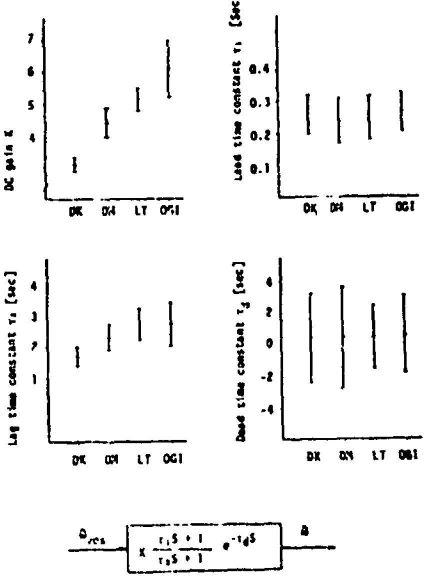

Figure 7b Parameter values of the describing function dependent on visual field type.

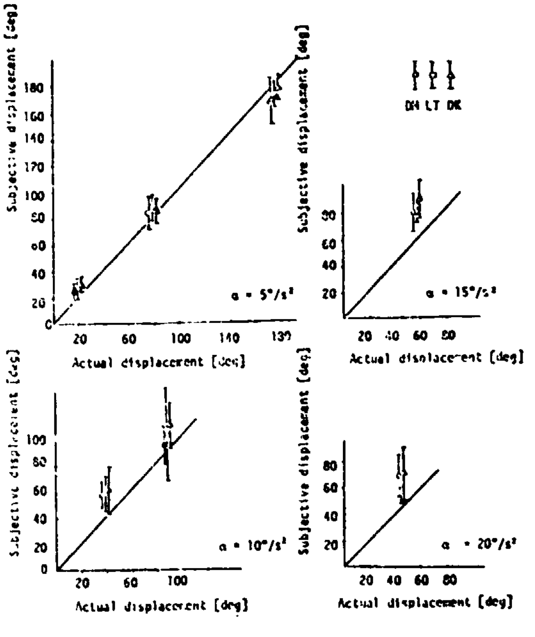

Figure 3. Annular displacement estimates obtained with triangular waveforms produced by different angular accelerations α.

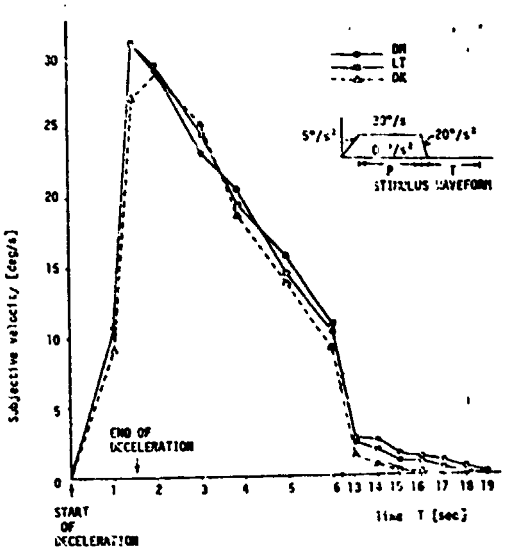

Figure 4. Subjective velocity (mean value) following a short constant deceleration of 20°/s² of the trapezoidal waveform.

threshold and has longer latency. The alertness of the subject in the DM and LT fields may also be a reason for the low threshold with the OGI.[3,7] Henn et al[9] showed that alertness changes, evident in eye movements, did not affect the vestibular nucleus units' response to angular acceleration. From Fig. 1, it can be seen that there is no significant difference between the DM and LT. For $0.5°/s^2$ acceleration, it is interesting that every subject showed a shorter latency time in DM. Higher illumination will increase the non-uniformity of the background and increase the sensation of stationarity of the stripes.[6] This may explain the higher threshold in LT and DM and also the higher thresholds in light found by Waespe et al.[14]

Closed-loop velocity nulling method: The gain in LT (or DM) is higher than in DK (Fig. 2a). The difference appears at frequencies below 0.06 Hz. Here, α is below $2.41°/s^2$ (from disturbance frequency spectrum), and the threshold is significantly lower in the DK with smaller α (Fig. 1). The oculogyral illusion presumably produces the lower threshold and results in greater sensitivity and a higher gain for nulling rotation in LT (or DM).

Open loop magnitude estimation method: With TRI stimulation, the magnitude estimates of the actual motion showed no significant difference between DK, DM and LT. Because ofthe strong stimulation and short duration, such a stimulus can be regarded as similar to a mid or high frequency sinusoidal stimulus. The vestibular system can sense the motion quickly and the judgment presumably does not rely upon the effect of visual input. These results are confirmed by those of the first experiment. For the TRZ stimulation, we found a quicker rising speed, larger subjective velocity, and longer duration of the after-rotation effect in the illuminated presentation than in the DK and we can expect to find greater differences with lower intensity stimulation.[13]

ORIGINAL PAGE IS
OF POOR QUALITY

CONCLUSIONS

All of the current results concerning detection and reaction to angular acceleration in the dark and with a fixed visual field show that, for low accelerations, the visual input enhances the sensitivity to self-motion Since the visual surround is fixed with respect to the subject, and might imply a "no motion" or null signal if interpreted as a circularvection input, it conflicts with the true rotation sensed by the semicircular canals and might be expected to inhibit the motion sensation. Furthermore, vestibular nucleus unit activity was shown[15] to be inhibited by a fixed visual surround in similar circumstances and compensatory eye movements are suppressed by visual fixation. We attribute the enhancement at low acceleration to the sensitive motion detectic ociated with the oculogyral illusion of relative motion of a fixed spot dur ject rotation.

Figure 5: Threshold for perception of angular acceleration about the vertical axis with DM, LT, and DK input.

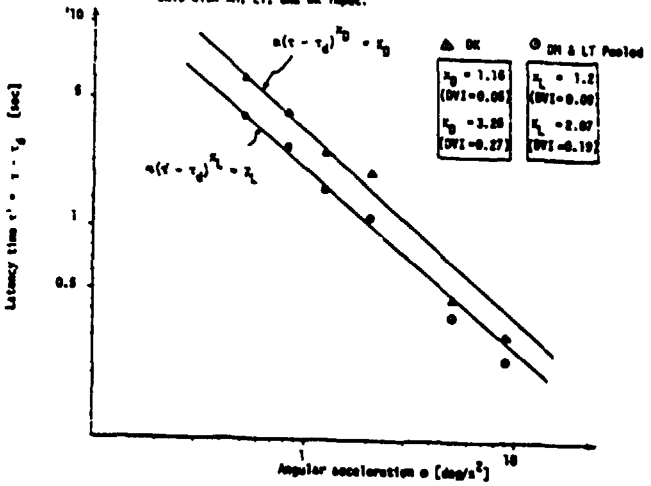

REFERENCES

1 Clark, B., Aerospace Med 38:443-450, 1967.
2 Clark, B., Stewart, J.D., Aerospace Med 33:1426-1432, 1962.
3 Clark, B., Stewart, J.D., Perception and Psychophysics 3:253-265, 1968.
4 Clark, B., Stewart, J.D., Aerospace Med 43:8-12, 1972
5 Dixon, W.T., BMD-Biomedical Computer Programs, University of California Press, 1973.
6 Graybiel, A., Hupp, D.I., J Aviat Med 17:3-27, 1946.
7 Guedry, F.E., In: Vestibular System Part II: Psychophysics, Applied Aspects and General Interpretation, H.H. Kornhuber (ed), 1974.
8 Guedry, F.E., Stockwell, C.W., Norman, J.W., Owens, G.G., Acta Otol 71: 439-448, 1971.
9 Henn, V.S., Young, L.R., Finley, C., Brain Res 71:144-149, 1974.
10 Marshall, J.E., Visual-Vestibular Interaction and Threshold for Angular Acceleration. USAMRL, Fort Knox, KY, 1967.
11 Meiry, J.L., The Vestibular System and Dynamic Space Orientation, Sc.D. Thesis, MIT, Cambridge, MA, 1965.

12 Melvill Jones, G., Young, L.R., Acta Otolar 85:45-53, 1978.
13 Parsons, R.D., J Exp Psychol 84:230-238, 1970.
14 Waespe, W., Waespe, B., Henn, V., Pflug. Arch ges Physiol 373 Suppl. R87, 1978.
15 Waespe, W., Henn, V., Exp Brain Res 33:203-211, 1978.
16 Zacharias, G.L., *Motion Sensation Dependence on Visual and Vestibular Cues*, Ph.D. Thesis, MIT, Cambridge, MA, 1977.

ORIGINAL PAGE IS
OF POOR QUALITY

N82 34056 D19

A Performance Analysis Study of A Complex G Field Experiment

D. W. Repperger
AFAMRL, Wright Patterson Air Force Base, Ohio 45433

Introduction:

When a human is subjected to a G field stress environment, the effect of this stress variable on tracking performance can be studied several ways. This paper will conduct a performance analysis on data from an experiment designed at the Air Force Aerospace Medical Research Laboratory by an effort in cooperation with the University of Connecticut. The details of this experiment have been well documented and this study has provided an interesting data base which illustrates the degradation of tracking performance as the human is subjected to the environmental stressor (1-4). The primary goal of this experiment was to obtain data for developing models utilizing the Optimal Control Model. Since this study has provided a data base which shows performance changes under the stress condition, the work conducted here is concerned with defining more explicitly the performance changes and examining statistical properties of human tracking with and without the stress effects.

The extant literature on the study of the effect on humans of acceleration stress is extensive. One measure of the amount of literature available can be seen in the classic work of Fraser (5) which lists 199 references in the area at that point in time. The paper by Brown (6) lists 100 references and quite interestingly defines human's performance under these stress fields in several different ways. The term performance can be used to describe tolerance limits, changes in reaction time, proprioceptive changes, visual perception loss, degradation in scores obtained from different motor related tasks, and a variety of physiological indicators or measurements under the stress condition on humans.

Since the definition of human performance has many interpretations in the acceleration stress area, it was decided in this paper to look at performance using an extension of a phase plane technique (7). There are two questions to be addressed here with respect to human tracking. First it is desired to better understand how human tracking changes under the exposure to the stress condition. One object of this investigation is to make explicit statements about the performance changes due to the stress exposure in lieu of making heuristic arguments using conventional measures of tracking performance. The goal here is to make some quantitative determination of how the stress effects the performance characteristics of human's tracking in the loop. The quantitative determination of stress effects on performance will be defined more explicitly in terms of parameters of a density function identified from the empirical data.

A second objective of this study is to determine exactly what the distribution functions are which characterize tracking in a phase plane representation of the closed loop error signal. The assumption in (7) was that the distributions of the error signal and its derivative in the phase plane were normal. The credibility of that assumption will be tested in this paper for a different tracking task and across a number of subjects. The data base (1-4) will be used to examine the distributions of the error signal and the first derivative of the error signal. This empirical data will be studied using a test for normality (8,9,10,11). The identified medians become the boundaries of the phase plane on their respective axes; the identified variances indicate the confidence in this estimate of the median value.

A z-statistic is used to determine if the medians and variances of the empirical data show a significant change (i.e. in the phase plane boundaries) between the stressed condition and the non-stressed condition. This test which has the property of being "distribution free", provides the framework to make a statement about the significant performance changes due to the stressed condition without the assumption of normality commonly used with t-tests. Also, using this formulation, it is possible to examine the assumption of normality of the distribution functions from the empirical data which characterize the phase plane boundaries. The assumption of normality for the distribution functions of the performance variables may not hold here because the forcing function used in this study is sum of sines which differs from the deterministic tracking task considered in (7).

The G Stress Field Experiment:

The experiment which gave rise to the data base used here has been extensively documented in (1-4). In this paper the data used in this analysis will consider two of the phases of this experiment Figure (1a) illustrates a block diagram of a human involved in this man-machine interaction. To describe this type of environmental stressor, the term "open loop stress" is used because the G stress field is applied to the human and he cannot change this stress field through his stick commands. Figure (1b) illustrates phase II of this experiment which is termed, "closed loop stress". In this case the human's stick commands increase the stress level and thus penalize the subject for making these stick commands in his tracking response. Figure (2) illustrates the conventional definitions of the G stress field vectors used in Air Force related applications. Using the vector definitions in figure (2), the open and closed loop portions of this experiment can be defined as follows:

Phase I:

Open Loop Stress: Gz=5.0, Gx=2.0, Gy=0.0; The target input consisted of a 95 second compensatory tracking task (sum of sines, zero mean, constant variance).

Phase II:

Closed Loop Stress: Gz= 5.0, Gx=2.0, with two levels of Gy defined as follows:

Low Level Gy: Gy ≅ ± 1 peak to peak (0.7 RMS) - Same Tracking Task
High Level Gy: Gy ≅ ± 2 peak to peak (1.4 RMS) - Same Tracking Task

During a daily run of the experiment, each subject tracked two 95 second tracking tasks (sum of sines) static and then experienced two stress exposures of 95 seconds each (with the same tracking task). After the stress exposure, the subject was required to track two post static runs of 95 seconds each. Chronologically, the tracking tasks were presented in the following sequence:

Table I - One Trial (One Days Run)

Experimental Condition	Length of Tracking Task
Pre Static 1	95 Seconds
Pre Static 2	95 Seconds
Stress 1	95 Seconds
Stress 2	95 Seconds
Post Static 1	95 Seconds
Post Static 2	95 Seconds

The subjects were trained until the performance scores showed asymptotic behavior (defined as less than 5% change in the mean square error for three consecutive replications) and also each subject maintained adequate tolerance to the stress level. This tolerance was determined through the subject's and medical monitor's evaluation as to his adaptation to the G stress level as well as observing the mean square performance scores during the stress phase of the experiment. In table I, during phase I, stress 1 and 2 were the open loop type stress described previously. In phase II the stress 1 and 2 were, respectively, one level of the low Gy value and a second level of the high Gy value. The orders of presentation of the Gy levels were alternated from trial to trial. A description of the performance aspects of this experiment is presented next.

Performance Analysis of The Data:

In the analysis of data from a man-machine experiment, many methods exist for assessing the closed loop tracking performance. With reference to figures (1a-b), it is desired to characterize measures of the tracking error which can be used to delineate performance changes with or without stress. The two common methods are e_{RMS}(Root Mean Square) and e_{Hit} Score defined as follows (7):

$$e_{RMS} = \sqrt{\frac{\sum_{i=1}^{N} e^2(t_i)}{N}} \quad (1)$$

where N is the number of samples at time instants t_i. $e_{Hit\ Score}$ or time on target can be defined in terms of when the error signal is smaller than a window of a specified size. By definition:

$$e_{Hit\ Score} = \text{The Number of Samples when } |e(t_i)| \leq K_1 \quad (2)$$

where K_1 is the window size. The time on target is defined by:

$$\text{Time on Target} = e_{Hit\ Score} * \text{Sampling rate (seconds)} \quad (3)$$

The use of hit score analysis is a valuable tool to assess performance changes; however, it is sometimes difficult to apply this performance metric to study large blocks of data over various window sizes and to draw comparisons between the different experimental conditions. An easier way to study the window problems (and to relate the ensuing phase plane analysis to the window study) is through the use of a Cumulative Distribution Function (CDF). Figures (3a-3b) illustrate the density function (assumed to be normal in the diagram) and its corresponding Cumulative Distribution Function (the first integral of the density function) defined as follows:

$$\text{Density Function} = \quad f(x) = 1/\sqrt{2\pi}\,\sigma \; e^{-(x-\mu)^2/2\sigma^2} \quad (4)$$

$$\text{Cumulative Distribution Function:} \quad F(x) = \int_{-\infty}^{x} f(s)\,ds \quad (5a)$$

$$= 1/\sqrt{2\pi}\,\sigma \int_{-\infty}^{x} e^{-(s-\mu)^2/2\sigma^2}\,ds \quad (5b)$$

$$= \mathrm{ERF}\,(\,x-\mu/\sigma) \quad (5c)$$

Where the definition of ERF in equation (5c) is represented by equation (5b). For a random variable x, the CDF has the property that:

$$F(K_o) = P\left\{x \leq K_o\right\} \quad (6)$$

That is, the probability that the error signal is smaller than a window of size K_o is equal to the value of the CDF function for that value of K_o. To illustrate the applicability of this approach for developing a better understanding of the performance aspects in man-machine systems, use can be made of the CDF to compare two trackers and two different control systems (figures 4a-4b).

In figure (4a), it is noted that the CDF (12,13) for a good tracker (one trial) is to the left of a poor tracker. This is true because the good tracker keeps all values of the error signal within a window of size K_1 while the poor tracker must have a window of size K_2 to contain all the samples of the error signal. To interpret window analysis from figure (4a), this is simplified by using the horizontal lines at a fraction of the CDF value. For example, for CDF=.5, it is noted that the good tracker keeps 50% of the error within a window of size K_3; however, the poor tracker keeps 50% of the error within a window of size K_4. A measure of comparison between the trackers is the distance K_4-K_3 which indicates how much of a window difference exists between these trackers 50% of the time. This analysis is then repeated for CDF=0.8 and from the CDF plots, the window of size K_6-K_5 illustrates the window difference for 80% of the error in the experiment.

The CDF is a valuable tool to assess aircraft performance as can be seen in figure (4b). In this diagram the shaded region A indicates the range of values that a control system may have an influence on the closed loop performance . The region A is shaded because it is assumed that some parameter of the control system is varied over a range of values to change the closed loop performance. The left side of the shaded region is the best case design, the right side of the shaded region is the worst case design. Control system B is illustrated by the shaded area B. This area B is to the right of the shaded region for the good control system which follows from the same argument made in figure (4a). The left and right hand sides of area B indicate, respectively, the best case and worst case design for system B. The real applicability of

ORIGINAL PAGE IS
OF POOR QUALITY

figure (4b) is in the comparisons between systems by projecting lines at specified values of the CDF function. For example, projecting the 0.5 CDF horizontal line across the diagram, one can determine the range of window values where each system is effected. From figure (4b), it is seen that control system A will have 50% error variations with window ranges K_1 to K_2. Control system B, however, has window ranges from K_3 to K_4, 50% of the time. The simple visual presentation in figure (4b) provides a valuable method for evaluating system performance when non-linearities are present in systems and comparisons are desired between the time domain response characteristics of these systems.

Figure (5) illustrates how to utilize the powerful techniques of the CDF to determine quite explicitly how the effects of stress on human tracking performance can be quantified. In figure (5), the assumption is made that a closed loop error phase plane is sufficient to describe human tracking performance in this type of tracking task. It is assumed here that along the $e(t)$ or $\dot{e}(t)$ axis, that there exists unknown density functions to describe the boundaries along the two axis. The median value of the density function is the unknown boundary point and this parameter as well as the variance of this density function, will be determined from the empirical data. From figure (5) it is seen that 4 unknown parameters exist which characterize the densities in the following manner:

$$f_i(x) = 1/\sqrt{2\pi}\,\sigma_i \quad e^{-(x-\mu_i)^2/2\sigma_i^2} \qquad (7)$$

where for no stress (i=2,4) and the four unknowns μ_i, σ_i are to be determined. For the stressed condition, (i=1,3) and the unknowns μ_i, σ_i will also have to be determined. In order to make explicit statements about performance changes, it will be necessary to first determine the parameters, μ_i, σ_i, i=1,4. Once these unknowns have been obtained, then the conclusions about the performance analysis can be stated. It is important at this point to understand what underlying assumptions are necessary to make an explicit statement about performance changes.

One could, conceivably, raise the question concerning the assumption that the densities $f_i(x)$ are normal. If they are not normal, the CDF table tests can still be used to establish statistically significant performance changes. However, there still would exist the uncertainty as to how the boundaries in figure (5) are characterized. The purpose of this paper is two fold. First it is desired to study the assumption of normality from the empirical data for this complex G field experiment. Secondly, it is desired to make explicit statements on the effect of the G stress on producing a degradation in tracking performance. In order to achieve the second goal, one must be careful to examine the underlying densities. The method considered here involves the Kolomogorov-Smirnov test on the density functions to study the normality question.

The Kolmogorov-Smirnov Test To Study The Densities:

The Kolmogorov-Smirnov Test is discussed here in an effort to make some statements about the underlying densities that characterize the phase plane boundaries in figure (5). The test can be defined as follows:

Definition-The K-S Test:

Given N samples of data from $\hat{F}_n(x)$ a Cumulative Distribution Function of the error signal (derived from the empirical samples) and $F(\hat{\mu}, \hat{\sigma})$ where:

$$F(\hat{\mu}, \hat{\sigma}) = 1/\sqrt{2\pi}\,\hat{\sigma} \int_{-\infty}^{x} e^{-(\bar{x}-\hat{\mu})^2/2\hat{\sigma}^2} d\bar{x} \qquad (8)$$

From equation (8), $F(\hat{\mu}, \hat{\sigma})$ is the theoretical or assumed CDF based on the sample estimates $\hat{\mu}$ and $\hat{\sigma}$ from the data. The purpose of this test is to consider two hypothesis:

Ho: f(x) is normal
H1: f(x) is not normal

It is desired to accept Ho at a desired level of significance α. The level of significance α is the risk of rejecting the hypothesized distribution if it is in fact the true distribution. The test statistic is the maximum distance a variable d obtains over the samples. The variable d is defined as follows:

$$d = \max_{x_i} \left| \hat{F}_n(x_i) - F(\hat{\mu}, \hat{\sigma}) \right| \qquad (9)$$

If α is specified at an .05 level, then d depends only on N the number of samples and can be determined from tables of values (8). The test statistic d is a random variable which satisfies:

$$0 \leq d \leq k_1 \qquad (10)$$

where k_1 is from the table of values (8). If equation (10) is not satisfied for a specified α level, then Ho is rejected. If (10) is true, then the hypothesized distribution cannot be rejected and it can be said that it is reasonable to assume that the hypothesized distribution is the true distribution.

To apply this test to the phase plane analysis, it is necessary to assume that the distribution of the boundary of the e(t) axis is identical for the positive axis as well as for the negative axis. This symmetry assumption seems reasonable in light of the fact that the tracking task is symmetrical (zero mean, constant variance, sum of sines) and also the stick has symmetrical response characteristics. Therefore we assume figures in the form of (6a-b) in which the density of e(t) is normal. This same argument holds for the $\dot{e}(t)$ axis.

Results From The Data:

As a preliminary investigation on this analysis, consider first the test for 1 subject, 1 trial, and 2 experimental conditions. Figures (7a-1,7a-2) illustrate the sample density function for e(t) and $\dot{e}(t)$, respectively, (related to the corresponding $\hat{F}(x_i)$) from the data samples for one trial in the prestatic condition. Figures (7b-1,7b-2) is the stress counterpart of figures (7a-1,7a-2) and shows the density obtained under the stress condition. It should be emphasized that figures (7a-b,1-2) all use the absolute values of the variables e(t) or $\dot{e}(t)$ which link the hit window concept with the phase plane diagram and the CDF approach used here.

Figure (8) displays the resulting CDF's obtained from the samples of e(t) data in figures (7a-b). One notices the degradation of performance level manifests itself by shifts to the right. From observation of figures (7a-b) and (8), one can now see how the two objectives of this paper relate to the empirical data base considered here. First it is desired to say whether figure (7a-b,1-2) can be approximated by normal densities. Secondly, from figure (8) it is desired to say something about how much performance change is introduced by the stress effect . Obviously with one trial, conclusions cannot be drawn. It is necessary to repeat this procedure across replications and across subjects. Figure (9) is drawn to illustrate the end product of this effort. The boundary points on the e(t) axis are determined by the median points of figures (7a-b) (the 0.5 point of the CDF). Likewise the same procedure is repeated for $\dot{e}(t)$. This yields the boundaries of figure (9) and the points obtained are illustrated in Table II:

Table II - Medians Obtained From 1 Trial of Each Condition

Experimental Condition	Variable e(t)	Variable $\dot{e}(t)$
Prestatic I	.060	0.25
Stress I (Phase II-High Gv Condition)	.11	0.33

This study will now extend this table for one subject across replications. Using the same subject as displayed in Table II, the analysis procedure is now extended to include 4 replications of the same experimental conditions. Table III is now constructed from these four replications of the phase II data. The data displayed in this table corresponds to that data used in final data analysis in (1,15,16):

Table III - One Subject - 4 Replications, 2 Experimental Conditions

Experimental Condition	Variable e(t)		Variable e(t)	
	mean	sd	mean	sd
Prestatic I	.065	.01	.27	.02
Stress I (Phase II - High Gv Condition)	.135	.015	.43	.10

Figure (10a-b) illustrates the CDF's obtained for the variables e(t) and $\dot{e}(t)$. To determine the phase plane boundaries, the 0.5 line is projected horizontally on figure (10a-b) and then projected downward on the window axis to determine the median points. Also from this projection, the variability in this estimate about the mean is obtained by plotting the one standard deviation envelope of this curve. Figure (11) can now be drawn. This represents the true stress regions and non-stress regions with the appropriate boundaries. The variability in the phase plane boundaries can be observed in figure (11) but they can also be tested using t-tests on the CDF's displayed in figures (10a-b). The next section will discuss the tests used.

Statistical Tests On The Empirical Data Base:

The first goal of this paper is to study the normality properties of the density functions obtained from the empirical data using the Kolomogorov-Smirnov test. This allows a better interpretation of the phase plane boundaries in figure (5). Using the data displayed in table III, the mean CDF is obtained for the stressed condition and the nonstressed condition for one subject and 4 replications. To better understand the K-S test, it is formulated here in a statistical framework.

Problem Formulation (Testing Densities For Normality):

Consider the following statistical problem with two alternative hypothesis:

$$H_o : \quad f(x) \text{ is normal } N(\hat{\mu},\hat{\sigma}) \qquad (11)$$

$$H_1 : \quad f(x) \text{ is not normal } N(\hat{\mu},\hat{\sigma}) \qquad (12)$$

where $\hat{\mu}$, $\hat{\sigma}$ are the sample mean and standard deviation, respectively. There are 4 elements of any statistical test for hypothesis testing. The two hypothesis listed above are the first two elements. The third element is the test statistic; the fourth element is the rejection or critical region. The test statistic for the K-S test is the random variable d defined in equation (9). It is noted in equation (9) that d is the maximum positive deviation between the two distribution functions $\hat{F}(x_i)$ and $F(\hat{\mu},\hat{\sigma})$. The CDF $F(\hat{\mu},\hat{\sigma})$ is the theoretical function given in equation (5b) with the sample data estimates $\hat{\mu}$, $\hat{\sigma}$ replacing μ and σ. The CDF $\hat{F}(x_i)$ is the sample CDF obtained from the accumulation of error scores over a variety of different window sizes.

The fourth element of this test is the determination of the rejection or critical region. For any hypothesis test, there exists two types of error. A type I error is the rejection of Ho when Ho is true. Let α denote the probability of a type I error. A type II error is the acceptance of Ho when H1 is true. Let β denote the probability of a type II error. Denoting Dn as the (14,17) critical value of d such that:

$$P\{d \quad D_n\} = 1-\alpha \qquad (13)$$

The expression given in equation (13) defines the rejection or critical region and thus provides the fourth element of the K-S test. It is noted that Dn is found in tables which only depend on N and α and not on the underlying density. The underlying density implicitly affects $F(\hat{\mu},\hat{\sigma})$ and must be continuous (8), but the K-S test is only performed on the distributions $F(\hat{\mu},\hat{\sigma})$ and $\hat{F}(x_i)$.

The manner in which the K-S test is applied here with respect to Table III is to estimate $\hat{F}(x_i)$ from the mean values of the four replications. $\hat{\mu}$ is obtained from the 0.5 projection onto the CDF curve. To determine $\hat{\sigma}$, the data is averaged over the 4 replications and $\hat{\sigma}$ satisfies:

$$\hat{\sigma}^2 = 1/(N-1) \sum_{i=1}^{N} (x_i - \hat{\mu})^2 \qquad (14)$$

ORIGINAL PAGE IS
OF POOR QUALITY

For each replication, the two CDF's are normalized as follows:

Let $y = (x_i - \hat{\mu}) / \hat{\sigma}$ (15)

Then:

$$F(\hat{\mu}, \hat{\sigma}) = 1/\sqrt{2\pi} \int_{-\infty}^{y} e^{-s^2/2} \, ds \quad (16a)$$

$$F(x_0) = \sum_{i} y_i / N \quad (16b)$$

Where $y_i = (x_i - \hat{\mu}) / \hat{\sigma}$ for $x_i \leq x_0$ (16c)

The results of the test for Table III can be illustrated as follows:

Table IV - Results of The K-S Test (N = 20)

Experimental Condition	d max theoretical	d max theoretical	d max theoretical	d max empirical
Prestatic e(t)	.264	.294	.356	.417
Stress 1 e(t)	.264	.294	.356	.442
Prestatic $\dot{e}$(t)	.264	.294	.356	.478
Stress 1 $\dot{e}$(t)	.264	.294	.356	.432

In this table the distance variable d refers to the definition given in equation (9). From the results of these tests for one subject, and 4 replications, we reject Ho and therefore conclude that we cannot accept the hypothesis that the densities are normal. It is noted from table V that the sample CDF obtained is outside the band which describes 99% of all sample CDF's from normal densities. This is a positive indication for this type of tracking task that another type of density is required.

Using this CDF representation, however, allows the determination of t tests for significance of performance changes. In addition, it will be of interest to study the minimum window sizes where stress effects appear to be significant. As a first guess on the performance changes between stress and non-stress, an analysis will be conducted on the data displayed in figures (10a-b). In both of these figures, horizontal lines are drawn at constant values of CDF=f1 and projected down on the window values for all points on the 1 σ envelope of the curves. The results of this projection are illustrated in table V:

Table V - Results of The Horizontal CDF Projections
(One subject - 4 Replications)

Experimental Variable	CDF= 0.2		CDF= 0.4		CDF= 0.6		CDF= 0.8	
	mean	s.d.	mean	s.d.	mean	s.d.	mean	s.d.
Static e(t)	.025	.004	.0563	.005	.0812	.006	.125	.007
Static $\dot{e}$(t)	.103	.010	.206	.012	0.30	.0125	.422	.018
Stress e(t)	.05	.012	.11	.018	0.16	.04	.27	.05
Stress $\dot{e}$(t)	.159	.028	.318	.056	.506	.0844	.72	.103

To determine values of minimum window size where stress shows effects on performance, the t statistic tests are computed as follows:

To compare the two hypothesis:

Ho : $\mu_x = \mu_y$

H1 : $\mu_x > \mu_y$

The t-statistic is computed as follows:

$$t = \frac{(\bar{x} - \bar{y}) - (\mu_x - \mu_y)}{\sqrt{N_x S_x^2 + N_y S_y^2}} \sqrt{\frac{N_x N_y (N_x + N_y - 2)}{N_x + N_y}}$$

where the assumption is made that $\mu_x = \mu_y$ and the number of degrees of freedom are

ORIGINAL PAGE IS
OF POOR QUALITY

$$\nu = N_x + N_y - 2 = 6 \qquad (17)$$

The results of the t tests are displayed in Table VI:

Table VI - t tests between experimental conditions
(One subject - 4 replications)

Comparisons of Experimental Conditions	CDF= 0.2	CDF=0.4	CDF= 0.6	CDF= 0.8
Static vs Stress $e(t)$	α level $\leq .01$ $t = 3.424$	α level $\leq .005$ $t=4.979$	α level $\leq .1$ $t=1.613$	α level $\leq .05$ $t=2.433$
Static vs Stress $\dot{e}(t)$	α level $\leq .025$ $t = 3.263$	α level $\leq .01$ $t=3.388$	α level $\leq .005$ $t=4.183$	α level $\leq .005$ $t=4.981$

One can see from Table VII that the effects of stress on performance are quite pronounced for one subject and 4 replications.

Summary and Conclusions:

A performance study has been conducted on human tracking under a complex G field. This paper illustrates three important points. First it shows the connection between the phase plane bondary points and window measures through the use of a CDF function on the data. Secondly, the effects of stress on tracking performance manifests itself via the t tests across CDF's under two experimental conditions. It is shown for one subject and 4 replications that there exists a significant performance degradation due to stress.

A third point made by this paper is that a K-S test on the distributions of the phase plane trajectories indicate the non-normality of the empirical density functions. This statement can be made with greater than 99% confidence. It is interesting in this case to have such a result hold for a tracking task which is sum of sines and to contrast this result to the deterministic case considered in (7).

References

(1) Korn, J., A. R. Ephrath, and D.L. Kleinman, "Human Operator Modeling For Aerial Tracking", TR-79-16, The University of Connecticut, November, 1979.

(2) Korn, J. and D. L. Kleinman, "Modeling Lateral Acceleration Effects on Pilot Performance in a Vector Force Fighter", The 1980 Annual Conference on Manual Control, May, 1980.

(3) Korn, J. and D.L. Kleinman, "Advances in Modeling Pilot Tracking Performance in The Presence of Sustained Linear Acceleration" Proceedings of the 15th. Annual Conference on Manual Control, 1979.

(4) Korn, J., Kleinman, D.L., and Repperger D.W., "Frequency Domain Measures of Human Performance Under G-Stress", Proceedings of The 18th Conference on Decision and Control, December, 1979.

(5) Fraser, T.M., "Human Response To Sustained Acceleration" NASDA SP-103, 1966.

(6) Brown J.L., "Acceleration and Human Performance " In H.W. Sinaiko (Ed), Selected Papers on Human Factors in The Design and Use of Control Systems, Dover Publications, Inc., N.Y., 1961.

(7) D.W. Repperger, S.L. Ward, E.J. Hartzell, B.C. Glass, and W.C. Summers, "An Algorithm To Ascertain Critical Regions of Human Tracking Ability" IEEE Transactions on Systems, Man, and Cybernetics, Vol. SMC-9, No. 9, No. 4, April, 1979, pp 183-196.

(8) Lilliefors, H.L., "On The Kolmogorov-Smirnov Test For Normality With Mean and Variance Unknown", The American Statistical Association Journal, June, 1976, pp. 399-402.

(9) Kim, P.J., "On The Exact and Approximate Sampling Distribution of The Two Sample Kolmogorov-Smirnov Criterion D_{mn}, m not greater than n", JASA, 64(328) 1969, 1625-1637.

(10) Feller, W., "On The Kolmogorov-Smirnov Limit Theorems For Empirical Distributions", Annals of Mathematical Statistics, 19, 177-189.

(11) Bradley, J.V., Distribution-Free Statistical Tests, Prentice-Hall, Inc. New Jersey, 1968, 367-369.

(12) R. Wood, M. Garland, and E. Meschko, "YF-16 Control Configured Vehicle (CCV) Operational Potential, Flying Qualities, and Performance Evaluation", AFFTC-TR-77-23, January, 1978.

(13) General Dynamics Corporation, "Fighter CCV Phase IV Report Volumn II-Flight Test Data Evaluation", AFFDL-TR-78-9, Volumn II, February, 1978.

(14) H. M. Walker, J. Lev, "Statistical Inference", Henry Holt and Company, 1953.

(15) J. Frazier, D.W. Repperger, V. Skowronski, and D. Toth, "Human Tracking Performance Changes During Combined ±Gz and ±Gy Stress", Preprints of the 1980 Aerospace Medical Association Meeting, May, 1980.

(16) D. Toth, D.W. Repperger, J. Frazier, "The Effects of Test and Training Intervals on Performance Evaluations in Acceleration Stress", preprints of the 1980 Aerospace Medical Association Meeting, May, 1980.

(17) P. G. Hoel, "Introduction To Mathematical Statistics", John Wiley & Sons, Inc., 1962.

ORIGINAL PAGE IS
OF POOR QUALITY

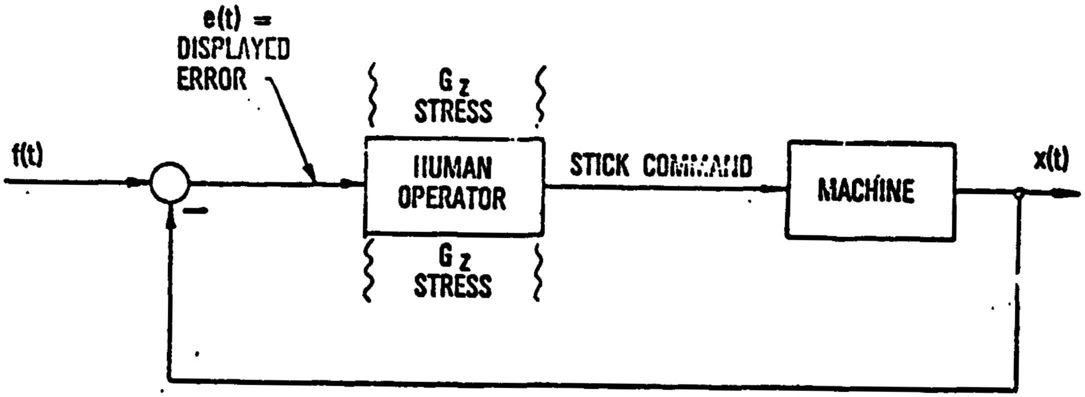
e(t) =
DISPLAYED
ERROR
f(t)
G_z
STRESS
HUMAN
OPERATOR
G_z
STRESS
STICK COMMAND
MACHINE
x(t)

FIGURE (1a) – OPEN LOOP STRESS

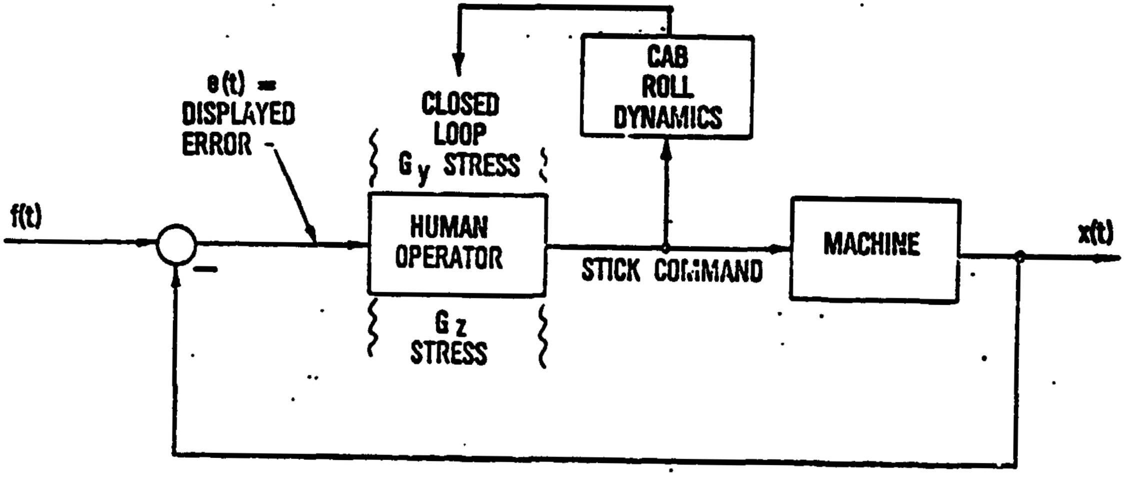
CAB
ROLL
DYNAMICS
e(t) =
DISPLAYED
ERROR
CLOSED
LOOP
G_y STRESS
f(t)
HUMAN
OPERATOR
STICK COMMAND
MACHINE
x(t)
G_z
STRESS

FIGURE (1b) – CLOSED LOOP STRESS

ORIGINAL PAGE IS
OF POOR QUALITY

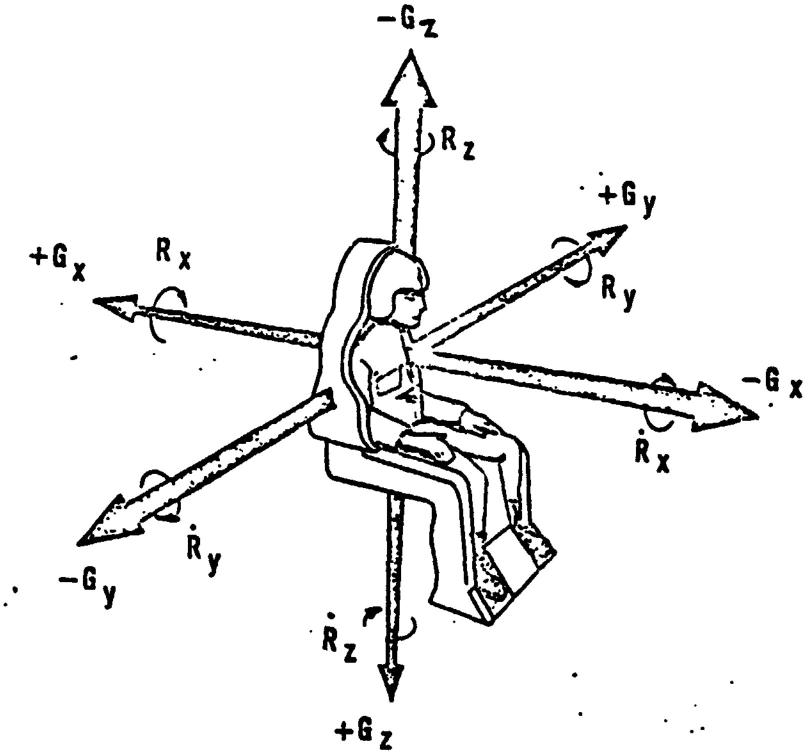
$-G_z$
R_z
$+G_y$
$+G_x$
R_x
R_y
$-G_x$
$\dot{R}_x$
$\dot{R}_y$
$-G_y$
$\dot{R}_z$
$+G_z$

FIGURE (2) – THE G STRESS FIELD VECTOR

FIGURE (3a) – THE DENSITY FUNCTION

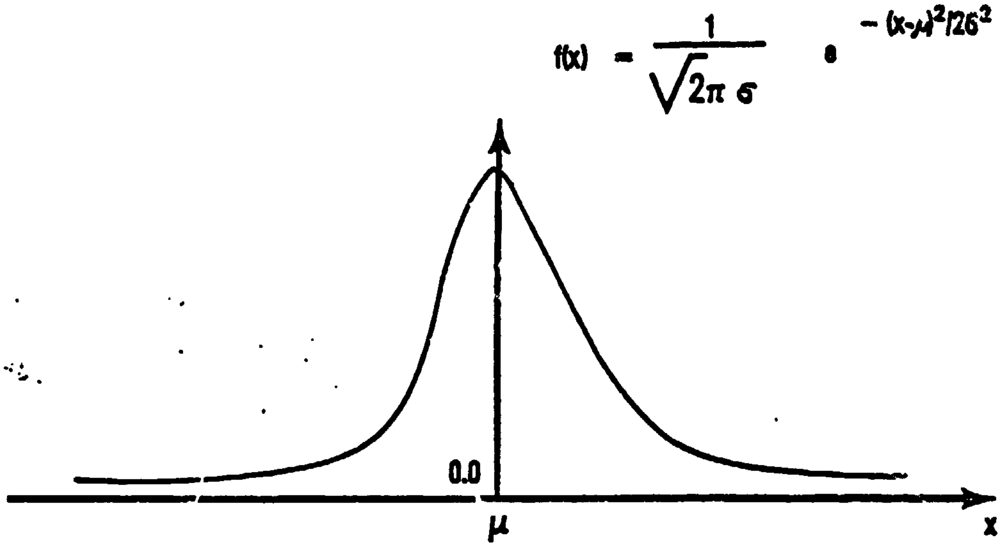

FIGURE (3b) – THE CUMULATIVE DISTRIBUTION FUNCTION

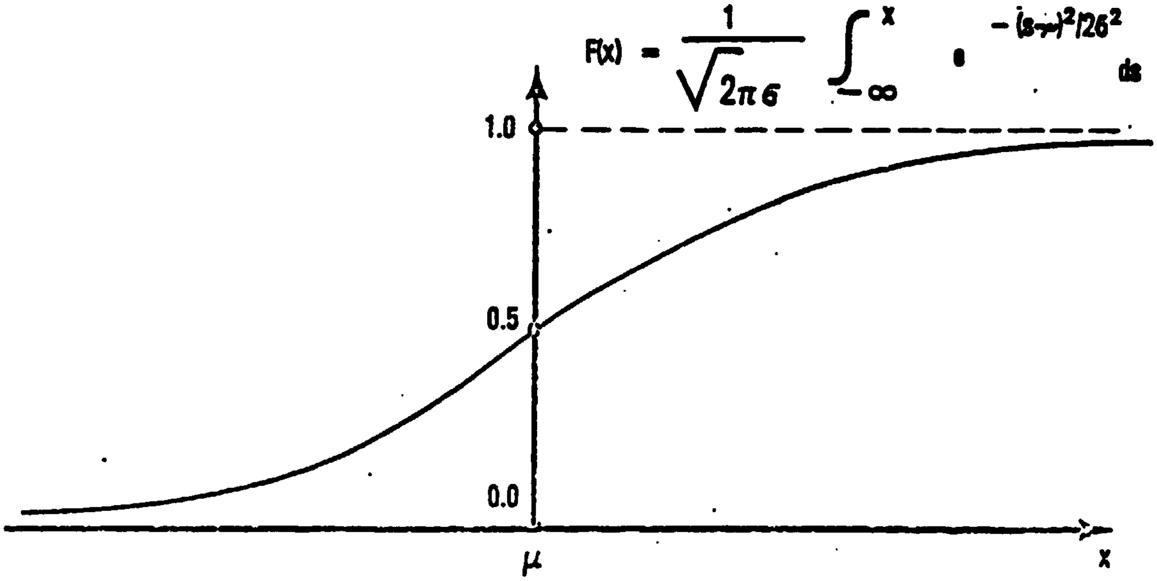

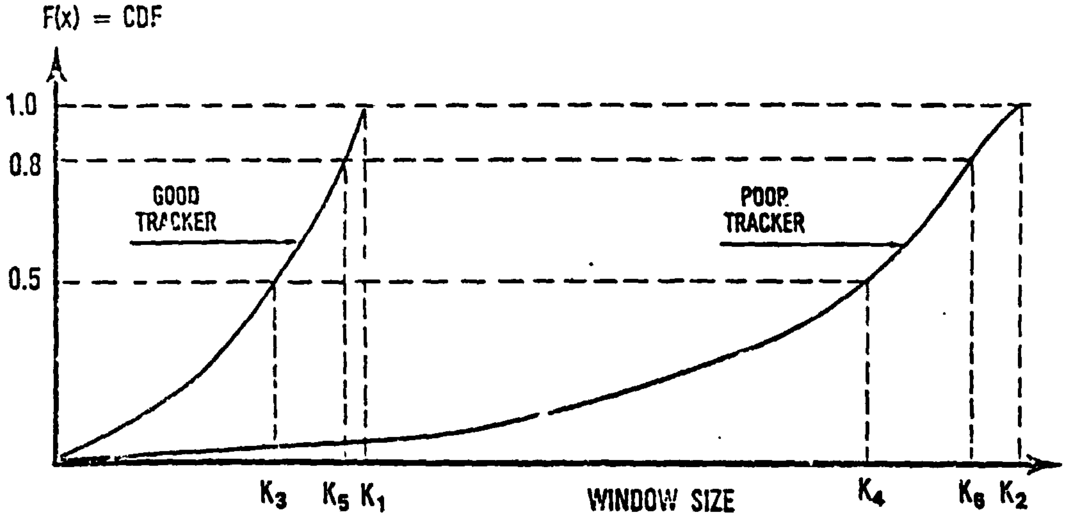

FIGURE (4a) – COMPARISON OF TWO TRACKERS USING CDF's

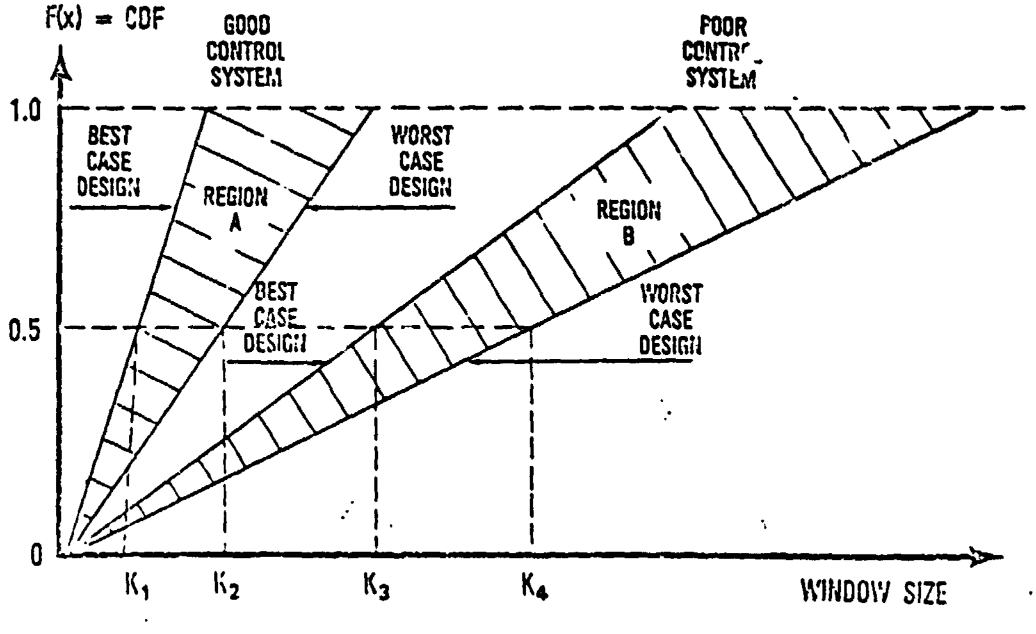

FIGURE (4b) – COMPARE TWO CONTROL SYSTEMS

ORIGINAL PAGE IS
OF POOR QUALITY

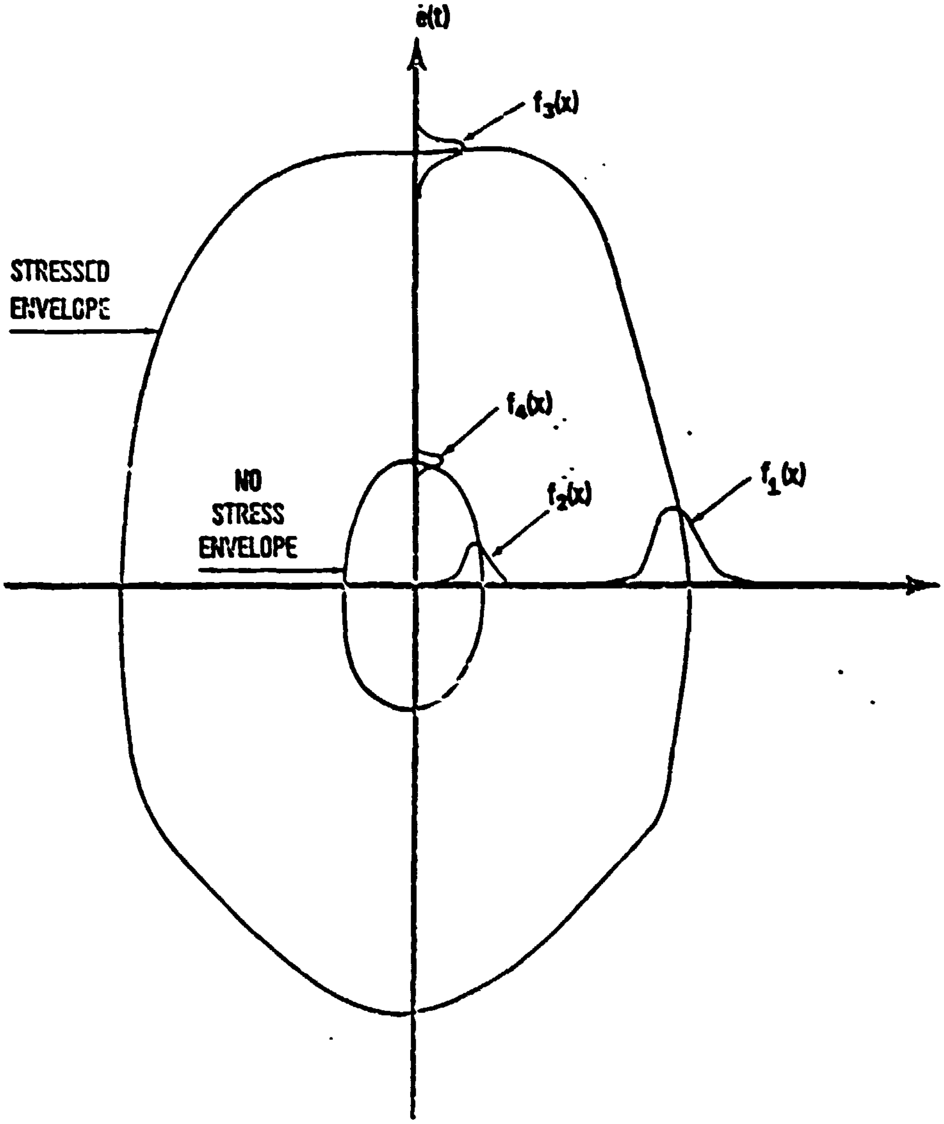

ė(t)
f3(x)
STRESSED ENVELOPE
f4(x)
NO STRESS ENVELOPE
f2(x)
f1(x)

FIGURE (5) – THE PHASE PLANE REPRESENTATION WITH AND WITHOUT STRESS

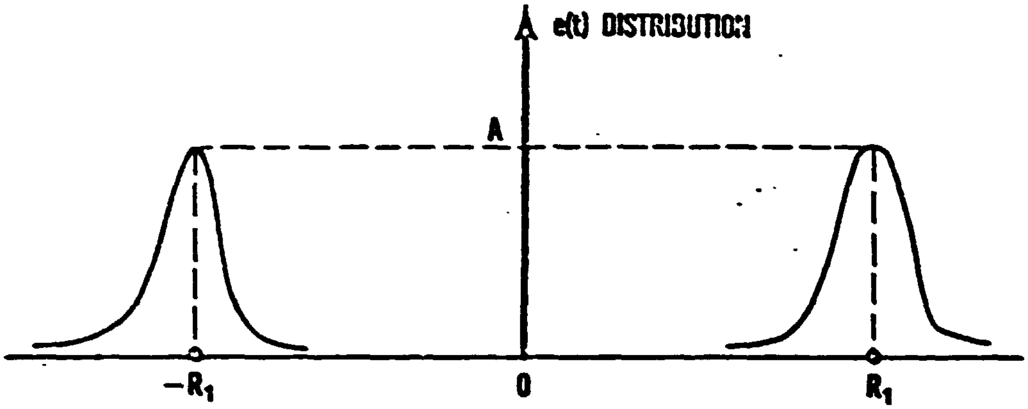

FIGURE (6a) – SIDE VIEW DISTRIBUTION OF THE PHASE PLANE

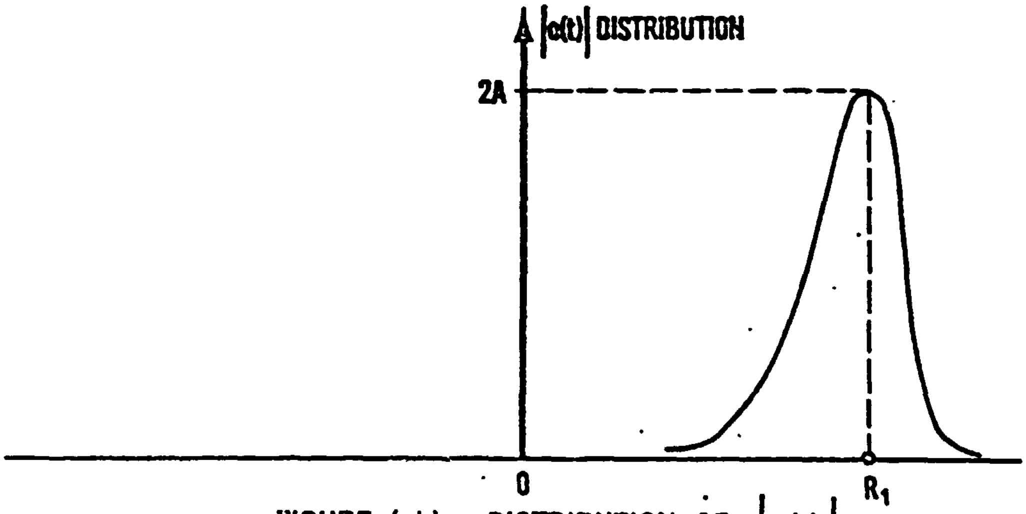

FIGURE (6b) – DISTRIBUTION OF $|e(t)|$

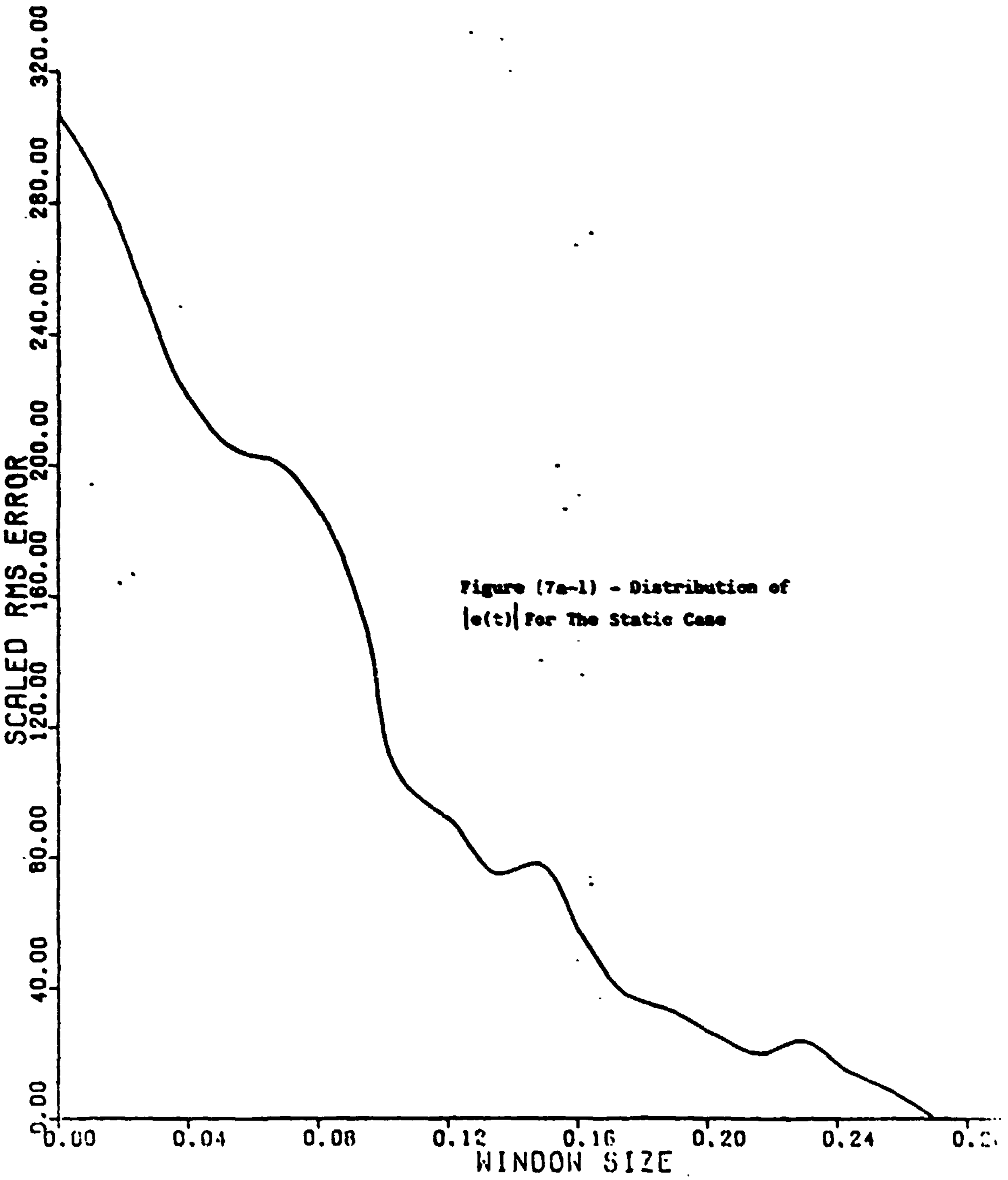

Figure (7a-1) - Distribution of $|e(t)|$ For The Static Case

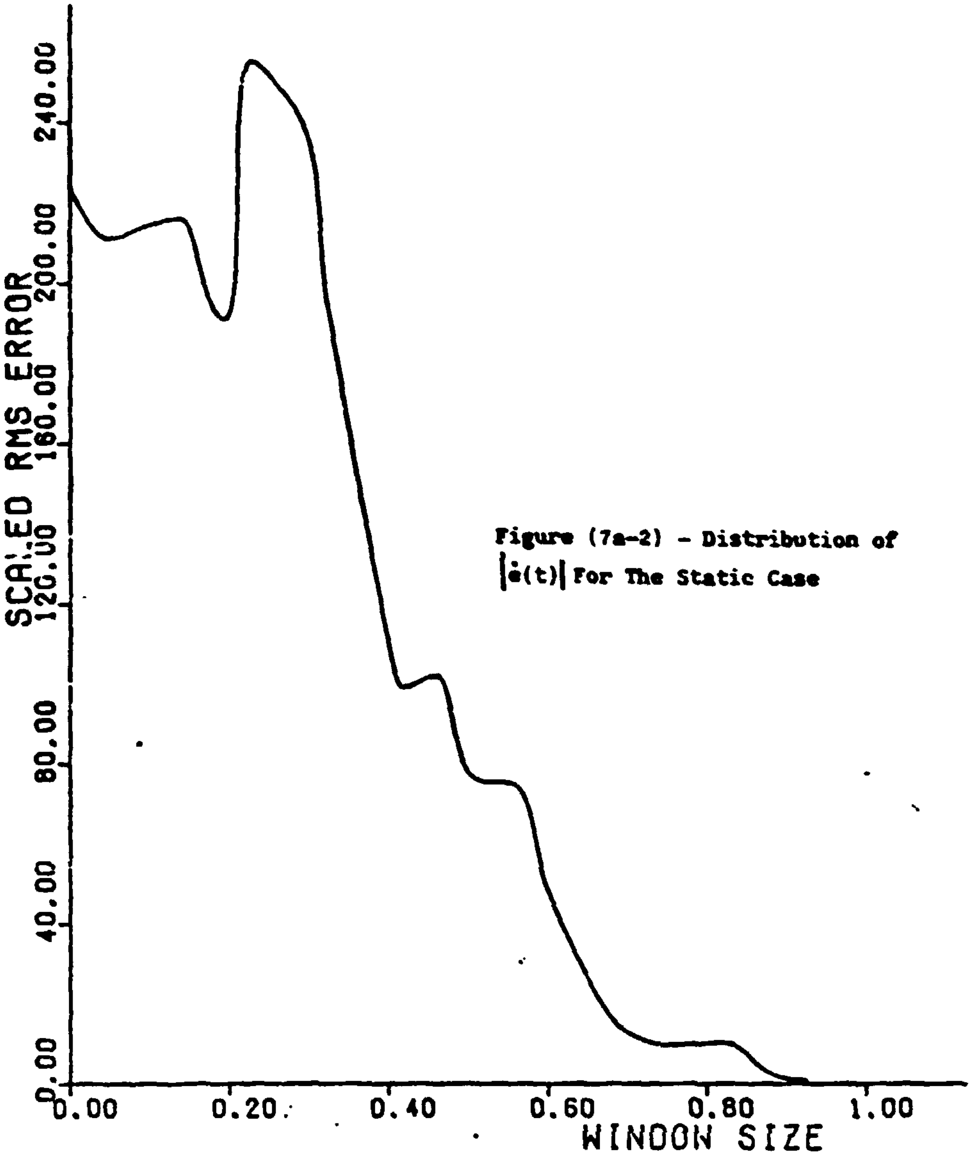

Figure (7a-2) - Distribution of $|\dot{e}(t)|$ For The Static Case

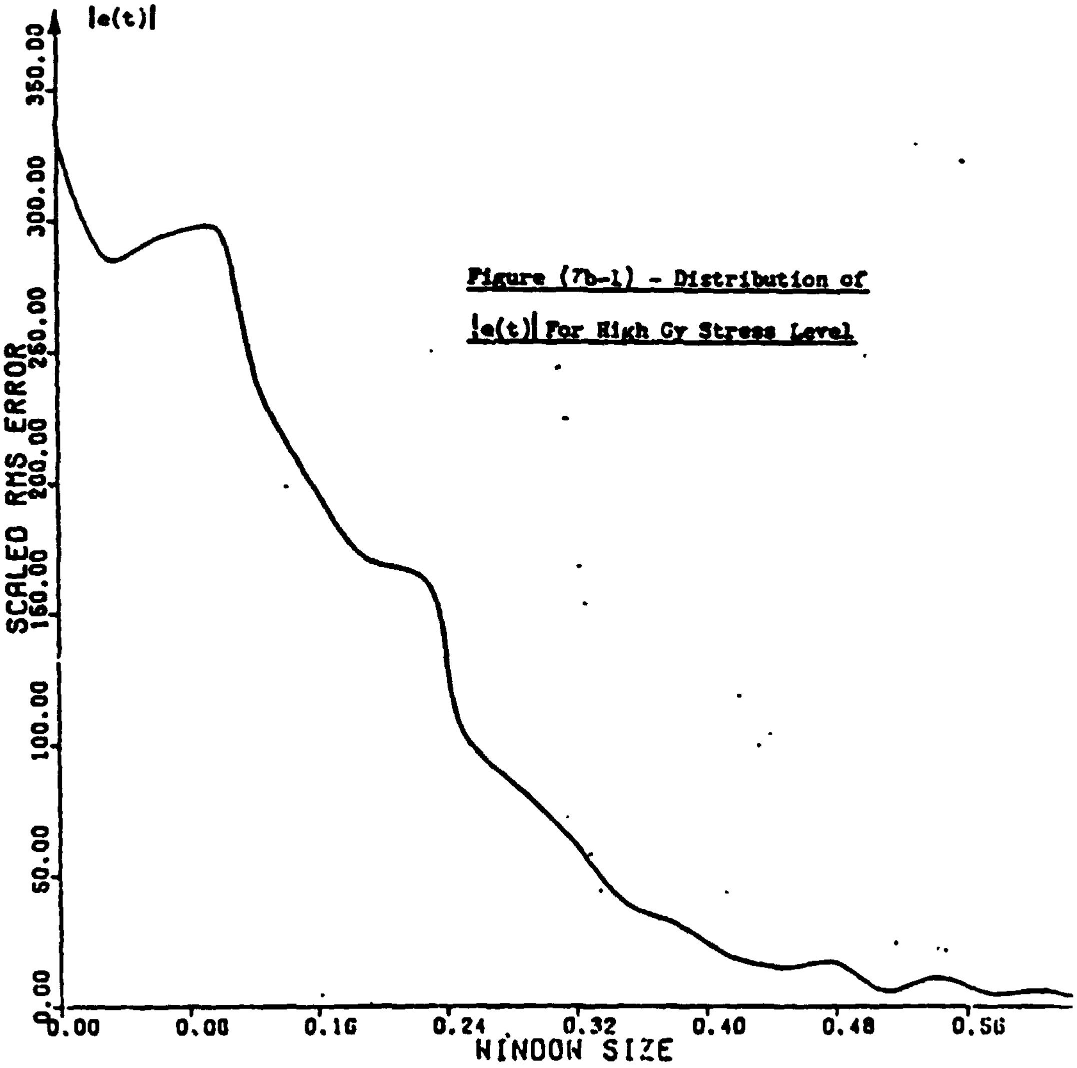

Figure (7b-1) - Distribution of |e(t)| For High Gy Stress Level

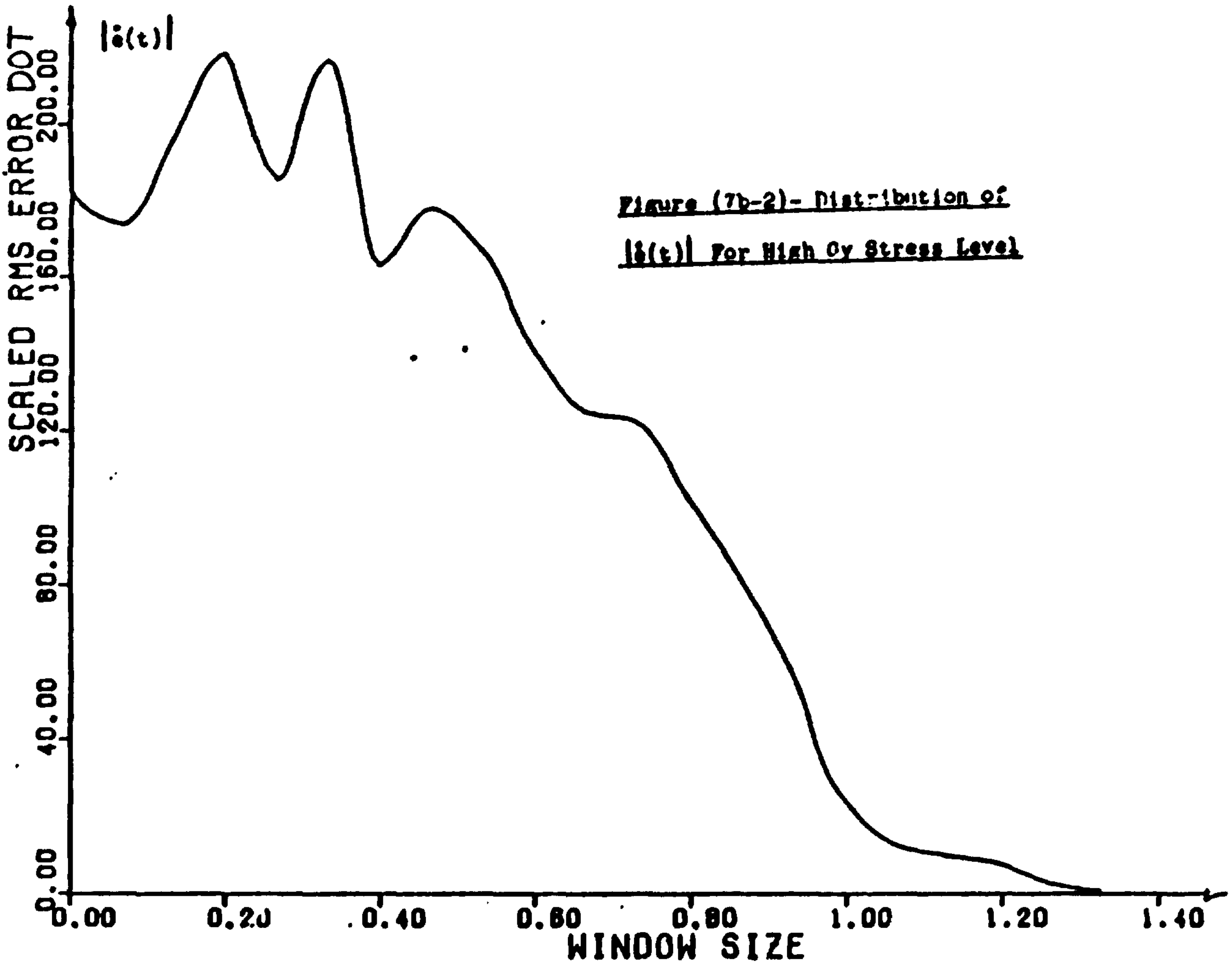

Figure (7b-2)- Distribution of $|\dot{e}(t)|$ For High σ_y Stress Level

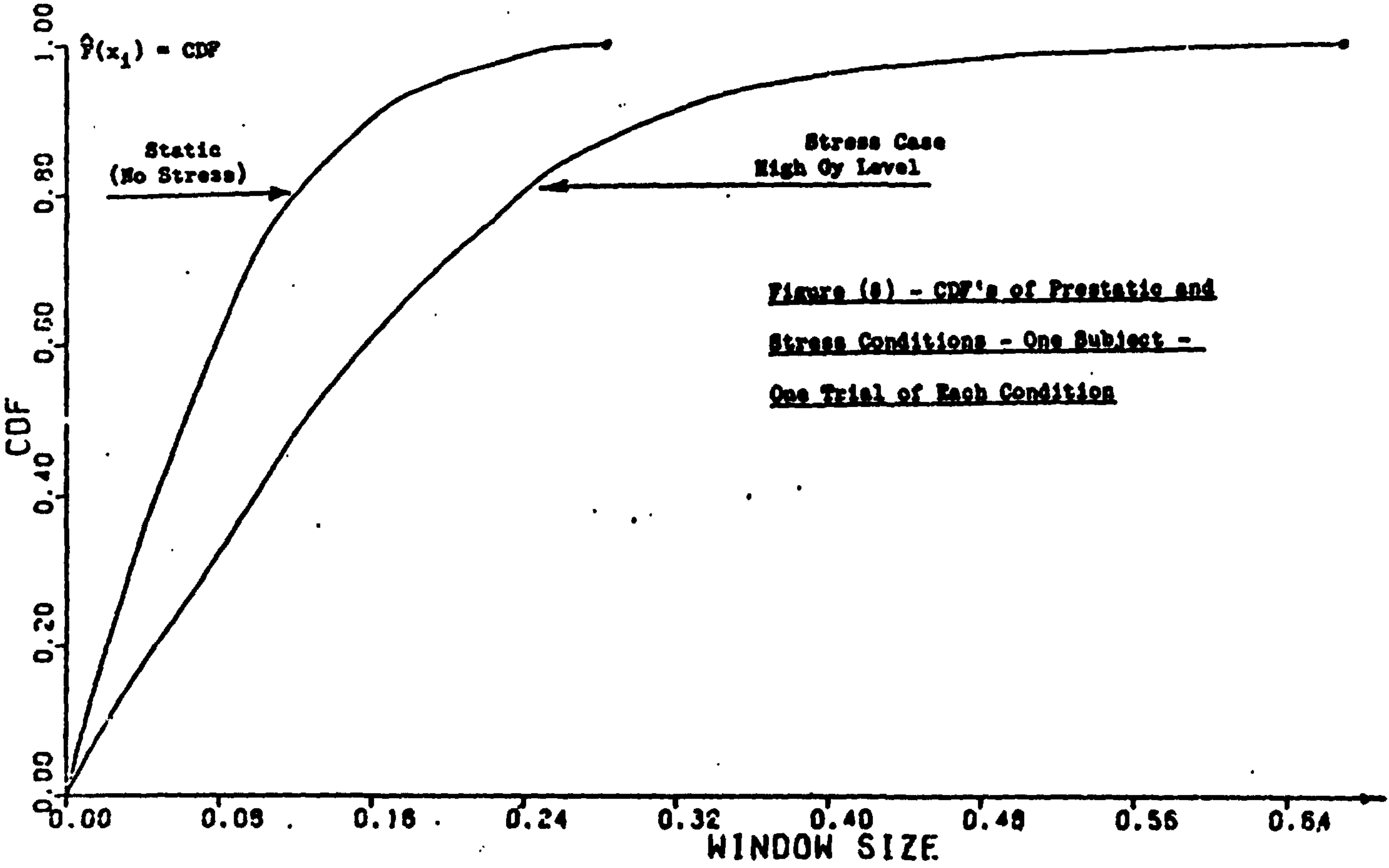

Figure (8) - CDF's of Prestatic and Stress Conditions - One Subject - One Trial of Each Condition

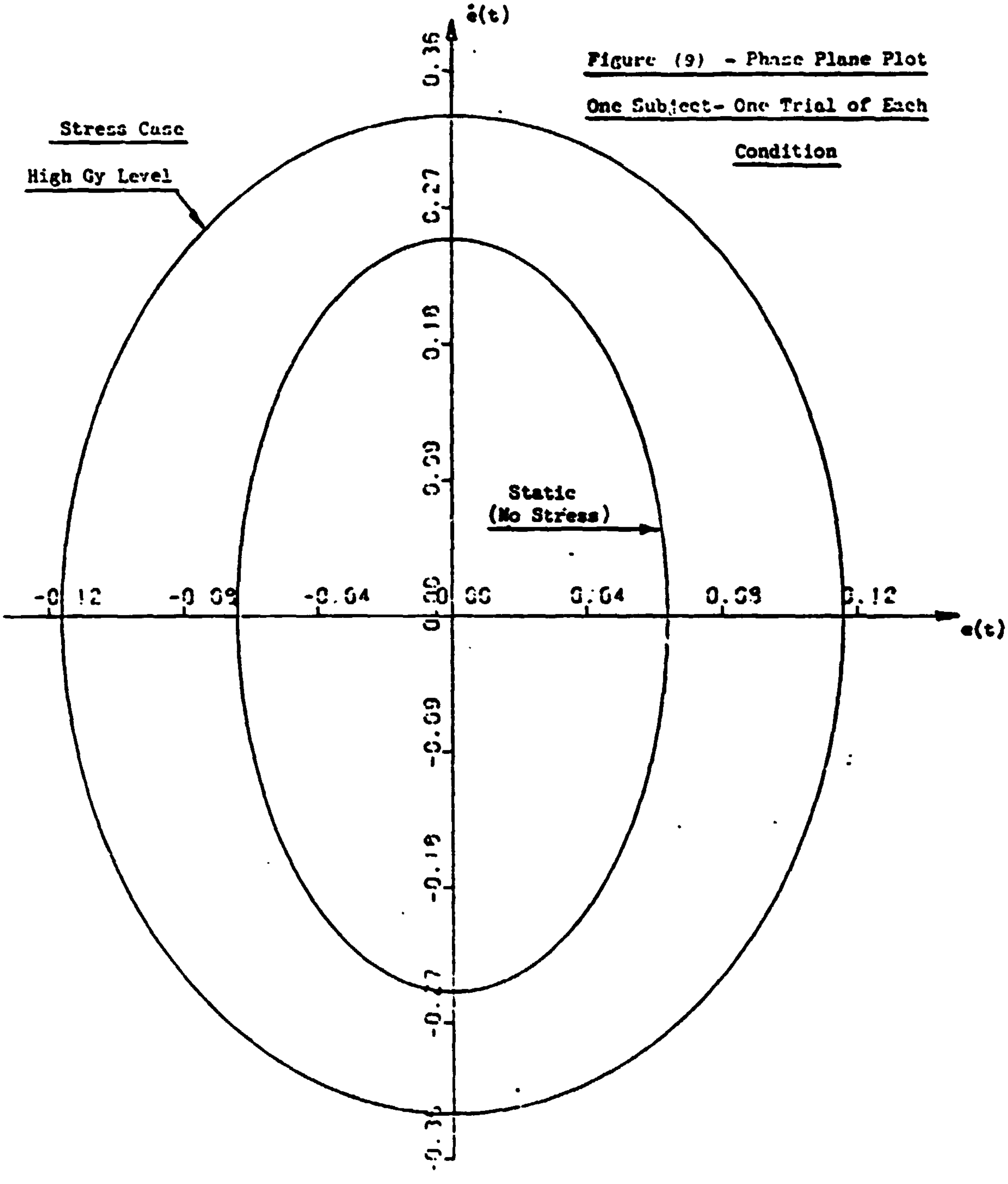

Figure (9) - Phase Plane Plot

One Subject- One Trial of Each Condition

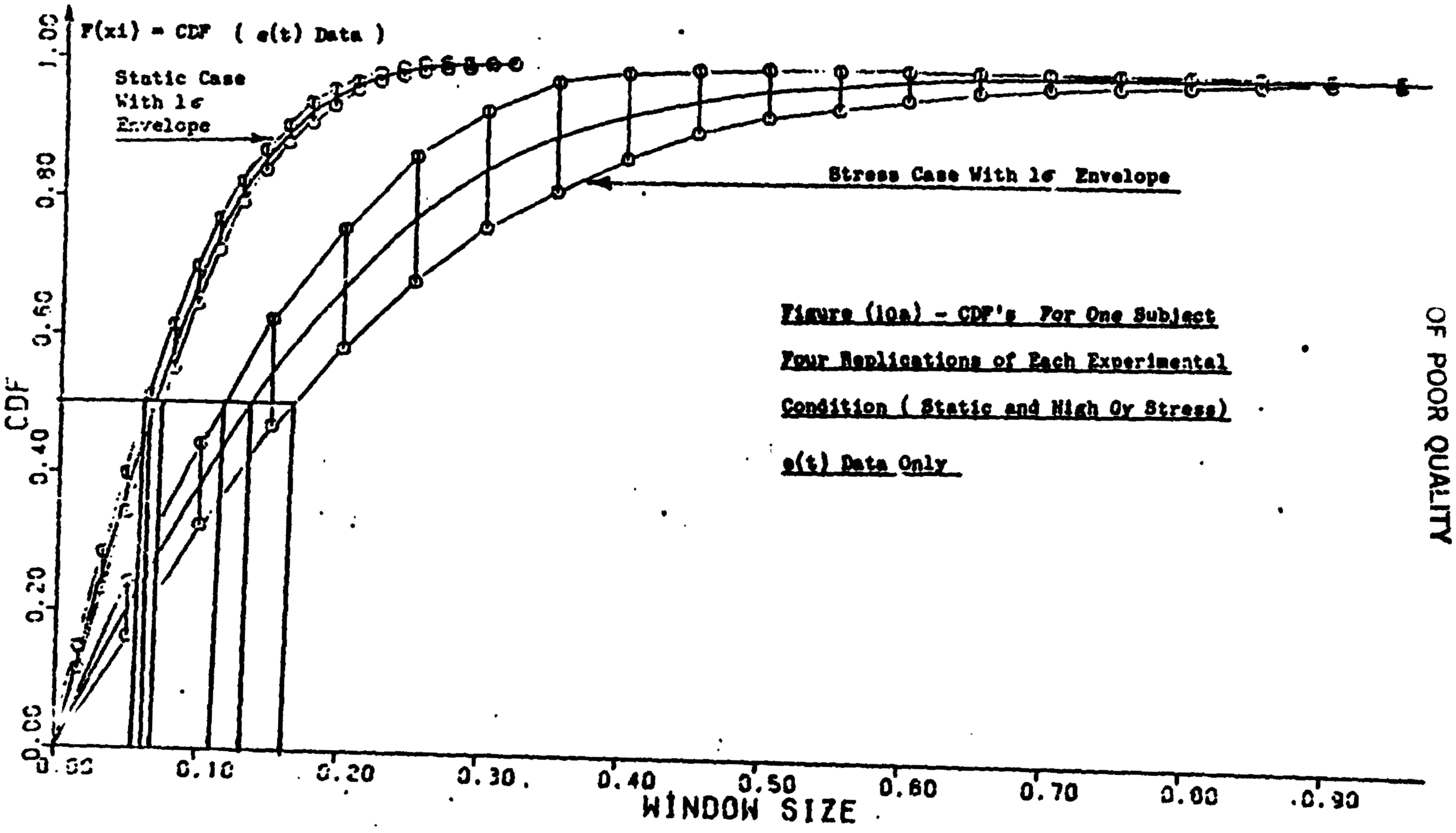

Figure (10a) - CDF's For One Subject
Four Replications of Each Experimental
Condition (Static and High Gy Stress)
e(t) Data Only

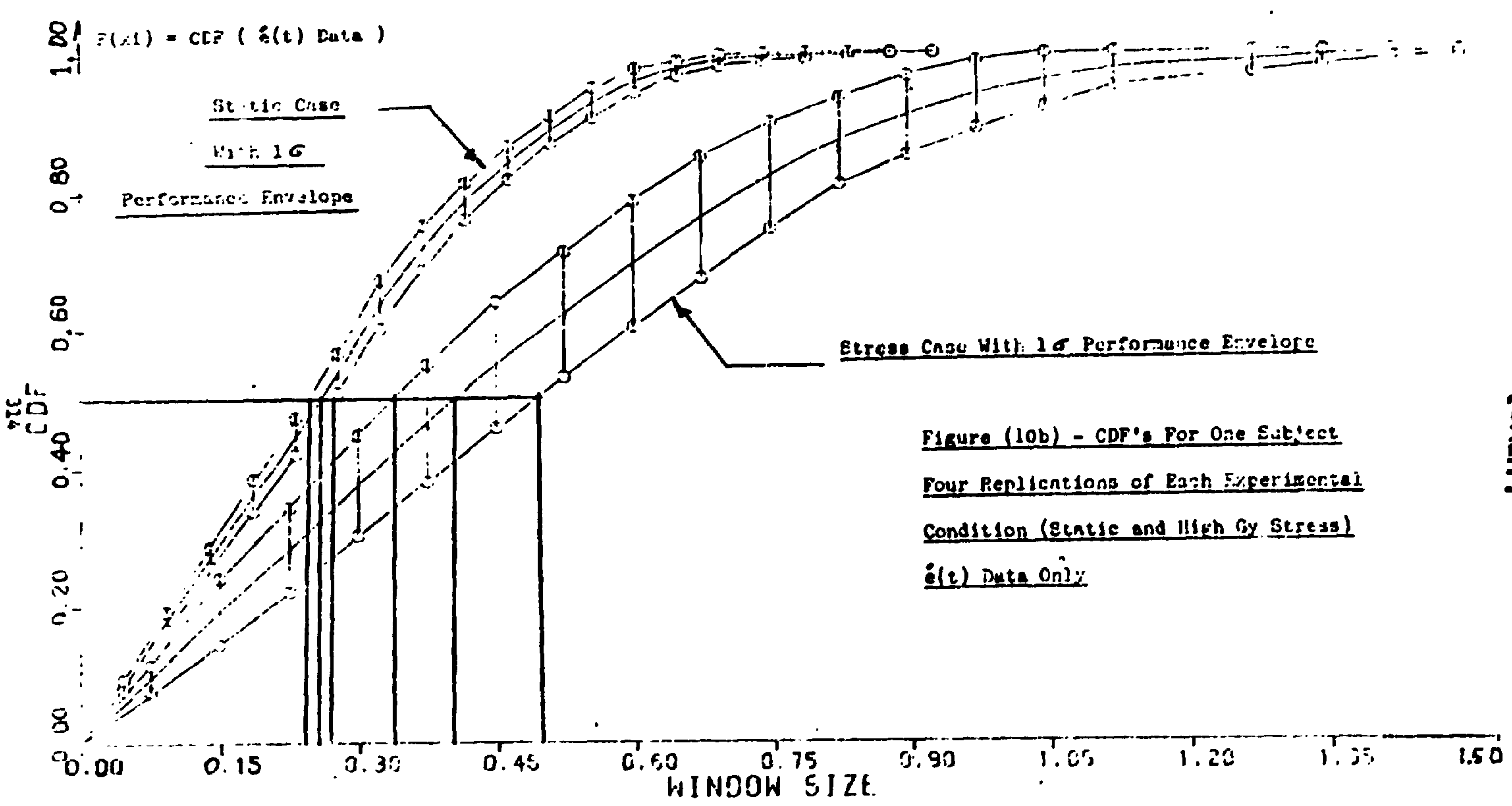

Figure (10b) - CDF's For One Subject
Four Replications of Each Experimental
Condition (Static and High Gy Stress)
ė(t) Data Only

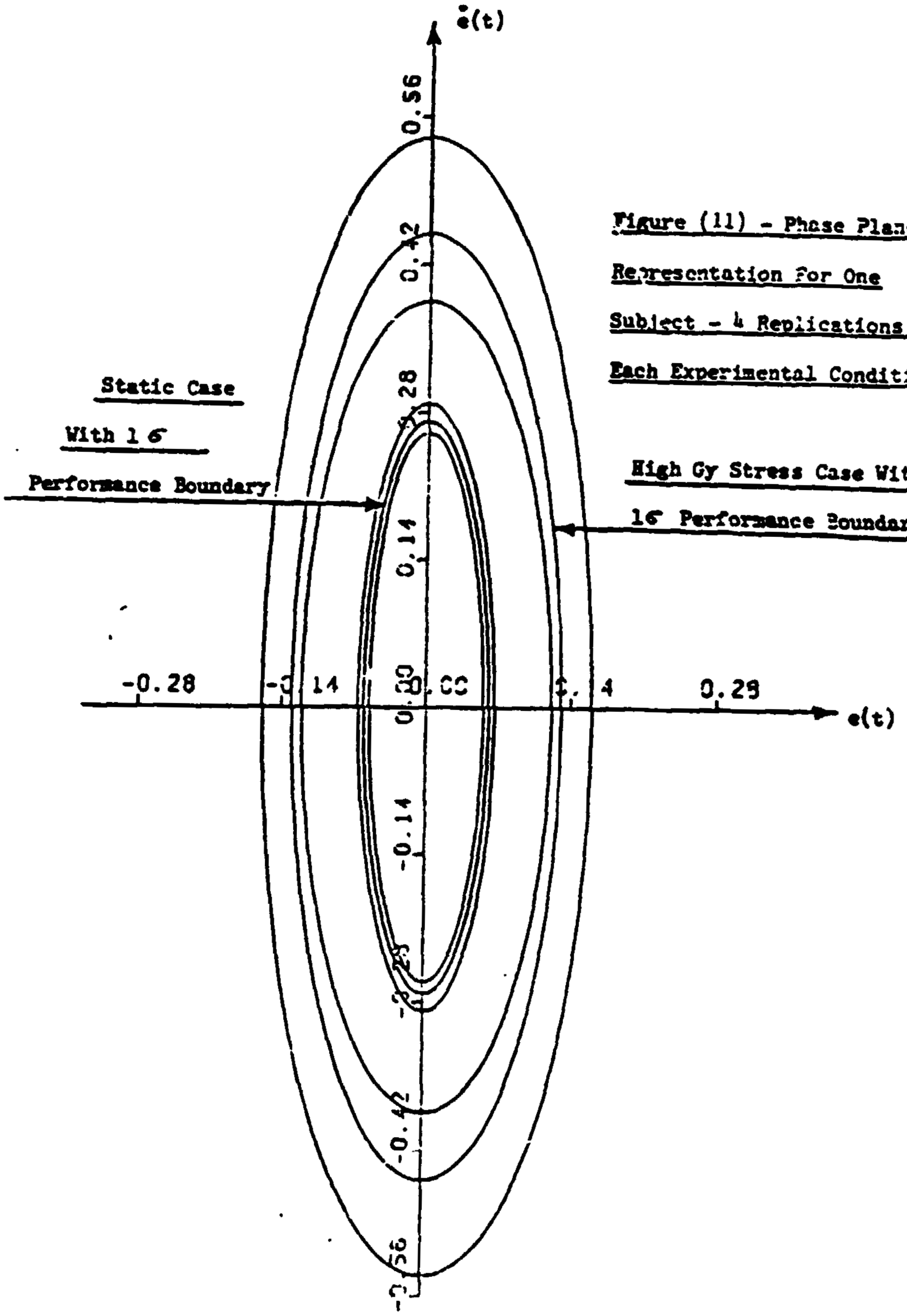

Static Case With 1σ Performance Boundary

High Gy Stress Case With 1σ Performance Boundary

Figure (11) - Phase Plane Representation For One Subject - 4 Replications of Each Experimental Condition

2117

ORIGINAL PAGE IS
OF POOR QUALITY

A LINEARIZED MODEL FOR VIBRATION EFFECTS ON THE EYE CONTROL SYSTEM

Raymond E. Magdaleno
Henry R. Jex

Systems Technology, Inc.
13766 South Hawthorne Boulevard
Hawthorne, California 90250

In a recent report* the authors presented a model "BIODYN-78", for the biomechanical effects of vertical vibration "feedthrough" to a pilot's control actions and head bobbing motions. The effects of the absolute and relative motions of the head and display on the eye's (image) motion were outlined there in block diagram form, but the element dynamics were not complete. In this paper we flesh out the block diagrams, based on a review of the data and models in the literature, and exercise the resulting model to illustrate some of the basic phenomena. Although the model presented here is for vertical (heave and pitch) vibration, its form is equally suitable for transverse (sway and yaw and roll) and fore-aft (surge and pitch) vibrations. In fact, much of the data on eye response to head motions comes from yawing experiments. The basic assumption is that the vibratory motions produce small perturbations around a "trimmed operator posture, so that the equations of sensorimotor control can be linearized about each operating condition.

The model formulation for vertical eye movements has been guided by work of Benson and Barnes (1977), Dallas and Jones (1963), and our interpretation of eye muscle dynamics from Robinson (1971). Dallas and Jones presented some frequency response data for eye response to both sine wave and random forcing functions. The low variability of the latter set justified using a proprietary model fitting procedure (MFP) to investigate model element forms involved in the fixation reflex.

The model is exercised to reveal qualitatively what happens in a number of special cases of frequent interest, such as: moving target with head fixed; moving head with target fixed, and both head and target moving (e.g., head mounted displays). The visual performance implications of the model's image motions are consistent with the related experimental data of Benson and Barnes (1978), on letter reading performance.

---

*Jex, Henry R., and Raymond E. Magdaleno, "Biomechanical Models for Vibration Feedthrough to Hands and Head for a Semisupine Pilot," Aviation, Space and Environmental Medicine, Volume 49, No. 1, Section II, January 1978

N82 34057

DESCRIPTION/DEMONSTRATION OF "BIODYN-80"

A Software Package for Evaluating the Transmissibility Between Vehicle Vibration and Motions of Hands (In Controls), Limbs, Head and Eyes*

Susan A. Riedel, Henry R. Jex, and Raymond E. Magdaleno
Systems Technology, Inc.
Hawthorne, California 90250

ABSTRACT

A user-oriented program for exercising the 1980 version of the STI biodynamic model "BIODYN-80" has been completed under the sponsorship of the USAF/AMRL, BioDynamic Branch. The user inputs (modifies) some 80-100 variables describing the assumed posture, interface characteristics (e.g., stick "feel" properties), and vestibular characteristics. The computer calculates the transfer functions between vibration input and various selected outputs of interest to the user. Another option is to output the operator's torso-limb-neuromuscular loop transmissibilities as seen at the stick, as required for the AMRL/BBN "PIVIB" computer program for computing tracking performance effects of vibration. Applications to some current problems will be demonstrated.

INTRODUCTION

BIODYN-80 is a computerized tool used to compute transmissibilities (transfer functions) between vertical and/or fore-aft vibration inputs and various biodynamic outputs, such as motions of the torso, head, eyes, arms or hands. The situation covers a seated pilot gripping an arbitrary angle stick and viewing a display, possibly engaged in a tracking task. The physical model uses an isomorphic, "lumped parameter," approach to represent the dominant whole-body joints and resulting modes of motion. The software model includes a chain of interacting parallel and serial second-order elements, with complex neuromuscular and force feedbacks at the arm and head. The resulting equations are in "second-order element" matrix form and are fairly general. A separate input file, which describes the particular set of parameters to be used, is created by the user (usually by modifying one of a cataloged set). This file is incorporated in the matrix to produce the linearized coefficients for perturbations about the selected equilibrium posture

---

*This research is sponsored by the Air Force Aeromedical Research Laboratory, Wright-Patterson AFB, under Contract F33615-79-C-0519; the technical monitor is Charles Harmon.

Cramer's rule is used to evaluate the desired transmissibility transfer functions, and these are written to a file in formats suitable for plotting or use in other programs. Typewriter-drawn frequency response plots (Bode format) are available to screen interesting results.

BIODYN-80 is one result of a several year development effort, reported in detail elsewhere.[1-6] It is based on vibration measurements made at AMRL/BBV and elsewhere. Most of the torso, limb and stick model elements have been validated by independent vibration measurements (e.g., Jex and Allen[5]), and the neck, head and eye effects show promising correlations with the few available measurements on image motion effects.[6] However, many aspects remain to be explored, validated or upgraded as more experiments are run and interpreted via BIODYN-80.

The possible applications of this interactive tool are many. It should be helpful in the early stages of experimental design for determining the optimal locations for vibration measurements and/or selection of frequencies. It can be used by development engineers for solving practical pilot-vehicle interface design problems such as pilot-induced oscillations and for choosing the best among design alternatives such as seating location, orientation and suspension parameters. Flight control system designers can make use of BIODYN output in optimizing vehicle/aircrew ride qualities and visual performance effects, possibly incorporating anti-vibration devices to improve the design. These are but a few of the wide range of potential applications for this computerized, interactive model.

One further application of BIODYN-80 deserves special mention. Its vibration-input to biodynamic parameter-output transfer functions are ideally suited as input to PIVIB, another software package which relates pilot tracking performance to the vibration environment.[7] Inputs to PIVIB require biomechanical transfer functions which are output by BIODYN-80. The details of the BIODYN-80/PIVIB interface are found in the BIODYN-80 user's manual.[8]

Figure 1 provides a functional block diagram description of the elements in BIODYN and its interface with PIVIB. The remainder of this report details the use of BIODYN-80, including the model used, the creation of the required input files, an example problem from start to finish, and a suggested interpretation of results.

OVERVIEW

The BIODYN-80 package is comprised of three programs. The first, called CREATE, interactively assembles the two input files used by BIODYN. The second, called BIODYN, is the actual "number cruncher," which sets up and solves the biomechanical equations and computes the desired transfer functions. The third, called PLOT, reads the file of BIODYN transfer functions, prints selected ones in a form readily comprehended by the user, and prepares "quick plot" Bode plots on the line printer, to facilitate a visual interpretation of the transfer function information. Both BIODYN and PLOT are designed as batch programs while, as stated above, CREATE is user-interactive.

A subsequent link in this series of programs is PIVIB. It is a large batch program with three modules. The first, BDMOD, computes the response

ORIGINAL PAGE IS
OF POOR QUALITY

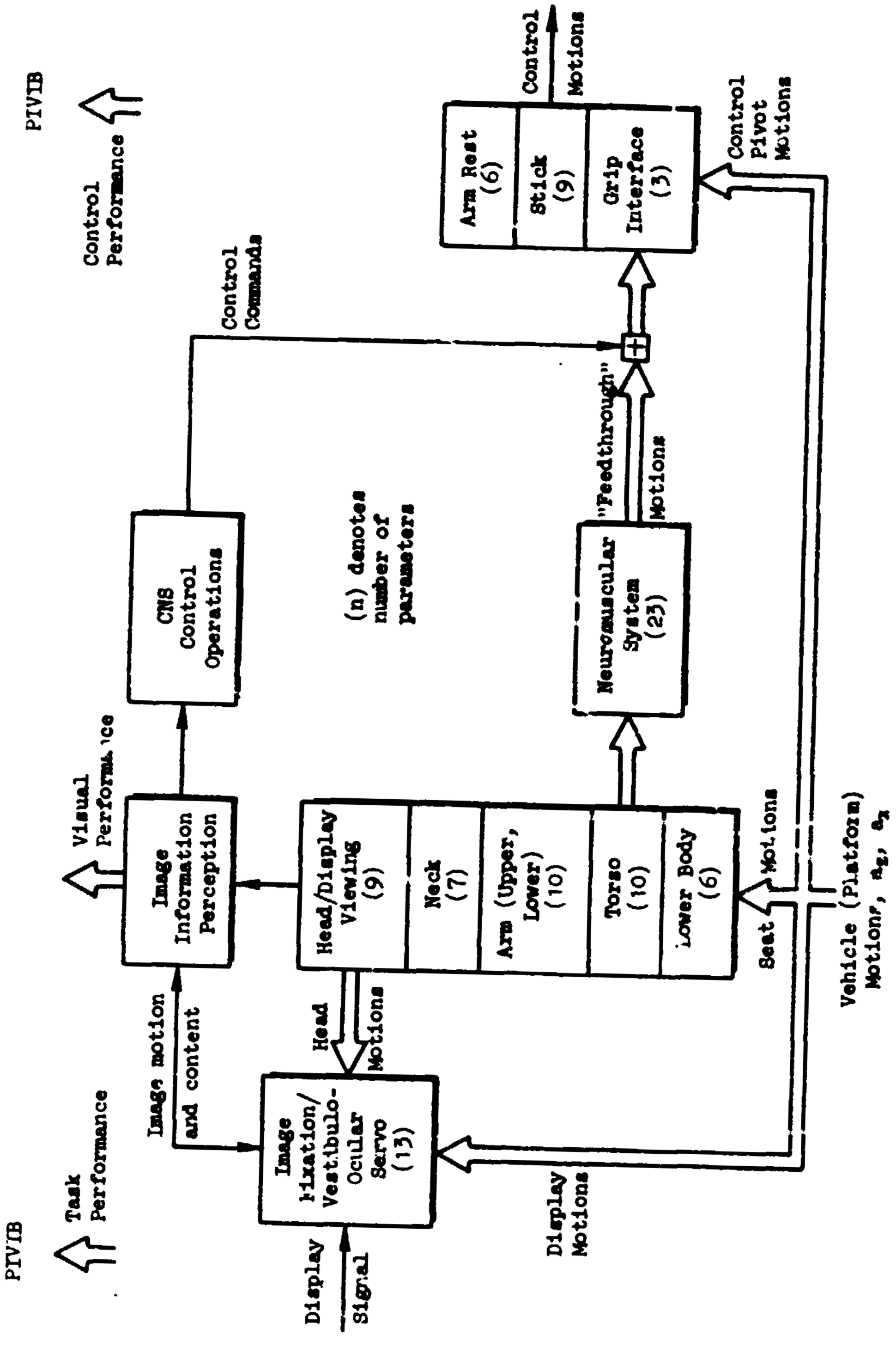

PTVIB
Control Performance
PTVIB
Task Performance
Visual Performance
Image Information Perception
CNS Control Operations
Control Commands
(n) denotes number of parameters
Arm Rest (6)
Stick (9)
Grip Interface (3)
Control Motions
Control Pivot Motions
"Feedthrough"
Motions
Neuromuscular System (23)
Head/Display Viewing (9)
Neck (7)
Arm (Upper, Lower) (10)
Torso (10)
Lower Body (6)
Seat Motions
Vehicle (Platform) Motions, a_z, a_x
Image motion and content
Head Motions
Image Fixation/ Vestibulo-Ocular Servo (13)
Display Motions
Display Signal

Figure 1. Overview of BIODYN-80

behavior of the various biomechanical subsystems. The second, PVMOD, uses the results of BDMOD and the BBN optimal control model to estimate pilot tracking performance within the vibration environment. The final module, VEXEC, provides the top level communication interface between BDMOD and PVMOD, and performs no actual computation. It is in the BDMOD module where biodynamic transfer functions must be specified, and this is the location of BIODYN-PIVIB interface. Further details may be found in the PIVIB user's manual.[7]

BIODYN-80 uses three separate files in the process of performing its computations. The PARAMETER file contains the set of 96 parameters used to define the specific pilot-posture-vibration-display configuration. CREATE is used to assemble this file and can modify an existing file or produce an entirely new file. The CHOICES file contains the list of desired transfer functions to be computed and output by BIODYN, as well as directives for producing the line printer Bode plots. Again, this CHOICES file is assembled by CREATE. Finally, the TF file is used to store the resulting transfer functions output by BIODYN, and is read by the PLOT routine for generating the Bode plots.

PIVIB employs a single large file to direct its flow of execution. This file defines the vibration environment, biomechanical transfer functions, tracking dynamics, tracking performance requirements, and pilot limitations (bandwidths, time delays, etc.). Currently, this file is assembled in the editor, using output from BIODYN-80 if desired.

BIODYN-80 and each of its predecessors were developed on the Tymshare, Inc., PDP-10 computers. BIODYN-80 has been adapted to the CDC 6600 computer at WPAFB in order to increase its availability to Air Force users, and to interact with PIVIB, also resident on the WPAFB CDC computer. The details presented here will address its use on the CDC machine.

Figure 2 presents a flow chart illustrating the use of BIODYN and PIVIB in a given session. Note that the flow of execution can be used to solve a single problem, by submitting a single batch request, or to iterate on a design by submitting a number of batch requests using the same CHOICES file and slightly altered PARAMETER files.

MODEL DESCRIPTION

Three distinct subsystem models are included in BIODYN-80. They are described individually below.

Biomechanical Model

Figure 3 (updated from Fig. 2 of Ref. 3) presents the biomechanical model and defines many of the necessary parameters that describe the nominal (or trim) situation. It utilizes an "isomorphic," or life-like representation, of the major body segments in their orientations, simplified to a minimum number of lumped parameter equivalents. The biomechanical features include:

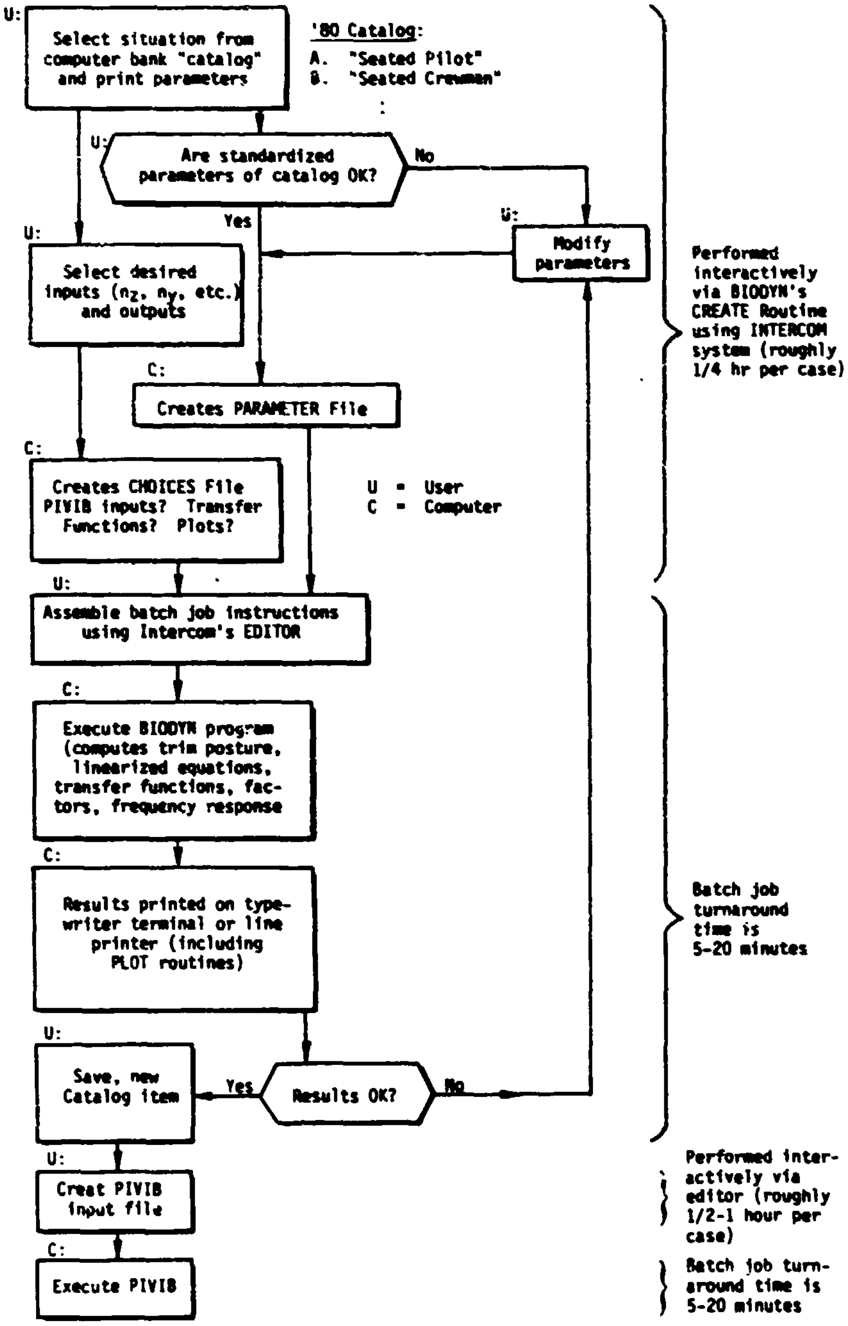
U: Select situation from computer bank "catalog" and print parameters
'80 Catalog:
A. "Seated Pilot"
B. "Seated Crewman"
:
U: Are standardized parameters of catalog OK?
No
Yes
U: Modify parameters
U: Select desired inputs (n_z, n_y, etc.) and outputs
C: Creates PARAMETER File
C: Creates CHOICES File PIVIB inputs? Transfer Functions? Plots?
U = User
C = Computer
Performed interactively via BIODYN's CREATE Routine using INTERCOM system (roughly 1/4 hr per case)
U: Assemble batch job instructions using Intercom's EDITOR
C: Execute BIODYN program (computes trim posture, linearized equations, transfer functions, factors, frequency response
C: Results printed on typewriter terminal or line printer (including PLOT routines)
Batch job turnaround time is 5-20 minutes
U: Save, new Catalog item
Yes
Results OK?
No
U: Creat PIVIB input file
C: Execute PIVIB
Performed interactively via editor (roughly 1/2-1 hour per case)
Batch job turnaround time is 5-20 minutes

Figure 1. BIODYN-80 Flow Chart

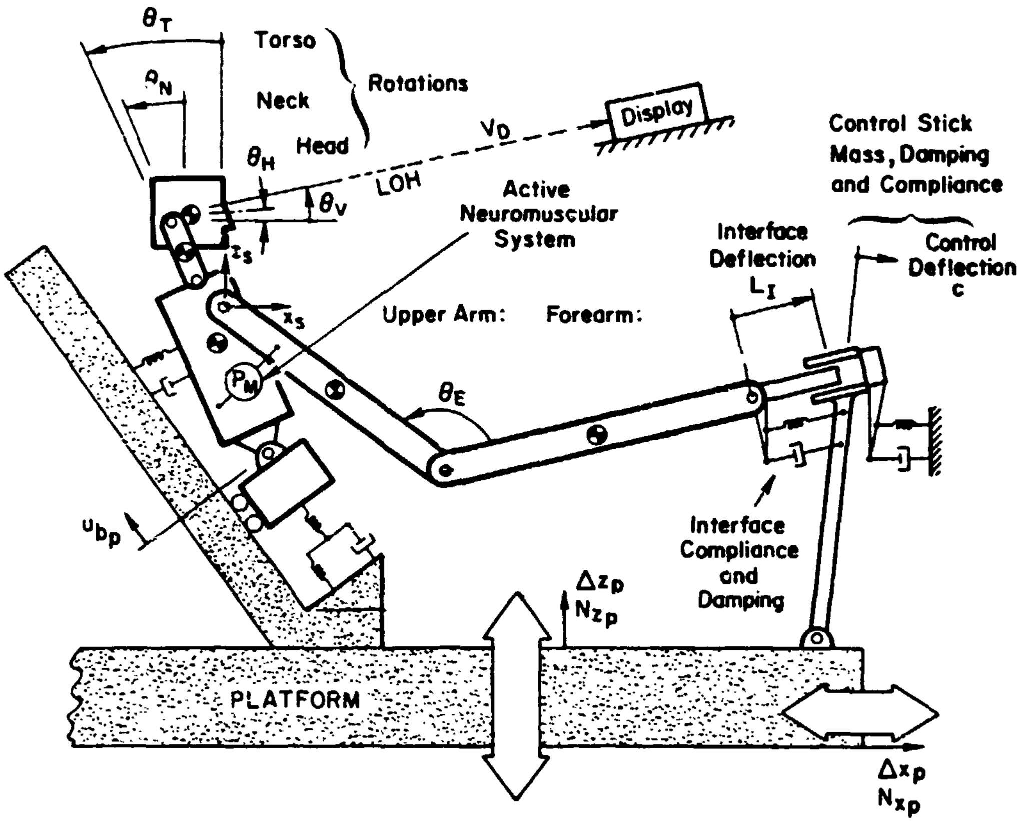
θ_T
Torso
θ_N
Neck
Head
Rotations
θ_H
V_D
Display
LOH
θ_V
Active Neuromuscular System
Control Stick Mass, Damping and Compliance
Interface Deflection
L_I
Control Deflection
c
z_s
x_s
Upper Arm:
Forearm:
P_M
θ_E
u_{b_p}
Δz_p
N_{z_p}
Interface Compliance and Damping
PLATFORM
Δx_p
N_{x_p}

Figure 3. Major Biomechanical Elements (Some Response Variables Are Identified)

- Semisupine torso; sliding hip plus rocking chest supported on a compliant buttocks/seat.
- Head bobbing on an articulated neck with passive compliance, or active neuromuscular system.
- Upper arm and forearm links plus grip-interface compliance, driven by an active neuromuscular system.
- Arm-rest restraints (optional).
- Stick "feel system" dynamics from zero to infinite stiffness, and any angle of stick or grip.

The simplified torso model was derived to describe the dominant motions of the head and arm elements; the "pin joint" node between upper and lower torso segments is not meant to represent any physical feature. In practice, the masses and inertias are obtained from tabulated biomechanical and anthropometric data for the appropriate sized person (e.g., Magdaleno[9]), the postural angles are based on the actual situation (preferably via a side-view photo), and the spring forces and damping coefficients are fitted to data or taken from other motions.[3,10]

Limb Neuromuscular Model

The active neuromuscular system noted on Fig. 3 is a schematic representation of the net effect of complex agonist/antagonist muscle pairs controlling the upper arm or head. An "NM switch" is defined in the PARAMETER file which causes this neuromuscular model to control the limb (NM = 0) or the head (NM = 1). A linearized representation of the limb neuromuscular model is shown in Fig. 4, while the head neuromuscular model is depicted in Fig. 5. This model relates the action of the muscle pairs to the effective (spindle) sensors of muscle length and force as well as proprioceptive senses from the stick-grip interface (in the case of the limb neuromuscular model) or the head-neck interface (in the case of the head neuromuscular model), to complete the loop through central nervous system processing.

Unless the neuromuscular properties are being investigated, it is recommended that the given values of the parameters[8] be used. They are representative of a normal person's arm-hand or head-neck system, and generally yield reasonably damped neuromuscular servo properties. The neuromuscular parameters[8] are characteristic of the largest muscles in the body (e.g., the legs) but experience has shown that the dynamic properties (torque/inertia ratios, damping ratios, natural frequencies, etc.) are about the same for all postural muscle pairs. Here, an empirical scale factor S (> 1.0) is used to scale the normalized muscle to a particular configuration, as though the muscle acted normal to the upper arm c.g. More detailed description of the neuromuscular model is given elsewhere.[11]

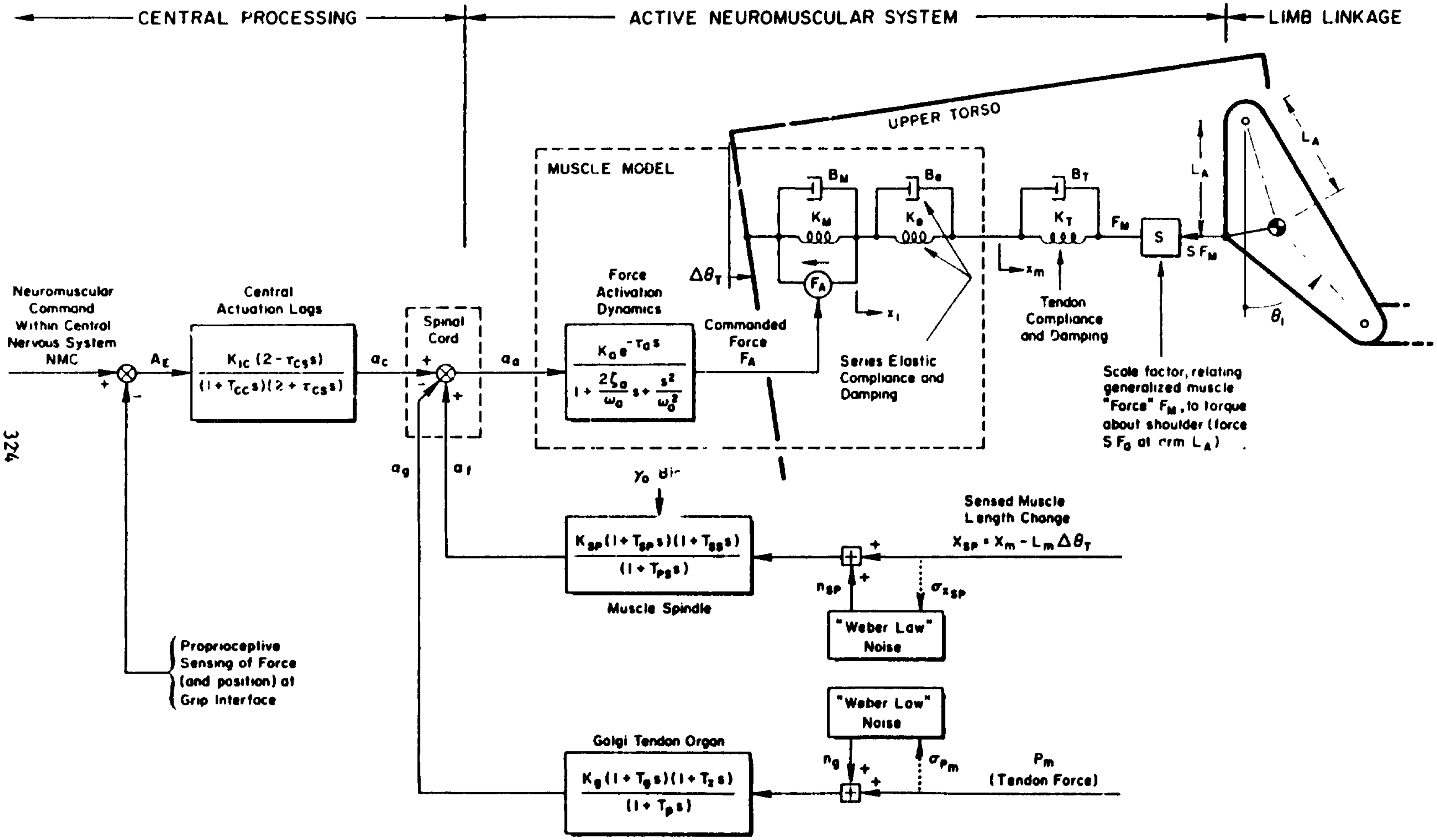
CENTRAL PROCESSING
ACTIVE NEUROMUSCULAR SYSTEM
LIMB LINKAGE
UPPER TORSO
MUSCLE MODEL
Neuromuscular Command Within Central Nervous System NMC
A_E
Central Actuation Logs
$\frac{K_{IC}(2-\tau_{CS}s)}{(1+T_{CC}s)(2+\tau_{CS}s)}$
a_c
Spinal Cord
a_a
Force Activation Dynamics
$\frac{K_a e^{-\tau_a s}}{1+\frac{2\zeta_a}{\omega_a}s+\frac{s^2}{\omega_a^2}}$
Commanded Force F_A
$\Delta\theta_T$
B_M
K_M
F_A
B_e
K_e
x_1
Series Elastic Compliance and Damping
B_T
K_T
x_m
Tendon Compliance and Damping
F_M
S
SF_M
L_A
L_A
θ_1
Scale factor, relating generalized muscle "Force" F_M, to torque about shoulder (force SF_a at arm L_A)
a_g
a_f
γ_o
$\frac{K_{SP}(1+T_{SP}s)(1+T_{SS}s)}{(1+T_{PS}s)}$
Muscle Spindle
Sensed Muscle Length Change
$x_{SP} = x_m - L_m\Delta\theta_T$
n_{SP}
$\sigma_{x_{SP}}$
"Weber Law" Noise
"Weber Law" Noise
Proprioceptive Sensing of Force (and position) at Grip Interface
Golgi Tendon Organ
$\frac{K_g(1+T_g s)(1+T_z s)}{(1+T_p s)}$
n_g
σ_{P_m}
P_m (Tendon Force)

Figure 4. Linearized Limb Neuromuscular System (When the Option NM ≡ 0)

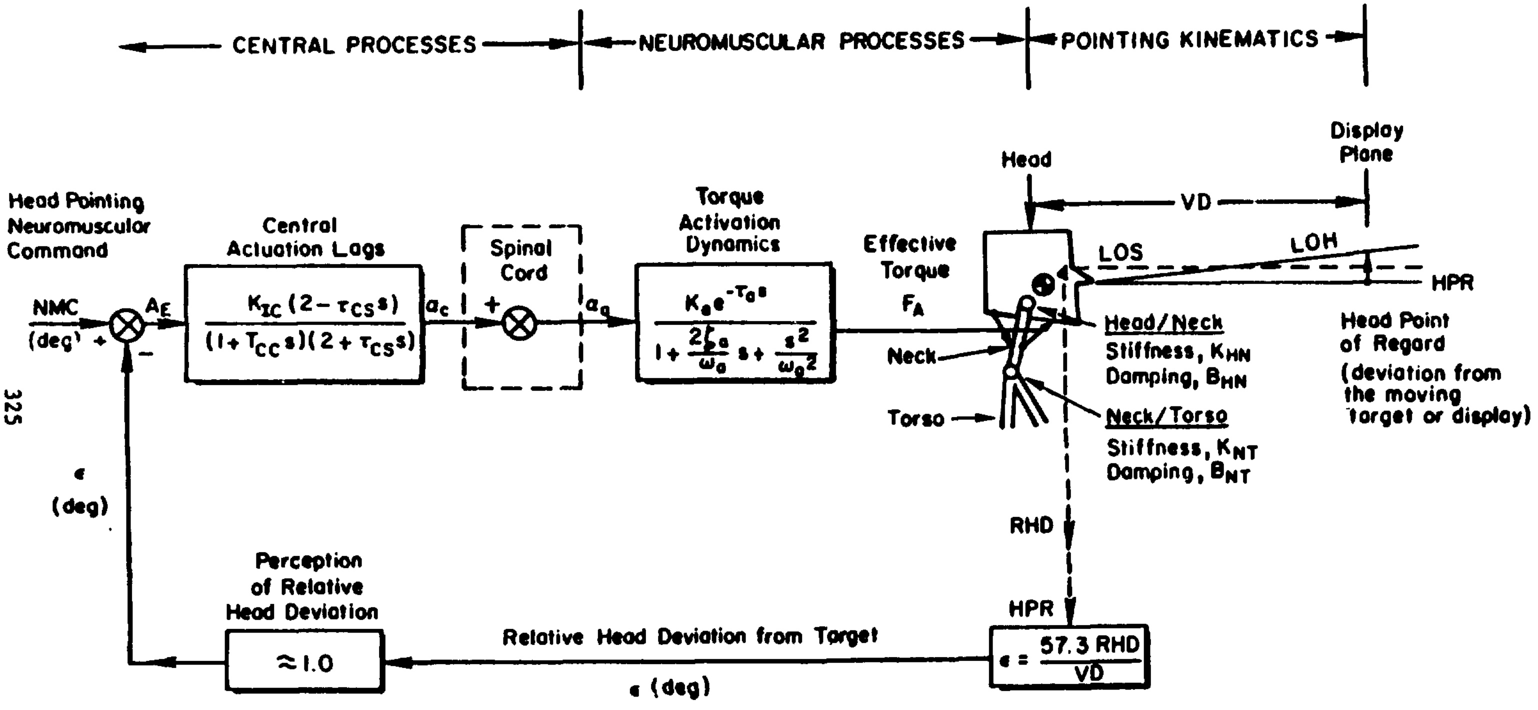
CENTRAL PROCESSES
NEUROMUSCULAR PROCESSES
POINTING KINEMATICS
Head Pointing Neuromuscular Command
NMC (deg)
+
−
A_ϵ
Central Actuation Lags
$\frac{K_{IC}(2-\tau_{CS}s)}{(1+T_{CC}s)(2+\tau_{CS}s)}$
a_c
Spinal Cord
+
a_a
Torque Activation Dynamics
$\frac{K_a e^{-\tau_a s}}{1+\frac{2\zeta_a}{\omega_a}s+\frac{s^2}{\omega_a^2}}$
Effective Torque F_A
Neck
Torso
Head
Display Plane
VD
LOS
LOH
HPR
Head/Neck
Stiffness, K_{HN}
Damping, B_{HN}
Neck/Torso
Stiffness, K_{NT}
Damping, B_{NT}
Head Point of Regard (deviation from the moving target or display)
RHD
HPR
$\epsilon = \frac{57.3\ RHD}{VD}$
Relative Head Deviation from Target
ϵ (deg)
Perception of Relative Head Deviation
≈1.0
ϵ (deg)

Notes:

When NM≡1, this simplified NM system is connected to the head to maintain head pointing at the vibrating target. The values of the parameters F_A, K_{IC}, K_a, etc. are different between the limb case (NM≡0) and head case (NM≡1)

Figure 5. Simplified Head Pointing Neuromuscular System (When Option NM = 1)

Neck/Head/Eye Model

Figure 6 illustrates the basic elements involved in the neck/head/eye model. Details involving validation and example use of this subsystem model are found in Ref. 6. The task is to keep the eye fixated on the target, i.e., null the relative eye (point of regard) deviation (RED) at the display. The moving base can produce image error disturbances, both from induced head rotation and translation as well as target motions. The "vestibulo-ocular reflex" ($G_V G_M$) is a "crossfeed" (or "feedforward") that rotates the eye oppositely to the head to compensate for head rotation, i.e., to maintain approximate inertial eye fixation.

The "Fixation Reflex" or feedback tracking loop ($G_E G_M$) involves the subject's efforts to null the image error θ_I by compensatory eye movements. The "Target Pursuit" path ($G_P G_M$) models the subject's "feedforward" operations on the perceived absolute target motions in inertial space (as distinct from the image error motions). For highly predictable and perceivable target motions the Target Pursuit path is capable of greatly reducing the image errors.

The linearized model formulation assumes that the target remains within the foveal area (3-4 deg field), and that angular velocities are small (i.e., less than 20 deg/sec) such that saccades are rare and can be ignored for most purposes. Additionally, the vibration-induced motions will always be small enough to permit linearization of all angular functions and allow a quasi-linear representation of the dynamic elements about each "operating point" (posture, view geometry, frequency).

The three subsystem models described above contain parameters which must be assigned values via the PARAMETER file, in order to describe the desired problem to BIODYN. These parameters are defined elsewhere.[8]

AN EXAMPLE PROBLEM

This section presents a typical terminal session in the Intercom 4.7 operating system, accessing the CSA mainframe at Wright-Patterson AFB's ASD Computer Center. The dialog is annotated so that a beginning user can follow the entire job from start to finish. All user responses are underlined.

This particular session on the computer was an investigation of the differences in the DTH/DXP and RHD/DXP transfer functions between a pilot in an erect orientation and a pilot in a semisupine orientation. Only two parameters are changed: in the erect posture, the angle between the torso-c.g.-to-hips pivot and vertical is 10 deg, while in the semisupine posture the angle is 65 deg; and in the erect posture, the angle between the head c.g. and head/neck pivot is 70 deg, while in the semisupine posture the angle is 110 deg.

The steps followed in the investigation are listed below:

1) Log in to Intercom.

2) Attach the PARAMETER file to be modified and name it TAPE20.

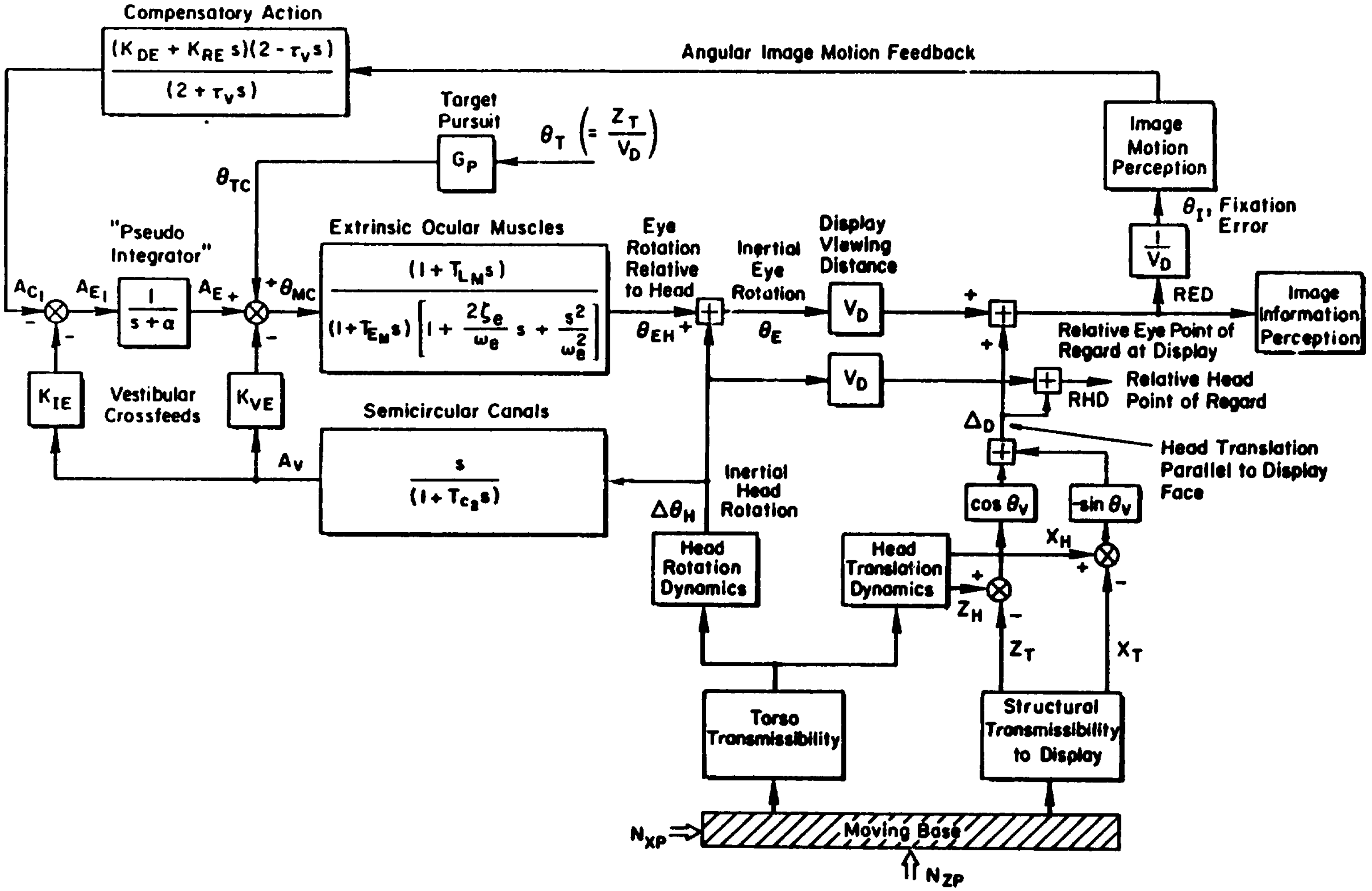
Compensatory Action
$\frac{(K_{DE} + K_{RE}s)(2 - \tau_V s)}{(2 + \tau_V s)}$
Angular Image Motion Feedback
Target Pursuit
G_P
$\theta_T \left(= \frac{Z_T}{V_D}\right)$
θ_{TC}
"Pseudo Integrator"
$\frac{1}{s+a}$
A_{C_I}
A_{E_I}
A_E
θ_{MC}
Extrinsic Ocular Muscles
$\frac{(1 + T_{L_M}s)}{(1+T_{E_M}s)\left[1 + \frac{2\zeta_e}{\omega_e}s + \frac{s^2}{\omega_e^2}\right]}$
K_{IE}
Vestibular Crossfeeds
K_{VE}
A_V
Semicircular Canals
$\frac{s}{(1 + T_{c_2}s)}$
Eye Rotation Relative to Head
θ_{EH}
Inertial Eye Rotation
θ_E
Display Viewing Distance
V_D
V_D
Inertial Head Rotation
$\Delta\theta_H$
Head Rotation Dynamics
Head Translation Dynamics
Torso Transmissibility
Structural Transmissibility to Display
Moving Base
N_{XP}
N_{ZP}
Z_H
Z_T
X_H
X_T
$\cos\theta_V$
$-\sin\theta_V$
Δ_D
Head Translation Parallel to Display Face
RHD
Relative Head Point of Regard
Relative Eye Point of Regard at Display
RED
$\frac{1}{V_D}$
θ_I, Fixation Error
Image Motion Perception
Image Information Perception

Figure 6. Block Diagram for Head, Eye, Vestibular Models and Display Kinematics

3) Attach the CREATE program, called EXECRT.

4) Run EXECRT, make changes to existing file, assemble new CHOICES file.

5) Assemble batch job to run BIODYN and PLOT, using the two PARAMETER files (old and modified) and the new CHOICES file.

6) Submit batch job to input queue.

7) When job completed, list the output file.

ADDITIONS TO BIODYN-80

Three areas of interest will be investigated to improve and update the software package described herein. These include:

- Validation of the head/eye/display model. BIODYN-80 will be exercised to verify that it correctly predicts past and current experimental data; in addition, new experiments will be suggested and performed for any remaining validation areas.

- Extension of model. The roll-sway modes of vibration will be incorporated in the BIODYN-80 model, so as to be responsive to experimental interest in lateral-directional vibration. Keen interest in helmet-mounted displays and helmet-mounted sights dictates that this capability also be incorporated into the model.

- Improved graphics outputs. Additional work in this area centers around constructing stick figure graphics on a CRT to display node shapes in a visually compelling manner.

ORIGINAL PAGE IS
OF POOR QUALITY

Typical INTERCOM Terminal Session

```
      LOGIN
ENTER PROBLEM NUMBER-L800015
███████████ ENTER PASSWORD-
```

1. Log in.

```
ENTER 3-DIGIT TERMINAL ID-000


03/20/80   LOGGED IN AT  15.21.27.
           WITH USER-ID CK
           EQUIP/PORT 13/000
COMMAND- REQUEST,TAPE7,*PF
```

2. Attach files.

```
COMMAND- REQUEST,TAPE8,*PF

COMMAND- ATTACH,TAPE20,BB19

 PF CYCLE NO. = 001
COMMAND- ATTACH,EXECRT
```

3. Attach EXECRT to run CREATE.

```
 PFN IS
 EXECRT
 PF CYCLE NO. = 001
COMMAND- EXECRT
```

4. Run EXECRT.

```
    NEW FILE ?
NO

    LISTING DESIRED?
YE

    (LO)NG OR (SH)ORT LISTING?
LI

    (LO)NG OR (SH)ORT LISTING?
LO
```

Get a listing of file to be modified. If response is not recognized, query repeats.

Session continues

Continuing

```
       STIFF  STICK

    PARAMETER DEFINITION        MNEMONIC     UNITS       VALUE

LOWER BODY MASS                   XMB       KG          14.0000
L. BODY SEAT CUSHION DAMPER       BB        N/M/S       1290.10
L. BODY SEAT CUSHION STIFFNESS    XKB       N/M         29585.0
SERIES SPRING GRAD.-LOWER BODY    GK1       N/M         71519.0
SEAT TILT ANGLE                   THL       DEG         13.0000
TRIM VERTICAL ACCEL.              G         M/S2        9.80000
TORSO MASS                        XMT       KG          18.0000
TORSO INERTIA                     ZIT       KGM2        .800000
TORSO DAMPING                     BTB       NM/R/S      16.7500
TORSO STIFFNESS                   XKTB      NM/R        500.000
ANGLE OF XLT FROM VERTICAL        THT       DEG         10.0000
TORSO CG TO HIPS PIVOT LENGTH     XLT       M           .150000
ANGLE OF XLTN                     THTN      DEG         5.00000
TORSO CG TO NECK/TORSO PIVOT      XLTN      M           .300000
ANGLE OF XLS                      THS       DEG         5.00000
TORSO CG TO SHOULDER LENGTH       XLS       M           .300000
NECK MASS                         XMN       KG         0.
NECK INERTIA                      ZIN       KGM2       0.
NECK/TORSO DAMPER                 BNT       NM/R/S      .250000
NECK/TORSO STIFFNESS              XKNT      NM/R        50.0000
ANGLE OF XLN                      THN       DEG        -20.0000
NECK LENGTH                       XLN       M           .100000
NECK CG TO NECK/TORSO PIVOT       XLN1      M           .500000E-01
HEAD MASS                         XMH       KG          4.34000
HEAD INERTIA                      ZIH       KGM2        .390000E-01
HEAD/NECK DAMPER                  BHN       NM/R/S     0.
HEAD/NECK STIFFNESS               XKHN      NM/R        1.00000
HEAD/NECK COMPLIANCE              CH        -          0.
ANGLE OF XLH                      [illegible]  DEG      70.0000
HEAD CG TO HEAD/NECK PIVOT LEN    XLH       M          0.
LINE OF SIGHT ANGLE               THV       DEG        -30.0000
VIEWING DISTANCE                  VD        M           .750000
UPPER ARM MASS                    XM1       KG          1.37200
UPPER ARM INERTIA                 Z1        KGM2        .120000E-01
UPPER ARM ANGLE                   T1        DEG         40.0000
UPPER ARM LENGTH                  D1        M           .290000
UPPER ARM CG                      R1        M/M         .440000
LOWER ARM MASS                    XM2       KG          1.01700
LOWER ARM INERTIA                 Z2        KGM2        .152000E-01
ELBOW ANGLE                       TE        DEG         145.000
LOWER ARM LENGTH                  D2        M           .305000
LOWER ARM CG                      R[illegible]  M/M     .500000
GRIP INTERFACE ANGLE              TIJ       DEG        0.
GRIP INTERFACE TIME CONSTANT      TIF       S           .100000E-01
GRIP INTERFACE COMPLIANCE         CI        M/N         .557810E-04
STICK MASS                        XMS       KG          .310000
STICK DAMPER                      BS        N/M/S       2.00000
STICK GRADIENT                    XKS       N/M         13900.0
STICK COMPLIANCE PARAMETER        CKS       -           1.00000
BOBWEIGHT SENSITIVITY TO NX       SX        N/G        0.
BOBWEIGHT SENSITIVITY TO NZ       SZ        N/G        0.
STICK ANGLE                       THC       DEG         90.0000
STICK LENGTH                      XLC       M           .610000
STICK OUTPUT SCALE FACTOR         XKSC      /M          13900.0
ARM REST DAMPER (NORMAL)          BAR       N/M/S      0.
ARM REST STIFFNESS (NORMAL)       XKAR      N/M        0.
ARM REST DAMPER (TANG)            BAT       N/M/S      0.
ARM REST STIFFNESS (TANG)         XKAT      N/M        0.
ELBOW TO ARM REST DISTANCE        XLER      M          0.
FRAC ARM WEIGHT ON ARM REST       ARMR      -          0.
SWITCH FOR CENTRAL AND F A.D.     NM        -          0.
OVERALL SF FOR MUSCLE ELEMENTS    SI        -           104.400
```

Session continues

Continuing

```
N/M ACTUATION GAIN                  XK1C     N/N          .204370E-01
N/M ACTUATION LAG                   TCC      S            .90909OE-01
N/M ACTUATION TIME DELAY            TCS      S            .898880E-01
GAIN OF F.A.D.                      XKAA     N/N          1.00000
DAMPING IN F.A.D.                   ZA       -            .800000
NATURAL FREQUENCY IN F.A.D.         WA       R/S          16.0000
TIME DELAY IN F.A.D.                TAA      S           0.
HILLS LAW DAMPER                    BM       N/M/S        1.00000
SPRING IN N/M SYSTEM                YKM      N/M          2.00000
SERIES ELASTIC ELEMENT DAMPER       BE       N/M/S        2.43120
SERIES ELASTIC ELEMENT GRAD         XKE      N/M          40.0000
TENDON DAMPER                       BT       N/M/S       0.   -
TENDON GRADIENT                     XKT      N/M          80.0000
SPINDLE MODEL GAIN                  XKSP     N/M          5.00000
SPINDLE LEAD TIME CONSTANT          TSP      S            .909000E-01
SPINDLE LAG TIME CONSTANT           TPS      S           0.
SPINDLE HI FREQ LEAD T.C.           TSS      S           0.
GOLGI MODEL GAIN                     KG      N/N          .500000
GOLGI LEAD TIME CONSTANT            .G       S            .555560E-01
GOLGI HI FREQ LEAD TIME CONST       TZ       S           0.
GOLGI LAG TIME CONSTANT             TP       S           0.
FIXATION ERROR GAIN                 XKDE     R/R          7.07950
FIXATION RATE GAIN                  XKRE     R/R/S       0.
TIME DELAY IN FIXATION LOOP         TV       S            .450000E-01
PSEUDO INTEGRATOR BREAK FREQ        ALPHA    R/S          .300000
TARGET PURSUIT GAIN                 XKF      R/R         0.
POSITION GAIN FROM VESTB SENSR      XKIE     -            .670000
VELOCITY GAIN FROM VESTB SENSR      XKVE     -            .100000
VESTIBULAR LAG                      TC2      S            .100000E-01
EOM LAG TIME CONSTANT               TEM      S            .100000
EOM LEAD TIME CONSTANT              TLM      S            .125000E-01
SWITCH FOR EOM FAST MODE            OE       -            1.00000
EOM DAMPING RATIO                   ZE       -            .650000
EOM NATURAL FREQUENCY               WE       R/S          316.230
    INPUT MNEMONIC(5 CHARS) AND VALUE FOR EACH CHANGE,
    TO EXIT, TYPE XXX.
ZHT  ,65.
WER  ,10.

    MNEMONIC WER   NOT PERMISSIBLE.  PLEASE REINPUT.
TH   ,1100.

    WARNING - RECOMMENDED RANGE FOR THIS PARAMETER IS
              -30.0000     TO  150.000     DEG
    DO YOU WANT TO CHANGE THE VALUE ?
YE

    PLEASE REINPUT
TH   ,110.
XXX

    TITLE IS STIFF  STICK
    CHANGE D IRED ?
YE

    NEW TITLE :
SEMI-SUPINE
```

Modify file

Error message if mnemonic not recognized. Warning if value

Title modified

Session continues

ORIGINAL PAGE IS
OF POOR QUALITY

Continuing

Listing of modified file

```
    LISTING DESIRED?
YE
    (LO)NG OR (SH)ORT LISTING?
SH
PARAMETERS FOR:

SEMI-SUPINE

LOWER BODY
 14.000      1290.1      29585.      71519.      13.000      9.8000
TORSO
 18.000      .80000      16.750      500.00
 65.000      .15000      5.0000      .30000      5.0000      .30000
NECK
0.          0.          .25000      50.000
-20.000      .10000      .50000E-01
HEAD/DISPLAY VIEWING
 4.3400      .39000E 01 0.          1.0000      0.
 110.00      0.         -30.000      .75000
ARM (UPPER, LOWER)
 1.3720      .12000E-01  40.000      .29000      .44000
 1.0170      .15200E-01  145.00      .30500      .50000
GRIP INTERFACE
0.           .10000E-01  .55781E-04
STICK
 .31000      2.0000      13900.      1.0000      0.          0.
 90.000      .61000      13900.
ARM REST
0.          0.          0.          0.          0.          0.
NEUROMUSCULAR SYSTEM
   0  104.40
 .20437E-01  .90909E-01  .89000E-01
 1.0000      .80000      16.000      0.
 1.0000      2.0000      2.4312      40.000      0.          80.000
 5.0000      .90900E-01 0.          0.
 .50000      .55556E-01 0.          0.
IMAGE FIXATION/VESTIBULO-OCULAR SERVO
 7.0795      0.          .45000E-01  .30000      0.
 .67000      .10000      .10000E-01
 .10000      .12500E-01  1.0000      .65000      316.23
```

Session continues

Continuing

```
    NEW CHOICES FILE ?                                              Assemble CHOICES file.
YE

    S:DDYN TFS DESIRED FOR PIVIB ?
NO

    TRANSFER FUNCTION INPUT :
    FIRST LINE-RESPONSE MNEMONIC, FORCING FUNCTION MNEMONIC        Instructions for input.
       (AAA,AAA) ; ENTER XXX TO STOP
    SECOND LINE-PLOTTING INFORMATION, 5 ITEMS :
       BODE LOWER FREQ. LIMIT
       BODE UPPER FREQ. LIMIT
       BODE UPPER PHASE LIMIT (0. DEFAULTS TO 200.)
       BODE LOWER PHASE LIMIT (0. DEFAULTS TO -400.)
       LIST (1. TO LIST TABLE, 0. FOR NO LIST)
    IF NO PLOT DESIRED, ENTER 0. FOR ALL ITEMS
RIN,RXF
1.,100.,0.,0.,0.                                                   Error message if
RNF,RXP                                                            mnemonic not found.

    RNF NOT PERMISSIBLE, PLEASE REINPUT
RNB,RXP
.1,200.,0.,0.,1.

    MAX FREQUENCY RANGE IS 3 DECADES                               Error message if
    PLEASE REINPUT ENTIRE LINE                                     frequency range > 3 decades
1.,100.,0.,0.,1.
XXX

     STOP                                                          EXECRT halts.
       .343 CP SECONDS EXECUTION TIME
```

Session continues

ORIGINAL PAGE IS
OF POOR QUALITY

Continuing

```
COMMAND- CATALOG,TAPE7,CHOICE,RP=999

 INITIAL CATALOG
 CT ID=  L800015 PFN=CHOICE
 CT CY= 001  00000064 WORDS.:
COMMAND- CATALOG,TAPE8,SEMI,RP=999

 INITIAL CATALOG
 CT ID=  L800015 PFN=SEMI
 CT CY= 001  00000256 WORDS.:
COMMAND- EDITOR
```

Catalog PARAMETER and CHOICES files.

```
..CREATE,S

ENTER LINES
SAR,CM150000,STCSA.   L800015,RIEBEL,(213)479-2281
ATTACH,TAPE7,CHOICE.
ATTACH,TAPE[illegible],BIO12.
ATT[illegible]IO.
EXEBIO([illegible]TPUT,TAPE7,TAPE8,TAPE19,TAPE21).
REWIND,TAPE19.
ATTACH,EXEPLT.
EX[illegible]TAPE19).
[illegible],EXEBIO,EXEPLT.
RETURN,TAPE8,TAPE19,TAPE21.
ATTACH,TAPE[illegible]MI.
EXE[illegible]TPUT,TAPE7,TAPE8,TAPE19,TAPE21).
REWIND,TAPE19.
EXEPLT(OUTPUT,TAPE19).
#EOR
=

..SAVE,GOBIO,NOSEQ

..STORE,GOBIO,BIODYN

 CT ID=   BIODYN PFN=GOBIO
 CT GY= 002  00000128 WORDS.:
..END
```

5. Use EDITOR to assemble batch job for running BIODYN (EXEBIO) and PLOT (EXEPLT).

   Note that BIODYN requires CM150000.

```
COMMAND- BATCH,GOBIO,INPUT,HERE

COMMAND- FILES

--LOCAL FILES--
 $TAPE8     $TAPE7     $INPUT     $OUTPUT    $TAPE20
 $EXECRT    $GOBIO
--REMOTE EXECUTING JOBS--
  SARCKQI
```

6. Submit batch job.

```
         FILES

--LOCAL FILES--
 $INPUT     $OUTPUT    $GOBIO
--REMOTE OUTPUT FILES--
  SARCKQI
COMMAND- BATCH,SARCKQI,LOCAL

COMMAND- EDITOR

..
YOU HAVE AN EXISTING EDIT FILE
EDIT,SARCKQI,S

LIN    TRUNCATED- CM= 72 CHARS, LONGEST LINE WAS  132
..L,  ,ALL,S
```

Recover output file.

Session continues

ORIGINAL PAGE IS
OF POOR QUALITY

Continuing

Stiff Stick

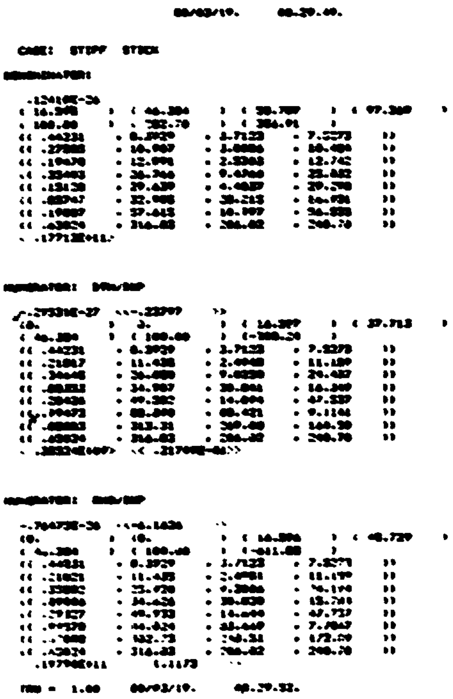

Semisupine

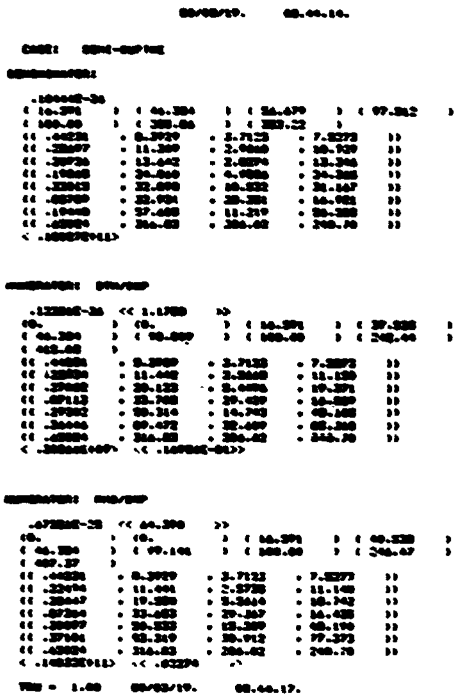

Session continues

ORIGINAL PAGE IS
OF POOR QUALITY

Continuing

Stiff Stick

```
BIODYN T.F.            [illegible]     [illegible]
STIFF  STICK

[illegible]
STN/[illegible]
[illegible]


BIODYN T.F.

BIODYN T.F.            [illegible]     [illegible]
STIFF  STICK

            STN/[illegible]
            [illegible]
FIRST-ORDER DIPOLES CANCELLED :
 [illegible]
 [illegible]

SECOND-ORDER DIPOLES CANCELLED :
 [illegible]     [illegible]
 [illegible]     [illegible]

NUMERATOR:

[illegible]
[illegible]        ( [illegible]     ) ( [illegible]   ) ( 37.713     )
(-[illegible]      )
(( [illegible]    [illegible]   [illegible]   [illegible]   ))
(( [illegible]    [illegible]   [illegible]   [illegible]   ))
(( [illegible]    [illegible]   [illegible]   [illegible]   ))
(( [illegible]    [illegible]   [illegible]   [illegible]   ))
(( [illegible]    [illegible]   [illegible]   [illegible]   ))
(( [illegible]    [illegible]   [illegible]   [illegible]   ))

DENOMINATOR:

( [illegible]   ) ( [illegible]   ) ( 97.360    ) ( [illegible]   )
( [illegible]   )
(( [illegible]    [illegible]   [illegible]   [illegible]   ))
(( [illegible]    [illegible]   [illegible]   [illegible]   ))
(( [illegible]    [illegible]   [illegible]   [illegible]   ))
(( [illegible]    [illegible]   [illegible]   [illegible]   ))
(( [illegible]    [illegible]   [illegible]   [illegible]   ))
(( [illegible]    [illegible]   [illegible]   [illegible]   ))
   [illegible]


BIODYN T.F.

BIODYN T.F.            [illegible]     [illegible]
STIFF  STICK

            STN/[illegible]
            [illegible]
```

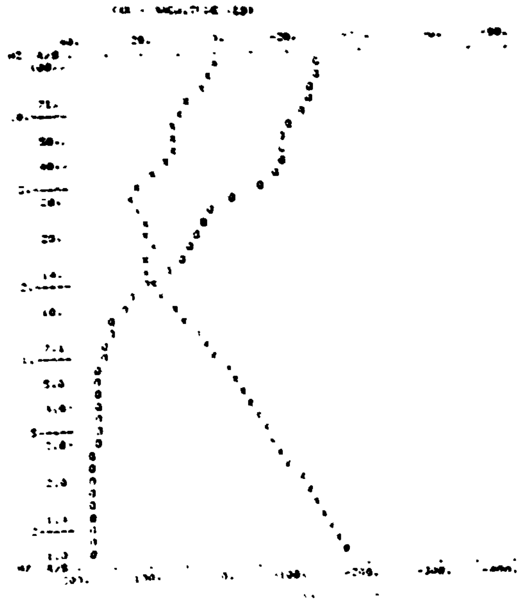

Semisupine

```
BIODYN T.F.            [illegible]     [illegible]
SEMI-SUPINE

[illegible]
STN/[illegible]
[illegible]


BIODYN T.F.

BIODYN T.F.            [illegible]     [illegible]
SEMI-SUPINE

            STN/[illegible]
            [illegible]
FIRST-ORDER DIPOLES CANCELLED :
 [illegible]
 [illegible]

SECOND-ORDER DIPOLES CANCELLED :
 [illegible]     [illegible]
 [illegible]     [illegible]

NUMERATOR:

[illegible]
([illegible]       ( [illegible]    ) ( [illegible]   ) ( [illegible]   )
( [illegible]     ) ( [illegible]   ) ( [illegible]   )
(( [illegible]    [illegible]   [illegible]   [illegible]   ))
(( [illegible]    [illegible]   [illegible]   [illegible]   ))
(( [illegible]    [illegible]   [illegible]   [illegible]   ))
(( [illegible]    [illegible]   [illegible]   [illegible]   ))
(( [illegible]    [illegible]   [illegible]   [illegible]   ))

DENOMINATOR:

( [illegible]   ) ( [illegible]   ) ( [illegible]   ) ( [illegible]   )
( [illegible]   )
(( [illegible]    [illegible]   [illegible]   [illegible]   ))
(( [illegible]    [illegible]   [illegible]   [illegible]   ))
(( [illegible]    [illegible]   [illegible]   [illegible]   ))
(( [illegible]    [illegible]   [illegible]   [illegible]   ))
(( [illegible]    [illegible]   [illegible]   [illegible]   ))
(( [illegible]    [illegible]   [illegible]   [illegible]   ))
   [illegible]


BIODYN T.F.

BIODYN T.F.            [illegible]     [illegible]
SEMI-SUPINE

            STN/[illegible]
            [illegible]
```

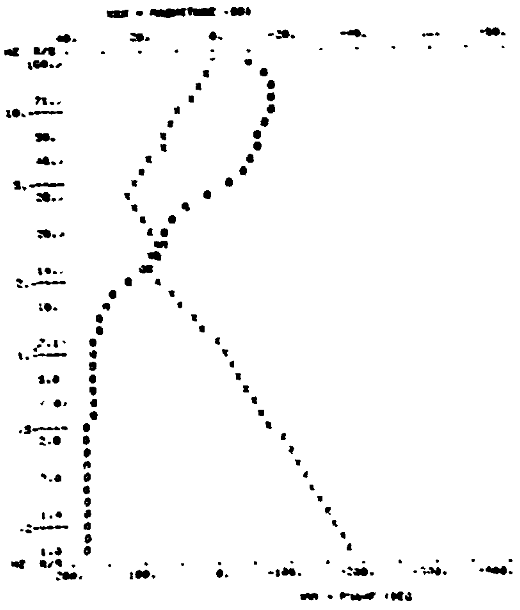

Session continues

ORIGINAL PAGE IS
OF POOR QUALITY

Continuing

Stiff Stick

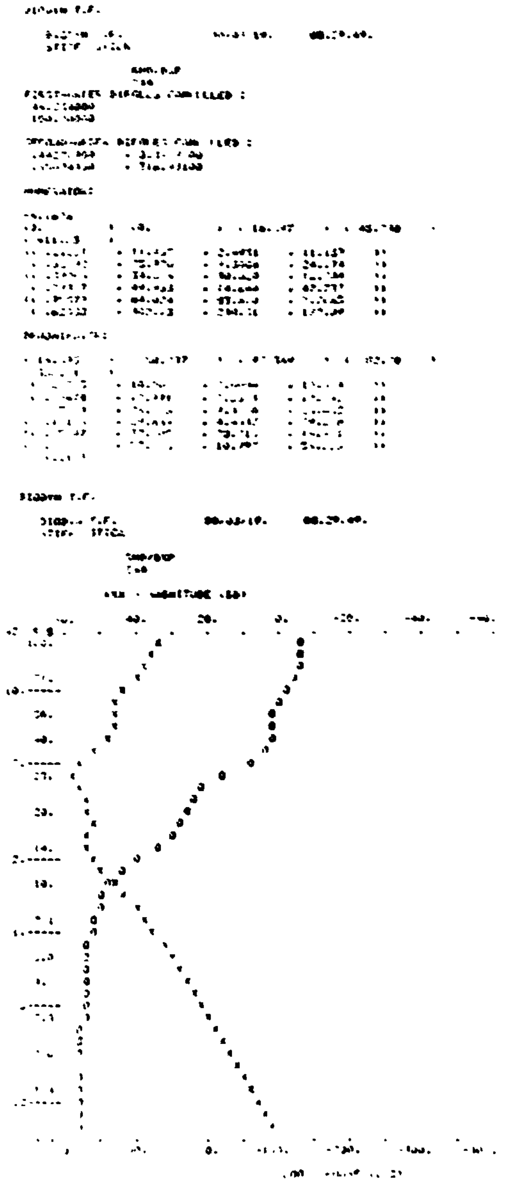

Semisupine

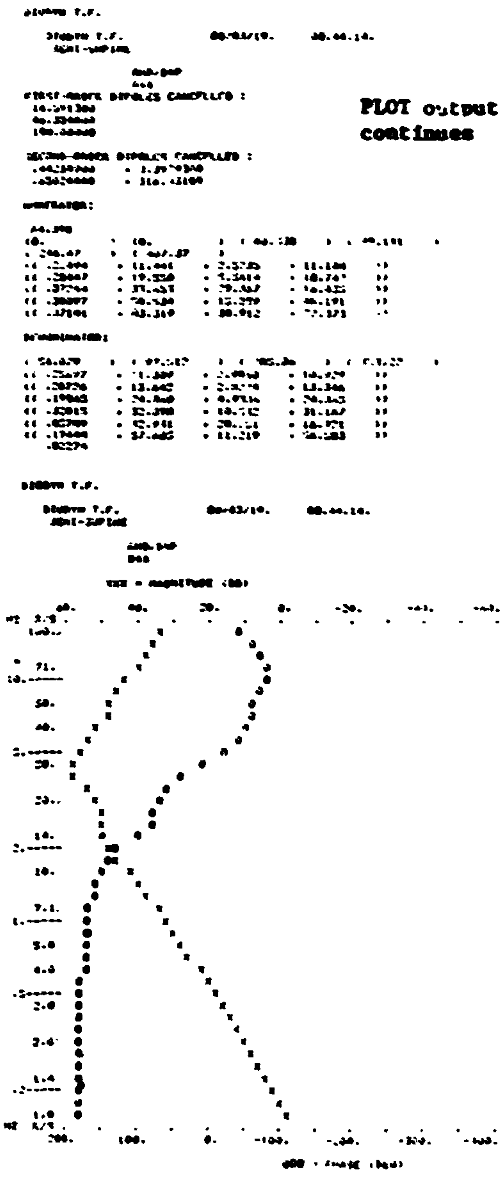

PLOT output continues

Session continues

Continuing

Stiff Stick

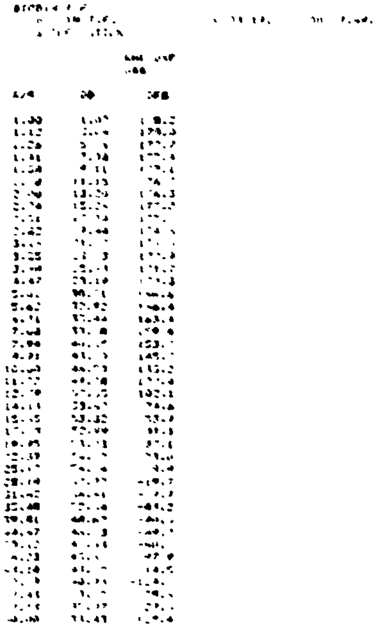

Semisupine

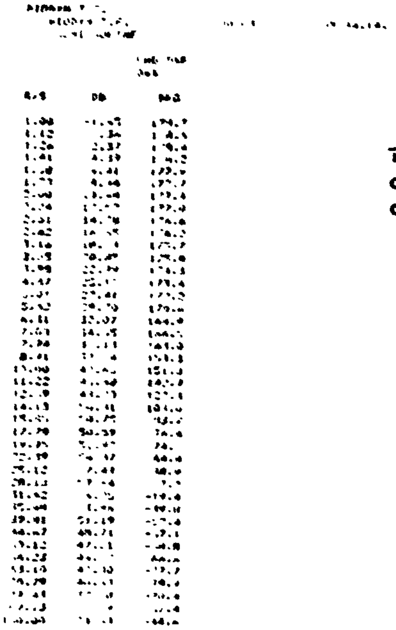

**PLOT
output
concluded**

Session concluded

REFERENCES

[1]Jex, H. R., and R. E. Magdaleno, Modeling Biodynamic Effects of Vibration, Fifth Year; Final Scientific Report, Systems Technology, Inc., SR-a037-1, Aug. 1979.

[2]Jex, H. R., and R. E. Magdaleno, "Progress in Measuring and Modeling the Effects of Low Frequency Vibration on Performance," Models and Analogues for the Evaluation of Human Biodynamic Response, Performance and Protection, AGARD CP-253, June 1979, pp. A29-1 through A29-11.

[3]Jex, H. R., and R. E. Magdaleno, "Biomechanical Models for Vibration Feedthrough to Hands and Head for a Semisupine Pilot," Aviation, Space and Environmental Med., Vol. 49, No. 1, Jan. 1978, pp. 304-316.

[4]Magdaleno, R. E., and H. R. Jex, User's Guide to BIODYN-78, An Interactive Computer Program for Modeling Biodynamic Feedthrough to a Pilot's Hands and Head, Systems Technology, Inc., TR-1037-2, July 1979.

[5]Jex, H. R., and R. W. Allen, "Evaluating Biodynamic Interference with Operational Crews," Vibration and Combined Stresses in Advanced Systems, AGARD CP-1 Mar. 1975, pp. B24-1 through B24-18.

[6]Jex, H. R., and R. E. Magdaleno, Modeling Biodynamic Effects of Vibration; Fourth Year Interim Scientific Report, Systems Technology, Inc., ISR-1037-4, Sept. 1978.

[7] Berliner, Jeffrey E., and William H. Levison, PIVIB: A Computer Program for Analysis of Pilot Biodynamic and Tracking Response to Vibration, Bolt, Beranek and Newman, Rept. 3457, Dec. 1976.

[8]Riedel, S. A., R. E. Magdaleno, and H. R. Jex, User's Guide to BIODYN-80; An Interactive Software Package for Modeling Biodynamic Feedthrough to a Pilot's Hands, Head and Eyes, Systems Technology, Inc., TR-1146-1, 21 Mar. 1980.

[9]Braune, W., O. Fischer, J. Amar, and W. T. Dempster, Human Mechanics; Four Monographs Abridged, AMRL-TDR-63-123, Dec. 1963.

[10]"Symposium on Biodynamic Models and Their Applications," Dayton, Ohio, 15-17 Feb. 1977, published in Av., Space and Environ. Med., Vol. 49, No. 1, Jan. 1978.

[11]Magdaleno, R. E., D. T. McRuer, and G. P. Moore, Small Perturbation Dynamics of the Neuromuscular System in Tracking Tasks, NASA CR-1212, Dec. 1968.

D21

N82 34058

ORIGINAL PAGE IS
OF POOR QUALITY

MODELING LATERAL ACCELERATION EFFECTS ON PILOT PERFORMANCE

Jonathan Korn and David L. Kleinman
Department of Electrical Engineering and Computer Science
University of Connecticut
Storrs, Connecticut 06268

[redacted]

CABS

Attendant to the direct side force [redacted] maneuver of a Vectored Force Fighter [redacted] is the transverse acceleration imposed on the pilot. This lateral acceleration (G_y), when combined with a positive G_z stress, is a potential source of pilot tracking performance impairment. A research effort to investigate these performance decrements includes experimental as well as analytical pilot performance modeling using the Optimal Control Model. [redacted]

CASA AUTHOR

I Introduction

The Vectored Force Fighter (VFF) is characterized by several new and unconventional features, specifically its capability to use direct side force (DSF) to institute a rapid transverse (lateral) maneuver independent of aircraft attitude. This maneuvering capability is potentially desirable in an air-to-air combat encounter, as it greatly increases the aircraft's mobility. On the one hand, the evading VFF provides peculiar visual cues that can not be readily interpreted by the attacker. Alternatively, the attacking VFF can significantly enhance the pilot's lateral tracking performance by virtually eliminating the time required to enter into a conventional turn.

Along with the desirable properties of the DSF maneuver, increased levels of lateral acceleration (G_y) are imposed on the pilot. This unfamiliar stress environment, which may be superimposed on the usual normal ($+G_z$) component, is an unavoidalbe result of the vectored force maneuvering. An analysis of the impact (on pilot control performance) of such uncommon acceleration is the subject of this paper.

Empirical research into the effects of off-normal acceleration stress on lateral tracking task performance was conducted by Loose, et al [1]. They found that it was "harder" to perform the task when under G_y stress, and sighted a 20% increase, from the fixed base condition, in the RMS tracking error values. These results have motivated further quantification of pilot performance under various levels of G_y stress, using tracking scores and other performance metrics. In addition, a normative pilot model, capable of predicting performance changes as a function of G_y levels has become a developmental goal. Consequently, a joint experimental/analytical program has been undertaken by the Aerospace Medical Research Laboratory (AMRL), WPAFB, and the University of Connecticut.

The experimental phase included compensatory tracking tasks in the lateral plane, and was conducted on the Dynamic Environment Simulator (DES) centrifuge. Of the various modes employed in the experiment, three are considered in this study: (1) Static - fixed base (ST); (2) Dynamic - moderate G_y stress (D1); and (3) Dynamic - strong G_y stress (D2). The experimental design and the subsequent data analysis are discussed in detail in Sections II and III.

The ensuing modeling phase resulted in a predictive performance model based upon the Optimal Control Model (OCM). The model has been modified to include the effects of a closed-loop side force combined with a constant G_z stress. The OCM parameters that are sensitive to G_y and/or G_z are identified and related quantitatively to the various accelerations. It is shown that the models developed are capable of reproducing human response characteristics such as pilot describing functions, control remnant and RMS tracking scores. Section IV details the modeling approach and results.

II Experimental Detail

The motion-visual loop used in the AMRL experiments is given in Figure 1.

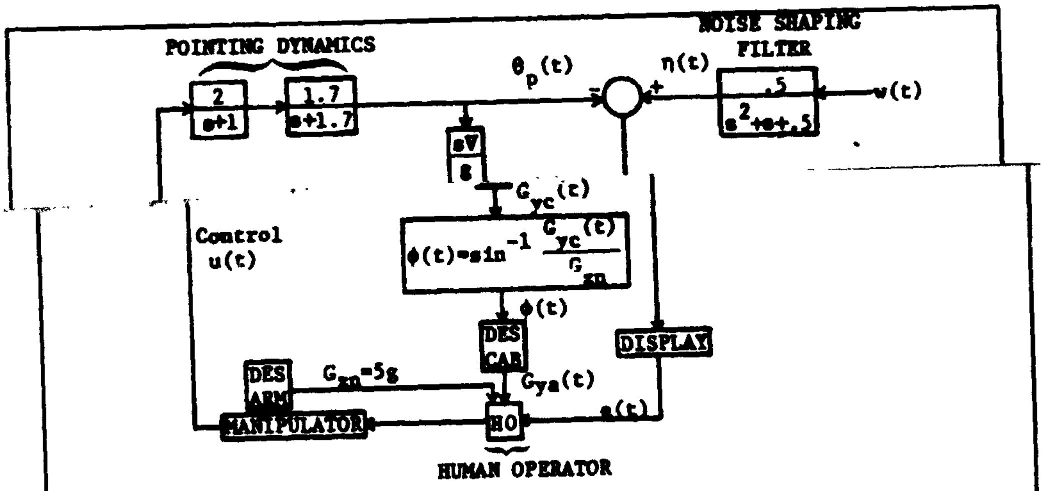

Fig. 1: THE MOTION-VISUAL LOOP

$\eta(t)$ - target excitation signal
$w(t)$ - white driving noise
$\theta_p(t)$ - vehicle pointing angle
$e(t)$ - tracking error = $\eta(t)-\theta_p(t)$
V - aircraft velocity

$G_{yc}(t)$ - commanded lateral acceleration
$G_{ya}(t)$ - attained lateral acceleration
G_{zn} - nominal normal component = 5g
$\phi(t)$ - cab commanded rotation angle
g = 32.2 ft/sec^2

Specifics concerning the lateral axis compensatory tracking task may be found in [2]. The major addition in the present experiment is the provision for the closed-loop DSF-induced motion. In order to simulate the lateral acceleration, it was necessary to centrifugate the subjects to a nominal vertical acceleration plateau ($G_{zn}=5g$), and to rotate the DES cab to produce an off-normal G_y component. The roll command input to the cab, $\phi(t)$, generated in conjunction with the pilot control signals, is directly related to the pointing angle rate, viz.,

$$\sin \phi(t) = \frac{G_{yc}(t)}{G_{zn}} , \quad G_{yc}(t) = \frac{V}{g} \dot{\theta}_p(t) \qquad (1)$$

The driving signal and the plant dynamics were designed to be in harmony with the DES capabilities.

Three experimental conditions were studied:

(1) ST mode - The control condition (static), no G_z/G_y acceleration present.

(2) D1 mode - Moderate G_y level. In this condition V=1500 ft/sec. and $G_z=G_{zn}=5g$. The resulting ensemble mean RMS level of G_{ya} was .49± .13g (see Section III).

(3) D2 mode - Strong G_y level: V=3000 ft/sec., $G_z=G_{zn}=5g$. The resulting G_{ya} RMS level was .76± .11g.

Each session included two static runs followed by a D1 run and by a D2 run. The order of employing the D1/D2 modes was alternated from one session to another in order to eliminate any possible interaction effects. Five subjects participated in a total of 20 sessions. With the removal of the outliers, ensembles of 37 static, 19 D1, and 19 D2 runs resulted.

III Data Analysis

Of the numerous time-histories that were recorded those that are pertinent to this study are the tracking error, e(t), the pilot control input, u(t), and the attained level of G_y, $G_{ya}(t)$. The data were transformed to obtain frequency domain measures which were then (across-subject) ensemble-averaged at the input frequencies. This procedure yielded the first- and second-order statistics of:

a. Pilot describing function, $H(j\omega)$ (magnitude and phase).
b. Pilot remnant, $R(\omega)$.
c. RMS scores of e(t), u(t) and $G_{ya}(t)$: s_e, s_u and $G_{y,rms}$ respectively†

It is possible now to relate modes D1 and D2 to the respective attained G_y levels. From the FFT analysis we obtain (1) D1: $G_{y,rms}=.49\pm .13g$, and (2) D2: $G_{y,rms}=.76\pm .11g$.

Figure 2 illustrates the differences in (average) pilot gain, phase, and remnant for the three experimental conditions. Table I lists the RMS scores (± one standard deviation). Multiple comparison type of ANOVA tests that have been performed on the reduced data reject a hypothesis of performance invariance among the three experimental conditions. Significant differences ($P<.05$) exist among the pilot gains, remnants and tracking error scores. These differences occur throughout virtually the entire frequency range. The phase exhibits significant differences only at the higher frequencies and no trends are evident in the control scores. Several observations are pertinent:

---

† The absolute values of s_e and s_u are determined, of course, by the driving noise (w(t)) covariance, W. In this study W=.36. For details see [2].

(1) Figure 2a clearly indicates that increased levels of lateral acceleration effect reduced pilot gains and lower control bandwidths. The gain decreases by as much as 3-4 dB between ST and D1 modes, and then further decreases an additional 3-4 dB in the D2 mode. This trend is likely a consequence of the closed-loop acceleration stress, as the subjects tend to decrease their control activity for which they are penalized by lateral jolting.

(2) An indication of a narrower control bandwidth is also manifested in Figure 2b, where increased lag at the higher frequencies with increased G_y stress, is evident. At the highest frequency (15.57 rad/sec), for example, the phase lag difference between the static and the D1 condition is as much as 26°, and up to 44° between the static and the D2 condition. In the modeling section (IV), we attribute this lagging tendency not only to a narrow control bandwidth, but also to an increased human reaction time delay.

It is our belief that the gradual pilot gain decrease and bandwidth narrowness is ascribed to G_y stress only, and that the normal acceleration component has no effect on this mode of human performance. This has been ascertained in a parallel research project reported in [3]; the control task was similar, but only G_z stress was employed—i.e. no off-normal accelerations were present. The resulting pilot transfer function (both gain and phase) remained unchanged in both control- and G_z stress condition†.

(3) Increased randomness in pilot control is another facet of the acceleration stress. Figure 2C indicates that with increasing G_y levels the pilot control remnant increases. The amount of increase is very significant: from the static condition to the D1 mode the increase is 3.9 dB on the average, and from D1 to D2—an additional 2.6 dB. This remnant increase is attributed to G_y, as well as to G_z stress. Based upon the results of [2,3], the moderate G_y level (D1) does not affect the remnant level, as in both D1 and the constant G_z stress condition [2,3] the remnant levels are precisely the same. Only the higher level of G_y stress (D2) further raises the remnant.

(4) Very significant ($P<.01$) increases in the RMS tracking error values in D1 and D2 are indicated in Table I, and depicted in Figure 6. The increase from the ST to the D1 condition is by 27% and from D1 to D2—by 18%. As in (3), these increases are partly attributed to the sustained G_z stress: a 13% increase in tracking scores was noted in the constant G_z condition in [2,3].

IV Modeling Results

The analytic model used in this effort is the OCM [4]; the modeling details are similar to those of [2,3]. The parameters in the OCM that are descriptive of human limitations are: (1) the neuromotor time constant τ_N, (2) the lumped time delay τ_D, (3) the motor noise ratio ρ_u, and (4) the error and error-rate observation noise ratios ρ_e and $\rho_{\dot{e}}$. The presence of the subject-commanded G_y acceleration, which correlates with the signal $\dot{\theta}_p$ in the visual loop, requires an additional parameter, (5) the error indifference threshold a_e. The inclusion of this parameter is based upon the assumption that a closed-loop stress increases the human's error indifference threshold. In another words, the human's consideration

---

† Reference [3] is an updated version of [2]. It has been suggested in [2] that some minor differences existed between the pilot gains in the static and the G_z stress conditions, but a subsequent statistical test did not sustain this assertion. The data base used in [3] is much broader than in [2], and these minor dissimilarities totally diminish.

ORIGINAL PAGE IS
OF POOR QUALITY

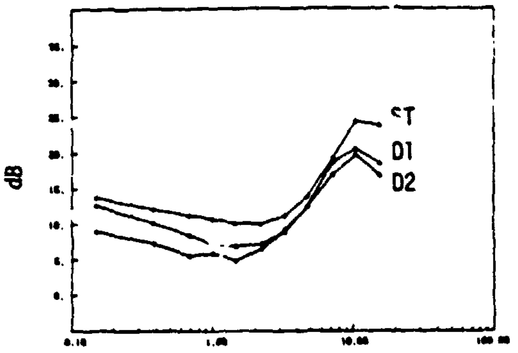

a. GAIN

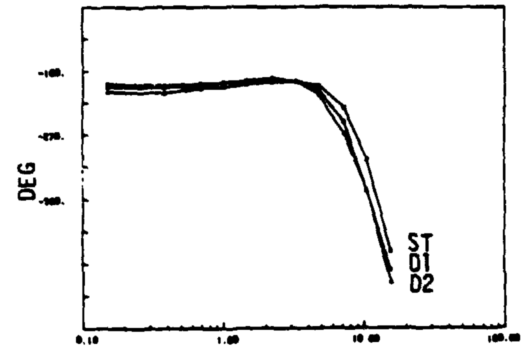

b. PHASE

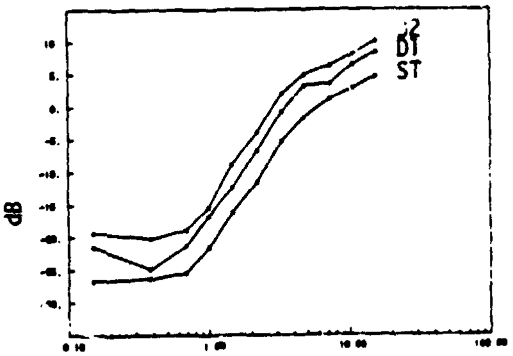

c. REMNANT

FIG. 2· COMPARISON OF MODES
ST, D1, D2

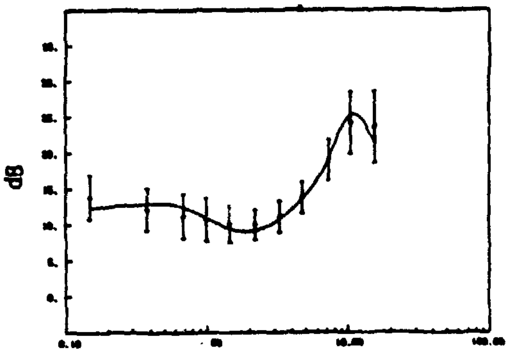

a. GAIN

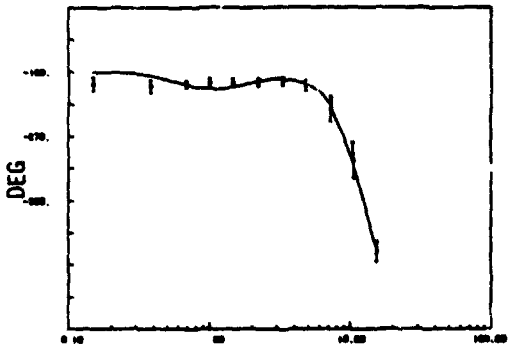

b. PHASE

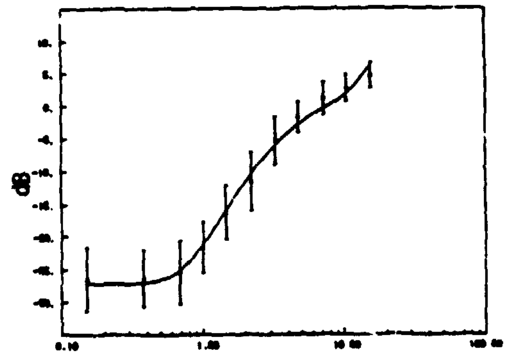

c. REMNANT

FIG. 3· MODEL-DATA COMPARISON
ST MODE.

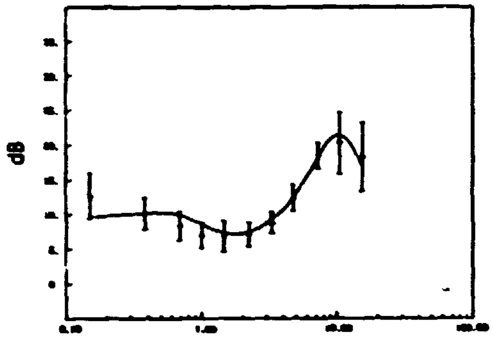

a. GAIN

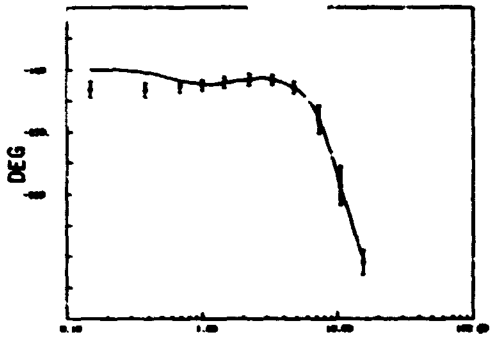

b. PHASE

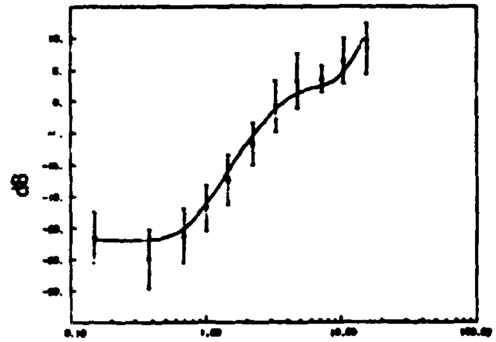

c. REMNANT

FIG. 4: MODEL-DATA COMPARISON
D1 MODE

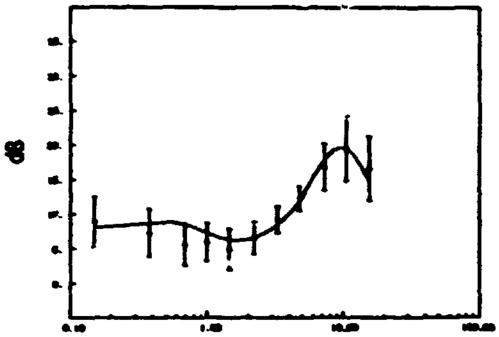

a. GAIN

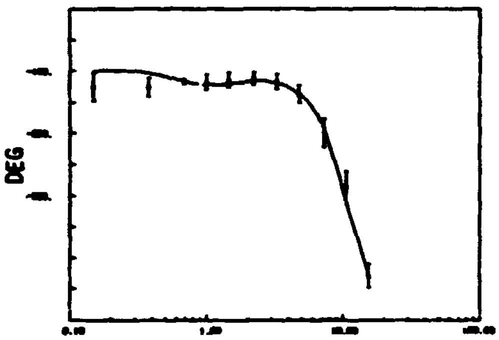

b. PHASE

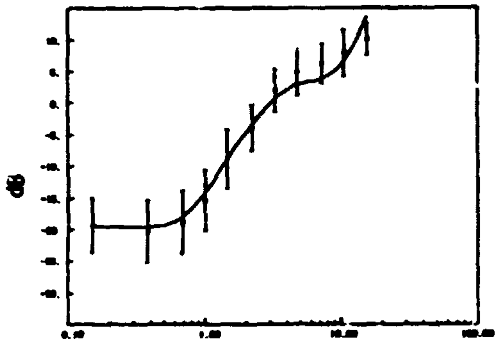

c. REMNANT

FIG. 5: MODEL-DATA COMPARISON
D2 MODE

for his own well-being is traded-off against the control task. A similar approach has been followed in another G_z closed-loop modeling effort [5].

In practice, the indifference threshold parameter is represented in the OCM by its equivalent Random Input Describing Function [6],

$$N(a_e/\sigma_e) = \sqrt{\frac{2}{\pi}} \int_{-\infty}^{-a_e/\sigma_e} e^{-\frac{x^2}{2}} \, dx \le 1. \qquad (2)$$

where σ_e is the predicted RMS tracking error. This function modifies the model in two ways [3,4,6]:

(1) Observation Noise: We replace the usual equation for computing the error observation noise V_e with

$$V_e = \frac{\pi\rho_e\sigma_e^2}{N^2(a_e/\sigma_e)} = \pi\rho_e^*\sigma_e^2 \; ; \quad \rho_e^* \triangleq \frac{\rho_e}{N^2(a_e/\sigma_e)} . \qquad (3)$$

Notice that the effective noise ratio, ρ_e^*, is the only identifiable parameter in Eq. (3).

(2) Cost Functional: The OCM assumes that the well-trained and motivated human operator adopts an optimal control strategy, subject to his inherent psychophysiological limitations. The mathematical interpretation of this statement is that the pilot, in the case at hand, will minimize the cost functional,

$$J(u) = E\left\{\lim_{T\to\infty} \frac{1}{T} \int_0^T \left[q_e e^2(t) + q_r \dot{u}^2(t)\right] dt\right\} , \qquad (4)$$

where q_e and q_r are the error and the control rate weightings. Nominally, we pick q_e=1, and adjust q_r to correspond to the requisite control bandwidth, τ_N^{-1}. Equation (4) is applicable in the absence at any threshold effects. When the error indifference threshold is no longer negligible, one should replace the displayed error in (4) with the perceived one. This yields a revised cost functional

$$J(u) = E\left\{\lim_{T\to\infty} \frac{1}{T} \int_0^T \left[q_e N^2(a_e/\sigma_e) \, e^2(t) + q_r \dot{u}^2(t)\right] dt\right\} . \qquad (5)$$

It is evident now that increased a_e effects lower weighting on the error, as should be expected. This in turn results in higher relative weighting on the control rate, and consequently an increase in the neuromuscular time constant τ_N.

Figures 3,4,5 and 6 present the identified model vs. data comparisons for the ST (control), D1, and D2 conditions. Shown are the pilot describing function magnitudes and phases, remnants, and RMS tracking errors (scores). The empirical tracking control scores (s_e, s_u) are also compared with their modeled counterparts (σ_e, σ_u) in Table I.

ORIGINAL PAGE IS
OF POOR QUALITY

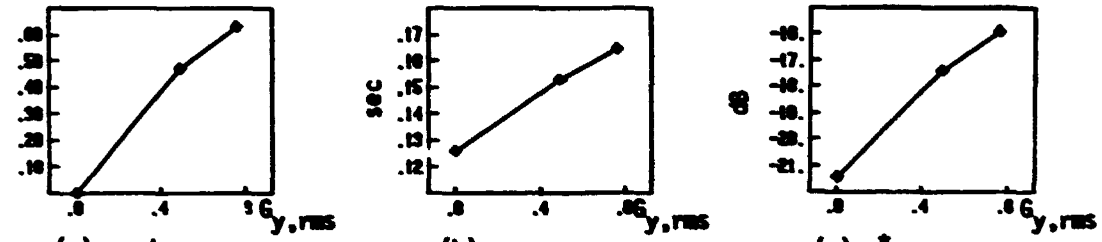

(a) a_e/σ_e (b) τ_N (c) ρ_e^*

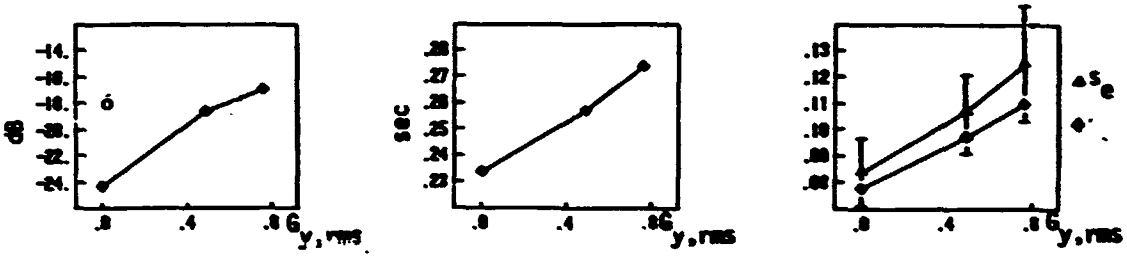

(d) ρ_u (e) τ_D (f) SCORES

FIG. 6: MODEL PARAMETERS & SCORES vs. $G_{y,rms}$
(o INDICATES OPEN LOOP G_z ONLY)

SCORES / MODE	s_e	σ_e	s_u	σ_u
ST	.083±.012	.078	.38±.10	.33
D1	.106±.015	.098	.36±.09	.32
D2	.125±.022	.110	.38±.11	.32

TABLE I RMS SCORES

PARAME / MODE	a_e/σ_e	τ_N, sec	ρ_e^*, dB	ρ_e, dB	ρ_u, dB	τ_D, sec
ST	0	.126	-21.4	-22.0	-24.3	.234
D1	.47	.153	-17.4	-21.5	-18.6	.257
D2	.63	.165	-15.9	-21.0	-16.9	.274

TABLE II MODEL PARAMETERS

The model parameters are listed in Table II, and plotted as a function of the RMS G_{ya} levels ($G_{y,rms}$) in Figure 6a-e. It is clear that almost all the parameters deviate from the static case, reflecting a performance degradation. These increases, however, can not be attributed to the G_y stress alone: the sustained positive acceleration of G_z=5g is an important factor in this performance impairment. The following is our proposed theory of how the various acceleration components affect the OCM parameters.

Error Indifference Threshold, a_e: According to our initial assumption, the threshold parameter is affected only by the closed-loop G_y stress. Figure 6a shows significant increases in the a_e/σ_e values in the D1 and D2 conditions, and it is clear that the subjects allow for larger tracking errors in order to minimize their jolting.

Neuromu... r Time Constant, τ_D: The subjects' tendency to limit their control bandwidth, under closed-loop lateral acceleration, is clearly manifested by the trend in τ_N. Figure 6b suggests a nearly linear dependence between τ_N and $G_{y,rms}$. As noted in Equation (5), the increase in τ_N is a direct result of the increase in a_e. The constant (open-loop) G_z stress has no effect on this parameter [2,3].

Observation Noise Ratio, ρ_e: Traditionally, positive acceleration stress (G_z) has been recognized as an antecedent to vision impairment. Tunnel vision, greyout, and blur are perhaps the most acknowledged symptoms of sustained G_z imposed on passive subjects (e.g. [7]). These symptoms, however, should diminish in a controlled tracking task, as the subjects perform straining maneuvers to maintain vision. We assign, therefore, the nominal value of $\rho_e = -21.4$ dB to all modes. This ρ_e value corresponds to $a_e=0$, but with the increase in the indifference threshold under G_y stress, the effective observation noise coefficient, ρ_e^*, exhibits a significant increase (Figure 6c).

Observation Noise Ratio, $\rho_{\dot{e}}$: There are insignificant variations in $\rho_{\dot{e}}$ in the three conditions. This parameter has proven to be insensitive to either G_y or G_z acceleration component, which is in agreement with [2,3].

Motor Noise Coefficient, ρ_u: This parameter mainly affects the pilot control remnant. As stated in Section III, we ascribe the remnant increase in the D1 condition to G_z stress only. Also, as shown in [3], the ρ_u value in a G_z stress situation (no G_y) is as high as in D1. It is possible, therefore, to conjecture that low to moderate levels of G_y have no substantial effect on the human's motor noise. Only increased levels of lateral acceleration (>.5g,rms) effect higher ρ_u. Higher remnant/ρ_u under G_z or G_z/G_y stress is a clear indication of decrements in motor performance. It has been widely reported that the operator psycho-motor performance is impaired under G_z stress (e.g. [8]), but no reference to G_y effects has ever been made.

Time Delay, τ_D: The reasons for the increased time-delay under G_y stress are not well understood. The increasing phase lags with increasing $G_{y,rms}$, as exhibited by the empirical data in Figure 2, clearly show the increasing response lag. However, there is no apriori reason to expect τ_D to depend on G_y. What one might be seeing is an increase in the effective delay as position information (e) is degraded relative to rate ($\dot{e}$) information. A similar phenomenon of increasing τ_D occurs when a tracking display is moved into the peripheral field.

V Conclusions

An investigation of the effects of a direct side force (DSF) maneuver on pilot tracking performance has been undertaken. The research includes G_y/G_z-stress tracking experiments, and pilot performance modeling using the OCM.

It is suggested that the human operator admits larger tracking errors, under closed-loop G_y stress, by increasing his error indifference threshold. Consequently, in an attempt to ameliorate his lateral acceleration, the subject adopts a control strategy that lowers his gain and constrains his bandwidth. In addition, an increased phase lag in the pilot transfer function is observed, when under G_y stress. The pertinent OCM parameters: the indifference threshold, the neuromotor time-constant, and the operator time-delay all increase, causing substantial performance degradation. We attribute these parameter deviations to G_y stress alone, as past research has shown that open-loop (and constant) G_z stress had no effect on these modes of human performance.

However, we surmise that the increase in pilot control remnant, as modeled by a commensurate increase in the motor noise parameter, is primarily ascribed to G_z stress. Based upon past research, we postulate that only the stronger G_y stress levels affect the operator motor performance, whereas low to moderate levels have no significant effect.

References

1. Loose, D. R., K. W. McElreath and G. Potor, Jr., "Effects of Direct Side Force Control on Pilot Performance," AMRL-TR-76-87, Aerospace Medical Research Laboratory, WPAFB, Ohio.
2. Korn, J., D. L. Kleinman and D. W. Repperger, "Frequency Domain Measures of Human Performance under G-Stress," Proceeding of the 18th IEEE Conference on Decision & Control, December, 1979.
3. Korn, J., "Modeling Human Operator Performance in Aerial Tracking Task," work in progress.
4. Kleinman, D. L., S. Baron and W. H. Levison, "A Control Theoretic Approach to Manned-Vehicle Systems Analysis," IEEE Transaction on Automatic Control, Vol. AC-16, No. 6, 1971.
5. Korn, J., H. S. Boal and M. M. Vikmanis, "Modeling Human Tracking Performance in a High G-stress Environment," Proceedings of the 1978 Conference on Decision and Control, January 1979.
6. Kleinman, D. L. and S. Baron, "Analytic Evaluation of Display Requirements for Approach to Landing," BBN Report 2075, Bolt Beranek and Newman, Inc., Cambridge, Mass. March, 1971.
7. White, W. J., "Variations in Absolute Visual Thresholds during Acceleration Stress," WADD Technical Report 60-34, Wright Air Development Division, WPAFB, Ohio.
8. Brown, J. L. and M. Lechner, "Acceleration and Human Performance," Aviation Medicine, February 1956.

N82 34059

D22

A COMPREHENSIVE SYSTEM MODEL FOR MOTION/SPACE SICKNESS — PRELIMINARY RESULTS*

Susan A. Riedel
Systems Technology, Inc.
Hawthorne, California

ABSTRACT

Recent motion sickness research literature puts forth several promising conceptual theories which attempt to "model" various portions of the motion/space sickness syndrome. Perhaps the most inviting of these is the "sensory conflict" theory, advanced by Reason and others, which suggests that the barrage of sensory orientation cues from the eyes, vestibular system, proprioceptors, etc., are interpreted and even modified by a central "comparator" in the brain, with respect to a "neural store" of expected correlations in normal experience. This theory qualitatively explains many of the observed motion/space sickness phenomena; yet, no comprehensive quantitative system model exists for researchers to exercise. Such a system model of motion/space sickness is needed to: categorize and order the observed facts into a rational structure; efficiently encode the measured data and dynamic processes; and reveal key experiments needed to predict and/or prevent motion sickness on earth and in space.

This paper reports a preliminary attempt to satisfy the first of these goals. It presents an "array of key facts" as assembled from the recent literature, consisting of a collection of motion/space sickness observations which should be accounted for in the comprehensive model. A model structure which is responsive to the "array of key facts," as well as to the other requirements of a working research tool (modularity, ease of use, conciseness, etc.) is also suggested.

INTRODUCTION

The seeming complexity of motion sickness in all of its manifestations has kept untold numbers of researchers busy for at least the past 40 years. An overwhelming amount of data has been collected, observations made, preliminary conclusions drawn. Research worldwide has covered a large range of interest, using human subjects and animal subjects, measuring physical, psychological, behavioral, and autonomic variables, with the goal of discovering causes and cures of this debilitating affliction. Even its most fundamental effect, nausea, is puzzling; as Treisman[1] points out, motion sickness symptomatology has no logical survival benefit in an evolutionary sense.

---

*This research is sponsored by the National Aeronautics and Space Administration under Contract NAS2-10430; the technical monitor is Melvin Sadoff.

Recently, a theory has been advanced by Reason[2], Benson[3], and others which appears to tie much of the motion sickness research results together. This so-called "sensory conflict" theory states that various physiological sensors combine with a set of psychological expectations, sometimes resulting in a sensory conflict: motion/space sickness. Qualitatively, this theory explains many of the observed phenomena associated with motion/space sickness. But the need still exists for a comprehensive, dynamic (time domain) model which predicts the time course of motion sickness as a function of the environmental inputs and mediating or ameliorative actions. Such a model should:

1) Quantitatively account for the key facts of the motion sickness syndrome which have been identified by research to date.

2) Catalog these effects in an orderly and efficient way.

3) Identify key experiments designed to validate and test the model in various ways.

4) Provide more precise measures and methods for predicting individual susceptibility.

5) Suggest treatments geared to prevent motion/space sickness.

These are the objectives of the modeling effort described here.

RESEARCH GOALS AND METHODOLOGY

In order to accomplish these goals, a three-year, three-phase research effort has begun at Systems Technology, Inc. The ultimate hope is to better understand, logically organize, and render predictive the large amount of data which has arisen out of the motion/space sickness research to date. To this end, the current research plan is structured as follows.

Phase I: Survey and Tentative Model Development

Three separate items comprise this phase. The first is a search of the available literature on motion/space sickness, concentrating on two major areas: key facts which describe motion sickness in a dynamic, quantified way; and all types of models developed in the past relating to motion sickness and its peripheral areas. Visits to several key research facilities are planned so that ongoing work may be incorporated in the model as well. These visits are also a first step in establishing open communication lines with the motion sickness research community so that the model will become an interactive basis for the exchange of ideas in this field.

The second work item will assemble the results of the literature search into an "array of key facts" which relate to motion sickness and must be accounted for and predicted by the comprehensive model. In constructing this fact array the following criteria will be used:

- Degree of concordance among investigators.
- Degree of ubiquitousness among various forms of motion sickness.
- Availability of appropriate quantitative input/output information.
- Existance of a model which accounts for this effect.
- Interrelation with other elements in the fact array.
- Priority of the effect within the array.

The final step in this first phase is to suggest a tentative model structure which accounts for the array of key facts and the interactions among the array elements. An eclectic policy will be adopted, such that the best and most appropriate type of model will be incorporated in each subsystem. Since many models already exist for various portions of the comprehensive model, the majority of effort in this task will be establishing the interconnections among these several parts.

Phase II: Validation, Refinement and Computerization

Validating the model developed in Phase I consists of obtaining the predicted set of outputs to a given set of inputs, such that the key facts assembled in Phase I are all taken into account. Validating the model is also tied in with model refinement as a three-step process: 1) exercise the model to match existing data or predict new results; 2) perform experiments to verify predicted results or obtain new results; and 3) update the model accordingly. Computerization of the comprehensive model satisfies the need for a user-oriented tool which is readily available to the entire research community. To this end, an interactive FORTRAN software package is envisioned such that the tool will be readily usable by a wide range of practitioners, who need not be familiar with the detailed mechanization. The Phase II goals can be realized only if a flexible, modular structure serves as the foundation for the comprehensive model.

Phase III: Applications, Space Experiments, and User's Guide

This phase covers the maturing stages of the model development as the tool is made available to researchers in the form of a User's Guide to the software. It is anticipated that once the model is used in a variety of applications, and from a wealth of different viewpoints, the maturing process will be hastened by new experiments and a constantly enlarging data base. Particularly interesting are potential applications of the model in 0 g environments (e.g., the Space Shuttle), since concerns centering around preventing space sickness among Space Shuttle crews originally motivated this search for a comprehensive motion/space sickness model.

The remainder of this paper presents work completed and ongoing in Phase I. Areas addressed are modeling principles, the array of key facts, and a preliminary model which incorporates some of the key facts. It is clear that this model-building effort would be enormous were it not for the solid groundwork provided by past researchers. Perhaps the significance of this past work will become more apparent when seen in the context of an overall dynamic process. The ultimate goal in constructing such a model is to provide an arena where the interrelationships can be observed and evaluated as a routine element in motion sickness research.

CONSIDERATIONS IN MODELING

Before the array of facts is assembled from the modeling viewpoint it is important to identify the major considerations in modeling. There are two important concerns which must be addressed: the types of models which will form subsections of the comprehensive model; and the characteristics essential to the proposed model. These concerns will be discussed next.

In defining the types of models to incorporate in the overall model the present point of view is that of a systems engineer describing the inputs and outputs of a complex dynamic process — the human subsystem involved in motion sickness. Thus, it is important to allow leeway in assembling the model, such that the best types of models are used where they are most appropriate. The model types include:

- Conceptual models. These are the most important starting points as they are a culmination of insight, mechanisms, and qualitative assessments of interacting elements. Since such models are not quantitative, however, they are of limited predictive value for specific problems.

- Input/output models. The logical extension of a conceptual model is a numerically exercisable "math" model which encodes known data in a veridical and efficient way. So-called "input/output" system models require knowledge of the functional relationships (statistical or signal correlations) of the system under study, although the detailed internal mechanisms need not be specified. Dynamic system models are appropriate for several motion sickness subsystems, and an existing arsenal of mathematical tools and system identification techniques can be brought to bear on the problem. Previous successes using this approach are evident in the literature.[4-8]

- Physical models. Whenever the fundamental physical processes of a given subsystem are well understood, a detailed physical math model can be constructed. For some of the human subsystems involved in motion sickness such models do indeed exist (e.g., semicircular canals and otoliths,[9-12]). Yet, for several reasons, other physical models which are desirable for the comprehensive model may be a long way off: mechanisms are poorly understood and not readily quantified; the process is partly psychological; the complexity necessary to capture essential details makes a complete physical model impractical.

- Living models. In motion sickness research, much use is made of animal models and human models in investigating environmental, psychological, and drug effects as manifested in motion sickness. When such models are feasible, they lend much insight into the motion sickness syndrome as a whole. This permits an important glimpse at the overall picture, but often imposes a problem when trying to sort out specific aspects, symptoms, causes, and effects. In addition, the use of animal models imposes the problems of scaling the effects between animal and human and of experimental protocol constraints.

The second consideration in modeling defines the characteristics desirable for the proposed comprehensive model. The key requirements are enumerated as follows:

- Modular. It is important to maintain a subsystem approach to facilitate updates, revisions, and corrections and also to aid in computerization.

- Dynamic. The time course of symptoms, adaptation, and habituation should be represented.

- Interactive. The modular interconnections are important here in understanding the overall motion sickness picture. And, in the other sense of "interactive," the computerized model will be user-oriented and user-interactive, both fundamental ingredients for a useful tool.

- Nonlinear. Many important aspects of motion sickness are best represented by nonlinear elements such as thresholds, saturations, and allocation algorithms.

- Quantitative. Validation of the model demands that key experimental results be predicted in a quantitative sense by exercising the model.

- Functionally Isomorphic. Architecturally, the subelements of the model will have a functional structure which is an isomorph with its human counterpart. This allows modules to be identified with distinct human elements (labyrinth, eyes, neck proprioceptors, etc.) even if a detailed physical model is not available for the particular element.

- Computationally Efficient. A comprehensive model which is difficult, time consuming, or expensive to exercise will find few users in the research laboratories, no matter how accurate it is. Care must be taken in constructing the software package and in preparing the user's guide so as to assure its efficiency for a wide range of users.

- Validated. The refinement and validation of the model is an ongoing process as new data are forthcoming, new experiments are suggested, and increased understanding of interconnections is gained. The model structure must be such as to readily acoomodate validation and subsequent refinement.

- Predictive. It is essential that the motion sickness model be predictive, so that its continued validation, refinement, and use be extended to new situations. Then it can serve as an integral part of motion sickness technology and not merely as a computerized "library" of experimental results.

- Insightful. The ubiquitousness of the motion sickness syndrome implies that some very basic cause-effect relationships are involved. It is hoped that the construction of this comprehensive model will illuminate these basic "motion sickness principles," which have heretofore been unclear.

The types of models which may potentially comprise the comprehensive model, and the fundamental characteristics to which the model must adhere, have been discussed. The final section suggests a start at encoding some key facts in motion sickness within the prescribed structural boundaries.

MODELING THE ARRAY OF KEY FACTS

As an example of the procedures involved in structuring t .omprehensive model, some of the key facts gleaned from a survey of motion s ckness literature have been used to construct a foundation for the model. An attempt is made to begin at the most fundamental levels, defined by those elements of the fact array which are most universally reported and agreed upon. Building from this baseline, embellishments and refinements are made which account for more elements in the array. When care is taken in modular construction, the formulation of this architectural hierarchy should progress smoothly.

The first four elements culled from the fact array serve as the baseline for the model:

1) Labyrinthine defective subjects are immune to motion sickness.[13-16]

2) Motion sickness symptoms can be induced by pure visual stimulus.[17-19]

3) Motion sickness symptoms can be induced by pure motion stimulus.[20-21]

4) Motion sickness symptoms can often be attenuated by drugs, training, and/or habituation.[13,31,32,41,53,59,60,61]

Together, these widely-agreed-upon and well-validated facts specify some of the key components in the model. In order to accommodate each of the facts, the model must include the vestibular system, the visual system, a neuro-chemical system whereon drugs may act, a "learning center" (presumably in the central nervous system) to include training and habituation effects and a nauseogenic system which actually produces the motion sickness symptoms. The sensory conflict theory discussed briefly in the Introduction appears to be an appropriate conceptual model which structures the elements and their interconnections in a global model, such as shown in Fig. 1.

In order to begin validating the model suggested by the Fig. 1 structure, the various element blocks must be replaced by mathematical models which can generate quantitative data for a given visual/motion environment. This necessitates a return to the fact array.

5) The vestibular system is composed of the semicircular canals, which respond to head angular acceleration and indicate head angular velocity, and the otoliths, which sense gravity and linear acceleration and indicate static head orientation with respect to vertical.[2,10,22-23]

6) The visual system senses linear and angular velocity.[19,24]

7) The semicircular canals may be modeled as a damped torsion pendulum.[10,23,25-26]

8) The otoliths may be modeled as linear accelerometers with threshold and neurological adaptation.[9,25-26]

These facts suggest replacement of the "vestibular system" and "visual system" blocks of Fig. 1 with the linearized approximate mathematical models shown in Fig. 2. As suggested in the discussion on modeling, the global model is separated into a set of modules, and Fig. 2 presents only the modules for the visual and vestibular systems. Note that the particular mathematical representations of the physical systems shown in the figure are only one example of the possible models which could be used. Also, important details such

ORIGINAL PAGE IS
OF POOR QUALITY

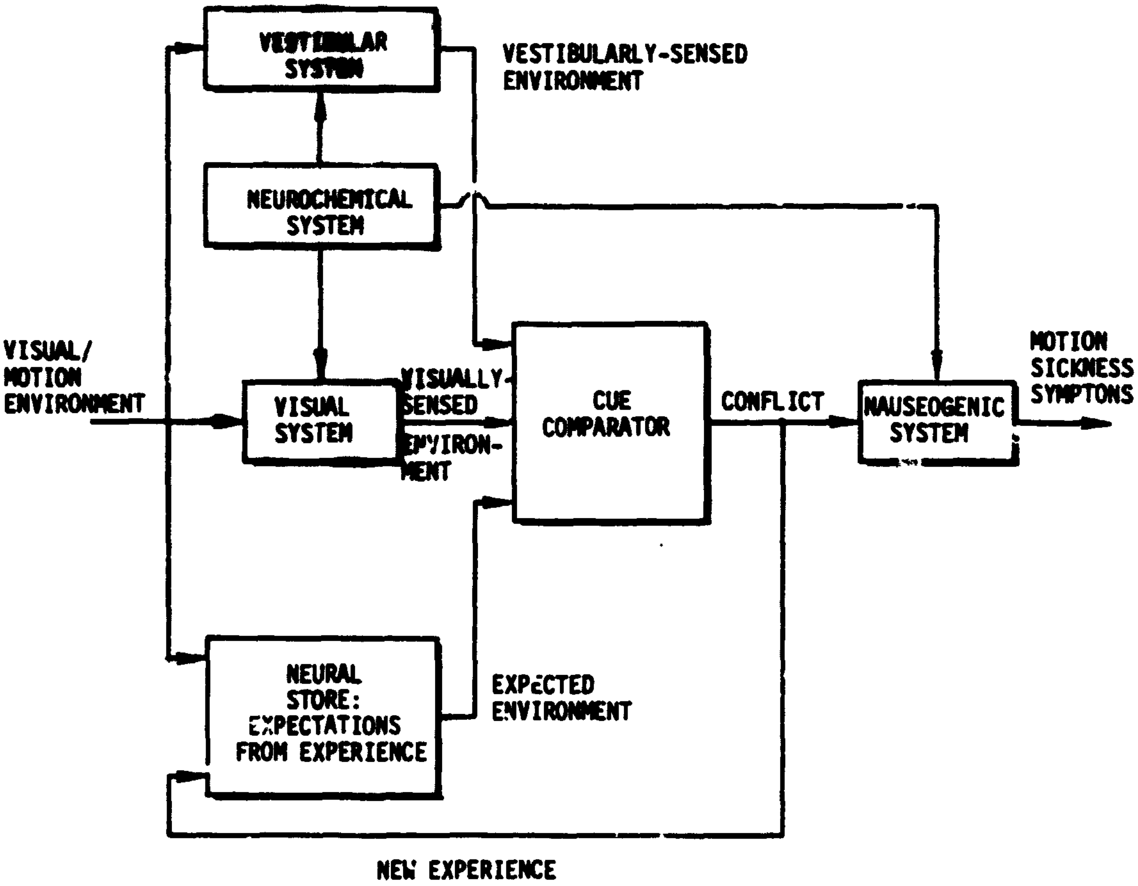
VESTIBULAR SYSTEM
VESTIBULARLY-SENSED ENVIRONMENT
NEUROCHEMICAL SYSTEM
VISUAL/ MOTION ENVIRONMENT
VISUAL SYSTEM
VISUALLY-SENSED ENVIRONMENT
CUE COMPARATOR
CONFLICT
NAUSEOGENIC SYSTEM
MOTION SICKNESS SYMPTONS
NEURAL STORE: EXPECTATIONS FROM EXPERIENCE
EXPECTED ENVIRONMENT
NEW EXPERIENCE

Figure 1. Comprehensive Model: Global Structure Based on Conceptual "Cue Conflict" Model

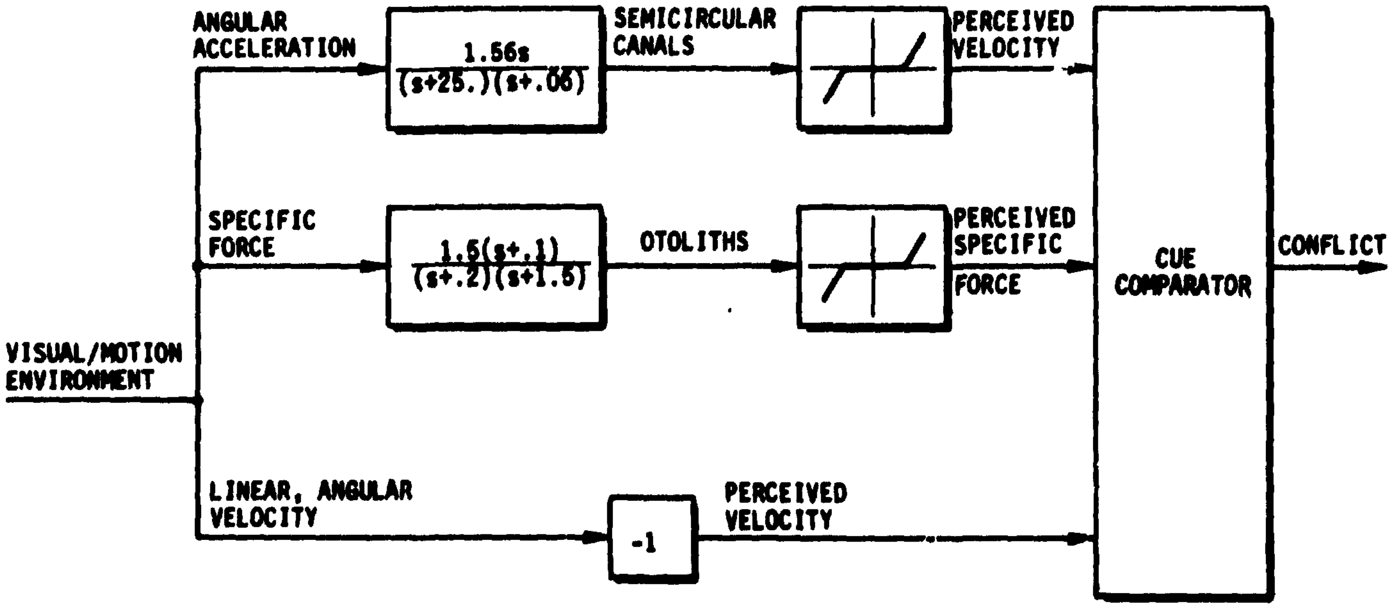
ANGULAR ACCELERATION
$\frac{1.56s}{(s+25.)(s+.06)}$
SEMICIRCULAR CANALS
PERCEIVED VELOCITY
SPECIFIC FORCE
$\frac{1.5(s+.1)}{(s+.2)(s+1.5)}$
OTOLITHS
PERCEIVED SPECIFIC FORCE
CUE COMPARATOR
CONFLICT
VISUAL/MOTION ENVIRONMENT
LINEAR, ANGULAR VELOCITY
-1
PERCEIVED VELOCITY

Figure 2. Comprehensive Model: Vestibular and Visual System Detail

C-5

as the vestibulo-ocular reflex (wherein eye movements may be evoked by purely vestibular stimuli) and the eye stabilization system have not yet been added.

As an example of an even finer level of detail, further key facts which more carefully explore the cue comparator structure are examined next.

9) Vestibular signals dominate in the short-term (high frequency) determination of acceleration, while visual signals provide long-term (low frequency) velocity information.[26,27]

10) When vestibular cues confirm visual cues, the vestibular cues are weighted slightly; when a conflict occurs, vestibular sensations dominate.[28]

11) Cross-coupled or Coriolis accelerations provoke motion sickness due to a canal-otolith conflict.[11,21,29]

12) Rapid head movements in weightlessness cause motion sickness, possibly due to absence of otolith indication of 1 g environment.[29-34]

These facts suggest a comparator structure composed of two separate elements: one which compares vestibularly perceived velocity with visually perceived velocity, and another which compares semicircular-canal-deduced orientation with otolith-deduced orientation. In each case the conflict can arise from two signals which conflict, or one signal which does not confirm the other signal (i.e., one signal is absent). Thus, the "comparator" not only compares the two signals against each other, but may also compare each signal against its "expected" value, which may be dependent on past experience, mental set, training, etc.

The comparator model has quickly become quite complex, but as an example, consider just the semicircular canal-otolith conflict, which manifests itself via the Coriolis acceleration motion profile. Figure 3 shows the three levels of comparison possible: direct canal-otolith comparison; comparison between actual and expected canal signals; and comparison between actual and expected otolith signals. The manner in which signals are weighted in the comparison process and the precise definition of "conflict" have not yet been included in the cue comparison module. In addition, a similar subsection of this module which compares vestibular and visual cues has not been shown in the figure.

SUMMARY

Only a brief sketch of the methodology for constructing a comprehensive motion/space sickness model has been presented. A global structure was established and more detailed specification of several component modules was undertaken. Much work remains, as suggested by the other elements in the key fact array. Areas of interest include the neuro-chemical system and attendant drug effects, the neural store as it is realized in habituation, training, adaptation, etc., and the various nauseogenic symptoms which arise from very different visual and motion environments. The appendix contains the full array

ORIGINAL PAGE IS
OF POOR QUALITY

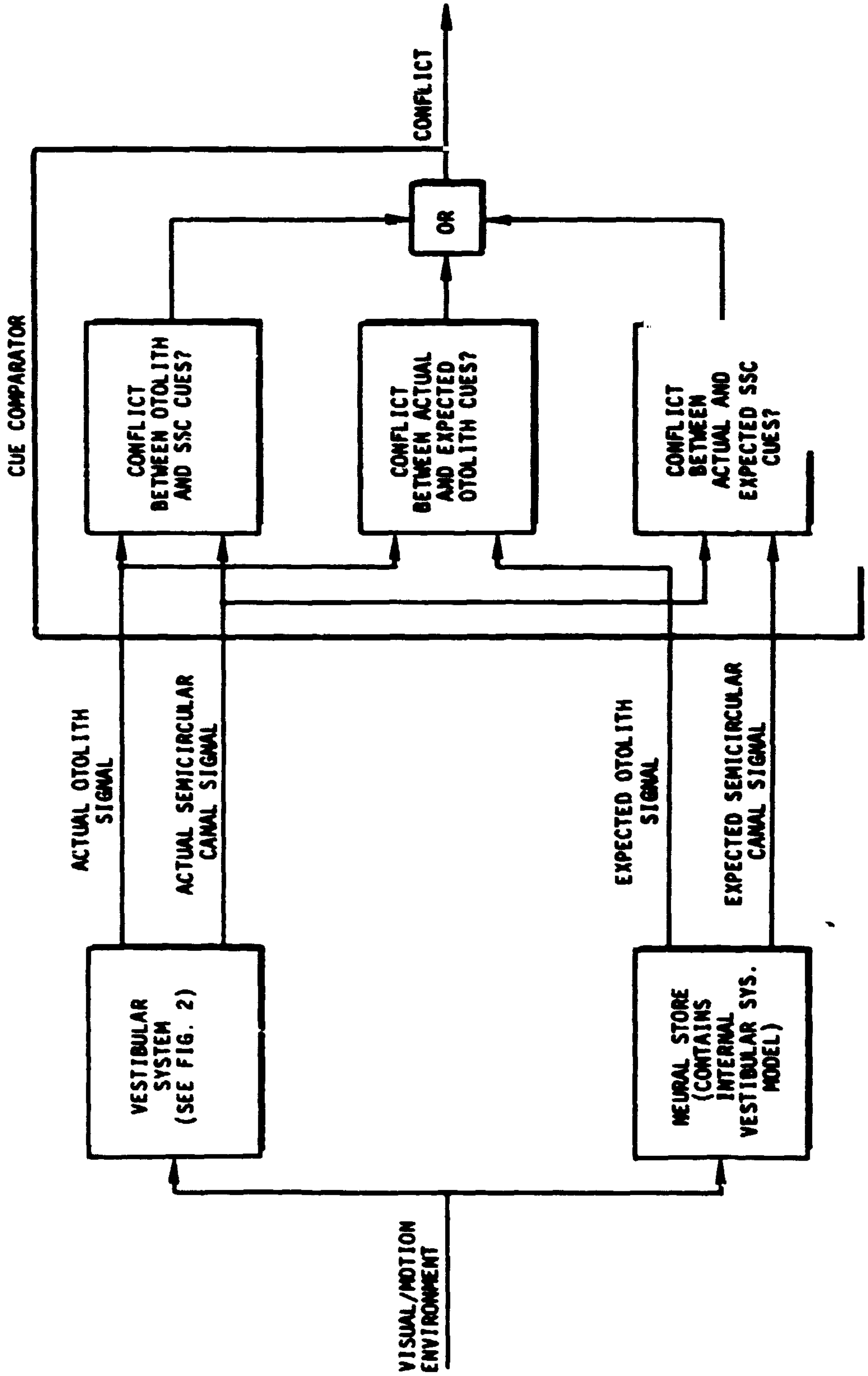
VISUAL/MOTION ENVIRONMENT
VESTIBULAR SYSTEM (SEE FIG. 2)
NEURAL STORE (CONTAINS INTERNAL VESTIBULAR SYS. MODEL)
ACTUAL OTOLITH SIGNAL
ACTUAL SEMICIRCULAR CANAL SIGNAL
EXPECTED OTOLITH SIGNAL
EXPECTED SEMICIRCULAR CANAL SIGNAL
CUE COMPARATOR
CONFLICT BETWEEN OTOLITH AND SSC CUES?
CONFLICT BETWEEN ACTUAL AND EXPECTED OTOLITH CUES?
CONFLICT BETWEEN ACTUAL AND EXPECTED SSC CUES?
OR
CONFLICT

Figure 3. Comprehensive Model: Cue Comparator Logic for Pure Vestibular Conflict

of key motion/space sickness facts assembled to this point; these facts and others from ongoing research will be employed in the continuation of this model-building effort.

APPENDIX

ARRAY OF KEY MOTION/SPACE SICKNESS FACTS

Role of the Vestibular System

Labyrinthine defectives (LDs) do not get motion sick.[15,16]

LDs never experience the inversion illusion.[14]

LDs exhibit greater levels of A- and E-phenomena bias than normals, and the patterns of apparent tilt vs. actual tilt are different.[35]

Motion Environments Causing Sickness (Canal-Otolith Conflict)

Coriolis acceleration: canals provide erroneous signals.[36]

Direct correlation exists between stressor induced by head movement and chair rotational velocity.[29]

Necessary parameters in predicting the magnitude of the cross-coupled angular acceleration disturbance are both the magnitude of the individual sensory cues and the magnitude of the geometric mismatches among them.[37]

Vertical oscillation: most nauseogenic frequency is around 0.2 Hz. Sickness diminishes above that and is nonexistent above 0.6 Hz.[2]

The probabilistic assumption that each component in a sum-of-sinusoids vertical oscillation profile acts independently, and thus their individual nauseogenic effects add, does not hold true.[38]

Aubert and Mueller effects (E- and A-phenomena): lateral tilt with no visual reference induces an overcompensating bias in subjective estimation of tilt angle at 15-20 deg (E-phenomena) and an undercompensating bias at larger angles (A-phenomena).[39]

The A- and E-phenomena angle estimation profiles vary as a function of g-level.[40]

Weightlessness/zero-g motion sickness may be induced merely by moving the head in zero g.[34]

Increased freedom of movement in a weightless environment causes increased susceptibility to motion sickness.[33]

Head movements are essential to produce motion sickness in zero g.[41,42]

Symptoms of motion and space sickness are virtually identical.[43]

Cross-coupled angular acceleration motions are particularly effective in inducing motion sickness in zero g.[29]

Return to normogravic environment from zero g is accompanied by feelings of instability and postural disturbance, rather than nausea and vomiting.[41,42]

In roller coaster flight (parabolic maneuvers) it is found that susceptibility to x-axis acceleration changes in higher than to z-axis acceleration changes in eliciting motion sickness.[48]

Correlation is found between modified Müller-Aubert-test, optokinetic nystagmus asymmetries, and susceptibility to roller coaster flight sickness.[48]

Visual Environments Causing Sickness (Visual-Vestibular Conflicts)

Visually induced sensation of motion can cause symptoms of motion sickness.[17]

Peripheral field must be stimulated in order to induce self motion.[44]

Background field stimulation dominates over foreground field stimulation.[33]

Spatial frequency determines the intensity of the self-motion illusion.[24]

Pitch and roll visually induced self motion is strongly dependent on head position, suggesting that these sensations are limited by otolith cue conflict.[45]

Subjects experience stronger sensations of pitching down than pitching up.[45]

Pitch asymmetry is fixed with respect to the head, rather than to the subjective impression of "down," indicating that its origin is visual rather than vestibular.[45]

Visually induced tilt presents a paradoxical illusion of continuous body and target movement combined with limited sensed displacement of both; this constrains the apparent induced shift.[46]

Circularvection: angular acceleration detection thresholds are increased when acceleration opposes circularvection direction, implying that the vestibular threshold is not purely mechanical.[28]

Linearvection: detection thresholds for backwards LV are consistently smaller than for forwards LV.[19]

Delay in LV onset is attributed to short term (high frequency) vestibular dominance (LV is most compelling when acceleration to constant velocity is below the vestibular threshold).[19]

Breakdown of the pursuit reflex and suppression of the vestibulo-ocular reflex occur over the same frequency region, implying a similarity of mechanisms.[47]

Vestibular Coriolis effects and optokinetically induced pseudo-Coriolis effects cannot be distinguished qualitatively.[18]

Optokinetic motion sickness symptoms are very different from those elicited via vestibular stimulation. Also, execution of head movements decreases self-rotation illusions and decreases motion sickness incidence.[49,50]

Combined Visual/Motion Environments Causing Sickness

Vestibular signals dominate in the short term determination of acceleration, while visual signals provide long-term velocity information.[27]

When vestibular cues confirm visual cues, the vestibular cues are weighted slightly; when a conflict occurs, the vestibular sensations dominate.[28]

Vestibular stimulation can modify the visual evaluation of image motion.[51]

Oculogravic illusion: apparent visual field motiondue to otolith stimulation.[26,52]

In weightlessness, objects viewed against a dark background appear displaced downward, while after-images move oppositely when the g-load is removed.[63-65]

Oculogyral illusion: apparent visual field motion due to semicircular canal stimulation.[26,66]

Drug Effects

Optokinetic and vestibular motion sickness are similarly affected by anti-motion-sickness drugs, implying a common pathway for both.[53]

Drug combinations which act synergistically to reduce motion sickness include an anti-cholenergic and a sympathemimetic.[13]

Anti-motion-sickness drug effects: increase subjective acceleration thresholds; diminish post-rotational nystagmus; most probable site of action is vestibular nucleic synapses.[53]

Drugs successful in treating motion sickness also seem to retard symptoms of dysmetric dyslexia and dyspraxia.[54]

ORIGINAL PAGE IS
OF POOR QUALITY

Psychological Factors

Field-independent subjects make a priori assumptions about a given motion environment based on past experience and, when confronted with a new situation, produce motor responses which may be inappropriate for the environment. Field-dependent subjects produce motor responses directly in response to the current environment. Field-independents are more susceptible than field-dependents to motion sickness.[55]

Field-independents are more likely to experience simulator sickness than field-dependents.[56,57]

Vestibular thresholds increase if workload increases.[58]

Vestibular thresholds decrease if subject has prior knowledge of motion profile.[58]

Adaptation, Habituation, Training

Active head/body movements are superior to passive in developing adaptation.[31,32,59,60]

Least disturbing/most efficient means to Coriolis acceleration adaptation is without visual reference.[21]

Adaptation to zero g occurs within 3-6 days and symptoms never recur.[32]

Coriolis accelerations are very provocative on the ground and in transient weightlessness, but after adaptation to zero g they are ineffective in producing motion sickness.[30,31]

Adaptation to zero g does not transfer to seasickness.[31]

Motion sickness susceptibility to Coriolis stimulus does not accurately predict susceptibility to space sickness.[36]

Autogenic feedback training is a compelling and successful technique for adaptation to motion-sickness-causing environments.[61]

Miscellaneous Facts

Visual cues dominate proprioceptive cues in determining limb and body position.[62]

REFERENCES

[1] Treisman, M., "Motion Sickness: An Evolutionary Hypothesis," Science, Vol 197, 1977. pp. 493-495.

[2] Reason, J. T., "Motion Sickness: Some Theoretical and Practical Considerations," Applied Ergonomics, Vol. 9, No. 3, 1978, pp. 163-167.

[3] Benson, A. J., Possible Mechanisms of Motion and Space Sickness, RAF Inst. of Av. Med., 1977.

[4] Jex, H. R., and R. E. Magdaleno, "Biomechanical Models for Vibration Feedthrough to Hands and Head for a Semisupine Pilot," Av., Space, and Environ. Med., Vol. 49, No. 1, Jan. 1978, pp. 304-316.

[5] McRuer, D. T., and E. S. Krendel, Mathematical Models of Human Pilot Behavior, AGARD-AG-188, Jan. 1974.

[6] McRuer, D. T., and H. R. Jex, "A Review of Quasi-Linear Pilot Models," IEEE Trans., Vol. HFE-8, No. 3, Sept. 1967, pp. 231-249.

[7] McRuer, D., "Human Dynamics in Man-Machine Systems," presented at 7th Triennial IFAC World Congress, Helsinki, June 1978.

[8] Kleinman, D. L., S. Baron, and W. H. Levison, "An Optimal Control Model of Human Response, Parts 1 and 2," Automatica, Vol. 6, 1970.

[9] Young, L. R., and J. L. Meiry, A Revised Dynamic Otolith Model, AMRL-TR-66-209, 1968.

[10] Ormsby, C. C., Model of Human Dynamic Orientation, NASA CR-132537, Jan. 1974 (also MIT, Ph.D. Thesis).

[11] Young, L. R., "A Control Model of the Vestibular System," presented at IFAC Symposium of Technical and Biological Problems in Cybernetics, Yerivan, Armenia, Sept. 1968.

[12] Van Egmond, A. A. J., J. J. Groen, and L. B. W. Jonkees, "The Mechanics of the Semicircular Canal," J. Physiology, Vol. 110, 1949, pp. 1-17.

[13] Money, K. E., "Motion-Sickness," Physiol. Rev., Vol. 50, Jan. 1970, pp. 1-35.

[14] Graybiel, A., and R. S. Kellogg, "The Inversion Illusion in Parabolic Flight: Its Probable Dependence on Otolith Function," Aerosp. Med., Vol. 38, 1967, pp. 1099-1103.

[15] Kellogg, R. S., R. S. Kennedy, and A. Graybiel, Motion Sickness Symptomatology of Labyrinthine Defective and Normal Subjects During Zero Gravity Maneuvers, AMRL, June

[16] Kennedy, R. S., A. Graybiel, R. C. McDonough, and F. D. Beckwith, *Symptomatology Under Storm Conditions in the North Atlantic in Control Subjects and in Persons with Bilateral Labyrinthine Defects*, Nav. Sch. of Av. Med., NSAM-928, May 1965.

[17] Miller, J. W., and J. E. Goodson, "Motion Sickness in a Helicopter Simulation," *Aerosp. Med.*, Vol. 31, 1960, pp. 204-212.

[18] Dichgans, J., and Th. Brandt, "Optokinetic Motion Sickness and Pseudo-Coriolis Effects Induced by Moving Visual Stimuli," *Acta Otolaryng.*, Vol. 76, 1973, pp. 339-348.

[19] Berthoz, A., B. Pavard, and L. R. Young, "Perception of Linear Horizontal Self-Motion Induced by Peripheral Vision (Linearvection): Basic Characteristics and Visual-Vestibular Interactions," *Exp. Brain Res.*, Vol. 23, 1975, pp. 471-489.

[20] Barnes, G. R., *Vestibulo-Ocular Responses to Head Turning Movements and Their Functional Significance During Visual Target Acquisition*, Univ. of Surrey, England, Ph.D. Thesis, 1976.

[21] Reason, J. T., and E. Diaz, *The Effects of Visual Reference on Adaptation to Coriolis Accelerations*, Flying Personnel Res. Comm., London, Rept. FPRC-1303, May 1970.

[22] Young, L. R., C. M. Oman, R. E. Curry, and J. M. Dichgans, "A Descriptive Model of Multi-Sensor Human Spatial Orientation with Applications to Visually Induced Sensations of Motion," AIAA Paper 73-915, 1973.

[23] Young, L. R., "The Role of the Vestibular System in Posture and Movement," in V. B. Mountcastle, ed., *Medical Physiology*, St. Louis, C. V. Mosby Co., 1974.

[24] Young, L. R., "Visually Induced Motion in Flight Simulation," presented at FMP Specialists Meeting on Piloted Aircraft Environment Simulation Techniques, Brussels, 24-27 Apr. 1978.

[25] Borah, J., L. R. Young, and R. E Curry, "Final Briefing: Sensory Mechanism Modeling Study," AFHRL, WPAFB, Contract F33615-76-6-0039, 1977.

[26] Peters, R. A., *Dynamics of the Vestibular System and Their Relation to Motion Perception, Spatial Orientation and Illusions*, NASA CR-1309, 1969.

[27] Young, L. R., "On Visual Vestibular Interactions," *Fifth NASA Symposium on the Role of the Vestibular Organs in Space Exploration*, NASA SP-314, 1970.

[28] Young, L. R., J. Dichgans, R. Murphy, and Th. Brandt, "Interaction of Optokinetic and Vestibular Stimuli in Motion Perception," Acta Otolaryng., Vol. 76, 1973, pp. 24-31.

[29] Miller, E. F. II, and A. Graybiel, "Motion Sickness Produced by Head Movement as a Function of Rotational Velocity," Aerosp. Med., Vol. 41, 1970, pp. 1180-1184.

[30] Graybiel, A., R. S. Kennedy, and R. S. Kellogg, Motion-Sickness Precipitated in the Weightless Phase of Parabolic Flight by Coriolis Accelerations, Nav. Aerosp. Med. Inst., NAMI-1061, 1969.

[31] Graybiel, A., E. F. Miller, and J. L. Homick, "Experiment M-131. Human Vestibular Function. 1: Susceptibility to Motion-Sickness," Proc. Skylab Life Sciences Symposium, NASA TM X-58154, Vol. 1, 1974, pp. 169-198.

[32] Berry, C. A., "Findings on American Astronauts Bearing on the Issue of Artificial Gravity for Future Manned Space Vehicles," Fifth Symposium on the Role of the Vestibular Organs in Space Exploration, NASA SP-314, 1973, pp. 15-22.

[33] Berry, C. A., and J. L. Homick, "Findings on American Astronauts Bearing on the Issue of Artificial Gravity for Future Manned Space Vehicles," Aerosp. Med., Vol. 44, 1973, pp. 163-168.

[34] Miller, E. F. II, and A. Graybiel, "Motion Sickness Susceptibility Under Weightless and Hypergravity Conditions Generated by Parabolic Flight," Aerosp. Med., Vol. 40, 1969, pp. 862-868.

[35] Miller, E. F. II, A. R. Fregley, and A. Graybiel, Comparison of Visual Horizontal Judgments by Subjects with Known Defects and Normal Persons Tilted with Respect to Gravity, Nav. Aerosp. Med. Inst., NAMI-989, 1966.

[36] Graybiel, A., E. F. Miller, and J. L. Homick, "Individual Differences in Susceptibility to Motion-Sickness Among Six Skylab Astronauts," Acta. Astronautica, Vol. 2, 155-174.

[37] Guedry, F. E., Jr., and A. J. Benson, "Coriolis Cross-Coupling Effects: Disorienting and Nauseogenic or Not?" Av., Space and Environ. Med., Vol. 49, No. 1, 1978, pp. 29-35.

[38] Guignard, J. C., and M. E. McCauley, "Motion Sickness Incidence Induced by Complex Periodic Waveforms," Proc. 1977 Annual Meeting of the Human Factors Society, 1977.

[39] Miller, E. F. II, A. R. Fregley, G. Van den Brink, and A. Graybiel, Visual Localization of the Horizontal as a Function of Body Tilt Up to ±90° from Gravitational Vertical, Nav. Sch. of Av. Med., NSAM-942, 1965.

[40] Miller, E. F. II, and A. Graybiel, "Magnitude of Gravito-inertial Force, an Independent Variable in Egocentric Visual Localization of the Horizontal," J. Exp. Psychol., Vol. 71, 1966, pp. 452-460.

[41] Homick, J. L., M. F. Reschke, and E. F. Miller, "The Effects of Prolonged Exposure to Weightlessness on Postural Equilibrium," Proc. Skylab Life Sciences Symposium, NASA TM X-58154, Vol. 1, 1974, pp. 221-238.

[42] Melvill Jones, G., "Adaptive Neurobiology in Space Flight," Proc. Skylab Life Sciences Symposium, NASA TM X-58154, Vol. 2, 1974, pp. 847-859.

[43] Graybiel, A., "Structural Elements in the Concept of Motion-Sickness," Aerosp. Med., Vol. 40, pp. 351-367.

[44] Held, R., J. M. Dichgans, and J. Bauer, "Characteristics of Moving Visual Scenes Influencing Spatial Orientation," Vision Res., Vol. 14, 1974, pp. 1-9.

[45] Young, L. R., C. M. Oman, and J. M. Dichgans, "Influence of Head Orientation on Visually Induced Pitch and Roll Sensation," Av., Space and Environ. Med., Vol. 46, 1975, pp. 264-268.

[46] Dichgans, J., R. Held, L. R. Young, and Th. Brandt, "Moving Visual Scenes Also Influence the Apparent Direction of Gravity," Science, Vol. 178, 1972, pp. 1217-1219.

[47] Barnes, G. R., A. J. Benson, and A. R. J. Prion, "Visual-Vestibular Interaction in the Control of Eye Movements," Av., Space and Environ. Med., Vol. 49, No. 4, 1978, pp. 557-564.

[48] von Baumgarten, R. J., B. Baldrighi, H. Vogel, and R. Theumber, "Physiological Responses to Hyper- and Hypogravity During Rollercoaster Flight," Av., Space and Environ. Med., Vol. 51, No. 2, 1980, pp. 145-154.

[49] Lackner, J. R., and R. A. Teixeira, "Optokinetic Motion Sickness: Continuous Head Movements Attenuate the Visual Induction of Apparent Self-Rotation and Symptoms of Motion Sickness," Av., Space and Environ. Med., Vol. 48, No. 3, 1977, pp. 248-253.

[50] Guedry, F. E., Jr., "Visual Counteraction of Nauseogenic and Disorienting Effects of Some Wide-Body Motions: A Proposed Mechanism," Av., Space and Environ. Med., Vol. 49, No. 1, 1978, pp. 36-41.

[51] Pavard, B., and A. Berthoz, "Linear Acceleration Modifies the Perceived Velocity of a Moving Visual Scene," Perception, Vol. 6, 1977, pp. 529-540.

[52] Graybiel, A., "The Oculogravic Illusion," Arch. Ophthal., Vol. 48, 1952, pp. 605-615.

[53] Brandt, Th., J. Dichgans, and W. Wagner, "Drug Effectiveness on Experimental Optokinetic and Vestibular Motion Sickness," Aerosp. Med., Vol. 45, No. 11, 1974, pp. 1291-1297.

[54] Frank, J., and H. N. Levinson, "Seasickness Mechanisms and Medications in Dysmetric Dyslexia and Dyspraxia," Academic Therapy, Vol. 12, No. 2, 1977, pp. 133-153.

[55] Alexander, R. A., and G. V. Barrett, "Relationship Between Perceptual Style and Responses to Visual Motion Under Active and Passive Viewing Conditions," J. App. Psychol., Vol. 60, No. 4, 1975, pp. 507-512.

[56] Barret, G. V., and C. L. Thornton, "Relationship Between Perceptual Style and Simulator Sickness," *J. Appl. Psychol.*, Vol. 52, 1968, pp. 304-308.

[57] Testa, C. J., *The Prediction and Evaluation of Simulator Illness Symptomatology*, UCLA, Unpublished doctoral dissertation, 1969.

[58] Hosman, R. J. A. W., and J. C. van der Vaart, *Vestibular Models and Thresholds of Motion Perception; Results of Tests in a Flight Simulator*, Delft Univ. of Tech., Rept. LR-265, 1978.

[59] Mikaelian, H., and R. Held, "Two Types of Adaptation to an Optically-Rotated Visual Field," *Am. J. Psychol.*, Vol. 77, 1964, pp. 257-263.

[60] Reason, J. T., and A. J. Benson, "Voluntary Movement Control and Adaptation to Cross-Coupled Stimulation," *Av., Space and Environ. Med.*, Vol. 49, No. 11, 1978, pp. 1275-1280.

[61] Cowings, P. S., "Autogenic Feedback Training for Controlling Vestibular Symptomatology," *Proc. of a Space Motion Sickness Symposium*, NASA/JSC, 1978.

[62] Lackner, J. R., and A. Graybiel, "Somatosensory Motion After-Effect Following Earth-Horizontal Rotation About the Z-Axis: A New Illusion," *Av., Space and Environ. Med.*, Vol. 48, No. 6, 1977, pp. 501-502.

[63] Gerathewohl, S. J., and H. D. Stallings, "Experiments During Weightlessness: A Study of the Oculo-agravic Illusion," *J. Aviat. Med.*, Vol. 29, 1958, pp. 504-516.

[64] Roman, J. A., B. H. Warren, J. I. Niven, and A. Brahbiel, "Some Observations on the Behavior of a Visual Target and a Visual After-Image During Parabolic Flight Maneuvers," *Aerospace Med.*, Vol. 34, 1963, pp. 841-846.

[65] Whiteside, T. C. D., A. Graybiel, and J. I. Niven, "Visual Illusions of Movement," *Brain*, Vol. 88, 1965, pp. 193-210.

[66] Graybiel, A., and D. I. Hupp, "The Oculo-Gyral Illusion, a Form of Apparent Motion Which May Be Observed Following Stimulation of the Semicircular Canals," *J. Aviat. Med.*, Vol. 17, 1946, pp. 3-27.

N82 34060-3

EVALUATION OF A TRAJECTORY COMMAND CONCEPT FOR MANUAL CONTROL OF CARRIER APPROACHES AND LANDINGS

Walter E. McNeill, Aerospace Engineer
G. Allan Smith, Jr., Aerospace Engineer
Ronald M. Gerdes, Aerospace Engineer and Pilot

National Aeronautics and Space Administration
Ames Research Center
Moffett Field, CA 94035

SUMMARY

A novel trajectory control system concept has been implemented to provide manual control of a conventional jet aircraft. This concept, called Total Aircraft Flight Control System (TAFCOS), utilizes an inverse model of the aerodynamic and propulsion characteristics and employs feedforward control to provide the required acceleration command. The concept requires on-board digital computations which can easily be handled by a modern airborne computer.

The system was studied in a piloted simulation of the carrier approach and landing task with primarily visual flight and guidance cues. The principal modes of vertical flight-path control investigated were vertical velocity command and vertical acceleration command. The study included manual carrier approaches with and without moderate ship motion and associated air disturbances, and tests of the effects of discrete gusts.

Manual control of flight path through this new concept was shown to be feasible as an addition to an automatic control system and to have potential as an improved mode of control over conventional control for the carrier approach task. The concept also offers several advantages, among which are design flexibility, automatic compensation for external disturbances, and prevention of abusive pilot control.

INTRODUCTION

Manual control of Navy shipboard aircraft during carrier approaches and landings is a demanding task which becomes increasingly difficult as external disturbances grow more severe. The problem of vertical flight-path, or "meatball", control is the one that presents the greatest difficulty, particularly near touchdown, where the ship's air wake and deck motion require close coordination of pitch attitude and engine thrust.

This paper reports the results of a piloted simulation study of an application of a novel feedforward trajectory - command flight control system to the manual carrier approach and landing task. On the basis of previous flight and unmanned simulation studies of such systems applied to automatic control, it appeared that improvements in manual carrier approaches could be achieved in terms of better flight-path control, reduced touchdown scatter, and reduced pilot workload.

This system, called Total Aircraft Flight Control System (TAFCOS) has been in development at Ames Research Center for the past five years [1,2,3] and has been tested successfully both in ground-based simulators and in flight with STOL aircraft. Adaptation to manual control is straightforward and provides an attractive and logical adjunct to an automatic control system, as TAFCOS was originally conceived. The advent in recent years of the airborne digital computer enables the basic system structure and the required additions to be programmed readily and inexpensively.

In the present study, manual control through TAFCOS was applied to the Navy A-7E attack aircraft performing straight-in visual carrier approaches and landings, to assess the feasibility of the concept for the task and to compare improvements in flight-path control and landing performance using different vertical command modes.

SYMBOLS

A_r	rough commanded attitude direction cosine matrix
A_s	smooth commanded attitude direction cosine matrix
$\hat{A}$	measured attitude direction cosine matrix
C_{D_c}	commanded drag coefficient
C_{L_c}	commanded lift coefficient
C_{ℓ_c}	commanded rolling-moment coefficient
C_{m_c}	commanded pitching-moment coefficient
C_{n_c}	commanded yawing-moment coefficient
C_{T_c}	commanded thrust coefficient
g	acceleration due to gravity
R_r	rough commanded position vector
R_s	smooth commanded position vector
$\hat{R}$	measured position vector
V_r	rough commanded velocity vector
V_s	smooth commanded velocity vector
$\hat{V}$	measured velocity vector
$\dot{V}_r$	rough commanded acceleration vector
$\dot{V}_s$	smooth commanded acceleration vector

$\dot{V}_T$	total commanded acceleration vector
α_c	commanded angle of attack
Γ_c	commanded vertical flight-path angle
ψ_c	commanded horizontal flight-path angle
ϕ_c	commanded roll angle
$\Delta\dot{V}_c$	perturbation acceleration command vector
ΔTh	perturbation thrust command
$\Delta\dot{\omega}_c$	perturbation angular acceleration command vector
δ_a	commanded aileron angle
δ_s	commanded stabilizer angle
δ_r	commanded rudder angle
δ_T	commanded throttle angle
ω_s	smooth commanded angular velocity vector
$\hat{\omega}$	measured angular velocity vector
$\dot{\omega}_s$	smooth commanded angular acceleration vector
$\dot{\omega}_T$	total commanded angular acceleration vector

CONTROL SYSTEM DESCRIPTION

System features. - TAFCOS uses a balance of open-loop feedforward control and closed-loop feedback control. The presence of detailed models of the aircraft force, moment and thrust characteristics in the feedforward path enable it to provide most of the control. Feedback is needed only to compensate for external disturbances and for differences between the models and the actual aircraft. The basic arrangement of these control loops is shown in figure 1.

In TAFCOS, pilot input commands of aircraft velocity, airspeed or acceleration are combined, smoothed, and limited to provide a smooth executable translational acceleration command vector in inertial axes. Then the system forces the aircraft to follow closely this acceleration command and the corresponding velocity and position trajectory.

Figure 1 shows that the feedforward path (solid lines) includes a trim map which is an inversion of the aircraft model. This trim map in series with the actual aircraft provides an approximate identity (i.e., output nearly equals input). The dashed lines indicate how the feedback is compared with the command to form an error signal which is then used to close the feedback loop. It should be noted that the feedback loop is closed ahead of the trim map so that it includes the identity; thus the feedback loop is linear and conventional linear techniques can be used in the design of the regulator.

Representation of variables by three-component vectors and angles by their three-by-three direction cosine matrices permits easy transformation of quantities between different coordinate systems. Pilot commands are in relative velocity axes and moment calculations are performed in body axes.

System structure.- Since the TAFCOS concept is different from conventional designs, a brief explanation of its structure will be helpful in understanding its operation. For the present application a manually-piloted stability augmentation system and trajectory command system has been created by additions to a completely automatic control system. This procedure is in contrast to the usual simplification of an automatic system to provide manual control. The increase in complexity is considered justified by potential performance advantages and by design flexibility. Advances in airborne digital computers have made these capabilities possible and relatively inexpensive.

Figure 2 is a signal flow diagram of TAFCOS. Again to emphazise the open-loop characterisitcs, the feedforward paths are shown by solid lines while the corrective feedbacks are shown by dashed lines. Most of the variables are three-component vectors; e.g., V_r is the rough commanded velocity vector in inertial axes and $\dot{\omega}_s$ is smooth commanded angular acceleration in body axes. The three pilot inputs are: (1) forward and aft movements of the control stick to command either vertical velocity or vertical acceleration in inertial axes; (2) left and right displacement of the stick to command rate of change of lateral acceleration in velocity axes; and (3) throttle lever position to command airspeed. All rough command signals are directly proportional to the magnitude of the control motion. For example, the first velocity axis is directed along the aircraft velocity vector with the second axis in the horizontal plane so that a constant lateral stick deflection commands a constant build-up of centripetal acceleration. When the stick is returned to neutral, a constant centripetal acceleration in the horizontal plane and perpendicular to the instantaneous velocity vector is commanded. The result is a circular flight path with a constant bank angle.

The trajectory time sequencer combines the various pilot signals and calculates a total rough commanded acceleration vector in three-dimensional inertial space. It also calculates corresponding inertial velocity and position vectors. These vector commands are rough in the sense that they may have excessive and abrupt rates of change and call for maneuvers that may not be executable by the aircraft within the desired stall margin, comfortable angular acceleration or attitude limits, or engine response and control surface limits.

The trajectory command generator smooths, limits, and rotates the rough commands to provide an executable commanded-acceleration vector $\dot{V}_s$ and corresponding velocity and position vectors V_s and R_s in velocity axes. Each channel of the trajectory command generator includes four integrators and appropriate internal feedback loops so that a specific dynamic response can be provided by pole placement or other linear techniques. The components of the smooth commanded velocity resolved back into inertial axes give the commanded horizontal and vertical flight-path angles ψ_C and Γ_C .

The force trim map accepts the commanded specific force vector and combines it with commanded dynamic pressure and wing area. It then calculates commanded total lift and drag coefficients which include the effects of engine thrust. An inverse interpolation of the aircraft lift and drag characteristics stored as tabular data then yields the angle of attack and thrust coefficient required to follow the trajectory. Figure 3 is a representation of the force trim map data. It is seen to be a family of lift-drag polars for several values of thrust coefficient C_{T_C} . An example is shown by the small circle. If a lift coefficient of 1.2 and a drag coefficient of zero are commanded, then an angle of attack of 12 degrees and a thrust coefficient of 0.2 would be the outputs. At this point the commanded input lift and drag coefficients are limited to the perimeter of the trim map or to a subperimeter to provide suitable safety margins.

The horizontal and vertical flight-path angles ψ_C and Γ_C , the roll angle ϕ_C , and the angle of attack α_C are combined in figure 2 to give the commanded direction cosine matrix from inertial to body axes A_T . This commanded aircraft attitude is the input to the attitude command generator.

The attitude command generator has a similar function to the trajectory command generator. It has two integrators and appropriate internal feedback loops. The output is a smooth, executable commanded angular acceleration vector $\dot{\omega}_S$, the corresponding consistent angular velocity vector ω_S , and the attitude matrix A_S .

The thrust coefficient from the force trim map C_{T_C} is processed by a power command generator and engine trim map to calculate the required throttle angle δ_T . The power command generator and engine trim map perform the same type of function as the trajectory command generator and force trim map. They provide a smooth command with suitable dynamics. The engine trim map involves inverse interpolation of a table of engine characteristics.

The moment trim map is the last element in the feedforward path. Its input is the commanded angular acceleration which is first multiplied by the aircraft inertia matrix to give the moment vector. It is then converted to moment coefficients by combination with dynamic pressure, wing area, chord and span. The moment trim map involves a calculation of the moment already commanded by angle of attack, engine thrust, and body rates to determine how much more moment must be supplied by the aerodynamic control surfaces. An inverse interpolation of the aircraft moment data yields the required control surface deflections.

This open-loop control system is then supplemented by feedback loops shown by the dashed elements in figure 2. The smooth translational position and velocity commands R_S and V_S are compared with the measured response $\hat{R}$ and $\hat{V}$ and combined with suitable gains and limits in the trajectory regulator to give a closed-loop perturbation translational acceleration vector $\Delta\dot{V}_C$. This vector is added to the open-loop signal $\dot{V}_S$ to give the total signal $\dot{V}_T$ as input to the force trim map. The gains in the regulator are chosen by a linear pole-placement technique to give a satisfactory dynamic response. The vector ΔV_c is generally a small fraction of V_s and the feedback loop is essentially linear. Similar techniques are used to determine the gains in the attitude regulator.

APPLICATION TO CARRIER APPROACH

Carrier approach task.- Figure 4 shows the normal manual carrier approach scenario. A level leg is established first, where visual line-up is achieved prior to tip-over. When the pilot receives the proper indication from the Fresnel Lens Optical Landing System (FLOLS) or from the SPN-41 shipboard tracking radar cross-pointers in the cockpit he begins a constant-rate descent which, for the present simulation conditions of airspeed 66.4 meters/second (129 knots), glide path 3.5° with respect to the ship, and wind over the deck of 15.4 meters/second (30 knots), was just over 3 meters/second (600 feet per minute). During the final descent, guidance is entirely visual with vertical flight path cues provided by the FLOLS.

For the present study, the FLOLS display information was calculated so that an on-glide-path approach resulted in the tail hook touching down midway between the second and third arresting wires, of which there were four, spaced 12.2 meters (40 feet) apart. The FLOLS was assumed to be line stabilized; i.e., glide path stabilized against ship pitching motion but not against heave.

Command modes studied.- The vertical velocity command (VVC) mode and the vertical acceleration command (VAC) mode were selected for study. In making this selection, one line of thought was that a given magnitude of stick input should command a given FLOLS "meatball" rate at a particular range. This reasoning led to VVC as the prime candidate for the carrier-approach control mode. In order to de-sensitize meatball response to vertical flight path changes near the ship, provision was made for decreasing command gain with decreasing range. Both this variable gain and a constant gain were investigated.

The terms VVC and VAC apply only to the rough commanded quantities proportional to stick displacement. Smooth commanded accelerations and velocities are always generated and used within TAFCOS.

Test facilities.- The study was conducted using a fixed-base simulator with a full complement of flight instruments and a set of hydraulically-loaded fighter/attack aircraft cockpit controls. A closed-circuit television landing display was used, complete with a scale model aircraft carrier with heave motion and a servo-driven mechanical representation of the FLOLS to display glide-path error. All simulation calculations were performed by a Sigma 9 general purpose digital computer.

RESULTS AND DISCUSSION

In the discussion which follows, time histories of control system and airplane behavior are presented for typical simulated straight-in carrier approaches. These approaches include one using vertical velocity command with ship motion and air disturbances, followed by a series of three which show comparisons between vertical velocity command and vertical acceleration command, then one that shows responses to discrete gust disturbances. Pilot comments are also presented, followed by discussions of numerical pilot ratings and touchdown performance data.

Aircraft Response during Carrier Approaches

Vertical velocity command with ship motion.- Figure 5 shows a time history of a manual carrier approach and landing with TAFCOS vertical velocity command mode selected. Ship motion consisted of +0.9 meter (+3 feet) of heave with a standard set of ship air wake (burble) disturbances. For this approach, tip-over was initiated at about 10 seconds after the start of the run. In order that the pilot would not have to hold his stick input to command a steady rate of descent following tip-over, a vertical velocity trim function was provided using the pilot's trim button. Thus, the total rough commanded vertical velocity was the sum of the trim input (third trace, fig. 5(a)) and a signal proportional to the stick input (second trace). The fifth trace shows the resulting vertical velocity, which closely followed the smooth command. The bottom trace shows that the aircraft height followed the commanded height (integrated vertical velocity) well within 0.3 meter (one foot) error, except during the last few seconds before touchdown. Additional details of the approach are shown in figure 5(b). The aerodynamic flight path angle (measured with respect to the air mass) is shown to change to about -3° , the angle that would be expected for 15.4 meters/second (30 knots) of wind over the deck. Pitch attitude changes generated by TAFCOS, though probably greater than a pilot would call for if he were controlling attitude directly, did not appear to be excessive.

Comparisons between command modes.- Figure 6 shows comparisons between vertical velocity command and vertical acceleration command as they influence the nature of the pilot inputs and the resulting airplane vertical response. For VVC with ship motion (fig. 6(a)) the stick deflection was characterized by more or less continuous activity as vertical velocity corrections were required following initial trimming at tip-over. As he approached the ship, the pilot's glide-path error information from the FLOLS improved and the need to tighten his control loop (especially in the presence of deck motion) became apparent. The increased frequency and magnitude of his inputs, beginning at about 37 seconds, are obvious. The complete stick deflection time history (in addition to the trim input) is reflected in the rough commanded vertical velocity. (Because the VVC mode was in use, rough commanded vertical acceleration was zero.)

Figure 6(b) shows the results using VAC, with the same time history of ship motion and air disturbances that was used for VVC. In this case, the stick inputs were applied more in the manner of pulses, with more time spent at zero deflection. The rough commanded vertical velocity took on more the appearance of a succession of ramps as the rough acceleration pulses were integrated. Again, the effects of following the deck motion are seen in the latter half of the rough commanded and actual vertical velocities.

Without ship motion (fig. 6(c)), the VAC inputs, again in the nature of individual pulses, were more infrequent than with ship motion. In this case, since there were no other disturbances, the pilot at any given time had only to apply small corrections to the aircraft motion resulting from his own previous inputs.

Response to gusts.- Figure 7 shows a time history of the airplane response to discrete 3 meter-per-second (10 foot-per-second) vertical gusts introduced during a manual approach with VVC selected and no ship motion or other disturbances. These gusts were more severe than any normally encountered in practice but they show how TAFCOS was able to respond and control flight path.

Vertical acceleration perturbations of 1.8 meters per second squared (6 feet per second squared or 0.2g) and angle of attack perturbations of 2.6 degrees due to the gusts are noted in figure 7(a). The resulting vertical velocity and the error between instantaneous and smooth commanded height (bottom trace) showed perturbations of only 0.76 meter per second (2.5 feet per second) and about 2 meters (6 feet), respectively. Some pilot stick response to the first (down) gust is noted; however, essentially no response was made to the onset of the second gust, while TAFCOS is seen to have corrected the height error in well under 10 seconds.

Figure 7(b) shows that pitch attitude underwent fairly large excursions (12.4° maximum to 6.5° minimum) in combined response to the gusts and the stabilizer deflections applied by TAFCOS. The power lever angle and thrust transients that were required to hold commanded airspeed were signficant in magnitude; however, recovery to a reasonably normal thrust level was made about five seconds prior to touchdown.

Pilot Comments

General comments.- Pilot comments indicated that general acceptability of manual trajectory control through TAFCOS was good. Lateral-directional maneuvering was natural, with no unusual or adverse characteristics. In roll entries and reversals, behavior was essentially that of a roll-rate command system. Lateral maneuvers to correct line-up were easy to make, with no lateral PIO tendencies noted.

Vertical flight-path control was good, with smooth response to commands. Somewhat exaggerated pitch attitude changes were noted as TAFCOS responded to the trajectory commands. These excursions seemed somewhat unnatural and annoying at first to the pilots (who are accustomed to having direct control of pitch attitude). It was found that pilots soon adapted to this response and it is believed that with practice carrier pilots would not find this characteristic objectionable. Speed control was considered excellent; response to speed change commands was prompt and precise.

Effect of ship motion and air disturbances.- Ship motion and air disturbances had a large effect on height control close to the ship, as reflected in the ability to keep the meatball centered. This difficulty in turn had a degrading effect on both touchdown precision and pilot rating (discussed later).

Effect of command mode.- With or without ship motion and air disturbances there did not appear to be any large differences in results using vertical velocity command or vertical acceleration command. With ship motion, VAC sometimes required excessive maneuvering during the final stages of the approach to keep the meatball centered, probably due to the pilot's not having a preset commanded vertical velocity to return to on relaxation of his control input, or his tendency to use a "pulse-and-wait" technique with VAC. The pilot also reported a need to mentally integrate his acceleration command inputs in an attempt to predict changes in vertical velocity. This effort was not a totally fruitful one since the smooth commands, not the rough commands, are the ones integrated within TAFCOS.

Although the VVC trim control provided a "standard".commanded rate of descent about which stick-commanded perturbations could be made, it constituted an additional (retrimming) step in the control procedure which was not required with VAC.

Effect of variable gain.- De-sensitizing the vertical velocity response by decreasing pilot input control gain with decreasing range did make it easier to effect small flight-path corrections near touchdown, but there were cases when large corrections were called for and full stick inputs were applied without obtaining sufficient corrective response from the airplane. Constant gain was prefereable to this situation.

Pilot Rating Data

Figure 8 shows pilot ratings obtained during the study using the Cooper-Harper scale.[4] The rating data, grouped according to absence or presence of ship motion and air disturbances, were based on 10-run samples. (For those cases with ship motion, the ship drive signal was initiated so that the vertical deck position at touchdown was not repeated from run to run.)

Effect of ship motion and air disturbances.- Figure 8 reflects to a larger degree the pilot comment made earlier regarding effect of ship motion by showing that the largest single factor affecting pilot rating was the absence or presence of ship motion and air disturbances. Although ±0.9 meter (±3 feet) of vertical deck travel would be considered moderate, it did (in combination with the standard air wake) add considerably to the pilot's task. If one considers the most favorably-rated case in each main group (i.e., TAFCOS with VVC, constant gain), a degradation of at least from 2 to 6 is noted. The reasons given by the pilot for this degradation were increased difficulty in keeping the meatball centered prior to touchdown and deterioration of touchdown point accuracy.

Effect of command mode.- Although the evaluation pilot did not report any large differences between command modes, the ratings in figure 8 with or without ship motion do show a degradation in going from VVC to VAC. The remarks under Pilot Comments for the case with ship motion, pertaining to not having a preset vertical velocity to return to, pilot use of a pulse-and-wait control technique, and attempted mental integration of his vertical acceleration command inputs apply also to the case without motion and appear to substantiate the observed changes in rating.

Effect of variable gain.- Figure 8 shows that without ship motion and air disturbances there was no effect on pilot rating of decreasing pilot control gain with decreasing range using VVC. However, with motion a degradation of rating across the 6-1/2 boundary occurred when going from constant gain to variable gain. The occasions when full stick inputs to make large corrections (see Pilot Comments) failed to generate sufficient airplane response apparently accounted for this degradation.

Approaches with standard A-7E with APC.- For comparison with conventional control, approaches were also made with the simulated A-7E airplane with standard control system and approach power compensator. Figure 8 shows less favorable ratings for the conventionally-controlled airplane than for any of the TAFCOS test cases. This indication was less apparent with ship motion than without motion, due to the severe effect that the motion had on all the ratings as a result of the increased difficulty in keeping the meatball centered close to the ship.

Touchdown Performance

Figure 9 shows mean and standard deviation of longitudinal touchdown point (based on the 10-run samples) for all the cases discussed previously. The line segments extending beyond the standard deviation bars indicate the total spread of data points for each case. The horizontal dashed lines show the locations of the four arresting wires. To give a standard for comparison, it is seen that the first and fourth wires were 18.3 meters (60 feet) from the desired touchdown point, which is shown by the horizontal axis. Thus a spread extending beyond these limits would mean often landing short or missing all the wires and executing a bolter.

Generally, the larger standard deviations shown here were reflected in the less favorable ratings in the previous figure, and vice versa. These relationships were fairly consistent throughout the study and the standard deviation data follow closely the pilot comments in support of the numerical ratings.

CONCLUDING REMARKS

Manual control of aircraft flightpath through the TAFCOS concept has been shown to be feasible as an addition to a pre-existing automatic control system and to have potential as an improved mode of control over conventional control for the carrier approach task. Further optimization and development studies need to be made to explore this potential fully and to determine what degree of improvement can be realistically expected.

REFERENCES

1. Smith, G. Allan, and Meyer, George: Application of the Concept of Dynamic Trim Control to Automatic Landing of Carrier Aircraft. NASA Technical Paper 1512, 1980.

2. Smith, G. Allan, and Meyer, George: Total Aircraft Flight-Control System - Balanced Open- and Closed-Loop Control with Dynamic Trim Maps. Proceedings of the Third Digital Avionics Systems Conference, Ft. Worth, Texas, Nov. 1979, IEEE Catalog No. 79CH1518-0.

3. Meyer, G., and Cicolani, L. S.: A Formal Structure for Advanced Automatic Flight-Control Systems. NASA TN D-7940, 1975.

4. Cooper, George E., and Harper, Robert P.: The Use of Pilot Rating in the Evaluation of Aircraft Handling Qualities. NASA TN D-5153, 1969.

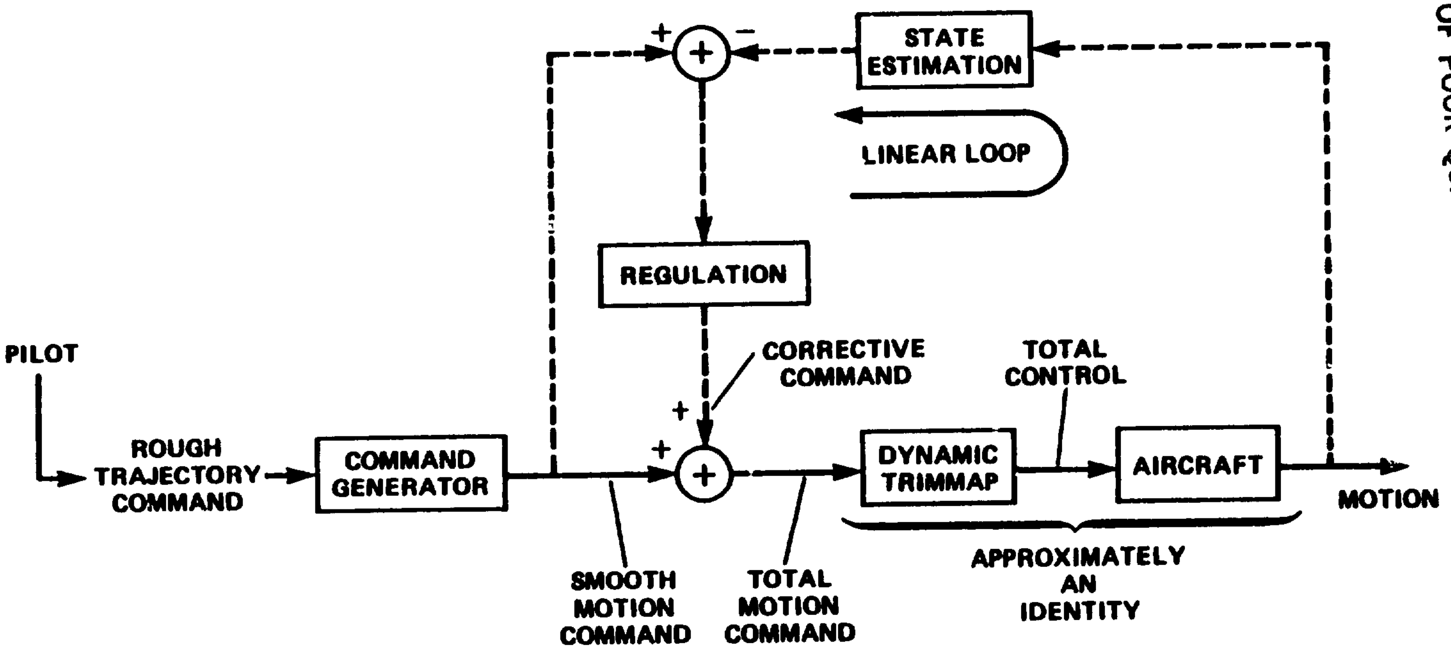
PILOT
ROUGH TRAJECTORY COMMAND
COMMAND GENERATOR
SMOOTH MOTION COMMAND
+
−
STATE ESTIMATION
LINEAR LOOP
REGULATION
CORRECTIVE COMMAND
+
+
TOTAL MOTION COMMAND
DYNAMIC TRIMMAP
TOTAL CONTROL
AIRCRAFT
MOTION
APPROXIMATELY AN IDENTITY

Figure 1.- TAFCOS structure - conceptual diagram.

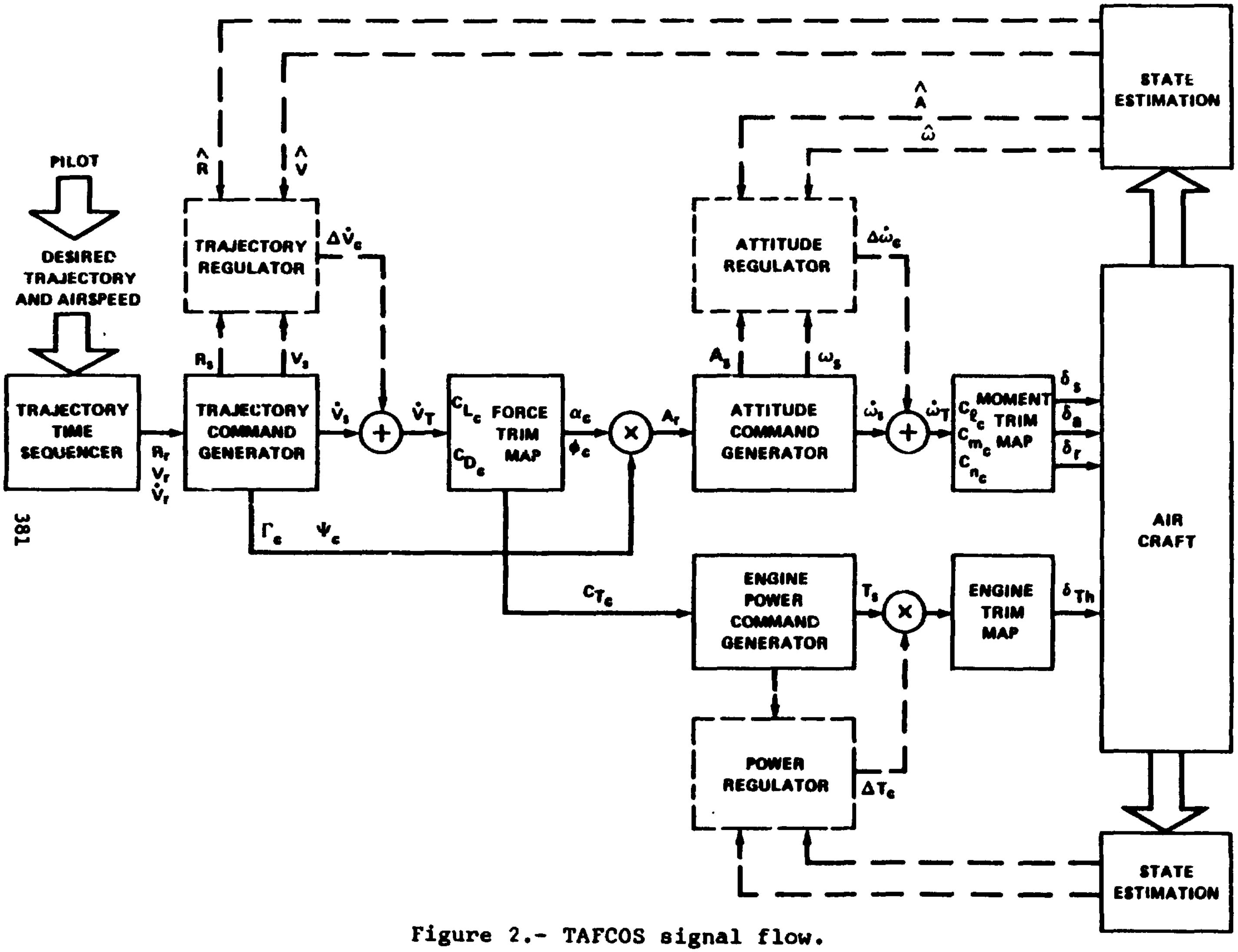
PILOT
DESIRED TRAJECTORY AND AIRSPEED
TRAJECTORY TIME SEQUENCER
R_r V_r $\dot{V}_r$
TRAJECTORY COMMAND GENERATOR
TRAJECTORY REGULATOR
$\hat{R}$
$\hat{V}$
R_s
V_s
$\Delta\dot{V}_c$
$\dot{V}_s$
$\dot{V}_T$
Γ_c
Ψ_c
C_{L_c} FORCE TRIM MAP C_{D_c}
α_c
ϕ_c
A_r
C_{T_c}
ATTITUDE COMMAND GENERATOR
ATTITUDE REGULATOR
$\hat{A}$
$\hat{\omega}$
A_s
ω_s
$\Delta\dot{\omega}_c$
$\dot{\omega}_s$
$\dot{\omega}_T$
MOMENT TRIM MAP C_{ℓ_c} C_{m_c} C_{n_c}
δ_s
δ_a
δ_r
ENGINE POWER COMMAND GENERATOR
POWER REGULATOR
T_s
ΔT_c
ENGINE TRIM MAP
δ_{Th}
AIR CRAFT
STATE ESTIMATION
STATE ESTIMATION

Figure 2.- TAFCOS signal flow.

ORIGINAL PAGE IS
OF POOR QUALITY

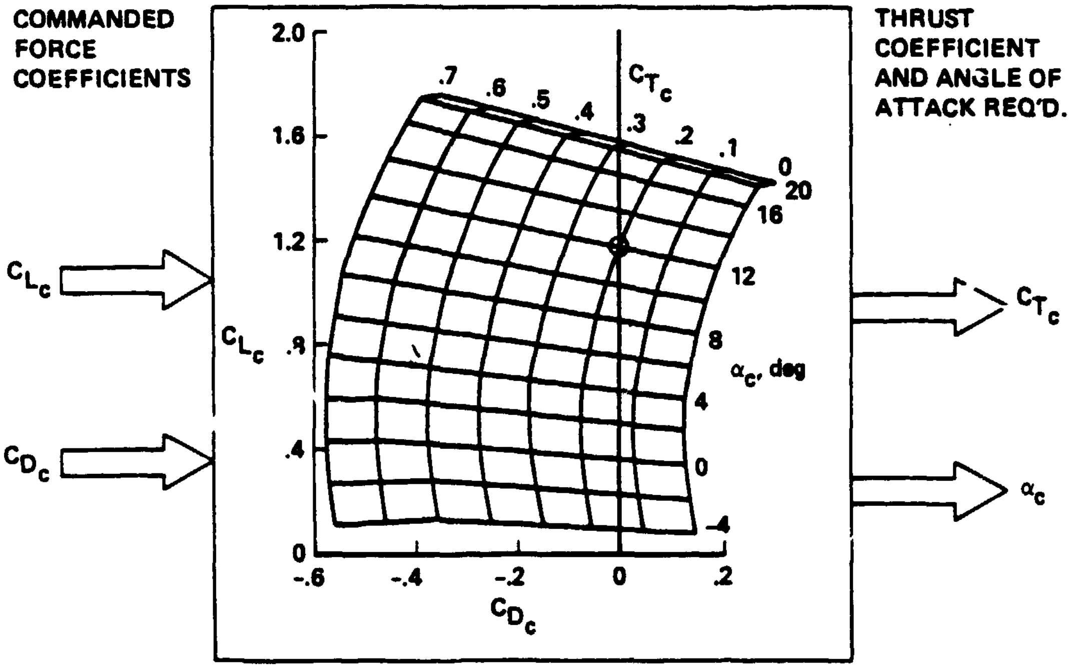

Figure 3.- Force trim map.

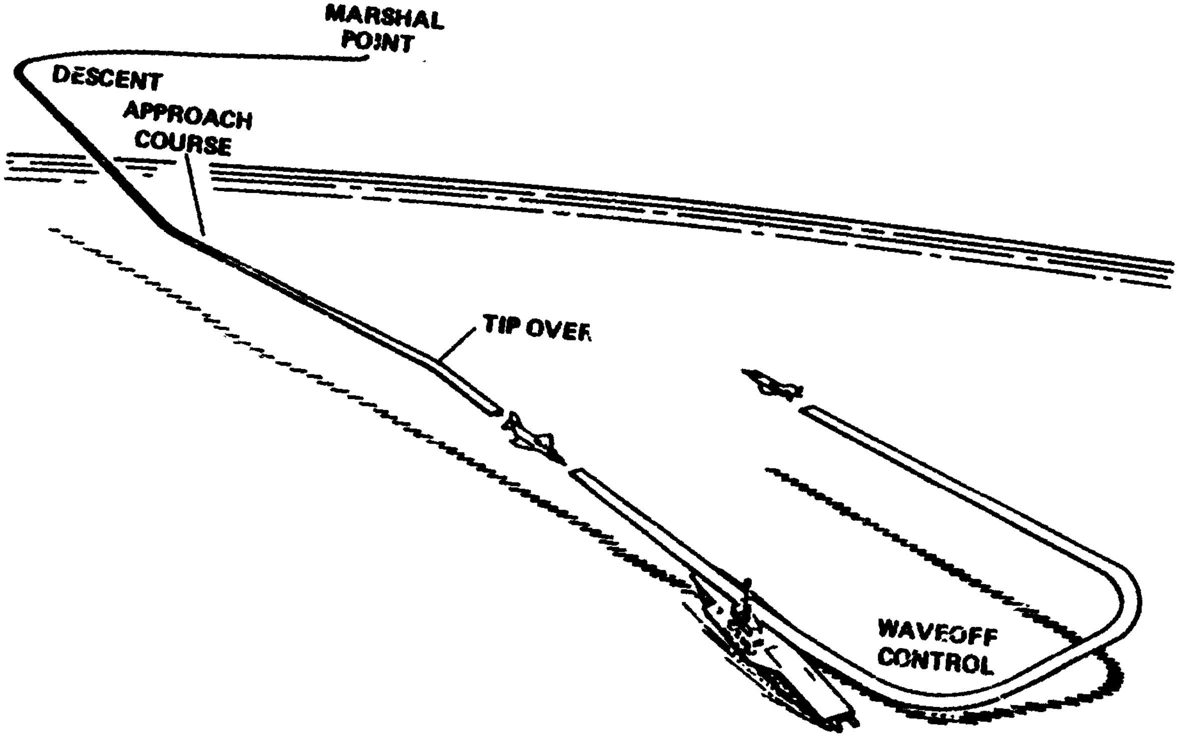
MARSHAL POINT
DESCENT
APPROACH COURSE
TIP OVER
WAVEOFF CONTROL

Figure 4.- Carrier landing situation.

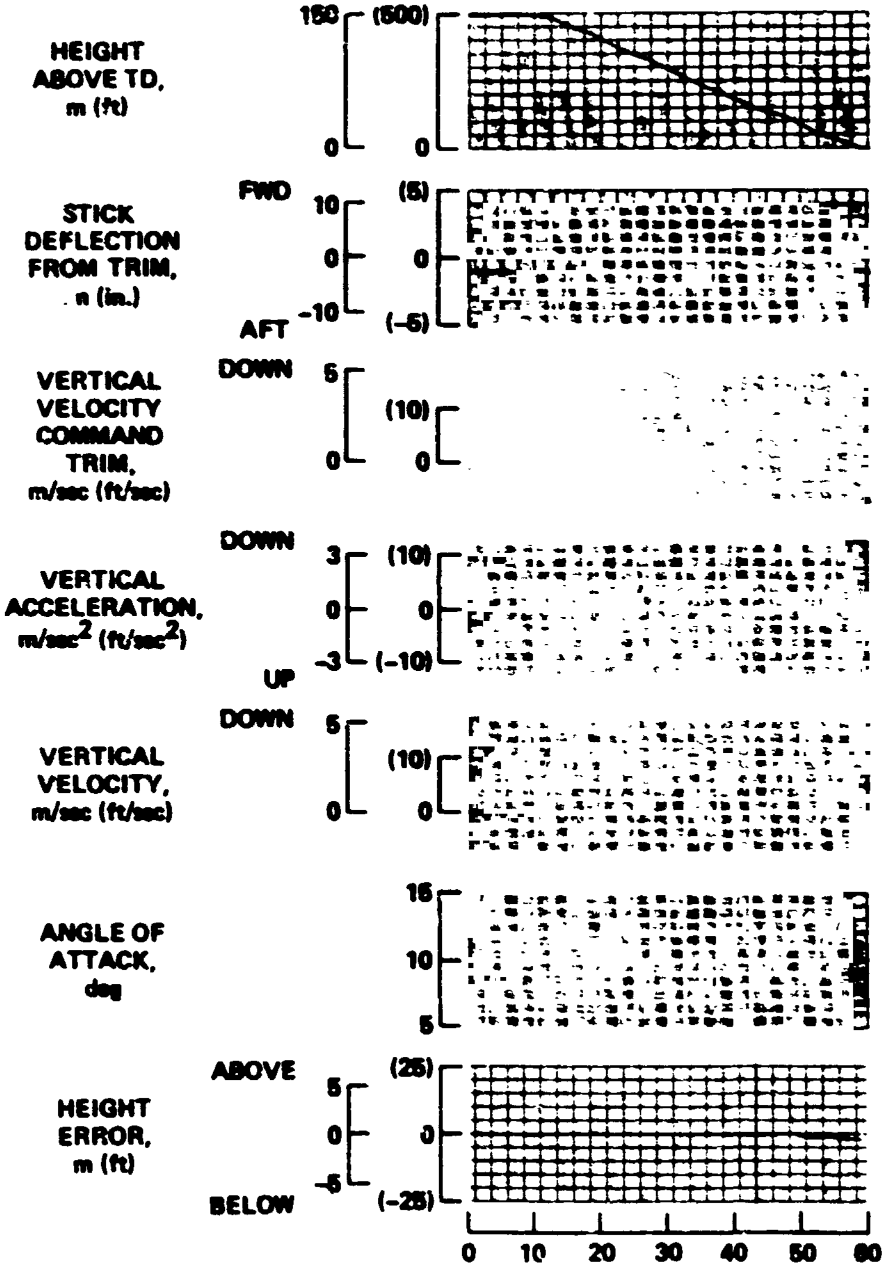

(a)

Figure 5.- Time history of a manual carrier approach with TAFCOS, vertical velocity command

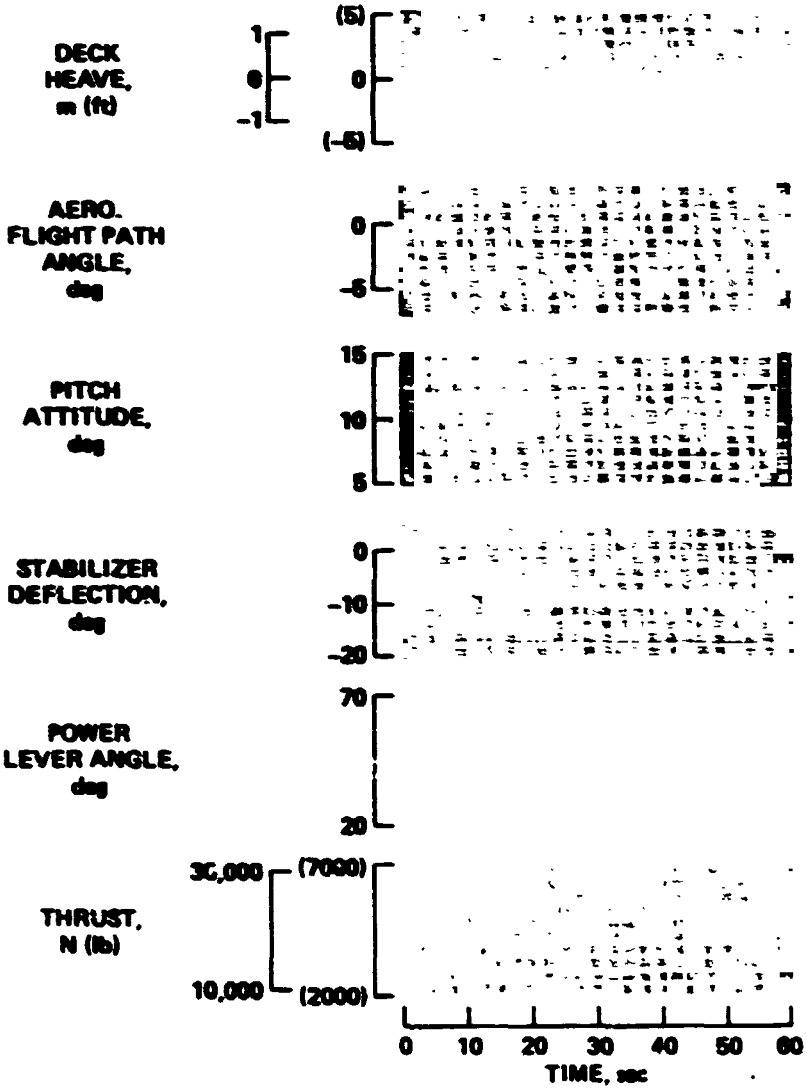

(b)

Figure 5.- Concluded.

ORIGINAL PAGE IS
OF POOR QUALITY

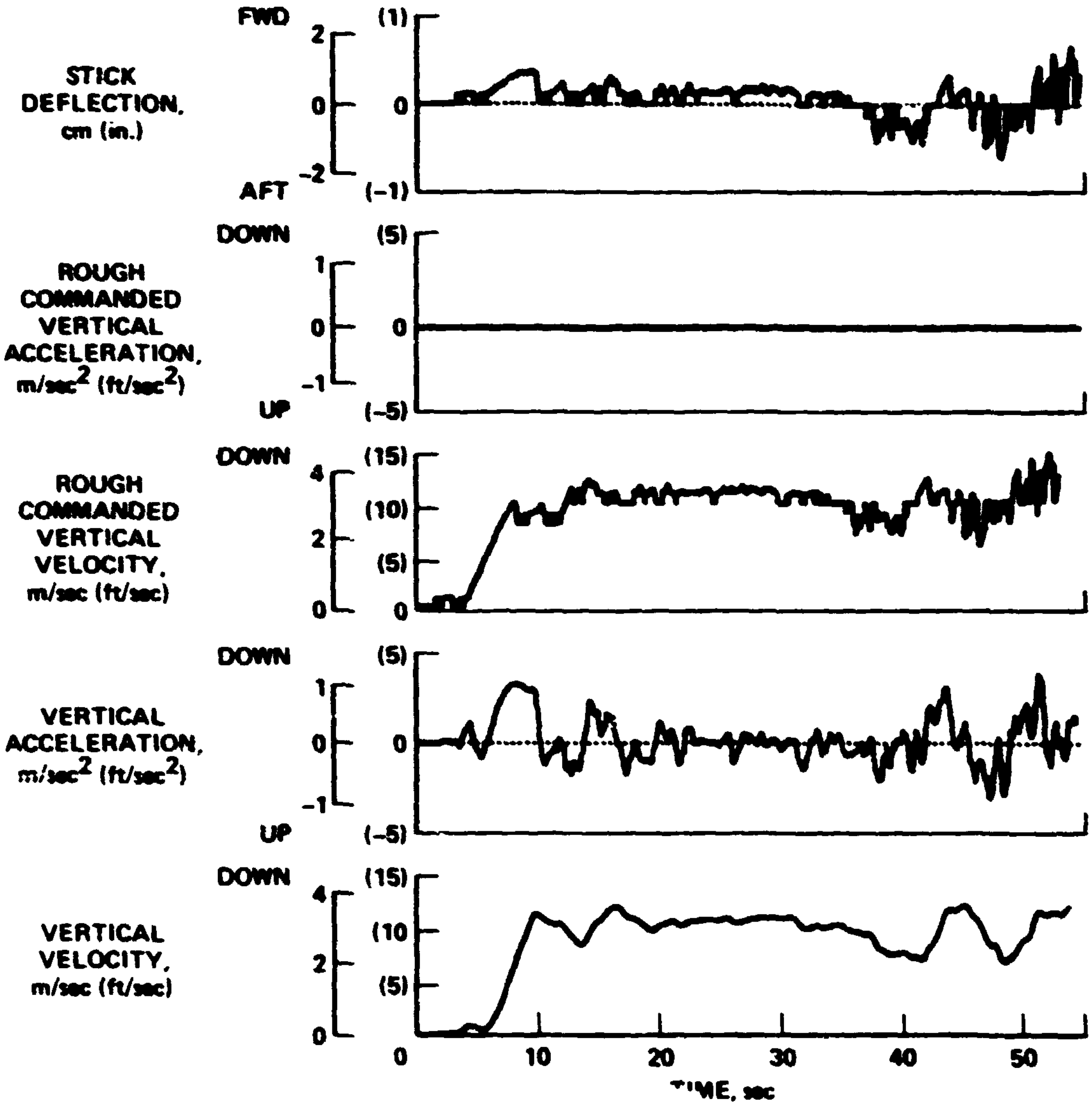

(a) Vertical velocity command, with ship motion.

Figure 6.- Comparison between TAFCOS vertical velocity command and vertical acceleration command.

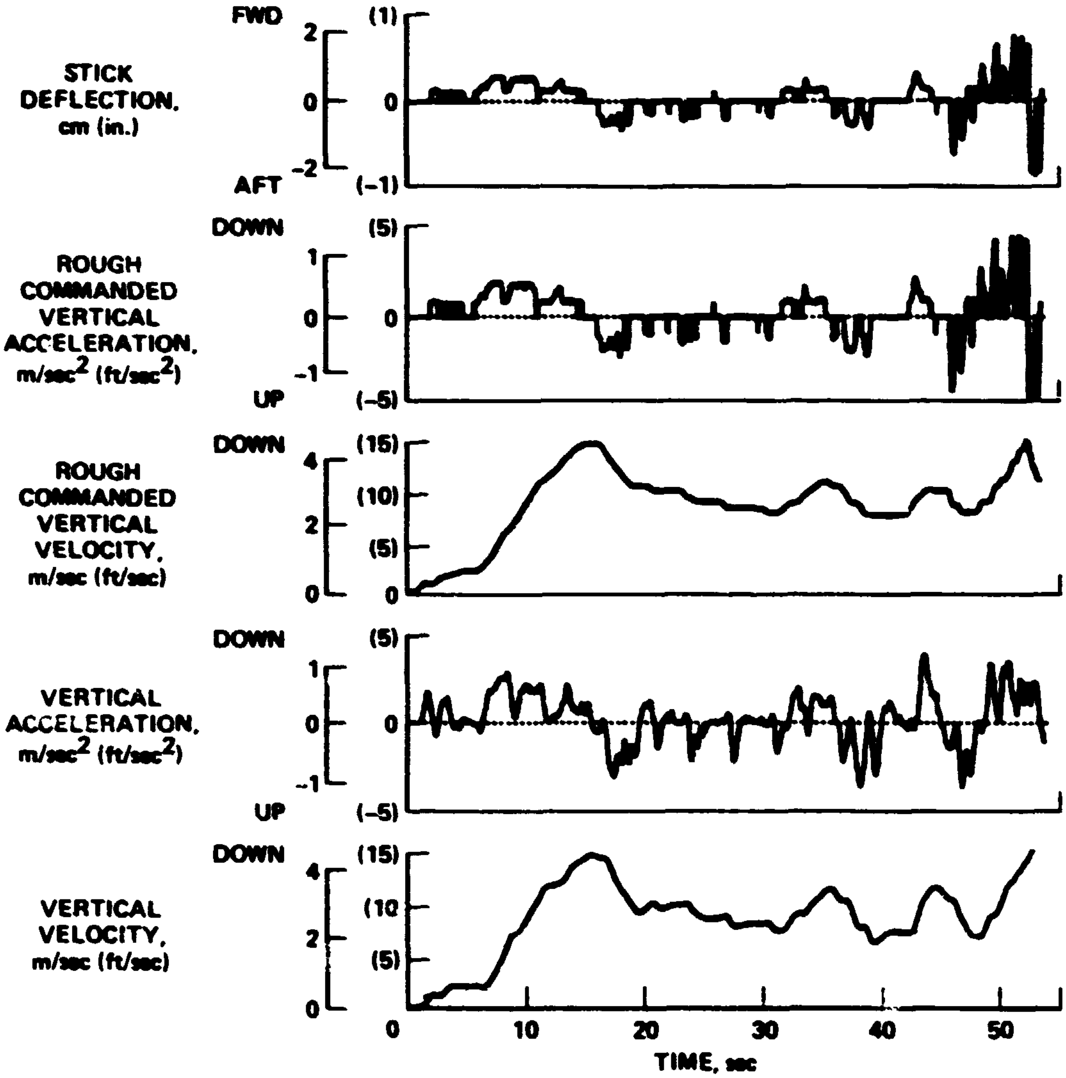

(b) Vertical acceleration command, with ship motion.

Figure 6.- Continued.

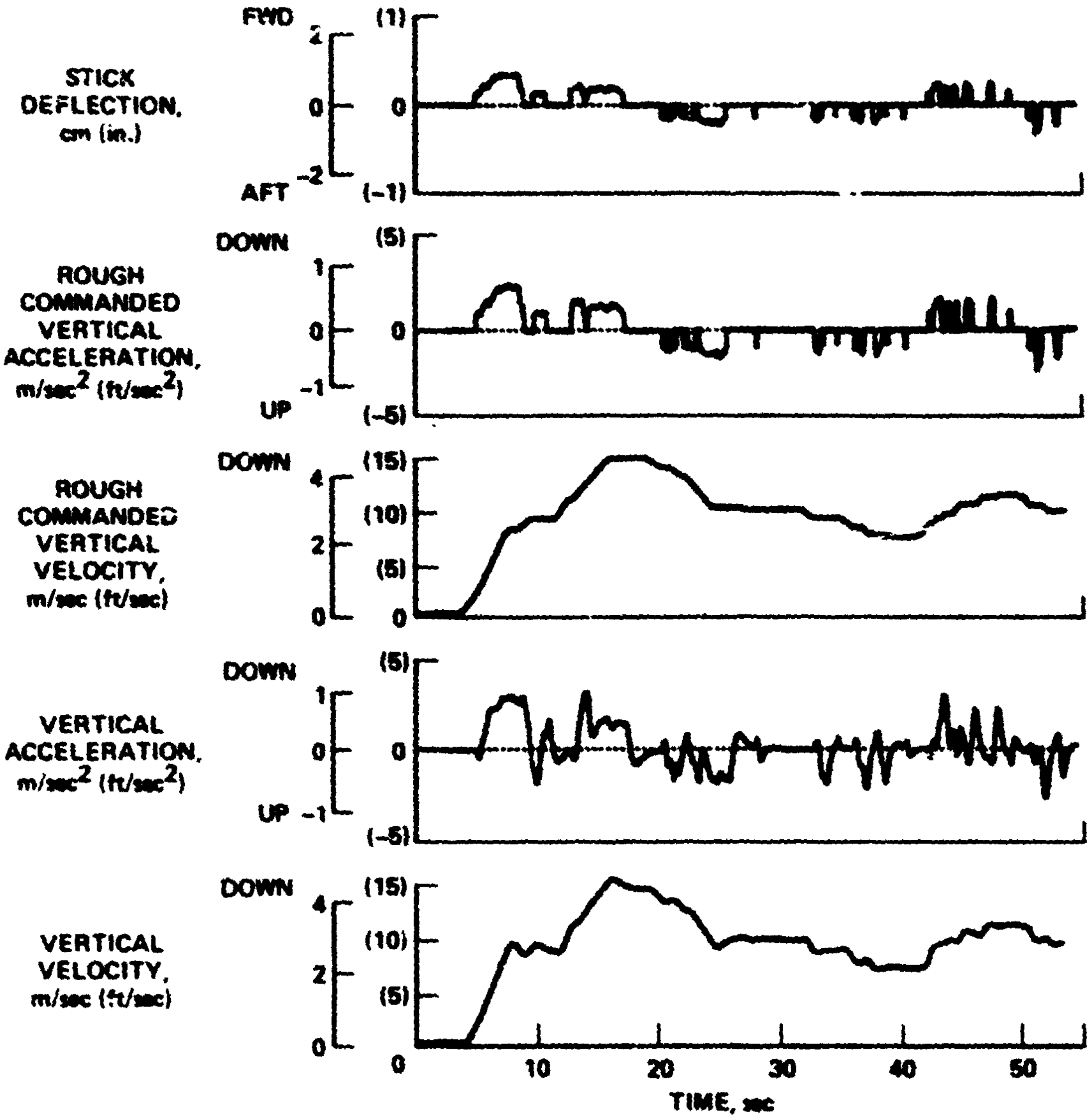

(c) Vertical acceleration command, without ship motion.

Figure 6.- Concluded

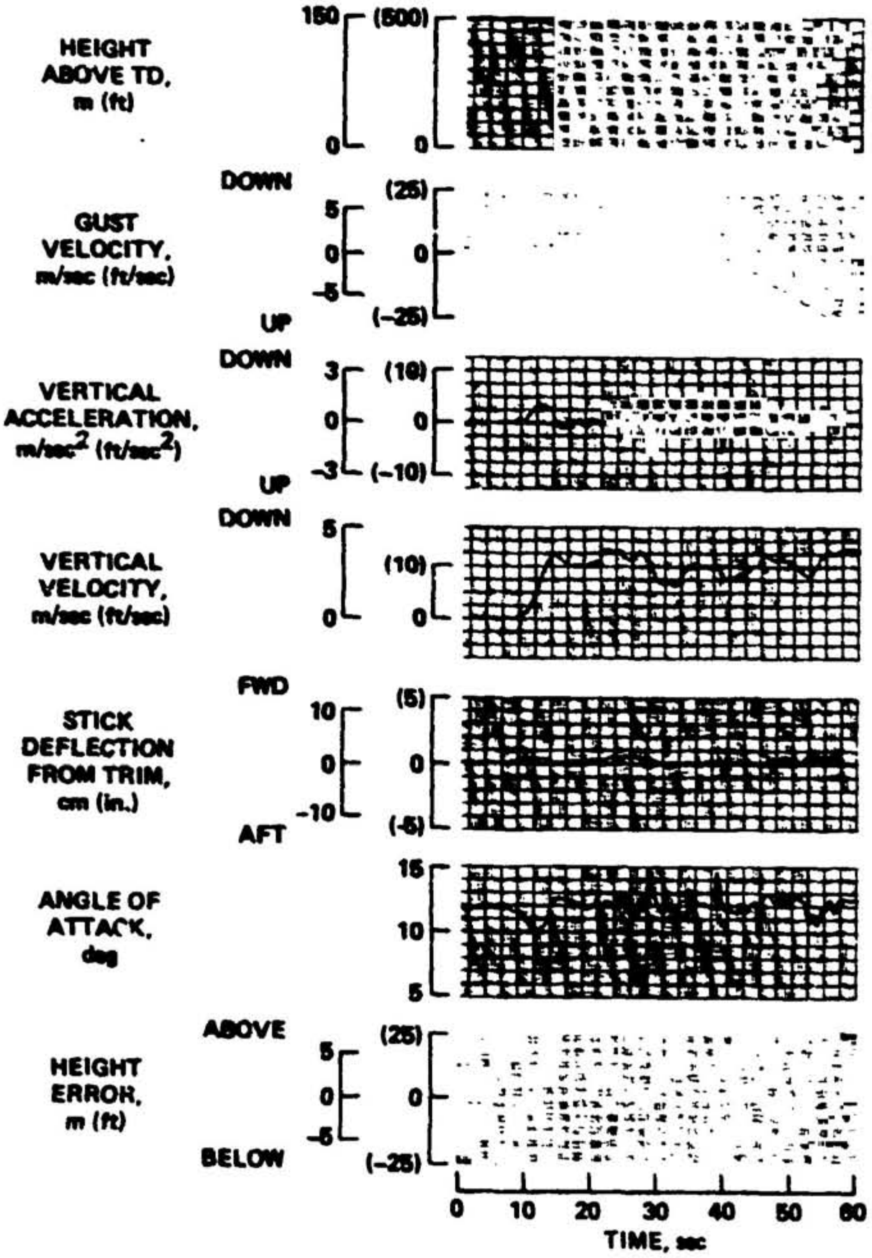

(a)

Figure 7.- Time history of response to discrete gusts.

ORIGINAL PAGE IS
OF POOR QUALITY

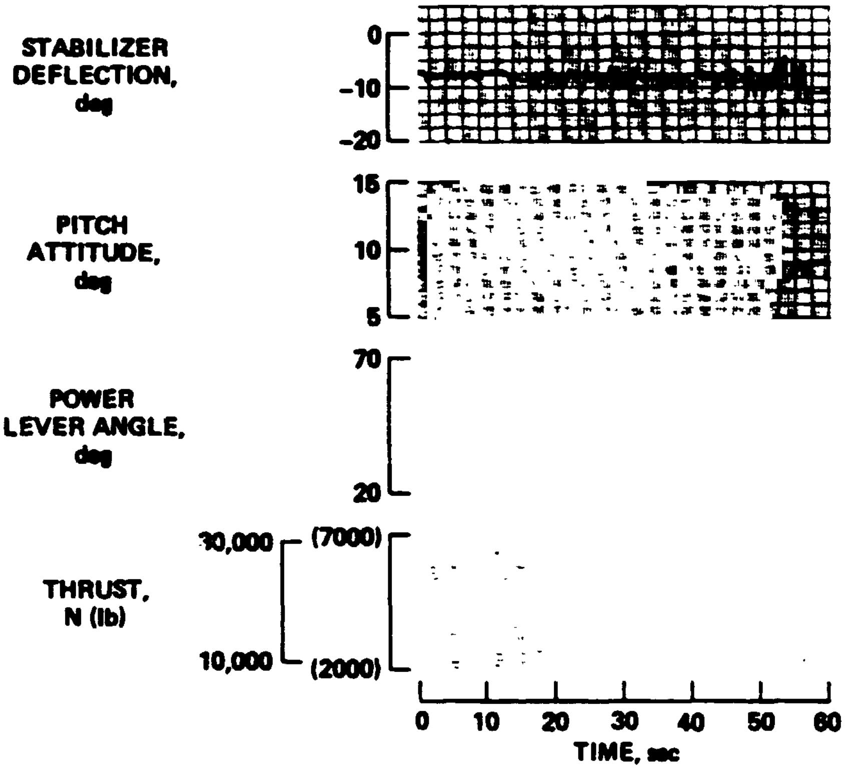

(b)

Figure 7.- Concluded

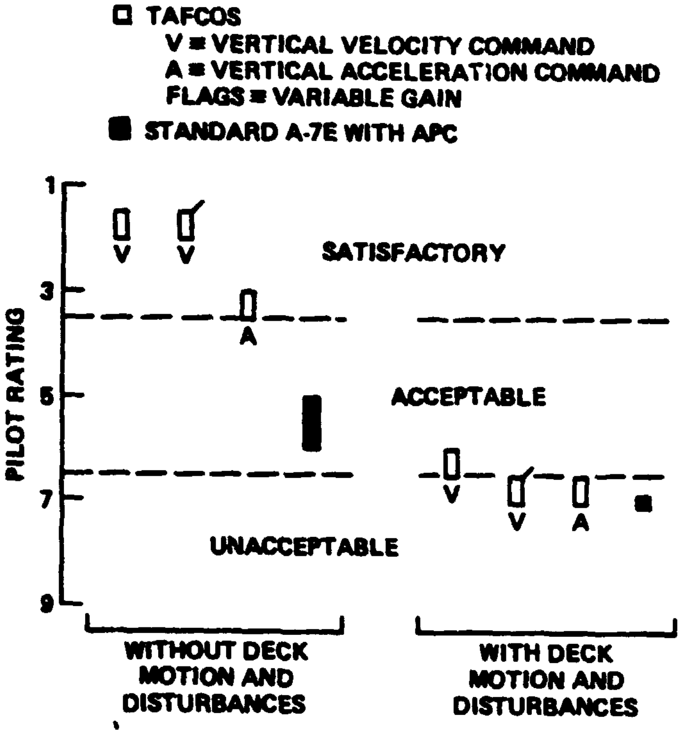

Figure 8.- Pilot rating data.

ORIGINAL PAGE IS
OF POOR QUALITY

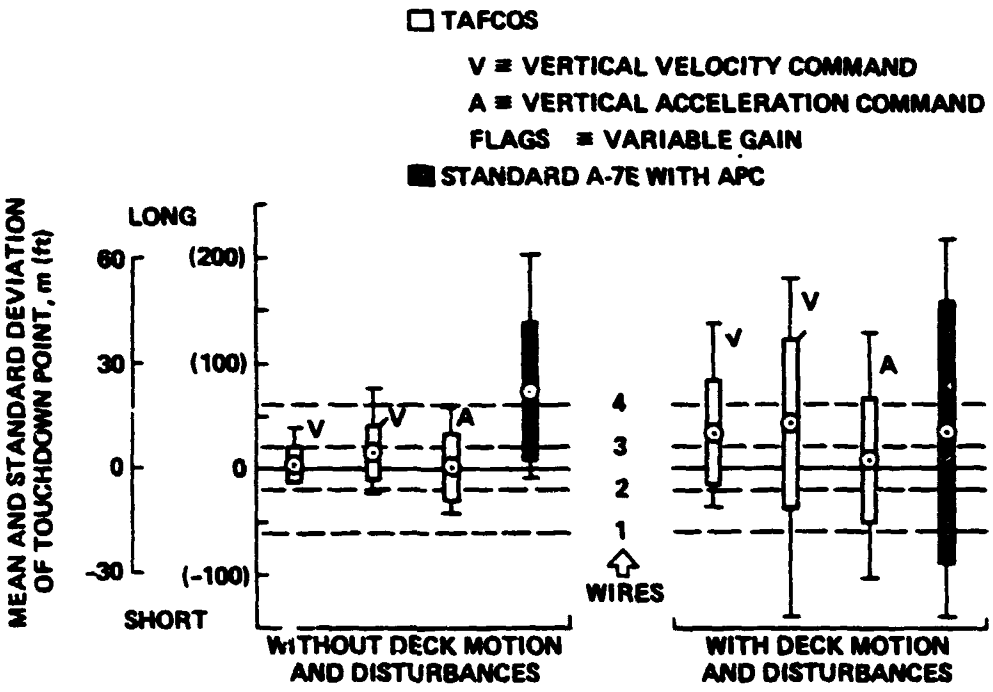

Figure 9.- Mean and standard deviation of longitudinal touchdown point.

ABSTRACT

Wind Shear Simulation Experiments

Mark Connelly
Information and Decision Systems Laboratory, M.I.T., Cambridge, MA

A set of simulation experiments has demonstrated the effects of various levels of horizontal wind shear and the presence of thunderstorm cells on instrument landing performance. A theoretical analysis was carried out showing what control inputs are necessary to compensate for vertical and horizontal wind shears. A final set of simulation experiments using the suggested control technique indicates that a substantial reduction in the effects of shear can be obtained by displaying the proper dynamic information to the pilot in a timely fashion.

ABSTRACT

Combined Use of Airborne Traffic Situation Displays And 4DRNAV In ATC

Two key tasks in the application of distributed management to the problem of providing adequate ATC capacity, safety, and efficiency at busy terminals are: (1) To follow a 3D terminal aerospace structure and arrive at fixed waypoints within the structure precisely at pre-scheduled times in the presence of a full range of wind conditions aloft (2) To monitor nearby traffic on an airborne traffic situation display to detect blunders and resolve conflicts in a safe manner. This paper describes a series of simulation experiments carried out to evaluate both of these functions.

N82 34061 D24

APPLICATION OF A PILOT CONTROL STRATEGY IDENTIFICATION TECHNIQUE TO A JOINT FAA/NASA GROUND-BASED SIMULATION OF HEAD-UP DISPLAYS FOR CTOL AIRCRAFT*

Wayne F. Jewell
Staff Engineer, Research
Systems Technology, Inc.
2672 Bayshore-Frontage Road
Mountain View, California 94043

ABSTRACT

A technique for measuring a pilot's control strategy has been developed, evaluated, and applied to a realtime ground-based simulation. The technique, called the Non-Intrusive Pilot Identification Program (NIPIP), estimates the pilot's input-output describing function and combined pilot-vehicle performance parameters such as crossover frequency and phase margin by using a time domain model of the pilot and a least-squares identification algorithm. NIPIP functions in realtime and uses a "sliding" time window to maintain freshness in the data; thus time-varying characteristics in the pilot's control strategy can be measured.

This paper describes the salient features of NIPIP, presents the results of a performance evaluation of NIPIP, and then describes the results of applying NIPIP to a realtime ground-based simulation of two competing concepts of head-up displays (HUD) for use in conventional take-off and landing (CTOL) aircraft. Differences in the pilot's control strategy used for the two HUDs and the head-down display are quantified in terms of differences in the pilots' describing functions and combined pilot-vehicle measurements. Conclusions based on the performance evaluation and application of NIPIP are presented and some recommendations on how NIPIP could be used in other manual control tasks are discussed.

INTRODUCTION

A technique for measuring a pilot's control strategy has been developed, evaluated, and applied to a joint FAA/NASA ground-based simulation of two competing concepts of head-up displays (HUD) for use in conventional take-off and landing (CTOL) aircraft. The technique, called the Non-Intrusive Pilot Identification Program (NIPIP), estimates the pilot's input-output describing function and combined pilot-vehicle performance parameters such as crossover frequency and phase margin by using a time domain model of the pilot and a least-squares identification algorithm. NIPIP functions in realtime and uses a "sliding" time window to maintain freshness in the data; thus time-varying characteristics in the pilot's control strategy can be measured.

---

* This work was sponsored by the Man-Vehicle Systems Research Division at the NASA Ames Research Center, Moffett Field, California, under contract NAS2-10385. The NASA contract technical monitor was Dr. Richard Haines. The ground-based simulation was a joint FAA/NASA head-up display concept evaluation project conducted under Task Order DOT-FA77 WAI-725 to Inter-Agency Agreement NASA-NMI 1052.151 dated March 9, 1977.

PRECEDING PAGE BLANK NOT FILMED

This paper is divided into the following sections:

- Description of the salient features of NIPIP
- Performance evaluation of NIPIP
- Application of NIPIP
- Conclusions and recommendations.

The treatments of each of the above topics in this paper are intentionally terse. More in-depth and detailed treatments will be presented in a forthcoming NASA contractor report[1].

SALIENT FEATURES OF NIPIP

The function of NIPIP is to estimate the describing function of the human operator (HO) while performing a multiloop control task such as flying an aircraft. NIPIP makes use of well-proven reduced-order models of the HO dynamics[2] and is well suited for easy implementation on modern, high speed digital computers.

One of the design criteria of NIPIP was that it be able to obtain measurements of the HO's control strategy in a realtime simulation environment on a non-interfering basis, which is why it is referred to as "non-intrusive." The result was an algorithm that is fast enough and efficient enough to coexist with the essential components of a realtime aircraft simulator. Furthermore, NIPIP is simple enough to use on a routine basis, without the use of special inputs, disturbances, or other alterations to the integrity of the simulation.

While there are a number of techniques available for identifying HO dynamics[3-7], NIPIP is unique in that it can identify the time-varying characteristics of the HO, does not require knowledge of the disturbance, and can function in realtime. This last attribute is advantageous because it allows a researcher to monitor the HO's dynamic behavior as he is performing the control task. The following text briefly describes the requirements for using NIPIP as well as the inputs and outputs of NIPIP.

The first step in using NIPIP is to synthesize a loop structure of the pilot-vehicle system. This can be based on control system analysis and/or observation of the HO behavior in performing the required task. The next step is to represent the elements of the human operator in the loop structure with discrete transfer functions. It is shown[8] that reduced order forms of the HO dynamics can be used for the discrete transfer functions. Then one writes difference equations using the loop structure and discrete transfer functions. The parameters of the difference equations are estimated by using a running multiple linear regression and a sliding time window.

The running multiple linear regression starts processing the time histories of the pilot's control actions and the variables to be controlled until it fills up a specified time window. Once the time window is filled up NIPIP slides the window along the time history, thus identifying any time varying characteristics in the pilot's control strategy. The raw outputs of NIPIP are the difference equations coefficients (DEC). It was discovered that the DEC would behave very strangely under certain circumstances (e.g., for time-varying behavior of the HO), but the frequency response of the HO was very well behaved. Thus the last step for NIPIP is to interpret the results in the frequency domain. It does this by computing frequency responses of the estimated elements of the HO in the loop structure (i.e., describing functions) and combined pilot-vehicle measures such as crossover frequency and phase margin.

A mathematical treatment of the NIPIP algorithm can be found[1], and will not be repeated in this paper. Instead we will present herein the results of a performance evaluation of NIPIP.

PERFORMANCE EVALUATION OF NIPIP

Figure 1 shows the construct used for the performance evaluation of NIPIP. The approach taken was to integrate NIPIP into a simulation of a Boeing 727 aircraft along with the control laws of the flight director and fast/slow speed error. Analog pilots were used to control the flight director with the control column and the fast/slow error with the throttle. Shaped white noise was used to simulate pilot remnant and injected into the control loop as shown in the figure. The pilot-vehicle system was disturbed with the Dryden model of atmospheric turbulence[9].

The construct shown in Fig. 1 permitted a comparison of the known parameters of the analog pilot to the estimated outputs of NIPIP in a known

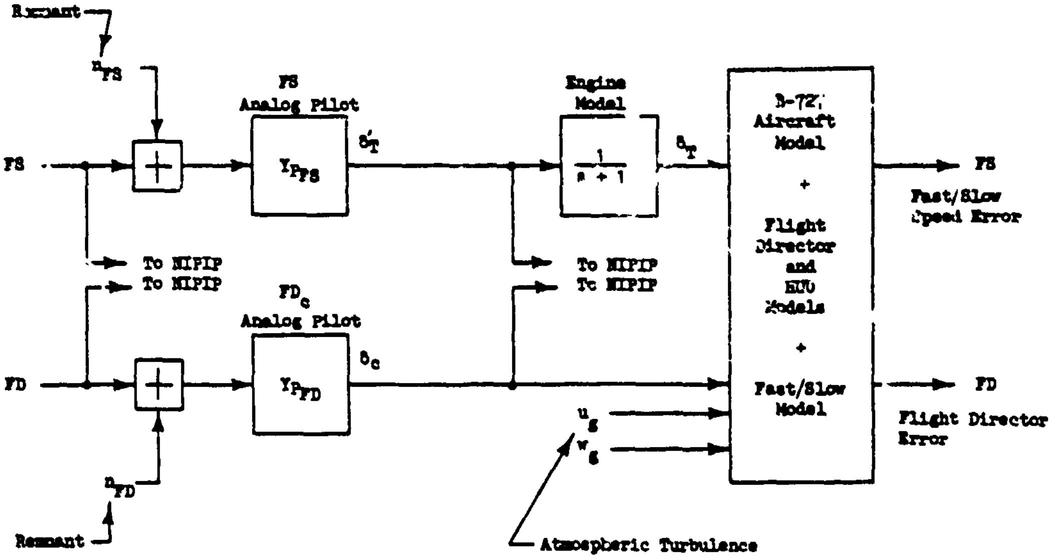
Remnant
n_{FS}
FS
FS
Analog Pilot
$Y_{P_{FS}}$
δ_T'
Engine
Model
$\frac{1}{s+1}$
δ_T
B-727
Aircraft
Model
+
Flight
Director
and
HUD
Models
+
Fast/Slow
Model
FS
Fast/Slow
Speed Error
To NIPIP
To NIPIP
To NIPIP
To NIPIP
FD_c
Analog Pilot
$Y_{P_{FD}}$
δ_c
FD
FD
Flight Director
Error
u_g
w_g
n_{FD}
Remnant
Atmospheric Turbulence

$$\hat{Y}_p = \frac{b_0 + b_1 z^{-1}}{1 - a_1 z^{-1} - a_2 z^{-2}}$$

$$\frac{\sigma_{n_{FS}}}{\sigma_{FS}} = \begin{Bmatrix} 0 \\ 0.15 \\ 0.30 \end{Bmatrix}, \quad \frac{\sigma_{n_{FD}}}{\sigma_{FD}} = \begin{Bmatrix} 0 \\ 0.22 \\ 0.44 \end{Bmatrix}$$

Figure 1. Construct Used for the Performance Evaluation of NIPIP

level of remnant. The amount of remnant was quantified in terms of noise-to-signal ratios. For example,

$$\frac{n}{s} = \frac{\sigma_n}{\sigma_s}$$

In addition to evaluating the effects of pilot remnant on the outputs of NIPIP, the effects of variations in the following items were also evaluated:

1. Length of the sliding time window, T_W. The larger the value of T_W the better the estimated $\hat{Y}_p$. The tradeoff to be considered is that the time-varying characteristics of $\hat{Y}_p$ are masked for larger values of T_W.
2. Time variations in Y_p. That is, NIPIP was used to identify controlled variations in the parameters of the analog pilot, Y_p.
3. Number of degrees of freedom (DOF) in $\hat{Y}_p$. If the number of DOF in $\hat{Y}_p$ differs from those in Y_p how does this affect NIPIP's ability to estimate $\hat{Y}_p$?
4. Pure time delay in Y_p. How does a pure time delay in Y_p affect the estimate of $\hat{Y}_p$?

All of the effects listed above are described in detail[1]. For brevity only the effects of pilot remnant will be discussed herein, the effects of which are summarized in Fig. 2. The figure contains the frequency responses of the actual analog pilot for the flight director loop and the estimated describing functions for three levels of simulated pilot remnant (for zero remnant the estimated and actual frequency responses are identical).

The procedure used to draw Fig. 2 was to use the sliding window in NIPIP to obtain a large number of estimates for $\hat{Y}_p$. This permitted us to specify bounds on the upper and lower limits of the estimated $\hat{Y}_p$ for a given level of remnant. The figure shows that the bounds are frequency dependent, with less than ± 1 dB error in $|\hat{Y}_p(j\omega)|$ at or below 1 rad/sec (the crossover frequency of the flight director loop was 1 rad/sec) and a maximum of about ± 3 dB error at 8 rad/sec. The frequency dependence of the error in $|\hat{Y}_p(j\omega)|$ is attributed to the low-band pass filters on both the atmospheric turbulence and the remnant. The maximum error in $\measuredangle \hat{Y}_p(j\omega)$ was about ± 5 deg and did not appear to be a strong function of frequency.

Also note from Fig. 2 that the effects of remnant are non-linear. Doubling the signal-to-noise ratio from 22 to 44 percent did not double the errors in $\hat{Y}_p(j\omega)$.

Wingrove[5] demonstrated that some identification techniques will not function properly when large amounts of remnant are present. There can be biases in the estimates or a tendency to identify the inverse plant. The results shown in Fig. 2 demonstrate that NIPIP is not subject to either of these problems.

APPLICATION OF NIPIP

NIPIP was applied to the simulator evaluation of three aircraft displays for use in terminal area navigation. Simplified sketches of the three displays and a summary of the display laws are shown in Figs. 3, 4, and 5.

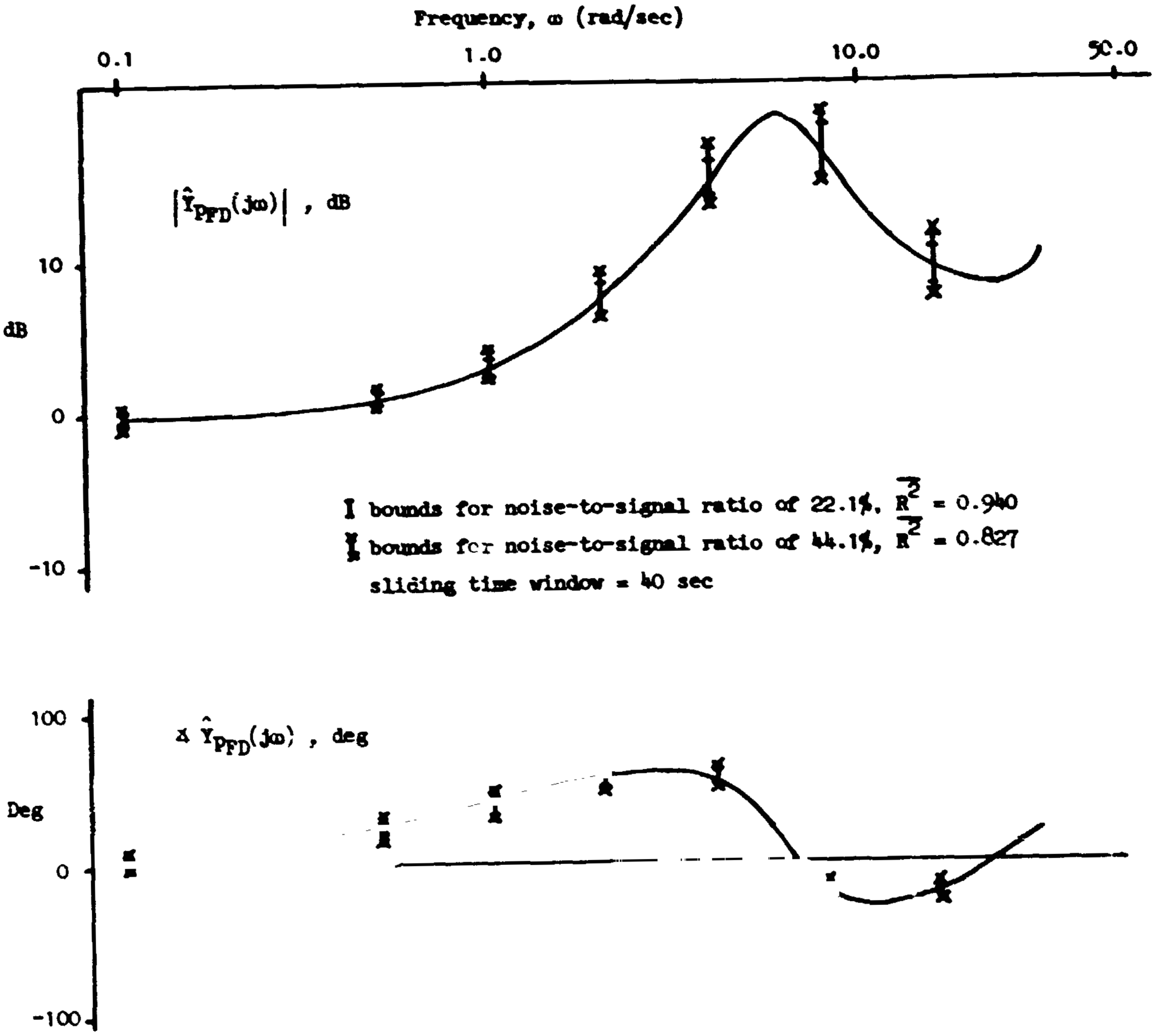

Figure 2. Effects of Pilot Remnant on Estimated Pilot Describing Function

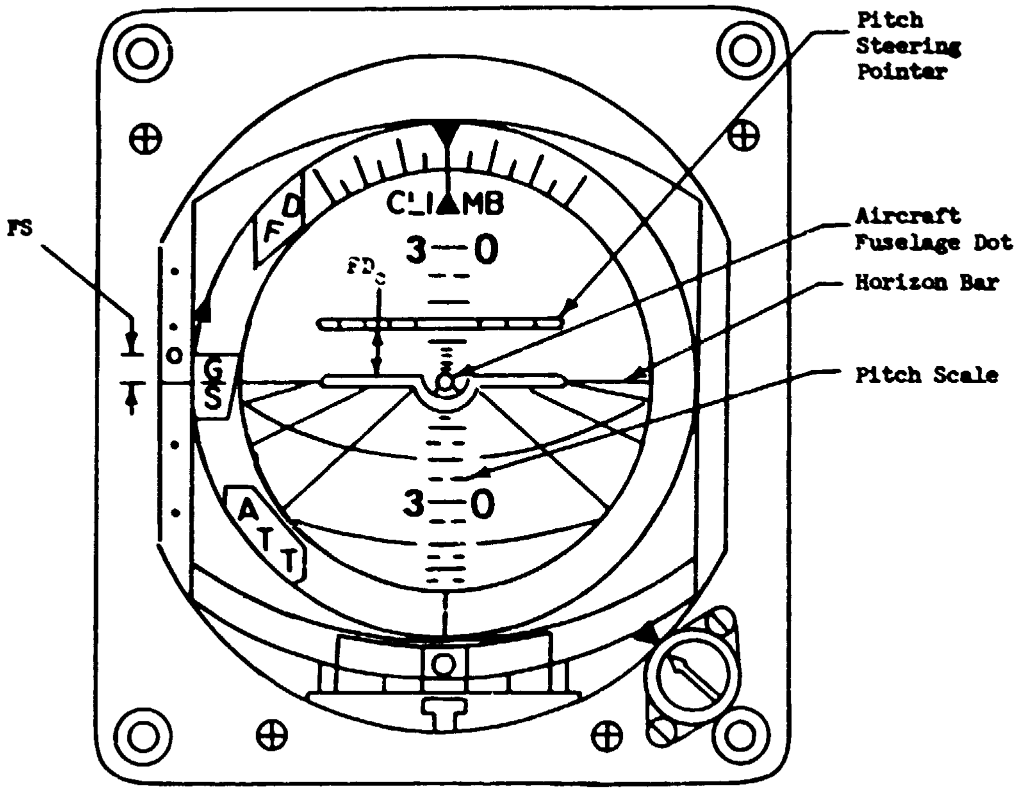
Pitch Steering Pointer
Aircraft Fuselage Dot
Horizon Bar
Pitch Scale
FS
FD
CLIMB
3—0
FD_c
G/S
ATT
3—0
O

Display control laws:

$$FD_c = K_{\epsilon_1} \epsilon_{G/S} + \frac{15.0\ s}{15.0\ s + 1} \theta$$

$$FS = \frac{1.0}{s + 1.0} (V - V_{ref})$$

Figure 3. Simplified Sketch of Head-Down Flight Director Display

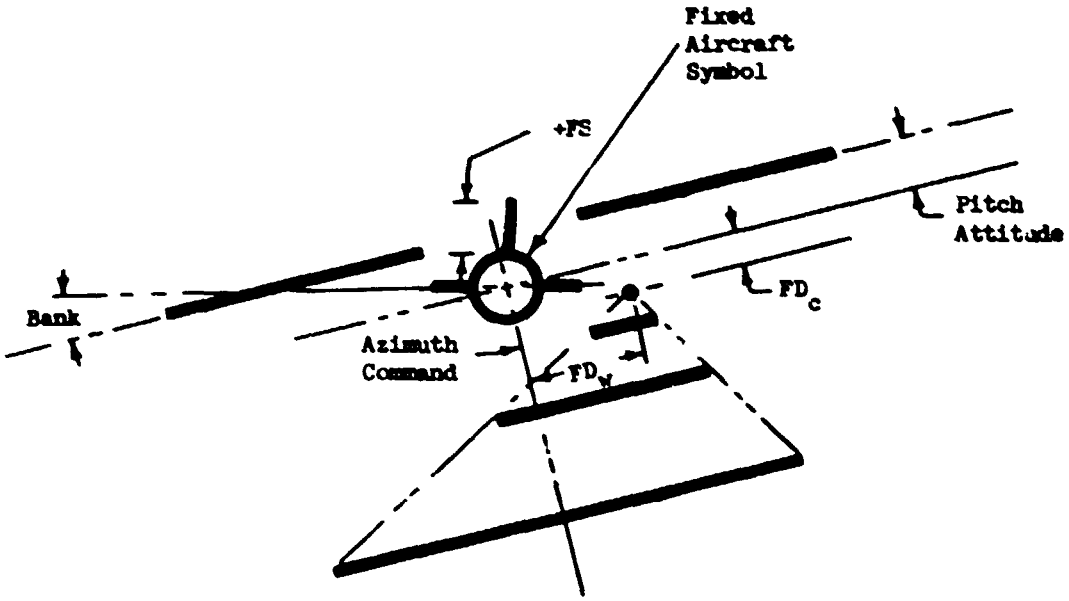
Fixed
Aircraft
Symbol
+FS
Pitch
Attitude
FD_c
Bank
Azimuth
Command
FD_V

Display control laws:

$$FD_c = \Delta\gamma_V + \frac{\ell_x}{V}\dot{\theta} + K_{\epsilon_2}\epsilon_G/S + \frac{0.4\,s}{s + 2.5}\,\theta$$

$$FS = \frac{1.0}{s + 1.0}\,(V - V_{ref})$$

Figure 4. Simplified Sketch of Flight Director HUD

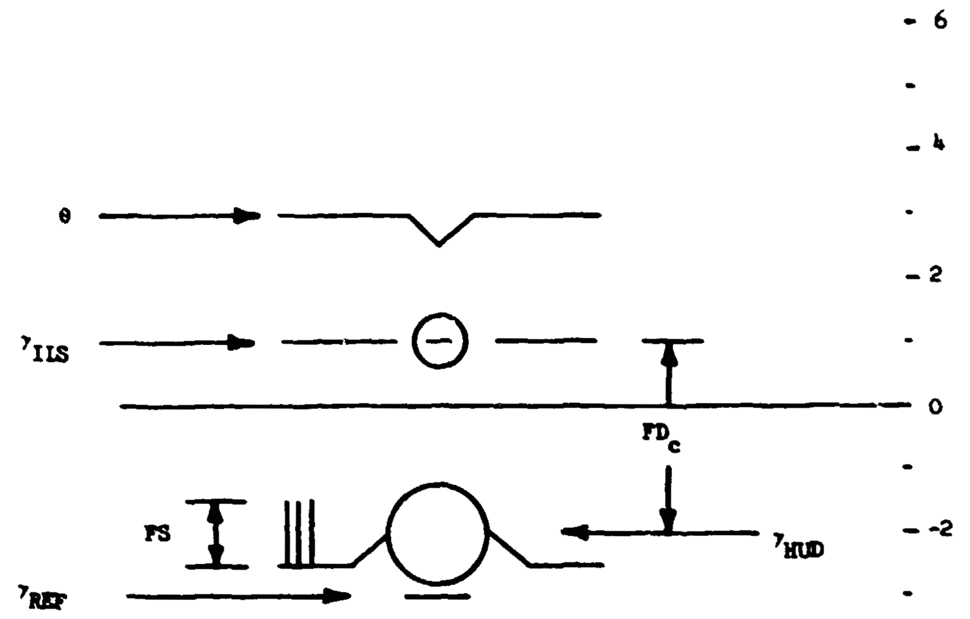

Display control laws:

$$FD_c = \Delta\gamma_V + \frac{\ell_x}{V}\dot{\theta} + K_{\epsilon_2}\epsilon_G/s + \frac{0.4\,s}{s + 2.5}\,\theta$$

$$FS = \frac{1.0}{s + 1.0}\,(V - V_{ref})$$

$$\gamma_{HUD} = \gamma_V + \frac{\ell_x}{V}\dot{\theta} + \frac{0.4\,s}{s + 2.5}\,\theta$$

$$\gamma_{ILS} = -\gamma_{REF} - K_\epsilon \epsilon_G/s$$

γ_{REF} = ILS glide slope (= 3.0 deg)

γ_V = Inertial flight path angle of aircraft

Status: Aircraft is pitched up 3 deg and on a 2 deg flight path angle. Glide slope is 3 deg above aircraft.

Figure 5. Simplified Sketch of Flight Director HUD

The reference display, Fig. 3, was a conventional head-down ADI/HSI with cross hairs used to display the flight director signals[10]. The head-down display included the normal complement CTOL instrumentation.

There were two competing concepts of head-up displays. The first was called the flight director HUD, Fig. 4, and used a fixed aircraft symbol and a moving dot to display the vertical and lateral guidance commands[11]. The second HUD was called the flight path HUD, Fig. 5, and used a conformal display of the aircraft flight path angle, the reference glide slope, and an angle that is proportional to the glide slope error[12]. For this display, an effective flight director signal can be formed by using the difference between aircraft flight path and glide slope angles.

The aircraft was a conventional jet transport and was simulated on a full six degrees of freedom motion simulator with a color visual display[13]. The simulation was restricted to terminal area navigation but the pilots did have to transition from a straight and level flight condition at 160 kt to a -3 deg flight path angle at about 130 kt (V_{ref} was chosen by the pilots). The data presented in this report was for an rms Dryden model turbulence level of 3.0 fps. No discrete wind shears were simulated.

The pilot subjects used in the simulation were eleven professional airline captains. Three of the subjects' data were selected for detailed analysis, the results of which are presented and discussed below.

The overall objectives of the simulation were to compare the CTOL head-down display to the two head-up displays and to document any advantage to using a head-up display. Many different types of data were collected and analyzed in support of these objectives. However, for the purposes of this paper, only those data related to the pilots' control strategy will be presented and discussed herein.

A summary of the experimental results related to the pilots' control strategy obtained from the simulation is shown in Table 1. A discussion of the results, and some of the data used to support these results, is contained in the following text.

TABLE 1

EXPERIMENTAL RESULTS

- Behavioral variation from display-to-display
- Behavioral variation from pilot-to-pilot
- Identification of time-varying behavior
- Detection of control strategy errors

Figure 6 shows a plot of crossover frequency, ω_c, plotted against phase margin, φ_m, for each of the three displays and three of the subject pilots. The head-down data is plotted separately from the HUD data because the display laws were different, which, of course, caused the controlled element dynamics to be different.

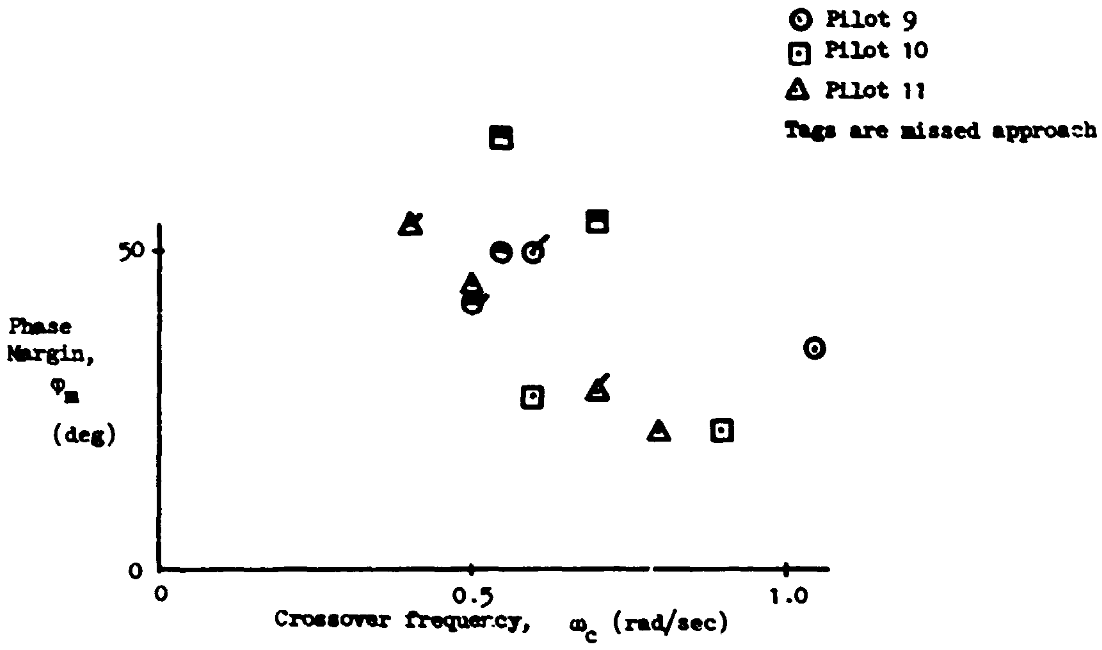

a. Flight Path HUD (open) and Flight Director HUD (top shaded)

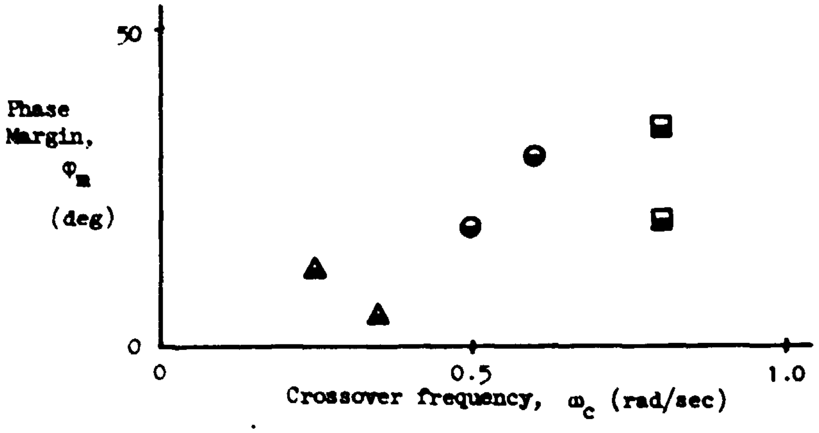

b. Head-Down Flight Director (bottom shaded)

Figure 6. Combined Pilot-Vehicle Measurements

It can be seen from Fig. 6 that similar pilot behavior for the two types of head-up displays was obtained although there was a definite trend toward flying the flight path HUD with a higher bandwidth and lower crossover frequency than with the flight director HUD. The variability among the three pilots was fairly low for the two head-up displays but quite large for the head-down display. However, within each pilot's data there was fairly low variability, which indicated that a pilot would adapt his own personal combination of ω_c and φ_m. Also note that the trends in the head-up versus the head-down displays were opposite. That is, increasing ω_c corresponded to decreasing φ_m for the head-up display but just the opposite for the head-down display. This difference was not surprising and is due to the difference in the controlled element dynamics.

Examination of the describing function data revealed that all the pilots were able to fly the head-up displays with a fairly high gain and use lead compensation in their control strategy. But the describing functions for the head-down display exhibited a low-bandwidth, and a very laggy type control technique. Some sample describing functions obtained from the simulation will be presented in a forthcoming NASA report[1].

Thus NIPIP was able to use combined pilot-vehicle and describing function measures to discern behavioral variations from display to display and from pilot to pilot.

The pilot's describing functions exhibited a trend in time-varying behavior when using the flight director HUD and head-down display but to a much less degree when using the flight path HUD. Usually what the pilots did was to increase their gain and decrease their control latency as they became closer to the minimum decision altitude. This effect is demonstrated in the describing functions shown in Fig. 7.

NIPIP was able to detect control strategy errors with the head-down display and the flight path HUD. These were due to control reversals with the head-down flight director and due to accidentally using the wrong element in the display with the flight path HUD. The time history of Fig. 8 shows how a control strategy error is manifested in the NIPIP measurements.

After "breaking out" (i.e., beneath the cloud cover) the pilot apparently became confused as to which symbol to track in the display. This caused an instability in the flight director loop. That is, positive feedback of the flight director to control column (viz., Item 6 in the figure). This sudden change in control strategy caused a sharp decrease in the amplitude and phase of Y_p, and corresponding decreases in crossover frequency and phase margin. The unstable condition lasted for only a few seconds but it was interesting that NIPIP responded to the control strategy error before the pilot was aware of it. In fact, when the pilot did become aware of it, he actually screamed and then rapidly applied the proper control action.

The time history of Fig. 8 also demonstrates how NIPIP converges after the transition from straight and level flight to a -3 deg glide slope (Item 8 in the figure). NIPIP's response to the flare and landing is also shown in Fig. 8.

CONCLUSIONS AND RECOMMENDATIONS

An empirical evaluation of the Non-Intrusive Pilot Identification Program (NIPIP) has demonstrated that accurate, unbiased estimates of a pilot's control strategy in performing manual control tasks can be obtained

ORIGINAL PAGE IS
OF POOR QUALITY

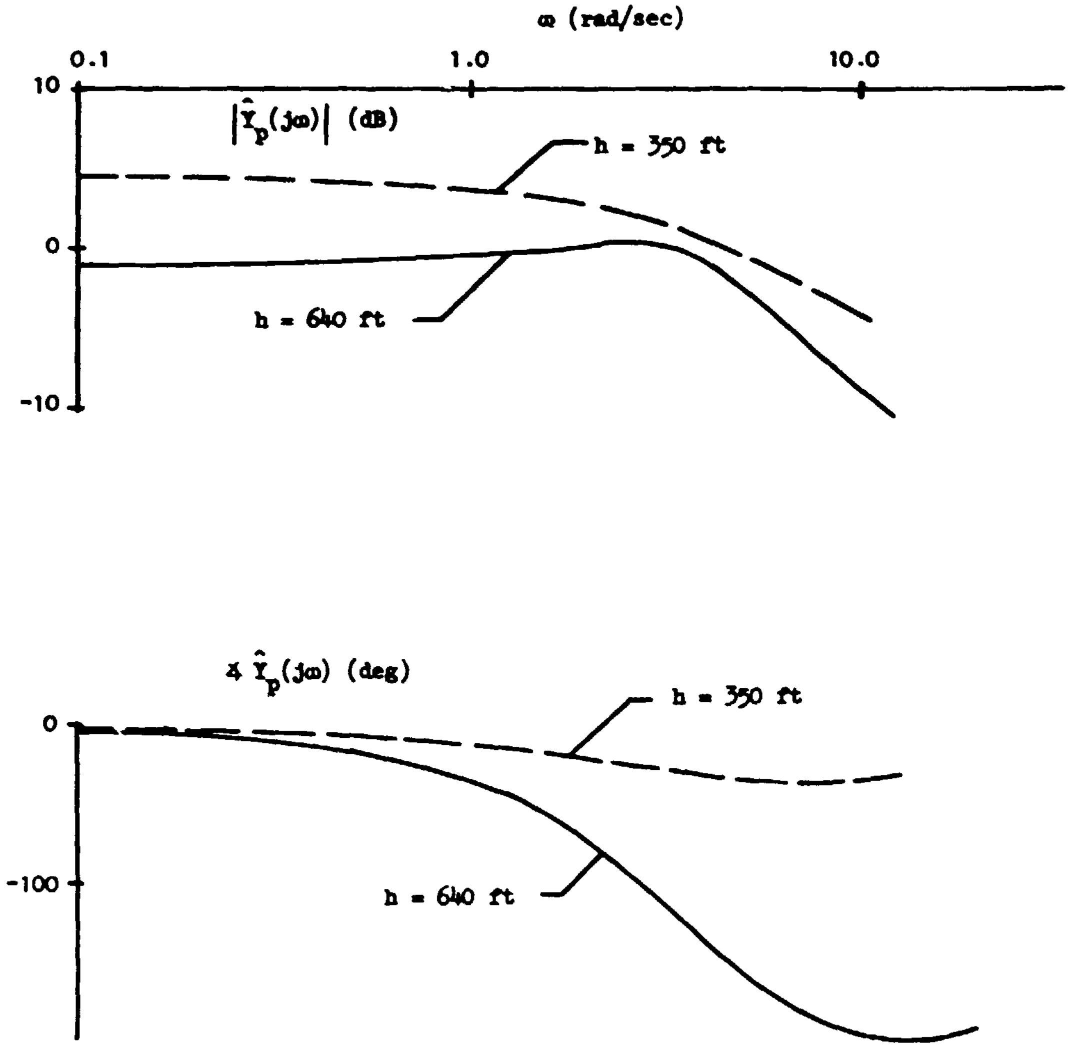

Figure 7. Describing Function Frequency Response Using Flight Director HUD (Pilot 9, Run 386)

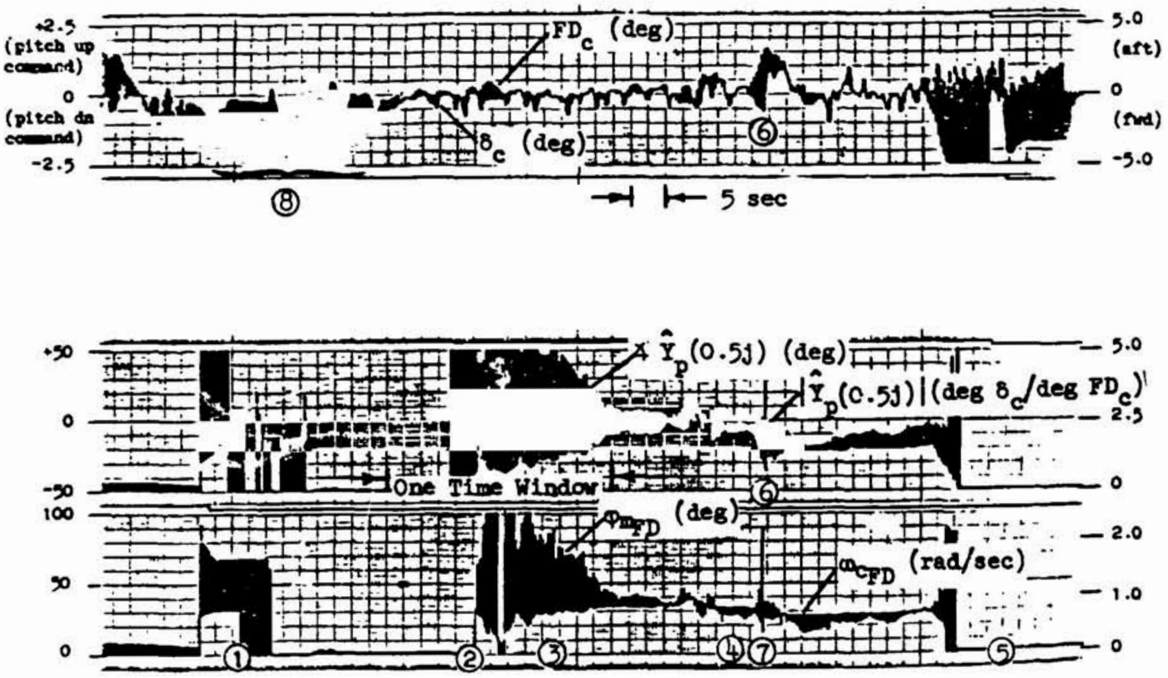

① Outer marker (NIPIP initialized)
② Time window full
③ Convergence time of NIPIP
④ Breakout (i.e., below cloud cover)
⑤ Touchdown
⑥ Pilot tracking incorrect symbol in HUD
⑦ Note the sudden change in phase margin
⑧ Precognitive maneuver

Figure 8. Time History on Final Approach for Run 335.
Flight Path HUD, Pilot 10

even in the presence of pilot remnant. Furthermore, it is possible to use NIPIP for multiloop control tasks without the use of special inputs or disturbances. Time-variations in the pilot's control strategy are identified by NIPIP through the use of a "sliding time window."

NIPIP was applied to a realtime ground-based simulation of two competing concepts of head-up displays and a conventional head-down display. It was shown that behavioral variations in the pilot's control strategy from display to display and from pilot to pilot could be measured by NIPIP. It was also shown that NIPIP could identify time-varying behavior in the pilot and detect certain types of control strategy errors.

For the simulation described herein no attempt was made to correlate the objective measures of NIPIP with subjective assessment of the task workload or pilot preference for a particular type of display. It is recommended that these types of subjective measurements be made in future applications of NIPIP in order to calibrate the objective measurements of NIPIP with pilot opinion data.

The application of NIPIP described herein was to a research project in a ground-based simulator. It would be possible to use NIPIP for many other types of manual control tasks, whether simulated or in actual flight. One such application is in the field of flight training. By using NIPIP, an instructor could monitor the performance and learning trends of the student pilot, instead of just the performance of the combined pilot-vehicle system. Improper or erroneous control techniques could be identified and the student informed of the problem.

REFERENCES

1. Jewell, Wayne F., and Ted M. Schulman, A Pilot Control Strategy Identification Technique for Use in Multiloop Control Tasks, (forthcoming NASA contractor report, May 1980).

2. McRuer, D. T., and E. S. Krendel, Mathematical Models of Human Pilot Behavior, AGARD-AG-188, January 1974.

3. Weir, D. H., and R. H. Klein, Measurement and Analysis of Pilot Scanning Behavior During Simulated Instrument Approaches, AIAA Paper No. 70-999, August 17-19, 1970.

4. Merhav, S. J., and E. Gabay, Identification of a Parametric Model of the Human Operator in Closed Loop Control Tasks, Technion - Israel Institute of Technology, Department of Aeronautical Engineering, TAE Report No. 291, June 1976.

5. Wingrove, Rodney C., Comparison of Methods for Identifying Pilot Describing Functions From Closed-Loop Operating Records, NASA TN D-6235, March 1971.

6. Balakrishna, S., Time Domain and Time Series Models for Human Activity in Compensatory Tracking Experiments, National Aeronautical Lab., NAL Technical Note TN-50, March 1976.

7. Astrom, K. J., and P. Eykhoff, "System Identification — A Survey," *Automatica*, Vol. 7, Pergamon Press, 1971, pp. 123-162.

8. Heffley, Robert K., and Wayne F. Jewell, *Development of a CTOL Piloting Technique Measurement Scheme for a Real-Time Simulator Environment*, NASA CR-152294, July 1979.

9. Chalk, C. R., T. P. Neal, T. M. Harris, et al., *Background Information and User's Guide for MIL-F-8785B (ASG), "Military Specification - Flying Qualities of Piloted Airplanes,"* AFFDL-TR-69-72, August 1969.

10. Hazen, M. R., and J. W. Kerrigan, *B-727-200 Simulation for SRI: Math Models and Checkout Data, Model 727*, Boeing Document No. D6-44608, 23 September 1977.

11. von Wieser, M. F., and F. M. Wilson, *Head-Up Display, Experimental Flight Test Programs*, 14th Corporate Aircraft Safety Seminar, Flight Safety Foundation Inc., Washington, D. C., May 14, 1969.

12. Bray, Richard S., *Head-Up Display Format No. 55*, unpublished document, August 20, 1979.

13. Sinacori, John B., Robert L. Stapleford, Wayne F. Jewell, and John M. Lehman, *Researcher's Guide to the NASA Ames Flight Simulator for Advanced Aircraft (FSAA)*, NASA CR-2875, February 1977.

OMIT
ACCESSIONED AS
81A29143

Pilot Reaction to Attitude Gyro Failure

-A Flight Experiment-

Richard L. Newman and David L. Quam

Aerospace Engineering
University of Dayton
Dayton, Ohio 45469

-Abstract-

Recently aviation safety workers have expressed concern about the ability of general aviation pilots to cope with a total vacuum system failure during flight in instrument meteorological conditions. Such a failures leaves the pilot with only a turn-rate gyro to maintain wings-level flight. Two difficulties lead to this concern. First, the pilot generally has some difficulty in flying the airplane by reference to the turn-rate gyro, the inclinometer, and the airspeed indicator (the so-called needle, ball, and airspeed). The second difficulty arose with the introduction of the turn coordinator which uses an outside-in presentation -- the reverse of the pilot's primary attitude gyro.

To evaluate the severity of the problem, a flight experiment was designed using a Cessna 172 airplane with the vacuum system modified to permit total failure of the attitude and directional gyros. Nine subject pilots, ranging in experience from 170 to 5100 hours, flew simulated (hooded) instrument missions with an unexpected gyro failure introduced at a critical point. All subjects, except for the 170 hour pilot, were instrument rated. (The 170 hour pilot was a private pilot working on his instrument rating.)

All of the subject pilots were able to maintain control of the airplane following the gyro failure. Only one subject exceeded the a priori criterion of losing a maximum of 250 feet of altitude. None of the subjects flew a satisfactory VOR approach following the failure; however all would have found the airport safely given a ceiling of 1000 feet or better.

-Introduction-

During flight in instrument meteorological conditions (IMC), the pilot is wholly dependent on his flight instruments for the cues necessary to control the airplane. In particular, the attitude and directional gyros provide vital cues the pilot needs to maintain orientation in the absence of a visual ground reference.

80-04

Both of these gyroscopic instruments are susceptible to damage from violent manuevers and to failures because of their common power supplies.

To prevent total loss of control if either or both gyros fail, a back-up instrument is required for flight in IMC. Light airplanes use a turn-rate indicator which shows the rate of yaw. This instrument relies on gyroscopic precession to deflect a needle and is therefore much more physically robust than conventional attitude and directional gyros. This means that it is much less likely to be damaged in a manuever. To preclude loss of control in the event of a power supply failure, turn-rate indicators are usually powered separately from the other two gyros. Most light airplanes use vacuum powered attitude and heading gyros (from an engine driven vacuum pump) and electric turn-rate indicators. However there is no requirement for separate power supplies in single-engine airplanes. These flight instruments and their characteristics are discussed in several instrument flight manuals published by the US government(1,2).

-Statement of the Problem-

It is much more difficult for a pilot to fly an airplane using the turn-rate indicator than the other two gyro instruments. This is well-known to any instrument rated pilot. The reasons are threefold. First, the dynamics of the turn indicator shows yaw rates, not roll information or heading. This has been partially compensated for in recent designs by tilting the axis of the gyro to produce some measure of roll rate information(3). Second, the turn-rate indicator provides no pitch attitude information. The pilot must obtain this from his airspeed or vertical speed indicator. While the airspeed can be used, these pressure instruments have built-in lags. Third, the display format is quite different from the normal presentation. The pilot must use several instruments to obtain his data. In addition, the tilted-rate-gyros in recent vogue use a format that appears superficially the same as the attitude gyro. However, the sense of the motion is reversed.

During initial instrument training, a great deal of time is spent drilling the student on flying with only the turn-rate indicator, the so-called partial panel. Virtually all of this training is accomplished by covering the attitude and directional gyros and having the student fly using only "needle, ball, and airspeed."

Although, the student is trained to fly by reference to the turn indicator, he is given no experience in detecting primary gyro failures. These failures can be described as precession, tumbling, or freezing. From a pilot's point of view, precession appears to be slightly erratic motions in both pitch and roll with a random input. The heading shown on the directional gyro slowly drifts. The cause of precession can be dirty bearings, a binding gimbal, or low gyro speed.

Tumbling is a violent precession, usually caused by a manuever that causes the gimbal to strike the stops. It can be caused by a complete power failure. To the pilot, this appears as if the attitude gyro were swimming in its display. The directional gyro simply spins. If the tumbling was caused by exceeding the gyro limits in pitch or roll, the erection mechanism will slowly return the gyros to normal operation.

Freezing of the gyros can be caused by mechanical b[illegible] or by a caging mechanism designed to prevent tumbling when power is removed. Thus, under some circumstances, a complete power failure will not result in tumbling, but will produce an unmoving display. This null failure can be quite difficult for the pilot to detect.

Failure of the common power supply (vacuum pump failure) can produce precession errors in both gyros if the failure is partial. It can produce tumbling (spinning) or freezing errors if the failure is complete. During the preliminary development of this paper, we undertook to observe an actual vacuum system failure. A Cessna 172 was flown to 12,500 ft and the engine shut down. Approximately four minutes later, passing through 9,000 ft, the attitude gyro failure. The failure mode was not apparent except by observing the outside visual reference. Holding zero pitch and roll on the indicator, the airplane rolled into a thirty degree bank spiral approximately five to ten degrees nose down. There was no indication of tumbling or failure of the gyro itself. The failure was fairly slow in developing.

The turn-rate indicator is also subject to errors. Because of its design as a rate gyro, precession is a normal event. The turn indication is simply a measure of the precession force caused by rotation about the airplane's vertical axis. The only possible malfunctions involve slowing or stopping of the gyro. These appear as decreased sensitivity or as no turn indication at all.

Several factors can influence the ability of the pilot to detect and cope with gyro failures. These are his proficiency, his training, and the instrument panel design.

Pilot proficiency includes recency of instrument flight experience, currency in the airplane, and proficiency in partial panel flight. While a proficient pilot can certainly fly a much smoother profile, it does not necessarily follow that he will be able to detect instrument failures more quickly just by virtue of his currency. However, a proficient pilot may have a lower workload than a non-proficient pilot for the same task, which may help. Recency of partial panel flying experience is more likely to be significant than the other factors, however.

Pilot training includes both initial training in instrument flying and any experience the pilot may have had in detectiing instrument failures. Obviously, few pilots at present have had any training in the recognition of a vacuum pump failure. Only those pilots who have either personally experienced an instrument failure or who have had a close associate who has experienced on will even be aware of the problem.

Instrument panel design includes such factors as warning devices (including vacuum gauges) and the design of the instruments themselves. One factor that makes partial panel flight more difficult is the different sense of motion in recent turn-rate indicators. These new instruments present the turn in an outside-in format as opposed to the conventional inside-out artificial horizon. The different sense of motion could have a negative effect both in detecting an attitude gyro failure and in flying the airplane afterwards.

Difficulties in coping with gyro failures were reported by the National Transportation Safety Board, who reviewed several fatal general aviation accidents during the period 1969 to 1973(4). In these accidents, which occurred during flight in IMC with instrument rated pilots, the Safety

Board cited vacuum systems or flight instruments as causal factors. The Safety Board noted:

> Pilots must be able to detect promptly instrument and equipment malfunctions. A successful transition from routine IFR flight to an emergency situation using only a partial instrument panel is compounded if the failure or malfunction is not recognized quickly. ... If a pilot relies too heavily on the pitch indicator, he may not crosscheck his other instruments as frequently or as efficiently as he should.(4)

This heavy reliance on the attitude indicator has been demonstrated in eye dwell experiments using experienced airline pilots during siumulated instrument approaches. Klein and Weir found that 90% of the eye dwell time was devoted to the attitude and horizontal situation indicators during simulated ILS approaches(5). If similiar eye dwell times apply to general aviation pilots, then the Safety Board's concern would seem to be well-founded.

In an attempt to determine if the problem is a severe one, a preliminary flight experiment was undertaken using a typical general aviation airplane and a sample of civilian and military pilots.

-Method-

Airplane A Cessna 172 was modified by inserting a length of plastic tubing into the vacuum line between the vacuum pump and the attitude and directional gyros. The plastic line was routed (out of sight of the left-seat pilot) to a point below and behind the right-front seat pilot. During flight, either the safety pilot or the rear-seat observer could pinch off the line and shut off the vacuum source to the gyros. The vacuum gauge was by-passed, thus eliminating this cue to the subject pilots. Two subjects noticed this during preflight runups and were told that the gauge was inoperative.

Subject Selection Most subjects were recruited from a University class in Flight Test Engineering taught at Wright-Patterson AFB. Additional subjects were recruited from local airports. Table I shows the pilots' experience and qualifications. All pilots completed a pre-experimental questionnaire and were told that the purpose of the experiment was to measure their tracking accuracy during VOR holding patterns or VOR approaches (as appropriate to the flight profile flown). All subjects except one were instrument qualified. All but one were current in either civilian or military aircraft.

Following the experiment, the subjects were told the real purpose of the experiment. (Most had guessed when the failure occurred.) They then completed a post-experiment questionnaire. Among other questions, this questionnaire asked for recency of partial panel flight and if they had ever experienced a similiar failure. None of the subjects had experienced such a failure in IMC.

Flight Profiles Two briefed profiles were flown. One consisted of a holding pattern at a VOR. The other was a VOR instrument approach to minimums. The subjects were given sufficient time to become comfortable before the final task. All reported that they felt ready for a performance measurement. The failures introduced in the holding pattern were all started at the point of reaching the VOR.

The subjects briefed to fly a VOR approach were instructed to call minimums at the appropriate point. Half were told to execute a missed approacn (with the vacuum line closed off at the same instant). The other half made a full-stop landing and the vacuum was failed during the taxi back. These subjects were given a complex routing to follow during the subsequent takeoff.

All ATC communications were simulated with the safety pilot acting as ATC.

The subjects continued to fly the prescribed patterns until they recognized the failure. If necessary, they were told to continue flying as if they were in actual weather conditions. Two military pilots with limited experience with vacuum systems had to have the common power supply for the attitude and directional gyros pointed out.

Following this, all subjects were provided a no-gyro radar steer by Dayton Approach Control to a VOR approach at a nearby airport. All had to perform the interception of final and final tracking without aid from ATC.

Data All data was hand recorded by the safety pilot and the rear seat observer who was carried on some flights. The subject's smoothness in controlling airspeed, altitude, heading, and track was evaluated before and after the failure. The level of turbulence present and the degree of ATC workload were also reported. The safety pilot for all flights was one of the authors (RLN), who is an experienced instrument instructor pilot with 1200 hours of flight instruction experience.

Also noted were the time to a failure indication on the gyro and the failure mode itself. The amount of altitude lost and the heading deviations during the failure were also noted.

The subject's post-experiment questionnaire also asked for his estimate of the excursions during the failure.

-Results-

In some ways the results were as predicted. None of the subjects was able to fly a consistent track over the ground. This was expected. However, none of the subjects lost control of the airplane. In no case did a subject pilot have any difficulty in maintaining wings-level flight. This is not to say that they flew within IFR tolerances, but they did retain control of the airplane.

ORIGINAL PAGE IS
OF POOR QUALITY

Table II shows the extent of airspeed, altitude, heading, and track excursions noted by the safety pilot and by the subjects themselves in the post experiment questionnaires. In general the track excursions were so bad that no consistent measure could be used by the safety pilot. Before the experiment was flown, we had decided that losing 250 ft would be considered "a loss of control." As can be seen in the table, only one subject exceeded this figure. In retrospect, this criterion was probably too strict.

Following detection of the failure, the subjects were required to fly a VOR approach. They were allowed a no-gyro vector to intercept the final approach course, but they were required to intercept and fly the final based solely on their own navigation. Table III shows the safety pilot's assessment their smoothness of control both before and following the failure. The smoothness "after failure" does not include the excursions during the initial part of the failure, just the flying "after settling down." One subject, S5, had better performance following the failure. This particular subject had not been on flying status for some time and was probably still on the learning curve. All of the other subjects did not do as well on the partial panel as on the full panel.

It is worth noting the different failure descriptions. The holding pattern failures took about six minutes to develop. These usually produced a pitch up error. That is, the gyro showed a pitch down leading the pilot to raise the nose. The directional gyro continued to run for some time after the attitude gyro failed in most cases.

During the failures introduced on takeoff or during a go-around, the failures occurred much more quickly. In these cases the failure modes were not at all consistent. The failure descriptions are shown in Table IV.

Table V shows additional responses to questions on the post-experiment questionnaire. The most common reply to "what cue did you use to detect or notice the failure?" was the attitude gyro. Actually, the subjects reported that it was discrepancies between this instrument and other instruments that first alerted them to a problem. Several cited inconsistent responses displayed on the artificial horizon as they applied control inputs.

The subjects did not feel that control was especially difficult following the failure. While they were sure that previous experience did help them to fly with a partial panel, they were much less sure about the value of this experience in detecting a failure. The failed gyros' motion did distract them during the partial panel flight.

In general the subject pilots felt that this was a realistic demonstration of instrument failure. A number of comments suggest that it would be a useful addition to intial and recurrent instrument training. These comments are shown in Table VI.

-Conclusions-

The primary conclusion is that the problem of general aviation pilots coping with vacuum pump failures is not as severe as initially believed when the experiment was designed. While the subject pilots were reasonably current, they had not practiced partial-panel flight for many years (in one case nineteen years). Nevertheless they were able to fly the airplane safely and would have made a safe recovery had the weather been a 1000 ft ceiling with one mile visibility. In spite of articles to the contrary (6), the general aviation pilot seems to be able to cope with the problem. The military pilots had more difficulty, primarily because of a lack of familiarity with the systems.

It did seem that the subjects had no clear-cut approach to flying a given track on partial panel, however. They did not attempt to fly a heading, but rather reacted simply to the motion of the deviation indicator. It would seem that this area could be added to initial instrument training.

We recommend that partial panel training for initial instrument ratings be improved to include failure modes of the primary instruments with subsequent tracking and at least one VOR approach.

-References-

1 *Instrument Flying*, USAF AFM-51-37, November 1971

2 *Instrument Flying Handbook*, FAA AC-61-27B, September 1970

3 G. J. Stinnet, C. T. Jackson, and P. D. Talbot, *The Turn Rate Indicator -- Its Interpretation as Affected by Installation and True Airspeed*, SAE Paper No. 710380, March 1971

4 "Inadequate Instrument Crosschecks and Untimely Detection of Instrument and Equipment Malfunctions," NTSB Safety Recommendations Nos. A-76-29 and A-76-30, March 1976

5 D. H. Weir and R. H. Klein, "Measurement and Analysis of Pilot Scanning Behavior During Simulated Instrument Approaches," *Journal of Aircraft*, *8*, 1971, 897-904

6 B. Schiff, "Gyro Failure," *AOPA Pilot*, October 1979, pp. 49-55

March 1980

ORIGINAL PAGE IS
OF POOR QUALITY

SUBJECT	FLIGHT EXPERIENCE		QUALIFICATIONS[(a)]		CURRENT AIRCRAFT	RECENT IFR EXPERIENCE			PROFILE FLOWN
						LAST 90 DAYS		PARTIAL PANEL(b)	
	TOTAL	INSTRUMENT	CIVIL	MILITARY		HOURS	APPRS		
S1	170	30	PP(c)	--	CE-172	15	10	1 month	Holding Pattern
S2	600	100	PP	--	CE-172	5	4	--	Holding Pattern
S3	600	165	CP/II	--	PA-28R	4	0	2 years	Takeoff
S4	615	93	CP	--	PA-28	2	4	1 year	Go Around
S5	1600	300	CP	IP	T-37(d)	0	0	3 years	Holding Pattern
S6	2300	130	CP/II	--	CE-172	4	5	5 years	Takeoff
S7	2380	1000	--	FE	C-135	22	30	6 years	Holding Pattern
S8	2500	600	CP	IP	C-135	15	10	Never	Holding Pattern
S9	5100	1200	CP	FE/FL	A-7D	15	12	19 years	Go Around

(a) Code: PP = Private Pilot; CP = Commercial Pilot; II = Instrument Instructor
IP = Instructor Pilot; FE = Stan/Eval Flight Examiner; FL = Flight Leader
All except S1 were instrument qualified.

(b) Time since subject last practiced partial panel flight.

(c) This subject had no instrument rating, but was training for it.

(d) This subject was not currently on flying status. He was previously a T-37 IP.

Table I

Subject Qualifications

ORIGINAL PAGE IS
OF POOR QUALITY

FLIGHT PROFILE	SUBJECT PILOT	MAXIMUM EXCURSIONS DURING GYRO FAILURE							
		SAFETY PILOT ASSESSMENT				SUBJECT PILOT ASSESSMENT			
		Airspeed	Altitude	Heading	Track	Airspeed	Altitude	Heading	Track
Holding Pattern	S1	+10	+200	30	-	UNK	200	25	O/S(a)
	S2	-10	+300 -200	50	-	±15	+200	±30	±30
	S5	-10	+200	50	-	10	150	30	20
	S7	0	+200 -150	360	-	-10	+200	-	-
	S8	0	+300	360	-	0	150	"bad"	-
Takeoff	S3	0	+350 -50	-	-	±20	±150	±20	-
	S6	0	[illegible]	10	-	0	0	20	-
Go Around	S4	+10 -20	+100 -300	20	-	-	-	10	5
	S9	±5	±80	±10	-	0	100	-	-

(a) O/S = Off Scale

Table II

Maximum Excursions During Gyro Failure

ORIGINAL PAGE IS
OF POOR QUALITY

FLIGHT PROFILE	SUBJECT PILOT	SAFETY PILOT ASSESSMENT OF SMOOTHNESS							
		BEFORE FAILURE				AFTER FAILURE			
		Airspeed	Altitude	Heading	Track	Airspeed	Altitude	Heading	Track
Holding Pattern	S1	8	5	5	5	5	5	3	3
	S2	7	6	6	5	6	5	3	3
	S5	5	5	4	4	6	5	4	4
	S7	9	8	7	7	5	3	1	1
	S8	9	9	8	8	7	4	1	1
Takeoff	S3	8	5	8	9	8	8	-	-
	S6	9	9	5	4	5	5	4	-
Go Around	S4	8	7	8	9	6	5	4	-
	S9	8	5	5	-	8	4	3	5

Table III

Smoothness of Flight Before and After Failure

FLIGHT PROFILE	SUBJECT PILOT	TURBULENCE	TIME TO FAILURE	DESCRIPTION OF FAILURE
Holding Pattern	S1	None	6:00	Pitch up
	S2	Light	6:00	Pitch up; one minute later, dimectional gyro Began to spin
	S5	None	6:00	Pitch up; one minute thirty seconds later attitude gyro tumbled
	S7	None	6:12	Pitch up; attitude indiator sluggish
	S8	None	5:51	Pitch up; followed by slow 360 degree rolls
Takeoff	S3	Light	--	Showed pitch-up
	S6	Light	4:30	Directional gyro froze; followed by attitude gyro pitch up and 360 roll
Go Around	S4	Moderate	4:30	Pitch down and left roll
	S9	Moderate	2:00	Sluggish attitude indicator, shows roll error Directional gyro did not fail until 6:00 after vacuum failure

Table IV

Failure Descriptions

QUESTIONS	NO.	RESPONSES
CUES USED TO DETECT FAILURE	8	Artificial Horizon
	3	Directional Gyro
	2	Sound Cues
	1	Airspeed
	1	Deviation on Course Indicator
	1	Altimeter
	1	Turn and Bank
	1	Vertical Speed
HOW DIFFICULT WAS CONTROL FOLLOWING FAILURE?	-	Very Easy
	2	Easy
	6	Medium
	1	Difficult
	-	Very Difficult
DID PREVIOUS PARTIAL PANEL EXP. HELP YOU		
TO DETECT THE FAILURE	3	Yes, Definitely
	2	Probably
	2	Uncertain
	2	Probably Not
	-	No, Definitely
TO FLY AFTER YOU WERE AWARE OF THE FAILURE	6	Yes, Definitely
	1	Probably
	-	Uncertain
	2	Probably Not
	-	No, Definitely
DID THE FAILED INDICATORS DISTRACT YOU	3	Yes, Considerably
	5	A little
	1	No
WAS THE FAILURE REALISTIC	9	Yes
	-	No

Table V

Additional Responses

SUBJECT PILOT	ADDITIONAL COMMENTS
S1	Need more practice like this.
S2	More of this type of thing should be done in the interest of flying safety.
S4	Good practice. I felt it was a valuable experience since I was totally ignorant that it was not a genuine failure. Should be required on Biannual.
S8	I hope it never happens to me in small aircraft. I never realized how much I used the other pilot's panel when this situation arose.
S9	Very insideous and realistic. The turn coordinator and the ADI turn in opposite directions.

Table VI

Subject Pilot Comments

Smit

PILOT INDUCED LONG PERIOD OSCILLATIONS CREATED BY CERTAIN DISPLAY CONFIGURATIONS

by

James J. Adams
NASA Langley Research Center
Hampton, Virginia

General aviation accident records show that the most dangerous period of an IFR flight is the approach to landing. One area of concern in this matter is the role that instrument display configurations play in the stability of the pilot-aircraft system. Pilot response studies and pilot modeling effort have shown that the pilot does respond much like a linear feedback control mechanism when controlling an aircraft, and that a definite stability characteristic does result in the pilot-aircraft system. Aircraft are designed so that in most cases this system stability is positive (damped), but occasions do arise when the system becomes unstable. Pilot induced oscillations have been an item of study for some time. Up until now these studies have usually centered around short period (around 2 to 3 seconds) instabilities. Long period unstable oscillations can also occur, involving large displacements from the desired flight path of the aircraft, which affect the safety of flight. There is evidence of such long period instabilities to be found in measurements made during instrument landing approaches. However, these instabilities usually do not have time to become well developed before the pilot goes visual, and then the instability disappears. The present study will emphasize the existence of these long period instabilities by special test techniques made possible by the flexibility of the simulation computer, and relate them to conventional general aviation instrument display configurations.

N82 34062 D25

DESIGN, SIMULATION AND EVALUATION OF ADVANCED DISPLAY CONCEPTS FOR THE F-16 CONTROL CONFIGURED VEHICLE

Robert W. Klein*
Guidance and Control Department
Grumman Aerospace Corporation
Bethpage, N.Y. 11714

Walter M. Hollister
Associate Professor, Department of Aeronautics and Astronautics
Massachusetts Institute of Technology
Cambridge, MA 02139

*research conducted at: Department of Aeronautics and Astronautics
Massachusetts Institute of Technology
Cambridge, MA 02139

ABSTRACT

The purpose of this study was to design, simulate and evaluate advanced display concepts to augment the tracking ability of the F-16 Control Configured Vehicle (CCV). A literature search reveals that historically CCV and display research has been conducted independently; the design of a display system for a CCV aircraft should take the unique CCV flight modes (i.e. direct force, pointing, translation) into consideration. This paper details the recent M.I.T. study which reviewed the F-16 CCV flight test program, reviewed current aircraft display research, and suggests task-oriented and compensatory displays to even further enhance the capability of the F-16 CCV.

The fixed-base M.I.T. 707 simulator was modified to represent the F-16 CCV. An isometric sidearm control stick and two-axis CCV thumb button were installed in the cockpit. The forward cockpit CRT was programmed to present an external scene (numbered runway, horizon) and the designed Heads Up Display. The cockpit interior was modified to represent a fighter and the F-16 CCV dynamics and direct lift and side force modes were programmed. Compensatory displays were designed from man:machine considerations.

Pilots evaluated the Heads Up Display and compensatory displays during simulated descents in the presence of several levels of filtered, zero-mean wind gusts. During a descent from 2500 feet to the runway, the pilots tracked a point on the runway utilizing the basic F-16, F-16 CCV, and F-16 CCV with advanced displays. Substantial tracking improvements resulted utilizing the CCV modes, and the displays were found to even further enhance the tracking ability of the F-16 CCV.

INTRODUCTION

The F-16 Control Configured Vehicle

The F-16 CCV was selected for the M.I.T. study based on the operational timeframe of the aircraft, recent flight test and evaluation by USAF pilots, and availability of aircraft dynamics data. In 1973 the Air Force Flight Dynamics Laboratory contracted with General Dynamics for an 87 flight, 125 hour test program of the F-16 CCV (ref. 1). This marked the first exploitation of decoupled six degree-of-freedom flight path control. Completed in June 1977, Edwards Air Force Base test pilots evaluated the CCV control modes

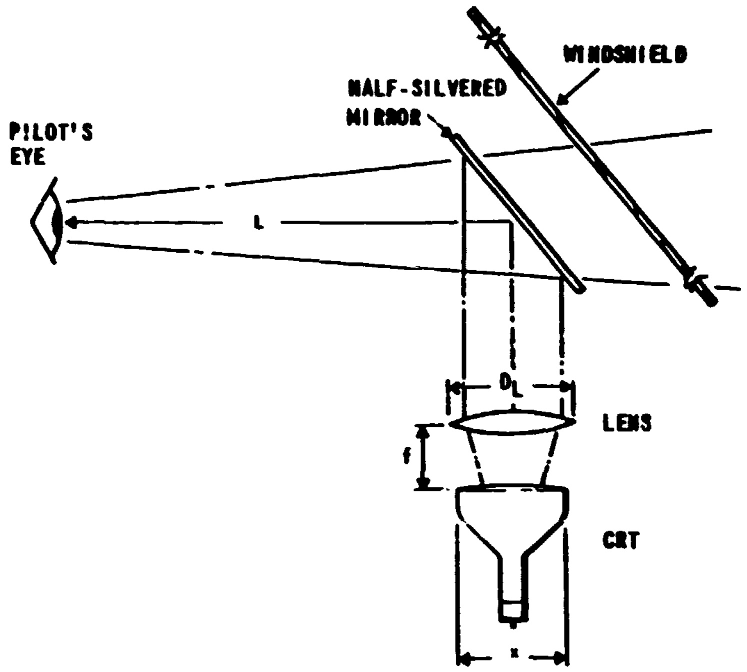
WINDSHIELD
HALF-SILVERED MIRROR
PILOT'S EYE
L
D_L
LENS
f
CRT
x

Figure 1. Heads Up Display (HUD) Optics

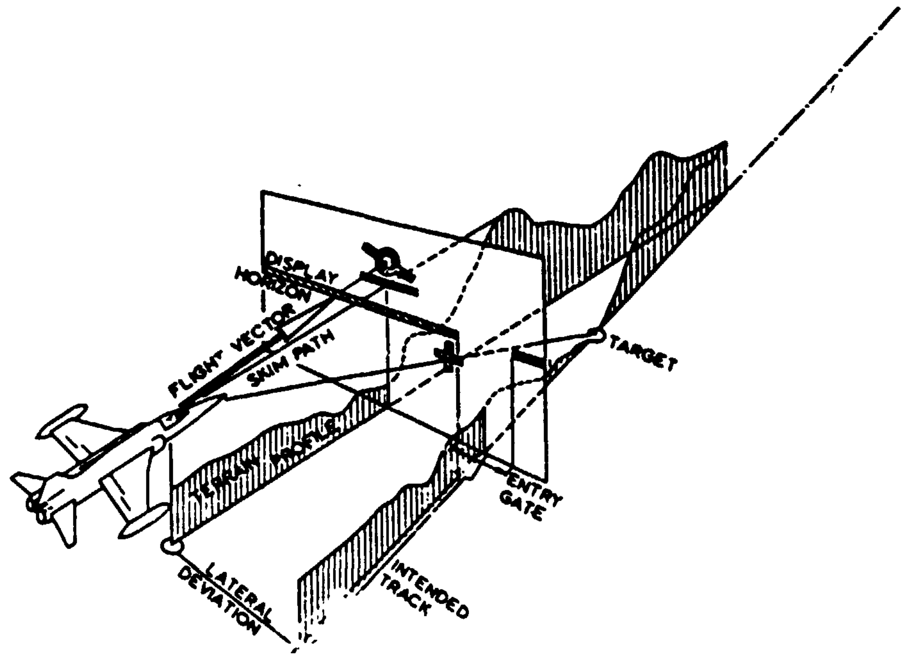
TRUE HORIZON
DISPLAY HORIZON
FLIGHT VECTOR
SKIM PATH
TERRAIN PROFILE
TARGET
ENTRY GATE
INTENDED TRACK
LATERAL DEVIATION

Figure 2. External Scene Appearance through the HUD

for air-to-air and air-to-ground missions. Recommendations made during the flight test program are incorporated in the M.I.T. display.

References 2,3, and 4 detail the F-16 CCV program. Modifications to the F-16 include canted canards on the forward fuselage and modification of the flight control system (FCS) to implement the direct force, pointing and translation modes. The trim button on the sidearm controller was replaced with a two-axis. force-operated thumb button. Thus in the direct force mode, left thumb pressure on the thumb button commands a left flat turn rate. Upward thumb pressure commands direct lift. In the direct force mode, pressure on the thumb button commands the rate of change of horizontal and vertical flight path angle. "Beeping" the thumb button increments the flight path angle for small tracking corrections. The CCV mode (direct force, pointing, translation) is selected on the cockpit control panel and commanded by the thumb button. Note that the pilot does not move his hands or feet from the conventional controls to utilize the CCV modes; they do not disturb normal aircraft operation and augment the fighter capability.

During the flight test program, gun camera films quantitatively recorded tracking performance and qualitative pilot comments were recorded. The pilots recommended higher authority modes (3 g's or greater). They noted that the flight path angle could be driven laterally without banking, eliminating the "pendulum effect" with the fixed recticle sight. Since the CCV aircraft effectively decouples the aircraft attitude and velocity vectors, attitude was no longer a cue for the aircraft's instantaneous destination. A Heads Up Display (HUD) presentation of the velocity vector was recommended to restore the attitude:velocity vector cue. Many of the modes enhanced fighter operations in air-to-air and air-to-ground tasks (ref. 3).

Advanced Displays

The decision to choose a Heads Up Display (HUD) to augment the CCV aircraft operation follows from analysis of the CCV aircraft/mode controller/pilot interface. The flight regimes in which the CCV modes will improve fighter performance is in air-to-air combat, air-to-ground weapons delivery and landing in variable weather conditions. In all these missions the pilot's attention is focussed outside the aircraft at another aircraft, a ground target, or the runway. The Heads Up Display allows the pilot to keep his attention oriented outside the canopy with his eyes focussed at infinity. The measured and displayed flight information appears in one-to-one correspondence with the outside world. A HUD presentation of the velocity vector overlayed on the external scene restores the lost attitude:velocity vector feedback and improves perception of the aircraft flight path. These reasons strategically point to the utilization of a Heads Up Display to fully realize CCV mode potential.

Figure 1 illustrates how a Heads Up Display operates. By projecting flight information through a lens on a half silvered mirror oriented inside the canopy, the pilot simultaneously views the outside world and flight data focussed at infinity. Delays are eliminated in continually refocussing from the heads down instruments to the external scene. The sheer distance and associated delay time in scanning from one instrument to another is signifigantly reduced since most of the relevant flight information is integrated on the HUD display.

Figure 2 shows how the flight information and outside scene appears through the HUD. The primary information a HUD should display is the flight vector, the horizon and the intended track or target superimposed on the external scene. Other information which can be displayed is an aircraft attitude symbol, reference angle-of-attack, limit angle-of-attack (stall) and potential path (aircraft path in accelerated flight). The potential path is used for thrust management. When the symbol is above the velocity vector excess thrust exists and when the symbols coincide velocity is stabilized. When the velocity vector is above the horizon the aircraft is climbing and when below the horizon it is losing altitude. When symbolic flight data is in one-to-one correspondence angularly with the outside view, aircraft states are more easily interpreted and controlled.

For example, if the velocity vector, horizon, and aircraft body axis are displayed on the HUD, the following angles are readily apparent:

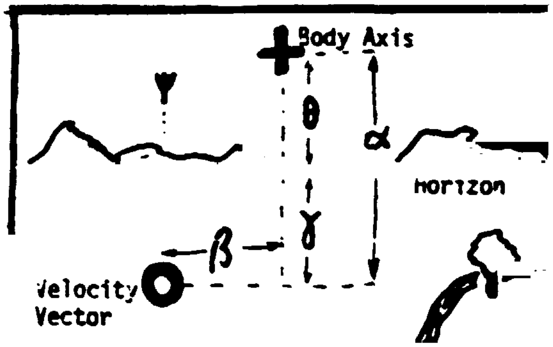

Heading ψ
Sideslip β
Angle-of-attack α
Flight Path Angle γ
Pitch Angle θ

Figure 3. Angular Data Perceptible from HUD Symbology

Flight information (such as velocity V, vertical velocity $\dot{h}$) can be visually deduced from angular relationships between the velocity vector, body axis and horizon overlayed on the real world. The pilot may steer the velocity vector towards an intended destination point. Any cross wind or wind gradient (shear) is immediately apparent since the background scene will drift with respect to the velocity vector. Immediate realization of these situations allow the pilot to make appropriate corrective control actions.

In general, a pilot can monitor seven to eight data items without difficulty, according to research carried out by the Royal Aircraft Establishment, Farnborough, England. Thus the display should be designed to show only those instrument readings necessary for a given mode of flight. The highest priority data should be close to the nominal field of view to reduce scan lag. Information should be displayed in the appropriate analog (compensatory) or digital (numerical) form to minimize pilot workload. Large eye movements should be minimized, and the display axes should physically correspond with the outside world (i.e. altitude along vertical axis, heading angle along the horizontal axis, etc.) in "natural display directions" (as viewed from the aircraft outward). It is also advantageous to have the altitude, airspeed, etc. information located in the normal "T" dashboard panel positions (airspeed upper left, altitude upper right, etc.) for crew transition to the HUD display. The nearness of data to the nominal point of view and its priority should follow a gaussian distribution (the most frequently scanned displays closest). Displaying information in the appropriate analog tape form or digital form should minimize interpretive and compensatory workload. The HUD field of view must be wide enough so that velocity, heading, and altitude may be peripherally displayed without interfering with target acquisition. Since angular relationships are preserved on the HUD, and the HUD is nominally located 19" from the pilot's eyes, a 10" HUD screen yields a 30° field of view. This is appropriate for the

± 5° pointing authority (a 10° authority square in a 30° by 30° field) and the angle-of-attack variation from high to low speed.

DISPLAY DESIGN FOR THE CCV AIRCRAFT

In designing an appropriate display to augment CCV aircraft performance one must consider the display as part of the total pilot/controller/aircraft closed loop system (figure 4). In conventional aircraft, the pilot must utilize several controls in a closed loop fashion to bring about a commanded state. The pilot adjusts his internal transfer function to effectively decouple the coupled system. In general, the human is not particularly efficient in decoupling multiple degrees-of-freedom systems. Such systems increase the workload and compensation a pilot must provide in bringing about a desired state. For instance, in making a heading change, the pilot utilizes the aileron, rudder and elevator to initiate the bank, to bank, and return to wings level flight once the desired heading change is achieved. The aircraft is strongly coupled lateral-directionally. The pilot must apply "lead" or anticipate when to roll out of the bank. The decoupling and lead the pilot must apply correspond to an increase in concentration during the maneuver and thus an increase in pilot workload.

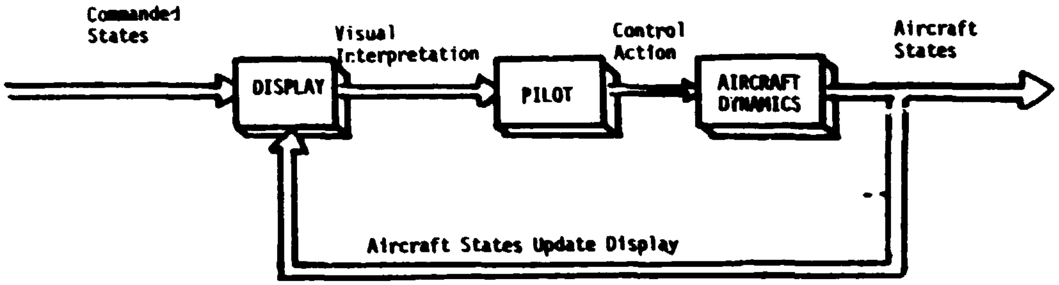

Figure 4. The Display System as part of the Total Pilot/Aircraft System

Herein lies the advantage of the CCV aircraft. One control may be utilized to command one state. In the above example, the CCV pilot could just "beep" a heading angle change using the direct side force mode The rate of change of heading is proportional to the lateral thumb force on the "Coolie Hat" thumb button. The response is decoupled, and the heading change is easily conducted, since the heading angle change is proportional to one input (single input: single output relationship). A similar analogy may be made with the sluggish phugoid mode which is controlled by thrust and elevator setting. The direct lift mode quickens the phugoid response and commands the flight path angle.

In designing a display for the CCV aircraft one notes that there are already features of conventional displays which augment CCV performance. The conventional system of crosshairs serves as an aid in compensatory tracking or nulling the diagonal offset of a target. If one crosshair axis is met, the human controller knows to translate purely along that axis (figure 5). The CCV slew rate responses to horizontal and vertical thumb button inputs are parallel to the crosshairs. In this way CCV display design has been reduced to human compensatory engineering analysis.

In nulling the pointing error the display should improve CCV performance if it displays aircraft slew rate magnitude and direction. These are sensed on the thumb controller (slew rate is proportional to force on thumb controller)

PRECEDING PAGE BLANK NOT FILMED

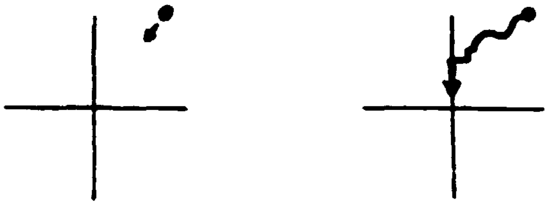

Figure 5. Nulling Offsets Utilizing Aircraft Crosshair System

but the authors believe that force magnitude and angle are not sensed accurately enough by the thumb. A proper display of CCV slew rates and direction of slew would augment CCV performance in air-to-air and air-to-ground tracking. One possibility is a vector display (figure 6) which shows the magnitude and direction of the slew rate. The human controller, visualizing the actual slew rate magnitude and direction, can change the force and direction exerted on the thumb controller to null the pointing error. The overall CCV tracking capability should improve since the display applies an additional more accurate feedback to the pilot than the force feedback from the thumb controller.

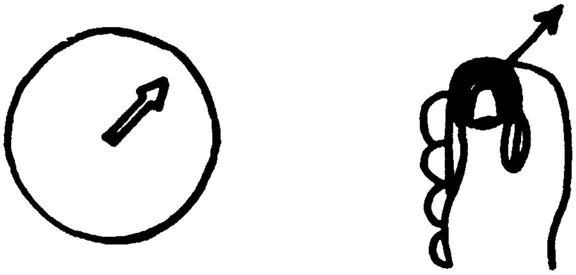

Figure 6. Vector Compensatory Display Showing CCV Magnitude and Direction

If there is concern that the arrow will interfere with target acquisition, another display could be a line showing the angular direction of the thumb force exerted on the "Coolie Hat" (figure 7). Angular data, rather than magnitude data, is presented since the thumb probably senses force level better than force direction, and thus it is force direction data that is incorporated in the display.

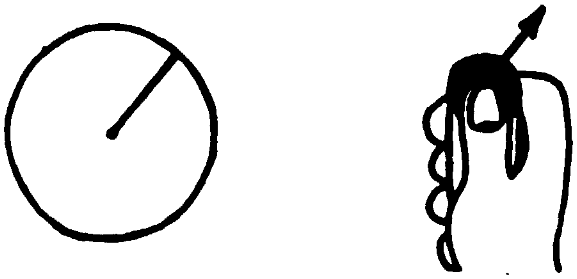

Figure 7. Angular Compensatory Format and CCV Mode Activation

Another feature which should be incorporated is an authority circle. With equal pointing capability in pitch and yaw, the circle illustrates the region in which CCV pointing modes may be utilized. No guesswork is necessary: once the pilot acquires the target within the authority circle, he may utilize the quick, decoupled CCV modes for precise aiming. Thus for the pointing mode, there are two candidate compensatory formats (figures 6 and 7).

Similar magnitude and direction information could be displayed for the direct force and translation modes (e.g. for acceleration, vector length and direction indicates magnitude and direction of acceleration, maximum vector length inside the authority circle corresponds to maximum CCV acceleration). The nominal velocity vector circle would serve as the vector origin with a deadband for small force inputs. Thus either figure 6 or 7 could be used for compensatory tasks involving the direct force, pointing or translational CCV mode, depending on which mode was presently in operation.

The next step is the display of numerical flight data. This includes airspeed, heading angle, altitude, Mach number, and rate-of-climb/sink. Tape scales of airspeed will be displayed along the left border, heading along the top, and altitude along the right border. The analog "tape" form is chosen since this is compensatory data and pilot workload is lower nulling tape errors rather than reading a digital format, interpreting the data and making an appropriate control action (rate information is lacking in the digital format). Digital values of Mach number and rate-of-climb/sink are displayed in boxes. In this case the numerical values are of most interest. An artificial horizon is also included in this integrated display. Based on the above analysis of CCV operation and advanced displays, the candidate Heads Up Displays in figures 8 and 9 are proposed.

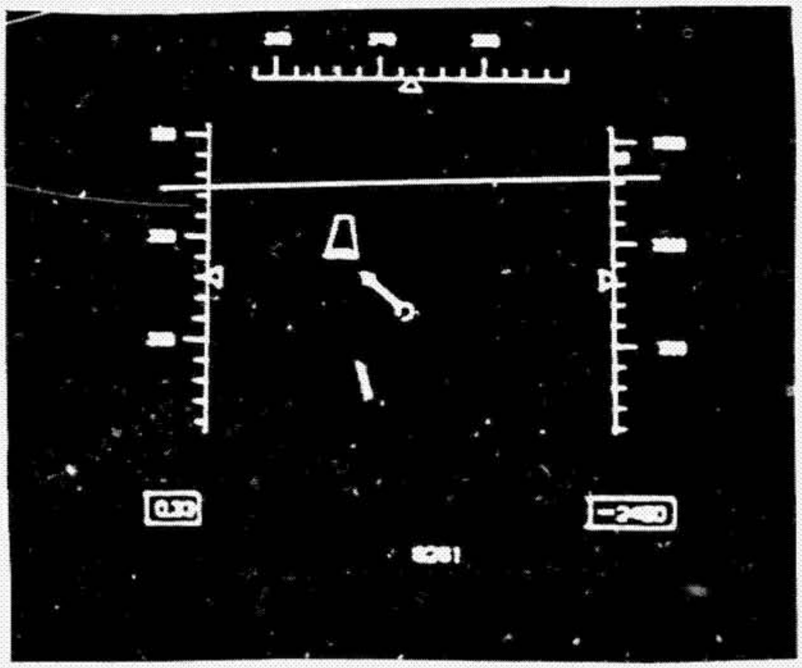

Figure 8. Candidate Heads Up Display with Compensatory Display (Arrow)

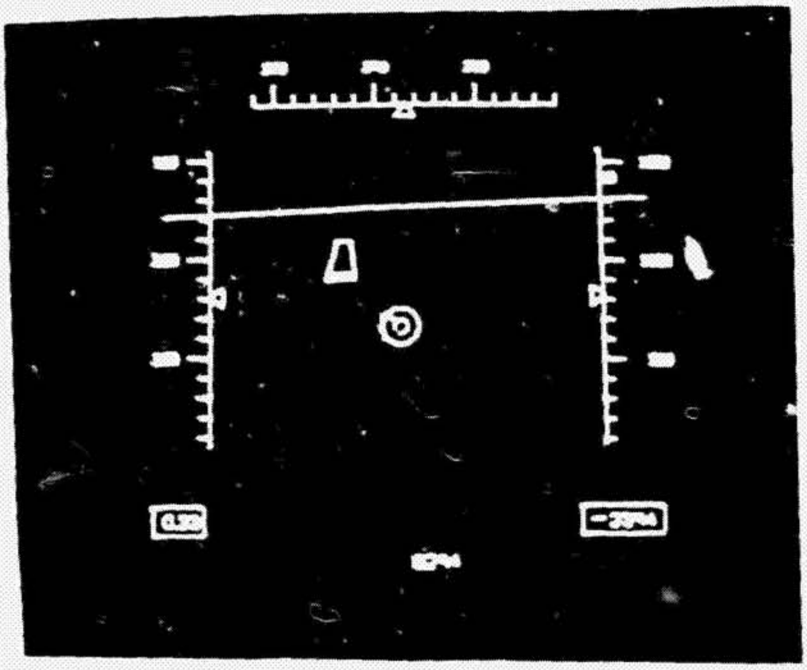

Figure 9. Candidate Heads Up Display with Compensatory Display (Angular)

CONVERSION OF THE 707 SIMULATOR TO THE F-16 CCV

In order to evaluate these concepts an existing 707 simulator (figure 10) was converted to an F-16 CCV simulator with an advanced Heads Up Display. Extensive modifications were made to the assembly language programs to accommodate the F-16 aircraft dynamics. The Heads Up Displays shown in figures 8 and 9 were programmed. A numbered runway and horizon line was added to represent the external scene during the flight simulation. The external scene enhanced the fidelity of the simulation by providing aircraft positional perspective with respect to the runway and attitude cues. The cockpit interior was modified to represent a fighter and isometric sidearm controller (as currently utilized on the F-16) with CCV isometric thumb button was installed in the right half of the cockpit. Figure 11 outlines the operation of the simulator. The simulator pilot, viewing the HUD and external scene, operates the controls (stick, CCV button, throttle, etc.) to bring about a change in aircraft states. These mechanical inputs are converted to electrical analog signals which are then sampled by an analog:digital converter. The signals are demultiplexed into appropriate channels for the assembly language programs. The Adage AGT-30 computer calculates the aircraft states and updates the HUD and external scene CRT display. An update occurs every 1/20 second with no perceptible flicker. The previous 707 simulator is the product of ten years of research at M.I.T.

A random, zero-mean wind gust program was written to study tracking performance in the presence of gusts and turbulence. The gusts were realistically generated by filtering Gaussian white noise with the Dryden spectra wind model. The RMS amplitude of the wind was set for three discrete levels during the test program.

Originally the compensatory displays were to indicate just the CCV input. This yielded somewhat encouraging tracking improvements. The decision was made

Figure 10. Modification of Right Half of Cockpit to Represent the F-16 CCV with Heads Up Display and External View

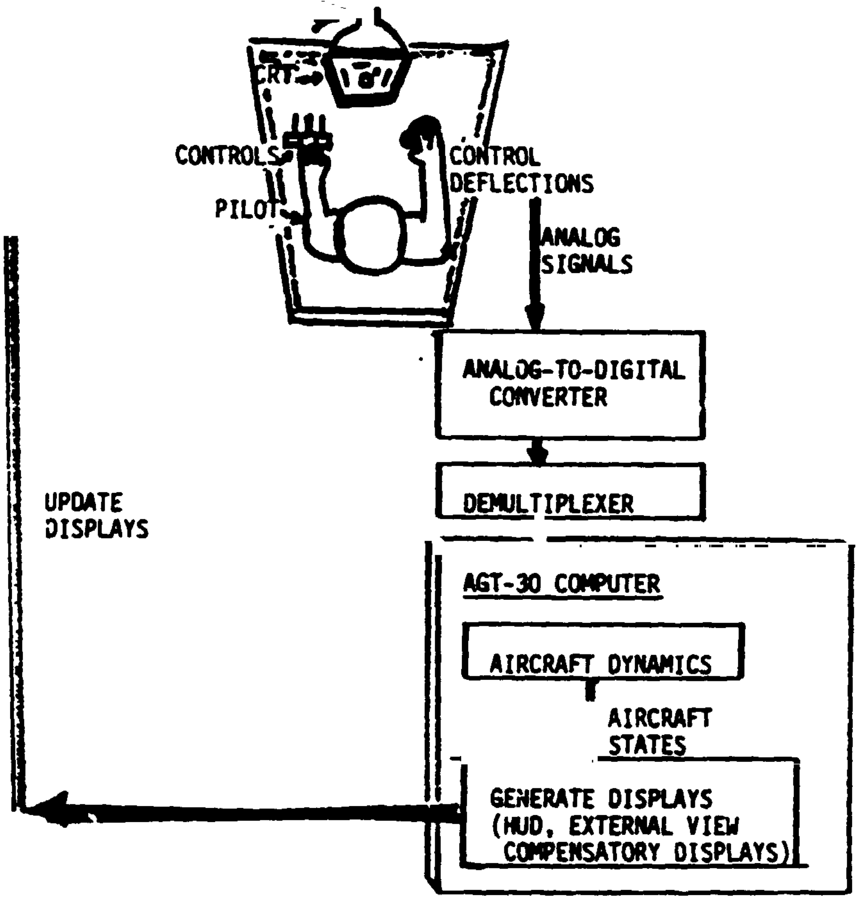
CRT
CONTROLS
PILOT
CONTROL
DEFLECTIONS
ANALOG
SIGNALS
ANALOG-TO-DIGITAL
CONVERTER
DEMULTIPLEXER
UPDATE
DISPLAYS
AGT-30 COMPUTER
AIRCRAFT DYNAMICS
AIRCRAFT
STATES
GENERATE DISPLAYS
(HUD, EXTERNAL VIEW
COMPENSATORY DISPLAYS)

Figure 11. Simulator Operation with AGT-30 Computer

to have the compensatory displays represent the vector sum of the direct force modes (thumb button input) and wind effects upon the aircraft. Thus the arrow and line represent the inertial aircraft acceleration. The displays therefore serve two purposes. By showing acceleration they provide lead to the pilot in the tracking task. The displays also provide an additional visual cue to the pilot so when a sudden gust affects the aircraft the pilot may respond immediately. The arrow represents the future position (in 3/10 second) of the velocity vector circle with respect to the external scene, and aids the pilot with or without wind.

TEST PROGRAM

The purpose of the test program was to utilize the F-16 CCV simulator to determine whether the CCV modes do improve tracking performance over the conventional aircraft flight modes and if the designed compensatory displays do indeed augment CCV tracking performance. A tracking task was programmed into the F-16 CCV simulator: tracking the aircraft velocity vector over the runway numbers. A program was written to determine the average tracking error (RMS) in degrees x 1000. Figure 12 shows the instantaneous error ERRT which is averaged over time (samplings occur every 1/20 second). The performance index or average RMS tracking error is

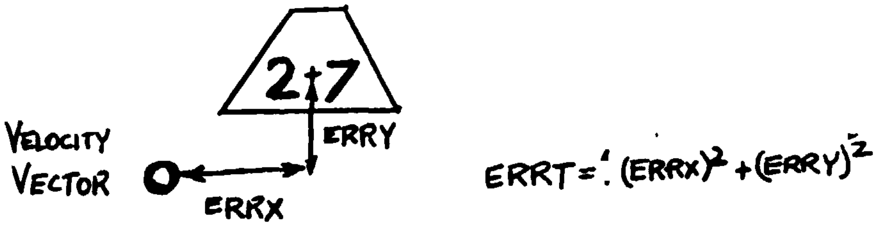

Figure 12. Diagram Showing Tracking Error Measure

$$P.I. = \frac{\int_0^{T_f} (ERRT)\,dt}{\int_0^{T_f} dt} = \frac{1}{T_f}\int_0^{T_f}\left[(ERRX)^2 + (ERRY)^2\right]^{1/2} dt$$

A run consists of tracking the velocity vector over the middle of the runway numbers during a descent from 2500 feet to sea level. At the end of each run the average RMS tracking error was recorded. Three runs totalling 6 minutes were made for each configuration (sampling time 1/20 second).

The four configurations of interest were the basic F-16, F-16 CCV, and F-16 CCV with each of the compensatory displays. Three runs were conducted for each configuration, in the presence of no wind, moderate winds (6.6 kts RMS, peak gust 18 kts) and severe winds (13.2 kts RMS, peak gust 37 kts). The pilots flew the basic aircraft, CCV aircraft, and CCV aircraft with compensatory displays in the presence of various wind levels for approximately 45 minutes for familiarization with the aircraft dynamics to minimize any bias during the testing due to learning. The tests themselves were conducted in several different orders to minimize learning curve bias.

WIND	CONFIGURATION
No Wind	Basic F-16
	F-16 CCV
6.6 kts RMS	Basic F-16
	F-16 CCV
	F-16 CCV w/ Display 1
	F-16 CCV w/ Display 2
13.2 kts RMS	Basic F-16
	F-16 CCV
	F-16 CCV w/ Display 1
	F-16 CCV w/ Display 2

Table 1. Test Run Matrix

Table 1 shows the test run matrix. Displays 1 and 2 were not tested for the no wind case since inputs do not exceed the deadband of the compensatory display. The pilots were not aware of their tracking performance until all the runs in the entire test matrix were completed. No affective comments (positive or negative) were made to the pilots to influence performance. Before quantitative tracking results were revealed, subjective comments were recorded and past flight experience outlined. The quantitative and qualitative results are given in the next section. The pilots did not have to adjust trim or thrust and therefore just utilized the stick and CCV thumb button during the conduction of the tests. The pilots were instructed that they would be rated purely on how well they tracked the velocity vector circle over the runway numbers. The pilots were alone in the simulator during the tests of various configurations and wind levels. Most of the pilots had combat experience in fighters.

SIMULATION RESULTS

The results of the test program are given in table 2. One notes the substantial improvement in tracking performance with CCV modes, and signifigant increase in performance with the designed displays. Table 2 shows the percent improvement with CCV modes over the basic aircraft and percent improvement of the F-16 CCV tracking with the advanced displays for each pilot. An approximately 40% improvement in tracking ability with the direct force modes compares favorably with gun camera films recorded during the Edwards Air Force Base flight test program.

A 10-15% reduction in pointing error is observed when the advanced displays are incorporated in the F-16 CCV simulation. There is little difference (1 standard deviation $\simeq$ 5%) in performance improvement between the two displays. Display 2 gives angular predictor information (both displays represent the sum of wind effects and CCV inputs) and display 1 gives magnitude as well as angular information. Since there is little difference between the two displays magnitude information in this case did not augment performance. This supports the earlier hypothesis that the thumb can sense magnitude information but cannot sense angular information well on the CCV button. It is the additional visual feedback of direction that the pilot uses to improve his tracking performance 10-15%. It is this predictor or lead cue the display gives of where the velocity vector circle will be superimposed in the next 3/10 second which augments the pilot:CCV aircraft system.

CONFIGURATION AND PERCENT IMPROVEMENT*	PILOT 1	PILOT 2	PILOT 3	PILOT 4	PILOT 5	PILOT 6	MEAN	STANDARD DEVIATION
NO WIND CCV over Basic F-16	20.0	57.7	23.7	55.6	48.5	43.8	41.6	14.5
WIND=6.6 kts RMS CCV over Basic F-16	47.9	63.5	54.8	15.1	36.7	30.9	41.5	16.0
F-16 CCV w/ Display 1	7.3	18.7	12.4	18.7	11.8	9.3	13.0	4.44
F-16 CCV w/ Display 2	7.2	15.5	15.2	19.4	13.0	10.5	13.5	3.77
WIND=13.2 kts RMS CCV over Basic F-16	15.5	52.4	50.3	3.1	22.8	36.0	30.0	18.0
F-16 CCV w/ Display 1	2.5	20.4	6.4	15.9	7.8	5.4	9.7	6.29
F-16 CCV w/ Display 2	12.6	17.6	18.4	4.8	6.9	9.8	11.7	5.08

Table 2. Summary of Tracking Improvements with CCV Modes over the Basic F-16 for Various Wind Levels (Random, Zero-Mean Gusts) and Summary of Improvement in CCV Tracking Performance with Compensatory Displays (Percentage)

CONCLUSIONS

Based on the test program utilizing the fixed-base F-16 CCV simulator with F-16 CCV dynamics, a Heads Up Display with an external view of a numbered runway and horizon, an isometric sidearm stick with two-axis thumb button to command the direct force modes, and a modified cockpit interior, the following conclusions were reached.

1. In the presence of no wind to moderate winds (6.6 kts RMS), the six pilots utilized the direct force modes to improve RMS tracking ability 40% over that attained with the basic aircraft.
2. In the presence of sever winds (13.2 kts RMS), the direct force modes improved tracking ability approximately 30%. The decrease from (1) is probably due to the fact that large CCV inputs are necessary in severe winds, which cause manual force coupling problems between the thumb button and sidearm stick.
3. The designed displays improved the tracking capability of the F-16 CCV 10-15%.
4. Subjectively most pilots preferred the arrow display (display 1) over the angular display (display 2); the latter was found to be more distracting.
5. Observing the tracking results, there was no statistically signifigant difference between the two displays. The angular display gave predictor information for direction. The arrow display gave magnitude and direction information. Thus the pilot primarily used direction information to improve his tracking performance; the additional magnitude information did not improve his performance appreciably. This correlates with the devel-

---

[*] Improvements in tracking performance with displays 1 and 2 are referenced to the F-16 CCV without the compensatory displays

oped hypothesis that the thumb could sense the magnitude of the CCV input well but not its direction. The purpose of the display was to show the direction of the input, which it did. Thus the magnitude cue was already available from the thumb button; the direction is now available from the display.

ACKNOWLEDGEMENT

This research was conducted under AFOSR Grant #78-3260, "Cockpit Display Concepts for New Control Capabilities", from the Air Force Flight Dynamics Laboratory of Wright-Patterson Air Force Base. Their support is greatly appreciated.

REFERENCES

1. "YF-16 CCV Operational Potential, Flying Qualities, and Performance Evaluation" Richard A. Wood, Project Engineer, Michael P. Garland, Flying Qualities Engineer, Edward T. Meschko, Major, USAF, Project Pilot; Final Report, Air Force Flight Test Center, Edwards Air Force Base, California, Air Force System Command, USAF January 1978
2. "Fighter CCV Phase II Report- Detail Design", General Dynamics/ Fort Worth, October 1976, March 1976, Air Force Flight Dynamics Laboratory, Air Force Systems Command, Wright-Patterson AFB, Ohio, AFFDL-TR-76-119
3. "Fighter CCV Phase IV Report- Vol. 1 - Program Summary", General Dynamics Corp., Fort Worth, Texas, February 1978
4. "Design Considerations for Implementing Integrated Mission-Tailored Flight Control Modes", James K. Ramage and Frank R. Swortzel, Air Force Flight Dynamics Laboratory, Wright-Patterson AFB, Ohio; 26th AGARD Guidance and Control Panel Symposium, May 1978
5. "The Impact of Electronic Displays on Aircraft Control", AGARD Conference Proceedings No. 58, Advanced Control Systems Concepts, P. Lowry, Elliot Bros., Ltd., Kent, England
6. "Control and Display Concepts for Combat Aircraft", Airborne Display Division, Marconi Avionics, Kent, England; AGARD Conference Proceedings No. 257, The Impact of Integrated Guidance and Control Technology on Weapon Systems Design, May 1978.
7. "Design, Simulation and Evaluation of Advanced Display Concepts for the F-16 Control Configured Vehicle" Robert W. Klein, Walter M. Hollister, Department of Aeronautics and Astronautics, Massachusetts Institute of Technology, February 1980

A complete bibliography of this research is contained in reference 7.

N82 34063-26

SEPARATION MONITORING WITH FOUR TYPES OF PREDICTORS ON A COCKPIT DISPLAY OF TRAFFIC INFORMATION

Sharon Jago and Everett Palmer
Ames Research Center, NASA

The concept of a cockpit display of traffic information (CDTI) includes the integration of air traffic, navigation, terrain and weather information in a single electronic display in the cockpit. The present study was conducted as part of a research project designed to develop a clear and concise display format for use in later full mission simulator evaluation of the CDTI concept. This experiment required airline pilots to monitor a CDTI and make perceptual judgments concerning the future position of a single intruder aircraft in relationship to their own aircraft (ownship). The main experimental variable was the type of predictor used to display future position of each aircraft. Predictors were referenced to the ground or to ownship and they either included turn rate information or did not. Other variables were the aircraft's separation distance when the judgment was required and the type of encounter (straight or turning). Results indicate that under these experimental conditions fewer errors were made when the predictor included turn rate information. There was little difference in overall error rate for the curved ground referenced and the ownship referenced predictors.

INTRODUCTION

Projected estimates of air traffic indicate a marked increase in congestion occurring over the next 20 years. This increase is expected to create a demand for greatly improved air traffic control services to maintain or improve present levels of safety. Relevant to the area of safety are concerns dealing with efficiency of flights into and out of capacity limited terminal areas. The concept of a cockpit display of traffic information (CDTI) is presently being considered to determine its role in the air traffic system.

The CDTI is displayed on a cathode-ray tube (CRT) located in the aircraft cockpit with a display created by a computer. The display allows the pilot to see other aircraft's position in relation to the pilot's own aircraft. The pilot's own position and direction of travel with respect to area navigation routes and terrain features are indicated by a heading-up moving map.

Prior experiments in this project were directed toward developing a clear and easy to use display (ref. 1, 2, 3, 4). Questions concerning the generic CDTI display were directed toward the display symbology and factors affecting perception of motion. Such variables as update rate, viewing time, background and methods of displaying past and future position of the aircraft have been considered. Additional studies have been made on how to display vertical situation information on a map display (ref. 5, 6).

The object of this experiment was to evaluate different predictors of aircraft motion in the horizontal plane. Four predictors were used. These were either ground referenced or ownship referenced with or without turn rate information. Also of interest was whether there was a difference in learning with the different predictors.

METHOD

Subjects. Sixteen airline pilots were paid to participate in this experiment. No pilot had prior experience using CDTI symbology, eliminating the possibility of previous learning affecting the results.

Apparatus. The pilots were seated in a two-place, fixed-base transport simulator. The only functioning parts of the simulator were the CRTs that displayed the traffic information. Responses were made on a hand-held instrument.

Visual display. The CDTI was displayed on a 18 cm X 18 cm CRT. The center of the screen was located 25 deg. (.44 rad) below the horizontal on the pilot's center line and .87 m from the subject's eye reference point. The width of the terrain displayed on the CRT was 10 nautical miles (18.5 km). With this map scale, 1 nautical mile (1.85 km) on the ground equals 1.2 cm on the display. The ownship was represented by a chevron symbol with the exact location of ownship being the top point of the symbol. The intruder was represented on the display by a circular symbol with a dot in the center indicating its present location. Both ownship and intruder were displayed with ground referenced history dots. Each of the eight dots indicated the past position of the aircraft over the ground at 4 sec intervals. These symbols were preferred by most pilots in Hart's studies of pilot preference for various types of CDTI symbols (ref 7, 8). An area navigation route map provided ground objects for the background.

Encounter variables. There were 48 different encounters. Figure 1 shows 12 of the 48 encounters. For example, encounter 1 displays the ownship in a heading up position. The intruder is approaching from the right. In Figure 1 all sketches show curved ground referenced predictors for the purpose of illustration. In 24 of the encounters the intruder ultimately passed in front of ownship. In the remaining 24 the intruder ultimately passed behind the ownship. In 24 of the encounters, both aircraft went straight and in the remaining 24 one or both aircraft turned. In 24 encounters the display stopped at 44 sec to the point of closest encounter. The remaining 24 encounters stopped at 28 sec to the point of the closest encounter. The parameters for the encounters are found in Palmer et. al.

Constant encounter parameters included: viewing time, 8 sec, separation distance at encounter, 3000 ft (.91 km), and update rates for ownship and intruder. Ownship's position and heading was

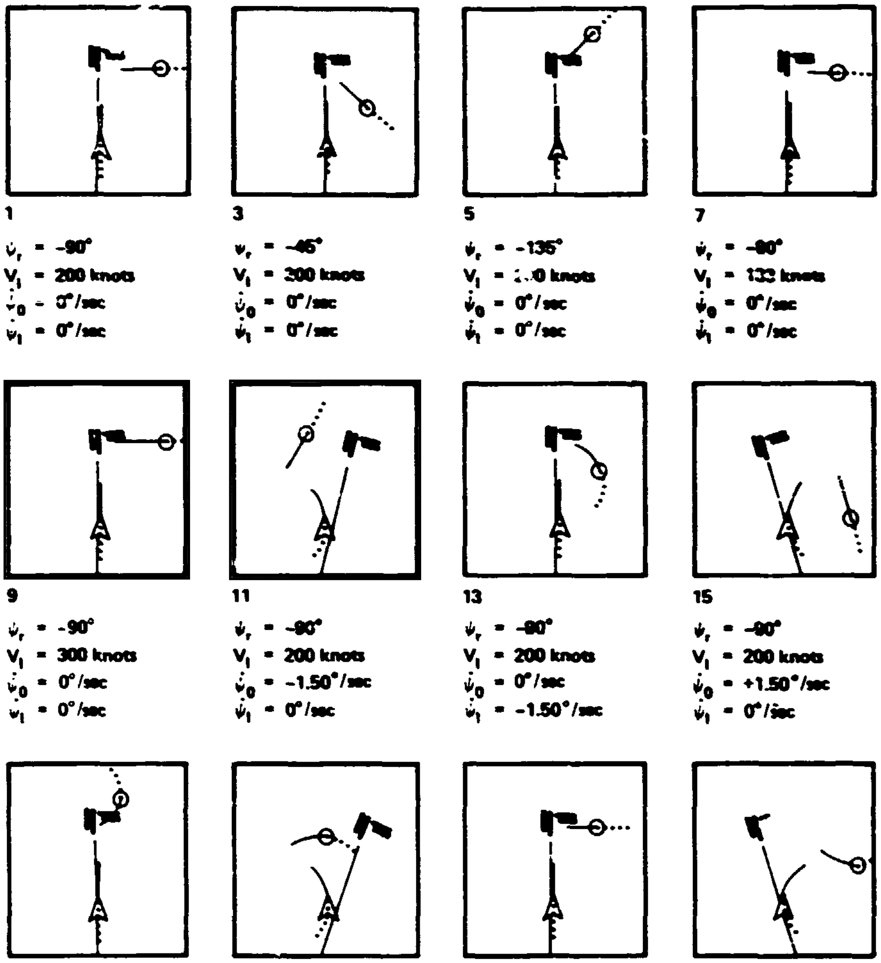

1

$\psi_r = -90°$
$V_I = 200$ knots
$\dot{\psi}_0 = 0°/\text{sec}$
$\dot{\psi}_I = 0°/\text{sec}$

3

$\psi_r = -45°$
$V_I = 300$ knots
$\dot{\psi}_0 = 0°/\text{sec}$
$\dot{\psi}_I = 0°/\text{sec}$

5

$\psi_r = -135°$
$V_I = 200$ knots
$\dot{\psi}_0 = 0°/\text{sec}$
$\dot{\psi}_I = 0°/\text{sec}$

7

$\psi_r = -90°$
$V_I = 133$ knots
$\dot{\psi}_0 = 0°/\text{sec}$
$\dot{\psi}_I = 0°/\text{sec}$

9

$\psi_r = -90°$
$V_I = 300$ knots
$\dot{\psi}_0 = 0°/\text{sec}$
$\dot{\psi}_I = 0°/\text{sec}$

11

$\psi_r = -90°$
$V_I = 200$ knots
$\dot{\psi}_0 = -1.50°/\text{sec}$
$\dot{\psi}_I = 0°/\text{sec}$

13

$\psi_r = -90°$
$V_I = 200$ knots
$\dot{\psi}_0 = 0°/\text{sec}$
$\dot{\psi}_I = -1.50°/\text{sec}$

15

$\psi_r = -90°$
$V_I = 200$ knots
$\dot{\psi}_0 = +1.50°/\text{sec}$
$\dot{\psi}_I = 0°/\text{sec}$

17

$\psi_r = -90°$
$V_I = 200$ knots
$\dot{\psi}_0 = 0°/\text{sec}$
$\dot{\psi}_I = +1.50°/\text{sec}$

19

$\psi_r = -90°$
$V_I = 200$ knots
$\dot{\psi}_0 = -1.50°/\text{sec}$
$\dot{\psi}_I = -1.50°/\text{sec}$

21

$\psi_r = -90°$
$V_I = 167$ knots
$\dot{\psi}_0 = 0°/\text{sec}$
$\dot{\psi}_I = 0°/\text{sec}$

23

$\psi_r = -90°$
$V_I = 200$ knots
$\dot{\psi}_0 = +1.50°/\text{sec}$
$\dot{\psi}_I = +1.50°/\text{sec}$

Figure 1 Twelve of the 48 encounters in which the intruder would ultimately pass in front of ownship. All displays show curved ground referenced predictors.

updated every .1 sec, while the intruder's position and heading was updated every 2 sec.

Display variables. There were four conditions of display predictors: (a) straight ground referenced, (b) curved ground referenced, (c) straight relative, and (d) curved relative. In the straight ground referenced predictors, the end of the vector indicated the projected position of the aircraft over the ground in 32 sec, assuming the aircraft maintained its current instantaneous ground track. The curved ground referenced predictor indicated the position of the aircraft in 32 sec, assuming the aircraft maintained its current turn rate. In curved encounters this predictor curved in proportion to the turn rate. With the straight relative predictor the end of the predictor indicated the intruder's position relative to the ownship position, direction, and speed if both aircraft maintain their current ground track. With the curved relative the end of the predictor predicts the position of the intruder relative to ownship if both aircraft maintain their current turn rates. In encounters where both aircraft are going straight the display appears the same with both straight and curved predictors. Figure 2 shows the same encounter with each of the four predictors. No radar noise or tracker lag were simulated.

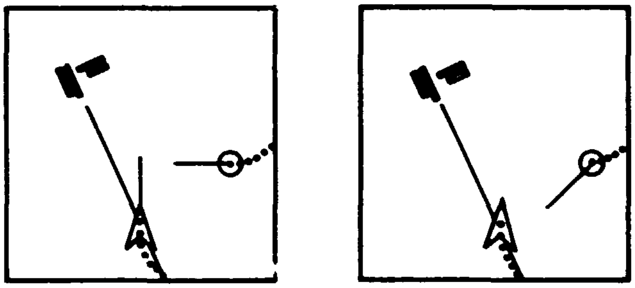

STRAIGHT GROUND-REFERENCED PREDICTORS ON BOTH AIR-CRAFT (STR GRP)

RELATIVE PREDICTOR ON INTRUDER AND NO PREDICTOR ON OWN SHIP (STR OPR)

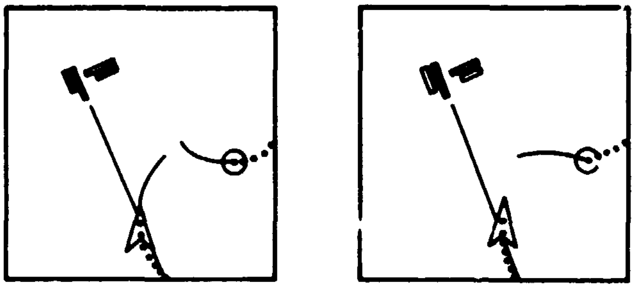

CURVED GROUND-REFERENCED PREDICTORS ON BOTH AIRCRAFT (CRV GRP)

CURVED RELATIVE PREDICTOR ON INTRUDER AND NO PREDICTOR ON OWN SHIP (CRV ORP)

Figure 2. The four display formats used in the experiment.

Procedure. The task for this experiment was to monitor the CDTI for 8 sec and predict whether the intruder aircraft would ultimately pass in front of or in back of the ownship. The subjects indicated their decisions by pressing the appropriate button on the hand held response switch. Two seconds after the initiation of the run, the intruder appeared on the CDTI with a position, velocity, track angle, and turn rate calculated so that the intruder ultimately passed either directly in front of or in back of ownship in 52 or 35 sec. After 8 sec of viewing time the CRT was blanked and replaced with a message asking whether the intruder would pass in front or in back of ownship. The pilot responded. The words "IN FRONT" or "IN BACK" then appeared on the screen indicating the correct judgment.

Four subjects were assigned to each of the four conditions. Initial oral instructions concerning the concept of the CDTI and the meaning of the various display symbols were given. After approximately one half hour of training, all pilots underwent a pretest block of 48 encounters with no predictors. At the conclusion of the pretest trial there was a 10-minute break. The pilots received additional training specific to the experimental condition. On Day 1, three blocks of the experimental condition of the 48 encounters were administered with a 10-minute break between blocks. On Day 2, the subjects received instructions on the meaning of the CDTI symbols for the experimental condition and three more blocks of 48 encounters of the experimental condition were given. The experiment concluded with a posttest block identical to the pretest block with no predictors. Presentation order was randomized. In addition, whether the subject saw a specific encounter or its mirror image was also randomized.

Results

Table 1 shows the percent error for each of the predictor conditions for straight and curved encounters at both distances. It can be seen in Figure 3 and Table 1 that fewer errors were made on curved encounters when the predictor indicated the future joint effect of current turn rate of both aircraft. Both ground referenced and ownship referenced predictors resulted in equally good performances on straight encounters. However the error rate on curved encounters was consistently lower for the conditions with curved ground or ownship referenced predictors that provided turn rate information. With turn rate information the error rate on the curved encounters was comparable to the error rate on straight encounters. The highest error rates occured when both aircraft were turning and the predictors did not include turn rate information.

An analysis of variance was conducted on transformed percent error rate over the four predictor conditions, separation distance at encounter and type of encounter (straight or turning). Table 2 shows the results of the ANOVA. Performances over the four predictor types, two separation distances and encounter types were significantly different as were the interactions of predictor type and separation distance and the interaction between predictor type and encounter type.

ORIGINAL PAGE IS
OF POOR QUALITY

Predictors	Encounters			
	Straight		Curved	
	28	44 sec	28	44 sec
None (pretest)	31	42	23	35
None (posttest)	23	29	25	35
Straight ground ref.	1	11	27	30
Curved ground ref.	2	10	2	7
Straight ownship ref.	1	8	14	35
Curved ownship ref.	0	0	0	10

Table 1. Percent error averaged over subjects and replications for straight and curved encounters. There were 96 trials each per cell for the pretest and posttest no predictor conditions and 288 trials each per cell for the four predictor conditions.

Source	SS	df	MS	F
P	3215.5	3	1071.8	20.2 *
D	1605.3	1	1606.3	178.3 *
E	1557.2	1	1557.2	75.6 *
P X D	13.2	3	4.4	<1
P X E	1292.6	3	430.8	20.9 *
D X E	2.6	1	2.6	<1
P X D X E	298.2	3	99.4	4.5 *

* $p<0.01$

Table 2. ANOVA over predictor conditions (P), separation distance (D), and encounter type (E).

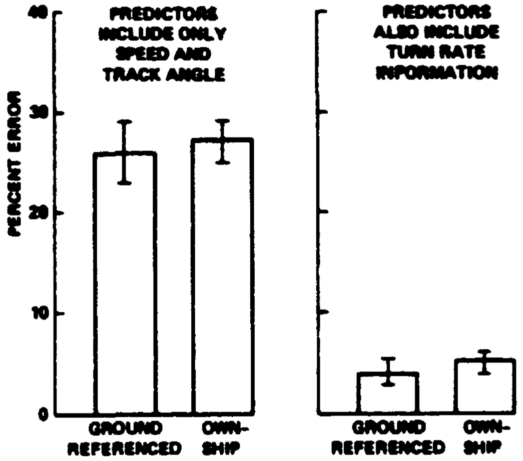

Figure 3. The effect of adding turn rate information to the predictor.

Figure 4 shows percent error collapsed over subjects for each of the predictors. The data are shown for each of the replications averaged over the two distances. It can be seen that replications with predictors do not improve performance on the no predictor posttest. There was no significant difference between the pretest and posttest means. There was evidence for learning for all predictors except the curved ownship referenced predictor which maintained an average error rate of 3%.

At the conclusion of the experiment the pilots were allowed to view the other predictor conditions. Their predictor preference was requested. All pilots preferred predictors with turn rate information included. The preference was evenly divided between ground referenced and ownship referenced predictors.

DISCUSSION

The main objective of this experiment was to investigate performances using different types of predictors. Evidence clearly shows that the addition of a predictor reduced the error rate. The percent error was further reduced when turn rate information was added to the predictor.

There still remains a question whether ground referencing or ownship referencing is the best method. The percent error data on the replications showed that there was little learning with the curved ownship referenced predictor. Although after six replications both curved ground referenced and curved ownship referenced predictor conditions had similiar low error rates.

The question of which method of referencing is best is further clouded by the fact that 50% of the error with the curved ownship referenced predictor was accounted for by two encounters. These two encounters (#11 and #19) are both encounters where the ownship is turning. Thus the curved ownship referenced predictor condition had a very low overall error rate when these two encounters are not considered. One could argue that ownship referencing is the best method. On the other hand, the curved ground referenced predictor condition had a more even distribution of error. One must also question how good a referencing method is if it can be so confusing on two of the encounters and not confusing on all the other encounters.

Results from the subjective data suggest that the method of referencing is an individual preference and not based on performance.

CONCLUSION

This experiment adds to a series of experiments designed to evaluate CDTI display symbology in a dynamic but controlled environment. The following are general observations based on the data from this experiment. 1) The addition of predictive information reduces error. 2) The best results were obtained when turn rate information was included in the prediction.

It is important that any conclusion the reader may draw from

ORIGINAL PAGE IS
OF POOR QUALITY

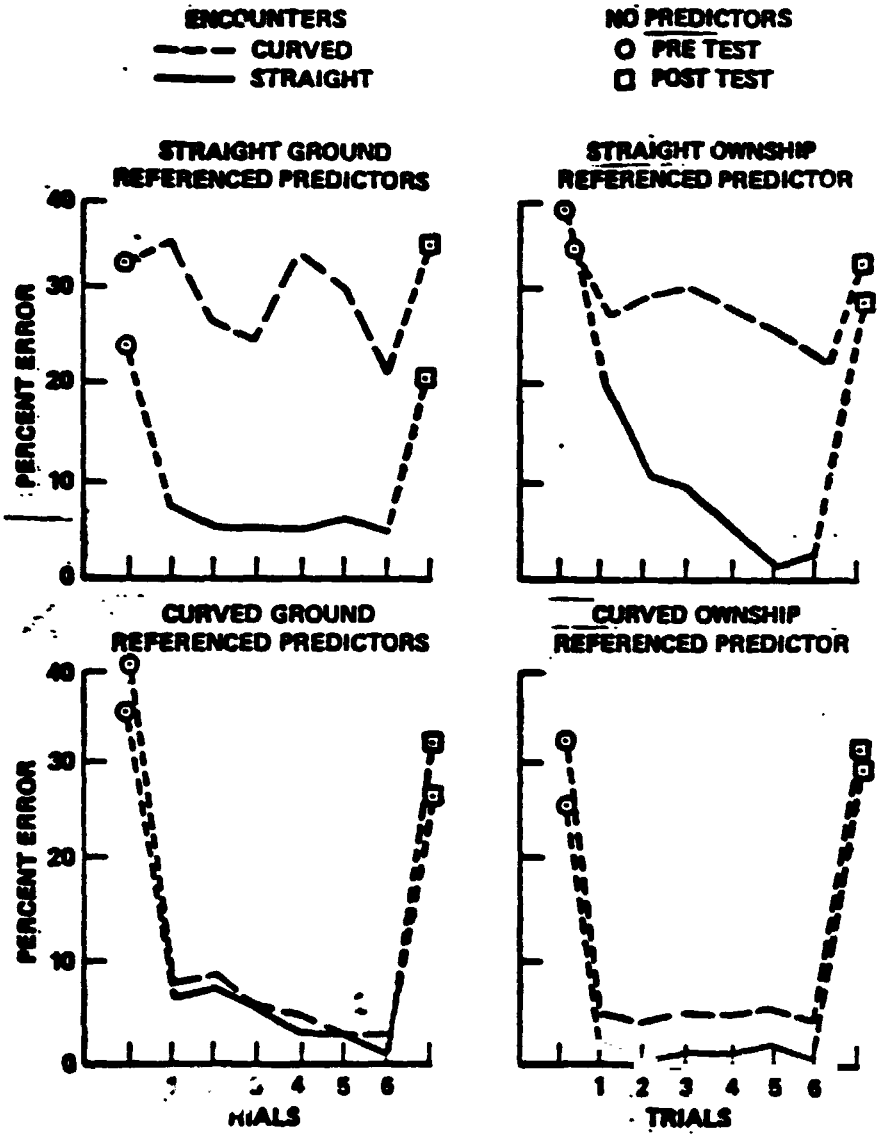

Figure 4. Learning performance with each predictor type. Percent error collapsed over subjects.

these results take into account the following limitations of the research method: (1) The pilots could devote their uninterrupted attention to the task for 8 sec; (2) neither aircraft changed its speed or turn rate during an encounter; (3) although the display was dynamic, the pilots could not interact with the display to ask for more information about the intruder or change the map scale; (4) pilots could not take over manual control of the aircraft; (5) the passive nature of the task and the large number of trials resulted in a task that quickly became routine. The first two items should lead to fewer errors than would be expected in a real aircraft. The last three items should lead to more errors than in a real aircraft. It is felt, however, that the relative difference between the displays will remain the same as the task is made more realistic.

References

1. Palmer, E. A., Baty, D. L., and O'Connor, S. L. Perception of aircraft separation with various symbols on a cockpit display of traffic information, Paper presented at the 15th Annual Conference on Manual Control, Wright State University, Dayton, Ohio, March 1979.
2. O'Connor, S. L., Palmer, E. A., Baty, D. L., and Jago, S. J. The effect of viewing time, time to encounter, and practice on perception of aircraft separation on a cockpit display of traffic information, NASA TM 81173.
3. O'Connor, S. L., Jago, S. J., Baty, D. L., and Palmer, E. A. Perception of aircraft separation with pilot preferred symbology on a cockpit display of traffic information, NASA TM 81172, in preparation.
4. Baty, D. L., Jago, S. J., O'Connor, S. L., and Palmer, E. A. The effect of display update rate, update type and background on perception of aircraft separation on a cockpit display of traffic information, NASA TM 81171, in preparation.
5. Hart, S. G. and Loomis, L. L. Evaluation of the potential format and content of a cockpit display of traffic information. To be published in a special issue of Human Factors, October, 1980.
6. Hart, S. G. and Loomis, L. L. Evaluation and prediction of the vertical situation from a horizontal simulation display. Presented at the 18th IEEE Conference on Decision and Control, Fort Lauderdale, Florida, December 1979.
7. Hart, S. G. and Wempe, T. E. Cockpit display of traffic information: airline pilots' opinions about content, symbology, and format, NASA TM 78601.
8. Hart, S. G. Content, symbology, and format of cockpit display of traffic information: general aviation pilot opinion. Presented at the 15th Annual Conference on Manual Control, Dayton, Ohio, March 1979.

N82 34064 D27

COMBINED DISCRETE NETWORK--CONTINUOUS CONTROL MODELLING OF OPERATOR BEHAVIOR

R. A. Miller
Dept. of Industrial & Systems Engineering
The Ohio State University
Columbus, Ohio 43210

and

Deborah J. Seifert
Airesearch Manufacturing Co.
P. O. Box 5217
Dept. 60-60
Phoenix, Arizona 85010

ABSTRACT

The class of systems of interest is that in which an operator is faced with a continuous control task plus one or more discrete information processing tasks. The objective is to explore a modelling approach which has the capability of realistically representing both types of tasks and the resulting interactions. The modelling approach utilizes discrete network models for the cognitive tasks and elements of an open-loop/closed-loop control representation for the continuous task.

The approach is demonstrated through its application to a simulated Digital Avionics Information System in which subjects were required to perform retrieval and processing tasks as well as flight control. This model differs from conventional models in that system status sampling is not necessarily continuous or periodic. Rather, the pilot is assumed to read system status displays only as time permits and operate in a so-called "open-loop" preprogrammed fashion between sampling.

INTRODUCTION

It is clear to anyone participating in this conference that research on supervisory control has been increasing during the last few years. This study, which was primarily exploratory and methodological in scope, follows in that trend and the results contribute to a better understanding of human-machine systems and supervisory control modelling.

Specifically, a computer simulation approach, which utilizes discrete network techniques to represent certain cognitive and decision making tasks and a novel control model for continuous tasks, was used to explore a number of supervisory control questions. A rather general simulation model of operator performance with a digital avionics information system (DAIS) was constructed and verified against data which had been collected in a previous man-in-the-loop study.[1,2] The resulting model was used to perform sensitivity analyses of flight control variables and explore a variety of questions about task organization and performance strategy. An outline of the model and some of the more interesting results are reported here.

It must also be mentioned that in addition to the above traditional modelling objectives, a major reason for the study was to explore the possible utilization of digital simulation methods for the design of expensive man-in-the-loop type experiments. A few suggestions toward this end are also presented.

DESCRIPTION OF THE DAIS SIMULATOR

The DAIS simulator cockpit replaced many of the traditionally dedicated instruments, displays, and subsystem controls with interactive multipurpose displays (MPD) and multifunction keyboard switching (MFK). The mock-up cockpit had a forward station configured simular to a single-engine, single-place, transonic light attack aircraft. The front panel of the cockpit was equipped with three CRT-type displays, two served multipurpose functions and the center display was used to present information concerning basic flight parameters in a moving tape format. The flight control display presented current readouts of the aircraft angle of attack, g-load, indicated airspeed, percent of total throttle, mach number, vertical velocity, and heading. Information storage and retrieval was achieved through the use of the multi-function keyboard and the alphanumeric keyboard located on the left side of the cockpit. The cockpit also contained a throttle with afterburner switch and a center-mounted joystick control which were used, in combination with the displayed flight information, to "fly" various maneuvers. Analog outputs from the stick, throttle, and MFK were processed by an A/D converter for input to a digital computer where further processing was performed. The nonlinear aircraft motion equations were simulated digitally and updated to respond to the positions of the stick and the throttle. Similarly, switching instructions communicated to the pilot via audio headsets were entered through the MFK causing the MPDs to be updated.

Flight control variables were recorded in terms of the error between the actual values and the command or desired levels. Performance scores were computed for both the flight control alone and flight control performed in conjunction with MFK switching configurations of the mission. These scores along with data collected concerning discrete information retrieval task times were used to compare and evaluate the information workload tradeoff of the proposed DAIS system.

This system was selected for this study for several reasons: (1) it appeared to be representative of many contemporary man-machine systems in that it required monitoring and discrete information processing behaviors as well as motor control tasks, (2) preliminary performance estimates were available, and (3) results of this endeavor had implications for ongoing research and experimental studies.

DESCRIPTION OF EXPERIMENT AND PROCEDURES

Seven different maneuvers were employed in the flight control task. They are identified in terms of command flight parameters as defined in Table 1.

TABLE 1
BASELINE FLIGHT CONTROL MANEUVERS

Maneuver	Altitude (ft)	Velocity (kt)	Vertical Velocity (ft/min)	G-Load
1 - straight and level	20,000	500	0	1.0
2 - left turn	30,000	500	0	1.5
3 - right turn	30,000	500	0	1.5
4 - turning dive	--	500	-2500	1.5
5 - stall	20,000	240	0	1.0
6 - turning ascent	--	500	2500	1.5
7 - high-g turn	30,000	600	0	3.0

The subjects were instructed to "maintain" these parameters for the duration of the mission (approximately 200 secs.). Flight control was scored as a function of the difference between the desired control parameters and the actual ones. These "delta" (Δ) values were computed every 200 milliseconds. The flight parameters on which scoring was based was chosen through consultation with pilots and other researchers who were able to specify on an experiential basis the minimum number of significant parameters for each mission, and the importance of a given amount of error in each parameter. Working from this basis, a formula was derived for each maneuver. The specific formulas chosen for the maneuvers used in this study are presented in Table 2.

TABLE 2
MANEUVER PERFORMANCE SCORES

Straight and Level Flying	(.01)Δaltitude + (.1)Δspeed
Dive/Climb	(.005) vertical velocity + (.1) speed
Diving/Climbing Turn	(.005)Δvertical velocity + (.1)Δ speed +Δg-load
Level Turn	(.01)Δaltitude + (.1)Δ speed + (1.1) g-load

NOTE: Δ represents the mean absolute error from the command value.

Four levels of task difficulty were utilized for the MFK switching tasks, which required approximately 4, 6, 8 or 12 push-button switch actions per task. The MFK task was scored on the basis of correct completion of the switching sequence, total time required for correct completion, and time per switch action.

ORIGINAL PAGE IS
OF POOR QUALITY

Three different configurations were considered: flight control alone, MFK alone, and the combination of flight control with switching. Four college students served as subjects for the experiments. Each received approximately 40 hours of training on the primary flight control task and at least 20 hours of training on both the secondary MFK and combined tasks. In every case, training was to asymptotic performance.

In the flight control alone segment, there were 28 trials per subject - four for each of the seven maneuvers. At the beginning of a trial the subject was told which maneuver he was to fly, including the flight parameter values to be maintained. Then he was allowed to "fly" the simulated aircraft until he was confident he was prepared to start the maneuver, which he indicated by pulling a trigger on the control stick, designated as the "hotswitch". At that point a 200-second trial began with automatic scoring and termination by the supporting computer program. There were 30-second intervals between trials.

In the MFK task alone, each subject was also given 28 200-second trials. There were seven trials for each of the four levels of MFK difficulty investigated. Thirty-second rest intervals separated trials. Four different MFK tasks of the given difficulty level were performed during each trial period. The subject received pre-recorded instructions via his earphones concerning the task he was to perform. The instructions were followed by a tone which was the signal to start the MFK task. The subject depressed a "stop" button on the left side panel to the right and ahead of the throttle, to indicate he had completed the MFK task. The experimenter monitored the duplicate displays at his station to ascertain the correctness of subject action on the MFK.

The combined flight control with MFK session was identical to the flight control single task condition except as follows. Thirty seconds after the subject's signal that he was reddy for scoring of the flight maneuver to start, the recoried instructions for the first MFK task were presented. Thus the flight control and MFK single task scenarios were "overlayed" so that each subject had to divide his attention between them throughout the standard 28 200-second trial periods. The subjects were instructed to give first priority to flight control. A more detailed description of the procedures can be found in references 1 and 2.

COMBINED SIMULATION MODEL STRUCTURE

Two basic maneuver types out of the seven employed in the DAIS real-time simulation were simulated: straight and level flying and a turning dive. These are considered to be the easiest and hardest flight maneuvers, respectively. An open-loop closed-loop control model for these maneuvers based on the flight equations employed in the DAIS simulation was developed. Conventional control models, in which the pilot is assumed to be sampling system status variables continuously (or periodically in the discrete time case), are termed "closed-loop" models. The proposed model differs from that above in that system status sampling is not necessarily continuous nor periodic, due to the secondary multi-function keyboard tasks imposed upon the pilot. Therefore, the pilot reads the system status displays only as time permits and operates in a

**ORIGINAL PAGE IS
OF POOR QUALITY**

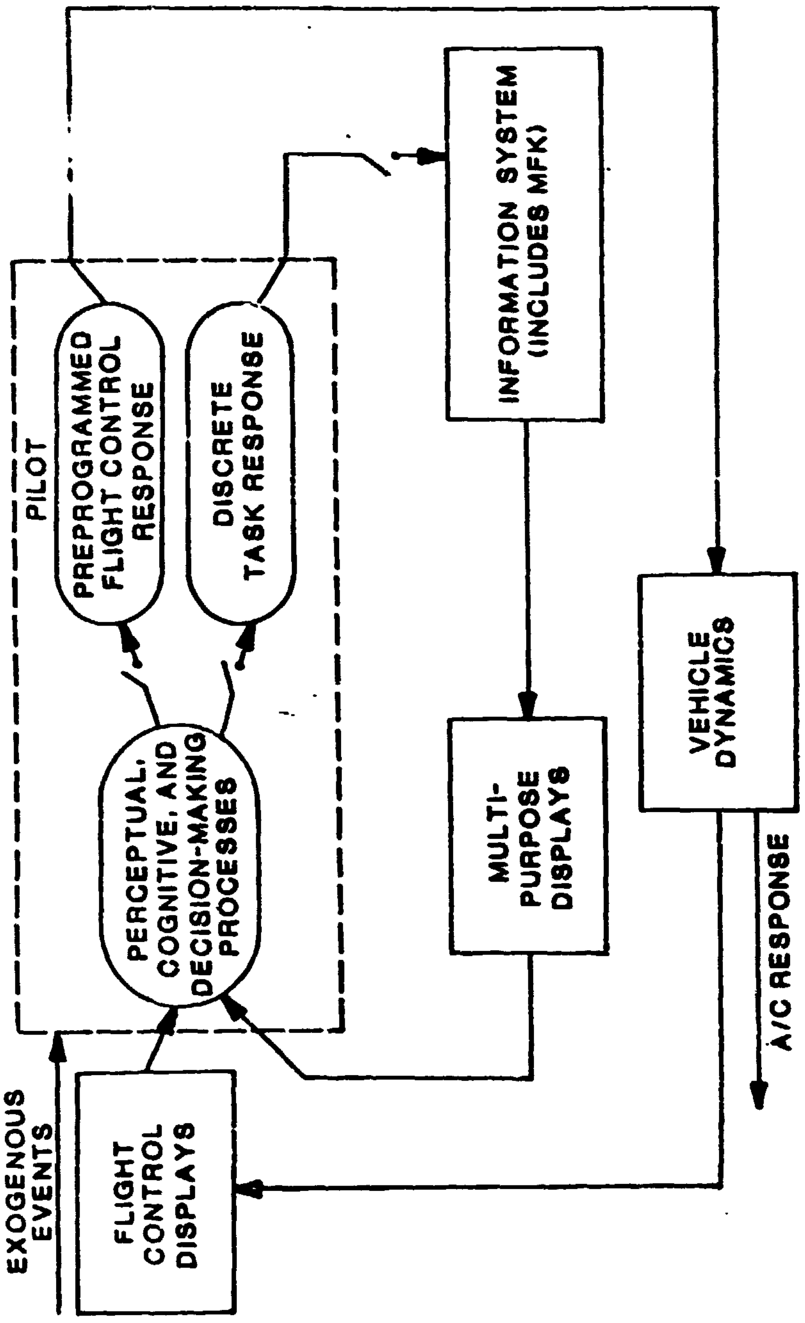
PILOT
PREPROGRAMMED FLIGHT CONTROL RESPONSE
DISCRETE TASK RESPONSE
PERCEPTUAL, COGNITIVE, AND DECISION-MAKING PROCESSES
INFORMATION SYSTEM (INCLUDES MFK)
MULTI-PURPOSE DISPLAYS
VEHICLE DYNAMICS
FLIGHT CONTROL DISPLAYS
EXOGENOUS EVENTS
A/C RESPONSE

FIGURE 1 OPEN-LOOP CLOSED-LOOP CONTROL SYSTEM STRUCTURE

C-6

so-called "open-loop" preprogrammed fashion between sampling.

Figure 1 depicts the structure of the open-loop closed-loop control system. The pilot must encode and process information from flight control displays, multipurpose displays, and exogenous events such as audio switching instructions. The pilot then evaluates this information as a function of system status demands, applying decision rules and priority requirements in determining his selected output control or switching actions. Some of these actions involve conscious decision-making on the part of the pilot; others are highly developed psychomotor skills required for flight control involving less conscious decision-making.

The operator is performing in a multi-task environment at several different behavioral levels. He is monitoring displays, processing information, making flight control inputs, and storing and retrieving information via the keyboard switching tasks. It is the modelling of these activities, along with the pilot's cognitive, decision-making processes, to which the models presented herein are addressed.

The decision-making process and the information system, including the multifunction switching tasks, are modeled via discrete network techniques. Because of the hierarchical structure of network models, the task activities of the pilot may now be represented at many different levels. For example, tasks may be used to indicate discrete button-pushing and dial setting operations. They may also be employed in representing sequential and/or stochastic information processing models. On a completely different level, network models are used here to achieve desired state variable sampling intervals and priority schemes. The network structure is designed to operate at many different levels simultaneously and thus is capable of representing sophisticated man-machine system behaviors. In its application here, the network also serves a supervisory role in interfacing with the open-loop optimal control model representation of the pilot's tracking task. These two modeling approaches are meshed together to form a combined discrete network-continuous optimal control model of the human operator.

The Control Model

The open loop-closed loop model is best described in linear systems terms. In the case where the operator is assumed to be sampling continuously, his control behavior is represented as a multivariate proportional plus integral control system operating on a noise corrupted displayed error input. The open loop-closed loop formulation presumes that control responses between samples of state variables are based on a conditional mean extrapolation of the system trajectory. The effect of sampling is to redefine or update the state of the extrapolation mechanism. The control response then is essentially continuous although the sampling and information processing required is discontinuous.

The model is most easily described in a closed loop form first and then extended to the open loop-closed loop version. The operator's response is presumed to be proportional plus integral and defined by a system of the following form:

$$\dot{Z}(t) = K\,(E(t) + Ed(t)) \qquad (1)$$

$$U(t) = Z(t) + G(E(t) + Ed(\ )) + Eu(\ ) \qquad (2)$$

where U(t) is the control vector (fore-aft stick movement, side-side stick movement, throttle); Z(t) is the dynamic portion of the control, also a three dimensional vector; E(t) is a six dimensional error vector representing the deviation from nominal values of the state variables (altitude, roll angle, heading angle, flight path angle, angle of attack, velocity); Ed(t) is a display reading error vector assumed to be white noise; and Eu(T) is a motor noise term also assumed to be white noise. This operator model is based on a linearized vehicle model of the form:

$$\dot{E}(t) = AE(t) + BU(t) + Ee(t) \qquad (3)$$

where E(t) and U(t) are as defined above, and Ee(t) is a process noise vector assumed to be white noise. The linearized model (actually two models, one for each maneuver) was used to define the control gains K and G via optimal control. In terms of the operator modelling problem equation (3) should be viewed as an internal model and it is not identical to the non-linear equations used to simulate the aircraft.

The open loop-closed loop model can now be defined. Equations (1), (2) and (3) form a stochastic process describing the response process that the operator would like to realize. In augmented form this process is described by:

$$\begin{bmatrix} \dot{E}(t) \\ \dot{Z}(t) \end{bmatrix} = \begin{bmatrix} A + BG & B \\ K & 0 \end{bmatrix} \begin{bmatrix} E(t) \\ Z(t) \end{bmatrix} + \begin{bmatrix} I & B & BG \\ 0 & 0 & K \end{bmatrix} \begin{bmatrix} Ee(t) \\ Eu(t) \\ Ed(t) \end{bmatrix}$$

which for convenience of notation is rewritten as

$$\dot{X}(t) = \hat{A}X(t) + FE(t) \qquad (4)$$

where

$$X(t) = \begin{bmatrix} E(t) \\ Z(t) \end{bmatrix}$$

Note that

$$U(t) = \begin{bmatrix} G & I \end{bmatrix} X(t) + \begin{bmatrix} 0 & I & G \end{bmatrix} E(t). \qquad (5)$$

Now, to obtain the open loop-closed loop form, let

$$Y(t) = (I \ \ 0)\ X(t) + Ed(t) \qquad (6)$$

represent the display reading process and define

$$M(t,\tau) + E(X(t)/Y(\tau)), \quad t \geq \tau.$$

M(t, τ) is then the conditional mean of the process based on a sample Y(t) at time τ. Clearly,

$$\frac{dM(t,\tau)}{dt} = \hat{A}M(t,\tau), \qquad (7)$$

and under the assumption that there is no memory or information processing associated with the sampling process

$$M(t,\tau) = Y(t) \qquad (8)$$

The operator's control response is then assumed to be of the form

$$U(t) = \begin{bmatrix} G & I \end{bmatrix} M(t,\tau) + Eu(t) \qquad (9)$$

which is basically equation (5) with the conditional mean substitutde for X(t) and the display error removed.

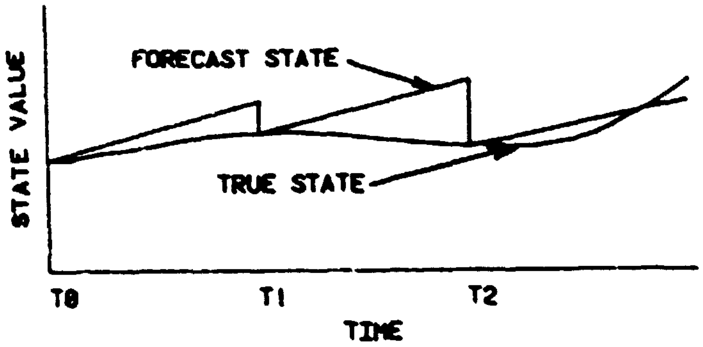

FIGURE 2
STATE VARIABLE SAMPLING

Equation (9) produces a somewhat discontinuous or episodic control response due to the resetting of the mean at sample points. A hypothetical response given samples at times t_0 , t_1 . . . is shown in figure 2 (drawn with the assumption that sampling is error free).

The interested reader is referred to Siefert[3] for more details on the model development and development of the covariance properties.

Baseline model parameters for each maneuver (control gains and noise statistics) were obtained largely by trial and error guided by methods and data found in the manual control literature. Initial control gains were estimated using state variable excursion limit methods[4] to postulate a quadratic regulator optimal control problem. These parameters were then adjusted to produce acceptable model performance (the model "flew" too well with the initial estimates). Noise parameters were estimated from signal to noise considerations of the DAIS data.

The overall model, including the network structure for discrete tasks, was implemented in SAINT[5].

RESULTS

The results consist of sensitivity analyses of the baseline model and some more exploratory analysis of alternative task strategies.

Baseline Model Runs

A series of model runs were made in a configuration in which all state variables were sampled every a time units. The assumption is that the multi-function switching tasks do not interfere with the flight control variable sampling. The flight control display variable sampling interval was varied over a range of 1. to 10. seconds for straight and level, and .5 to 2. seconds for turning dive. The resulting overall score for three different initial random number seeds are displayed in Tables 3 and 4. Each random number seed corresponds to a new sample from the ensemble of mission scores. A graphical representation of the first data appears in Figure 3. The three symbols displayed in the graph denote the three different samples taken at that sample interval. Of some importance is the sensitivity of the scores to the sampling interval. In the straight and level maneuver the scores appear to be increasing almost linearly with the sample interval, with the exception of the 4.5 and 5.0 time intervals. At 5. the score jumps dramatically to .89. This would

ORIGINAL PAGE IS
OF POOR QUALITY

TABLE 3
AIGHT AND LEVEL CASE 1 SCORES

SAMPLE INTERVAL (SEC)	RUN #		
	1	2	3
1	.1228	.1217	.1227
2	.1745	.1658	.1598
3	.2105	.2107	.2037
4	.2529	.3237	.2601
4.5	.5389	.6241	.3600
5	.8483	.8913	.5772
6	.3594	.4828	.3562
7	.4068	.4253	.4094
10	.6056	.5075	.5161

TABLE 4
RISING DIVE CASE 1 SCORES

SAMPLE INTERVAL (SEC)	RUN #		
	1	2	3
.5	3.259	2.564	2.810
.6	3.146	3.332	2.402
.75	2.940	2.134	2.859
.8	2.578	2.097	2.997
1.0	9.915	8.892	9.660
1.4	4.515	4.716	7.646
1.6	5.980	3.652	5.945
1.8	8.825	7.101	9.399
2.0	11.510	17.680	11.810

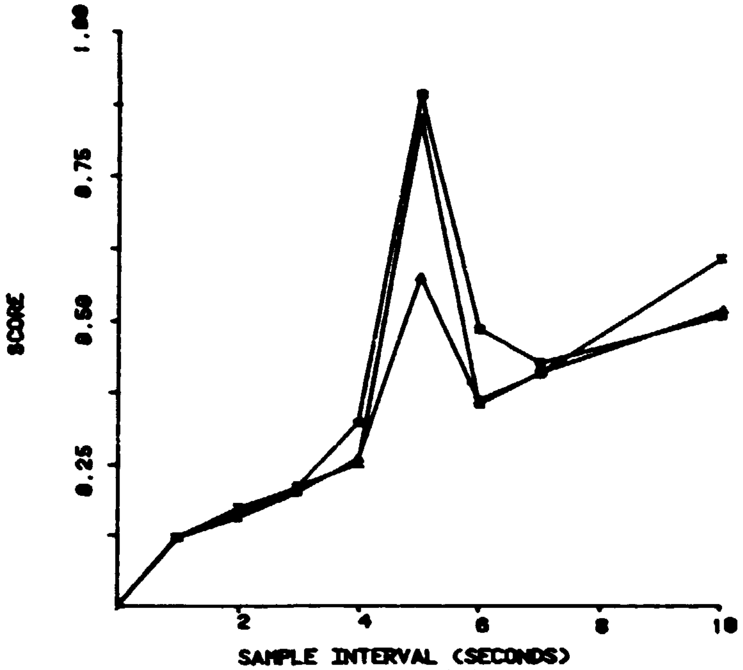

FIGURE 3
STRAIGHT AND LEVEL
SCORES VS SAMPLE INTERVAL

not be so surprising except that at a time interval of 6. seconds, the score drops down to a range between .35 and .48. It gradually increases for the 7. and 10. second sampling intervals.

A similar phenomenon occurs in the turning dive case. Between .5 and .8 the score is relatively insensitive to the sample interval. At 1.0 the score jumps to almost 10. Again, at higher sample intervals the scores drop down; at 1.6 the score ranges between 3.6 and 5.98. Like the straight and level case, the scores begin increasing, this time not quite so gradually.

These peaks in the scores at .5 in straight and leve, and 1.0 in turning dive, were not expected. Closer analysis of the model suggests one plausible explanation for this behavior. Plots over time of the state variable mean statistics produced by the forecasting system are revealing. These distributions have peak errors at the identical points in time where the scores peak. After this time, the forecasting system generally stabilizes, although with higher errors than in the early portion of the sample interval (less than 4.0 in straight and level and 0.8 in turning dive). There appears to be a tradeoff between obtaining estimates of flight control states at peak error points and using the "internal" estimates of state variable values.

Comparison to DAIS Results

The results appear to reflect fairly well the performance of the DAIS subjects. In the straight and level flight alone maneuver, DAIS subjects averaged a score of .72[illegible] with a standard deviation of .219. Experimenters indicated that the highly motivated pilots consistently performed at the .5 level. This suggests that the model sampling interval could span up to 10 seconds and still maintain scores within one standard deviation of the DAIS subjects. Likewise, comparable scores can be obtained in the turning dive maneuver with sample intervals up to 1.6 seconds where the DAIS experimental results produced a mean score of 5.495 with a 1.135 standard deviation.

Analysis of Task Priority

It is probably quite unrealistic to assume that the MFK tasks do not interfere with the flight control variable sampling; nor is it apparent that the pilot operates in a strict priority mode. He more likely "time shares" between flight control and switching, appearing to operate almost in parallel. This behavior is difficult to represent in a simulation model. One possible approach (Case 2) is to use an interleave scheme during the switching task period in which the pilot alternates between an MFK subtask and a flight control display update. With no sampling permitted during the individual MFK tasks.

An alternate sampling scheme gives switching priority over flight control. In this formulation (Case 3), the pilot would under no condition interrupt a keyboard task to update his control task. This represents an extreme or "worst" case in terms of the amount of time devoted to flight control.

Models of Cases 2 and 3 were exercised for both maneuvers. Table 5 contains a summary of the score statistics for all three cases. In Case 2, state variable sampling is performed between each of the eight MFK tasks, each of which have mean durations of 1.08 seconds. During the "flight alone" segments of the mission, sampling is performed at the regular specified interval. Thus for intervals greater than 1.08, Case 2 sampling would actually occur more frequently than in the Case 1 condition,

TABLE 5
STRAIGHT AND LEVEL AVERAGE SCORES

SAMPLE INTERVAL (SEC)	CASE 1 (AVERAGE)	CASE 2 (AVERAGE)	CASE 3 (AVERAGE)
1	.1224	.1330	.2059
2	.1667	.1599	.2553
3	.2083	.1972	.2819
4	.2789	.2551	.4618
5	.7723	.3293	1.1880
6	.3995	.3127	.5549
7	.4138	.3451	.5148
10	.5431	.3976	.5028

and lower scores would be expected. This is precisely what occurred. At the 1 sec. sample interval, the Case 2 average score of .1330 is higher than the Case 1 score of .1224. At all the other intervals (2 through 10), the Case 2 score is lower, as anticipated. It is also of interest to note that the peak at 5 sec. is barely noticeable due to the increased sampling.

In Case 3 no sampling is performed during the MFK switching sequence, which has an average duration of 8.64 secs. The Case 3 results for sample intervals between 1 and 7 secs. indicate scores which in all instances are higher than the Case 1 scores.

Results for turning dive were similar.

SENSITIVITY ANALYSIS OF COMPONENTS OF ERROR

Three separate flight performance scores were recorded for each mission: (1) flight alone phase, (2) flight and MFK switching phase, and (3) overall mission scores. In Case 3 the intuitive notion was that the scores would be much worse (higher) during the combined flight control and switching segments than during the flight alone segments, since no sampling was permitted during these sequences. However, this was not generally true. It was decided to examine flight performance in more detail than that afforded by the three averaged scores. The simulation was rerun with a moving window scoring procedure based on the previous seven points.

A graph of the scores for the turning dive, Case 3, appear in Figure 4. The Δ's indicate when MFK switching is occurring. No clear

ORIGINAL PAGE IS
OF POOR QUALITY

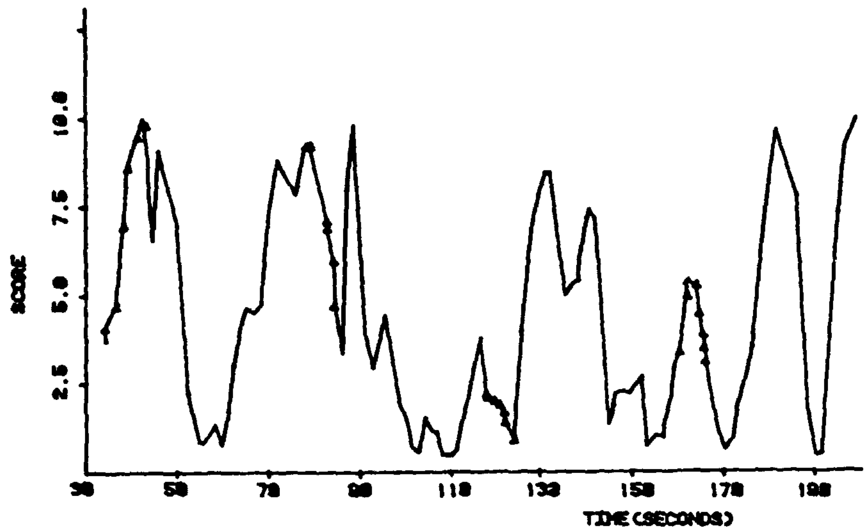

FIGURE 4
TURNING DIVE SCORES

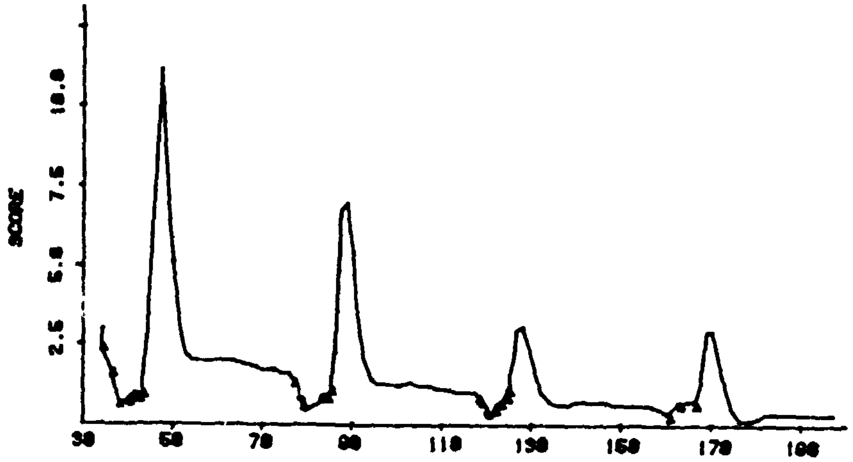

FIGURE 5
TURNING DIVE SCORES
(NO ERRORS)

patterns or trends exist. There appears to be a great deal more variability in the scores than was expected, certainly more than can be ascertained from "mean" data. The extreme range of the scores is also of concern. At some instances the vehicle is very well controlled; at other points in time, control is much less well established.

In an attempt to determine if these characteristics were just anomalies of the simulation model, a similar graph was prepared for a "typical" turning dive maneuver from the real-time experiment. It showed the same degree of variability as the model outputs and also indicated approximately the same range of scores. It appears that the model is duplicating fairly well the performance of the DAIS subjects.

An attempt was made to determine the nature of this variability. The same turning dive Case 3 condition as depicted in Figure 4 was rerun with all the display and control input error distributions removed. The surprising, but logical, results are contained in Figure 5. It appears that the vehicle is in good control upon entering the MFK task. Even though no sampling occurs during the MFK task, the aircraft does not go out of control. However, immediately following the switching task, the pilot reads the displays, determines he has deviated from the command values, and begins to correct his flight path. He grossly overcompensates, causing the peaks in the score, and takes approximately 10 seconds to recover.

The decreasing magnitude ofthe peaks over time is also of interest. This suggests that the system is still undergoing a stabilization period 200 seconds into the mission. This has implications on man-in-the-loop experimental procedures. Allowing the subject sufficient time to achieve stabilization before initiating scoring could produce results which are overly optimistic.

Next, the display errors were added back in. The results of this run indicated the same trend as the "no-error" case. Additing the u_1 (angle of attack) and u_2 (roll angle) control errors individually and in conjunction with the display errors produced no significant changes. Adding u_1 and u_2 together produced generally the same results. Including display errors with u_1 and u_2 also results in the same trend. Adding u_3 errors, however, produces more variability and is never really in a stable mode. It more closely resembles the full error condition. This suggests that the largest contributor to the problem is the difficulty in controlling throttle (u_3), with some additional problems with the other two control variables, u_1 and u_2. Discussions with DAIS experimenters and more detailed examination of the data proved this to be true. It was apparent that vertical velocity was not well controlled in either maneuver, but particularly not in turning dive. While vertical velocity is a function of all three control variables, it is most heavily determined by throttle. It was known for some time that there were physical problems with the response characteristics of both the stick and the throttle. The stick in particular had an extensive amount of "dead space" around the center point. It is hypothesized, based on the above results and conversations with DAIS experimenters, that the DAIS subjects had an exceptionally difficult time controlling the stick and throttle, resulting in extensive variability of flight parameters, vertical velocity in particular. This could very well be the reason why no significant effects were reported between the "flight alone" and "flight plus MFK" conditions. The high variability caused by poor stick and throttle hardware, coupled with inadequate scoring techniques based on averages, may have masked the true effects.

In an attempt to determine what might have happened in more realistic experiments, the model was exercised with reduced error noise. The results indicated much more sensitivity and showed significant differences between sampling strategies.

While these runs certainly did not "prove" that significant differences would have been found in the real-time man-in-the-loop experiment had the stick and throttle been better engineered, it does demonstrate the extreme sensitivity of the system to these parameters, and indicates how main effects may very well have been hidden by their variability. It makes a case for employing a model such as this one for determining how well-behaved such system components must be constructed to perform in order to produce desired system characteristics.

This analysis also points to the need for examining alternate scoring formulations other than the "overall" mission score employed. Ignoring the peaks in the scores immediately following the MFK switching sequence, and using only "averaged" scores, necessarily mask the true effects due to the secondary tasks. One cannot help but to postulate that the outcome of the man-in-the-loop experiment would have been different had the controls been better and the scoring been more sensitive.

Summary of Additional Analyses

In addition to the above analysis, several additional task organization and strategy questions were examined. Two of these are briefly outlined below.

Eye movement data were used to incorporate into the model a probabilistic finite state system which controlled scanning behavior. The model results showed little sensitivity to information gathering strategy during straight and level flight as long as velocity and altitude variables were regularly updated. For turning dive maneuvers, flight control required much more attention and g-load, velocity and vertical velocity were the key variables.

A second sampling strategy termed "probability out of limit" was also examined. In this case the variable with the highest probability of falling outside some specified window was sampled. Probability estimates were based on the mean and covariance produced by the linear model. The sampling algorithm also required that every state variable be sampled periodically.

In straight and level, altitude and velocity were the two primary variables sampled- Vertical velocity and g-load were seldom sampled between the 10 second, "sample everything", intervals. The mean scores for all three cases fall approximately between the 3 and 4 second time intervals of the reduced error case results.

ORIGINAL PAGE IS
OF POOR QUALITY

In the turning dive maneuver, vertical velocity, g-load, and velocity were all sampled, with vertical velocity being sampled most frequently. The other three state variables were sampled together every 5 seconds. In comparing these results to the reduced error, equal-interval sampling scores, it was found that these results fell just slightly above the 0.8 second interval scores. This suggests that similar scores can be obtained by sampling everything 0.8 seconds or by sampling one of three variables every 0.2 seconds.

Closer examination of the individual runs produced additional insights. In the equal-interval sampling runs, the standard deviation of the score is approximately equal to the mean overall score. Thus there is a great deal of variability in flight control performance, as evidenced by the peaks immediately following the MFK task sequence. This is not true in the "probability out of limits" sampling case. There are no sharp peaks and the variances of the scores are much lower. These trends may be important in analyzing workload issues. In peak workload or stress situations, it may be critical that the score (as an estimate of the level of flight control) not go above a certain level at any given time, even though the average performance score is well within limits. If this type of behavior is required, one may opt for the "probability out of limits" type sampling approach. This type of sampling also appears to be more representative of actual pilot flight performance in that the variable which deviates the most from the allowable range is the one attended to. Thus, in a sense, a built-in priority scheme is exercised.

SUMMARY AND CONCLUSIONS

The feasibility of employing a combined modeling approach was demonstrated through successful application to the DAIS system. This modelling approach reduces the weaknesses of employing either network or continuous control techniques independently in modelling monitoring and supervisory control systems. The discrete task activities and decision-making processes of the human operator were explicitly represented along with his continuous tracking behaviors.

The approach's utility as an analysis tool in the design of man-in-the-loop experiments was demonstrated. It can be used to evaluate and establish operator procedures and the experimental protocol or scenario prior to actually running the experiment. For example, results of the DAIS analysis indicated that the aircraft required a relatively long stabilization period and, hence, provided direction for the appropriate collection of data and the sequencing of maneuvers. This effort also demonstrated how the technique can be employed in determining optimal hardware configurations and accuracy requirements. The DAIS simulator stick and throttle devices were known to have defects. The simulation outputs indicated the severity of these defects and could be used to assess accuracy requirements in order to achieve predetermined levels of system performance.

1. Brandt, W. E., Jr. and Wartluft, D. L., *Program Documentation for the DAIS Triple Task*. Aerospace Medical Research Laboratory, AMRL-TR-75-24, Wright-Patterson AFB, Ohio, 1975.

2. Crawford, B. M., Pearson, W. H. and Hoffman, M.S., *Multipurpose Digital Switching and Flight Control Workload*. Aerospace Medical Research Laboratory, Wright-Patterson AFB, Ohio, AMRL-TR-78-43, 1978.

3. Seifert, D. J., *Combined Discrete Network -- Continuous Control Modelling of Man-Machine Systems*, Ph. D. Dissertation, The Ohio State University, Columbus, Ohio, 1979.

4. Baron, S. and Levison, W. H., A Display Evaluation Methodology with Application to Vertical Situation Displays for STOL Aircraft. *Proceedings of Ninth Annual NASA-University Conference on Manual Control*, M.I.T., May 1973.

5. Duket, S. D., Wortman, D. B., Seifert, D. J., Hann, R. L., and Chubb, G. P. *Documentation for the SAINT Simulation Program*. Aerospace Medical Research Laboratory, Wright-Patterson AFB, Ohio, AMRL-TR-77-63, July 1978 (a).

6. Spicuzza, R. J., Pinkus, A. R., and O'Donnell, R. D., *Development of Performance Assessment Methodology for the Digital Avionics Information System*. Systems Research Laboratories, Inc., 1974.

N82 34065 28

A MODEL OF HUMAN DECISION MAKING IN MULTIPLE PROCESS MONITORING SITUATIONS(1)

Joel S. Greenstein
Department of Industrial Engineering and Operations Research
Virginia Polytechnic Institute and State University
Blacksburg, Virginia 24061

William B. Rouse
Department of Mechanical and Industrial Engineering
Coordinated Science Laboratory
University of Illinois at Urbana-Champaign
Urbana, Illinois 61801

ABSTRACT

Human decision making in multiple process monitoring situations is considered. It is proposed that human decision making in many multiple process monitoring situations can be modeled in terms of the human's detection of process related events and his allocation of attention among processes once he feels events have occurred. A mathematical model of human event detection and attention allocation performance in multiple process monitoring situations is developed. An assumption made in developing the model is that, in attempting to detect events, the human generates estimates of the probabilities that events have occurred. An elementary pattern recognition technique, discriminant analysis, is used to model the human's generation of these probability estimates. The performance of the model is compared to that of four subjects in a multiple process monitoring situation requiring allocation of attention among processes.

---

(1)This research was supported by the National Aeronautics and Space Administration under NASA-Ames Grant NSG-2119.

INTRODUCTION

There are many situations in which the human operator must monitor various processes and decide whether and when to direct his attention to one of them. Examples of such multi-task situations include the monitoring of industrial plants, power systems, and air traffic. Product inspection and aircraft piloting tasks provide additional examples. As the complexity and performance demands of such situations increase, the operator must supervise more processes of greater variety. There is consequently an increased probability that he will encounter situations in which there arise more tasks than he can acceptably perform.

One means of maintaining the operator's workload at a satisfactory level is the introduction of automation capable of performing some of the operator's tasks. Models of the operator's task performance would be of use in predicting the performance gains to be expected from the introduction of such aids. Further, in systems in which the responsibilities for some tasks are shared by the operator and an automated decision maker, these models might also be used within the system to coordinate the actions of the two decision makers.

Senders (1) and Smallwood (2) have modeled human decision making in multiple process monitoring tasks. Senders employed an information theory approach to determine how often and for what duration the human must sample each display. Smallwood proposed that the human operator forms an internal model of the processes he is monitoring and of the environment relevant to his task as a result of his past perceptions of them. Carbonell (3,4) and Senders and Posner (5) have proposed queueing theory approaches to the modeling of human decision making in multiple process monitoring tasks. Kleinman and Curry (6) have applied control theoretic techniques to develop models of human performance in such tasks.

The models cited above emphasize the monitoring of displays, rather than the decisions or actions that result from the human operator's perception of the displayed values. The operator's motivation for monitoring the displays is the possibility that an event which requires his action will occur. The multi-task decision making problem addressed in this paper concerns the event detection and action selection decisions the operator makes on the basis of the information he gains through monitoring.

Human decision making in such multi-task situations, then, might be modeled in terms of the manner in which the human detects events related to the processes and the manner in which he allocates his attention among the processes once he feels events have occurred. Gai and Curry (7) have developed a model of the human monitor in a failure detection task. The model has two stages, the first a Kalman filter which estimates the states and observations of the monitored process, and the second a decision mechanism which operates on the Kalman filter residuals using sequential analysis concepts. Sheridan and Tulga (8) have modeled the manner in which the human operator allocates his attention among various tasks. They address a situation in which events present themselves unequivocally and use a dynamic programming approach to determine the action sequence which maximizes the operator's earnings.

Rouse (9) has investigated the issue of allocation of decision making responsibility between a human operator and an automated decision maker. He presents a mathematical formulation of multi-task decision making situations appropriate to modeling either decision maker. Based on displayed information, the decision maker is assumed to generate probabilities that events have occurred in his tasks. He also generates density functions which characterize his perceptions of what might occur in his tasks while his attention is diverted to a particular task and how long his attention will be diverted should he decide to take a given action. Given the estimates of event occurrence probabilities and the perceptions of density functions of interarrival and action times, the decision maker is assumed to choose actions so as to minimize an appropriate cost criterion.

This formulation has been applied to the design of a computer aided decision making system within a queueing theory framework (10,11). Two experiments within a flight management context were used to illustrate the value of this multi-task formulation. It was found that the queueing theory model provided a quite reasonable description of multi-task decision making in terms of task waiting times and utilization (i.e., fraction of time busy) of decision makers. The nature of the flight management task employed in this research, however, allowed avoidance of the issue of how the human decision maker detects events.

A MODEL OF HUMAN DECISION MAKING

In this section we propose a model of human decision making in a multiple process monitoring situation. The model assumes that the human uses a weighted linear combination of various features to generate estimates of the probabilities of event occurrences. A discriminant analysis approach (12,13) is employed to model the human's generation of these probability estimates. This pattern recognition technique is amenable to real-time, adaptive implementation. A computer aiding scheme based on such a model would have the capability of learning to generate appropriate event occurrence probability estimates through observation of the human operator's task performance. The model might then assume decision making responsibilities when the human becomes overloaded.

For each process, it is assumed that the human extracts various features X_j, $j=1,2,\ldots,p$, from his observations. These features are properties of the observations that characterize (or are believed to characterize) the presence or absence of events related to the process. Following the extraction of a set of features, the value of a linear discriminant function

$$Y = v_1X_1 + \ldots + v_pX_p \qquad (1)$$

is calculated. Based on previous experience with the process, estimates are made of the discriminant function coefficients v_j, $j=1,2,\ldots,p$, with which to combine the feature values X_j to obtain the discriminant function score Y that best differentiates observations of events from the rest of the process related observations. Estimates of the mean and variance of the discriminant function over observations of events and over the rest of the observations are also formed. The a posteriori probability that an event has occurred is generated using the value of the discriminant function score, the estimates of the means and variances of this score over events and "non-events", and an estimate of the a priori probability of the event. The reader is referred to (12) for a development of the mathematics through which we determine the discriminant function coefficients, the means and variances of the resulting discriminant function, and finally, the a posteriori probability that an event has occurred conditioned upon the value of this function.

If a process of unknown state (event present or not present) is observed, features X_j, $j=1,2,\ldots,p$, are extracted from the observations, and the value of the discriminant function Y is calculated as prescribed by Eq. (1), the a posteriori probability that an event has occurred is given by

$$P(e/Y) = \exp(-x_2^{\,2}/2) \Big/ \sum_{k=1}^{2} \exp(-x_k^{\,2}/2) \qquad (2)$$

where

$$x_k^{\,2} = \quad - \bar{Y}^{(k)}]^2/D_k(y) + \ln D_k(y) - 2 \ln p_k \qquad k = 1, 2 \qquad (3)$$

$\bar{Y}^{(k)}$ and $D_k(y)$ are the group means and variances, respectively, of the discriminant function based on previous observations taken at times at which no event related to the process was present (k=1) and at times at which a process related event was present (k=2). p_k is the a priori probability of no event (k=1) or an event (k=2).

If the human operator is forced to make a yes/no response on the presence of an event, we might assume that he chooses the response which maximizes his expected reward. We can then express his decision in a signal detection manner and state that he should respond "yes, an event related to process i has occurred" if the following inequality holds:

$$P(e/Y)/[1 - P(e/Y)] > [V_{CR} + C_{FA}]/[V_H + C_M] \qquad (4)$$

$P(e/Y)$ is the a posteriori probability that a process related event has occurred and is generated as described above. V_{CR} is the value of correctly responding "no event" (a correct rejection). C_{FA} is the cost of incorrectly responding "event" (a false alarm). V_H is the value of correctly responding "event" (a hit), and C_M is the cost of incorrectly responding "no event" (a miss).

It is predicted, then, that if the operator is forced to make a yes/no decision on the presence of a process related event, he calculates the likelihood ratio of the event (the left hand side of Eq. (4)). He compares the magnitude of the likelihood ratio with a threshold determined by the values of correct responses and the costs of incorrect responses (the right hand side of Eq. (4)). He responds "event" if the likelihood ratio exceeds the threshold.

In many situations, however, the decision maker is not forced to make yes/no decisions with respect to each of the processes. He is instead faced with a situation in which the decision to take action with respect to a process implies the allocation of attention to that process for some amount of time and the diversion of attention from other processes during that time. If we consider this decision making problem in the context of the mathematical formulation presented in Rouse (9) and Rouse and Greenstein (14), another modeling approach suggests itself. It was assumed in that formulation that the human operator has perceptions of the probabilities that events have occurred in the processes, $p(./\underline{Z})$, the joint probability density function of the time between events in the processes, $f(./\underline{Z})$, and the joint probability density function of the action times for the processes, $g(./\underline{Z})$. The operator is to decide which actions of the set $a_0, a_1, \ldots, a_N$ should be performed. He might choose a_0 (the decision to continue monitoring) in order to obtain new information with which he can update $p(./\underline{Z})$. If he chooses a_i, $i \neq 0$, he services process i for some amount of time and is unable to monitor or attend to the other N-1 processes until servicing of process i is completed.

The operator might be modeled as deciding whether to continue monitoring all processes or to divert his attention to some of the processes by utilizing his perceptions of $p(./\underline{Z})$, $f(./\underline{Z})$, and $g(./\underline{Z})$ to determine a sequence of actions which minimize an appropriate cost criterion. If we want to penalize deviations of process state $\underline{x}_i$ from some desired state, then we might formulate the criterion so as to allow use of control theoretic techniques. On the other hand, if we are interested in minimizing the average time from occurrence of a process failure to completion of service to that process, queueing theory provides an appropriate methodology. Because the general multiple process monitoring situation does not inherently involve processes whose states can be described by linear dynamic systems, we will consider a criterion involving minimization of the costs of delays in service to failed processes. In particular, let us consider the following cost criterion as one which the operator might seek to minimize:

$$E[C/T] = (1/T)E[c_1w_1 + c_2w_2 + \ldots + c_Nw_N] \qquad (5)$$

where w_i is the delay experienced by process i and includes the waiting time until initiation of service and the servicing time, c_i is the cost per unit time of delay in service to process i, and T is the amount of time for which the operator's attention is diverted from his displays as a result of his action sequence.

Throughout the remainder of this paper we will assume independence among processes. That is, it will be assumed that the probabilities of events having occurred in the processes are independent among processes. Thus

$$p(\cdot/\underline{Z}) = p(\underline{e}_1/\underline{z}_1)p(\underline{e}_2/\underline{z}_2) \cdots p(\underline{e}_N/\underline{z}_N) \tag{6}$$

Similarly, the time between events and the time required to attend to a process are independent among processes. Thus

$$f(\cdot/\underline{Z}) = f_1(\underline{t}_e/\underline{z}_1)f_2(\underline{t}_e/\underline{z}_2) \cdots f_N(\underline{t}_e/\underline{z}_N) \tag{7}$$

and

$$g(\cdot/\underline{Z}) = g_0(t_a/\underline{Z})g_1(\underline{t}_a/\underline{z}_1) \cdots g_N(\underline{t}_a/\underline{z}_N) \tag{8}$$

Consideration of interdependencies among processes would complicate the analysis substantially. It should be noted however, that the assumption of independence among processes is, in many realistic situations, difficult to justify.

Let us approach the problem by evaluating each c_iw_i component of Eq. (5) for a candidate action sequence. Proceeding from Eqs. (6), (7), and (8), let us now, for the sake of simplicity, assume that only one type of event in each process is of interest. Let us also assume that the time between events in a process and the time required to attend to a process is independent of the observations, $\underline{Z}$. Then

$$f(\cdot/\underline{Z}) = f_1(t_e)f_2(t_e) \cdots f_N(t_e) \tag{9}$$

and

$$g(\cdot/\underline{Z}) = g_0(t_a)g_1(t_a) \cdots g_N(t_a) \tag{10}$$

If the human chooses to perform action a_j $(i \neq j)$, then the cost due to ignoring process i for time t_a, given that an event e_i has occurred is

$$c_i t_a$$

and the cost due to ignoring process i if an event e_i occurs after initiation of action a_j is

$$\begin{array}{ll} c_i(t_a - t_e) & t_a > t_e \\ 0 & t_a \leq t_e \end{array}$$

Therefore, if the human chooses to perform process a_j, $(i \neq j)$, then

$$E[c_i w_i / a_j] = p(e_i/\underline{z}_i) c_i \int_0^\infty t_a g_j(t_a) dt_a$$

$$+ [1 - p(e_i/\underline{z}_i)] c_i \int_0^\infty \int_0^{t_a} (t_a - t_e) f(t_e) g(t_a) dt_e dt_a \qquad (11)$$

where the first term is the expected cost of ignoring process i for time t_a due to an event e_i that has occurred, while the second term is the expected cost due to an event e_i occurring during t_a.

If event interarrival times in process i are exponentially distributed with mean $1/\lambda_i$ and action times are constants t_j, $j=0,1,\ldots,N$, then

$$E[c_i w_i / a_j] = p(e_i/\underline{z}_i) c_i t_j$$

$$+ [1 - p(e_i/\underline{z}_i)] c_i \int_0^{t_j} (t_j - t_e) \lambda_i \exp(-\lambda_i t_e) dt_e \qquad (12)$$

And, upon carrying out the indicated integration,

$$E[c_i w_i/a_j] = p(e_i/\underline{z}_i)c_i t_j$$

$$+ [1 - p(e_i/\underline{z}_i)]c_i[t_j - (1/\lambda_i)(1 - \exp(-\lambda_i t_j))] \qquad (13)$$

Assume that the human plans ahead two actions, a_j and a_k, $(i \neq j,k)$. Then

$$E[c_i w_i/a_j,a_k] = p(e_i/\underline{z}_i)c_i(t_j + t_k)$$

$$+ [1 - p(e_i/\underline{z}_i)]c_i \int_0^{t_j+t_k} (t_j + t_k - t_e)\lambda_i \exp(-\lambda_i t_e)dt_e$$

$$= p(e_i/\underline{z}_i)c_i(t_j + t_k)$$

$$+ [1 - p(e_i/z_i)]c_i[t_j + t_k - (1/\lambda_i)(1 - \exp(-\lambda_i(t_j + t_k)))]$$

Generalizing to action sequences of length N, we have

$$E[c_i w_i/a_j, \ldots , a_l] = p(e_i/\underline{z}_i)c_i(t_j + \ldots + t_l)$$

$$+ [1 - p(e_i/\underline{z}_i)]c_i$$

$$\cdot[t_j + \ldots + t_l - (1/\lambda_i)(1 - \exp(-\lambda_i(t_j + \ldots + t_l)))]$$

$$i \neq j, \ldots , l \qquad (14)$$

Suppose action a_i is performed. If the waiting time w_i is measured from the time of failure to the time of service completion and it is assumed that servicing of process i precludes the possibility of failures during servicing, then

$$E[c_i w_i/a_i] = p(e_i/\underline{z}_i)c_i t_i \qquad (15)$$

Suppose after action a_i other actions $a_m,\ldots,a_n$ are performed. The cost to process i incurred by these actions is due only to the cost of ignoring process i if an event e_i occurs after completion of service to process i (since process i is in the normal state upon completion of service to it). Therefore

$$E[c_i w_i/a_m, \ldots, a_n] =$$

$$c_i[(t_m + \ldots + t_n) - (1/\lambda_i)(1 - \exp(-\lambda_i(t_m + \ldots + t_n)))] \tag{16}$$

So, the expected cost in process i incurred by an action sequence $a_j,\ldots,a_l,a_i,a_m,\ldots,a_n$ can be expressed as

$$\begin{aligned}
E[c_i w_i/a_j, \ldots, a_l, a_i, a_m, \ldots, a_n] = {} \\
& p(e_i/\underline{z}_i)c_i(t_j + \ldots + t_l) \\
& + [1 - p(e_i/\underline{z}_i)]c_i \\
& \quad \cdot[t_j + \ldots + t_l - (1/\lambda_i)(1 - \exp(-\lambda_i(t_j + \ldots + t_l)))] \\
& + p(e_i/\underline{z}_i)c_i t_i \\
& + c_i[(t_m + \ldots + t_n) \\
& \quad - (1/\lambda_i)(1 - \exp(-\lambda_i(t_m + \ldots + t_n)))]
\end{aligned} \tag{17}$$

The total cost incurred by an action sequence $a_j,\ldots,a_l,a_i,a_m,\ldots,a_n$ over the time duration of the action sequence is then given by the summation of costs over the total number of tasks, N. Thus,

$$E[C] = \sum_{i=1}^{N} E[c_i w_i/a_j, \ldots, a_l, a_i, a_m, \ldots a_n] \tag{18}$$

and the expected cost per unit time incurred by the action sequence (which is the cost criterion, Eq. (5), under consideration) is therefore

$$E[C/T] =$$

$$\left(\sum_{i=1}^{N} E[c_i w_i / a_j, \ldots, a_l, a_i, a_m, \ldots a_n]\right) / (t_j + \ldots + t_n) \qquad (19)$$

We have thus far expressed the expected cost per unit time for an action sequence in terms of $p(./\underline{Z})$, $f(./\underline{Z})$, and $g(./\underline{Z})$, and carried through the development of this expression for the case of exponentially distributed event interarrival times and constant service times. Let us now suggest a specific model of human decision making which considers the expected cost per unit time of certain action sequences and selects from among these candidate sequences the action sequence which minimizes this cost criterion.

We suggest that the operator might be modeled as initially estimating the expected cost per unit time incurred by the decision to continue monitoring for a period of time. If acting with respect to any one process before monitoring would not result in a lower expected cost per unit time (over the time interval required to act on the process and then monitor), the operator simply elects to continue monitoring.

If acting with respect to a process before monitoring results in a lower expected cost per unit time than monitoring alone, the operator determines the action which results in the minimum expected cost per unit time and assigns to it the first position in his action sequence. He then determines whether acting with respect to any of the remaining processes before monitoring would lower the expected cost per unit time of his action sequence further. If it will not, he responds to the one process he has placed in his action sequence and then continues monitoring.

If acting with respect to one of the remaining processes before monitoring does lower the expected cost per unit time of his action sequence, the operator determines the action which results in the minimum expected cost per unit time and assigns to it the second position in his action sequence. The procedure continues until the addition to the sequence of an action with respect to any of the remaining processes does not lower the expected cost per unit time of the sequence or until actions with respect to all the processes have been included in the sequence.

EXPERIMENTAL SITUATION

An experimental situation was developed to facilitate the study of human decision making in a specific multiple process monitoring task. The task involves the simultaneous monitoring of nine dynamic processes for the occurrence of abnormal events, a situation representative, for example, of monitoring tasks in complex industrial plants.

Figure 1 illustrates the display observed by subjects within the experimental situation. The display is static and is generated on a Tektronix 4010 storage tube display by a time-shared DEC-System 10 digital computer. The display depicts the measured values of the outputs of nine processes over 100 sampling intervals (i.e., 101 measurements are depicted on the display for each process). A time unit on the display corresponds to the interval between successive samples of the process outputs.

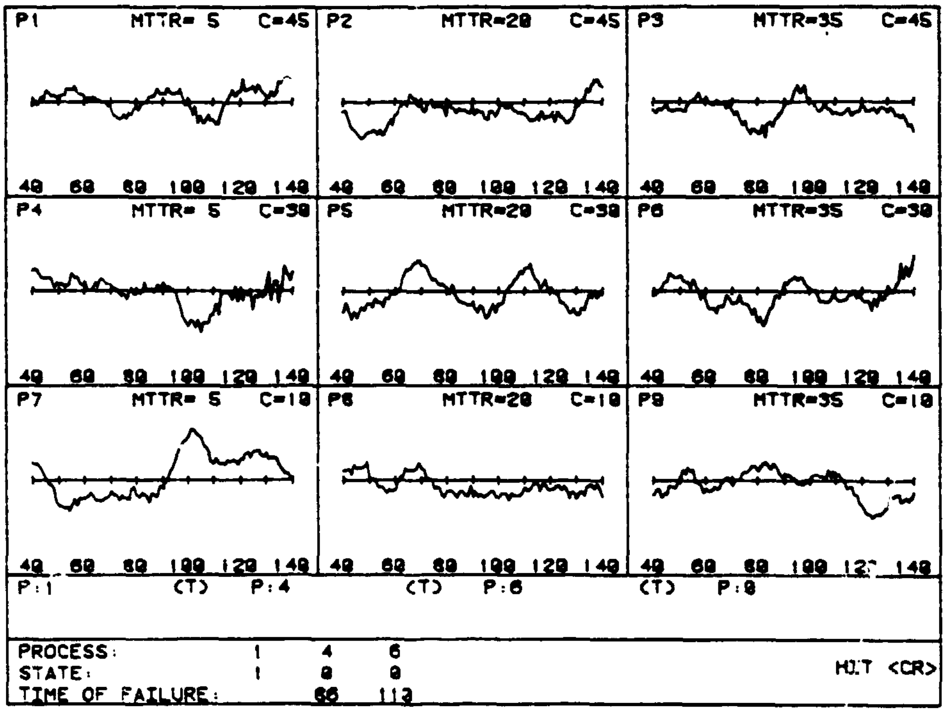
P1 MTTR= 5 C=45
P2 MTTR=20 C=45
P3 MTTR=35 C=45
P4 MTTR= 5 C=30
P5 MTTR=20 C=30
P6 MTTR=35 C=30
P7 MTTR= 5 C=10
P8 MTTR=20 C=10
P9 MTTR=35 C=10
40 60 80 100 120 140
P:1 <T> P:4 <T> P:6 <T> P:0
HIT <CR>

PROCESS: 1 4 6
STATE: 1 0 0
TIME OF FAILURE: 86 110

Figure 1: The multiple process monitoring situation

(Processes 4 and 6 have failed at times 86 and 110, respectively. Processes 1,4, and 6 have been selected for service.)

The processes have identical second order system dynamics with a natural frequency of 0.15 rad/time unit and a damping ratio of 0.5. The inputs to the processes are zero-mean Gaussian white noise sequences of identical variance. The displayed measurements are obtained by corrupting the process outputs with additive zero-mean Gaussian white noise sequences which normally have identical variance. The measurement noise variance is normally selected to yield measurements with signal-to-noise ratios of 25.0.

An abnormal event or process failure is defined by a gradual increase in the measurement noise variance following process failure such that the signal-to-noise ratio of each measurement is decreased to 95% of the signal-to-noise ratio of the immediately preceding measurement. A process failure manifests itself, then, by an exponential decay of the signal-to-noise ratio for measurements following the time of failure. Thus, failures become more pronounced with each measurement following their occurrence. This is illustrated in Figure 2: all nine processes have failed at various points within the time range depicted on the display. The points at which these failures occurred have been denoted in the figure by solid vertical lines. These lines did not appear on the display during the experiment.

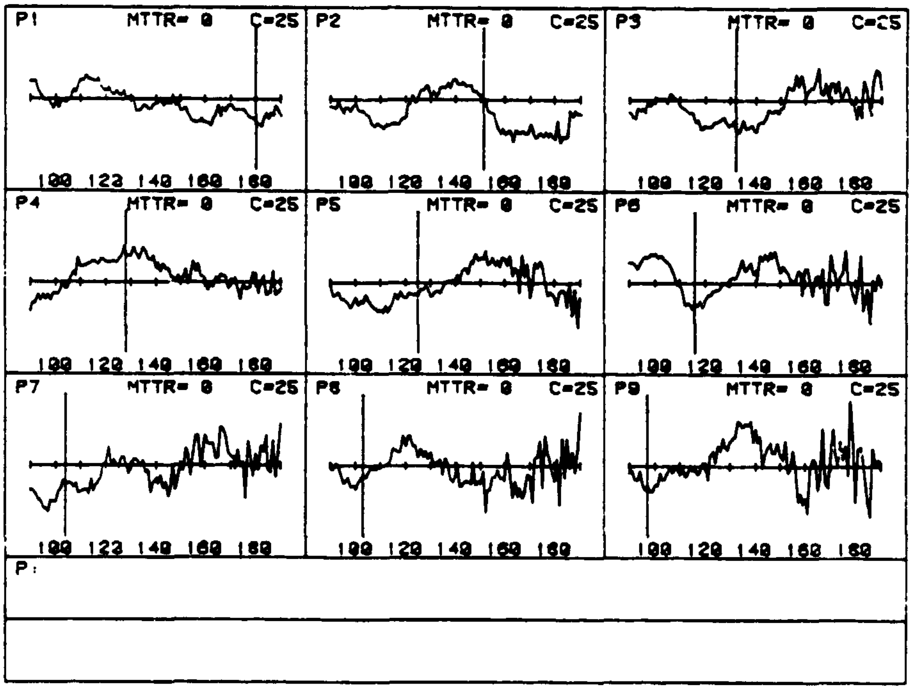

Figure 2: A display in which all processes have failed

While the exact nature of the subject's task in this experimental situation differs with the nature of the decision making being investigated — simple event detection or action selection involving allocation of attention among the processes — in all cases the subject seeks to detect events in processes and service these processes so that they are returned to the normal state. The amount of time required to service a process can be varied across the processes. If the amount of time required to service a process is nonzero, servicing of the process implies a diversion of attention from the other processes for this time. The cost of delaying service to a process can also be varied from process to process.

The above aspects of the situation are quantified by associating a set of two parameters with each of the nine processes — the mean time to repair the process (MTTR), and the cost per unit time of delay of service to a failed process (C). If the times required to repair a process are assumed constant or exponentially distributed, then MTTR completely specifies the distribution of service times for that process.

After scanning the nine process histories depicted on the display, the subject is given an opportunity to key in the numbers of processes which he has decided to service. He also uses a graphic cursor to enter estimates of times at which he believes failures have occurred. Upon completion of his entries, the processes he has entered are serviced in the order in which he entered them. The first process entered by the subject is serviced over an interval which begins with the last time point displayed on the screen and extends forward the number of time units equal to the MTTR associated with the process. At the completion of this service the process is reset to normal if it has failed before this point and service is begun on the next process entered by the subject. When all processes entered have been serviced, the subject is given feedback regarding the state of each serviced process at the instant before servicing of that process was completed ("1" indicating the normal state, "0" indicating the failed state). An iteration in an experimental trial ends with erasure of the display and the scoring of the subject's performance on the iteration.

Another iteration is then begun by generating a new display depicting the process histories advanced in time by an amount equal to the sum of the service times (MTTRs) of the processes entered on the preceding iteration plus an additional constant increment. The additional increment is included to represent the interval of time required to monitor the processes each time they are displayed (this increment will be referred to as the mean time to monitor the processes, MTTM). The display which would follow that shown in Figure 1 is illustrated by Figure 3. The MTTRs associated with the processes are depicted in the figure. The MTTM employed in the situation illustrated is 10 time units. It should be noted that Figs. 1 and 3 presented here as illustrations of the experimental situation represent iterations or displays which would fall somewhere in the middle of a subject's experimental trial. The first iteration or display viewed by the subject in an experimental trial would depict the measured values of the nine processes' outputs over a time span beginning at time t=0 (as labeled on the horizontal axes) and ending at time t=100.

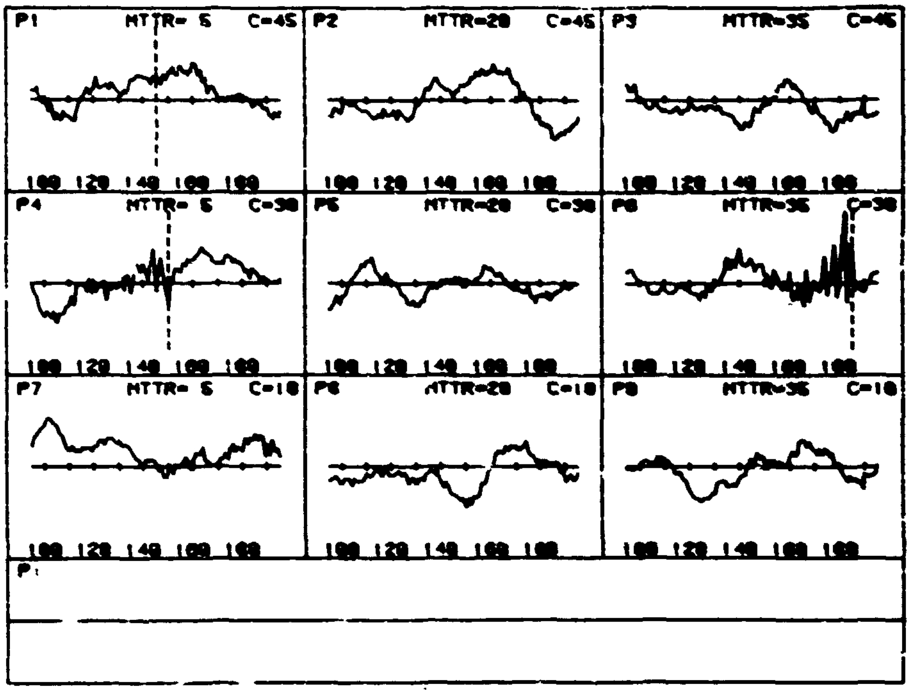

Figure 3: The display which follows that shown in Fig. 1

(The dashed vertical lines indicate to the subject the point at which service of each process was last completed.)

EXPERIMENT

An experiment was conducted employing the multiple process monitoring situation described in the preceding section. The task of the subject in this experimental situation was to service, or allocate attention to, processes in a manner which minimized the total cost incurred due to delays in the servicing of failed processes.

Four subjects were given six trials with the experimental situation over a period of four to six days. Each trial consisted of 25 iterations (an initial display followed by 24 updated displays) and was of approximately 45 minutes duration. Three levels of MTTR and C were employed across the nine processes. The values of MTTR and C associated with each of the processes were as depicted in Figs. 1 and 3. The value of MTTM employed in the experiment was 10 time units. These values were held constant across all trials. The interarrival times of the failures scheduled to occur in each process were exponentially distributed with a mean time between failures (MTBF) of 175 time units in all processes. Not all scheduled failures actually occurred. If a failure was scheduled to occur in a process in which a previous failure had not been attended to, the scheduled failure was deleted from the trial. The interarrival times used to schedule failures on the successive trials given a subject differed from trial to trial.

Prior to beginning the six trials with the experimental situation described above, the subjects were given four trials in which the MTTRs were set to zero and the Cs to one for all processes. With zero MTTR and equal C for all processes, the decision to allocate attention to one process involved no diversion of attention from the other processes and a delay in servicing one process was no more costly than a delay in servicing any other process. After scanning the process histories depicted on the display, the subject simply entered the numbers of processes in which he had decided failures had occurred. These trials provided the subjects with experience in the detection of process failures without the additional task of deciding how to allocate attention among processes with different attentional requirements and costs. Subjects were also given several iterations of training before these trials and the later six trials. During these training iterations, solid vertical lines were included on the process histories to mark when and where events had occurred (see Fig. 2). Subjects were not given any information regarding the dynamics of the processes, but were told that they could expect the processes to exhibit similar characteristics when operating normally. They were also not told what parameter changes defined events, but were told that all events would generally exhibit similar characteristics and all would become more pronounced as time passed.

APPLICATION OF THE MODEL TO THE EXPERIMENTAL SITUATION

The decision making model suggests that the human operator in the experimental situation just described extracts various features from his observations of the process measurements. He attempts to select features which characterize the presence or absence of task related events. Through his experience with the processes, the operator has formed estimates of the discriminant function coefficients with which to combine the features to obtain a discriminant function score. He has also formed estimates of the means and variances of this score over observations of events and over the rest of his observations. The operator generates the a posteriori probability that an event has occurred based on the value of the discriminant function score, his estimates of the means and variances of the score, and his estimate of the a priori probability of an event occurrence.

Four features of the process measurements were selected for use with the event detection model. Selection of these features was guided by the comments of experimental subjects in a similar situation regarding the characteristics of the process measurements they found useful in event detection. The first feature involves the magnitude changes between successive measurements in a sequence of the most recent measurements. The second feature involves the presence of reversals in direction in this sequence (changes from positive slope to negative, or vice versa, of the line segments connecting the measurements of the sequence). The third feature tests for the simultaneous occurrence of large magnitude changes and reversals. The fourth feature, like the first, is a measure of magnitude changes, but it is much more local in that it involves only the four most recent measurements of the process output.

Given that events become more pronounced with time following their occurrence, it seems reasonable that the most recent process measurements would be of greater use in event detection than older measurements. Therefore, in extracting features from the process measurements, the values of the features over recent measurements are weighted more heavily than the values over earlier measurements. The weight decreases exponentially with the age of the measurement and the rate of this decrease is a free parameter. The value of the first feature, for example, a measure of the magnitude changes between successive measurements in a sequence of the n most recent measurements of a process's output, is given by

$$X_1 = \{\sum_{k=1}^{n-1} |z(k+1) - z(k)| \cdot \exp[-\beta(n-1-k)]\} \Big/ \sum_{k=1}^{n-1} \exp[-\beta(n-1-k)] \qquad (20)$$

where z(k) is the k th measurement in the sequence, z(n) is the most recent measurement, and β is the free parameter governing the relative weighting of the feature's value over recent and earlier measurements in the sequence.

The estimation of discriminant function coefficients requires a representation of normal and abnormal process measurements. This representation was formed using the process histories displayed to the subject on his last event detection trial (i.e., the fourth of the four trials given in which the MTTRs were all zero and the Cs all one). The process histories are separated into two groups of sequences -- normal and abnormal. Sequences of measurements beginning at the point at which a process was returned to the normal state and ending at the point at which an event occurred (or, alternatively, the point at which the subject estimated an event occurred) are defined to be normal. Sequences of measurements beginning at the point at which an event occurred (or the point at which the subject estimated an event occurred) and ending at the point at which the process was returned to the normal state are defined to be abnormal. In obtaining the results to be presented here, the points at which the subject estimated events occurred, rather than the actual points of occurrence, were used to define the final points of normal sequences and initial points of abnormal sequences. This was done to test the ability of the model to perform adequately in situations in which true event times are unknown and a human operator's identification of events and estimates of occurrence times represent the only event time data available. This decision is consistent with our long term goal of developing a computer aided process monitoring system.

The representation of normal and abnormal process measurements formed using the process histories of the subject's last event detection trial are used to determine discriminant function coefficients and the means and variances of the resulting discriminant function scores. If the model is then to be used to generate the a posteriori probability of an event in a process at a given iteration of an experimental trial, the number of process measurements over which the features are to be calculated must be defined. It is reasonable to assume that the measurement sequence ends with the last measurement displayed for the process on that iteration. However, the cutoff length which indicates when the measurement sequence begins is a free parameter. Values of the features over process measurements taken earlier than the cutoff are not calculated (or, effectively, are assigned zero weight).

Generation of the a posteriori probability of events in the tasks using the discriminant analysis approach requires estimates of the a priori probabilities of event occurrences in the tasks. We can approximate the time between consecutive event arrivals to a process as an exponential distribution with parameter 1/MTBF. (This is an approximation because not all scheduled events occurred. Thus, the true mean time between failures is somewhat larger than the nominal value used to schedule the arrivals.)

If we let U(t) be the number of failures in a process by time t (t>0), where time 0 designates the instant at which the count begins, then

$$p(U(t) = n) = [(t/MTBF)^n \exp(- t/MTBF)]/n! \qquad n = 0, 1, \ldots ; \qquad (21)$$

Thus,

$$p(U(t) = 0) = \exp(- t/MTBF) \qquad (22)$$

and the a priori probability that an event occurs in the process at or before time t is

$$p(U(t) \neq 0) = 1 - \exp(- t/MTBF) \qquad (23)$$

We model the subject's estimate of the time t that has elapsed since the process was last reset to normal (and during which a failure may have occurred) as the minimum of the time since service to the process was last completed and the time since the first measurement presented on the current display. We thus assume that if service of a process was last completed at a time point earlier than the earliest time point shown on the current display, the subject uses the earliest time point on the display as his estimate of the first point at which a new failure may have occurred in the process.

Before concluding this section we would like to consider a modification to the basic model. Application of the model as we have outlined it to data obtained in the experiment presented in the preceding section reveals a disparity between the performance of the model and that of the experimental subjects. Specifically, the model tends to respond to lower MTTR and higher C processes more often than the subjects, while it tends to respond to higher MTTR and lower C processes less often than the subjects. In an attempt to deal with this disparity while retaining the potential robustness of the model, we will incorporate two additional parameters into the model.

The first parameter is a lower probability threshold. If the probability that an event has occurred in a process j is lower than this threshold, than process j is not considered for inclusion in the action sequence, even if inclusion would result in a lower expected cost per unit time than omission of the action or inclusion of some other action. This parameter is introduced to reduce the tendency of the model to respond to some processes more often than the human operator.

The second parameter is an upper probability threshold. If, after the determination of an action sequence by the concatenation of actions which successively lower the expected cost per unit time of the sequence, there remain outside the sequence processes for which the probability of an event occurrence is greater than this threshold, these processes are added to the action sequence. Of these processes, that whose addition results in the smallest increase in the expected cost per unit time is added to the sequence first. The remaining processes are then added to the sequence in the same manner. This parameter is introduced to reduce the tendency of the model to respond to some processes less often than the human operator.

There are, then, four free parameters in our application of the model to the experimental situation -- β , specifying the relative weighting assigned to feature values calculated over recent and older process measurements, the cutoff length, specifying the number of measurements over which features are extracted, and two probability thresholds used to exclude or include actions in the action sequence on the basis of event probability alone.

RESULTS

The decision making performance of the model was compared with that of each subject by supplying the model with the MTTRs and Cs associated with each of the processes and with estimates of the a priori and a posteriori probabilities of failures in each of the processes at the time they were displayed to the subject. The model was used to generate action sequences for each display viewed by each subject on his last three trials (a total of 75 displays with 9 processes/display for each subject). These action sequences were compared on a sequence by sequence basis with the corresponding action sequences entered by the subject.

In generating the a posteriori probabilities of failures in each of the processes, β and the cutoff length were fixed at intuitively reasonable values of 0.2 and 10, respectively. No attempt was made to determine the values of β and cutoff length which yield the best performance of the model across all subjects. Although it seems reasonable to conjecture that better performance could be obtained by determining the optimal β -cutoff length pair for each subject, our goal of a simple computer aiding scheme motivated the decision to fix these parameters.

In evaluating the model's performance we are concerned with two aspects of decision making. First, when did the model include a specific process in its action sequence and how does the timing of this action compare with that of the subject's response to the process? Second, for those processes included in both the model's and the subject's action sequences for a given display, how many of the model's orderings of actions within the sequence differ from the subject's orderings?

Regarding the timing of the model's responses relative to that of the subject, there is some difference in the utility of modeling those responses of the subject to processes which actually require service (hits) and those responses to processes which are not failed and do not require service (false alarms). We would be particularly concerned that the model respond to those processes requiring service that the subject responds to, and would prefer that the model also respond to these processes at the same time as the subject. We are less concerned with the correspondence of the model's and subject's false alarms, provided the model does not make more false alarms than the subject.

Table 1 compares the performance of the model with the performance of each of the four subjects. In each case, the lower and upper probability thresholds of the model were varied to achieve the best fit of the model's performance to the subject's performance. The best fit was defined in terms of the difference of two performance measures: the number of detections by the model made only at the exact same time as the subject's detections and the number of detections made by the subject and missed by the model. The latter measure was subtracted from the former and the threshold was varied to maximize the resulting quantity. The maximization was done subject to the constraint that the number of false alarms by the model not exceed the number of false alarms by the subject. Thus, we sought to maximize the number of times the model and subject responded to failed processes at exactly the same time. We sought to minimize the number of times the model did not respond to a failed process to which the subject did respond to. And we did not permit the model to make more false alarms than the subject. It should be noted that, during the experimental trials given the subject, processes entered by the subject for service on a given iteration were serviced and reset to normal before the generation of a display for the next iteration. Because of this, when we compare the model's actions with those of the subject, it is not possible for the model to take action with respect to a failed process on an iteration later than the one at which the subject acted.

TABLE 1

Comparison of model's performance with subjects' performance

Subject	T_L	T_U	NHIT_s	NHIT_{sm}	NHIT_{co}	NHIT_{so}	NFA_s	NFA_m
S1	0.39	0.60	110	97	85	13	17	17
S2	0.63	0.94	117	109	92	8	28	27
S3	0.32	0.38	83	72	56	11	18	12
S4	0.79	0.99	120	110	102	10	16	16

T_L: lower probability threshold
T_U: upper probability threshold
NHIT_s: # detections by the subject
NHIT_{sm}: # detections by the subject also made by the model (at the same time or earlier)
NHIT_{co}: # detections by the model at the exact same time as the subject and only at that time
NHIT_{so}: # detections by the subject missed by the model
NFA_s: # false alarms by the subject
NFA_m: # false alarms by the model

Table 1 reveals that, through the variation of the threshold parameters alone, it was possible to obtain a high degree of correspondence between the model's performance and the performance of the subjects on their last three trials.. Within the constraint that the model make no more false alarms than the subject, the model responded to 90% of the process failures responded to by the subjects. It responded to 78% of the process failures responded to by the subjects on the iteration of the subject's response and only on that iteration. And, as shown, in Table 2, for those processes included in both the model's and the subject's action sequences, only 17 of the model's 240 ordering decisions differed from those of the subjects.

TABLE 2

Comparison of the model's ordering decisions with those of the subject (for responses common to model and subject)

	Subject			
	S1	S2	S3	S4
# Consistent decisions	53	73	33	81
# Inconsistent decisions	3	8	2	4

CONCLUSION

The decision making model has been shown to provide a good fit to data obtained using a specific multiple process monitoring situation. The use of discriminant analysis to model the human's generation of event probabilities permits the model to be used in situations in which explicit models of the processes being monitored are unavailable. It also allows the model to be applied with relative ease to situations in which specific event probability estimation algorithms are available, but unwieldy. In the application described in this paper the nature of the events to be detected resulted in displayed process histories of a nonstationary nature. Four simple features of the process measurements were used to discriminate between the presence and absence of events. These features were suggested by the comments of subjects attempting to detect the events. In providing the model with examples of the values these features took on when events were present and absent, subjects' estimates of the event occurrence times were used to define events. Reasonably good performance was obtained without the availability of true event occurrence times to define events for the model. Thus, the model performed well despite the fact that it only had subjects' qualitative descriptions of what events looked like and when they occurred.

Although the model generally exhibited performance similar to that of the experimental subjects, analysis of the ordering decisions made by the subjects indicated that several of the subjects occasionally scheduled actions with respect to processes they didn't feel yet required attention. These processes required diversion of attention from other processes for only a small amount of time and thus, permitted the subject to act with little risk on the possibility that the processes might require attention by the time it was available for them. The model we have presented allocates attention only to processes for which the probability of process failure is above a threshold. It thus does not model this aspect of the subjects' performance well.

In this paper, we have postulated a multi-task situation in which the human simultaneously monitors multiple dynamic processes for action evoking events. The processes may differ in priority and the human cannot attend to all processes simultaneously, but instead must allocate his attention among the processes. Our goal is the development of models of human decision making amenable to use in the design and implementation of a computer aided process monitoring system. This goal dictates several specifications for such models. First, the models have to be simple enough to implement in a real-time environment. Second, they have to be capable of adapting to changing process dynamics and decision making criteria. Finally, they would hopefully be capable of learning the task by "watching" the human. We feel that the model proposed in this paper meets these specifications.

In this paper, the model was applied to an experimental situation involving the monitoring of nine independent processes which characteristically exhibited only one type of failure or action evoking event. In applying the model to this situation, very little fitting of parameters to data was required. Some parameters of the model were fixed at values considered to be intuitively reasonable. Features were selected in similar fashion, although he comments of other experimental subjects performing decision making tasks within a similar situation were also instructive. Two threshold parameters were varied to achieve a good fit of model to subject in a situation involving event detection and attention allocation decisions.

It is clear, however, that the models would have to be extended and validated for situations much different from the one to which it has been applied. The development, for example, was carried through assuming independence among processes, an unrealistic assumption in many potential applications. In situations in which some processes are interdependent, the distributions of event interarrival times and action times within these processes might depend upon the instantaneous configuration of the interdependent processes. While such interdependencies complicate the problem substantially, the general approach we have proposed is still applicable.

REFERENCES

1. Senders, J. W., "The Human Operator as a Monitor and Controller of Multidegree of Freedom Systems," IEEE Trans. Human Factors in Electronics, vol. HFE-5, no. 1, pp. 2-5, Sept. 1964.

2. Smallwood, R. D., "Internal Models and the Human Instrument Monitor," IEEE Trans. Human Factors in Electronics, vol. HFE-8, no. 3, pp. 181-187, Sept. 1967.

3. Carbonell, J. R., "A Queueing Model of Many-Instrument Visual Sampling," IEEE Trans. Human Factors in Electronics, vol. HFE-7, no. 4, pp. 157-164, Dec. 1966.

4. Carbonell, J. R. Ward, J. L., and Senders, J. W., "A Queueing Model of Visual Sampling: Experimental Validation," IEEE Trans. Man-Machine Systems, vol. MMS-9, no. 3, pp. 82-87, Sept. 1968.

5. Senders, J. W. and Posner, M. J. M., "A Queueing Model of Monitoring and Supervisory Behavior," in T. B. Sheridan and G. Johannsen, Eds., Monitoring Behavior and Supervisory Control, New York: Plenum 1976, pp. 245-259.

6. Kleinman, D. L. and Curry, R. E., "Some New Control Theoretic Models for Human Operator Display Monitoring," IEEE Trans. Systems, Man, and Cybernetics, vol, SMC-7, no. 11, pp. 778-784, Nov. 1977.

7. Gai, E. G. and Curry, R. E., "A Model of the Human Observer in Failure Detection Tasks," IEEE Trans. Systems, Man, and Cybernetics, vol. SMC-6, no. 2, pp. 85-94, Feb. 1976.

8. Sheridan, T. B. and Tulga, M. K., "A Model for Dynamic Allocation of Human Attention Among Multiple Tasks," Proceedings of the Fourteenth Annual Conference on Manual Control, University of Southern California, April, 1978, NASA CP-2060, pp. 569-592.

9. Rouse, W. B.: "Human-Computer Interaction in Multitask Situations," IEEE Trans. Systems, Man, and Cybernetics, vol. SMC-7, no. 5, pp. 384-392, May 1977.

10. Walden, R. S. and Rouse, W. B., "A Queueing Model of Pilot Decisionmaking in a Multitask Flight Management Sitution," IEEE Trans. Systems, Man, and Cybernetics, vol. SMC-8, no. 12, pp. 867-875, Dec. 1978.

11. Chu, Y. Y. and Rouse, W. B., "Adaptive Allocation of Decisionmaking Responsibility Between Human and Computer in Multitask Situations," IEEE Trans. Systems, Man, and Cybernetics, vol. SMC-9, no. 12, pp. 769-778, Dec. 1979.

12. Tatsuoka, M. M., Multivariate Analysis. New York: Wiley, 1971.

13. Afifi, A. A. and Azen, S. P., Statistical Analysis. New York: Academic Press, 1972.

14. Rouse, W. B. and Greenstein, J. S., "A Model of Human Decision Making in Multi-Task Situations: Implications for Computer Aiding," Proceedings of the 1976 International Conference on Cybernetics and Society, Washington, DC: IEEE Systems, Man, and Cybernetics Society, November 1976, pp. 425-433.

N82 34066 D29

PROCRU: A MODEL FOR ANALYZING FLIGHT CREW PROCEDURES IN APPROACH TO LANDING *

S. Baron, G. Zacharias, R. Muralidharan, R. Lancraft

Bolt Beranek and Newman Inc.
50 Moulton Street
Cambridge, MA 02138

The approach and landing task involves a wide range of human behaviors and activities, both cognitive and perceptual-motor. These include monitoring and information-processing, flight control, decision-making, execution of standard procedures, and communication with other crew members and with ATC. The goal of the research reported here was to develop a model for this complicated process that would provide a means for systematic exploration of questions concerning the impact of procedural and equipment design and the allocation of resources in the cockpit on performance and safety in approach-to-landing.

Given the objectives we have for the model and the nature of the issues we hope to analyze with it, several general implications for modelling the task emerge. First, it is clear that a system model is needed; one that accounts for the interactions of crew, procedures, vehicle, approach geometry, and environment. Second, the issues of interest revolve principally around allocation of tasks in the cockpit and crew performance with respect to the cognitive aspects of the tasks. The model must, therefore, deal effectively with information processing and decision-making aspects of human performance. Third, despite the high cognitive content of the approach task, a large portion of the crew's activities involves highly structured, standard procedures. These must be modelled at a level that is adequate for determining how performance on these tasks interferes with other tasks (and vice-versa) and for evaluating the consequences of failure to execute important procedures. Fourth, communication among crew members and between the crew and ATC must be considered in the model, at least with respect to accounting for the transfer of information and the load imposed by such communication. Finally, to examine the impact of various system conditions and assumptions, it must be possible to compute performance parameters of interest.

---

*This work was performed under Contract NAS2-10035. NASA, Ames Research Center sponsored the research with Dr. Renwick Curry as technical monitor.

PROCRU (Procedure Oriented Crew Model), is a simulation model for examining crew procedures in approach to landing, developed with the above requirements in mind. It includes a system model and a model for each crew member. The crew is assumed to be composed of three members: pilot flying (PF), pilot not flying (PNF) and second officer (SO). In the present implementation of PROCRU, the SO model does not include any information processing or decision-making components. Rather, the SO is modelled as a purely deterministic program that responds to events and generates requests. PF and PNF, on the other hand, are each represented by complex human operator models which have the same general form but differ in detail.

Briefly, PF and PNF are each assumed to have a set of "procedures" or tasks to perform. The procedures include both routines established "by the book" (such as checklists) and tasks to be performed in some "optimizing" fashion (such as flying the airplane). The particular task chosen at a given instant in time is the one perceived to have the highest expected gain for execution at that time. The gain is a function of mission priorities and of the perceived estimate of the state-of-the-world at that instant. This estimate is based on monitoring of the displays, the external visual scene and auditory inputs from other crew members. PROCRU draws heavily on the concepts and submodels of the Optimal Control Model (OCM) for the human operator[1] for its information processing and control representation. However, there are many novel aspects and features of the model that constitute new developments.

In the remainder of this paper we present an overview of the PROCRU model and some results illustrating its operation. More details may be found in reference 2.

1. Model Description

The basic structure of the PROCRU model for either PF or PNF is illustrated in Figure 1. The system model is the same for both crew members and is discussed first.

1.1 System Model

Vehicle Dynamics

The representation of vehicle dynamics must be sufficient to capture the essential aspects of the task but there is an incentive (computational cost) to keep it as simple as possible. Certainly, the equations of motion must be adequate to describe the position and velocity of the aircraft relative to the nominal approach path, but for the issues to be addressed by PROCRU (at least, initially), linearized equations can be used and inner-loop (high-frequency) dynamics ignored, to a first approximation. Thus, we use as a basis for the dynamic calculations in PROCRU standard point mass equations for the vehicle trajectory.[2]

These equations may be written in the general form

$$\dot{\underline{X}} = \underline{f}\ (\underline{X},\underline{U},t) \tag{1}$$

where $\underline{X}$ is the vehicle state vector and $\underline{U}$ is the control input.

The scheme utilized to "integrate" the above equations and to provide the linearized equations needed for implementing the control and estimation portions of PROCRU is somewhat novel and, we believe, is in keeping with the manner in which approach trajectories are flown. Briefly, five "nominal trajectory" segments, corresponding to five standard maneuvers, are defined:

1) straight and level flight
2) deceleration at constant flight path angle
3) turn at constant rate
4) flare (constant rate of change of flight path at constant speed and heading))
5) descend at constant sink-rate

It is possible to determine, algebraically, for each maneuver the "trim" or "nominal" controls $\underline{U}_N$, necessary to achieve the desired condition and, moreover, to integrate the corresponding equations of motion exactly to obtain $\underline{X}_N(t)$.[2] The equations can then be linearized about the particular segment to yield equations of the form

$$\underline{x} = \underline{A}_{N_i}\underline{x} + B_{N_i}\,\underline{u} \tag{2}$$

where

$$\underline{X}(t) = \underline{X}_{N_i}(t) + \underline{x}(t)$$
$$\underline{U}(t) = \underline{U}_{N_i}(t) + \underline{u}(t)$$

$$A_{N_i} = \frac{\partial f}{\partial x}\bigg|_{N_i}, \quad B_{N_i} = \frac{\partial f}{\partial U}\bigg|_{N_i} \tag{3}$$

and the subscript N_i means that the quantity is evaluated along the N_i'th segment.

We note that it is not necessary for a nominal segment to start at a particular place. In addition, because the system matrices change from segment to segment (and from moment to moment in a turn or segment), the linearized equations (3.3) will be time-varying (piecewise constant) over the approach trajectory. Finally, we may generalize (2) to include wind and other possible disturbances by rewriting it as

$$\dot{\underline{x}} = \underline{A}_{N_i}\,\underline{x} + \underline{B}_{N_i}\underline{u} + \underline{E}_{N_i}\,\underline{w}_{N_i} + \underline{F}_{N_i}\underline{z}_{N_i} \tag{4}$$

where w_{N_i} is a zero-mean white noise with covariance $\underline{W}_{N_i}$ and $\underline{z}_{N_i}$ is a deterministic disturbance that is unknown to the pilot. Equation 4 is in a form that is standard for applying the Optimal Control Model (OCM) of the human operator.[1]

Subsystems:

Aircraft subsystems, such as engines, hydraulics, etc., are not modelled in any detail. Subsystem operation, when required by procedures, is accomplished, or not, as determined by the models for the crew.

ATC Communications:

Air Traffic control vectoring commands are preprogrammed as part of the approach scenario. They take the form of auditory guidance commands, to be processed and executed by the PF.

Instrument Landing System:

The instrument landing system model includes the glide slope, localizer, outer marker and middle marker. Computed vehicle position is used to compute "activation" of any of these ILS signals and to determine glide slope and localizer errors in "dots". The model does not presently include any beam errors but these could be added without difficulty.

Information Sources:

We assume that four basic sources or "clusters" of information are available to a crew member: external visual scene information, visual information concerning vehicle state from the flight instruments, visual information concerning subsystems and auditory information.

The information from the external visual scene depends on the position and attitude of the aircraft relative to the airfield. Geometric analysis allows us to define how the "displayed" quantities, $\underline{y}_E$, depend on vehicle state and scene content.[3,4]

The information on the instrument panel can relate to vehicle status information (from flight instrumentation), command information (from flight directors) and subsystem information (including subsystem status and visual "alarms"). The information may be discrete as well as continuous. We assume this information is separated into two clusters, one for vehicle state related information, $\underline{y}_I$, and one for subsystem information. For the PROCRU analysis conducted herein, the flight displays are assumed to indicate air speed, heading, altitude, rate-of-climb and, after beam intercept, localizer and glide slope error. The subsystem displays are not modelled with respect to information content but serve as an attention distraction or "sink" when a procedure requiring subsystem operation is being performed (see below).

Auditory information includes command information from ATC, auditory alarms, and communications from other crew members such as callouts, requests, etc.

1.2 Human Operator Models

The models for the human operator (PF or PNF) contain submodels for monitoring, information processing, decision-making (procedure selection) and action. These are discussed below.

Monitoring

The monitor sub-model accounts for the operator's sensory limitations as well as for monitoring decisions (i.e., allocation of attention). The visual sensory limitations are modelled in the same manner as in the OCM,[1,3] except that the perceptual delay is neglected. In particular, an observation noise and a threshold are associated with each observed visual quantity. The thresholds are particularly important for external visual scene perception; for example, in limiting the quality of available vertical guidance information.

Auditory information is assumed to be heard correctly. It is stored in a memory buffer for subsequent processing.

The operator cannot process all sources of information simultaneously and must, therefore, decide which source to "attend to." In the case of visual information there is a fundamental choice as to where to fixate, on the external world or on the instrument panel. If the instrument panel is chosen, the operator must decide upon which instrument to fixate. We shall also assume that the auditory information similarly "competes" with the visual information for operator attention.

Thus, when auditory or subsystem information is requested by a procedure, attention is diverted from the flight displays and no information concerning the vehicle's state is obtained (except if it comes via the auditory channel from another crew member). When flight displays are being observed, either for flying the airplane (for PF) or for status monitoring (for PNF), attention is assumed to be shared among the displays on a continuous basis instead of being restricted to a single display at a time. PROCRU employs sub-optimal attention-allocation algorithms to compute the appropriate attention-sharing strategies.[2] However, if a crew member selects a procedure that results in a "monitoring request" for a given display (e.g., check airspeed), then the fraction of attention corresponding to that flight display is set to (approximately) one, and the remaining attentions are set to (approximately) zero.

Information Processing

The information processor portion of the model consists of two sub-models, an "estimator" and a "discrete event detector". The estimator is identical to that used in the OCM and is a time-varying Kalman filter. The internal model for the filter changes with changes in dynamics resulting from alteration of the "nominal" or from flap or gear extensions or with changes in disturbance characteristics.

The outputs of the estimator are the estimate of the perturbed state, $\hat{\underline{x}}$, the covariance of the estimation error, Σ, and, perhaps, the innovations sequence, and its covariance.* We will assume that the probability distribution for $\underline{x}$ is normal, in which case $\hat{\underline{x}}$ and $\underline{\Sigma}$ are sufficient statistics for determining the conditional density of $\underline{x}$ based on past observations $\underline{y}$, $P(x|y)$. Thus, the estimator produces status information, $\hat{\underline{x}}$, needed for control and "subjective" probability estimates that can be used for decision-making or detection. Note that the error covariance, Σ, is a measure of the operator's uncertainty in the estimate $\hat{\underline{x}}$ and will be a major factor in determining monitoring decisions, as will be seen below.

The discrete event detector is intended to model those aspects of operator information processing other than vehicle state estimation. Typically, it is concerned with determining or detecting that an event has occurred which "enables" a subsequent procedure execution. The event may be a failure (that did or did not result in an alarm), a request for action (say from ATC), or some annunciated condition (e.g., crossing OM, glide slope active or, passing through some altitude). The inputs to the event detector are outputs of visual alarms, auditory information, and the outputs of the state estimator. The state information is used to detect state related events such as a destabilized approach condition.

---

* In the present implementation of PROCRU, it is assumed that the nominal state $\underline{X}_n(t)$ is known to the crew.

Highly sophisticated models exist for certain types of failure detection based on state estimation, and these might eventually be incorporated in the event detector model.[6] We did not get so sophisticated initially. Instead, we assumed, simply, that the occurrence of an event is detected with a specified, finite probability by the crew.* However, the nature of the event is assumed to be unknown until the procedure for decoding messages (see below) is invoked. The selection of this procedure can be delayed by the requirements to perform other tasks, thus delaying the effective time of event detection. Once the message associated with the event is decoded, it will generally result in the "enabling" or "triggering" of an appropriate procedural response.

Procedure Definition and Selection

The operator is assumed to have a number of procedures or tasks that may be performed at each instant.

The definition of these procedures is an essential step in the formulation of PROCRU. All crew actions, except for the decision as to which procedure to execute, are determined by the procedures. We emphasize that we use the term procedure here to apply to tasks in general; a procedure in these terms could have considerably more cognitive content than might normally be considered to be the case.

Procedure Categories

Table 1 categorizes the approach to landing flight procedures for the PF and PNF. For each crewman, six categories are shown, and for each category, specific types of procedures are itemized. We briefly discuss these categories and types in the following paragraphs.

The vehicle control procedures assigned to the PF are broken down into three types: maneuvering control, regulatory control and retrimming control. The first involves the determination of appropriate maneuver rates, setting trim control values to effect these rates, and monitoring for maneuver termination. In effect, open-loop maneuver control provides a means of generating the "nominal" trajectory of Eqn. 3. Regulatory control, on the other hand, involves monitoring the display perturbations away from the nominal, estimating the corresponding vehicle state perturbations, and generating an appropriate perturbation control to control out the variations. Closed-loop regulatory control ensures proper execution of the desired maneuver and is modelled using standard OCM techniques[1]. Finally, retrimming control provides a means of retrimming the vehicle after a flap or gear setting change has altered the vehicle trim conditions.

---

* The probability is chosen to be one for this study, for simplicity.

The vehicle monitoring procedures assigned to the PNF are also broken down into two types: monitoring for vehicle status, and monitoring for event or failure detection. The former involves determining an appropriate monitoring strategy for attention sharing among the available displays, estimating the corresponding vehicle state, and evaluating the approach progress based on the current state estimate. The latter involves a similar process, but is centered on detecting events or failures.

Requests and callouts made by the PF and PNF, respectively, involve verbal responses based on estimates of current vehicle status. The flap, gear, and checklist requests made by the PF involve determining the vehicle's approach progress in terms of one or more trajectory/instrument parameters, and making the request based on the progress and in accordance with a well-defined set of request procedures. The position and altitude callouts made by the PNF involve a similar process. The approach stability and runway-in-sight (RWIS) callouts, also made by the PNF, involve the additional requirement of determining when the vehicle is in an appropriate "window" for making or not making the callout.

Subsystem monitoring and control actions made by both pilots are assumed to be event driven, and involve discrete control actions and/or diversion of attention from flight displays for appropriate subsystem servicing. For the PF, servicing the altitude alert subsystem is distinguished from the servicing of all other subsystems, because of the interactive nature of setting the trigger point, responding to the alarm, and resetting it. For the PNF, the flap and gear subsystems are called out because of their impact on approach progress, their unique status of being driven by requests from the PF, and because of the need for subprocedures involving validation of the request, and setting and checking of the subsystem involved.

Verbal acknowledgements made by the PF and PNF are driven by checklist item prompts generated by the SO. These require the checking of an appropriate subsystem (attention-diversion) and making the appropriate verbal response. The PNF is also assigned the duty of acknowledging the receipt of ATC vector requests.

The SAP/MAP terminal procedures provide for appropriate callouts, head-up/head-down switching strategies, and missed approach initiation during the terminal phase of either the Standard Approach Procedure (SAP) or the Monitored Approach (MAP).[2] Although this category of procedures could be allocated item by item to the other categories, it has been found to be more convenient to treat it as a uniform procedural category, both for the purpose of modelling, and for discussion.

The miscellaneous procedures shown are primarily for the purpose of modelling convenience, and are not intended to directly represent "by-the-book" or actual procedures engaged in by the crew. They include processing and decoding of verbal communications, auditory alarms, and discrete visual events. In addition, for the PF, they involve selection of appropriate landing configuration parameters.

Procedure Selection

We assume that the operator knows what is to be done and, essentially, how to accomplish the objective. However, he must decide what procedure to do next. This is a decision among alternatives and the procedure selected is assumed to be the one with the highest expected gain for execution at that time. The Expected Gain for executing a procedure, EGP, is a function that is selected to reflect the urgency or priority of that procedure as well as its "value". In addition, the EGP can be a function of the "enabling" state of the procedure. Thus, if a procedure were not "enabled" it would have zero gain and would not be chosen; if the enabling event had a non-zero probability of occurrence, the procedure might then be selected.

In PROCRU, we have assumed the EGP functions have the following general form (specific expressions are given in reference 2):

$$\mathrm{EGP}(I) = G(I) + G_0(I), \quad I=1,\ldots,N \tag{5}$$

where I denotes the Ith procedure, G(I) is a function that reflects the "situational relevance" of the procedure and $G_0(I)$ is a constant that depends on the relative "value" of the procedure. For procedures that are triggered by the operator's internal assessment of a condition related to the vehicle state-vector, the G(I) functions are appropriate subjective probabilities, based on $\hat{\underline{x}}$ and Σ, as determined by the information processing portion of the model. Procedures that are triggered by events external to the operator, such as ATC commands, communications from the crew, etc., are characterized by G's that are explicit functions of time. For either type of function, the gain for performing a procedure will increase, subsequent to the perception of the triggering event, until the procedure is performed or until a time such that the procedure is assumed to be "missed" or no longer appropriate for execution.

The G_0 terms have two principal purposes. First, they are used to establish a "default" procedure for each operator by assigning a base value for BGP for that procedure that is greater than for any other one. (The G(I) for any other procedure must exceed this base value before the procedure can be selected.) For PF the default is flying the airplane, whereas for the PNF it is monitoring the vehicle's status. The second purpose of the G_0 term is to establish priorities among procedures that might have the same situational relevance at a given time.

Procedures may be comprised of a number of sub-procedures, so that at the completion of each sub-procedure, a decision to continue must be made. This will permit interruption of such a procedure, depending on the outcome of the decision.

We believe that this model for procedure selection captures many important aspects of human performance in a multi-task environment, and is directly relevant to investigating the efficacy of flight crew procedures. It allows for procedures to be missed and/or interrupted: even flying the airplane may be neglected, as can happen. Although we do not expect sub-procedural steps to be performed out of order with this modelling approach, it would be possible to preprogram such errors if desired.

Procedure Execution

The selection and execution of a procedure will result in an action or a sequence of actions. Three types of actions are considered: control actions, monitoring requests and communications. The control actions include continuous manual flight control inputs to the aircraft and discrete control settings (switches, flap settings, etc.). Monitoring requests result from procedural requirements for specific information and, therefore, raise the attention allocated to the particular information source. We note that verifying that a variable is within limits may not require an actual instrument check, if the operator already has a "confident" internal estimate of that variable. Communications are verbal requests or responses as demanded by a procedure. They include callouts, requests or commands, and communications to ATC.

Associated with each procedural action is a time to complete the required action. (It is possible to modify PROCRU to allow for a probabilistic distribution of action times). When the operator decides to execute a specific procedure, it is assumed that he is "locked in" to the appropriate mode for a specified time. For example, if the procedure requires "checking" a particular instrument and it is assumed that it takes t seconds to accomplish the check, then the "monitor" will not attend to other information for that period, nor will another procedure be executed.

In PROCRU procedural implementation is modelled as essentially error free. However, errors in execution of procedures can occur because of improper decisions that result from a lack of information (quantity or quality) due to perceptual, procedural and workload limitations. If the effects of action errors are also to be analyzed, this is accomplished by deliberately inserting such errors directly into the model. It should also be pointed out that verbal communication is modelled directly as the transfer of either state, command or event information.

2. Model Outputs

PROCRU generates a number of outputs that are useful for analyzing crew procedures and performance. First, one can obtain full trajectory information. This information is provided at any time in terms of the total state (TSTATE xt) (and/or the nominal state) and the perturbation or deviation (DSTATE x) from the nominal. In addition to this information, one can obtain each crew member's estimate of the state (xh) and the standard deviation of the estimation error (SDEV), the attentional allocation (AT) at that time and PF's control inputs (u). These data, along with significant events, etc., are tabulated in a file as illustrated in Figure 2. PF is crew member 1 and PNF crew member 2.

In addition to the trajectory output, PROCRU provides three separate time lines: a procedural time line (PTL), a message time line (MTL), and a milestone time line (TL). Table 2 lists the mnemonics used for these time lines. The procedural time-line, illustrated in Figure 3 for the nominal approach conditions, provides a listing of the procedures (PROC) being executed by each crew member, the gain for doing that procedure (EGP) and the information cluster and display being attended to at a given time. Also provided for each crew member is the procedure that has the next highest gain for execution at that time.* Thus, for example, at time 915.4 seconds, PF was flying on instruments (scanning) and no other procedures were competing for attention. At the same time, PNF was monitoring the altimeter in order to make an altitude callout (at t=919.6), while the default monitoring task was the task with the next highest priority. Shortly thereafter (920.8 sec), PF diverts attention from regulating about the nominal to process the callout and PNF has reverted to basic monitoring.

---

* Procedure numbers used in the PTL correspond to those in reference 2, Table 4.20.

The message time line (MTL) is a record of all the communication traffic and auditory signals that occur in the simulated cockpit. Figure 4 is a message time line for the nominal approach. The type of message (Signal name), the source of the message and its destination, its processing status, its time of origin and processing, as well as an indication of the signal content are all presented using mnemonics that are fairly transparent. For example, on the message time line, we see the communication activity noted above. The 500′ altitude callout is made by the F/O (PNF) at 919.6 seconds and directed to the CAPT (PF). It is processed (i.e. used to update PF′s altitude estimate) at 921.0 seconds.

The milestone time line (TL), illustrated in Figure 5, contains selected trajectory variables of interest (altitude, speed and heading), an indication of crew activity and a listing of important flight milestones and events. Note that the time marker given in the TL, t_{go}, is the time-to-go, computed simply as 980s minus the event time. This provides a fair approximation to the actual time-to-go.

3. An Example

The milestone time line in Figure 5 presents an overview of crew activity for a nominal and even-paced approach and will be discussed in detail.

The time-line begins with the vehicle at 10,000 ft altitude, on a 210 deg heading, proceeding at 190 kts. In the first 50 seconds, three ATC requests, for a heading change, deceleration, and descent, are processed by both the PF and PNF. As shown in both Figure 5 and Figure 4, each request involves: a) a message generated by ATC sent to both the PF and PNF; b) message processing by the PF, resulting in a new maneuver (e.g., "Prcsd Turn"); and c) message processing by the PNF, resulting in a verbal confirmation of the ATC request (e.g., "ATCcn"). Note that Figure 4 shows that each confirmation message (from PNF to ATC) is ignored by ATC, since the ATC module used in this simulation operates in a time-locked open-loop fashion. Naturally, a more sophisticated module would take into account the procedural activity of ATC, and incorporate the verbal confirmatory feedback provided by the crew.

The descent request made by ATC at t_{go} = 930s triggers a number of crew activities. As just noted, it triggers a verbal confirmation by the PNF. It also triggers the generation of a three-segment maneuver (flare/descent/flare) by the PF, in accordance with the procedure defined for such a maneuver. Thus, a flare to -6 deg flight path is initiated at t_{go} = 926s, and constant sink rate is maintained until t_{go} = 707s, at which point a flare-out is initiated, and completed at t_{go} = 676s. The ATC descent request also triggers an altitude alert setting by the PF ("AAon" at t_{go} = 922s).

As the vehicle approaches the requested 3500 ft altitude, the PF makes a verbal request for the initial approach checklist ("IACR" at t_{go} = 686s) which, as shown by Figure 4, is processed by the S/O at t = 294s. This then initiates the series of IAC prompts by the S/O, shown in the next few minutes of the time-line. Each such prompt (e.g., "IAC 1" at t_{go} = 666s) results in a requirement on the PF or PNF to process that prompt (e.g., "Procsd IAC 1" at t_{go} = 663s), and verbally echo the prompt back to the S/O. Subsequent processing of the confirmation by the S/O (e.g., "Prcsd IACX1" at t_{go} = 659s), initiates generation of another prompt by the S/O (e.g., "IAC X2" at t_{go} = 639s). The IAC is concluded at t_{go} = 533s by a "IACfn" message generated by the S/O.

The descent to 3500 ft also triggers the altitude alert (AA) subsystem. Thus, at h = 4019 ft the AA becomes active, which requires the PF to turn it off at t_{go} = 709s, which, in turn deactivates the AA at the next time step in the simulation. Note that this occurs prior to the flare-out initiated by the PF, thus providing an appropriate warning to begin the flare-out.

After the PF levels off near the requested 3500 ft altitude, ATC requests a deceleration to 160 kt. As before, this triggers a maneuver by the PF and a message confirmation by the PNF. Note that completion of this maneuver triggers a 5 deg flap request by the PF (t_{go} = 656), in accordance with the flap/speed management procedures.

Following an ATC-requested turn to 180 deg (t_{go} = 540s), a second descent to 2000 ft is initiated (t_{go} = 498s). The same activity sequence is followed as in the first descent, except that ATC makes a 120 deg turn request (t_{go} = 450s) while the vehicle is descending. The message is processed by both crew members (as shown in Figure 4), and confirmation is provided by the PNF. The PF, however, does not act on this request, but merely stores it in his memory. Once he levels off to the requested 2000 ft altitude (t_{go} = 383s), he then immediately initiates the turn to 120 deg.

As in the initial descent, the PF requests the checklist during his levelling off to his assigned altitude ("FACR" at t_{go} = 390s). Again, this initiates a series of S/O prompts and PF and PNF confirmations, lasting until checklist termination by the S/O ("FACfn" at t_{go} = 183s).

While the PF is turning to the requested 120 deg heading, ATC notifies the crew that they are cleared to land (t_{go} = 375s). This message is processed by both the PF and PNF, and "enables" a series of velocity, altitude, and heading management procedures designed to ensure proper touchdown performance.

The first of these is a deceleration to 150 kt, following completion of the turn to 120 deg (t_{go} = 363s). Once this speed is reached, 15 deg flaps are requested and set, by the PF and PNF respectively (t_{go} = 349s). Shortly thereafter, the localizer becomes active, which results in an announcement by the PNF, which, in turn, triggers a turn to final by the PF.

During the turn, the glide slope becomes active (t_{go} = 326s), and is announced by the PNF. After the turn is completed, the vehicle has achieved its final inbound heading, with a small localizer error (not shown on the time-line). Shortly thereafter, a 2 dot low glide slope error (also not shown), triggers a gear-down request from the PF, which is acted on by the PNF (t_{go} = 273s).

As the vehicle approaches the glide slope, the PF initiates two decelerations in accordance with the velocity maneuver procedures, one to 140 kt at 1.5 dots low, and the second to the final approach speed of 139 kt, at 1 dot low. Each of these trigger new flap requests and settings (to 25 and 30 deg) in accordance with the flap/speed management procedure.

When the vehicle is 0.5 dots below the glide slope, the PF initiates a pitch down (t_{go} = 218s). This flare sets up the final descent followed for the remainder of the approach.

During the descent, the PNF announces OM activity ("OMann" at t_{go} = 151s), and makes the required 1000 ft, 500 ft, and "approaching minimum"s (300 ft) callouts. He is also monitoring out-the-window, and, with the 250 ft ceiling simulated, makes the appropriate RWIS callout at t_{go} = 35s.

While the PNF is monitoring for this RWIS callout, the MM alert sounds, and both pilots process this message. The PNF should announce MM activity during this time, but is engaged in monitoring the altimeter for his required "minimums" callout at 200 ft. He makes the altitude callout slightly early (at h=215ft and t_{go} = 31s), and by the time he can attend to making the MM announcement, the MM becomes inactive (at t_{go} = 30s). Since the announcement procedure, as programmed, requires the MM to be active for an announcement to be made, the PNF remains silent.

The PF begins decelerating to the required threshold speed of 134 kt slightly early (at t_{go} = 26s) and 10 ft above the 150 ft altitude specified for the nominal approach.[2] The final flare is initiated about 1 sec late and 10 ft below the 50 ft altitude desired for the maneuver. During this flare the GS signal turns off because of the flare away from the glide slope beam, and the LOC signal turns off at touchdown, as required by the LOC characteristics modelled in this simulation.

The time-line just discussed can be correlated with the other outputs of PROCRU to provide a fairly detailed look at the landing approach. Though the particular approach just simulated was relaxed in tempo, it is clear that more demanding scenarios can also be studied.[2] For these cases, where the demands of the task and the procedures and equipment employed interact in complex and significant ways, a model of PROCRU's breadth should prove most useful.

4. Concluding Remarks

PROCRU, a new simulation model for analyzing crew procedures in approach to landing, has been described. The model is a system model that can account for vehicle dynamics, environmental disturbances and crew activities in information processing, decision making, control and communication. Crew sub-tasks are defined based on a time-line analysis of nominal procedures. Information processing and control behavior is modelled after the approach utilized in the Optimal Control Model. Decision making behavior is based on maximizing subjective expected gain. The result is a complex, stochastic model for analyzing the impact on approach and landing of system, procedure and crew variables.

The PROCRU model has not been validated experimentally, though the information processing and control parts of it have been tested for manual control experiments. IN addition, for this initial implementation, several important aspects of human behavior have been simplified or neglected. Nonetheless, it is likely that even in its present state of development, with some upgrading of wind models and vehicle dynamics, PROCRU could be used to analyze many questions of interest regarding procedures for approach and landing.

REFERENCES

1. Kleinman, D. L., S. Baron and W. H. Levison, "A Control Theoretic Approach to Manned-Vehicle Systems Analysis", IEEE Trans. on Auto. Control, Vol. AC-16, No. 6, December 1971.

2. Baron, S., C. E. Feehrer, and G. L. Zacharias, "Analysis and Modeling of Flight Crew Procedures in Approach and Landing", BBN Interim Report No. 4112, July 1979.

3. Baron S., and W. H. Levison, "Display Analysis with the Optimal Control Model of the Human Operator," Human Factors, Vol. 19, No. 5, Oct. 1977.

4. Wewerinke, P. H., "A Theoretical and Experimental Analysis of the Outside World Perception Process," Fourteenth Annual Conference on Manual Control, NASA Conference Publication 2060, Nov. 1978.

5. Levison, W. H., J. I. Elkind, and J. L. Ward, "Studies on Multi-Variable Manual Control Systems: A Model for Task Interference, NASA CR-1746, May 1971.

6. Gai, E. G. and R. E. Curry, "A Model of the Human Observer in Failure Detection Tasks," IEEE Transactions on Systems, Man and Cybernetics, SMC-6, No. 2, Feb. 1976.

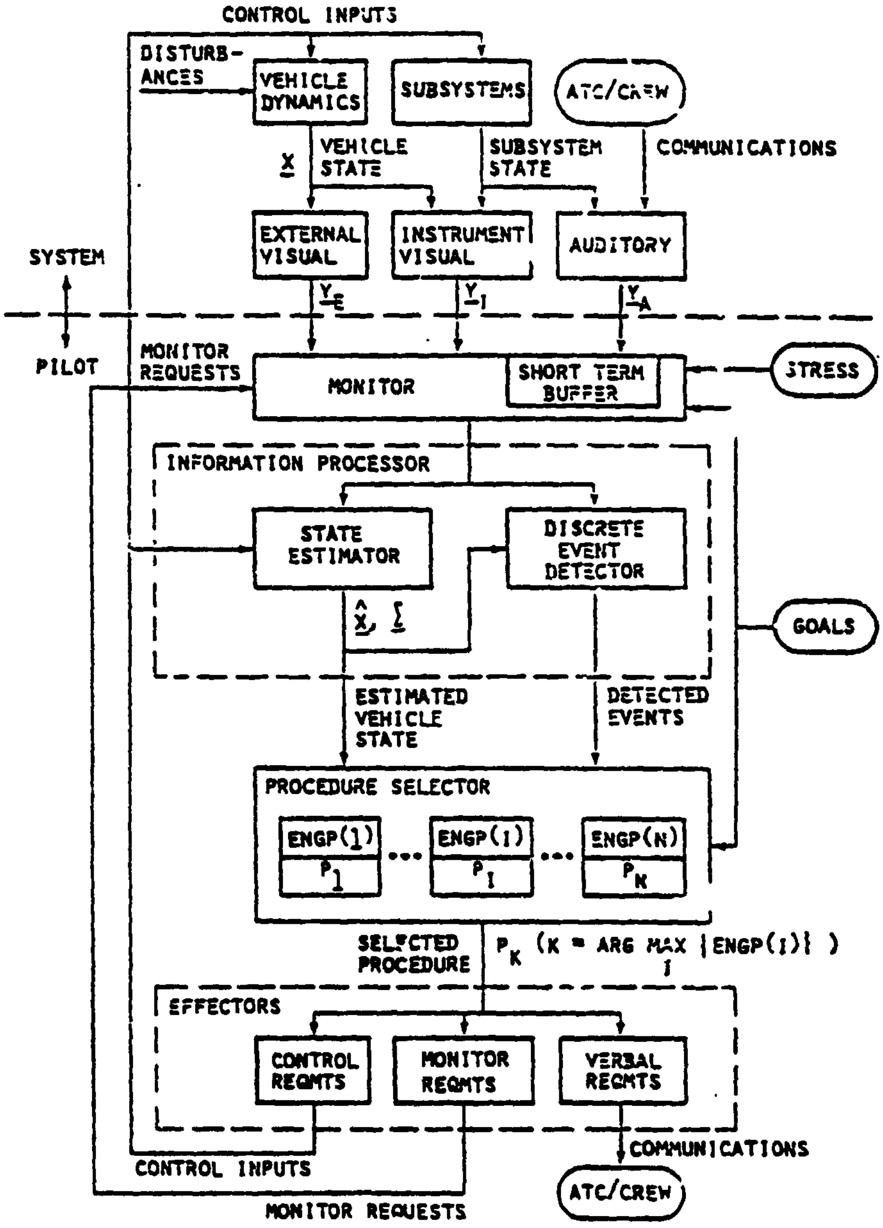
CONTROL INPUTS
DISTURBANCES
VEHICLE DYNAMICS
SUBSYSTEMS
ATC/CREW
$\underline{X}$
VEHICLE STATE
SUBSYSTEM STATE
COMMUNICATIONS
EXTERNAL VISUAL
INSTRUMENT VISUAL
AUDITORY
SYSTEM
PILOT
$\underline{Y}_E$
$\underline{Y}_I$
$\underline{Y}_A$
MONITOR REQUESTS
MONITOR
SHORT TERM BUFFER
STRESS
INFORMATION PROCESSOR
STATE ESTIMATOR
DISCRETE EVENT DETECTOR
$\hat{\underline{x}}, \underline{\Sigma}$
GOALS
ESTIMATED VEHICLE STATE
DETECTED EVENTS
PROCEDURE SELECTOR
ENGP(1)
P_1
ENGP(I)
P_I
ENGP(N)
P_N
SELECTED PROCEDURE
P_K ($K = \underset{I}{\text{ARG MAX}} \{\text{ENGP}(I)\}$)
EFFECTORS
CONTROL REQMTS
MONITOR REQMTS
VERBAL REQMTS
COMMUNICATIONS
CONTROL INPUTS
MONITOR REQUESTS
ATC/CREW

Figure 1: Model Structure for Crew Member Analysis

ORIGINAL PAGE IS
OF POOR QUALITY

Figure 2: Sample PROCRU Trajectory Information File (case ILS)

```
*** TIME= 5.816E+02 ***
Tstate xt. 1.489E+04-8.619E+04 2.091E+03 1.599E+02 1.799E+02-2.942E+00
Dstate x:  [illegible]78E-01 3.205E-01 1.832E-01-8.564E-02-7.831E-02 3.503E-02
xh1 k|k:   [illegible].263E+00 1.221E+00-2.772E-01 1.923E-02 5.370E-02-2.596E-02
xh2 k|k:   9.636E-01-3.556E+00-4.201E-01 5.574E-02-7.441E-03 3.323E-02
SDev1 k|k: 1.251E+02 1.092E+02 7.846E+00 1.971E-01 3.031E-01 8.459E-02
SDev2 k|k: 1.227E+02 1.081E+02 5.643E+00 2.192E-01 2.753E-01 1.084E-01
AT1:       V:   .015 PSI: .240 H:   .010 Hdot: .713 LOC: .010 GS:  .010
AT2:       V:   .086 PSI: .629 H:   .112 Hdot: .153 LOC: .010 GS:  .010
***** Altitude Alert Active *****
GUIDE: " Executing FLARE to  0.000E+00  deg  at  2.001E-01 deg/s."
Total u:  -8.950E-02 2.574E+00 9.398E+03 Flaps=  5. Gear is UP


*** TIME= 5.818E+02 ***
Tstate xt: 1.483E+04-8.619E+04 2.088E+03 1.599E+02 1.799E+02-2.864E+00
Dstate x:  1.605E-01 3.879E-01 2.360E-01-1.082E-01-6.467E-02 7.293E-02
xh1 k|k:   1.260E+00 1.172E+00-2.823E-01-4.249E-04 5.151E-02 1.534E-02
xh2 k|k:   1.432E+00-5.007E+00-1.348E-01 1.177E-02 4.980E-02 6.501E-02
SDev1 k|k: 1.251E+02 1.092E+02 7.847E+00 1.972E-01 3.080E-01 8.745E-02
SDev2 k|k: 1.227E+02 1.081E+02 5.644E+00 2.192E-01 2.753E-01 1.085E-01
AT1:       V:  0.000 PSI:0.000 H:  0.000 Hdot:0.000 LOC:0.000 GS: 0.000
AT2:       V:   .086 PSI: .628 H:   .112 Hdot: .154 LOC: .010 GS:  .010
***** Altitude Alert Inactive *****
GUIDE: " Executing FLARE to  0.000E+00  deg  at  2.001E-01 deg/s "
Total u:  -8.586E-02 1.955E+00 9.502E+03 Flaps=  5. Gear is UP

*** TIME= 5.820E+02 ***
Tstate xt: 1.478E+04-8.619E+04 2.086E+03 1.599E+02 1.799E+02-2.852E+00
Dstate x:  1.955E-01 4.469E-01 2.933E-01-9.887E-02-6.040E-02 4.449E-02
xh1 k|k:   1.258E+00 1.124E+00-2.789E-01 1.015E-02 4.942E-02-7.861E-03
xh2 k|k:   1.234E+00-4.404E+00-2.945E-02 1.631E-02 2.031E-02 5.046E-02
SDev1 k|k: 1.252E+02 1.092E+02 7.848E+00 1.972E-01 3.128E-01 9.021E-02
SDev2 k|k: 1.227E+02 1.081E+02 5.644E+00 2.192E-01 2.753E-01 1.085E-01
AT1:       V:  0.000 PSI:0.000 H:  0.000 Hdot:0.000 LOC:0.000 GS: 0.000
AT2:       V:   .086 PSI: .628 H:   .112 Hdot: .153 LOC: .010 GS:  .010
GUIDE: " Executing FLARE to  0.000E+00  deg  at  2.001E-01 deg/s "
Total u:  -8.236E-02 2.301E+00 9.606E+03 Flaps=  5. Gear is UP
```

Figure 3: Sample PROCRU Procedure Time Line (case ILS)

	CAPTAIN				FIRST OFFICER			
TIME	PROC:EGP	CLUST	DISP	PROC:EGP	PROC:EGP	CLUST	DISP	PROC:EGP
0.0	26: .30	Instr	Scan	0: .00	22: .30	Instr	Scan	0: .00
1.2	1: .32	Audio	SBsys	26: .30	1: .32	Audio	SBsys	22: .30
1.4	26: .30	Instr	Scan	5: .14	22: .30	Instr	Scan	10: .04
2.2	5: .32	Instr	Scan	26: .30	22: .30	Instr	Scan	10: .22
2.6	5: .32	Instr	Scan	26: .30	10: .32	SBsys	SBsys	22: .30
3.6	5: .32	Instr	Scan	26: .30	22: .30	Instr	Scan	0: .00
4.2	26: .30	Instr	Scan	0: .00	22: .30	Instr	Scan	0: .00
22.2	4: .97	Instr	Scan	26: .30	22: .30	Instr	Scan	0: .00
24.2	26: .30	Instr	Scan	0: .00	22: .30	Instr	Scan	0: .00
31.2	1: .32	Audio	SBsys	26: .30	1: .32	Audio	SBsys	22: .30
31.4	26: .30	Instr	Scan	5: .14	22: .30	Instr	Scan	10: .04
32.2	5: .32	Instr	Scan	26: .30	22: .30	Instr	Scan	10: .22
32.6	5: .32	Instr	Scan	26: .30	10: .32	SBsys	SBsys	22: .30
33.6	5: .32	Instr	Scan	26: .30	22: .30	Instr	Scan	0: .00
34.2	26: .30	Instr	Scan	0: .00	22: .30	Instr	Scan	0: .00
51.2	1: .32	Audio	SBsys	26: .30	1: .32	Audio	SBsys	22: .30
51.4	26: .30	Instr	Scan	5: .14	22: .30	Instr	Scan	10: .04
52.0	4: .33	Instr	Scan	26: .30	22: .30	Instr	Scan	10: .17
52.6	4: .33	Instr	Scan	26: .30	10: .32	SBsys	SBsys	22: .30
53.6	4: .33	Instr	Scan	26: .30	22: .30	Instr	Scan	0: .00
54.0	5: .85	Instr	Scan	26: .30	22: .30	Instr	Scan	0: .00
56.0	9:1.00	Audio	SBsys	26: .30	22: .30	Instr	Scan	0: .00
58.0	26: .30	Instr	Scan	0: .00	22: .30	Instr	Scan	0: .00
83.4	4: .36	Instr	Scan	26: .30	22: .30	Instr	Scan	0: .00
85.4	26: .30	Instr	Scan	0: .00	22: .30	Instr	Scan	0: .00
269.4	1:1.00	Audio	SBsys	26: .30	22: .30	Instr	Scan	1: .10
269.6	26: .30	Instr	Scan	24: .04	22: .30	Instr	Scan	1: .14
270.4	26: .30	Instr	Scan	24: .22	1: .32	Audio	SBsys	22: .30
270.6	26: .30	Instr	Scan	24: .27	22: .30	Instr	Scan	0: .00
270.8	24: .32	Audio	SBsys	26: .30	22: .30	Instr	Scan	0: .00
272.8	4:1.00	Instr	Scan	26: .30	22: .30	Instr	Scan	0: .00
274.8	26: .30	Instr	Scan	0: .00	22: .30	Instr	Scan	0: .00
294.2	2: .31	Audio	SBsys	26: .30	22: .30	Instr	Scan	0: .00
295.2	26: .30	Instr	Scan	0: .00	22: .30	Instr	Scan	0: .00
302.6	4: .75	Instr	Scan	26: .30	22: .30	Instr	Scan	0: .00
304.6	26: .30	Instr	Scan	0: .00	22: .30	Instr	Scan	0: .00
311.2	1: .32	Audio	SBsys	26: .30	1: .32	Audio	SBsys	22: .30
311.4	26: .30	Instr	Scan	5: .14	22: .30	Instr	Scan	10: .04
312.2	5: .32	Instr	Scan	26: .30	22: .30	Instr	Scan	10: .22
312.6	5: .32	Instr	Scan	26: .30	10: .32	SBsys	SBsys	22: .30
313.6	5: .32	Instr	Scan	26: .30	22: .30	Instr	Scan	0: .00
314.2	26: .30	Instr	Scan	0: .00	22: .30	Instr	Scan	0: .00
315.6	26: .30	Instr	Scan	0: .00	1: .32	Audio	SBsys	22: .30

•
•
•

Figure 3 (cont.)

•

•

•

```
872.2   26: .30  Instr Scan    0: .00     22: .30  Instr Scan    0: .00
915.4   26: .30  Instr Scan    0: .00     24: .33  Instr H      22: .30
919.6   26: .30  Instr Scan    0: .00     24:1.00  Audio SBsys  22: .30
920.8    1: .32  Audio SBsys  26: .30     22: .33  Instr Scan    0: .00
921.0   27:1.00  Audio SBsys  26: .30     22: .30  Instr Scan    0: .00
921.2   26: .30  Instr Scan    0: .00     22: .30  Instr Scan    0: .00
935.2   26: .30  Instr Scan    0: .00     25: .37  Instr H      22: .30
938.6   26: .30  Instr Scan    0: .00     25:1.00  Audio SBsys  22: .30
939.8    1: .32  Audio SBsys  26: .30      6: .55  SBsys SBsys  22: .30
940.0   27:1.00  Audio SBsys  26: .30      6: .55  SBsys SBsys  22: .30
940.2   26: .30  Instr Scan    0: .00      6: .55  SBsys SBsys  22: .30
942.6   26: .30  Instr Scan    0: .00      6: .55  Extnl Scan   22: .30
945.2   26: .30  Instr Scan    0: .00      6: .55  SBsys SBsys  22: .30
945.4    1:1.00  Audio SBsys  26: .30      6: .55  SBsys SBsys  22: .30
945.6   26: .30  Instr Scan    1: .10      6: .55  SBsys SBsys  22: .30
946.6    1: .32  Audio SBsys  26: .30      6: .55  SBsys SBsys  22: .30
946.8    8:1.00  SBsys SBsys  26: .30      6: .55  SBsys SBsys  22: .30
948.2    8:1.00  SBsys SBsys  26: .30      6: .55  Instr Scan   22: .30
948.4    8:1.00  SBsys SBsys  26: .30      1:1.00  Audio SBsys  26:1.00
948.6    8:1.00  SBsys SBsys  26: .30     26:1.00  Audio SBsys  22: .30
949.8    8:1.00  Extnl Scan   26: .30     22: .30  Instr Scan    0: .00
950.0    1: .37  Audio SBsys  26: .30     22: .30  Instr Scan    0: .00
950.2   27:1.00  Audio SBsys  26: .30     22: .30  Instr Scan    0: .00
950.4   26: .30  Extnl Scan    0: .00     22: .30  Instr Scan    0: .00
954.0   23: .33  Extnl Scan   26: .30     22: .30  Instr Scan    0: .00
956.0   26: .30  Extnl Scan    0: .00     22: .30  Instr Scan    0: .00
963.6    4: .39  Extnl Scan   26: .30     22: .30  Instr Scan    0: .00
964.4    4: .39  Extnl Scan   26: .30     22: .30  Instr Scan    0: .00
964.8    4: .39  Extnl Scan   26: .30     22: .30  Instr Scan    0: .00
965.6   18: .75  Extnl Scan   26: .30     22: .30  Instr Scan    0: .00
967.6   26: .30  Extnl Scan    0: .00     22: .30  Instr Scan    0: .00
974.6    4: .34  Extnl Scan   26: .30     22: .30  Instr Scan    0: .00
```

Figure 4: Sample PROCRU Message Time-Line (case 1LS)

SIGNL NAME	SOURC CODE	DESTN CODE	PROCS STATS	TIME ORIGN	TIME PROCs	SIGNL CONTs
Turn	A.T.C	Capt.	Prcsd	0.0	2.2	270.
Turn	A.T.C	FO	Prcsd	0.0	2.6	270.
ATCcn	FO	A.T.C	Ignrd	3.4	3.6	
Decel	A.T.C	Capt.	Prcsd	30.0	32.2	170.
Decel	A.T.C	FO	Prcsd	30.0	32.6	170.
ATCcn	FO	A.T.C	Ignrd	33.4	33.6	
ChAlt	A.T.C	Capt.	Prcsd	50.0	54.0	3500.
ChAlt	A.T.C	FO	Prcsd	50.0	52.6	3500.
ATCcn	FO	A.T.C	Ignrd	53.4	53.6	
AAon	Capt.	Annoc	Ignrd	57.8	58.0	3500.
AltAl	SBsys	Capt.	Prcsd	269.2	270.8	3500.
AltAl	SBsys	FO	Ignrd	269.2	270.4	3500.
AAoff	Capt.	Annoc	Ignrd	270.8	271.0	
IACR	Capt.	SO	Prcsd	294.2	294.4	
IACst	SO	Annoc	Ignrd	294.4	294.6	
Decel	A.T.C	Capt.	Prcsd	310.0	312.2	160.
Decel	A.T.C	FO	Prcsd	310.0	312.6	160.
ATCcn	FO	A.T.C	Ignrd	313.4	313.6	
IAC#1	SO	FO	Prcsd	314.4	317.0	
IAC#1	FO	SO	Prcsd	320.8	321.0	
FlapR	Capt.	FO	Prcsd	324.0	326.6	5.
FlapS	FO	Annoc	Ignrd	326.6	326.8	5.
IAC#2	SO	FO	Prcsd	341.0	343.5	
IAC#2	FO	SO	Prcsd	347.4	347.6	
IAC#3	SO	FO	Prcsd	367.6	370.2	
IAC#3	FO	SO	Prcsd	374.0	374.2	
IAC#4	SO	FO	Prcsd	394.2	396.8	
IAC#4	FO	SO	Prcsd	400.6	400.8	
IAC#5	SO	FO	Prcsd	420.8	423.4	
IAC#5	FO	SO	Prcsd	427.2	427.4	
Turn	A.T.C	Capt.	Prcsd	440.0	442.2	180.
Turn	A.T.C	FO	Prcsd	440.0	442.6	180.
ATCcn	FO	A.T.C	Ignrd	443.4	443.6	
IACfn	SO	Annoc	Ignrd	447.4	447.6	
ChAlt	A.T.C	Capt.	Prcsd	480.0	482.2	2000.
ChAlt	A.T.C	FO	Prcsd	480.0	482.6	2000.
ATCcn	FO	A.T.C	Ignrd	483.4	483.6	
AAon	Capt.	Annoc	Ignrd	486.0	486.2	2000.
Turn	A.T.C	Capt.	Prcsd	530.0	532.2	120.
Turn	A.T.C	FO	Prcsd	530.0	532.6	120.
ATCcn	FO	A.T.C	Ignrd	533.4	533.6	
AltAl	SBsys	Capt.	Prcsd	578.4	581.6	2000.
AltAl	SBsys	FO	Ignrd	578.4	579.6	2000.
AAoff	Capt.	Annoc	Ignrd	581.6	581.8	
FACR	Capt.	SO	Prcsd	589.6	589.8	
FACst	SO	Annoc	Ignrd	589.8	590.0	
FAC#1	SO	FO	Prcsd	594.8	597.4	
FAC#1	FO	SO	Prcsd	601.2	601.4	
ClrFL	A.T.C	Capt.	Prcsd	605.0	606.2	

Figure 4 (cont.)

ClrFL	A.T.C	FO	Prcsd	605.0	607.6	
ATCcn	FO	A.T.C	Ignrd	608.4	608.6	
FlapR	Capt.	FO	Prcsd	628.8	631.4	15.
FlapS	FO	Annoc	Ignrd	631.4	631.6	15.
LOCon	SBsys	Capt.	Prcsd	635.2	636.4	
LOCon	SBsys	FO	Prcsd	635.2	635.4	
Loc A	FO	Capt.	Ignrd	636.8	639.6	
GSon	SBsys	Capt.	Prcsd	653.6	654.8	
GSon	SBsys	FO	Prcsd	653.6	653.8	
GslpA	FO	Capt.	Ignrd	655.2	656.4	
GearR	Capt.	FO	Prcsd	704.8	707.4	1.
GearD	FO	Annoc	Ignrd	707.4	707.6	
FAC#2	SO	Capt.	Prcsd	707.6	710.2	
FAC#2	Capt.	SO	Prcsd	712.0	712.2	
FlapR	Capt.	FO	Prcsd	738.2	740.8	25.
FlapS	FO	Annoc	Ignrd	740.8	741.0	25.
FlapR	Capt.	FO	Prcsd	748.4	751.0	30.
FlapS	FO	Annoc	Ignrd	751.0	751.2	30.
FAC#3	SO	FO	Prcsd	751.2	756.4	
FAC#3	FO	SO	Prcsd	760.2	760.4	
FAC#6	SO	FO	Prcsd	785.4	788.0	
FAC#6	FO	SO	Prcsd	791.8	792.0	
FACfn	SO	Annoc	Ignrd	797.0	797.2	
OMon	SBsys	Capt.	Prcsd	827.2	827.4	
OMon	SBsys	FO	Prcsd	827.2	827.4	
OMann	FO	Capt.	Ignrd	828.8	830.0	
AltCo	FO	Capt.	Prcsd	870.6	872.0	1000.
AltCo	FO	Capt.	Prcsd	919.6	921.0	500.
AltCo	FO	Capt.	Prcsd	938.6	940.0	300.
MMon	SBsys	Capt.	Prcsd	945.2	945.4	
MMon	SBsys	FO	Prcsd	945.2	948.4	
RwisC	FO	Capt.	Prcsd	945.2	946.8	
AltCo	FO	Capt.	Prcsd	948.6	950.2	200.

Figure 5:   Sample PROCRU Milestone Time-Line (Case ILS)

```
-----------------------------------------------------------------------
 TIME  VEHICLE STATE          CREW ACTIVITY          FLIGHT MILESTONES
TGo   Alt    Vel Head  Captain   FOfficer SOfficer
                         (PF)     (PNF)
-----------------------------------------------------------------------
                                                  ATC:TURN to 270. deg
980.0 10000 190 210
                                                  End S & L Begin TURN
                                                  to  270.0  deg
                       PrcsdTurn
977.8 10000 189 210
                                 PrcsdTurn
977.4  9999 189 211
                                 ATCcn
976.6  9999 190 213
                                                  End TURN  Begin S & L
957.8 10000 190 270
                                                  ATC:DECELto 170. kts
950.0 10002 189 270
                                                  End S & L Begin DECEL
                                                  to  170.0  kts
                       PrcsdDecel
947.8 10003 189 270
                                 PrcsdDecel
947.4 10003 189 270
                                 ATCcn
946.6 10004 188 270
                                                  ATC:DSCNDto3500. ft
930.0 10001 172 270
                                                  End DECEL Begin S & L
927.6 10001 170 270
                                 PrcsdChAlt
927.4 10001 170 270
                                 ATCcn
926.6 10001 170 270
                                                  End S & L Begin FLARE
                                                  to   -6.0  deg
                       PrcsdChAlt
926.0 10001 170 270
                       AAon
922.2  9995 170 270
                                                  End FLARE Begin DSCNT
                                                  to 3947.0   ft
895.6  9541 170 270
                                                  AA active
710.8  4019 170 270
                       AAoff
                       PrcsdAltAl
709.2  3972 170 270
                                                  AA inactive
709.0  3966 170 269
```

Figure 5   (cont.)

```
                                                  End DSCNT Begin FLARE
                                                  to    0.0  deg
707.2  3912 170  269
                       IACR
685.8  3500 170  269
                                           IACst
                                           PrcsdIACR
685.6  3498 170  269
                                                  End FLARE Begin S & L
676.6  3466 169  269
                                                  ATC:DECELto 160. kts
670.0  3465 170  269
                                                  End S & L Begin DECEL
                                                  to  160.0  kts
                       PrcsdDecel
667.8  3465 170  269
                                 PrcsdDecel
667.4  3465 169  269
                                 ATCcn
666.6  3465 168  269
                                           IAC#1
665.6  3465 167  269
                                 PrcsdIAC#1
663.0  3465 165  269
                                 IAC#1
659.2  3465 161  269
                                           PrcsdIAC#1
659.0  3465 161  269
                                                  End DECEL Begin S & L
657.6  3465 159  269
                       FlapR
656.0  3466 159  269
                                                  Flaps at  5.0
                                 FlapS
                                 PrcsdFlapR
653.4  3467 159  270
                                           IAC#2
639.0  3464 160  270
                                 PrcsdIAC#2
636.4  3464 160  269
                                 IAC#2
632.6  3465 159  269
                                           PrcsdIAC#2
632.4  3465 159  269
                                           IAC#3
612.4  3467 159  269
                                 PrcsdIAC#3
609.8  3467 159  269
                                 IAC#3
606.0  3467 159  269
                                           PrcsdIAC#3
605.8  3467 159  269
                                           IAC#4
585.8  3463 160  270
```

PRECEDING PAGE BLANK NOT FILMED

Figure 5 (cont.)

```
                                 PrcsdIAC#4
583.2  3463 160 270
                                 IAC#4
579.4  3463 160 270
                                           PrcsdIAC#4
579.2  3463 160 270
                                           IAC#5
559.2  3465 159 270
                                 PrcsdIAC#5
556.6  3464 159 269
                                 IAC#5
552.8  3463 160 270
                                           PrcsdIAC#5
552.6  3463 160 270
                                                  ATC:TURN to 180. deg
540.0  3462 160 270
                                                  End S & L Begin TURN
                                                  to  180.0  deg
                       PrcsdTurn
537.8  3463 160 270
                                 PrcsdTurn
537.4  3463 160 268
                                 ATCcn
536.6  3464 159 266
                                           IACfn
532.6  3464 160 254
                                                  End TURN  Begin S & L
507.8  3464 160 180
                                                  ATC:DSCNDto2000. ft
500.0  3465 159 180
                                                  End S & L Begin FLARE
                                                  to   -3.2  deg
                       PrcsdChAlt
497.8  3465 159 180
                                 PrcsdChAlt
497.4  3465 159 180
                                 ATCcn
496.6  3464 159 180
                       AAon
494.0  3457 160 180
                                                  End FLARE Begin DSCNT
                                                  to 2118.5   ft
481.2  3334 160 180
                                                  ATC:TURN to 120. deg
450.0  2866 159 179
                       PrcsdTurn
447.8  2834 159 179
                                 PrcsdTurn
447.4  2828 159 179
                                 ATCcn
446.6  2815 159 179
```

```
                  Figure 5   (cont.)

                                                   AA active
401.6  2138 159 179
                                                   End DSCNT Begin FLARE
                                                   to    0.0  deg
399.4  2105 159 179
                        AAoff
                        PrcsdAltAl
398.4  2091 159 179
                                                   AA inactive
398.2  2088 159 179
                        FACR
390.4  2008 159 179
                                            FACst
                                            PrcsdFACR
390.2  2007 159 179
                                            FAC#1
385.2  1988 159 180
                                                   End FLARE Begin TURN
                                                   to  120.0  deg
383.0  1987 159 180
                                  PrcsdFAC#1
382.6  1987 159 178
                                  FAC#1
378.8  1987 159 167
                                            PrcsdFAC#1
378.6  1987 159 167
                                                   ATC:Cleared to land
375.0  1988 159 156
                        PrcsdClrFL
373.8  1989 159 152
                                  PrcsdClrFL
372.4  1989 159 148
                                  ATCcn
371.6  1990 159 146
                                                   End TURN  Begin DECEL
                                                   to  150.0  kts
363.0  1986 159 120
                                                   End DECEL Begin S & L
352.8  1988 149 120
                        FlapR
351.2  1988 149 120
                                                   Flaps at 15.0
                                  FlapS
                                  PrcsdFlapR
348.6  1985 149 120
                                                   LOC: on  -2.5 dots
344.8  1981 149 120
                                  PrcsdLOCon
344.6  1981 149 120
                        PrcsdLOCon
343.6  1980 149 120
```

Figure 5   (cont.)

```
                                 Loc A
343.2  1980 149 120
                                                  End S & L Begin TURN
                                                  to   90.0  deg
342.4  1979 149 120
                                                  GS: on  -2.9 dots
326.4  1975 150 111
                                 PrcsdGSon
326.2  1975 150 111
                       PrcsdGSon
325.2  1975 150 110
                                 GslpA
324.8  1975 150 110
                                                  End TURN  Begin S & L
286.6  1978 150  89
                       GearR
275.2  1977 150  90
                                                  Landing gear down
                                 GearD
                                 PrcsdGearR
272.6  1977 150  90
                                           FAC#2
272.4  1977 150  90
                       PrcsdFAC#2
269.8  1978 150  90
                       FAC#2
268.0  1979 150  90
                                           PrcsdFAC#2
267.8  1979 150  90
                                                  End S & L Begin DECEL
                                                  to  140.0  kts
253.6  1980 149  90
                                                  End DECEL Begin S & L
243.4  1979 139  90
                       FlapR
241.8  1978 139  90
                                                  Flaps at 25.0
                                 FlapS
                                 PrcsdFlapR
239.2  1976 140  90
                                                  End S & L Begin DECEL
                                                  to  139.0  kts
233.6  1976 140  90
                                                  End DECEL Begin S & L
232.4  1976 138  90
                       FlapR
231.6  1976 138  90
                                                  Flaps at 30.0
                                 FlapS
                                 PrcsdFlapR
229.0  1976 138  90
                                           FAC#3
228.8  1976 138  90
```

Figure 5   (cont.)

```
                                      PrcsdFAC#3
223.6  1976 138  89
                                      FAC#3
219.8  1976 138  89
                                                PrcsdFAC#3
219.6  1976 138  89
                                                       End S & L Begin FLARE
                                                       to   -2.5  deg
217.8  1976 138  89
                                                FAC#5
194.6  1881 138  90
                                      PrcsdFAC#6
192.0  1858 138  90
                                      FAC#6
188.2  1821 138  90
                                                PrcsdFAC#6
188.0  1819 138  90
                                                       End FLARE Begin DSCNT
187.4  1813 138  90
                                                FACfn
183.0  1766 139  90
                                                       OM active
152.8  1458 139  89
                            PrcsdOMon
                                      PrcsdOMon
152.6  1456 139  89
                                      OMann
151.2  1443 139  89
                                                       OM inactive
150.6  1437 139  89
                                      AltCo
109.4  1016 139  90
                            PrcsdAltCo
108.0  1002 139  90
                                      AltCo
 60.4   510 139  90
                            PrcsdAltCo
 59.0   497 139  90
                                      AltCo
 41.4   315 139  89
                            PrcsdAltCo
 40.0   300 139  89
                                                       MM Active
                                      RwisC
 34.8   248 139  89
                            PrcsdMMon
 34.6   246 139  89
                            PrcsdRwisC
 33.2   233 138  90
                                      PrcsdMMon
 31.6   217 138  90
                                      AltCo
 31.4   215 138  90
```

Figure 5   (cont.)

```
                                                    MM inactive
30.4   205 138   90
                     PrcsdAltCo
29.8   199 138   90
                                                    End DSCNT Begin DECEL
                                                    to  134.0  kts
26.0   160 138   90
                                                    End DECEL Begin DSCNT
15.2    49 133   89
                                                    End DSCNT Begin FLARE
                                                    to    0.0  deg
14.4    41 133   89
                                                    GS  off
12.0    20 133   90
                                                    LOC off
 8.2     0 133   89
```

Table 1: PF and PNF Procedures

PF	PNF
1. Vehicle Control Procedures	1. Vehicle Monitor Procedures
a) Maneuver	a) Vehicle status determination
b) Regulate	b) Failure detection and identification
c) Retrim	
2. Request Procedures	2. Callout Procedures
a) Flap request	a) Vehicle position callout
b) Gear request	b) Altitude callout
c) Checklist initiate request	c) Approach stability callout
3. Subsystem Procedures	3. Subsystem Procedures
a) Altitude alert monitor/control	a) Flap monitor/control
b) Misc. subsystem monitor/control	b) Gear monitor/control
	c) Misc. subsystem monitor/control
4. Acknowledgement Procedures	4. Acknowledgement Procedures
a) Checklist item acknowledgement	a) Checklist item acknowledgement
	b) ATC request acknowledgement
5. SAP/MAP Terminal Procedures	5. SAP/MAP Terminal Procedures
6. Miscellaneous Procedures	6. Miscellaneous Procedures
a) General message processing	a) General message processing
b) Landing parameter selection	

Table 2: Mnemonics for Time Lines

FlapR	Flap request
GearR	Gear request
DCR	Begin descent checklist request
IACR	Begin initial approach checklist request
FACR	Begin final approach checklist request
OMA	Outer marker active callout
LOCA	Localizer capture callout
GslpA	Glide slope alive callout
AltCo	Altitude callout
AppDs	Approach destabilization callout
RwisC	Runway in sight callout
ATCcn	Confirmation of ATC msg.
DC#1	Descent checklist item #1
IAC#1	Initial approach checklist item #1
IAC#2	Initial approach checklist item #2
IAC#3	Initial approach checklist item #3
IAC#4	Initial approach checklist item #4
IAC#5	Initial approach checklist item #5
FAC#1	Final approach checklist item #1
FAC#2	Final approach checklist item #2
FAC#3	Final approach checklist item #3
FAC#6	Final approach checklist item #6
SBck	Speed brakes armed - check.
SBSon	Seat belt sign on announcement
FlapS	Flaps set announcement
Gear D	Landing gear down announcement
ILLon	Inboard landing lights on announcement

Table 2: (Cont.)

SBarm	Speed brakes armed announcement
NSSon	No smoking sign on announcement
ASon	Anti skid on announcement
GPWon	Ground proximity warning system on announcement
AAon	Altitude alert on announcement
AAoff	Altitude alert off announcement
LOCon	Localizer on
GSon	Glide slope on
OMon	Outer marker on
MMon	Middle marker on
GPWSa	Ground proximity warning system alert on
AltAl	Altitude alert on
Decel	Decel command
Turn	Turn command
Flare	Flare command
ChAlt	Change Altitude command
DCst	Starting descent checklist announcement
IACst	Starting initial approach checklist announcement
FACst	Starting final approach checklist announcement
DCfn	Finished descent checklist announcement
IACfn	Finished initial approach checklist announcement
FACfn	Finished final approach checklist announcement
ClrFl	Cleared for landing announcement
CIgON	Continuous ignition on announcement
MMa	Middle marker active callout
ChgRl	"taking control" announcement

omit 30

A MODEL FOR REAL-TIME HUMAN DECISION-MAKING IN A MULTI-TASK ENVIRONMENT

P. Krishna-Rao
Arye R. Ephrath
David L. Kleinman

The University of Connecticut
Storrs, Connecticut 06268, USA

ABSTRACT

A dominant thrust in future man-machine systems appears to be away from manual control to partial, if not full, automation. In this direction, the role of the human operator is shifting from that of a direct system controller to one of a monitor of multiple tasks, or a supervisor of several semi-automated subsystems. The operator's primary task in these systems is to extract information from his environment and integrate it for action selection and implementation. However, the human brings to the man-machine system various inherent limitations, such as reaction time delays, limited resolving power and randomness, that limit his ability and degrade the overall system performance. In order to properly analyze and evaluate a man-machine system, a clear understanding of human's capabilities as a real-time decision maker is indispensable.

The present research has sought to understand human decision-making and task selection procedures in dynamic multi-task environment. The approach has been to assimilate the results of a joint experimental and analytic program into a normative optimal decision model (ODM) for predicting human task sequencing performance. To this end, a general multi-task paradigm is developed wherein tasks of different value (priority), duration (processing time), and deadline (opportunity window) compete for the attention of the human operator. This is the type of situation

the human operator encounters in AAA target selection, Air-traffic control, multi-targetting, production scheduling, etc.

The optimal decision model (ODM) consists of two separable blocks: information processor and decision-maker. The information-processor estimates the statistics of the 'decision state' which provides the complete running summary of past actions and estimates. These estimates, along with the task values, are used in a myopic decision strategy, based on semi-Markov decision process (SMDP) formulation, to obtain optimal decisions. A novel feature of our modeling approach is that it explicitly incorporates human limitations into the information-processing and decision-making stages. The model can be exercised either in a sample-path or in a covariance propagation mode.

The data are obtained using human subjects. The model-data validation effort consisted of comparing (i) the probability of acting on a task at time t; (ii) the probability of completing a task by time t; (iii) the incremental reward earned at time t; (iv) the accumulated reward earned by time t; and (v) the probability that the human commits an error (i.e., starts on a task he can not complete). Excellent model-data agreement was obtained for several experimental conditions.

N82 34067 D20

APPLICATION OF OPTIMAL CONTROL PRINCIPLES TO DESCRIBE THE SUPERVISORY CONTROL BEHAVIOR OF AAA CREW MEMBERS

Chris Hale
Systems Research Laboratories, Inc.
Dayton, Ohio

Capt. George J. Valentino
Air Force Aerospace Medical Research Laboratories
Wright-Patterson AFB, Ohio

ABSTRACT

Supervisory decision making and control behavior within a C^3 oriented, ground based weapon system is being studied. The program involves empirical investigation of the sequence of control strategies used during engagement of aircraft targets. An engagement is conceptually divided into several stages which include initial information processing activity, tracking, and ongoing adaptive control decisions.

Following a brief description of model parameters, two experiments which served as initial investigation into the accuracy of assumptions regarding the importance of situation assessment in procedure selection are outlined. Preliminary analysis of the results upheld the validity of the assumptions regarding strategic information processing and cue-criterion relationship learning. These results indicate that this model structure should be useful in studies of supervisory decision behavior.

INTRODUCTION

Principles of an optimal control model are currently being applied in the study of supervisory decision processes in a simulated AAA setting. The control model currently being developed in our program at AFAMRL is divided into three major stages; a display processor, an information processor, and a procedure processor. A diagram of the model organization is given in Figure 1. In the display processing stage, certain display components are selected and differentially weighted to yield a subjectively optimized display for further evaluation. The information processor then uses this display subset to generate a current estimate of system state and to detect specific events which may influence subsequent system operation. Finally, the procedure processor selects an appropriate procedure based on the combination of system state and detected events, and implements that procedure verbally and/or manually. This procedure selection is the stage which we are primarily interested in investigating.

We are currently concentrating our efforts on the operation of what we feel is the major aspect of procedure selection; the situation assessment process. This is considered to be of major importance because the tactical decisions concerning system operation are based on the outcome of this process. Figure 2 depicts a flow chart description of the selection of a system operating mode. Inspection of this figure reveals the importance of the situation assessor in this process. State estimate and event information enter the assessor from the Kalman filter. A perceived situation is output and this serves as data in subsequent processes. An outcome computer estimates p_K and p_S for each mode alternative. Each of the modes is then

OPERATOR MODEL

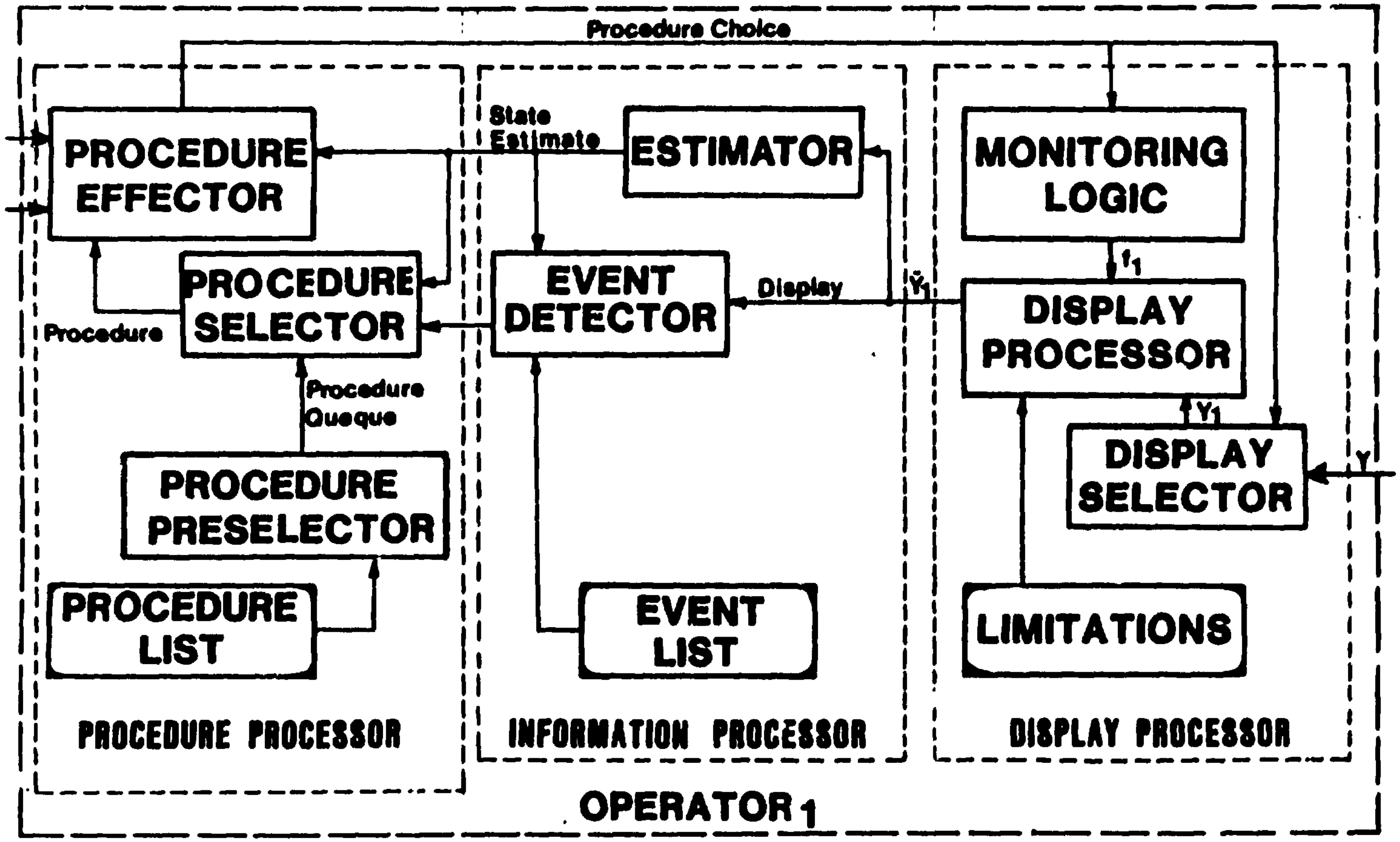
Procedure Choice
PROCEDURE EFFECTOR
PROCEDURE SELECTOR
Procedure
Procedure Queque
PROCEDURE PRESELECTOR
PROCEDURE LIST
PROCEDURE PROCESSOR
State Estimate
ESTIMATOR
EVENT DETECTOR
Display
EVENT LIST
INFORMATION PROCESSOR
$\hat{Y}_1$
MONITORING LOGIC
f_1
DISPLAY PROCESSOR
Y_1
DISPLAY SELECTOR
Y
LIMITATIONS
DISPLAY PROCESSOR
OPERATOR 1

FIGURE 1

MODE SELECTION PROCEDURE

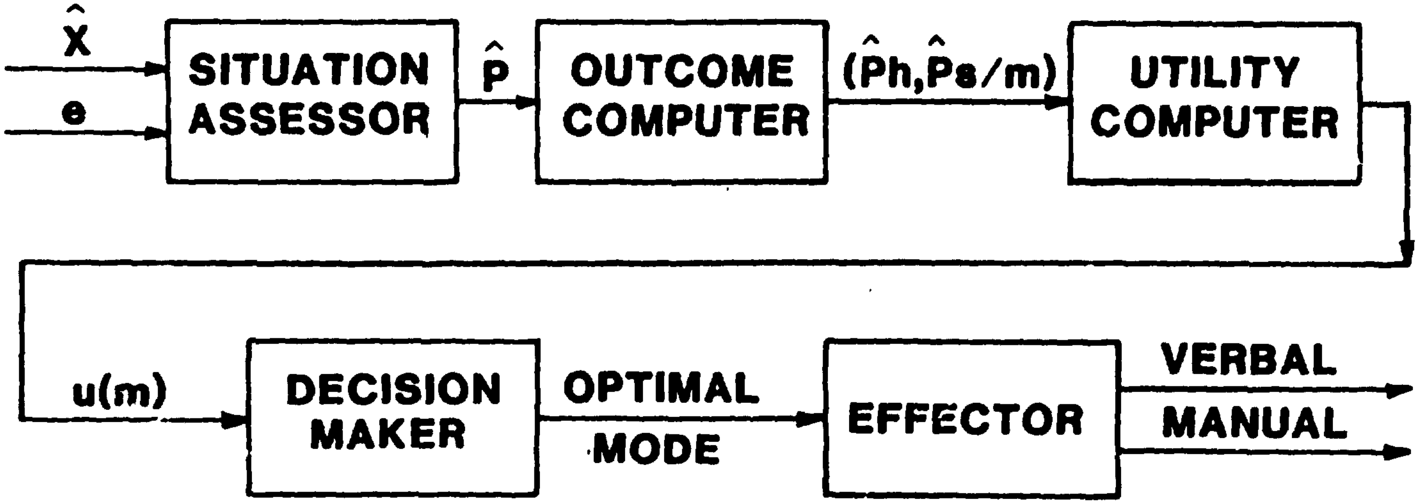
$\hat{X}$
e
SITUATION ASSESSOR
$\hat{P}$
OUTCOME COMPUTER
$(\hat{P}h,\hat{P}s/m)$
UTILITY COMPUTER
u(m)
DECISION MAKER
OPTIMAL MODE
EFFECTOR
VERBAL
MANUAL

FIGURE 2

assigned a weight on the basis of expected utility, and the decision maker selects the most optimal mode based on this measure.

One of the major tasks engaged in by the AAA commander in assessing a situation is the learning of the variety of relationships that exist between the display subset associated with an incoming target and his system's probability of successfully engaging that target. The information upon which these relationships depend is usually probabilistic, and often incomplete or contradictory. It is critical that strategies which allow accurate predictions of target behavior be developed quickly. The development of such strategies can often be impeded for two reasons. First, as mentioned above, is the probabilistic nature of the available data. Second, the value of the available information is usually not constant. Since information is differentially valuable, the absence of certain types of information from a total display may be more damaging to rapid and efficient control performance than the absence of other types of information. Two experiments were conducted to explore the implications of these two assertions.

EXPERIMENT I

One way of rapidly and efficiently assessing a situation is to utilize only a subset of the total information display which is manageable, and yet, approaches some optimal level of informativeness. Such a display would vary in form o[illegible]ial to trial. That is, the amount of information necessary for an optimal decision might change across trials, but more importantly, the type of specific information needed might change over trials due to the conditional and interdependent nature of information. If, when placed under a time constraint, a commander engages in strategic information processing in order to assess a situation, the results should be detectable as conditional information hierarchies. The purpose of this study was to attempt to expose such hierarchies which subjects might form when exposed to time constrained information search requirements. Subjects were to select an operating mode and target choice which was appropriate to the information present on that trial. In order to make these choices, it was necessary for the subject to request the information sequentially. The task was structured such that it was not possible to access all available information before the end of a trial. Thus, the subjects had to search for an optimal informational configuration on each trial by building the display element by element. We expected that this requirement would result in differential display construction. This is because the nature of the situation process requires a display which possesses enough information for an optimal choice among alternatives, while at the same time keeping the amount of information within manageable limits. These two conditions are satisfied only when the display conforms to certain configurations defined by the interrelationships of the information present on that given trial. Because of this, receipt of each new piece of information should influence requests for subsequent information such that a pattern of informational interrelationships should emerge.

Information was displayed on a Vector General CRT and consisted of four categories; trajectory of the target (flyby, zigzag, jink), and presence or absence of ECM, OCM, and ARM. In order to obtain specific information, subjects had to activate a series of category request buttons. Information requests could occur only at 5-second intervals. Specific information received following each request was randomly determined.

On half the trials, one target was present and on the other half, two targets were present. On double target trials, appearance of the second target followed the first at an interval of between 2 seconds and 14 seconds. Whenever a second target appeared, the potential information set doubled in size.

The results of each trial were represented according to a decision tree format (Figure 3). Analysis indicated that optimal display construction did indeed follow a pattern which resulted in displays characterized by conditional interim dependence. That is, the ordinal relationships between category requests were conditional upon the specific information received at each request. This supports the idea that situation assessment is a process characterized by search strategies resulting in displays which allow optimal state estimation and subsequent procedure selection. Further analysis, although still in progress, has resulted in estimation of conditional probabilities of category request which supports these qualitative observations.

EXPERIMENT II

The purpose of the second experiment was to examine the effects of probabilistic and incomplete information of the subjects' ability to optimize system performance. The level of system performance was determined by the subjects ability to learn the relationships that existed between the given information and his/her subsequent control behaviors. These cue-criterion relationships were revealed by a feedback metric which indicated a momentary measure of the level of performance, thus allowing within-trial control modifications which, if correct, could result in performance improvement. The metric itself consisted of a measure of the probability of kill (p_K) based on the range of actions that the commander must take during the course of an engagement. These include selection of operating mode, firing range, and burst duration.

On each trial subjects received probabilistic information regarding the presence of countermeasures (ECM, OCM, ARM), as well as identification of the target's trajectory, and target position information. Countermeasure probability information ranged from 0 to 1.00 and was normally distributed ($\bar{x}$ = .50; SD = $\mp$ .20). At some predetermined range the probabilities changed to either 0 or 1.00 to indicate absence or presence of the countermeasure. The trajectory of the target was made available at a range of 7.5 km and was either a flyby, zigzag, or jink. Target position information included range, azimuth, and altitude and was available in proportions of either .33, .66, or 1.00. On each trial the subjects task was to select an operating mode, a burst duration, and a firing range. When firing was initiated, burst duration and a 1-second forced delay between bursts were computer controlled. During firing, subjects received an instantaneous p_K score which was updated each second. The score was based on the characteristics of the target, the burst duration, mode chose, and range at each second of fire. At any time during firing, subjects could stop fire and

FIGURE 3a

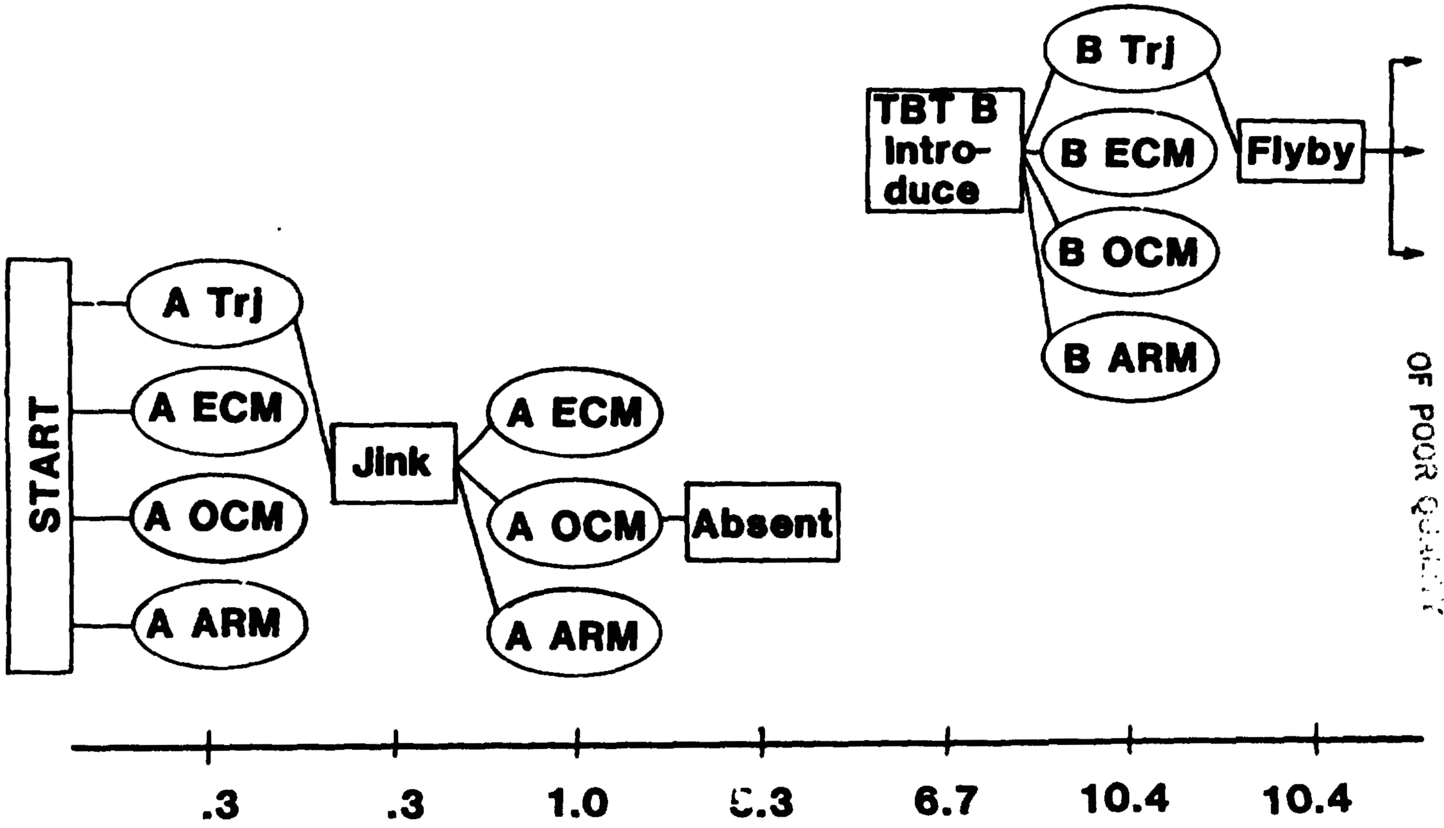
START
A Trj
A ECM
A OCM
A ARM
Jink
A ECM
A OCM
A ARM
Absent
TBT B Intro-duce
B Trj
B ECM
B OCM
B ARM
Flyby
.3
.3
1.0
5.3
6.7
10.4
10.4

FIGURE 3b

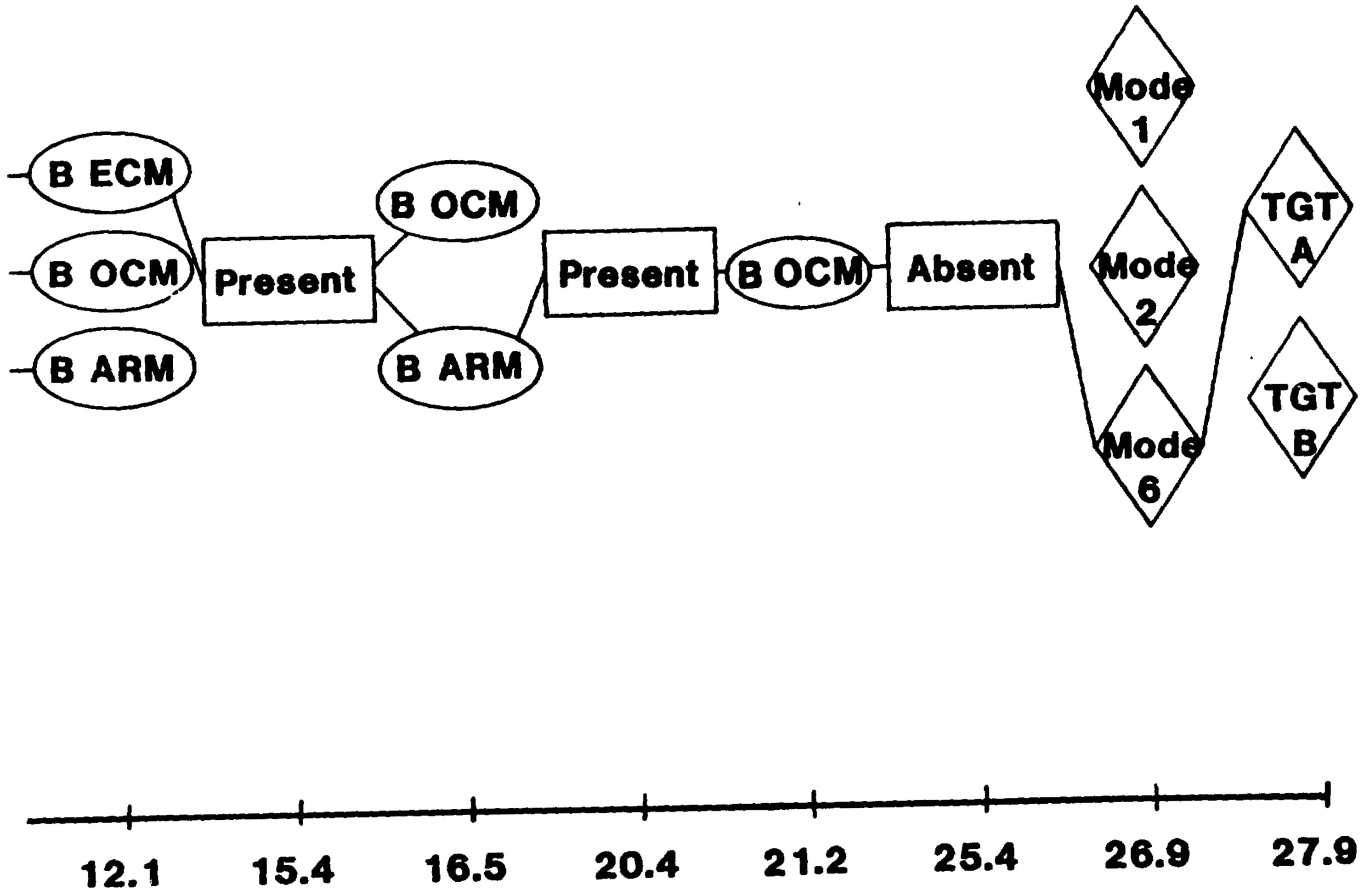
B ECM
B OCM
B ARM
Present
B OCM
B ARM
Present
B OCM
Absent
Mode 1
Mode 2
Mode 6
TGT A
TGT B
12.1
15.4
16.5
20.4
21.2
25.4
26.9
27.9

execute any series of actions; changes in mode, firing rate, etc. At the end of each trial, a cumulative p_K based on intratrial performance was displayed.

The analysis of this data was based on the following assumption. When presented with suboptimal displays subjects possess the capability of learning the relationships between these displays and the control actions which will result in optimal system performance. This deductive capability would be realized as an ability on the part of the subject to discriminate among the alternatives available to him/her. Such discriminative ability should be sensitive to statistical analysis. Accordingly, two discriminante analyses were performed using the display elements as predictors and mode choice as the variable to be discriminated.

RESULTS

The first analysis considered only the presence or absence of target position information, in addition to trajectory and countermeasure probabilities. A stepwise analysis was performed using the minimum D squared selection criteria. Seven of the eight variables entered the equation; the only variable not contributing significantly to discriminative power was altitude information. The two discriminant functions resulting from this analysis accounted for all of the mode selection variability, with the first function explaining 94.09 percent of this variability. Both the final weights attached to each prediction, and the order in which variables were entered into the equation, support the idea that subjects were engaging in a selective information evaluation process, the intent of which was to evaluate the utility of each available alternative, eliminate those which were inappropriate, and select the one which would yield the highest expected performance.

The final function, with seven of the eight variables considered, revealed that trajectory name was the most heavily weighted variable, followed in order, by the probabilities of ECM, ARM, and OCM. The presence or absence of target position information resulted in low, although still significant, weightings. These weights indicate that subjects were comparing the alternatives against one another primarily on the basis of that information which would allow the most rapid discrimination among, and elimination of, modes in terms of their defining characteristics.

This interpretation is supported by the order of entry. At the initial step of the analysis, the variable providing the most discriminating power was the probability of OCM. This seems to indicate the subjects were initially evaluating the alternative set on the basis of the utility of radar capability under the conditions present, thus allowing an initial crude evaluation of mode utilities in terms of the most salient separating feature of the mode set. Step 2 of the analysis (probability of ECM entered), implies that the subject is attempting to further discriminate among radar vs. nonradar utilities. The entry of trajectory name on the third step, and probability of ARM on the fourth step, confirms this idea. At this point, the subject is now able to discriminate maximally between all three mode alternatives in terms of the usefulness of each. Further entrance of predictors into the equation results in little increase in discriminative power.

A classification table indicated that a total of 79.25 percent of the cases were placed into the appropriate group membership category by the discriminant functions. The major source of error in the overall classification was due to a complete inability to correctly classify mode 2 selections into the appropriate group. Only 2.1 percent of such cases were correctly classified. This is compared to correct classifications for modes 1 and 3 of 61.8 percent and 90.5 percent, respectively.

The second analysis considered those trials on which the actual values of the position information was available. The outcome of this analysis took a somewhat different form than did the first analysis. With regard to variable weightings, two types of position information, along with trajectory name, assumed the most importance. These two were azimuth and altitude information. The order of entry was also different from the first analysis. Azimuth information was the first to enter the analysis. This is not surprising, since the presence of this value allows subjects to accurately infer the trajectory of the target, as well as obtaining azimuth information. Given this knowledge, the next three most important types of information were the probabilities of ECM, ARM, and OCM, respectively. Again, this is in line with the idea that subjects were attempting to eliminate alternatives, and thus uncertainty on the basis of defining characteristics of the modes. Thus, on those trials when ECM probability was low, the next most important consideration was the probabiliy of ARM. Once this probability had been evaluated, OCM probability, by virtue of its influence on mode 6 usefulness, was evaluated. Inspection of the level of discriminability revealed that, beyond this point, the entry of other predictors contributed very little discriminative power.

The classification table for this analysis revealed a successful group membership prediction of 83.47 percent. Again, the major source of classification error was the inability to correctly predict mode 2 membership. Of the mode 2 selections, 4.30 percent were incorrectly classified as belonging in the mode 1 group, and 95.70 percent were incorrectly placed in the mode 6 group. Seventy-six percent of the mode 1 selections were correctly classified in this analysis, and 90.90 percent of the mode 6 choices were placed correctly.

Finally, we feel that some comments are warranted concerning one of the most striking aspects of this experiment, that is, the complete inability to accurately predict mode 2 selections on the basis of the information available to the subject. Some reflection on the properties and capabilities of the three modes indicates that, perhaps, this result should not have been totally unexpected. Activation of mode 2 requires that the subject utilize aspects that are indigenous to both modes 1 (radar range information) and 6 (manual az and el estimation). Thus, mode 2 can be thought of a falling along a continuum between modes 1 and 6. Since the information that is being weighted most heavily by the subject has the greatest effect on either mode 1 (trajectory, ECM, ARM) or mode 6 (trajectory, OCM), and since the strategy of the subjects seems to be based on rapid, and somewhat noncompensatory, elimination of alternatives, mode 2 is often eliminated from consideration along with elimination of the mode whose defining characteristics are being matched against target attributes at that step in the decision process. This leads to the result that, in the few cases in which mode 2 is selected, it is almost impossible to classify correctly because the variables used for classification are not considered to apply primarily to mode 2. In short, it appears that conceptually mode 2 has no unique defining characteristics.

CONCLUSIONS

Preliminary analyses of these data indicate that the following conclusions are possible.

1. In order to assess a situation optimally, subjects will engage in strategic information search designed to extract maximum usefulness from a display, which limits that display to a size that is within human processing limitations. This will result in a limited number of display structures characterized by hierarchies which are defined by the interdependencies of the information set.

2. Subject's control decisions are based upon an ability to infer the relationship between information displays possessing suboptimal validity and a subsequent outcome. This capability manifests itself as an ability to discriminate, from among a set of alternatives, that alternative which will maximize the cue-criterion relationship, as indexed by outcome feedback.

Subsequent work in our laboratories related to these two experiments will focus on the structuring of the various information search and processing strategies employed by the commander and on the factors which influence the activation and use of these various strategies. Additionally, we plan to investigate variables effecting the cognitive activity involved in the commander's utilization of the relationship between external conditions and his knowledge and creative use of system capabilities.

N82 34068

DOES MAN ALWAYS CLOSE THE LOOP IN TRYING TO PILOT A LARGE SHIP?

Douglass R. Arnott
13 Devonshire Place
Huntington Station
New York 11746

T. Govindaraj
School of Industrial Engineering
Purdue University, Grissom Hall
West Lafayette, IN 47907

ABSTRACT

Control of a slowly responding complex dynamic system such as a large supertanker poses special problems for the human. Forming an internal model of such a system is more difficult than that of systems whose response characteristics match those of the humans more closely. For instance, due to slow response, quick control actions such as those required in flying an aircraft are not needed. Instead control actions must be based on information over a longer time span. The model should have appropriate features to handle such situations. It is not clear as to what types of display aids might be helpful in forming the internal model and/or for better control. Experiments were conducted to study this problem. Experienced ship's crew members maneuvered a simulated ship in real time. The simulation was performed using a graphics display run by a PDP 11/40 minicomputer. The maneuvers consisted of piloting a large ship along a narrow waterway. Preliminary results suggest that the human operates as a feedforward controller utilizing the preview information for 'gross changes' in heading, and as a feedback controller for correcting small deviations. The instruments displayed on the deck do not seem to be helpful in all situations. In fact, evidence seems to indicate that some of the displays might even interfere with the pilot's attempt to form a good internal model.

INTRODUCTION AND MOTIVATION

Traditionally, in ship simulators and in crew training the basic operating hypothesis has been based on task behavior training. The crew were trained in operations where they could respond to a set of stimuli in a pre-determined fashion. This had its origins, perhaps, in airplane simulators, and other operations where enough time was usually not available for detailed analysis of the state of the system. When sufficient time is not available for thinking through the problem it becomes necessary to use strategies whereby conditioned responses substitute for fast and timely actions.

Such a situation does not prevail in the operation of a ship due to the slow changes in speed and heading. If the crew has sufficient training it is possible to have a good internal model of the ship and be able to control it based on the actual state. In fact, in aircraft operations it is well known that the pilot operates as if he has a good internal model. Usually, the human operator uses information provided by the system as feedback to correct for errors and, generally for improving the performance.

However, in slow systems such as piloting a ship, feedback may not always be helpful. Feedback could prevent the formation of the internal model initially, and/or interfere with the operation of the internal model later. When the operator has an insufficient model of the system under control, it is possible that he fails to analyze the situation carefully and acts impulsively based on the feedback information. Under these conditions, it may be advantageous to remove some (or most) of the feedback displays so that he is forced to think through the situation and act accordingly. Even in cases where feedback is helpful, proper form of feedback is essential. Relevance of various instruments, and quantities to be measured and displayed must be carefully chosen. Understanding what components are important, what the input/output relationships are etc are important. Experiments were conducted to study various factors discussed above. Modeling efforts are being made to understand better the various quantities involved, and how they affect performance.

Depending upon the familiarity of the human with the system under control one or more of the following modes of information may be used by the human. The operation could be open loop or closed loop, or some form of feedback and/or feedforward information could be used. Instruments may reflect commanded quantities and response quantities. These are some of the issues to be considered in the experiments and in modeling.

EXPERIMENT

Dynamics of a large supertanker of 250,000 dwt was simulated on a PDP 11/40 computer with the VT11 Graphics system. A mock up of the ship's console was used to control the dynamics of the ship. The console had a ship's wheel and throttle control. The equations of motion were taken from Comstock[1].

The display generated by the computer is shown in Figure 1, and is similar to the view from the bridge of a large supertanker. The ship's bow remained fixed and the background moved past the ship. A three dimensional view was presented corresponding to the observer's height of 80 feet. The instruments available for display were: compass, rate of turn indicator, tachometer, rudder angle indicator, speed indicator, and time display. Any combination of the displays could be included in any particular experiment.

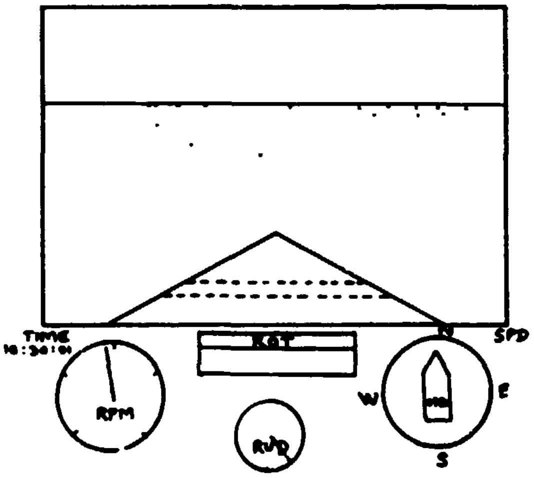

Figure 1

The maneuvering area of the ship was based on the Savannah River, with some modifications to accomodate a supertanker, and to take into account the limited capabilities of the computer. The essential details were included however, and the scenario provided opportunites for a number of different maneuvers within a 2 1/2 hour time period.

The subjects were instructed about the operation of the ship, and were shown the lay out of the buoys that define the course. During the experiment, they had access to a chart of the course. The basic maneuvers to be performed by the subjects were:

1. Accelerate and enter the main buoyed channel from a stopped position.
2. Turn in the channel at various angles and speeds.
3. Enter a buoyed channel, decelerate and remain at a slower speed.
4. Maintain a set heading of the vessel.

The experiment consisted of four phases. In the first phase, all the displays were available. The passage was up the river. The subjects were instructed in the proper use of the controls to obtain desired response. Some of the important characteristics were explained. In particular, the subjects were instructed as follows:

1. A stream of water over the rudder is needed to produce a radial acceleration. This could be achieved either by a forward velocity of the ship or by an increase in propeller RPM. For a given forward velocity, an increase in RPM would increase the velocity of the stream of water over the propeller.
2. Control of the ship could be achieved by acceleration. Rate of Turn (ROT) and speed reflect d any changes in control.

In addition, maximum rudder rate and RPM acceleration were pointed out to the subjects (3 deg/sec and 2 RPM/sec respectively.) The subjects were also aware of a slight instability in the ship's dynamics.

In the second phase, the subjects were allowed two instruments of their choice. The remaining instruments were not available. As in the first phase, the passage was up the river. The subjects were trained in such a way that most of the instruments became unavailable for feedback. At the end of this phase, usually lasting a single run, the subjects had enough training to be able to maneuver the ship without any instrument.

No instruments were available for the third phase. Hence, it was not possible to apply some input and watch the effect on the instrument display. The only feedback was by observing the view from the bridge after any control input. Due to the inherent slowness of the dynamics of the ship, the controls had to be carefully chosen, based on analysis of the situation. Since 30-40 seconds would have elapsed before the results of some response would be evident in the view from the bridge, immediate feedback would be all but impossible.

In the fourth phase, instruments were not available, and the passage was down the river. This forced the subjects to approach the turns at different speeds using different plans for the maneuvers. Therefore the course seemed quite different to the subjects. This phase was used as the final testing of the subjects' control behavior.

During the experiment, information concerning inputs (rudder angle and throttle (RPM) requests), and the position of the ship (coordinates) was collected. The data were collected for all phases except for the second phase when the subjects were trained to pilot the ship without the use of feedback displays (instruments). At the end of every maneuver, the subjects were also asked to fill out a questionaire concerning the efforts in performing that maneuver.

Since the lateral control was achieved by changes in radial acceleration, produced either by using the rudder angle or by changing the RPM of the propeller (or a combination of both), the control input of the subject was converted into an equivalent rudder input. For a given combination of rudder and throttle inputs, the equivalent rudder input was calculated as that input that would produce the same rate of turn if rudder alone were to be applied. This is based on the assumption that the subject used a combination of controls to get some desired radial acceleration. It is presumed that the input applied was chosen mainly to get the desired radial acceleration.

THE SUBJECTS

Four subjects participated in the experiment, involving more than fifty hours of simulated operation. In terms of US Coast Guard Licenses, two (GSA,RPH) were "Third Mates of Steam Vesssels of Any Tonnage, Upon Oceans". In addition, they were licensed "Third Assistant Engineers of Steam and Motor Vessels of any Horse Power". One of them (RPH) also had the classification of "Chief Engineer of Uninspected Towing Vessels of Any Horsepower, Upon Rivers." The third subject (FEG) was "Chief Mate of Steam Vessels of Any Tonnage, Upon Oceans." The most experienced subject (DAH) is "Master of Steam Vessels of Any Tonnage, Upon Oceans." Since all of them had a lot of experience in real ships, their transition to the simulator was smooth and fast.

POSSIBLE MODES OF CONTROL

The main control characteristics of interest concern • lateral motion of the ship along the channel. At various points in the course of the maneuver, the ship had to make turns at various angles and at various speeds. It is our desire to be able to model the control behavior in terms of some analytical methods. Possible modes of control are: open loop control without making use of any form of feedback (utilizing only the feedforward information about the desired course), closed loop control with feedback from instantaneous feedback from the instruments on the bridge, closed loop control based solely on the information obtained from observations on the deck, and a combination of various feedback and feedforward controls. It is also possible that the controller is capable of separating the controls into one or more regions, and identifying proper course of action. Appropriate controls can then be applied to get the desired performance.

In a purely open loop system, for changes in heading, the control action would be based on the difference between the feedforward information and some fixed reference. The resulting control would consist of a single pulse or a step of finite duration to initiate a turn, and a similar action in the opposite direction to bring the ROT back to zero. Unless the control system is calibrated to compensate for any directional instabilities, no additional control actions will be involved in the operation of such a system.

On the other hand, in a closed loop system, the control actions would be based on the error between the desired heading and the actual heading. Since there would be some error until the desired heading is reached, continuous control will result. In practice, this would manifest itself as a number of pulses closely spaced together. Control would be zero only when the error becomes zero.

It is also possible that the subject merely functions as an open loop (feedforward) controller as long as the error remains within some tolerance limit. When this limit is exceeded, action is taken to reduce the deviation and limit the drift. Depending upon the tolerance the subject has for the error or deviation there could be additional control pulses along the course of the turn. This situation would result in a control behavior having a number of pulses at various points in time. This would be somewhere between the completely open loop and completely closed loop systems.

EXPERIMENTAL RESULTS

The discussions of the previous section are meant to provide a framework for analyzing the results of the experiment. In this section, results for all four of the subjects are discussed. (Detailed results are given in Arnott[2].) Each subject will be considered separately in an effort to understand the possible mode(s) of operation.

From the results for subject FEG, it appears that he behaved as a feedforward-feedback controller most of the time. Though only feedforward control is used initially (open loop), apparently error builds up rapidly, and there appears to be a need to compensate for the error by using proper amount of control almost continuously. Equivalent control inputs increase after an initial open loop-like behavior. He could control the ship without using any of the instrument displays, though the control effort appeared to be much more than that required when feedback from the instruments were available. But according to the response from to the questionaire, his stress level was lower when there were no instruments. Apparently this indicates that his visual workload was reduced when instrument displays were removed. The performance in holding a steady course did not suffer when the displays were absent. Removal of the feedback displays did not seem to affect his performance in any of the phases.

In turns, DAH seemed to perform as a feedforward-feedback device. However, in some turns his controls were almost continuous, similar to that of a closed loop controller. His ability to hold a steady course without the instruments was not as good as having them to aid in control. Apparently it was difficult to get sufficient information about the course of the ship without the aid of displays. In fact, the information in the questionaire suggests that he might be trying to obtain the information from the display of the environment. The response to the questionaire suggests that he could be using the information more efficiently by analyzing the situation more carefully and using the internal model more effectively.

There was a tendency for GSA to act as a closed loop controller when instrument displays were available for feedback, and also when he transitioned into a mode with feedback displays removed. Apparently he could not develop a sufficiently accurate internal model and had to rely on feedback information either from the instruments or from the view from the bridge. As experience increased, he started to act more like an open loop controller or a combination of feedback-feedforward controller. From the questionaire and from the data on control and track, it appears that the feedback displays interfered with the formation of a good internal model. He devoted so much time to the information dislayed on the instruments that he could not think about the consequences of any action.

When the displays provided the feedback, the subject RPM was controlling more like an open loop controller. Later, with more experience, he started to act more like a feedforward-feedback controller. His performance did not suffer appreciably when feedback information provided by the instruments was absent.

DISCUSSION AND POSSIBLE APPROACHES TO MODELING

Though the experiments were rather detailed, the results are preliminary. These results seem to suggest that a combination of feedforward and feedback information is used by the subjects to control the ship in lateral motion. From the results obtained when the instruments were available it appears that they were not always helpful for control. In fact, during some phases they might have been a hindrance because of the misleading information about control resulting from the responses of the instruments themselves. They might also have increased the subject's workload.

When information concerning the future trajectory is available for some time it has been found that the human uses a combination of feedback and feedforward controls. In particular, the work of Donjes[3] on modeling the car driver seems relevant. He found that gross changes in direction were controlled as if the control was open loop and minor deviations from the desired trajectory were then corrected in a closed loop fashion. In a preview control task, Govindaraj and Rouse[4] obtained similar results. It was found that some form of feedforward and feedback information was used for control. It was also found that control was applied only when the perceived error exceeded a certain tolerance level. Control was therefore intermittent. This type of control behavior was characteristic of many of the subject runs in our experiment.

Modeling efforts are underway to study this type of control. In particular, it will be interesting to find out if there are thresholds for errors and/or controls. This might give an indication of the relative amounts of feedback and feedforward information. Detailed experiments will then be conducted to verify the modeling results. The model might also be helpful in understanding which of the feedback displays are more useful and which might even be harmful in the development of good control habits.

It is possible that there is a hierarchical control approach that the pilot uses in control. Depending upon the relative importance of various errors (or some other information) control might take different forms. Different levels in the model might be able to take care of appropriate phases in the information. Delegation of authority for control to different levels might be done by some simple device such as a combination low pass-high pass filter or some other complex mechanism. These and other possible methods will be explored in greater detail. Models developed will be validated by running detailed experiments.

OR[illegible]
OF [illegible]Y

ACKNOWLEDGEMENT

The coefficients in the equations used for the simulation were provided by Marine Safety International, and are their proprietary property. Their help and cooperation is gratefully acknowledged.

REFERENCES

[1] Comstock, J. P., Ed., Principles of Naval Architecture, The Society of Naval Architects and Marine Engineers, New York, 1967.

[2] Arnott, D. R. "Evaluating Man as an Open Loop Control Device in a Slow, Complex, Dynamic System", M.S. Thesis, Department of Mechanical and Industrial Engineering, University of Illinois at Urbana-Champaign, 1980.

[3] Donjes, E. "A Two-Level Model of Driver Steering Behavior", Human Factors, Vol.20, No.6, December 1978.

[4] Govindaraj, T. and Rouse, W. B. "Human Controller Modeling in Environments that Include Non-Control Tasks", Proceedings of the 18th IEEE Conference on Decision and Control, Fort Lauderdale, Florida, December 12-14, 1979.

N82 34069

Supervision of dynamic systems:
Monitoring, decision-making and control.

Ted N. White *
DELFT UNIVERSITY OF TECHNOLOGY
The Netherlands

ABSTRACT

Effects of task variables on the performance of the human supervisor by means of modelling techniques are discussed. The task variables considered are: The dynamics of the system, the task to be performed, the environmental disturbances and the observation noise.
A relationship between task variables and parameters of a supervisory model is assumed. The model, reported by Kok and Van Wijk consists of three parts: (1) The observer part is thought to be a full order optimal observer, (2) the decision-making part is stated as a set of decision rules, and (3) the controller part is given by a control law.
The observer part generates, on the basis of the system output and the control actions, an estimate of the state of the system and its associated variance. The outputs of the observer part are then used by the decision-making part to determine the instants in time of the observation actions on the one hand and the controls actions on the other. The controller part makes use of the estimated state to derive the amplitude(s) of the control action(s).

In addition to the identification of the model parameters, by a random search method, a more psychologically oriented method is used, primarily based on statistics. The psychological approach deals with a direct comparison of the number of control actions, the amplitudes of those control actions, and the number of observation actions generated by the operator as a function of the task variables mentioned before.

The system theoretical and the psychological approach will be discussed and a comparison of the results, using both approaches, will be given.

---

* This research is sponsored by the Netherlands Organization for the Advancement of Pure Research (ZWO).

INTRODUCTION

Due to the ever increasing automation in industry the task of the human operator has shifted from direct manual control to supervisory control. However, this task still can be considered as a control task, but on a higher mental level and of a discrete character. This means that only when deviations of the observed variables beyond the specified boundaries are detected, due to failures and/or disturbances in the automated system, corrective actions are initiated. Therefore, the task involves monitoring the system, as well as decision making and control.
For the optimal design of man-machine interface (MMIF) a profound understanding of the supervisor's behavior is necessary. This can be obtained by modeling the human operator's behavior, for instance during supervision of a system in a steady state mode. For this purpose descriptive models, or normative models, can be used.

DESCRIPTION OF A SUPERVISORY MODEL

In this paper we consider the verification of a normative model describing the human operator control of slowly responding complex systems.
The model is based on the concepts of the Optimal Control Model [Baron, Kleinman 1969; Kleinman, Baron, Levison, 1971] and was proposed by Kok and Van Wijk [3].
The purpose of the model is to describe human behavior in relationship with a set-point controlled process in a steady state mode.
The model is based on the hypotheses that the operator has knowledge about:
o the system dynamics,
o the statistical properties of the disturbances acting on the system and
o the task to be performed.
It is assumed that the operator's knowledge is perfect, that the model can be described by a set of linear differential equations and that the system is relatively slow in comparison to the neuro-muscular system of the human being.
The structure of the model is further based on the hypotheses that the operator estimates the state of the system independent of the control task.
So, the separation theorem of optimal linear filtering and control is accepted here as a basic mechanism of the operator's behavior.
The model then consists of an observer part, a controller part and a decision making part (see Fig. 1).

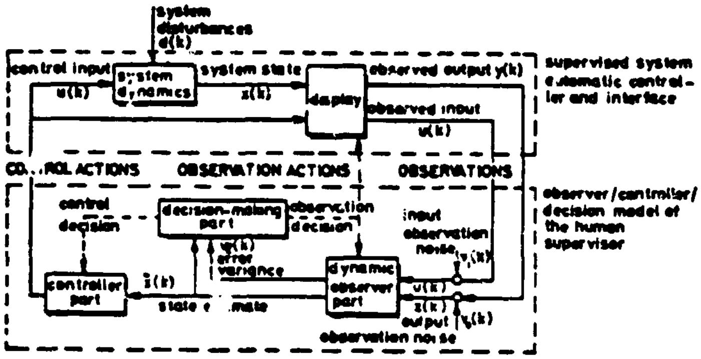
system disturbances d(k)
control input
u(k)
system dynamics
system state
x(k)
display
observed output y(k)
observed input
u(k)
supervised system automatic controller and interface
CONTROL ACTIONS
OBSERVATION ACTIONS
OBSERVATIONS
control decision
decision-making part
observation decision
input observation noise $v_i(k)$
w(k) error variance
controller part
$\hat{x}(k)$
state estimate
dynamic observer part
u(k)
x(k)
output observation noise $v_y(k)$
observer/controller/decision model of the human supervisor

Fig. 1 The model of the human operator

ORI[illegible]
OF P[illegible]TY

The observer part models the observation behavior of the supervisor. Based on the knowledge of the system dynamics, the values of the observed output variables, the noise statistics and the applied inputs on the system, a reconstruction or estimate $\hat{x}(t)$ of the process state and its associated variance $V_{\hat{x}}$ is generated by the observer part. The reconstruction mechanism is modeled by a Kalman predictor algorithm.

The controller part determines the amplitude of the discrete control actions based on the estimated value of the state.

The function of the decision making part is twofold. Using the estimated value of the state and its associated variance, the decision making part determines the instants in time that new observation actions are to be taken as well as the instants in time that a controller action should take place.
The decision making part for the observation actions (D.O.) is modeled by a hyperbolic decision line, whereas the decision making part for the controller actions (D.C.) is modeled as a straight decision line.
See Fig. 2 and 3.

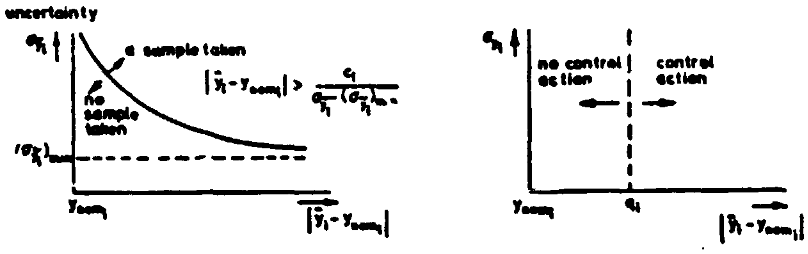

Fig. 2,3 Structure of the Decision Making Part

The parameters are; c_i - the curve parameter of the decision line, $\sigma_{\hat{y}_i min}$ - the minimal accepted uncertainty and q_i - the upper or lower tolerance related to the nominal output value, where i denotes the i-th output variable and $\hat{y}_i$ the estimated output variable.

MODEL HYPOTHESES

For the verification of the model we consider the so-called task variables in relation to the outputs of the model.
The (independent) task variables are:
- o the dynamic of the system
- o the noise parameters
- o the display structure and
- o the supervisory task to be performed

From the behavior of the operator there are quantities which can be measured directly such as:
- o the number of observation actions
- o the number of control actions and
- o the amplitude of the control actions

Since the quantities measured are the observed outputs of the supervisor, they should be related to the structure of the model.

As variations in the display structure can only effect the human pattern recognition and reconstruction of the state, it is postulated that:

o the effect of the task variable "variations of the structure of the display" will be reflected in the number of observation actions and not in the number of controller actions.

It is further postulated that:

o the effect of the task variable "variations of the intensity of the system disturbances" will be reflected in the number of control actions and in an additional number of observation actions.
  It will, however, not be reflected in the mean of amplitudes of the controller actions. See Table 1.

Table 1

	Number of Obs.Act.	Number of Contr.Act.	Amplitude of Contr.Act.
Variations of the intensity of the system disturbances	X	X	
Variations of the display structure	X		

In a later phase hypotheses with regards to the parameters of the three different parts of the model will be postulated and verified.

DESCRIPTION OF THE PROCESS

To verify the model hypotheses a computer simulation of a linear slow responding more or less complex system was developed. We took an example studied by Campbell and Shirley [4] from the Foxboro Company. The setpoint controlled process (utility plant) consists of a boiler, a backpressure turbine and a condensing turbine. The process has three inputs (a high pressure controller, a flow controller of the low pressure steam and a power controller) and three outputs (the pressure of the high pressuresteam, the flow of the low pressure steam and the total amount of electricity produced. See fig. 4.
The process is disturbed by first order filtered white noise.

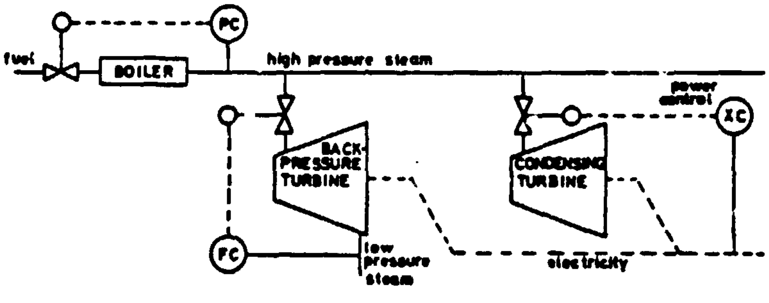

Fig. 4 Structure of the process

EXPERIMENTAL CONDITIONS

The task of the operator is to keep the three digitally displayed outputs within the specified boundaries using one or more of the three setpoint control inputs.
High pressure steam is displayed continuously, the flow and power are displayed on request during 5 seconds.
Four task conditions have been specified.
The system disturbances and the display structure were varied both on two levels, keeping the task to be performed and the system dynamics the same for all experiments.
The conditions are indicated as follows. a_1 b_1, a_1 b_2, a_2 b_1 and a_2 b_2.
a_1 represents a low level of system disturbances and a_2 a high level.
b_1 stands for local alarm which means that the operator knows exactly which output is out of the boundary specified and in what direction.
The actual value of the flow and the power can be obtained by taking a sample. b_2 stands for central alarm. This means that the operator only knows that one or more outputs are beyond the limits. Additional information in terms of the requested samples is required to determine the actual state of the system. It has been assumed before that the supervisor has a perfect internal representation, which means that his behavior should be stationary and that he should not be in a learning phase anymore.
Fig. 5 shows 86 sessions of the total of 123 sessions of 45 minutes with one subject. Due to learning effects only the last nine sessions of each condition have been used to verify the postulated hypotheses.

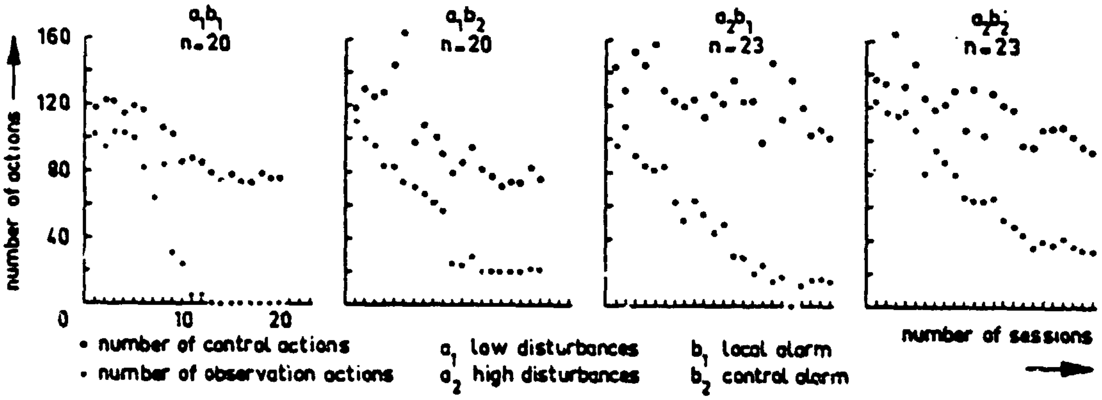

Fig. 5

RESULTS

Both the hypotheses postulated with respect to sampling and with respect to control actions were found to be true. For the results of the statistical analysis of the data we refer to Table 2. The null hypotheses related to the mean μ (number of samples and control actions per run) is tested
H_0: $\mu_1 \neq \mu_2$. Since it is not known whether the two groups to be compared have the same variance, an F-test or analysis of variance of the sample variance is performed. The null hypotheses is now H_0: $\sigma_1^2 = \sigma_2^2$ and a significance level of α = .01 is accepted here.
If the probability [illegible] for the value is greater than α then the null hypotheses H_0:$\sigma_1^2 = \sigma_2^2$ is accepted. The significance of H_0 : $\mu_1 \neq \mu_2$ is then based on the probability value for the pooled variance estimate. If the probability

ORIGINAL PAGE IS
OF POOR QUALITY

for F is less than or equal to α then the null hypotheses $H_0 : \sigma_1^2 = \sigma_2^2$ is rejected. The significance of $H_0 : \mu_1 \neq \mu_2$ is extrapolated from the separate variance estimate.

Table 2 T-TEST

VARIABLE		NUMBER OF CASES	MEAN	STANDARD DEVIATION	STANDARD ERROR	F VALUE	2-TAIL PROB.	POOLED VARIANCE ESTIMATE T VALUE	DEGREES OF FREEDOM	2-TAIL PROB.	SEPARATE VARIANCE ESTIMATE T VALUE	DEGREES OF FREEDOM	2-TAIL PROB.
[illegible]	GROUP [illegible]		[illegible]	[illegible]	[illegible]	2.10	[illegible]	-17.19	16	[illegible]	-17.19	[illegible]	[illegible]
	GROUP [illegible]	9	21.6667	[illegible]	[illegible]								
[illegible]	GROUP [illegible]	9	77.2222	[illegible]	[illegible]	[illegible]	[illegible]	[illegible]	16	[illegible]	[illegible]	[illegible]	[illegible]
	GROUP [illegible]	9	[illegible]	[illegible]	[illegible]								
[illegible]	GROUP [illegible]	9	[illegible]	[illegible]	[illegible]	[illegible]	[illegible]	[illegible]	16	[illegible]	[illegible]	[illegible]	[illegible]
	GROUP [illegible]	9	14.7778	[illegible]	[illegible]								
[illegible]	GROUP [illegible]	9	77.2222	[illegible]	[illegible]	[illegible]	[illegible]	[illegible]	16	[illegible]	[illegible]	[illegible]	[illegible]
	GROUP [illegible]	9	[illegible]	[illegible]	[illegible]								
[illegible]	GROUP [illegible]	9	[illegible]	[illegible]	[illegible]	[illegible]	[illegible]	[illegible]	16	[illegible]	[illegible]	[illegible]	[illegible]
	GROUP [illegible]	9	[illegible]	[illegible]	[illegible]								
[illegible]	GROUP [illegible]	9	[illegible]	[illegible]	[illegible]	[illegible]	[illegible]	[illegible]	16	[illegible]	[illegible]	[illegible]	[illegible]
	GROUP [illegible]	9	[illegible]	[illegible]	[illegible]								
[illegible]	GROUP [illegible]	9	21.6667	[illegible]	[illegible]	[illegible]	[illegible]	[illegible]	16	[illegible]	[illegible]	[illegible]	[illegible]
	GROUP [illegible]	9	14.7778	[illegible]	[illegible]								
[illegible]	GROUP [illegible]	9	[illegible]	[illegible]	[illegible]	[illegible]	[illegible]	[illegible]	16	[illegible]	[illegible]	[illegible]	[illegible]
	GROUP [illegible]	9	[illegible]	[illegible]	[illegible]								
[illegible]	GROUP [illegible]	9	21.6667	[illegible]	[illegible]	12.71	[illegible]	[illegible]	16	[illegible]	[illegible]	[illegible]	[illegible]
	GROUP [illegible]	9	[illegible]	[illegible]	[illegible]								
[illegible]	GROUP [illegible]	9	[illegible]	[illegible]	[illegible]	[illegible]	[illegible]	[illegible]	16	[illegible]	[illegible]	[illegible]	[illegible]
	GROUP [illegible]	9	[illegible]	[illegible]	[illegible]								
[illegible]	GROUP [illegible]	9	14.7778	[illegible]	[illegible]	[illegible]	[illegible]	[illegible]	16	[illegible]	[illegible]	[illegible]	[illegible]
	GROUP [illegible]	9	[illegible]	[illegible]	[illegible]								
[illegible]	GROUP [illegible]	9	[illegible]	[illegible]	[illegible]	[illegible]	[illegible]	[illegible]	16	[illegible]	[illegible]	[illegible]	[illegible]
	GROUP [illegible]	9	[illegible]	[illegible]	[illegible]								

Fig. 6 shows the 99% reliability interval of a T-Student distribution for each of the four conditions.
The same effects have been found on a 95% reliability interval with a less trained subject.
From these results the separate effects of the levels of the two task variables on the behavior of the supervisor are clear.
Comparing Figs. 6 and 7, it also follows that the subject increases his number of control actions when the system is more disturbed, but he does not change the amplitudes of the control.
The average amplitude of the control actions seems to be a fixed quantity based on the system dynamics and the given task; however, these task variables have not been varied during the four conditions.
Using the Analysis of Variance for each input, it also follows that for the given set of measurements no differences in the mean amplitude can be found (See Fig. 7).

We can conclude that changing the display structure does not influence the number of samples. Changing the level of the disturbances does have an

C-7

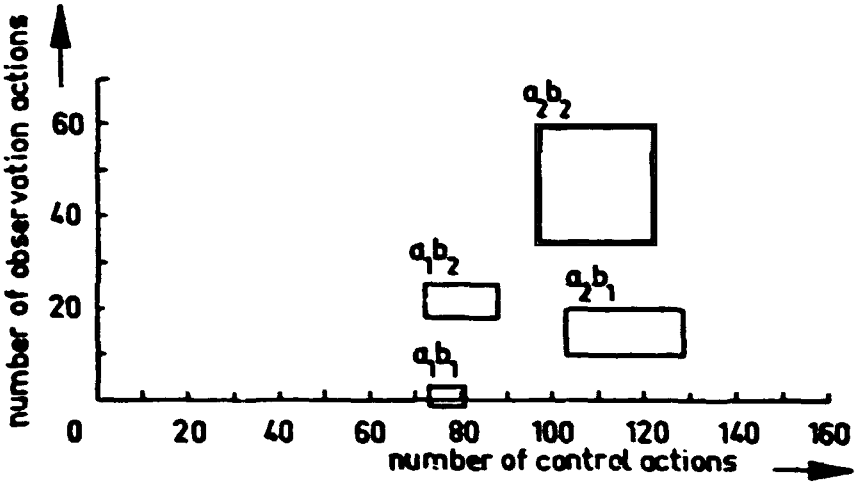

Fig. 6

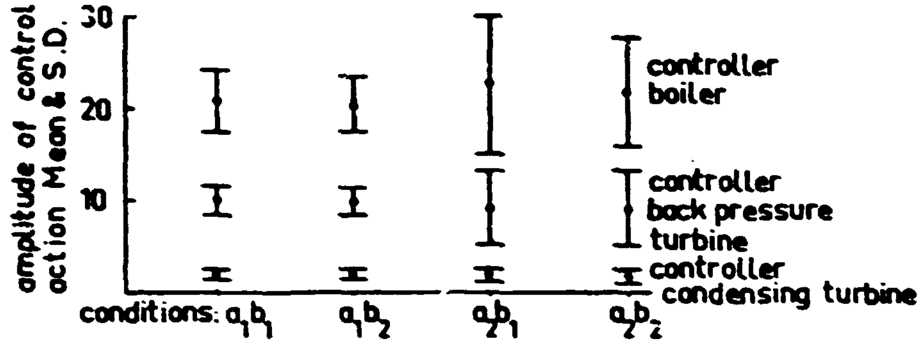

Fig. 7

influence on the sampling behavior and the number of control actions. The mean amplitude will not change for each condition: only some change of the standard deviation due to the disturbances do occur.

FURTHER RESEARCH

In this paper the stated hypotheses were tested and found to be true. In fact the survey dealt with a 2 x 2 x 1 x 1 design. Because the 'task requirements' and the 'system dynamics' have not been changed within the four conditions, we plan to change the task requirements for the next experiments. The boundaries specified will be decreased while keeping the other conditions as before.
On the basis of the structure of the model, new hypotheses have been postulated to relate the parameters of the different parts of the model to the task variables mentioned before.
These model hypotheses are:

- the parameters of the observer part are independent of the supervisory task and are only a function of the dynamics of the system, the structure of the display and the noise parameters.
- the parameters of the controller part are independent of the observation

process and are only a function of the dynamics of the system and the supervisory task.

Table 3 represents the postulated relationship between task variables and the parameters of the different parts of the model. The cross X means dependency.

Table 3

	Obs.P.	D.O.	D.C.	Contr.P.
a) Variations of the system disturbances	x	x		
b) Variations of the display	x	x		
c) Variations of the task requirements			x	x
d) Variations of the system dynamics	x	x	x	x

Next to the the parameter identification, more subjects will be investigated to increase the statistical significance of the results The final part of this results will be dealing with the last task variable mentioned; "the system dynamics". By then a complete 2 x 2 x 2 x 2 experimental design will be accomplished.

REFERENCES

[1] S. Baron and D.L. Kleinman, "The Human as an Optimal Controller and Information Processor", IEEE Trans. Man-Machine Syst., Vol. MMS-10, No. 1, pp. 9-17, March 1969.

[2] D.L. Kleinman, S. Baron, W.H. Levison, "A Control Theoretic Approach to Manned-Vehicle Systems Analysis", IEEE Trans. on Automatic Control, Vol. AC-16, No. 6, pp. 824-832, December 1971.

[3] J.J. Kok, R.A. van Wijk, "Evaluation of models describing human operator control of slowly responding systems", 1978, Dr.-thesis, DUP.

[4] B.D. Campbell, R.S. Shirley, "An Industrial Utility Model for Research in Man-Process Control", Annual Manual 1979.

omit

ORIGINAL PAGE IS
OF POOR QUALITY

EFFECT OF INFERENTIAL MONITORING AND VIGILANCE

Janice J. Wrye and Renwick E. Curry
NASA Ames Research Center, Moffett Field, CA

Advancements in automating man-machine systems will change the role of the human monitor. Many traditional vigilance studies are not broad enough to expose the decision-making processes involved in inferential monitoring of complex vigilance tasks. In order to investigate vigilance problems in modern man-machine systems, a paragigm has been designed to assess both simple and inferential monitoring. The paradigm consists of a simulated heat-regulator system that can be manually or automatically operated. The system's indicators will allow monitors to be aware of system malfunctioning which can be inferred from multiple information sources.

The experimental situation will allow varying degrees of automation in a set of control and monitoring tasks. The tasks will involve detection of malfunctions and varying levels of decision-making to correct the malfunctions. The level of decision-making will depend on the level of automation allocated to the computer or to the human monitor. The first set of experiments will address how decision-making (in terms of reaction time and errors) is affected by task complexity and knowledge of results. Subjects will monitor 1-hour of simple system operation with no inferential task required. The simple monitoring will be a detection task only. They will also monitor 1-hour of system operation requiring operational decision making in a diagnostic task. Three levels of KR will be assigned to three groups; no KR, partial KR, and total KR.

The initial study is designed to provide information about the following questions with respect to operational monitoring tasks:
a) Does performance change, indicated by an increase in number of errors and response time, during a 1-hour inferential monitoring task?
b) Will performance differ between simple detection task and inferential diagnostic task?
c) Does KR have an effect on the number of errors and RT during a 1-hour inferential monitoring task?

Eighteen naive college men will serve as paid volunteers for this study. Each subject will be randomly assigned to one of three groups: no KR, partial KR, and total KR. Analysis of the data will be a design of 2(task complexity) x (feedback) x 6(time segments) analysis of variance with repeated measures on task complexity and time. There will be two sets of experimental data. The first will be the total errors for each temporal block. The second will be the latency of each response. The basic data will be collected by the PDP-12 computer.

N82 34070 D33

EFFECTS OF MOTIVATION ON CAR-FOLLOWING

Tom Bösser

Psychologisches Institut der
Westfälischen Wilhelms-Universität
Schlaunstr.2, D-44 Münster
West-Germany

ABSTRACT. Speed- and distance control by automobile-drivers is described best by linear models when the leading vehicles speed varies randomly and when the driver is motivated to keep a large distance. A car-following experiment required subjects to follow at 'safe' or at 'close' distance. Transfer-characteristics of the driver were extented by 1 octave when following 'closely'. Nonlinear properties of drivers control-movements are assumed to reflect different motivation-dependent control strategies.

INTRODUCTION. The automobile driver's capability to control speed and distance to other cars is of considerable importance for traffic-safety, traffic flow, the usable capacity of the highway-system, and partly determines fuel-consumption. Automatisation of this task can not be expected in the foreseeable future, even then a servo-system must be adapted to existing traffic and thus requires the identification of human control-behaviour in this task.

Investigations of car-following by DREYER (1979) and HARTWICH (1971) showed that driver's control of speed and distance in real and simulated car-following-experiments can be described adequately by

PRECEDING PAGE BLANK NOT FILMED

linear models, where speed-difference between leading and following vehicle and distance are considered to be the inputs to the driver. From observations of driving behaviour under natural conditions on the motorway in an instrumented vehicle we concluded that under these conditions driver's speed-control is predictable only to a small extent by linear describing functions.

This is partly due to the variability of traffic conditions, which require only part of the time to follow a leading vehicle. Also distances between cars on average are much shorter than those observed in other experimental investigations, which excludes the neccessity to use high-frequency control-behaviour in order to avoid collisions. Linear models of car-following seem to describe driver's behaviour best, when the speed variations of the leading vehicle can not be predicted from traffic further ahead or from the course of the road, which under ordinary driving conditions is possible most of the time. Linear models seem to be deficient in that they can not represent responses to step-like changes in the input variables, which occur rarely, but are of great importance for safe driving. Secondly they do not represent the fact that performance-criteria for speed- and distance control in driving are determined by the driver's motivational state, where safety considerations, haste, comfort, risk-taking and cost are considered and an optimal course is determined.

Manual control experiments and control of more expensive vehicles like airplanes differ from driving an automobile in that motivation can be controlled and held constant in these situations. The aim of the investigation reported here is to explore the influence of motivational processes on car-following performance.

PROCEDURE. Experiments were carried out in an average saloon-car which was instrumented to allowed recording of speed, throttleposition, and other variables not considered here, on PCM-tape. In addition the traffic-situation ahead was recorded on video-tape, which was used to determine distance to the leading vehicle by an online photometric technique. For analysis data were filtered and stored with a sampling rate of 2.93 Hz.

A car-following experiment was conducted on an infrequently used part of the motorway during times of low traffic. The leading car varied its speed between 70 and 90 km/h according to a 5-level PRBS with a length of 63 intervals and a clock-frequency of 0.2 Hz, thus representing a frequency range of .1 to .006 Hz.

The properties of this test-sequences were selected to allow identification of behaviour in the high-frequency-range. Eight subjects (experienced drivers) followed this course four times, twice with the instruction to follow at a 'safe' distance and twice at 'close' distance.

Data obtained were analyzed in the frequency-domain with FFT-Procedures (BENDAT & PIERSOL, 1971).

RESULTS. The functions shown are averages of 8 subjects. Distance between cars is much lower under 'close' condition (Fig. 1. Note that measurement of short distances was limited by the field of view of the video camera, thus zero-distance represents a distance ⩽ 3m.) Power spectral density of distance is reduced accordingly over the whole frequency-range represented in the signal under the 'close' condition (Fig. 2). Power spectral density of speed shows that the 'close' condition introduces more high-frequency variance and reduces low-frequency variance (Fig. 3). Throttle position, which is the essential output-variable of the driver for speed- and distance-control, shows a probability-distribution with a lower peak and more frequent occurrence of extreme throttle-positions (Fig. 4), indicating maximum-force control and a time-optimal strategy. Power spectrum of throttle position (Fig. 5) shows that high-frequency-power is increased by the instruction to follow closely. Coherence between the distance to the leading vehicle - the essential input variable for the driver - and throttle position shows that the transfer-characteristics of the driver are extended through the instruction to follow at close distance by approximately one octave (Fig. 6).

DISCUSSION. Results demonstrate that human control-behaviour depends on motivation, which was varied in this case by instructing the driver. In the present experiments the transfer-characteristics of the driver extended to a higher frequency-range than was found in other investigations. This can be assumed to be due to the fact that in these investigations different input-signals to the driver were generated, where through preview the driver was able to control speed adequately by avoiding the neccessity for high-frequency control behaviour. This was not possible in the present case, as speed variations of the leading vehicle were not predictable.

Distances between vehicles under natural driving conditions are more similar to distances observed under the 'close' condition. This can also be attributed to the fact that normal traffic-conditions allow prediction of speed-changes ahead and thus allow drivers to be confident of their ability to control these short distances without neccessity of high-frequency control-behaviour.

Whereas in the low-frequency range driver's control movements can be approximated by linear models, a large proportion of the high-frequency power contained in the signals recorded is not related in a linear fashion to the input signal. This may be due to nonlinear control-strategies, e.g. 'bang-bang'-control or adaptive processes like those proposed by COSTELLO (1968). It is highly plausible to assume a nonlinear asymmetric weighting of the error in the control of distance between vehicles - a large distance does not lead to undesirable consequences, short distance however represents a highly dangerous situation and may introduce a nonlinear strategy to avoid this situation.

Although the instruction to follow 'closely' introduces high-frequency power into the throttle-signal, a considerable proportion is contained in the signal under the 'safe' conditions. The throttle-signal was predicted from the estimated nonparametric transfer-function and the distance to the leading car. Fig. 7 shows this for one subject under 'close' and 'safe' following. It can be seen that high-frequency variations under the 'safe' condition are present, but not related linearly to distance. In comparison under the 'close' conditions these high-frequency actions are highly correlated with the input-signal, as is represented by the coherence-function. This indicates that the change in control-activity can be described partly by the synchronisation of the high-frequency control movements to the input-signal. All subjects reported driving under the 'close' condition to be highly strainful and much more difficult than normal driving. We can therefore conclude hypothetically, that drivers adjust their control-activities to the input-signals in such a way as to make high-frequency control unnecessary. This can be achieved by increasing the set point for distance to the leading vehicle and giving low weight to deviations of distance from setpoint. Nonlinear properties of control behaviour with 'safe' distance may reflect a control strategy reducing workload, whereas nonlinear properties of 'close' following represent a time-optimal strategy.

Motivational variables can be assumed to limit the adaptability of the driver to traffic-conditions and to properties of the vehicle and the road beyond the limitations represented by the perceptual-motor system.

Bendat, J.S., Piersol, A.G.
Random Data: Analysis and Measurement Procedures, New York: Wiley, 1971

Costello, R.G.
The Surge Model of the Well-Trained Human Operator in Simple Manual Control. IEEE Trans. Man-Machine Systems, Vol. MMS-9 (1968), pp. 2-9

Dreyer, W.
Längsdynamische Untersuchung des Regelkreises Fahrer-Fahrzeug.
Bericht Nr. 525 des Instituts für Fahrzeugtechnik, TU Braunschweig 1979

Hartwich, E.
Längsdynamik und Folgebewegung des Straßenfahrzeugs und ihr Einfluß auf das Verhalten der Fahrzeugschlange, Dissertation, Darmstadt 1971

M. Artmann, L. Cremers, A. Isfort, E.M. Melchior and H. Zeissig participated at various stages of the investigation. This work was supported by Deutsche Forschungsgemeinschaft (Bo 642/1,2). Technical support from Audi-NSU A.G., Volkswagen A.G. and Opel A.G. is gratefully acknowledged.

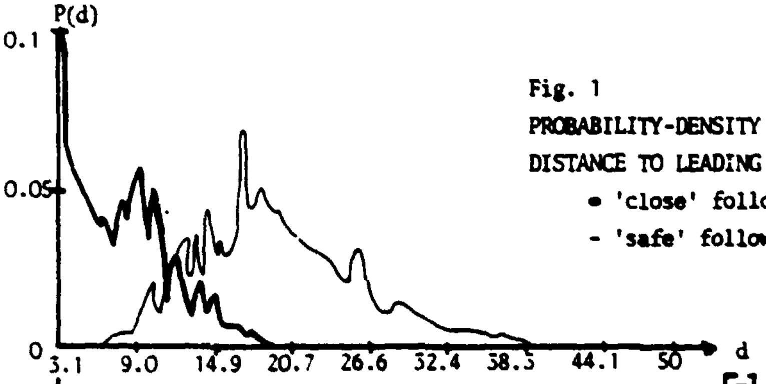

Fig. 1
PROBABILITY-DENSITY
DISTANCE TO LEADING VEHICLE
- ● 'close' following
- – 'safe' following

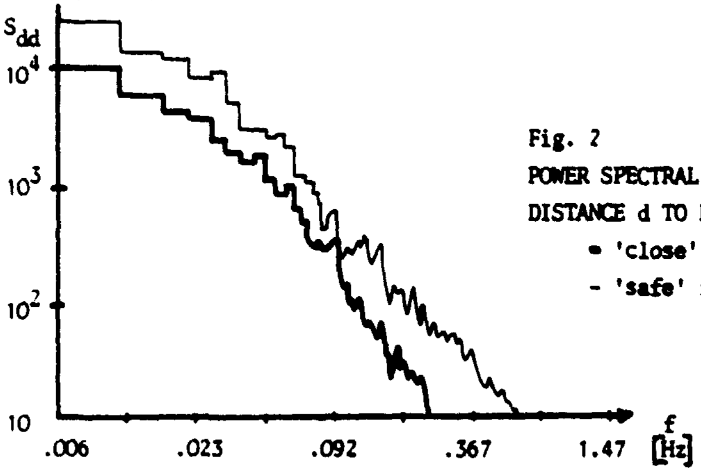

Fig. 2
POWER SPECTRAL DENSITY
DISTANCE d TO LEADING VEHICLE
- ● 'close' following
- – 'safe' following

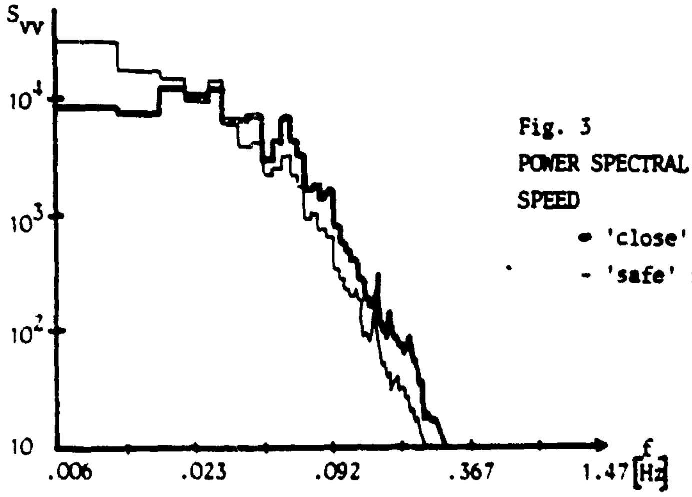

Fig. 3
POWER SPECTRAL DENSITY
SPEED
- ● 'close' following
- – 'safe' following

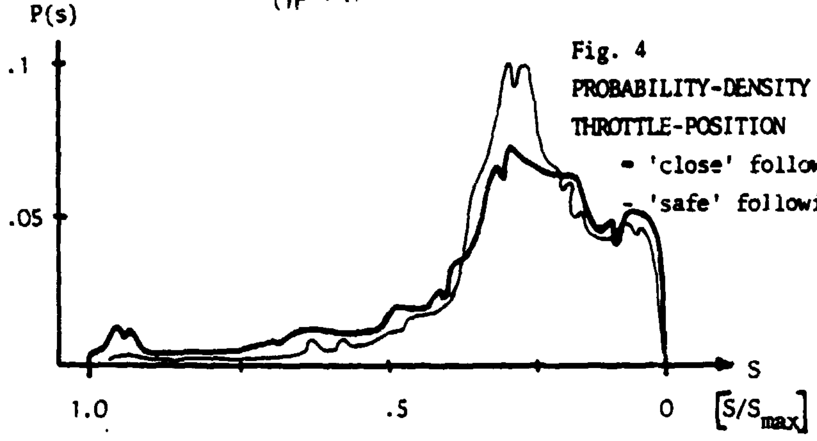

Fig. 4
PROBABILITY-DENSITY
THROTTLE-POSITION
- 'close' following
- 'safe' following

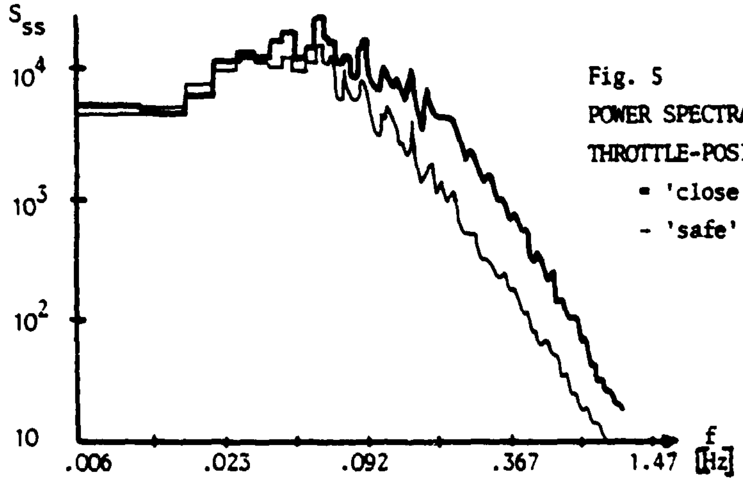

Fig. 5
POWER SPECTRAL DENSITY
THROTTLE-POSITION
- 'close' following
- 'safe' following

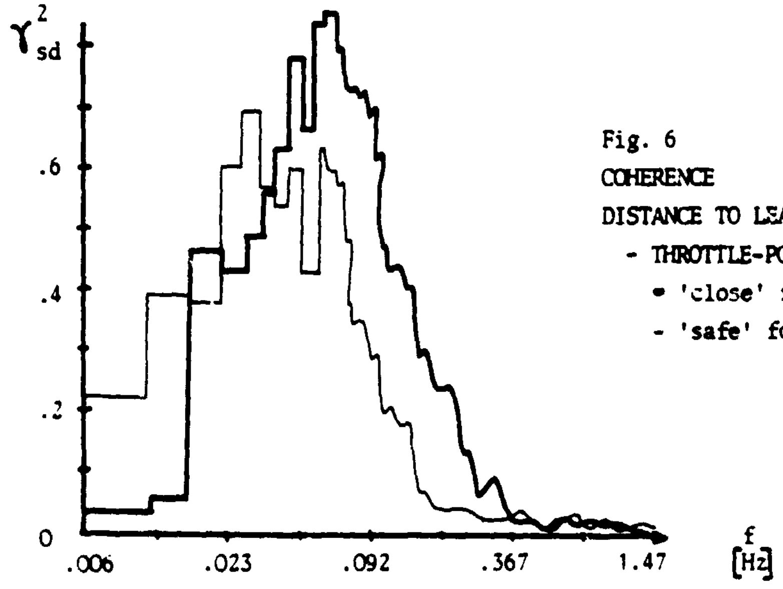

Fig. 6
COHERENCE
DISTANCE TO LEADING VEHICLE
- THROTTLE-POSITION
- 'close' following
- 'safe' following

ORIGINAL PAGE IS
OF POOR QUALITY

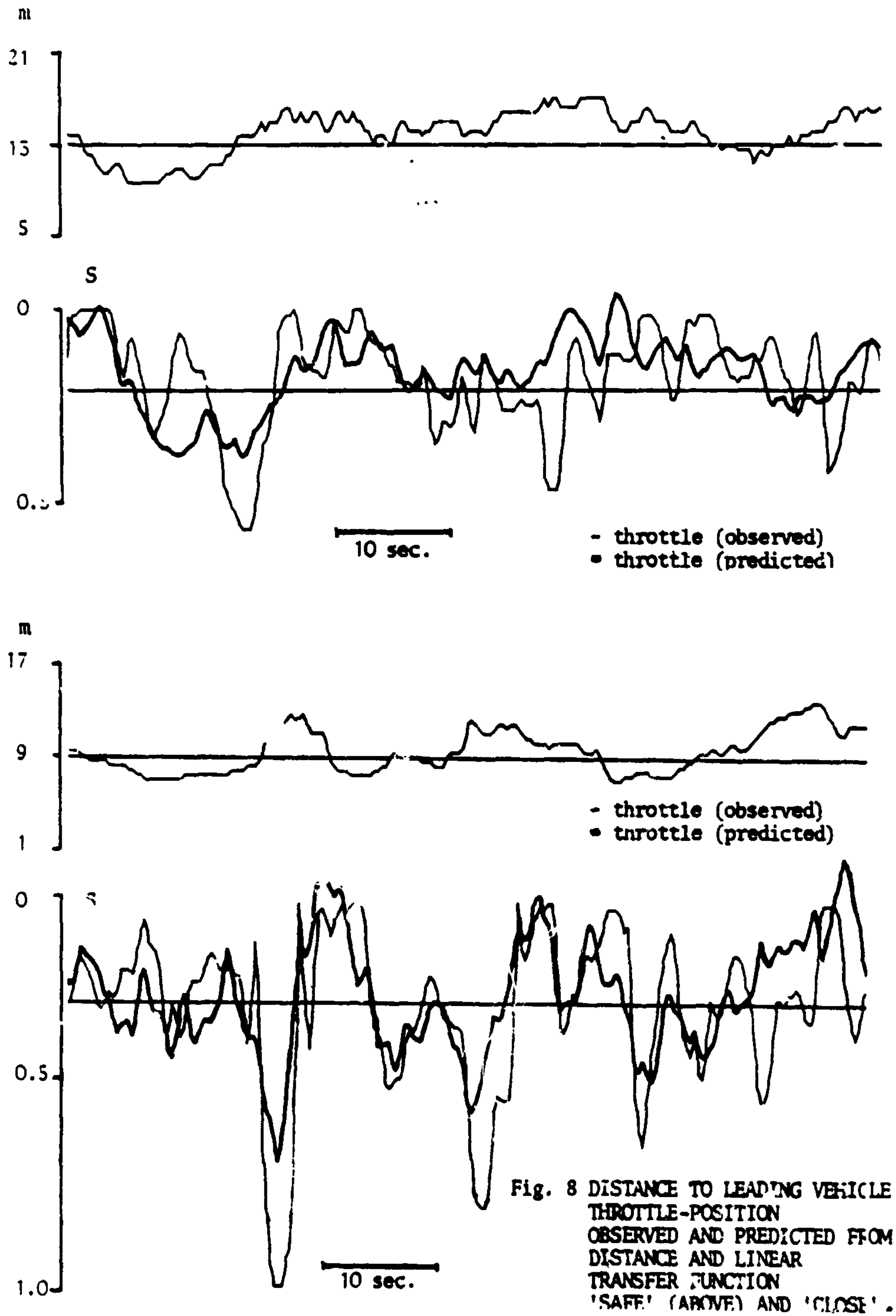

Fig. 8 DISTANCE TO LEADING VEHICLE
THROTTLE-POSITION
OBSERVED AND PREDICTED FROM
DISTANCE AND LINEAR
TRANSFER FUNCTION
'SAFE' (ABOVE) AND 'CLOSE'
(BELOW) FOLLOWING

N82 34071 -34

LEVELS OF STEERING CONTROL: REPRODUCTION OF STEERING-WHEEL MOVEMENTS

Hans Godthelp
Institute for Perception TNO
Soesterberg
The Netherlands

ABSTRACT

A schematic description of the steering control process is presented. It is shown that this process can be described in terms of levels of control. Level of control will depend on driver's skill in making use of 'clever' strategies which may be related to knowledge about the path to follow (input) and/or the vehicle under control. This knowledge may be referred to as an internal model of a particular task element. Internal information, as derived from these internal models will probably be used together with proprioceptive feedback. It is hypothesized that the efficiency of the higher levels of control will be dependent on the accuracy of both the internal and proprioceptive information. Based on this research philosophy a series of experiments is carried out. Two preliminary experiments were done in order to analyse subjects' ability to reproduce steering-wheel positions and movements without visual feedback. Steering-wheel angle amplitude, steering force and movement frequency were involved as independant variables.

1. INTRODUCTION

The design of a safe traffic system requires a good understanding of the elements in the system. In automobile driving these elements are the driver, the vehicle and the roadway environment. The latter two elements serve as the system to be controlled by the driver. Vehicle and environmental characteristics can be given in mathematical terms and the understanding of both these elements is fairly good. However, optimization of vehicle and environmental characteristics can only be made given sufficient knowledge about driver's capabilities. It is useful to distinguish three main aspects of a driver's task: navigation, guidance and vehicle control. Navigation deals with route selection. Guidance involves the processing of information on other vehicle motions, obstacle location, road geometry etc. leading to the desired vehicle speed and path. Finally, vehicle control implies the processes of speed and path (or steering-) control itself. We will mainly pay attention to the driver's capabilities in steering control.

Steering control tasks can be described in terms of levels of control (Krendel and McRuer[1], Pew[2], McRuer et al.[3], Donges[4]). Levels of control are related to the use of more or less 'clever' strategies. Strategies could be of a perceptual nature, for example when preview is used. Strategies could also be of a cognitive origin when drivers use internal representations or models about the vehicle under control and/or about environmental properties such as road geometry.

The diagram in Fig. 1 gives a hypothesized, schematic description of the steering control process (see also Krendel and McRuer[1]). Drivers estimation I about the input or path commands will be based on visually perceived, external information i_e and/or internal input information i_i which is derived from the Internal Model about the Input characteristics IMI. External input information may contain preview. Internal information will also allow the driver to make predictions about i.

Drivers estimation 0 about the output or vehicle motions o will be based on visually perceived, external information o_e and/or on internal input information o_i. This latter type of information will be a result of an interplay between manual feedback information m and driver's Internal Model about the Vehicle (V) characterictics IMV_o.

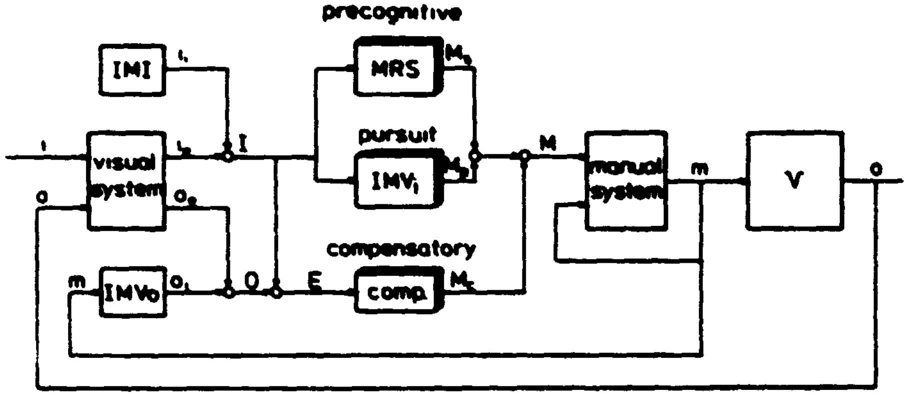

Fig. 1 Schematic description of the steering control process.

It is hypothesized that level of control in a particular steering task will mainly be governed by the availability of the above-mentioned types of information. At the highest, precognitive level drivers make use of their experience with the same type of task conditions, i.e. their internal models about the input and the vehicle properties. This experience will lead to the development of a Motor Response Scheme (MRS) which stores the specifications M_s of the manual control actions that should be made under the particular conditions. Although Schmidt[5] limits the validity of his scheme theory to the learning of discrete movements it is assumed here that comparable principles will play a role in continuous tasks. When the predictability of I is limited - due to the structure of i_e or due to absence of IMI - drivers may still use their knowledge about the vehicle characteristics. Control will take place at the pursuit level under these circumstances. Here drivers will generate desired manual control actions M_p using I (with its reduced predictability) as input and relying on the internal model about the dynamics of the vehicle under control (IMV_i) as a means of weighting between I and M_p.

It may be hypothesized that drivers primarily will generate control actions m based on M_s or M_p. Only when these control modes lead to vehicle motions O that - compared to I - show an error E which is beyond driver's criterion, the compensatory level of control comes into operation. It is at this lowest level of control that drivers generate corrections M_c on the desired manual control actions.

It is suggested that the attentional demands of a particular steering task depend on level of control. At the highest level steering is as an automatic or

'open loop' process, whereas at the lower levels steering is more 'closed loop' or under conscious control. Compensatory steering has been studied in many tasks and control behaviour at this level is rather well known (Pew[2], McRuer et al.[3]). The characteristics of the pursuit level in steering an automobile were illustrated by McRuer et al.[3] and Donges[4]. Further description especially with regard to the relative importance of the pursuit and compensatory level are necessary.
Very little is known about steering tasks in which motor programs are used. "It is at this level that our understanding and models are most incomplete" (Pew[2]).

In the present study the precognitive and pursuit levels of control will be subjected to further analysis. Special attention will be given to proprioceptive feedback, thereby considering the role of steering force or 'control feel' in particular. Few quantitative data are available on this latter point and it is expected that the described model will give the opportunity to quantify the role of control feel as a part of the proprioceptive information on m. Related to this is the question of the relative importance of visual and proprioceptive feedback at the different levels of control. Can the interplay between the proprioceptive system and the MRS and IMV-blocks reduce the load put on the visual system? Conversely it can be questioned how the amount of visual attention required for a particular steering task can be influenced by selecting the proper input and/or vehicle characteristics.
Let us again consider the diagram of Fig. 1. In the process of transferring inputs i into manual control actions m, three major subprocesses are - hypothetically - distinguished:

1. On the perceptual side there is the transformation from input i and output o into the estimation I and O.
2. These estimations should be translated into the specifications for the desired manual control actions M. Specifications may involve manual force, position, velocity (timing) and acceleration. At this central part of the process the MRS and/or IMV_i blocks will play a role.
3. Finally on the motor side, the transformation from desired (M) to actual (m) control action takes place. As shown in Fig. 1 it is suggested that a proprioceptive feedback path is in operation at this point, making compensatory corrections on the transformation from M to m.

The operators' skill in each of these subprocesses will ultimately determine the efficiency of the precognitive and/or pursuit level of control.
Experiments under way now deal with tracking predictable and unpredictable inputs under partially occluded conditions. In this way the degree to which internal and external information are available (and thus level of control) is experimentally varied.
The present paper describes two preliminary experiments which were done in order to get quantitative data about subjects' ability to transform desired (M) to actual (m) manual control actions. In a reproduction task subjects reproduced discrete and continuous steering-wheel movements. These relatively simple tasks were chosen to get a first impression of the influence of the following independent variables: steering-wheel movement amplitude, frequency and steering force.

2. EXPERIMENT I: REPRODUCTION OF DISCRETE STEERING-WHEEL MOVEMENTS

2.1 Background

Experiment I was designed to collect quantitative data about the M to m transformation in a discrete positioning task.
In a reproduction experiment subjects learned a discrete steering-wheel move-

ment and the ability to reproduce this movement was measured. As indicated in the introduction the results of this M to a transformation might be useful in evaluating the role of the precognitive and pursuit levels of control in steering tasks.

Literature shows a number of experiments in which subjects had to reproduce hand/arm movements under constrained conditions. The purpose of most of these experiments was to analyze the function of several types of feedback cues. A distinction can be made between position, amplitude, time, velocity and force as components of individual representation of a movement. Gundry[6] illustrated that with long (in terms of distance) movements subjects use mainly position information, while with short movements amplitude (time x velocity) information becomes more pronounced. Adams et al.[7] analyzed the relative importance of visual and proprioceptive (force) feedback in learning a discrete manual movement. In their experiment the role of the force cue as a component of subject's skill in reproduction was illustrated. However, it appeared that the efficiency of this feedback cues might be attenuated when learning takes place with visual and proprioceptive feedback combined. The present experiment was designed such that the effect of movement length and steering force on the accuracy of movement reproduction could be evaluated.

2.2 Method

2.2.1 *Subjects*

Twelve male subjects (Ss) participated in the experiment, all of them university students. Ss ranged in age from 20 to 34 years. All Ss had their driving license for at least two years. All Ss were right-handed, although three subjects indicated that this priority was not very pronounced.

2.2.2 *Instrumentation*

The experiment was carried out in the mock-up of the driving simulator of the Institute for Perception. This mock-up is a Volvo 144 with its original steering wheel with a 0.22 m radius. Spokes are mounted in the wheel at 56.5 degrees to the left and to the right from the axis connecting the upper and lowest point of the wheel. The angle between the steering-wheel plane and the vertical axis through the centre of the wheel is 15 degrees. The steering wheel axis is connected with a potentiometer which measures the steering-wheel angle continuously. Steering force is generated by means of an electric torque motor, Axem MV19, which is connected with the steering wheel axis by a gearbelt drive.

2.2.3 *Experimental conditions*

In a within-subjects design, Ss reproduced four steering-wheel positions. The positions were 30° to the left ($\delta_s = -30^\circ$) and 10°, 30° and 50° to the right ($\delta_s = 10^\circ, 30^\circ, 50^\circ$). The movements had to be reproduced in combination with three steering-wheel rim force levels i.e. 0 N, 7.5 N and 15 N, giving a total number of 12 movement conditions. For the steering-force conditions the relation between steering-wheel angle and steering force was linear, i.e. the wheel was spring-centered.

2.2.4 *Procedure*

Subjects were blindfolded during the experiment. The seat was adjusted so that Ss could comfortably hold the steering wheel with their arms slightly bent. Ss were instructed to hold the steering wheel such that their thumbs rested on the upper left and right spokes.

PRECEDING PAGE BLANK NOT FILMED

The experiment took six days with two Ss participating on each day. Each day was divided in 24 blocks. The two Ss alternatively performed a block. In a block the same movement was presented and reproduced for 40 consecutive trials. Sequence of movement conditions was randomized over Ss. In all conditions the centre position of the steering wheel (δ_s = 0°) served as the starting point. In each trial S actively moved the steering wheel to a stimulus position marked by an auditory signal. Actually, the signal marked an area of plus and minus ½° around the stimulus angle. Then Ss moved the steering wheel back to the starting position which was marked by a stop. Next to this stimulus presentation Ss were required to reproduce the movement as accurately as possible without the aid of the warning signal. Thus one trial consisted of a criterion (or *stimulus*) movement and a subsequent reproduction (or *response*) movement. A block of 40 trials of a particular movement condition lasted about 15 min.

2.2.5 *Data analysis*

Both stimulus and response angle were recorded. Means and standard deviations for the stimulus and response angles as well as the algebraic error were calculated over the last 25 trials of each block. The difference between stimulus and response within a trial was taken as algebraic error. Performance on the first 15 trials was not taken into the final analysis in order to overcome habituation and/or transfer effects and for the sake of correspondence with the data analysis of experiment II. Differences in means and standard deviations were tested by analysis of variance (ANOVA).

2.3 Results

Results showed no differences between the 30° movement to the left and the right. Therefore, only the results for the rightward movement will be discussed, see Fig. 2. The general overshoot effect for the means turned out to be significant ($p<0.01$). Analyzing the algebraic errors it turned out that the tendency exists for the overshoot effect to be about equal for the 30° and 50° movements and less for the 10° movement. An ANOVA on the algebraic errors indicated that the interaction, steering-wheel angle x steering force, was not significant. However, when only the 10° movement conditions were considered a significant effect ($p<0.05$) of steering force was found, indicating an increased overshoot tendency with the greatest steering force.

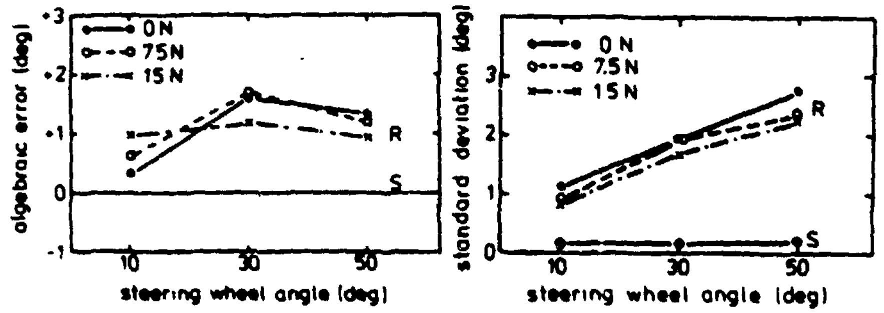

Fig. 2 Means and standard deviations of the stimulus (S) and response (R) movements for the movement conditions in Experiment I.

Fig. 2 also gives the variation of the standard deviations as a function of movement condition. For the responses the increase of the SD with steering angle was significant ($p<0.01$). Besides, a significant overall effect of steering force ($p<0.01$) indicates that standard deviations in responses decrease when steering force is available.

2.4 Discussion

The purpose of experiment I was to measure the effect of movement length and steering force on performance in reproduction. Subjects' performance during reproduction should be considered as a process of generating a control action m thereby using the desired action M as a reference. Therefore the reproduction data give an overall description of the M to m transformation as well as the accuracy of M. The results show a small but significant overshoot effect. The overall dependancy on movement condition of this effect was not significant. Only at the 10° movements, steering force resulted in a small increase of the overhoot tendency as compared with the no steering force condition. Obviously, the overshoot tendency in steering-force reproduction, as found before (Pepper and Herman[8]) is of most relevance with the shortest movement' length, i.e. with the largest steering force - steering-wheel angle gradient. As stated in par. 2.1 it may be expected that with short movement lengths control of movement velocity is very important. The steering force effect with short movement reproduction suggests that steering force leads to an increase in movement velocity. With regard to reproduction accuracy the data on variability in reproduction are of great importance. Both steering-wheel angle (movement length) and steerance. Standard deviations show a remarkable increase over the range of steering-wheel angles taken into consideration. However, this increase in response variability with steering-angle amplitude is less than proportional. The availability of steering force as an additional cue proved to diminish response variability. The relative importance of this effect is highest with the small steering-wheel angle. The process underlying the steering force effect will have its origin in a combination of movement length and steering force effects. Further experiments are needed to give detailed explanations.

The effects of steering-wheel angle and steering force as illustrated here might be of importance when considering the efficiency of the precognitive and pursuit level of control in continuous steering tasks. As a step from discrete towards continuous tasks an experiment will be discussed now in which reproduction of continuous movements was studied.

3. EXPERIMENT II: REPRODUCTION OF CONTINUOUS STEERING-WHEEL MOVEMENTS

3.1 Background

Experiment II was carried out in order to analyze the M to m transformation in a continuous task. Ss learned an isolated sine wave shaped movement with visual input (stimulus). Ss' ability in reproducing this movement (response) under occluded conditions was analyzed. Steering-wheel angle amplitude, steering force and steering-wheel movements frequency were taken as the independent variables. Response behaviour will again depend on the accuracy of M and that of the transfer from desired (M) to actual (m) control actions. Velocity and/or timing errors could also play a role.

ORIGINAL PAGE IS
OF POOR QUALITY

Vossius[9] analyzed timing aspects of precognitive control under occluded conditions. Ss learned a continuous movement pattern under visual pursuit conditions and reproduced the movement with 'lights out'. The 'open loop' generated movement pattern lasted about 10% longer than the stimulus movement. The question remained whether this timing-overshoot effect is related to:

1. correct movement velocity/position overshoot or
2. movement velocity undershoot/correct positioning.

Experiment II should give more data on this point.

In 'conventional' sine-wave tracking experiments it has been illustrated (Pew et al.[10], Magdaleno et al.[11]) that below frequencies of 0.5 Hz error detection and correction mechanisms play an important role, while at higher frequencies tracking behaviour becomes more and more autonomous i.e. with the aid of pattern-generation mechanisms. Although both frequency and movement amplitude (together resulting in a specific movement velocity) will be of importance, it may be expected that these phenomena will affect precognitive control. As a consequence it may be suggested that in 'rapid' movements the loss of visual guidance (occlusion) will be less detrimental than in slow movements. Besides, it may be expected that the role of the proprioceptive system in the overall accuracy of responses will be limited in the more rapid movements. Consequently, the availability of an additional cue like steering force could be most effective in slow movements. Whether this suggestion is valid will, of course, depend on the role of steering force in rapid movements. From a perceptual point of view this role may be limited. However, the functioning of steering force in rapid movements is largely unknown and steering forces could have a stabilizing effect on the execution of this type of movements.

3.2 Method

3.2.1 *Subjects*

Twenty-four male Ss participated in the experiment. All of them were university students. Ss ranged in age from 20 to 30 years. All Ss had their driving license for at least two years. None of them took part in Experiment I. All Ss were right-handed, although four Ss indicated that this priority was not very pronounced.

3.2.2 *Instrumentation*

The experiments were carried out in the same mock-up as used in Experiment I. As stimulus movement a visual pursuit tracking task was used. Visual presentations were made with the aid of a TV projector which was situated above the car. Two vertical lines, were projected on a screen situated at 2.90 m in front of Ss' head position. The upper vertical line served as the target while the lower was controlled by the S. The lines were projected just above and below Ss' eye height, this latter height being 1.20 m. The height of the vertical lines was 19 cm with an interspace of 2 cm. Line width was 3.5 cm. The gain between Ss' cursor and steering-wheel angle was 1.12 cm lateral displacement (0.22 degrees of visual angle) per degree of steering-wheel angle.

3.2.3 *Experimental conditions*

In a partly within- partly between-subjects design Ss reproduced six steering-wheel movements. The movement pattern was based on a sine wave with a modification at the start and end of the movement. Fig. 3a shows the movement pattern described in terms of steering-wheel angle amplitude SA and frequency F. The

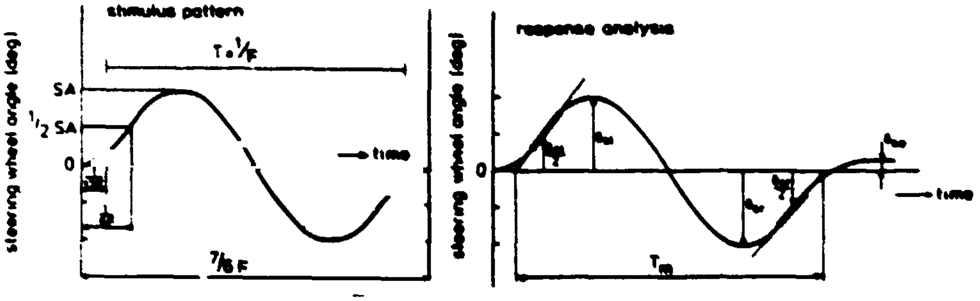

Fig. 3 Stimulus pattern and response analysis for movements in Experiment II.
SA = steering-wheel angle amplitude;
F = frequency (Hz);
ω = frequency (rad/sec);
T_m = calculated movement time (s)

Stimulus pattern can be described as:

$0 < t < 1/6F\ :\ \delta_s = SA\ (1 - \cos \omega t)$
$1/6F < t < 1/F:\ \delta_s = SA \sin (\omega t - \pi/6)$
$1/F < t < 7/6F:\ \delta_s = SA\ \{\cos(\omega t - \pi/3) - 1\}$

first part of the movement was to the left. Begin and end modifications were made in order to have a smooth movement pattern. Three amplitudes i.e. 10°, 30° and 50° and two frequencies i.e. 0.2 Hz (0.4 π rad/s) and 0.5 Hz (π rad/s) were taken into consideration, giving a total number of six steering-wheel movement patterns. Durations of the 0.2 Hz and 0.5 Hz movements were 5⅚ sec and 2⅓ sec respectively. Frequency served as the between-subjects variable so that 12 Ss reproduced the 0.2 Hz movements, while the other 12 Ss reproduced the 0.5 Hz movements. All of the movement patterns were reproduced at each of three steering-wheel rim force levels i.e. 0 N, 7.5 N and 15 N. As in Experiment I the relation between steering force and steering-wheel angle was linear. Steering-wheel angle amplitude and steering force were used again as the within-subject variables.

3.2.4 *Procedure*

Ss' seat and handgrip were adjusted as in Experiment I. The experiment took 12 days with the 0.2 Hz movements carried out in the first six days and the 0.5 Hz movements on the last six days. To Ss participated per day. Each day was divided into 18 blocks. The two Ss alternatively performed a block. In a block the same movement was presented and reproduced for 40 consecutive trials. Sequence of movement conditions was randomized over Ss for the within-subjects part of the experimental design. Pursuit tracking of the movement pattern served as the *stimulus* phase of each trial. The starting position of both the target line and Ss' cursor were in correspondence with the centre position of the steering wheel. The starting moment of the target movement could be anticipated with the aid of a warning signal.
This signal was a light spot that was projected on the screen at 20 cm to the right of the target line. Before the start of the target movement this spot moved to the left (20 cm/sec). The target movement started as soon as the light

spot touched the target line. After tracking the stimulus movement Ss had to close their eyes and reproduce the movement as accurately as possible without the aid of visual feedback. After this *response* movement Ss released the steering wheel. Then the steering wheel was set in the starting position again by the experimenter. Thus, Ss did not get feedback about the terminal position of the response movement. A block of 40 trials was carried out in about 15 min and 10 min for the 0.2 Hz and 0.5 Hz movements respectively.

3.2.5 *Data analysis*

Both stimulus and response movements were recorded continuously with a sample rate of 105 samples for each movement. Means and standard deviations were calculated for movement-amplitude errors to the left (δ_{sl}), to the right (δ_{sr}) and at the end of the movement (δ_{se}), both for the stimulus and response movement (Fig. 3b). Algebraic error between actual movement amplitude and ideal movement amplitude was taken as error score. Timing accuracy was measured by determining the movement time T_n, for which the start and end of each movement were calculated by way of a least square fit, thereby constructing a regression line through the eight data points surrounding the point $\delta_s = \frac{1}{2}\delta_{sl}$ (start) and $\delta_s = \frac{1}{2}\delta_{sr}$ (end) (see Fig. 3b). Timing accuracy was calculated in relation with the same type of movement time of the 'ideal movement. Therefore timing accuracy is presented in terms of percents too slow or too fast. Means and standard deviations were calculated for these percentages as well.
Performance under stimulus conditions was measured by determining the integrated error score during pursuit tracking. An evaluation of these data indicated that most of the habituating, learning and/or transfer effects occurred during the first 15 trials of each block. For that reason means and standard deviations of amplitude and timing accuracy were calculated over the last 25 trials of each block. Differences in means and standard deviations were again tested on their statistical significance by ANOVA.

3.3 Results

As shown in Table I the primary part of the movement (to the left) has a remarkable overshoot tendency ($p<0.01$) A SR x SA[*] interaction ($p<0.05$) points to the fact that the overshoot effect is less pronounced for the 10° movement conditions. In the second part of the movement (to the right) the overshoot effect is less (0.2 Hz condition) or even disappeared (0.5 Hz condition). In the latter condition an undershoot effect can be noted for the 50° movement condition. Steering force does not heavily influence the overshoot/undershoot effect. Only in the 0.2 Hz condition the steering-force level of 15 N tends to result in less overshoot as compared with the 0 N condition.

The standard deviations of the movement amplitudes show more or less the same effects for the movement parts to the left and the right. Standard deviations are highly dependent on movement amplitude with the largest deviations for the largest movement amplitudes (see Fig. 4). The F x SA x SR interaction indicates that for the 0.2 Hz condition the slopes of the S and R curves differ significantly ($p<0.01$), whereas for the 0.5 Hz condition the S and R curves are rather parallel. The availability of steering force leads to a decrease in amplitude standard deviations. For the movement to the left this effect holds for both the stimulus and response movement. For the movement to the right steering

---

[*] SR = stimulus response
SA = steering-wheel angle amplitude
SF = steering force
F = frequency

ORIGINAL PAGE IS
OF POOR QUALITY

Table I Mean algebraic movement-amplitude error for the movement conditions in Experiment II (l = leftward, r = rightward part of the movement, overshoot positive).

Movement amplitude (deg.)	Force amplitude (N)	0.2 Hz				0.5 Hz			
		l		r		l		r	
		S	R	S	R	S	R	S	R
10°	0	0.45	3.06	0.27	1.69	0.32	2.80	0.33	0.96
	7.5	0.29	4.13	0.19	2.95	0.11	3.04	0.07	1.61
	15	0.14	2.89	-0.03	1.37	0.42	4.16	0.06	1.53
30°	0	0.22	6.06	0.11	3.22	-0.02	4.30	0.01	-0.60
	7.5	0.02	5.83	-0.19	1.57	-0.63	4.15	-0.43	0.57
	15	-0.05	5.21	-0.20	1.50	-0.46	4.70	-0.36	1.05
50°	0	-0.43	7.82	0.09	5.65	-1.17	4.16	-0.40	-0.86
	7.5	-0.44	5.86	-0.11	3.87	-1.38	1.94	-0.88	-4.76
	15	-0.39	3.72	-0.40	2.27	-1.61	2.16	-0.85	-0.53

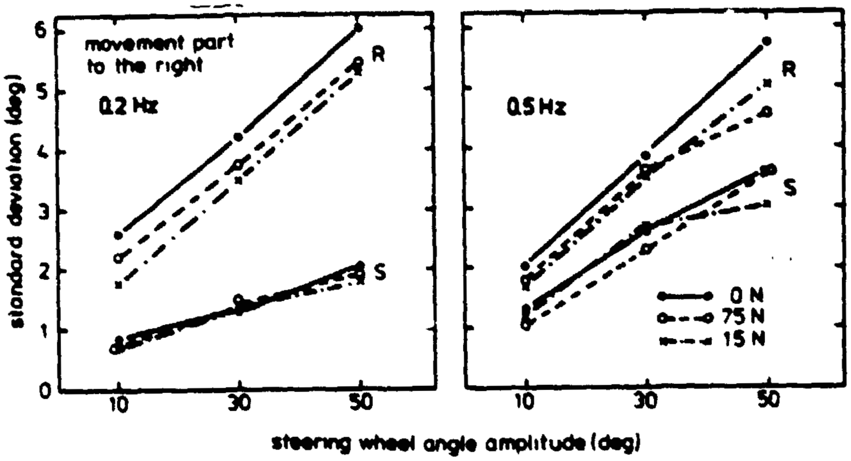

Fig. 4 Standard deviation of the steering-wheel angle amplitude for the movement conditions in Experiment II.

force mainly influenced the standard deviations of the response movements (SF x SR interaction).

Means and standard deviations of the relative errors in timing are shown in Fig. 5. Timing accuracy under stimulus conditions is rather good. Both movement amplitude and steering force influence timing accuracy in reproduction. In most conditions reproduction times are too long, especially with the 30° and 50° amplitudes. Only in the movements with the lowest velocity levels (0.2 Hz, small amplitudes) and with steering force available the tendency to reproduce movement times too long disappears. Movement times may be too short in these conditions. The effect of steering force in shortening movement time in reproduction is rather general and influences all of the movement conditions. The relative error in timing accuracy in responses is somewhat larger under 0.5 Hz conditions as compared with the 0.2 Hz condition.

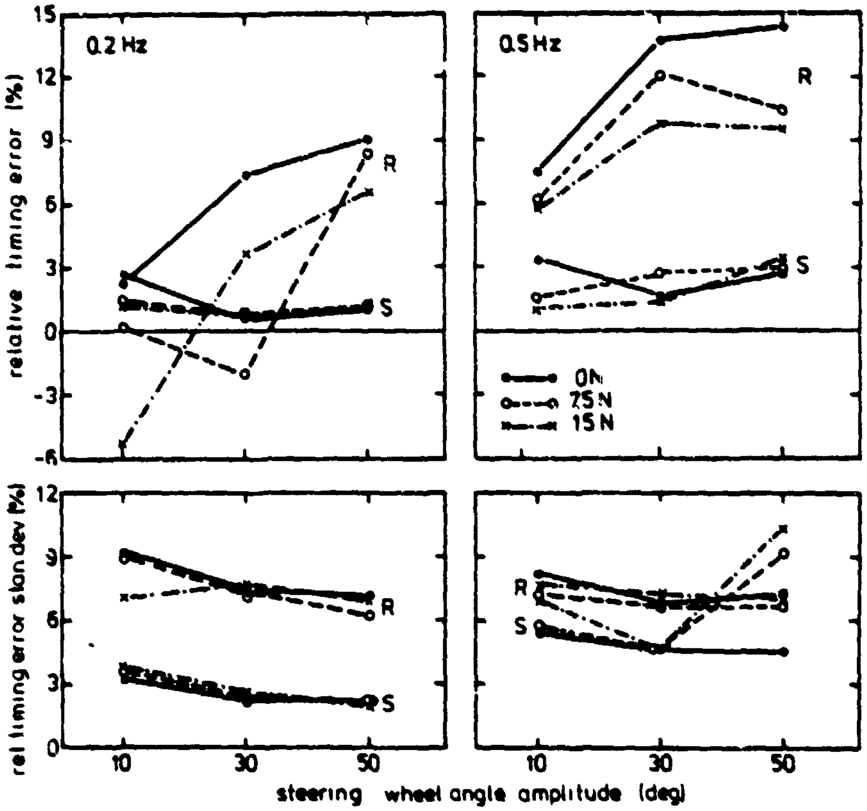

Fig. 5 Means and standard deviations of the relative errors in timing for the movement conditions in Experiment II.

Regarding the standard deviations of the timing error the F x SR interaction (p<0.01) indicates that differences between stimulus and response movements are less in the 0.5 Hz condition as compared with the 0.2 Hz movement. This effect is in correspondence with the effect that was noted for the standard deviations of the movement amplitude.

3.4 Discussion

The purpose of Experiment II was to investigate the efficiency of the M to m transformation in a continuous task and to measure the effects of movement amplitude, frequency and steering force on reproduction performance in this type of task.
Means and standard deviations for the criterion or *stimulus* movements may be considered as a maximum of Ss' accuracy in generating the desired manual control actions M. The results indicate that with regard to the amplitude and timing overshoot/undershoot tendency the stimulus movements were rather accurate. Amplitude standard deviations for stimulus conditions (Fig. 4) show that the variability increases slightly with movement amplitude and frequency. These data suggest that the variability in stimulus movements is mainly dependent on movement velocity. Fig. 6 may serve as an illustration and presents amplitude standard deviations (primary movement part) under stimulus conditions as a function of movement velocity. The maximum value of the velocity in the primary

ORIGINAL PAGE IS
OF POOR QUALITY

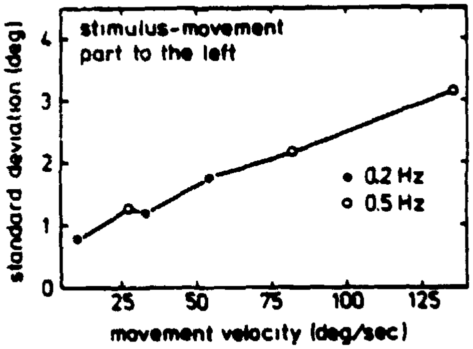

Fig. 6 Standard deviations of the steering-wheel angle amplitude under stimulus conditions for the d[illegible]ent movement velocity conditions [illegible] were taken over steering forc[illegible]ls.

part of the movement is taken as movement velocity. The steering force effect on amplitude standard deviations indicates that the variability of the stimulus movements is slightly decreased when steering force is available.
Timing standard deviations under stimulus conditions (Fig. 5) show that the variability in timing for the 0.5 Hz movement is about twice that of the 0.2 Hz movement, which points to the fact that timing variability is rather constant in seconds i.e. about 150 msec.

Behaviour in *responses* may be considered as Ss' accuracy in generating the actual control actions m when using the M respresentation as a reference. The response data should therefore again be considered as an overall description of the M to m transformation and the accuracy of M. Means of amplitude and timing behaviour under response conditions are influenced by movement conditions. Fig. 7 gives mean relative amplitude and timing errors as a function of movement velocity.

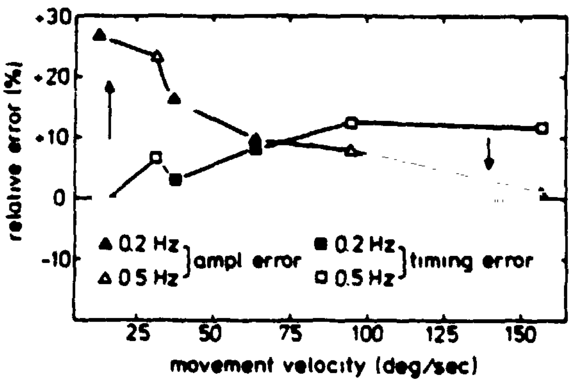

Fig. 7 Relative amplitude and timing errors for the different movement velocity conditions. Means were taken over steering-force levels.

Note in Fig. 7 that amplitude errors are presented as relative errors, i.e. as a percentage of the movement amplitude. Relative amplitude errors were calculated by taking the sum of the algebraic error of the leftward and rightward part of the movement divided by twice the movement amplitude. Maximum velocity between the leftward and rightward part of the movement was taken as movement velocity.
Three areas can be distinguished in Fig. 7:

A With low movement velocity timing errors are small, amplitude shows a major overshoot effect and movement velocity is too high.

B In the area of moderate movement velocity both timing and amplitude show a slight and about equal overshoot effect whereby movement velocity is largely correct.

C With high movement velocities relative amplitude errors are small. Therefore the timing overshoot tendency in this area indicates that movement velocity in responses were too low, i.e. a velocity undershoot tendency.

Steering force reduces timing overshoot or may even result in timing undershoot. Analyzing this effect leads to the suggestion that for the low velocity movement conditions steering force results in a decrease of the positioning overshoot tendency without influencing movement velocity. For rapid movements steering force mainly influences movement velocity witnout influencing positioning. As a result the velocity undershoot effect as noted under C is reduced with steering force available. This latter effect may have also played a role for the 10° movement condition in Experiment I.

Amplitude standard deviations under response conditions (Fig. 4) show a remarkable increase with movement amplitude. For the 0.2 Hz movement condition the difference between stimulus and response movements can largely be explained by the positioning accuracy data from Experiment I. This explanation does not completely hold for the 0.5 Hz movement condition. In the latter condition the variability under stimulus conditions is greater as compared with the 0.2 Hz movements. Nevertheless the response variability for the 0.5 Hz movements is about the same as for the 0.2 Hz movements. This effect should be considered in relation with the rather high accuracy of the means of the 0.5 Hz movement amplitudes. Together these data suggest that with slow movements both positioning and velocity (in)accuracy are of importance, whereas with rapid movements behaviour is controlled by velocity and timing accuracy.
The main steering force effect in reducing amplitude variability holds for both the 0.2 Hz and 0.5 Hz movement conditions. The data from Experiment I illustrated the functioning of steering force in reducing positioning variability. Experiment II indicated that steering force may also influence movement velocity. Therefore, the steering-force effect on amplitude variability may be a result of a reduction in both positioning and velocity variability for slow movements. With rapid movements steering force probably mainly reduces velocity variability.

In summary it can be stated that the combined results of Experiment II show that at the lower movement velocities the positioning accuracy of continuous movements under time constraint is worse when compared with that of discrete movements without time constraints. The additional role of velocity overshoot was illustrated. For rapid movements a velocity undershoot effect may occur, which - together with a slight timing overshoot tendency - leads to the situation that the positioning accuracy for rapid movements may be better than those for slow movements.
Movement velocity proved to be a major factor which largely determines the relative importance of positioning, velocity and timing accuracy. The role of steering force can be divided in three parts. Firstly, steering force decreases positioning overshoot effects of low velocity movements. Secondly, steering force reduces the velocity undershoot effect of rapid movements and finally steering force reduces positioning variability.

As mentioned in the introduction the relevancy of the present data will be tested further in an experiment on precognitive and pursuit tracking. In this latter experiment tracking of predictable and unpredictable inputs will be analyzed under conditions with and without occlusion. Thus the role of the internal representations IMV and MRS as functioning in combination with the proprioceptive system may be evaluated in more detail.

REFERENCES

1 Krendel, E.S. and McRuer, D.T. (1968). Psychological and Physiological Skill Development - A control engineering model. *Proceedings Fourth Annual Conference on Manual Control.*

2 Pew, R.W. (1974). Human Perceptual Motor Performance. B.H. Kantowitz (Ed.), In: *Human Information Processing*, Chapter 1, 1-39.

3 McRuer, D.T., Allen, R.W., Weir, D.H. and Klein, R.H. (1977). New results in Driver Steering Control Models. *Human Factors*, 19 (4), 381-397.

4 Donges, E. (1978). A Two-Level Model of Driver Steering Behavior. *Human Factors*, 20 (6), 691-707.

5 Schmidt, R.A. (1975). A schema theory of discrete motor skill learning. *Psychological Review*, 82, 225-260.

6 Gundry, J. (1975). The use of location and distance in reproducing different amplitudes of movement. *Journal of Motor Behavior*, Vol. 7, No. 2, 91-100.

7 Adams, J.A., Gopher, D. and Lintern, G. (1977). Effects of visual and proprioceptive feedback on motor learning. *Journal of Motor Behavior*, Vol. 9, No. 1, 11-23.

8 Pepper, R.L. and Herman, L.M. (1970). Decay and interference effects in the short-term retention of a discrete motor act. *Journal of Experimental Psychology*, Monograph Supplement, Vol. 83, No. 2, Part 2.

9 Vossius, G. (1965). Der kybernetische Aspect der Willkurbewegung. *Progress in Cybernetics*, New York, Elsevier Publishing Company.

10 Pew, R.W., Duffendack, J.C. and Fensch, L.K. (1967). Sine-wave tracking revisited. *IEEE Transactions on Human Factors in Electronics.* Vol. HFE-8, No. 2, 130-134.

11 Magdaleno, R.W., Jex, H.R. and Johnson, W.A. (1969). Tracking quasi-predictable displays; subjective predictability gradations, pilot models for periodic and narrowband inputs. *Proceedings Fifth Annual Conference on Manual Control.*

"The Role of Antagonist Coactivation in the Control of Natural Movement"

by

Neville Hogan, Ph.D.

Assistant Professor, Mechanical Engineering
Massachusetts Institute of Technology

ABSTRACT

The control of the impedance about the joints of the natural musculoskeletal system by coactivation of antagonist muscle groups is described. The consequences of the ability to control joint impedance are discussed. Based on the ability to control impedance an explanation of the crucial role played by two-joint muscles in the control of natural movement is proposed. The implications with respect to the control of manipulators and the modeling of the human operator are discussed.

Submitted to the Sixteenth Annual Conference on Manual Control, 1980

INTRODUCTION

The work presented in this paper is part of an ongoing project whose object is to control externally powered assistive devices such as prostheses and orthoses using bioelectric signals such as the electrical activity of muscle. Substantial progress has been made on the signal acquisition problem,(1) and the major focus of present efforts on this project is the correct interpretation of the acquired signals. Our objective is to determine from the available bioelectric signals what the operator's motor intent is and to deduce what the natural limb would have done in response, then generate the appropriate command signals so that the assistive device will do what the natural limb would have done. Our work has yielded new insights into the control of movement, some of which are presented in this paper.

TUNING IMPEDANCE BY ANTAGONIST CO-ACTIVATION

Correct interpretation of bioelectric signals is derived from a knowledge of muscle mechanics and functional anatomy. In addition to generating the forces which cause movement, muscles behave as tunable springs. If the length of a muscle is fixed, the isometric contractile force increases as a function of the activation level of muscle. However, if the length of the muscle is allowed to change, the stiffness of the muscle (or more generally, its mechanical impedance) also increases with increasing muscle activation(2&3). Anatomically, muscles are arranged about the joints in antagonist or opposing pairs. A puzzling aspect of muscular coordination is that under many circumstances antagonist muscles are active simultaneously. Because co-activation costs input chemical energy but does not contribute to the mechanical work output of the limb, it represents an energy diseconomy. Under the reasonable assumption that the majority of movements are tailored so as to minimize energy costs while accomplishing the task objectives, the purpose of co-activation needs to be explained. As shown in Figure 1 co-activation of antagonist muscles permits independent control of the torque about a joint and the rotational stiffness or impedance about the joint. Thus the co-activation of antagonist muscles provides an important vehicle for adaptive tuning of the system parameters which is independent of feedback, that is, open-loop.

Polit and Bizzi(4) have shown that deafferented monkeys can perform target-acquisition movemets in the presence of external mechanical disturbances and in the absence of any afferent feedback. This is possible because a given level of co-activation of antagonist muscles defines an equilibrium condition for the joint. Displacement of the limb from this equilibrium position results in the generation of a restoring torque which is a function of the mechanical properties of the muscle and is independent of afferent feedback. Furthermore, if the activities of the antagonist muscles are increased simultaneously, the equilibrium condition of the joint can remain unchanged while the stiffness about that equilibrium condition is increased (See Figure 1).

KINEMATICALLY CONSTRAINED MOVEMENTS

The ability to tune the mechanical impedance of the joints can simplify movements made against external kinematic constraints. For example consider the problem of turning a crank handle or opening a door: If the stiffnesses about the joints are high, as is the case in most manipulators, the end point of the manipulator must be moved in the required circular arc with high positional accuracy or high interface forces will result. This is difficult because it requires accurate knowledge of the location of the hinge and of the

MUSCLE:

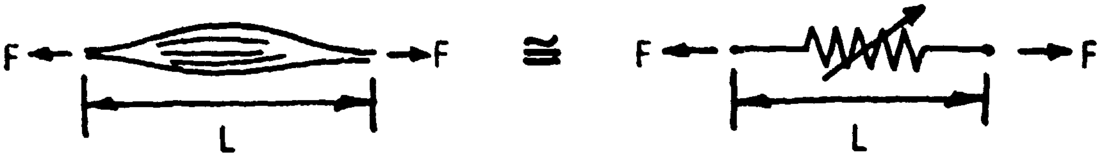

Assume linear force-length relation: $F = u\,k\,(L - L_e)$; $\partial F/\partial L = u\,k$
(F: force; L: length; L_e: rest length; u: neural input; k: constant)

JOINT:

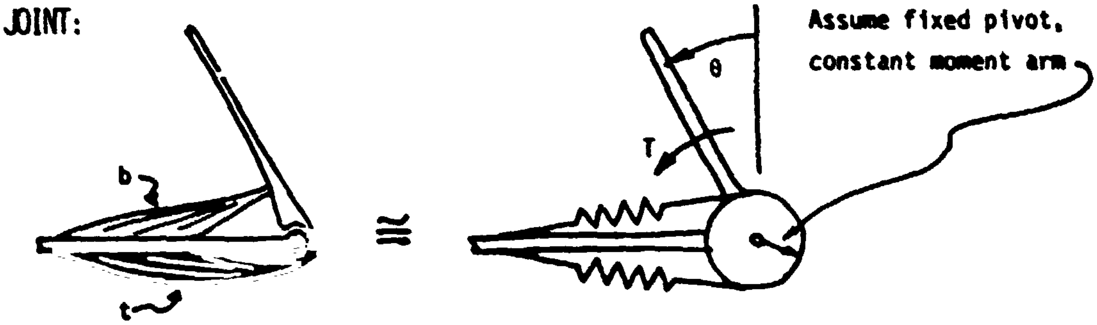

Assume fixed pivot,
constant moment arm

Scale variables such that: $T_b = u_b(1 - K\theta)$; $-T_t = u_t(1 + K\theta)$
$0 < u_b < 1$; $0 < u_t < 1$; $T_b > 0$; $-T_t > 0$; for $-\pi/2 < \theta < \pi/2$
(T; torque; K: constant; θ: joint angle)

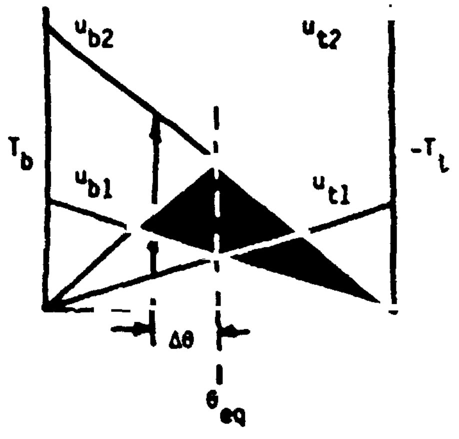

The net torque, T_n, is the difference between the agonist and antagonist torques.

$$T_n = \underbrace{(u_b - u_t)}_{\substack{\text{torque}\\ \text{control}}} - \underbrace{(u_b + u_t)K\theta}_{\substack{\text{stiffness}\\ \text{control}}}$$

If external torque is zero, $T_n = 0$ at equilibrium. Thus:

$$\theta_{eq} = \frac{(u_b - u_t)}{(u_b + u_t)K} = \frac{(u_b/u_t - 1)}{(u_b/u_t + 1)K}$$

if $u_t \neq 0$

FIGURE 1: CONTROL OF JOINT STIFFNESS BY ANTAGONIST CO-ACTIVATION

the perpendicular distance between the hinge and the handle, in addition to the ability to control the position of the end point accurately. In contrast if the stiffnesses about the joints are low, as is the case in the natural limb, the end effector need only exert a force in the general direction of the movement, allowing the kinematic constraint to determine the details of the end point trajectory. However, a target-acquisition movement such as that required to grasp the handle will require high positional accuracy and this in turn may dictate high stiffnesses about the joints. The ability to tune the stiffnesses about the joints permits the manipulator to operate successfully under both conditions.

Successful manipulation against kinematic constraints requires not only that the impedance about the manipulator joints be tunable but that the impedance of the end effector be controllable. That is, manipulation will be simplified if it is possible to specify the movement of the end effector in response to arbitrary disturbance forces. Consider the problem of inserting a peg into a hole: Under the action of the lateral forces resulting from the misalignment of the peg with respect to the hole the end effector must move in a direction so as to reduce these forces. Under the action of the torques which could cause wedging and jamming the end effector must rotate so as to reduce these torques. However, disturbance forces in the direction of insertion of the peg into the hole must be overcome. Thus we have specified the desired values of the elements of the stiffness matrix or tensor which relates the applied forces and torques to the resulting positional and angular movements. It has been shown (5) that provision of appropriate stiffness or compliance in an industrial manipulator considerably simplifies tasks involving manipulation of objects againt kinematic constraints such as, for example, the insertion of a shaft into a bearing.

END EFFECTOR STIFFNESS CONTROL

The question now is: If the stiffness about each joint (or along each degree of freedom) can be dictated, can the stiffness tensor which determines the motion of the end effector in response to arbitrary force inputs be specified? To address this question we consider the movements of a planar, two-degree-of-freedom, cartesian-coordinate manipulator as shown in Figure 2. The actuators which produce the movements of the cursor are depicted as springs. The stiffness tensor for the cursor is most easily investigated by finding the potential energy stored in the spring as a function of the deviation of the cursor from its equilibrium position which is assumed to be at the origin of the coordinate system. If we let the stiffness of the horizontal springs of the manipulator shown in Figure 2 become very large while the stiffness of the vertical springs becomes very small then the potential energy function is a very long, narrow "valley" oriented along the vertical axis. Conversely, if the vertical springs become infinitely stiff while the horizontal springs become infinitely compliant the potential energy function becomes a long, narrow "valley" oriented along the horizontal axis. If the vertical and horizontal stiffnesses are finite and equal, the energy function becomes a bowl-shaped depression with its lowest point at the equilibrium position. For a given set of spring stiffnesses the contours of constant potential energy are ellipses. The orientation of the potential energy "valley" is given by the principal eigenvector of the stiffness tensor and the width, or aspect ratio, of the potential energy "valley" is given by the ratio of eigenvalues of the stiffness tensor.

If the stiffness tensor could be completely specified then the "valley" of the potential energy function could be pointed in any direction and could be

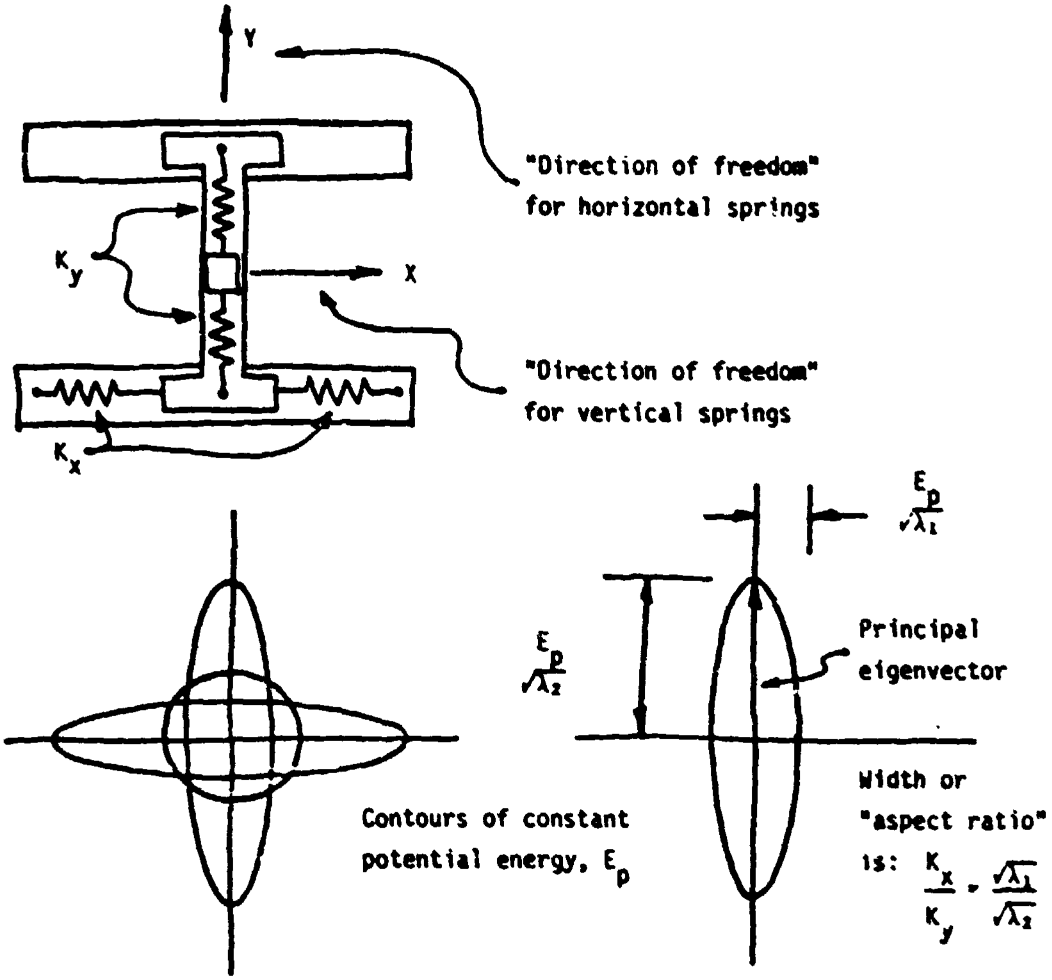
Y
"Direction of freedom" for horizontal springs
K_y
X
"Direction of freedom" for vertical springs
K_x
$\frac{E_p}{\sqrt{\lambda_1}}$
$\frac{E_p}{\sqrt{\lambda_2}}$
Principal eigenvector
Contours of constant potential energy, E_p
Width or "aspect ratio" is: $\frac{K_x}{K_y} = \frac{\sqrt{\lambda_1}}{\sqrt{\lambda_2}}$

$$\begin{bmatrix} F_x \\ F_y \end{bmatrix} = \begin{bmatrix} K_x & 0 \\ 0 & K_y \end{bmatrix} \begin{bmatrix} X \\ Y \end{bmatrix} \qquad E_p = \begin{bmatrix} X & Y \end{bmatrix} \begin{bmatrix} K_x & 0 \\ 0 & K_y \end{bmatrix} \begin{bmatrix} X \\ Y \end{bmatrix}$$

FIGURE 2. HYPOTHETICAL PLANAR CARTESIAN-COORDINATE MANIPULATOR

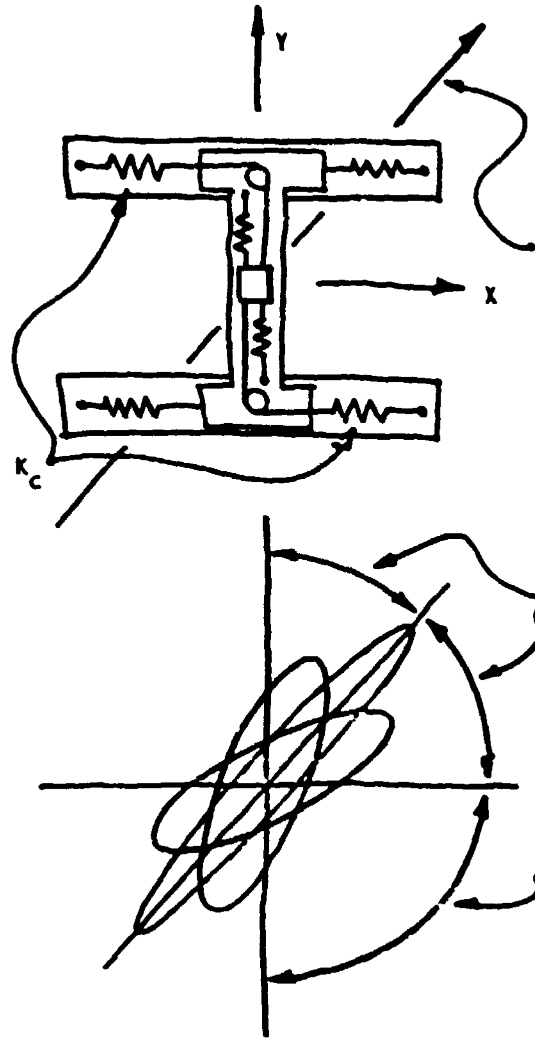

"Direction of freedom" for coupling springs

Principal eigenvector can point in any of these directions, but unless it coincides with one of the "directions of freedom" the aspect ratio is restricted.

Principal eigenvector cannot point in these directions.

$$\begin{bmatrix}F_x\\F_y\end{bmatrix} = \begin{bmatrix}K_x+K_c & K_c\\K_c & K_y+K_c\end{bmatrix}\begin{bmatrix}X\\Y\end{bmatrix} \qquad \varepsilon_p = \begin{bmatrix}X & Y\end{bmatrix}\begin{bmatrix}K_x+K_c & K_c\\K_c & K_y+K_c\end{bmatrix}\begin{bmatrix}X\\Y\end{bmatrix}$$

FIGURE 3. PLANAR MANIPULATOR WITH COUPLING SPRINGS

given any desired width. This cannot be achieved with the system shown in Figure 2. The principal eigenvector of the stiffness tensor can only be pointed along one or the other of the coordinate axes. However, if we add the pair of coupling springs shown in Figure 3 the situation changes. If the stiffness of these springs is made large while the stiffnesses of other springs are allowed to approach zero then the cursor will be free to move only along the diagonal shown. This is the "direction of freedom" associated with this pair of springs. The "directions of freedom" associated with the horizontal and vertical springs are the vertical and horizontal axes respectively. It is clear that the principal eigenvector of the stiffness tensor for the cursor can now be oriented along this diagonal direction of freedom. Furthermore, the width of the potential energy "valley" can be specified at will. In addition, it can readily be shown that the principal eigenvector of the stiffness tensor can be oriented along any of the directions shown in Figure 3 between the directions of freedom. However, if the principal eigenvector does not coincide with one of the three directions of freedom then the ratio of eigenvalues of the stiffness tensor is constrained such that a lower limit is placed on the width of the potential energy valley; that is, the valley cannot be made infinitely narrow. In general it can be shown that if the angle between two directions of freedom is less that 90 degrees then the principal eigenvector of the stiffness tensor can be oriented along any direction between these two directions of freedom. The more acute the angle between the directions of freedom the narrower the potential energy function valley can be made when the principal eigenvector of stiffness tensor is oriented midway between the two directions of freedom.

ROLE OF TWO-JOINT MUSCLES

The analogy between the "manipulator" of Figure 2 and 3 and the musculoskelatal system is direct: The presence of the two-joint muscles means that the principal eigenvector of the stiffness tensor of the end effector can be oriented in almost all directions. This cannot be achieved using the single-joint muscles alone. If we consider motions of the upper limb in a horizontal plane and model the upper limb as a two-link kinematic chain then we can define directions of freedom as in the case of the cartesian-coordinate manipulator. If the single-joint elbow muscles (e.g. brachialis, medial and lateral heads of triceps, etc.) are made infinitely stiff while all other muscles are made infinitely compliant the direction of freedom is a circular arc centered about the shoulder axis (See Figure 4a). If the single-joint shoulder muscles (e.g. anterior and posterior deltoid, etc.) are made infinitely stiff while all other muscles are made infinitely compliant the direction of freedom is a circular arc centered about the elbow axis (See figure 4a). The direction of freedom associated with the two-joint muscles (e.g. biceps, long head of triceps) will be a function of the precise anatomical connections of the muscles to the limbs. For simplicity we make the quantitatively inaccurate but qualitatively correct assumption that the two-joint muscles act with fixed and equal moment arms about the shoulder and elbow joint. Under these assumptions, if the two-joint muscles are made infinitely stiff while the single-joint muscles are infinitely compliant then a kinematic constraint has been imposed upon the values of the shoulder and elbow angles such that the absolute angle of the forearm with respect to the thorax is fixed. As a result the end effector describes a ciruclar arc as shown in Figure 4b. This is the direction of freedom associated with the two-joint muscles. If we look at the effect of the single and double-joint muscles taken together we can see that for a wide range of positions in the movement space the directions of freedom intersect one another at acute angles such that the principal eigenvector of the stiffness tensor of the end effector can be oriented along any direction (See Figure 4c). This is not possible with the single-joint muscles alone.

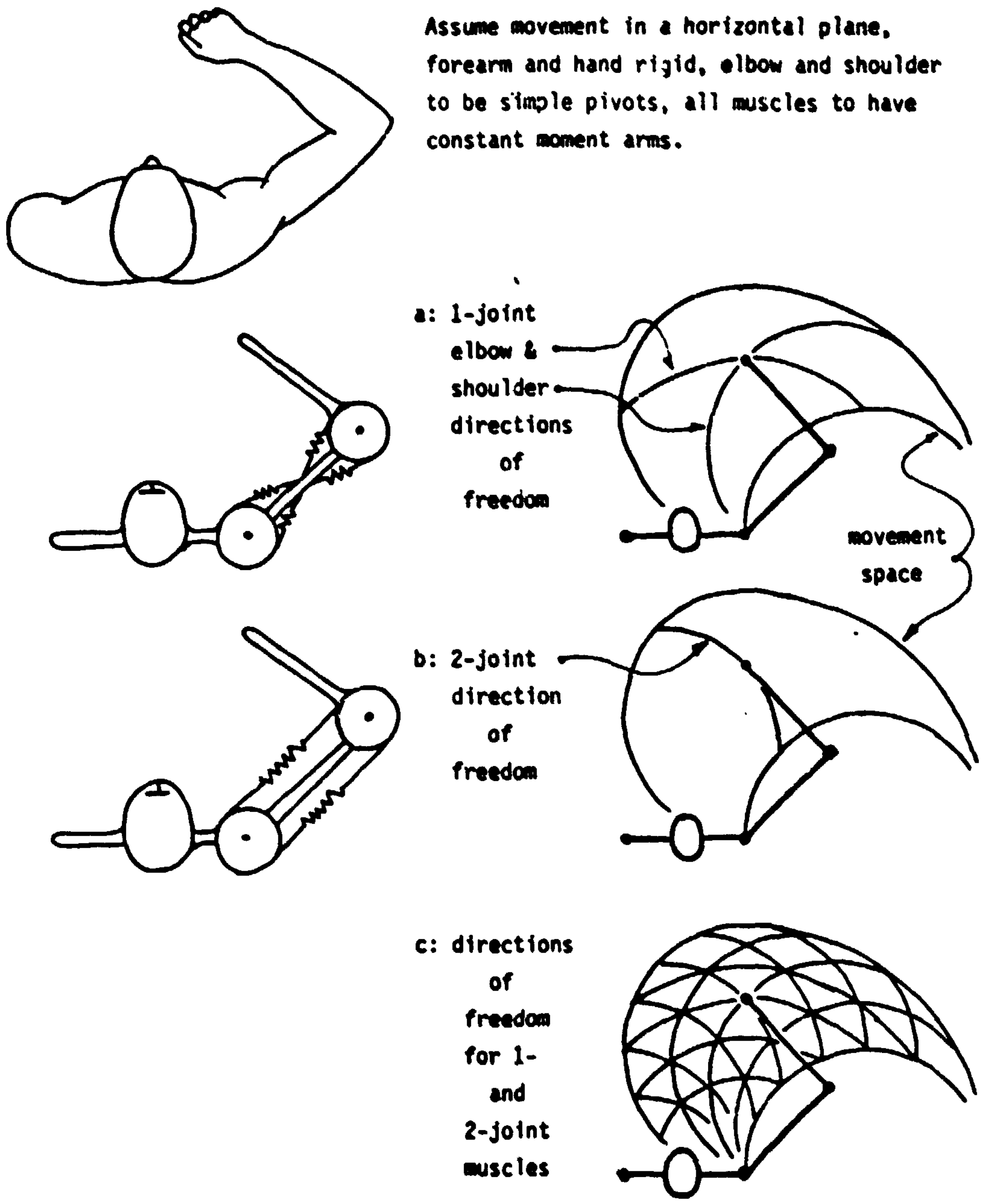

Assume movement in a horizontal plane, forearm and hand rigid, elbow and shoulder to be simple pivots, all muscles to have constant moment arms.

a: 1-joint elbow & shoulder directions of freedom

b: 2-joint direction of freedom

c: directions of freedom for 1- and 2-joint muscles

FIGURE 4. "DIRECTIONS OF FREEDOM" FOR THE UPPER LIMB

FINAL POSITION CONTROL

One of the fascinating consequences of the springlike properties of muscle is that in the case of motion about a single joint the entire movement could be controlled simply by specifying the final equilibrium position(4). The biocontroller would merely specify the appropriate set of muscle activities required to define the equilibrium position of the joint and allow the inherent mechanical properties of the musculo-skeletal system to take care of the details of the movement. It is not suggested that this is the only or even the predominant mode of natural movement, but it could be significantly advantageous to the central nervous system as the biocontroller need only intervene in the control of movement once every several hundred milliseconds or so thus allowing the higher levels of the central nervous system to be focused on other tasks. The question now arises: Could a similar control scheme work for multiple-degree-of-freedom movements? It is easy to show that if only single-joint muscles are used then for a large number of reasonable combinations of start positions and target (final) postions it is not possible to achieve the almost-straight-line trajectory between start and target which is typically observed for unconstrained movements. For example, if the start position and target position lie on an arc such that in both the start and target positions the angle of the upper arm is identical, only the angle of the forearm being different, then if the muscles are activated such that the equilibrium condition for the limb is at the target position the shoulder muscles can generate no torque about the shoulder joint when the limb is at rest in the start position. Thus the net force vector at the end effector due to the springlike properties of the musculo-skeletal system must point in a direction such that it intersects the shoulder joint (See Figure 5a). This will result in a movement which swings wide of the typically observed path between the start and target positions. However, the addition of the two-joint muscles considerably changes matters: For the combination of start and target positions described above the two-joint muscles provide the necessary freedom to allow the force vector at the end effector to point directly at the target position (See Figure 5b). Furthermore, the potential energy function for deviations about the equilibrium (target) position can be set up such that the energy function is a narrow "valley" running from the equilibrium position to the start position. This would mean that the end effector would tend to follow the "valley bottom" and move along an approximately straight line trajectory. Again, this opens up the intriguing possibility that large portions of the time history of the motion of the end effector could be controlled by the inherent properties of the musculo-skeletal system with only minimal intervention from the higher levels of the central nervous system.

RELEVANCE TO MANIPULATOR CONTROL AND HUMAN OPERATOR MODELING

From the foregoing analysis it follows that if the stiffness or impedance tensor for the end effector of any manipulator is to be fully controllable then it will be necessary to provide adaptable coupling between two or more degrees of freedom of the manipulator. This coupling may be provided mechanically, as in the natural limb, or electronically via feedback. Either way, the coupling should provide an adaptable kinematic constraint similar to that imposed by the multi-joint muscles in the natural limb. As mentioned earlier, controlling the end effector impedance will considerably simplify manipulation against external kinematic constraints. Another perspective is that impedance provides a convenient and natural "language" for the communication of motor intent between the controller and the effector (i.e. the manipulator). Two common modes of manipulator control are position control and "force" control. The former, in which the desired position or trajectory of the manipulator is specified, works well for free manipulations, the movements being relatively insensitive to ex-

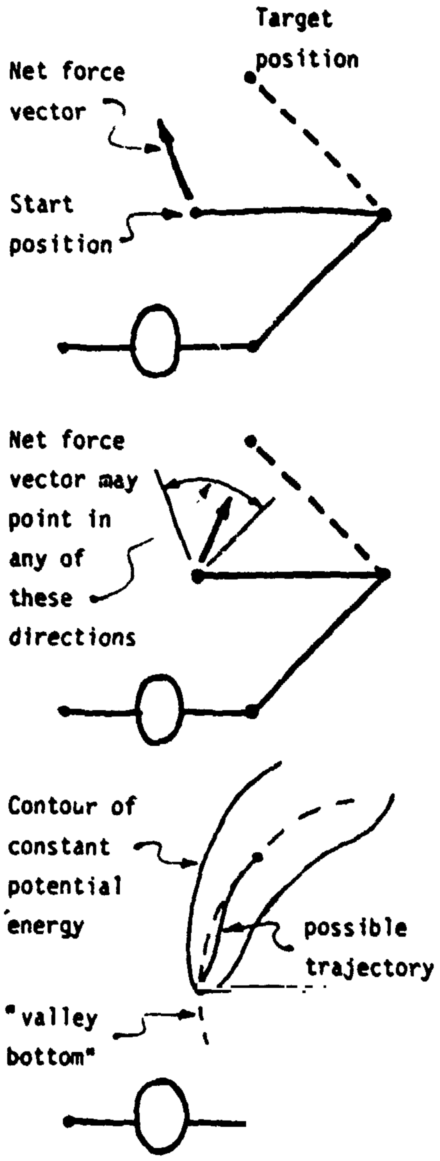
Target
position
Net force
vector
Start
position
Net force
vector may
point in
any of
these
directions
Contour of
constant
potential
energy
possible
trajectory
"valley
bottom"

Assume the muscle activities are set up such that at equilibrium the end effector is in the target position.

a: If only the 1-joint muscles are used the net force vector at the end effector when it is in the start position must point as shown.

b: If 1- and 2-joint muscles are used the net force vector may point directly at the target, or in any of the directions shown.

c: If the potential energy function is set up appropriately then the end effector may tend to follow the approximately straight trajectory shown.

FIGURE 5. TWO-JOINT FINAL POSITION CONTROL

ternal disturbances, but causes difficulty when dealing with external kinematic constraints. The latter, in which forces or torques are commanded, is better suited to manipulation against constraints, but does not perform well on free movements. In the former the movement "primitives" are positions; in the latter they are forces or torques. However, the foregoing analysis indicates that the "directions of freedom" associated with each of the manipulator actuators should be regarded as the movement "primitives". In other words, the "controlled variable" should not be position nor force, but impedance (or stiffness). Looked at from the point of view of impedance control, position control and force control are simply degenerate or extreme cases of impedance control. That is, position control implies very high stiffnesses or impedances, while force control implies very low (zero) stiffnesses or impedances. A manipulator with controllable impedance should have far greater capabilities than either a force-controlled or a position-controlled manipulator and should be equally successful at constrained manipulation and free movement.

The human ability to control impedance must be included in models of the human operator. Essentially the human operator is capable of adjusting his own mechanical system parameters to optimise performance on a task. This will be most evident in manipulation of tools or machine controls. For example, high levels of co-activation may yield good positional control over a tool or joystick due to increased mechanical coupling (good "grip"), but the same mechanical coupling implies increased transmission of vibration and shock loads. In a vibratory environment the skilled operator may tune his mechanical impedance to find the optimum trade off between these effects.

Co-activation costs input chemical energy to the muscles without yielding output mechanical work and undue co-activation will lead to early fatigue. An unskilled operator, being unable to predict any external disturbances, may co-activate excessively to reduce their effects on his movemetns. A skilled operator, more familiar with the nature of external disturbances, may elect for lower levels of co-activation and as a result avoid fatigue. However, even the skilled operator might opt for high co-activation in less familiar circumstances such as emergencies. Thus co-activation of antagonists may prove useful as a measure of movement skill and mental workload.

ACKNOWEDGEMENTS

The work reported in this paper was supported by the National Sciences Foundation under Grant #PFR-7917348.

REFERENCES

1. Hogan, N. and Mann, R.W., "Myoelectric Signal Processing: Optimal Estimation Applied to Electromyography, Part I & II," IEEE Transactions on Biomedical Engineering (in press)

2. Mason, P., "Dynamic Stiffness and Crossbridge Action in Muscle," Biophys. Struct. Mechanism, Vol. 4, pp. 15-25 (1978)

3. Zahalak, G.I. and Heyman, S.J., "A Quantitative Evaluation of the Frequency-Response Characteristics of Active Human Skeletal Muscle in Vivo," Journal of Biomechanical Engineering, Vol. 101, pp. 28-37 (February 1979)

4. Polit, A. and Bizzi, E., "Characteristics of Motor Programs Underlying Arm Movements in Monkeys," Journal of Neurophysiology, Vol 42 No. 1, pp. 183-194, (Jan., 1979)

5. Nevins, J.O. and Whitney, D.E., "Computer Controlled Assembly," Scientific American, Vol. 238, No. 2 pp. 62-74 (Feb., 1978)

N82 34072

A COMPARISON OF CONTROL MODES FOR TIME-DELAYED REMOTE MANIPULATION

GREGORY P STARR

I. INTRODUCTION

Transmission time delay in the communication channel of a manual control system degrades performance by preventing the human operator from immediately seeing the results of his actions.

A time delay can exist in remote manipulation systems, caused by long communication distances or bandwidth limitations. Ferrell [1] conducted the first research in time-delayed manipulation using a two degree-of-freedom manipulator. His subjects, working at time delays of 1.0, 2.1, and 3.2 s, could accomplish tasks even requiring great accuracy. The subjects spontaneously adopted a pattern of moving cautiously, then waiting to see the results of their actions. In experiments with a six degree-of-freedom master-slave manipulator system and time delays of 1.0 to 6 s, Black [2] saw that subjects tried to use the move-and-wait strategy; but there were often difficulties. The subjects seemed to have a problem in holding the master arm stationary while waiting for feedback. Any undesired drifting of the master arm introduced a discrepancy between the positions of the master and slave. This discrepancy was not perceived because of the time delay. The subject would then begin his next move with an inherent error.

The difficulty of effectively using the move-and-wait strategy with a master-slave manipulator suggested that rate control might be a more effective control mode with time delay. Manipulator rate controllers are usually multiaxis joysticks or switchboxes and are invariably constructed so that when the operator wishes to hold the manipulator stationary, he can simply remove his hand from the controller. This eliminates the possibility of undesired manipulator motion and should aid the operator in using the move-and-wait strategy.

The research summarized in this paper was conducted to compare master-slave and rate control of a manipulator. Four time delays were used. These delays (0.0, 0.33, 1.0, and 3.0 s) allowed us to examine the effect of time delay on control-mode performance. A peg transfer task was used, with automated data acquisition.

II. CONTROL-MODE IMPLEMENTATION

The NASA-Ames manipulator, designed by Vykukal *et al.* [3], was used in all experiments. This manipulator consists of conical fiberglass sections connected by rotational joints. The motion of these joints resembles the twisting of nested sections of stovepipe. There are seven rotational joints, plus the parallel-jaw end effector.

The master arm used with this manipulator is geometrically similar to the slave, although slightly scaled down. The operator's arm is inserted into the master arm, and analog position servos control the slave position.

The master had several undesirable characteristics. Foremost was preference for motion in certain directions, caused by the static and viscous joint friction combined with the master's unusual geometry. In addition, the operator could not move the master through its full range of motion.

Due to the peculiar geometry of the Ames arm, it was necessary to use resolved motion rate control (RMRC), conceived by Whitney [4]. In RMRC, a digital computer coordinates the individual joint rates. The operator specifies direction and speed of the hand without concerning himself with the individual joint rates.

A six degree-of-freedom isometric joystick was used as the rate controller. Using this joystick, the operator could command hand translational and angular velocity along axes of a Cartesian coordinate system fixed in the hand itself. See Figure 1. For a complete description of this rate control implementation, see Starr [5].

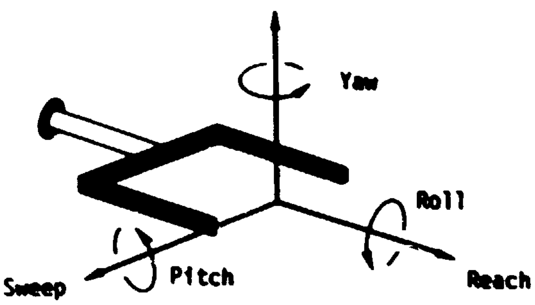

Fig. 1. Hand-mounted coordinate system.

The joystick had a small but noticeable amount of crosstalk, making it difficult to cause motion in only one direction. To permit motion along only one axis, an operator-activated switch was provided which selected only the largest output signal.

III. THE EXPERIMENT

Task

A peg transfer task was used to compare the two control modes. The operator extracted the peg from the left-hand receptacle, placed it in the right-hand one, removed it from the right and replaced it back in the left one. The subject was required to fully insert the peg before releasing it.

The receptacles were placed 8 in (20 cm) apart, and both were mounted on a table which was tilted back towards the manipulator at an angle of 32° with the horizontal. Furthermore, the right-hand receptacle was tilted away from the left at an angle of 17°, thus requiring a reorientation of the peg before insertion.

Three pegs were used with this task. All were 4-in (10.2 cm) long, and were 0.75-, 0.90-, and 0.99-in diameter (19.1-, 22.9-, and 25.1-mm). The clearance between the pegs and the 1-in (25.4-mm) hole was 0.25, 0.10, and 0.01 in (6.35, 2.54, and 0.25 mm), respectively.

Data Acquisition

The division of a task into simpler subtasks has been shown to be useful in industrial engineering research. Such a division of completion time was attempted by Blackmer [6] in a peg transfer manipulation task. The time division was done by the subject using a foot switch, and Blackmer acknowledged that the results were not precise enough to permit any conclusions.

The overall completion time in the peg transfer task described here, from peg liftoff to touchdown, was divided into three separate completion times, each representing a subtask. These subtasks were withdrawal, transport, and adjustment/insertion, defined as follows.

Withdrawal began at peg liftoff and ended when the peg left the receptacle.

Transport began when the peg left the receptacle and ended when the peg was 2 cm from the edge of the target hole.

Adjustment/insertion began when the peg was 2 cm from the edge of the hole and ended at touchdown of the peg.

The state of the task was monitored by a computer which accumulated the subtask completion times and recorded them on magnetic tape. These times were accurate to within 1/30 s.

The withdrawal time gives an indication of effectiveness in manipulation with external contact forces where terminal accuracy is not crucial. The transport time represents effectiveness in coarse positioning. Finally, the adjustment/insertion time reflects performance in two types of motion: an unconstrained fine-position segment where terminal accuracy is the goal (adjustment), and an externally constrained segment where force accommodation may be necessary.

Experiment Design

A factorial experiment design was used, the variables being control mode C, time delay T, peg size P, and task direction D (left-to-right or right-to-left). Because of time constraint plus equipment failures, we were able to use only one subject.

Procedure

After learning, the subject performed 20 replications of the task at each combination of variables, for a total of 960 replications. Peg size and time delay were randomized within each control mode. At the 1.0- and 3.0-s time delays, the subject complained of fatigue and frustration when using master-slave control.

IV. RESULTS AND DISCUSSION

Withdrawal

The withdrawal times versus time delay for each peg size appear in Figs. 2-4, along with least square regression lines. The vertical lines through the data points are ± one standard deviation.

Comparing the regression lines at each peg size, one can see the degradation of master-slave control as peg size increases. With peg 1, which had the greatest clearance, master-slave control resulted in lower withdrawal times at each delay. These times were significantly different at the 1 percent level.

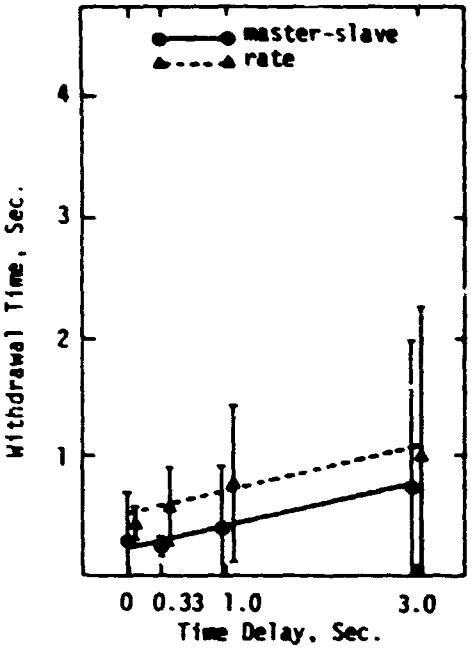

Fig. 2. Withdrawal time versus time delay, peg 1.

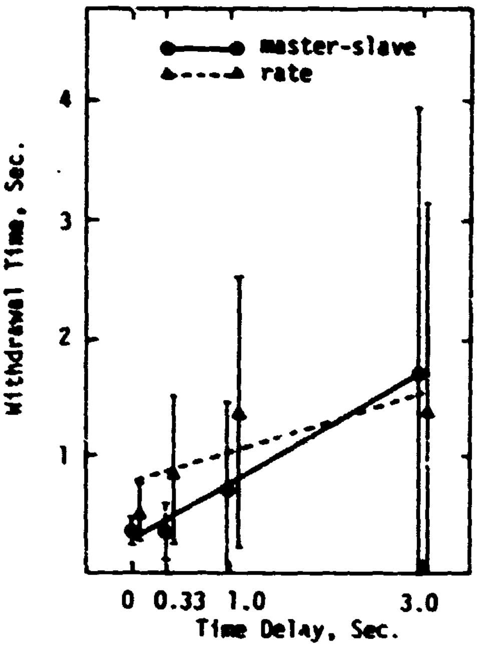

Fig. 3. Withdrawal time versus time delay, peg 2.

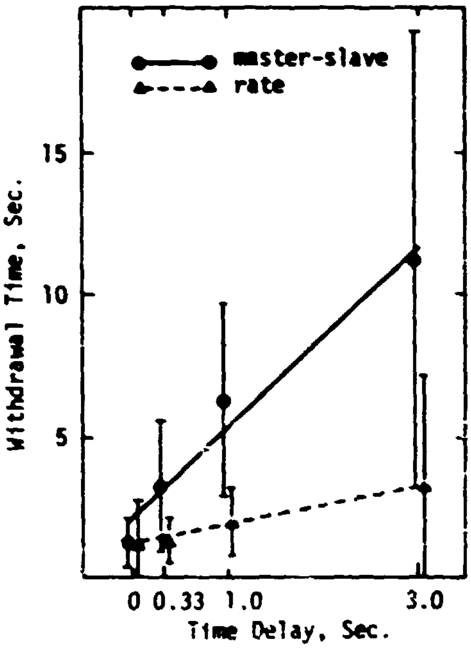

Fig. 4. Withdrawal time versus time delay, peg 4.

ORIGINAL PAGE IS
OF POOR QUALITY

With peg 2, master-slave control was superior at the lower three delays (1% significance level), but at the 3.0-s delay, rate control had a lower withdrawal time, although not significant. With peg 3, rate control had lower withdrawal times at all delays with 1% significance. The standard deviations of the master-slave withdrawal times with peg 3 were more than twice as large as those of rate control, indicating that jamming may have occurred with master-slave control.

The superiority of master-slave control in withdrawal of pegs 1 and 2 both with and without time delay can be explained by considering the type of motion necessary. With these pegs the clearance is large enough so that a perfectly axial withdrawal is not needed to avoid binding. Withdrawal becomes a coarse motion, emphasizing speed rather than directional accuracy. The master-slave system had higher speed capability than the rate control system, due to the rate gain we used. Thus master-slave would be expected to have lower withdrawal times with pegs 1 and 2. With peg 3, however, the withdrawal changes character. The clearance of 0.01 in (0.25 mm) between peg and hole results in a withdrawal segment stressing directional accuracy.

The angular clearance, or wobble angle, shows the directional accuracy needed for withdrawal better than the radial clearance. Wobble angle versus insertion depth for the three pegs is shown in Fig. 5. Peg 3 has a much smaller wobble angle than pegs 1 and 2, especially as it nears bottom.

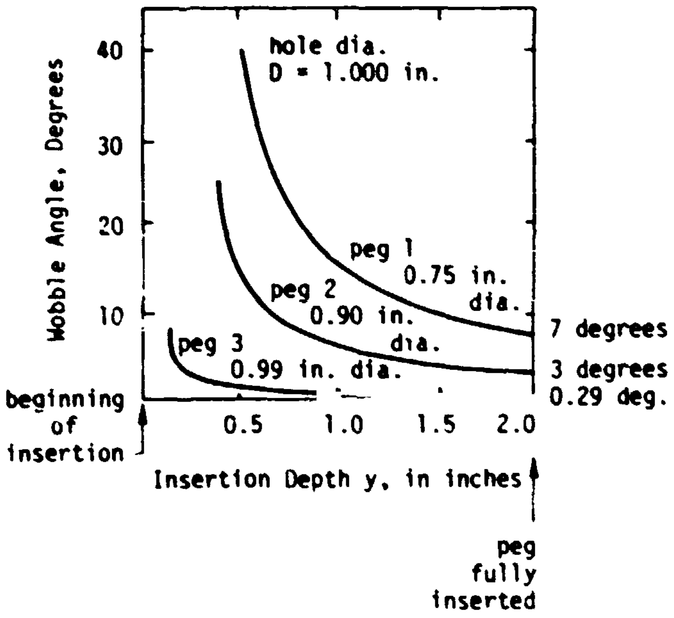

Fig. 5. Wobble angle versus insertion depth for three pegs.

When a time delay was present, the subject had to move open-loop. The withdrawal times suggest that the rate control system had better open-loop cirectional accuracy. With rate control, the subject oriented the hand parallel to the top of the block, grasped the peg, and issued a pure "lift" command. The hand would move back along the hole axis and extract the peg cleanly. The operator-controlled switch enabling generation of a pure command was helpful during withdrawal.

When using master-slave control, the subject had to monitor and attempt to null contact forces between the peg and the receptacle. Active force feedback would have been very helpful, but Ferrell [7] has shown that active force feedback can cause instability when a time delay is present.

Transport

Fig. 6 shows transport time versus time delay for each peg size and control mode. The regression lines are pooled over peg size. Transport time does not appear to vary consistently with peg size for either control mode.

A t-test made on the transport times pooled over peg size showed that master-slave control produced significantly lower transport times at all time delays. This is to be expected considering the higher speed capability of master-slave and the importance of speed during transport.

Fig. 7 shows transport time versus time delay for each control mode and task direction. The transport times for master-slave control, direction 2, are far lower at all delays than for direction 1, and lower than rate control in either direction.

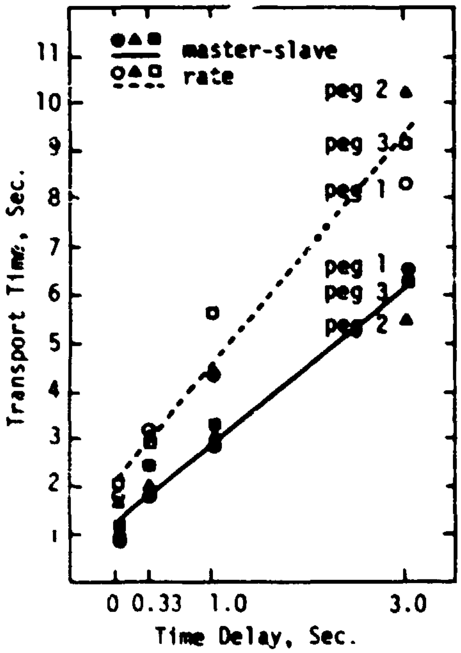

Fig. 6. Transport time versus time delay, all pegs.

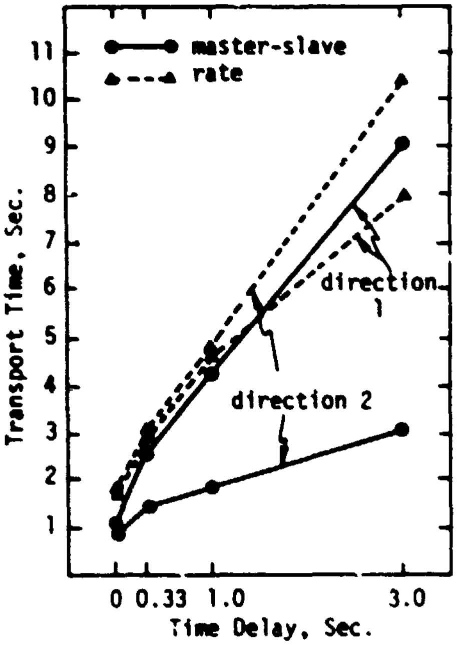

Fig. 7. Transport time versus time delay, directions 1 and 2.

The most likely explanation for this difference is the varying mechanical impedance of the master. Since the master has seven degrees of freedom, its joint rotations during direction 2 were not necessarily the reverse of those during direction 1. Transport in direction 1 apparently involved more joint rotation and did not match one of the master's low-impedance directions. The nonisotropic nature of this master-slave system is not true of resolved rate control, which decouples the operator from the geometry of the arm and permits motion in any direction with equal ease.

Adjustment/Insertion

Figs. 8-10 show that the adjustment/insertion times follow a pattern similar to the withdrawal times, with rate control degrading less with time delay. The similarity is because insertion is the reverse of withdrawal, since we required the subject to guide the peg to the bottom of the hole.

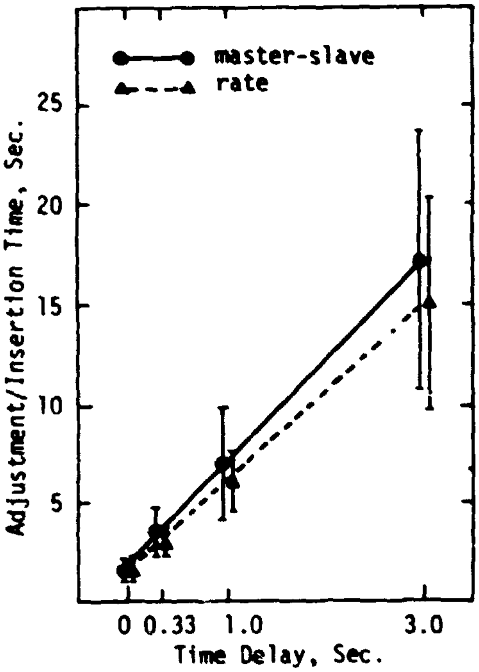

Fig. 8. Adjustment/insertion time versus time delay, peg 2.

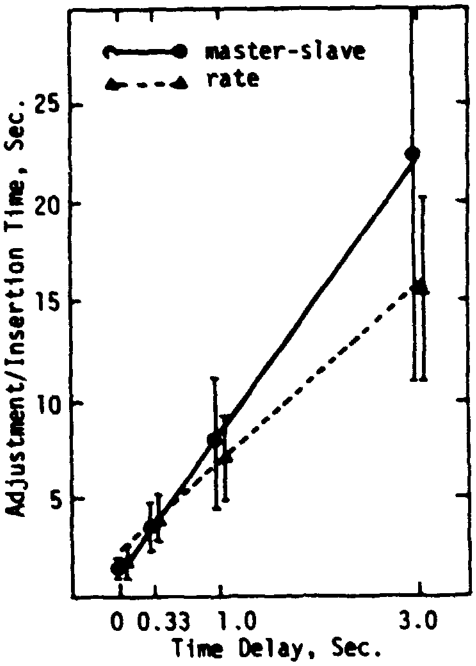

Fig. 9. Adjustment/insertion time versus time delay, peg 3.

V. CONCLUSIONS

Judging from these results, which are certainly inconclusive due to the use of only one subject, resolved motion rate control appears to be more effective than master-slave control for those parts of a time-delayed manipulation task emphasizing accuracy. Master-slave control was superior to rate control with no time delay, but degraded more rapidly with delay. This is partially due to the ease of holding the manipulator stationary with rate control, thus allowing motionless pauses to receive feedback. However, some

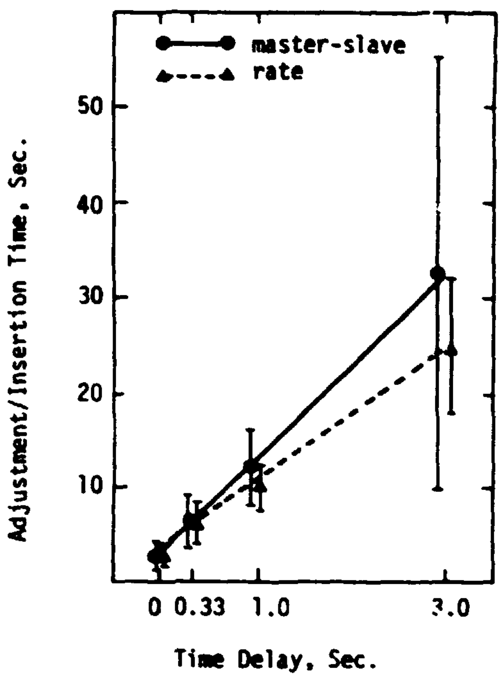

Fig. 10. Adjustment/insertion time versus time delay, peg 3.

of rate control's superiority may be the result of better open-loop positioning accuracy, which was not directly measured.

Also significant was the difficulty of the task as reported by the subject. When performing with the 3.0-s time delay, he became physically and mentally fatigued much more quickly than with master-slave control.

These results suggest that perhaps combined master-slave/rate control would be more appropriate for time-delayed manipulation. Master-slave control would be used for coarse positioning, and rate control for fine positioning.

We recognize that the results of this experiment apply only to the NASA-Ames manipulator system. For example, a fully counterbalanced master would reduce the subject's physical workload and may increase open-loop positioning accuracy. Nevertheless, it has been shown that rate control has advantages in time-delayed manipulation.

REFERENCES

[1] W. R. Ferrell, "Remote manipulation with transmission delay," NASA TN D-2665, Feb. 1965.

[2] J. H. Black, Jr., "Factorial study of remote manipulation with transmission time delay," M.S. thesis, MIT, 1970.

[3] H. C. Vykukal *et al.*, "An anthropomorphic master-slave manipulator," *Proc. 1st Conf. Remotely Manned Systems*, Calif. Inst. of Tech., 1972.

[4] D. E. Whitney, "Resolved-motion rate control of manipulators and human prostheses," *IEEE Trans. Man-Machine Syst.*, vol. MMS-10, no. 2, pp. 47-53, 1969.

[5] G. P. Starr, "A comparison of control modes for time-delayed remote manipulation," Ph.D. dissertation, Dept. Mech. Engr., Stanford Univ., 1978.

[6] R. H. Blackmer *et al.*, "Remote manipulators and mass transfer study," AFAPL-TR-68-75, Wright-Patterson AFB, Nov., 1968.

[7] W. R. Ferrell, "Delayed force feedback," *Human Factors*, vol. 8, no. 5, pp. 449-455.

N82 34073

EXPERIMENTAL EVALUATION OF THE CONCEPT OF SUPERVISORY MANIPULATION

T.L. Brooks
Robotics and Teleoperator Group
Jet Propulsion Laboratory
California Institute of Technology

T.B. Sheridan
Man-Machine System Laboratory
Massachusetts Institute of Technology

Abstract

A computer-controlled teleoperator system which is based on task-referenced sensor-aided control has been developed to study supervisory manipulation. This system, called SUPERMAN, is capable of performing complicated tasks in real-time by utilizing the operator for high-level functions related to the unpredictable portions of a task, while the subordinate machine performs the more well-defined subtasks under human supervison.

To determine whether supervisory control schemes such as these offer any advantage over manual control under real-time conditions, a number of experiments involving both simple and complicated tasks were performed. Six representative tasks were chosen for the study: (1) obtaining a tool from a rack, (2) returning the tool to the rack, (3) removing a nut, (4) placing samples in a storage bin, (5) opening and closing a valve, and (6) digging with a shovel. The experiments were performed under simulated conditions using four forms of manual control (i.e., switch rate, joystick rate, master-slave position control, and master-slave with force feedback), as well as supervisory control. Through these experiments the effectiveness and quality of control were evaluated on the basis of the time required to complete each portion of the task and the type and number of errors which occurred.

Even under the "best" control conditions (i.e., no degraded sensor or control loops due to time delays, restricted bandwidths, etc.) supervisory control was found to improve performance for all forms of manual control except force-reflecting master-slave which was found to be slightly faster than supervisory control, but more prone to errors. With degraded sensor or control loops it is fairly predictable that supervisory control will show even more advantage, through the latter experiments are yet to be done.

1. INTRODUCTION

Teleoperators have traditionally relied on relatively simple and direct man-machine interfaces for control. However, with the advent of microcomputers and advanced sensor techniques it is now possible to design and build a hierarchical control system in which the operator is responsible for the higher-level functions related to the unpredictable portions of the task, while the subordinate machine performs the more well-defined subtasks under human supervision. Control based on a supervisor-subordinate relationship such as this is called "supervisory control" [1]. In general, the human operator communicates intermittently with the computer, and the computer, in turn and continuously in time, controls the sensors and actuators of the vehicle and manipulator. In essence, the teleoperator system acts as an autonomous "robot" for short periods while in the pursuit of task goals previously programmed by the operator or updated on the last cycle of communication. This mode of control promises more precision for certain tasks, less susceptibility to failure in the event of communication channel breakdown, and greater efficiency than direct human control.

To investigate the relative merits of supervisory control applied to teleoperators, a task-referenced sensor-aided supervisory system, called SUPERMAN, was built and experiments were performed. This paper will evaluate those experiments and by comparison of various conventional control modes with supervisory control, demonstrate that supervisory manipulation does improve performance in the majority of cases.

2. METHOD

Apparatus

The major elements of the SUPERMAN system are a modified Argonne E2 master-slave manipulator with six degrees-of-freedom, a dedicated control interface (DASI), and an Interdata 70 computer. Designed for efficient man-machine interaction with both analog and symbolic control inputs, the system can be commanded by a variety of conventional control modes as well as supervisory. In addition, time delay and/or noise can be added for experimental purposes.

Using both analog and symbolic commands, a manipulation can be taught and/or demonstrated to the computer. Trained manipulations can be transformed from one coordinate system to another so that once the generic characteristics of a task have been learned, the machine can perform similar tasks in different locations without further training. When the human operator requires a particular trained manipulation he simply "initializes" the new coordinate system relative to the old by moving the teleoperator hand to the starting point of the task (e.g., grasping a nut or valve handle) and signals for execution. Certain objects in the task environment can, of course, maintain their original coordinates. For a complete development of task transformations related to supervisory control see refs. 2 and 3.

Since the manipulator can sense the forces generated during the task, supervisory programs can call for repeated movements which, upon certain touch conditions becoming true, branch into other movements. For example, repeated hand movements can grasp a nut, unscrew it by one revolution, pull back to test whether it is off and, if it is, place it in a bucket or, if it is not, repeat the operation. Similar supervisory programs have been applied to attaching a nut to a bolt, opening and closing a valve, scooping dirt and so on. Further information on the SUPERMAN system can be found in ref. 3.

The manipulator laboratory was arranged as shown in fig. 1 during the experiments. To simulate remote conditions the operator viewed the task environment through either a mono or 2-view television system. The video system consisted of two black and white high-resolution 9 in. monitors, a fixed camera with wide angle lens, and a zoom camera with pan & tilt.

Figure 2 shows the manipulator environment and the experimental tasks designed for this study. The tool rack and sample buckets remained in the locations shown throughout the experiments since these pieces of equipment are usually rigidly attached to the teleoperator vehicle in real applications. Also shown in the figure are the movable task hub and task board on which representative tasks such as valves, bolts, etc were mounted. The location of the task hub and board were changed throughout the study to simulate the random task/vehicle relationships which are typical of the arbitrary environments found in marine and space applications.

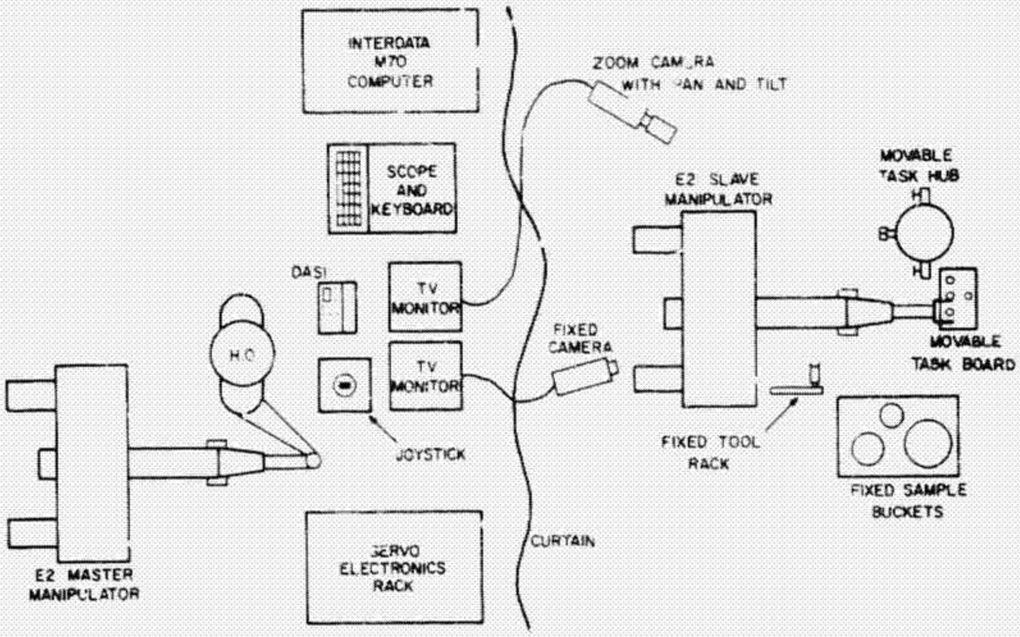
INTERDATA
M70
COMPUTER
SCOPE
AND
KEYBOARD
DASI
TV
MONITOR
TV
MONITOR
H.C.
JOYSTICK
SERVO
ELECTRONICS
RACK
E2 MASTER
MANIPULATOR
ZOOM CAMERA
WITH PAN AND TILT
FIXED
CAMERA
CURTAIN
E2 SLAVE
MANIPULATOR
MOVABLE
TASK HUB
MOVABLE
TASK BOARD
FIXED TOOL
RACK
FIXED SAMPLE
BUCKETS

Fig. 1: Schematic of Experimental Layout

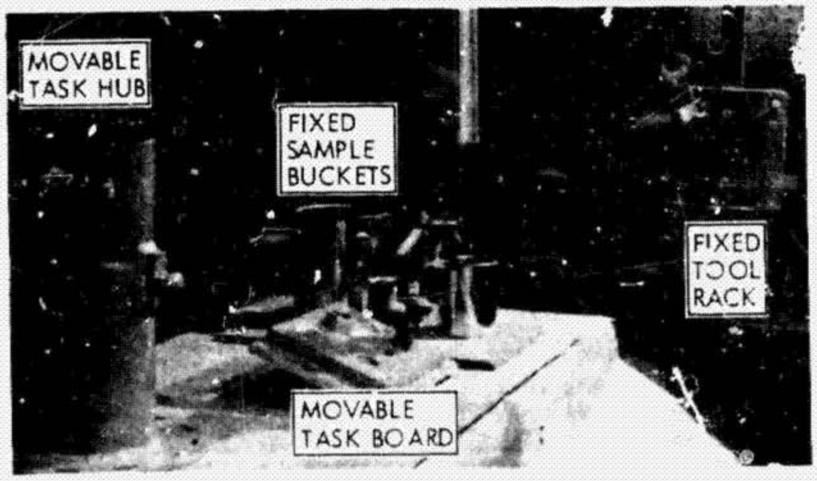
MOVABLE
TASK HUB
FIXED
SAMPLE
BUCKETS
FIXED
TOOL
RACK
MOVABLE
TASK BOARD

Fig. 2: Task Hub, Task Board, Sample Buckets, and Tool Rack

Experimental Design

Six basic tasks were identified for experimental investigation:[1] (1) tool retrieval; (2) tool return; (3) taking a nut off; (4) grasping an object and placing it in a container; (5) opening/closing a valve; and (6) digging. In addition, four manual control modes were delineated as important experimental parameters: (1) switch fixed rate; (2) joystick variable rate; (3) master-slave position control; and (4) master-slave position control with force reflection. With regard to the video arrangement, both mono and 2-view conditions were tested for comparison. Due to time constraints only three subjects were used for four of the tasks (tool retrieval, tool return, nut-off and sampler), and only one subject was used for the remaining two (open/close valve and digger). Each experiment was performed 5 times by each subject to obtain a statistical mean and standard deviation. Both manual and supervisory control were used.

These conditions result in a total of 1120 experimental runs. Since this would require an inordinate amount of time, the experimental load was reduced to 680 runs by noting that some of the tasks, or portions of the tasks, had constant computer execution times (see ref. 3 for details).

Subjects and Training

Three classes of subjects were used for these experiments, one experienced, four well trained, and two untrained subjects.

The well trained subjects had an average of 20 hours training given in 15 minute intervals for each of the control modes. Generally, after the subjects practiced for 15 minutes with a particular control mode a simulated task was performed. When the subjects appeared to show a plateau, experiments were begun. Since the experiments usually stretched over a period of several days, the subjects were asked to "reperform" some of the tasks due to a "mistake". If the subjects showed marked improvement the tasks were performed again until the learning curve levelled off. The four trained subjects were given incentives to perform well in the form of bonuses which would be awarded to the best combined time and error rates in any control category.

The first author was used as the baseline experienced subject. With over 200 hours of practice on manipulator systems and intimate knowledge of the SUPERMAN system, it may be reasonably assumed that the experienced subject underwent little or no learning. The experienced subject performed all of the tasks without a "warm-up" period.

The untrained subjects had a total of 3 hours training time for all control modes (i.e., 30 minutes per control mode and viewing condition). The learning curves of the untrained subjects were not observed. The only requirement placed on their training sessions was to insure that each control mode was given equal training time. After the 3 one-hour familiarity and adjustment periods were over the subjects were allowed 24 hours of rest and the experiments were begun.

---

[1] Although it may appear that the tool retrieval and return tasks are simply the reverse procedure of one another, these tasks do have fundamentally different requirements. To clarify, consider that the retrieval task required the subjects to locate a 7/8 x 3/4 inch tool handle with the end effector docking plate while the return task required the subjects to mate two 1/8 inch pins and holes.

Procedure

The experiments were scored on the basis of recorded time and errors. The subjects were not given specific instructions to minimize either quality, but only to weigh them equally. Each subject was, however, given a criterion by which successful completion of the task would be measured (these criteria will be specified on the following pages). The experiments were not redone when errors occurred, regardless of the magnitude, unless it was impossible to proceed with the task (e.g., a collision with an object that blew a fuse, etc.). The tasks were randomized whenever possible to negate the effects of variables which the experimenters were not aware of (e.g., particularly easy or difficult task positions, short term learning effects, etc.). All tasks started from a prespecified position so that comparisons of supervisory initialization times could be made across control modes.

The procedure for each of the representative tasks was as follows:

a) Tool-Retrieval Task - The first task required the subject to start with the end effector positioned near the task hub. On the experimenter's signal, the subject moved the end effector to the tool rack, obtained the tool, being sure it was properly seated in the hand, and returned with the tool to the starting postion. The subjects were told that the success or failure of the task was measured by whether a solid connection between the tool handle and end effector was achieved. Execution of this task under supervisory control simply involved a button push.

b) Tool-Return Task - For the second task the subject started from a position next to the task hub with the tool in hand, and on the experimenter's signal, moved to the rack, replaced the tool insuring that it was properly seated, and returned to the initial position. The operators were told that the success or failure of the task was determined by whether or not the tool was properly replaced on the rack. To properly seat the tool on the rack required that both of the 1/8 inch rack pins were engaged in the handle and that the tool was completely pushed onto the pins. This task was executed under supervisory control through a simple button push.

c) Nut-Removal Task - This experiment began with the end effector positioned over the valve on the task hub. On the experimenter's signal, the subject moved the end effector from the valve to the nut, oriented the hand, and removed the nut. The general procedure used by the subjects and computer was to turn 180°, pull back to test if the nut was off, and then either reverse 180° and continue, or remove the nut. Prior to the task, the operators were told that the task would be considered successfully completed if the nut could be removed without losing it. Under supervisory control the operator initialized the task by moving from the starting position to the nut, orienting the hand with the rotational axis of the nut, and signaling the computer to remove it.

d) Sampling Task - The fourth task required the subject to pick-up thirteen randomly placed samples and put them in one of two buckets according to their size. The subjects were told that their success or failure to complete the task would be measured by how many samples were successfully placed in the proper buckets. Under supervisory control the operator initialized the task by placing the end effector over the sample and signaling the computer to place it in the appropriate bucket. The computer returned control to the subject at the location were the sample was grasped. The operator then moved to another sample, initialized, and continued until all 13 samples were in the buckets.

e) Open/Close Valve Test - This experiment required the subject to position the end effector over the nut on the task hub, and then, on the experimenter's signal, the subject moved to the valve, oriented the hand, and opened or closed the valve as required (opening and closing tasks were switched after each experiment). The subject was required to continue until the valve operation was complete. To initialize this task under supervisory control the operator oriented the end effector on the rotational axis of the valve and signaled the computer either to open or close it as required. The computer checked the rotational torques to determine if the task had been completed.

f) Digging Task - The final task required the subject to remove a specified amount of soil from a box by filling a bucket with a shovel. This task is composed of a number of subtasks: (1) the shovel is positioned to remove the soil, (2) the shovel is pushed into the soil and lifted out, and (3) the soil is transported to the bucket and dropped in. The subject was required to continue until the bucket was filled. Under supervisory control the positioning of the shovel was performed manually (i.e., the operator decided when and where to dig) while the scooping and dropping actions were executed by the computer.

3. RESULTS

It has been shown by a number of investigators that the time required to perform a task can be attributed to a number of distinctly different motions. For example, one classification divides the task time for control with a time delay into segments related to get, transport, and position motions [4]. For a peg-in-the-hole task Hill [5] has shown that there are two independent motions which determine the total task time under manual control - gross travel and precision. This paper will use a similar scheme to describe the task completion time for a supervisory system:

$$t_{TT} = t_I + t_P$$

where

t_{TT} = Task Time

t_I = Time required by the human operator to initialize the task. This time is primarily a function of the initial hand/task locations and the manual control mode used to locate the task.

t_P = Time required by the computer to perform the task. This time is primarily a function of the task complexity.

The determination of these times is rather simple due to the discontinuity in control which occurs during the trade from manual initialization to computer execution (this "discontinuity" is a desired result since trading of control should be "apparent" [3,6]).

Figures 3-6 are plots of typical data (see legend below for figure abbreviations). The data recorded during the supervisory experiments have been divided into initialization and performance times to indicate the time spent by each action. Each of the time bars is the result of data averaged over two trained subjects, except for fig. 6 which is averaged over three trained subjects. The lines to the left of the manual control bars give the range over which the trained subjects performed the task. For comparison, the average time for an inexperienced subject to perform the first three tasks is also given (denoted by triangles). The mean times of the untrained subjects were always above the maximum value of the trained subjects for the same task and control mode. The lower portion of each figure (figs. 3b-6b) plots the mean number of errors which occurred under manual and supervisory control (for a specific breakdown of the individual errors see ref. 3).

LEGEND: Key to Abbreviations Used in Text

MS - Master-slave with force feedback
MS NO FFB - Master-slave without force feedback
JVRC - Joystick variable rate control
SVRC - Switch fixed/variable rate control

4. EVALUATION

Manual Control

Predictably, the task completion time increased with control complexity for all tasks. Viewing conditions (mono and 2-view) appeared to affect tasks which required precision movements (e.g., return tool and nut-off), but had little or no effect on the less precise tasks (e.g., sampling). In general, the number of errors increased as the control complexity increased from master-slave to switch rate. However, for some of the tasks a sharp decrease in errors was noticed between joystick and switch rate control (e.g., see figs. 5b and 6b). This effect is attributable to two factors: (1) the increased attention and care each operator exhibited during switch rate control modes (i.e, to move from point A to point B requires considerable thought and effort with switch rate control, but under joystick control the desired movement only requires a push on the stick), and (2) the coincidental matching of the task degrees of freedom and control degrees of freedom (e.g., in the valve or nut-off tasks the axis of rotation corresponded with the hand axis of rotation).

Table 1 gives the ratio of task completion times for each control mode with respect to the "best" control case, master-slave with force feedback. The ratios are given for each subject, task and viewing condition. The untrained subjects are denoted by U1 and U2, the trained subjects are denoted by T1, T2, T3 and T4, and the experienced subject is denoted by E1. The table shows a number of interesting trends: (1) the ratios increase with increasing control complexity, (2) the ratios are approximately constant across subjects (both trained and untrained) within a given task, (3) the ratios are constant across viewing conditions, and (4) the ratios are not constant across tasks (the tasks have been arranged in the table so that the ratio increases as the page is read from top to bottom). A number of other investigators have found similar trends [7,8,9,10].

ORIGINAL PAGE IS
OF POOR QUALITY

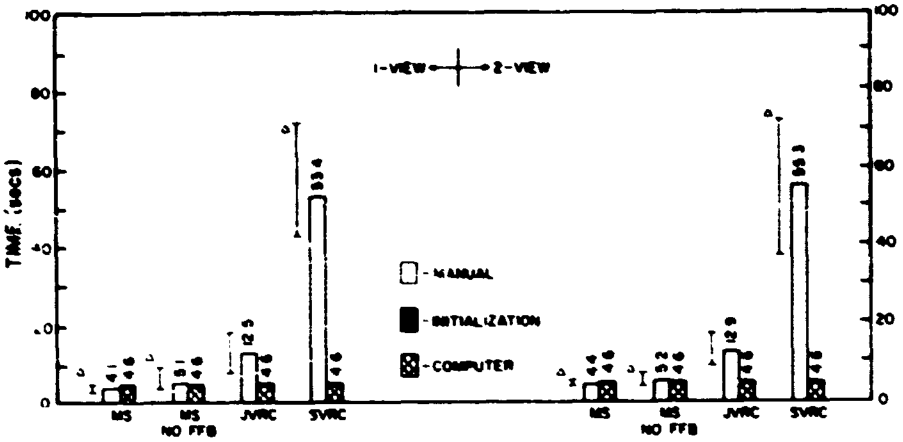

Fig. 3a: Average Tool-Retrieval Time. Each bar gives the average time of two subjects. The Δ symbol represents the mean time for an untrained subject. The capped lines show the total range of data for the trained subjects.

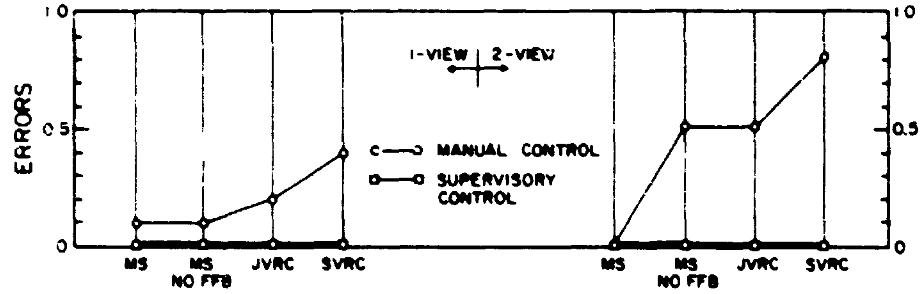

Fig. 3b: Expected Number of Tool-Retrieval Errors. Each data point represents the average error rate of two trained subjects. Possible errors included collisions, dropping the tool, and not seating the handle in the end effector properly.

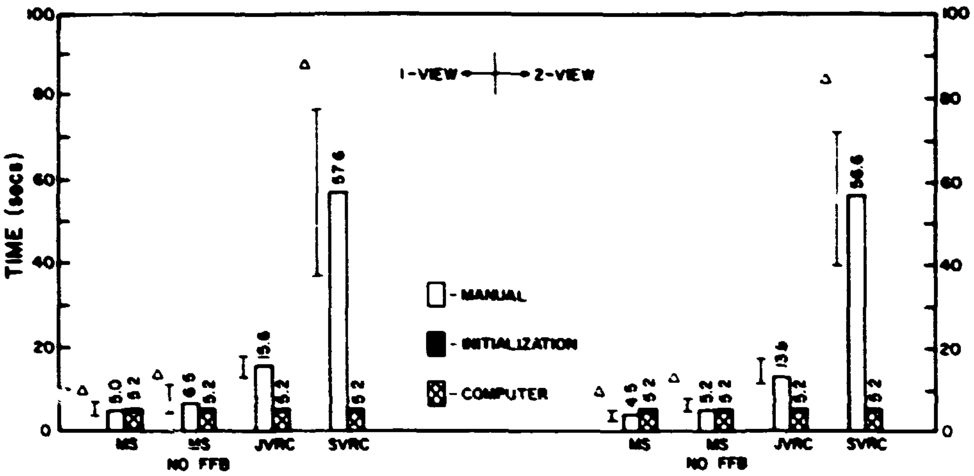

Fig. 4a: Average Tool-Return Time. Each bar represents the average time of two trained subjects and each Δ gives the mean time for an untrained subject. The capped lines represent the total range of data for the trained subjects.

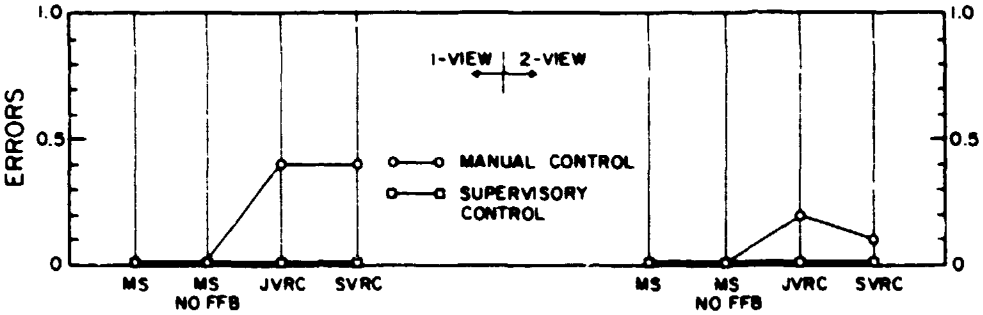

Fig. 4b: Expected Number of Tool-Return Errors. Each data point represents the average error rate of two trained subjects. Possible errors included collisions, dropping the tool, and not seating the handle on the rack properly.

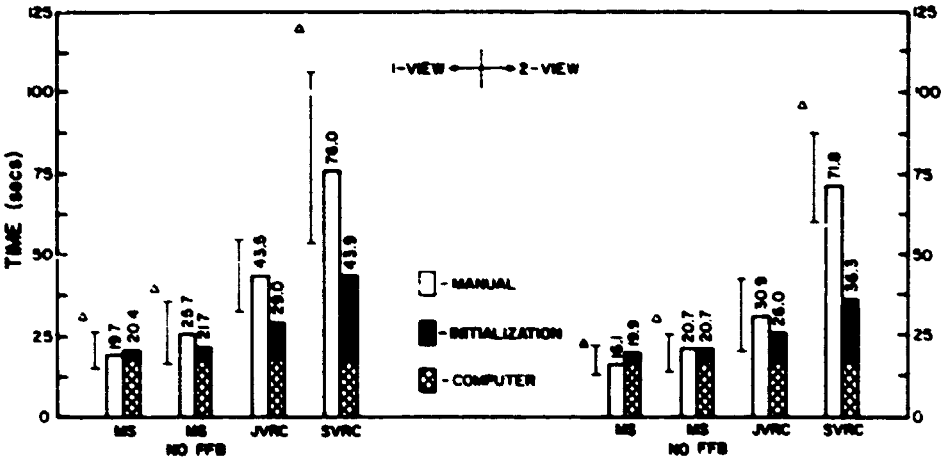

Fig. 5a: Average Nut-Removal Time. Each bar represents the average time of two trained subjects and each Δ gives the mean time for an untrained subject. The capped lines represent the total range of data for the trained subject.

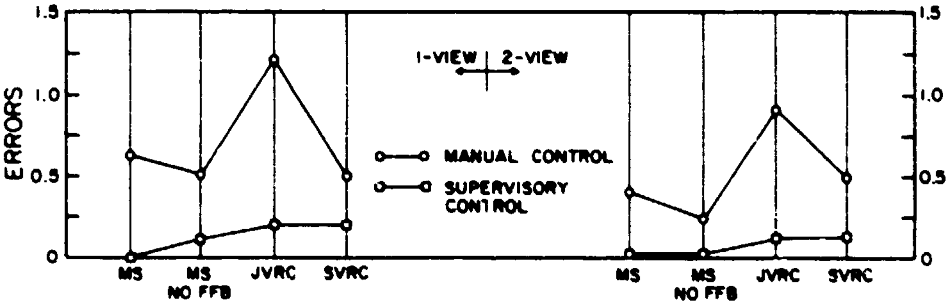

Fig. 5b: Expected Number of Nut-Removal Errors. Each data point represents the average error rate of two trained subjects. Possible errors included collisions and dropping the nut.

ORIGINAL PAGE IS
OF POOR QUALITY

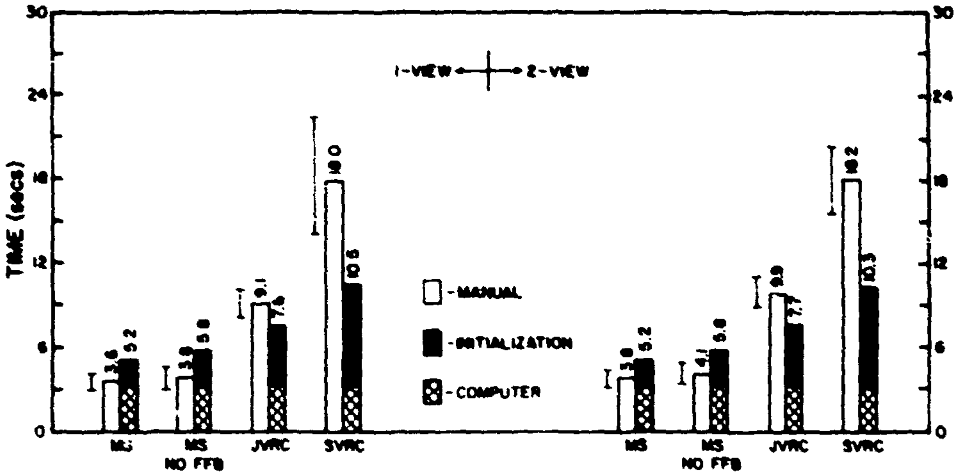

Fig. 6a: Average Sampling Time. Each bar represents the mean time of three trained subjects. The capped lines represent the total range of data for the subjects.

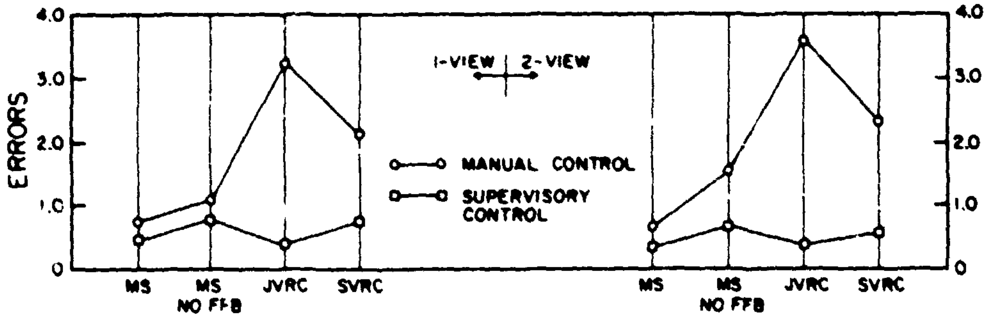

Fig. 6b: Expected Number of Sampling Errors. Each data point represents the average error rate of three trained subjects for 13 sampling actions. Possible errors included collisions, missed buckets, lost samples, and (under supervisory control) pressing the wrong button.

Table 1: Ratio of Time to Perform Task Under Given Control Mode to Time to Perform Task Under Master-Slave with Force Feedback (CM/MS).

	1-VIEW				2-VIEW				
	MS	MS NO FFB	JVRC	SVRC	MS	MS NO FFB	JVRC	SVRC	
VALVE 1-DOF	1.0	1.2	1.4	3.6	1.0	1.1	1.6	3.9	E1
CUT-OFF 2-DOF	1.0 1.0 1.0	1.2 1.4 1.3	2.2 2.2 *	4.3 3.3 3.9	1.0 1.0 1.0	1.3 1.2 1.4	2.0 1.9 *	4.4 4.5 4.3	T1 E1 U2
SAMPLER 3-DOF	1.0 1.0 1.0	1.1 1.0 1.0	2.5 2.8 2.4	5.1 5.3 4.7	1.0 1.0 1.0	1.1 1.0 1.1	2.7 2.5 2.6	4.4 5.1 4.9	T2 T3 E1
SCOOPER ?-DOF	1.0	1.1	3.9	10.6	1.0	1.2	3.9	10.9	E1
RETURN-TOOL 6-DOF	1.0 1.0 1.0	1.1 1.4 1.4	3.6 2.7 *	10.7 12.2 9.0	1.0 1.0 1.0	1.2 1.3 1.4	3.4 2.7 *	12.1 13.3 9.7	T4 E1 U1
GET-TOOL 6-DOF	1.0 1.0 1.0	1.1 1.4 1.4	3.8 2.4 *	13.0 13.0 8.3	1.0 1.0 1.0	1.2 1.2 1.3	3.3 2.6 *	12.1 13.2 11.8	T4 E1 U1

Supervisory Control

As would be expected, the time required by the computer to perform its portion of the task remained fixed regardless of the manual control mode from which the human operator issued the execution command. Also, since the only action required of the operator to initiate the tool-retrieval and return tasks was a button push, the absence of initialization times in figs. 3a and 4a was not surprising. The remaining tasks, including those not shown in this paper, had initialization times associated with the overall task time. As seen in figs. 5 and 6 the initialization times increased with control complexity.

Table 2 gives the ratios of the task completion times under manual control to the times under supervisory control. The ratios are given for each subject, task and viewing condition. The ratios relative to computer control (Table 2) do not show the same trends as those relative to master-slave control (Table 1). It is interesting to note that in contrast to the consistent ratios of Table 1, the computer control ratios of the untrained subjects are significantly higher than the trained subjects: clearly, untrained subjects gain more from supervisory control than trained subjects. Gains from supervisory control for any manual mode are seen to be most significant for tasks which do not require initialization procedures other than a button push (i.e., tool-retrieval and tool-return). The control mode columns clearly indicate the results of the SUPERMAN experiments: (1) master-slave with force feedback rarely benefits from supervisory control, (2) master-slave without force feedback can profit from supervisory control in tasks which require force feedback, and (3) both forms of rate control can be aided by supervisory routines regardless of the task.

ORIGINAL PAGE IS
OF POOR QUALITY

Table 2: Ratio of Time to Perform Task Under Manual Control to Time to Perform Task Under Supervisory Control (MC/SC).

	1-VIEW				2-VIEW				
	MS	MS NO FFB	JVRC	SVRC	MS	MS NO FFB	JVRC	SVRC	
VALVE 1-DOF	1.1	1.3	1.2	2.0	0.8	0.9	1.1	2.0	E1
SHUT-OFF 2-DOF	1.0 0.9 1.5	1.2 1.2 1.9	1.6 1.4 *	2.0 1.5 2.1	0.8 0.8 1.1	1.1 0.9 1.5	1.2 1.1 *	2.1 1.9 2.0	T1 E1 U2
SAMPLER 3-DOF	0.7 0.7 0.6	0.7 0.7 0.6	1.2 1.2 1.2	1.8 1.6 1.7	0.8 0.7 0.7	0.8 0.7 0.7	1.3 1.3 1.3	1.9 1.7 1.8	T2 T3 E1
SCOPPER 2-DOF	0.5	0.6	1.9	4.8	0.5	0.6	1.9	4.9	E1
RETURN-TOOL 6-DOF	0.9 1.1 1.9	1.0 1.5 2.6	3.2 2.8 *	9.4 12.8 16.9	0.9 0.9 1.7	1.0 1.1 2.4	3.0 2.3 *	10.6 11.3 16.3	T4 E1 U1
GET-TOOL 6-DOF	0.8 1.0 1.8	0.9 1.3 2.6	3.2 2.3 *	10.8 12.5 15.3	1.0 0.9 1.4	1.2 1.1 1.7	3.2 2.4 *	11.7 12.4 16.0	T4 E1 U1

In all cases the error rates for supervisory control were less than manual control. However, an interesting error was noted during the sampling experiments - occassionally the subjects pressed an incorrect button sending the sample to the wrong bucket.

5. DISCUSSION

Theoretically there is no reason why master-slave with force feedback should be any faster than supervisory control. Consider that the computer could simply mimic the human operator's best trajectory, and hence, be at least as fast. Unfortunately, in practice there is always a certain overhead associated with retransformation of coordinates, trajectory calculations and sensor logic. Also, it was generally observed that the subjects were making adaptive, orchestrated motions, whereas the computer was limited to more rigidly defined trajectories and states. In light of these observations it can be said that the faster master-slave times make more of a statement about the direction that future studies dealing with supervisory control should take than they do about its potential in teleoperator systems.

Although the experiments were not designed to measure the effectiveness of supervisory control during extended periods of manipulation, an interesting observation was made after the experiments had been completed - the manual experiments had been performed with rest periods between each run because the subjects complained of fatigue and boredom, while the supervisory experiments had been unintentionally run back-to-back since fatigue and boredom were not noted. From these observations it could be surmised that as a task becomes more involved and complex, boredom and fatigue will become increasingly important factors, tipping the scales even further in favor of supervisory control. However, experiments to validate this statement have yet to be performed.

6. CONCLUSION

Even under "ideal" control conditions supervisory control was found to be more efficient and effective (as determined from the task completion times and manipulation errors) than switch rate control, joystick rate control, and master-slave position control. Bilateral force-reflecting master-slave was found to be slightly faster than supervisory control, but more prone to errors. Since the experiments were performed under "ideal" conditions, it can be reasonably predicted that supervisory control will show even more advantage when used with degraded sensor or control loops (e.g., time delays, limited bandwidth, etc.), though the latter experiments remain to be done. In addition, an a posteriori observation of the experimental procedure appears to indicate that the effects of operator fatigue and boredom during extended periods of manipulation can be significantly reduced through supervisory control.

Acknowledgement

The research described in this paper was carried out at the Massachusetts Institute of Technology under Sea Grant No. 04-7-158-44079 and ONR No. N00014-77-C-0256. The presentation is sponsored by the Jet Propulsion Laboratory, California Institute of Technology under NASA contract No. NAS7-100.

References

1. Ferrel, W.R., and Sheridan, T.B., "Supervisory Control of Remote Manipulation," IEEE Spectrum, Vol. 4, No. 10, October 1967, pp. 81-88.
2. Brooks, T.L., "Supervisory Manipulation Based on the Concepts of Absolute vs Relative and Fixed vs Moving Tasks," to appear in the Proceedings of ASME International Computer Technology Conference, San Francisco, California, August 12-14, 1980.
3. Brooks, T.L., and Sheridan, T.B., "SUPERMAN: A System for Supervisory Manipulation and the Study of Human/Computer Interactions," MIT Sea Grant Report No. MITSG 79-20, July 1979, Massachusetts Institute of Technology.
4. Black, J.H., "Factoral Study of Remote Manipulation with Transmission Time Delay," Master's Thesis, M.I.T., December 1970.
5. Hill, J.W., "Two Measures of Performance in a Peg-in-Hole Manipulation Task with Force Feedback," Thirteenth Annual Conference on Manual Control, Cambridge, MA, June 1977.
6. Sheridan, T.B. and Verplank, W.L., "Human and Computer Control of Undersea Teleoperators," Man-Machine Systems Laboratory Report, Massachusetts Institute of Technology, July 1978.
7. Pesch, A.J., Hill, R.G., and Klepser, W.F., "Performance Comparisons of Scuba Divers vs. Submersible Manipulator Controllers in Undersea Work," Offshore Technology Conference, Houston, TX., 1971.

8. Mullen, D.P., "An Evaluation of Resolved Motion Rate Control for Remote Manipulators," Master's Thesis, M.I.T., January 1973.

9. Pesch, A.J., Bertsche, W.R., "Performance Measurement for Undersea Systems," Performance Evaluation of Programmable Robots and Manipulation, NBS Special Publication #459, October 1976.

10. Freedman, L.A., Crooks, W.H., and Coan, P.P., "TV Requirements for Manipulation in Space," Mechanism and Machine Theory, 1977, Vol. 12, pp. 425-438.

N82 34074 37

EVALUATION OF "SMART" SENSOR DISPLAYS FOR MULTIDIMENSIONAL PRECISION CONTROL OF SPACE SHUTTLE REMOTE MANIPULATOR

A. K. Bejczy
Member of the Technical Staff
Jet Propulsion Laboratory
California Institute of Technology
Pasadena, California 91103

J. W. Brown
Aerospace Engineer

J. L. Lewis
Section Head

Crew Station Design Section
Lyndon B. Johnson Space Center
Houston, Texas 77058

Abstract

An enhanced proximity sensor and display system has been developed at the Jet Propulsion Laboratory (JPL) and tested on the full scale Space Shuttle Remote Manipulator at the Johnson Space Center (JSC) Manipulator Development Facility (MDF). The sensor system, integrated with a four-claw end effector, measures range error up to 6 inches, and pitch and yaw alignment errors within ±15 deg., and displays error data on both graphic and numeric displays. The graphic display shows pitch and yaw errors with 1 deg. resolution and range error with 0.2 inches resolution in an integrated format. The numeric display resolution is 0.1 inch for range error and 0.5 deg. for pitch and yaw errors. The errors are referenced to the end effector control axes through appropriate data processing by a dedicated microcomputer acting on the sensor data in real time. Both display boxes contain a green lamp which indicates whether the combination of range, pitch and yaw errors will assure a successful grapple. More than 200 test runs were completed in early 1980 by three operators at JSC for grasping static and capturing slowly moving targets. The test goal was to investigate methods to minimize terminal range and alignment errors by utilizing range, pitch and yaw error information from the sensor displays. Reduced errors will reduce preload on payload grapple fixture. The test runs aided by sensor displays were contrasted with test runs without sensor display aids. The paper describes the enhanced sensor and display system, the test runs and results. The tests have indicated that the use of graphic/numeric displays of proximity sensor information improves precision control of grasp/capture range by more than a factor of two for both static and dynamic grapple conditions.

1. INTRODUCTION

Manual control of the 15.2 m. (50 ft.) long Space Shuttle Remote Manipulator System (RMS) requires a delicate balance in the information and control conditions. This requirement is particularly delicate when the target is near the grasp envelope of the end effector: a precise knowledge of small range or alignment errors can have a large effect on the success of or preload associated with the grasp.

Previously (Ref. 1), a proximity sensor system was developed at the Jet Propulsion Laboratory (JPL) and integrated with a four-claw end effector of Johnson Space Center (JSC). The sensor system consists of four proximity sensors, and was designed to supplement the visual information for control. It provides guidance data to the operator when the target is near the end effector's grasp envelope where visual perception of range, pitch and yaw errors are poor. In previous ground tests at the JSC Manipulator Development Facility (MDF), the use of the sensor system was restricted to the verification of a "successful grasp state" before the operator initiated the grasp. Even the use of restricted proximity sensor information proved to be valuable for improving control performance.

In order to extend the utility of proximity sensor information for grasp or capture control, two new "smart" displays (a graphic and a numeric) have been developed at JPL and tested at JSC recently. The purpose of the new displays is to show the operator the values of range, pitch and yaw errors referenced to end effector axes, in addition to indicating whether the combination of these three errors will assure a successful grasp of the target. The display of range, pitch and yaw error values was anticipated to aid the operator to fine-control the grasp with respect to these three errors within the grasp envelope. The tests have verified the anticipated utility of the detailed displays of error information, but raised a number of questions regarding a useful integration of proximity sensor and visual information.

2. "SMART" DISPLAYS

The new displays are being used with the proximity sensor system developed for the previous tests in 1978 and described in detail in (Ref. 1). However, the effective sensing range of the sensor system has been extended electronically from 5 to 6.5 inches. The effective depth of the grasp envelope of the four-claw end effector is about 3 inches. Consequently, the sensor system can look ahead of the grasp envelope by 3.5 inches. The use of this sensor system implies that the two lateral and roll misalignment errors within the grasp envelope are controlled visually.

The graphic display has been built from 10-element linear LED displays encapsulated in one chip, with individual addressable anode and cathode for each element in the chip. The graphic display resolution is 0.2 inches)0.508 cm) per display element in depth, and 1 degree per display element in pitch and yaw errors. (See Fig. 1.) The quantitative value of each error bar is increasing away from the center green lamp. Hence, zero error for each bar is at the center of the display. This focuses the operator's attention to a single "goal point" on the display towards which all error bars should be decreased and where the "green light" would be on for successful grasp.

Note that depth error is indicated with two identical bars converging in a parallax-type view arrangement towards the center green lamp. This renders the display more symmetric and facilitates the distinction between angular and depth-error bars. The green light "on" condition indicates that the existing combination of depth, pitch and yaw errors will allow a successful grasp.

The graphic display also contains a tone generator. It provides a "success tone" (a short beep tone, - distinguished in frequency from the "success tone") when the target reaches the sensing range or leaves the sensing range. The maximum depth sensing range shown on the display is 6 inches (or 15 cm). Pitch and yaw errors are indicated in the range of ±15 deg. Actually, the warning beep tone provides an advance warning since it is activated at a distance of about 6.3 inches which is not shown on the display. The display is activated only at 6 inches distance.

The numeric display resolution is 0.1 inch (0.254 cm) in depth error and 0.5 deg in angular errors. It also has the "green success lamp". The numeric display can also be applied to performance evaluation by the use of a hold/reset switch. This switch can be connected to the grasp control circuit. Hence, it can automatically register the residual depth, pitch and yaw errors at the moment of grapple.

The new displays are driven by a single board Intel 80/20 microprocessor which linearizes the sensor data and processes the linearized data through a preselected "success algorithm". An appropriate "success algorithm" can be selected in the computer through a BCD switch. The algorithms can be referenced to alternative roll orientations of the end effector pitch and yaw axes, and can utilize altenative numeric definitions for "successful grapple envelope" in terms of maximum and minimum values of allowable depth, pitch and yaw errors. Altogether 32 display drive program combinations have been implemented: 2 algorithm alternatives, with 4 alternative sets of parameters used in 4 alternative reference frames. The basic "success algorithm" is the conic algorithm (described in Ref. 1) using all four or only three out of four sensors. The four sets of trapezoid parameters are listed in Table 1 together with the BCD program select switch assignments.

Algorithmic selection of pitch and yaw reference axes by four 90 deg. rotation steps (see digit X on the BCD dial in Table 1) allows four alternative end effector mountings/viewings, keeping the pitch and yaw error display format unchanged in the display boxes. Furthermore, for a fixed end effector mounting/viewing, the algorithmic rotation of pitch and yaw reference axes by 180 deg. will change pitch and yaw error polarity in the display format. This allows two alternative correlations between displacement direction of hand controller and corresponding change in error bar length. The two alternative correlations are: the error bar changes length a) in the direction or b) opposite to the direction of the hand controller displacement.

Figure 2 summarizes the sensor, control and display reference frames together with the actual pitch and yaw error states for digit X = 0 on the BCD dial switch. The mathematics related to these transformations is summarized in the Appendix.

Figure 3 shows a target approach sequence as seen on the "smart" displays. In Figure 3.a the four-claw hand is outside the grasp envelope at 4.3 inches; the center green lamp is off. In Figure 3.b the four-claw hand is inside the grasp envelope at 2.0 inches, and the combination of range, pitch and yaw errors allows successful grasp; green lamp is on. In Figure 3.c the four-claw hand is inside grasp envelope with greatly reduced errors allowing a fine-controlled grasp; green lamp is on. Figure 4 shows the algorithmic rotations of pitch and yaw error axes in the displays by 90 degree steps for a fixed end effector mounting/viewing.

The display boxes contain the appropriate decoding and LED drive electronics.

3. GROUND TESTS

More than 200 test runs were completed in early 1980 by three operators for grasping static and capturing slowly moving targets using the simulated full scale Shuttle manipulator arm at the JSC MDF. The overall test goal was to investigate methods to minimize terminal range and misalignment of the manipulator end effector by utilizing quantitative information from the range, pitch and yaw error sensor displays. Reduced errors will reduce preload on the payload grapple fixture. The operators were asked to observe a predefined error margin within the grasp envelope. The test runs aided by sensor displays were contrasted with test runs with restricted or no sensor display aids. In this last case the operator had to rely upon direct vision and/or TV information. The TV information was enhanced with visual target cues.

OF POOR QUALITY

Table 1. Parameter sets for conic algorithm with trapezoid formula, and program select dial for display drive algorithms

Digit Y	H_A	H_B	H_C	H_D	C*	K
1 or 5	0.1	0.8	1.7	2.4	1.4	2.0
2 or 6	0.3	1.0	1.7	2.4	1.4	2.0
3 or 7	0.2	0.9	1.9	2.6	1.4	2.0
4 or 8	0.4	1.1	1.9	2.6	1.4	2.0

$\underbrace{\text{min} \quad \cdots \quad \text{max}}_{\text{distance (inches) for successful grasp}}$

Program select dial

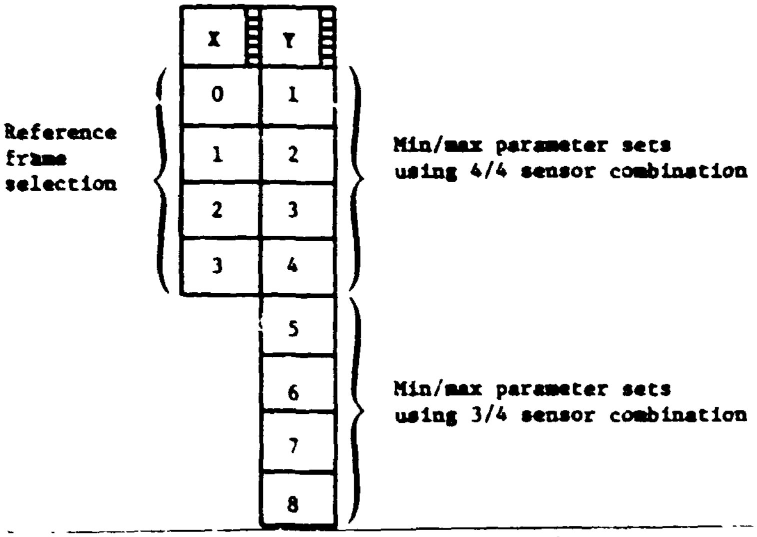
X
Y
0
1
2
3
1
2
3
4
5
6
7
8
Reference frame selection
Min/max parameter sets using 4/4 sensor combination
Min/max parameter sets using 3/4 sensor combination

The test facility and equipment have been described in detail in (Ref. 1).

The grapple target mounted on the payload represented the unit used in the RMS flight system. The target is used in conjunction with the Closed Circuit TV (CCTV) camera mounted on the wrist of the manipulator, which is controlled in the end effector coordinate system. This reference system allows for the operator to control the tip position and attitude of the end effector using only the CCTV camera feedback in a "fly-to" manner: a command right moves the end effector to the right along its Y axis, a negative roll command rotates the end effector counterclockwise (viewed down the arm) about its longitudinal axis.

The visual target, mounted above the grapple fixture, is designed to permit alignment of the end effector to within ±4 in. and ±15 deg. of the grapple fixture. The visual target and its relation to the grapple fixture is shown schematically in Fig. 5. The center rod of the visual target provides cues for linear alignment (i.e., horizontal and vertical) when used with a crosshair symbol on the CCTV monitor, as well as angular alignments of pitch and yaw. Roll cues are available from the radial lines when used with the CCTV monitor horizontal reference marks. Range information is determined by matching the 14 in. horizontal target lines to the roll reference marks on the CCTV monitor. Understandably, range is the most difficult parameter to determine from the visual cues, especially during dynamic grappling.

The test runs are summarized in Table 2. In addition to the test runs, an equal amount of training runs were also conducted.

In the static tests, the payload was located in the Shuttle payload bay as shown in Fig. 6. The RMS operator, positioned at the aft cabin workstation, attempted to align the end effector with the payload grapple fixture using alternative combinations of visual and sensor display aids as summarized in the test run matrix given in Table 2. The operators were asked to position the end effector by 0.2 in. off the grapple fixture with minimum (zero or near-zero) alignment errors. When the operator indicated that the positioning and alignment was as accurate as possible, the test conductor locked the numeric display by a

Table 2. Test run matrix

Run No.	Motion	Visual Access	No. Operators	No. Runs/ Operator
1	static	*DV only	3	3
2	static	DV + sensor	3	3
3	static	DV/TV only	3	3
4	static	DV/TV + sensor	3	3
5	static	TV only	3	3
6	static	TV + sensor	3	3
7	dynamic	TV only	3	6**
8	dynamic	TV + go/no-go	3	6
9	dynamic	TV + go/no-go + range/att. info.	3	6

NOTES:

1. Each operator received a training session to familiarize with the display devices and alignment operations prior to data taking. Training sessions were conducted for both static and dynamic phases of the test.
2. Each data session included some warm-up runs.

*DV - direct vision
TV - closed circuit television
**3 runs each at 0.1 and 0.2 ft/sec

remote switch, thereby measuring range, pitch and yaw accuracy achieved by the operator. The data were recorded manually for analysis.

In the dynamic tests, the task was to capture a payload translating at 0.1 and 0.2 ft/sec speed across the MDF air bearing floor. The payload (a black box equipped with the grapple fixture and visual target) was mounted on an air sled which was pulled across the floor using a motorized pulley system. The pulley system was placed at about 10 deg. angle relative to the payload bay. The operators were asked to position the end effector as close as possible to the grapple fixture (preferably by 0.2 in. from the grapple fixture) with minimum alignment error. During the dynamic tests, the display locking circuit was linked to the RMS grasp control switch so that the command to execute grasp locked the range, pitch and yaw error values shown on the numeric display. The data were recorded manually for analysis.

The sensor displays were located near the TV monitor as shown in Fig. 7. Figure 7 shows a static grasp test scene. The error values shown on the displays are the actual errors of the pre-grasp state that can be seen directly through the cabin aft window. The visual assessment of range, pitch and yaw errors is quite poor relative to the actual error values shown on the displays. Figure 8 shows the operators using the TV and sensor displays during the tests. Figure 9 shows a dynamic test scene viewed from the air bearing floor. Figure 10 shows a precision controlled range positioning for dynamic capture. The visual target described in Fig. 5 is presented in Fig. 10.

The following data were collected during the tests: time to align/capture; grapple success; grapple alignment errors (pitch, yaw, range); subjective operator comments; video taping; movie and still photography.

4. TEST DATA AND EVALUATION

Table 3 presents a brief quantitative summary of the static test data. However, caution must be exercised in drawing conclusions from data related to a statistical population of three test operators. As seen in Table 3, the use of the graphic and numeric sensor displays improves precision positioning performance by more than a factor of two. This result applies to the training runs as well as to the final runs. The average errors are computed relative to the 0.2 in. off-range from the grapple fixture the operators were asked to observe. Hence, the true individual errors are plus/minus errors. The 100% green lamp "on" result indicates that, using the sensor displays, the operators never went below the requested 0.2 in. off-range. Without sensor displays, the operators could control this condition only with 63% success. That is, in one out of three cases they went below the 0.2 in. off-range. Note also that training has a considerable effect on the final results. The final run data are in each case better by a factor of two as compared to the training run data.

Table 4 presents a brief quantitative summary of the dynamic test data. In this table, the average errors are computed relative to a true zero-level error. As seen again, the cumulative (total) result is that the use of the graphic and numeric sensor displays improves precision positioning performance by a factor of two. However, in the dynamic case there are interesting individual (human factors) variances. For one operator, the graphic/numeric display did not help too much; he obtained the factor of two performance improvement by using only the "green lamp" sensor display. But for another operator, the use of the graphic/numeric displays actually helped to improve the precision positioning performance

Table 3. Summary of static test data

	Using sensor displays		Without sensor displays	
	Average range error (in.)	Green success lamp "on"	Average range error (in.)	Green success lamp "on"
27 Training runs	0.23	no data	0.48	no data
27 Final runs	0.075	100%	0.2	63%

Table 4. Summary of dynamic test data

	Using graphic and numeric sensor displays	Using only "green lamp" sensor display	Without sensor displays
Operator	Average range error (in.)	Average range error (in.)	Average range error (in.)
No. 1, 6 runs each	0.4	1.3	1.4
No. 2, 6 runs each	0.5	0.8	1.1
No. 3, 6 runs each	0.9	0.5	1.0
Total of 18 runs	0.6	0.9	1.2

by more than a factor of three. Note also that there is a factor of two variation between operators' performance within each column of Table 4 related to the use of graphic/numeric and only "green lamp" displays, while the column related to test runs without sensor displays does not show that much variation between operators.

It is interesting to compare the dynamic and static tests. In general, the precision positioning performance in the static tests is better by a factor of six as compared to the positioning performance in the dynamic tests. Obviously, the time pressure and tracking demand in the dynamic capture tasks have a great impact on precision positioning performance.

The individual operator comments can be summarized as follows:

(1) In general, the sensor displays are useful and helpful.

(2) The pitch and yaw error bars should be colored different from the range error bars on the graphic display.

(3) In the dynamic tests, the dominant help came from a peripheral perception of the graphic error bars and "green lamp." The numeric display could not be used effectively during the dynamic capture tasks.

(4) In the static tests, the numeric display proved to be useful and provided an extrareassurance over the graphic display.

(5) The "multi-piece" and "multi-area" display organization can be counterproductive when there are time constraints. An integrated display organization should be preferred, e.g., within the frame of the TV monitor.

(6) A control strategy is needed to effectively utilize the error information obtainable from the displays.

(7) Often, the controllability of the manipulator did not allow to correct for errors shown on the displays.

5. CONCLUSIONS

The tests demonstrated the utility of the end effector proximity sensor and display system in facilitating accurate range positioning and in reducing alignment errors during grapple of a static payload. The advantages of a simple "go/no-go" signal ("green lamp") or a more qualitative "graphic" display during dynamic capture were underscored. The test also demonstrated the importance of learning curve considerations, as well as the emphasis of operator control strategies in using and integrating available information within reasonable workload ranges. The tests also demonstrated the need for developing more integrated displays, such that the operator can achieve a better visual concentration. The development of integrated displays for qualitatively different and multidimensional information raises interesting challenges as discussed in (Ref. 2).

Acknowledgment

The sensor and display development work has been carried out at the Jet Propulsion Laboratory, California Institute of Technology, under NASA Contract No. NAS7-100. The contribution of H. C. Primus and R. S. Dotson to the display hardware and software development, respectively, is acknowledged. The tests were supported by the Spacecraft Design Division of JSC.

References

1. A. K. Bejczy, J. W. Brown and J. L. Lewis, Evaluation of Proximity Sensor Aided Grasp Control for Shuttle RMS, Proceedings of the 15th Annual Conference on Manual Control, Wright State University, Dayton, Ohio, March 20-22, 1979.

2. A. K. Bejczy, Kinesthetic and Graphic Feedback for Integrated Operator Control, Proceedings of the 6th Annual Advanced Control Conference, Man-Machine Interfaces for Industrial Control, Purdue University, W. Lafayette, Indiana, April 28-30, 1980.

APPENDIX

Transformation of Error Variables

Among the three "success" algorithms implemented for the previous tests, the "conic" algorithm proved to be the most useful one. Therefore, only the "conic" success algorithm has been used for the 1980 tests in both variations: for all four sensors and for any three out of the four sensors. For easy reference, the algorithm is repeated here using the symbols explained below.

Square-Symmetric Configuration of Four Proximity Sensor on JSC Four-Claw End Effector

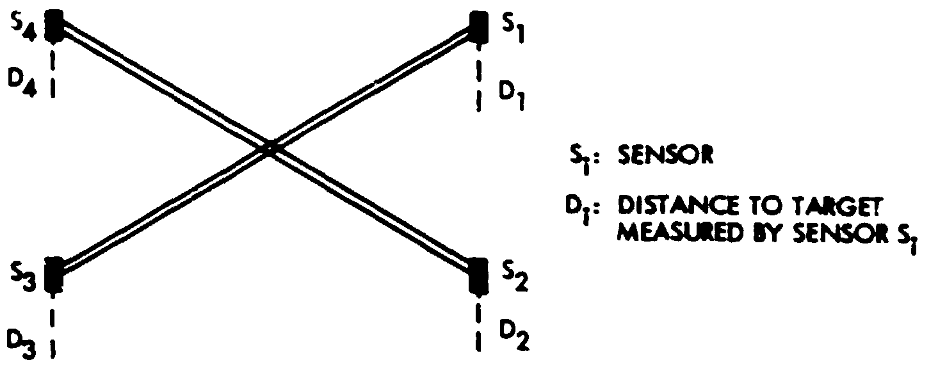
S_4
D_4
S_1
D_1
S_3
D_3
S_2
D_2
S_i: SENSOR
D_i: DISTANCE TO TARGET MEASURED BY SENSOR S_i

Measurements and Trapezoid Formula:

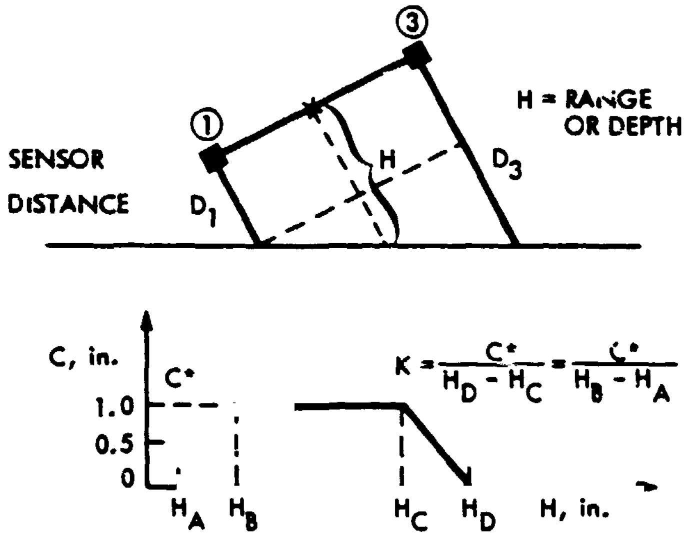
③
①
H = RANGE OR DEPTH
SENSOR DISTANCE
D_1
H
D_3
C, in.
C*
1.0
0.5
0
H_A
H_B
H_C
H_D
H, in.
$K = \frac{C^*}{H_D - H_C} = \frac{C^*}{H_B - H_A}$

C IS A MEASURE FOR PITCH AND YAW ERRORS; C = f(h)

H_A, H_B, H_C, H_D AND K (AND IMPLICITLY ALSO C*) ARE PRESET CONSTANTS

f(H) IS GIVEN BY THE TRAPEZOID FORMULA SHOWN ABOVE

The end effector range relative to the grapple fixture is referenced to the center of the end effector which is also the center of the end effector coordinate frame. Therefore, the range (H) computations defined below and applied in the previous tests are invariant to the coordinate frame rotations:

$$H = 1/2\ (D_1 + D_3) \text{ or } H = 1/2\ (D_2 + D_4) \tag{1}$$

$$\text{Alternatively, } H = 1/4\ (D_1 + D_2 + D_3 + D_4) \tag{2}$$

The trapezoid formula and the quadratic condition (conic expression) are also invariant to the coordinate frame rotations. Therefore, the quadratic condition (Eq. 3) can be used without transformation to drive the success display:

$$(D_1 - D_3)^2 + (D_2 - D_4)^2 \leq L = [f(H)]^2 \tag{3}$$

Consequently, the "conic" success algorithm can be stated in a form identical to the one implemented for the previous tests:

① $H_A \leq H \leq H_D$

WHERE $H = 1/2\ (D_1 + D_3)$

$1/2\ (D_2 + D_4)$

② $(D_1 - D_3)^2 + (D_2 - D_4)^2 \leq L$

WHERE $L = C^2 = [f(H)]^2$

IF BOTH CONDITIONS ARE TRUE
THEN LIGHT/BUZZER ARE ON,
OTHERWISE OFF

"True" (or "light/buzzer on") means that the existing combination of depth, pitch and yaw errors will allow a successful grasp.

For the "three out of the four sensors" variation of the conic algorithm (that is, when any one of the four sensor signals is missing), the computation of the missing D_i measurement from the existing three sensor signals is identical to the one implemented for the previous tests.

The display of pitch and yaw errors referenced to the end effector pitch and yaw control axes requires to transform the differenced sensor data, (D_1-D_3) and (D_2-D_4), from the sensor reference frame to the end effector reference frame. The four transformations specified subsequently will correspond to four possible rotational mountings of the end effector to the wrist, and will also allow to select pitch and yaw error polarity in the fixed graphics display format.

As a convenient initial reference, we define pitch and yaw error polarities measured in the sensor frame and shown in the graphic display frame (Figs. 1, 2) as follows:

$$D_3 - D_1 \triangleq D_{31} = E_p^s \tag{5}$$

$$D_4 - D_2 \triangleq D_{42} = E_y^s \tag{6}$$

If the pitch and yaw control axes were identical with the sensor reference axes, the definitions given by Eqs. 5 and 6 would correspond to the case when the error bars in the display frame are changing length in the direction of the hand controller displacement.

The relation between sensor and end effector reference axes is shown in Fig. 2. This figure shows the view looking from the wrist towards the end effector. Note that A, B and yellow strip are existing marks on the claws. Note also that the end effector control axes, AA and BB, are along the claws.

The basic transformation of pitch and yaw error vectors from the S_1S_3 and S_2S_4 axes to the AA and BB axes is as follows:

$$\begin{pmatrix} a & -a \\ a & a \end{pmatrix} \begin{pmatrix} D_{31} \\ D_{42} \end{pmatrix} = \begin{pmatrix} E_{AA} \\ E_{BB} \end{pmatrix} = \begin{pmatrix} E_p^o \\ E_y^o \end{pmatrix} \quad ; \; a = 1/\sqrt{2} \tag{7}$$

Hence,

$$E_p^o = a(D_{31} - D_{42}) \tag{8}$$

$$E_y^o = a(D_{31} + D_{42}) \tag{9}$$

Note that E_p^o and E_y^o are in the graphic display reference frame.

Suppose that the end effector (together with the sensors) is rotated by 90 deg. ccw. when mounted to the wrist, without changing the physical direction of pitch and yaw axes as defined in the graphic display frame (Fig. 1). This requires the following transformation:

$$\begin{pmatrix} 0 & 1 \\ -1 & 0 \end{pmatrix} \begin{pmatrix} E_p^o \\ E_y^o \end{pmatrix} = \begin{pmatrix} E_y^o \\ -E_p^o \end{pmatrix} = \begin{pmatrix} E_p^1 \\ E_y^1 \end{pmatrix} \tag{10}$$

Hence, for 90 deg. rotation we have:

$$E_p^1 = E_y^o = a\ (D_{31} + D_{42}) \qquad (11)$$

$$E_y^1 = -E_p^o = -a\ (D_{31} - D_{42}) \qquad (12)$$

Note again that E_p^1 and E_y^1 are in the graphic display reference frame.

If the end effector (together with the sensors) is rotated by 180 deg. ccw. when mounted to the wrist, and the physical direction of pitch and yaw axes are kept fixed as shown in the graphic display frame, then we have to perform the following transformation:

$$\begin{pmatrix} -1 & 0 \\ 0 & -1 \end{pmatrix} \begin{pmatrix} E_p^o \\ E_y^o \end{pmatrix} = \begin{pmatrix} -E_p^o \\ -E_y^o \end{pmatrix} = \begin{pmatrix} E_p^2 \\ E_y^2 \end{pmatrix} \qquad (13)$$

Hence, for 180° deg. rotation we have

$$E_p^2 = -E_p^o = -a\ (D_{31} - D_{42}) \qquad (14)$$

$$E_y^2 = -E_y^2 = -a\ (D_{31} + D_{42}) \qquad (15)$$

270 deg. rotation, having the same conditions as for the 90 degree or 180 degree rotations, will require the following transformation:

$$\begin{pmatrix} 0 & -1 \\ 1 & 0 \end{pmatrix} \begin{pmatrix} E_p^o \\ E_y^o \end{pmatrix} = \begin{pmatrix} -E_y^o \\ E_p^o \end{pmatrix} = \begin{pmatrix} E_p^3 \\ E_y^3 \end{pmatrix} \qquad (16)$$

Hence, for 270 deg. rotation we have:

$$E_p^3 = -E_y^o = -a\ (D_{31} + D_{42}) \qquad (17)$$

$$E_y^3 = E_p^o = a\ (D_{31} - D_{42}) \qquad (18)$$

Note that E_p^2, E_y^2, E_p^3, and E_y^3 are in the graphic display reference frame.

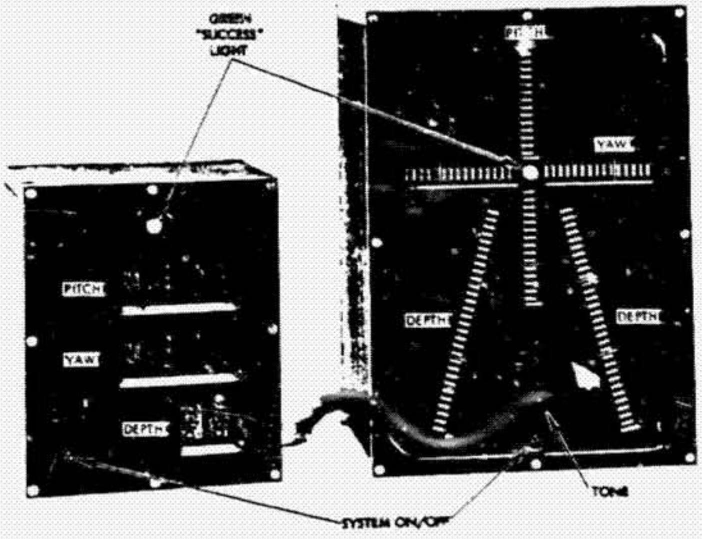
GREEN "SUCCESS" LIGHT
PITCH
YAW
DEPTH
PITCH
YAW
DEPTH
DEPTH
TONE
SYSTEM ON/OFF

Figure 1. Event-driven graphic and numeric displays of data from proximity sensor system integrated with four-claw end effector

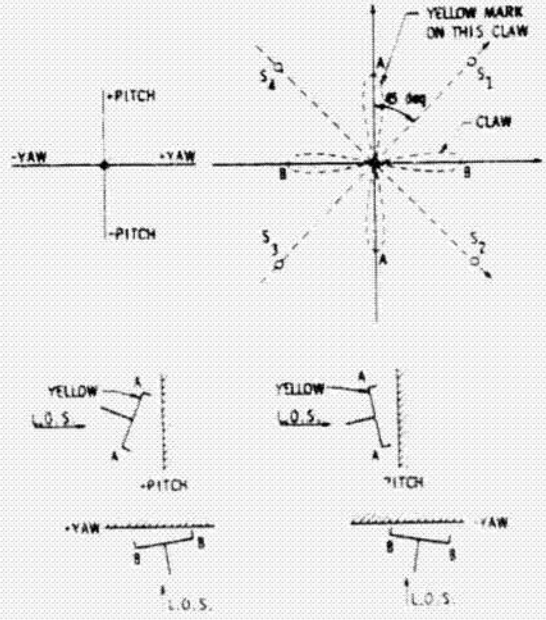
YELLOW MARK ON THIS CLAW
+PITCH
-YAW
+YAW
-PITCH
S_4
S_1
S_3
S_2
45 deg
CLAW
A
A
B
B
YELLOW
L.O.S.
A
A
+PITCH
YELLOW
L.O.S.
A
A
-PITCH
+YAW
B
B
L.O.S.
-YAW
B
B
L.O.S.

View: looking from wrist towards end effector.

Figure 2. Sensor, control and display reference frames: error states for X = 0 on the BCD dial switch

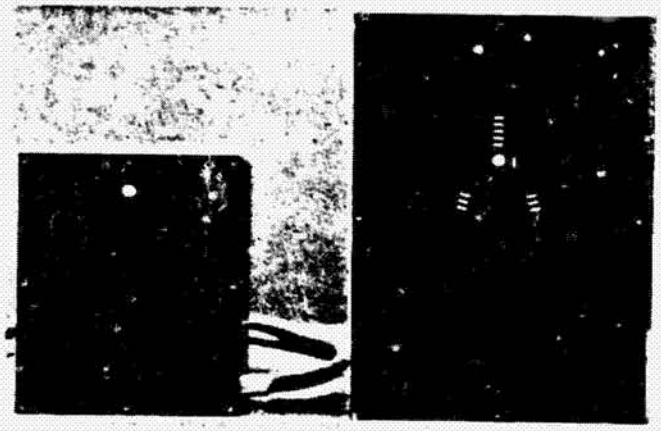

c) INSIDE GRASP ENVELOPE WITH GREATLY REDUCED ERRORS FOR A FINE-CONTROLLED GRASP; GREEN LAMP ON.

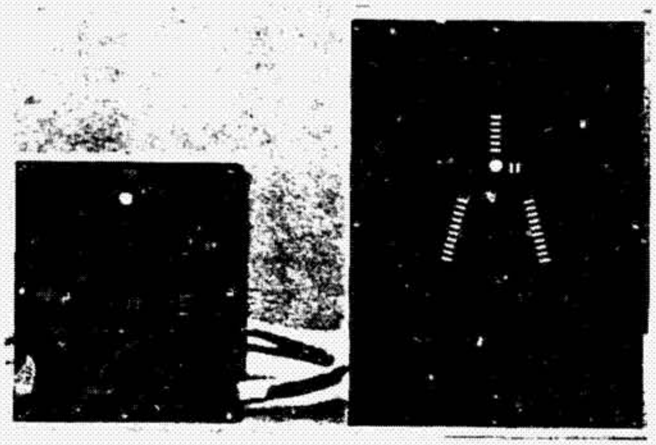

b) INSIDE GRASP ENVELOPE. ERROR COMBINATION ALLOWS SUCCESSFUL GRASP; GREEN LAMP ON.

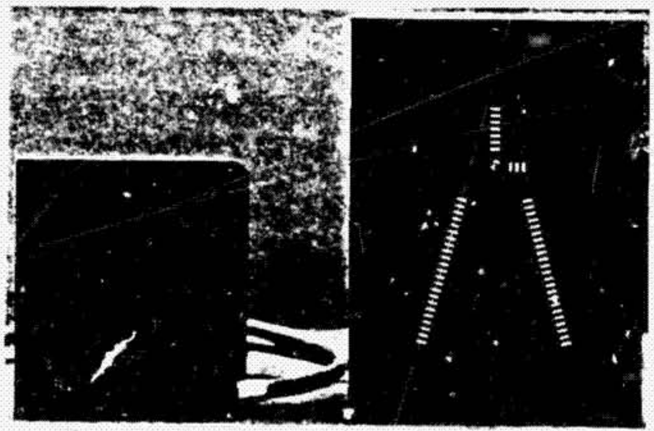

a) OUTSIDE GRASP ENVELOPE AT 4.5 inches RANGE; GREEN LAMP OFF.

Figure 3. Target approach sequence as seen on the "smart" displays. (Sequence from bottom to top.)

a) 0 deg (BASE FRAME)

b) 90 deg ROTATION

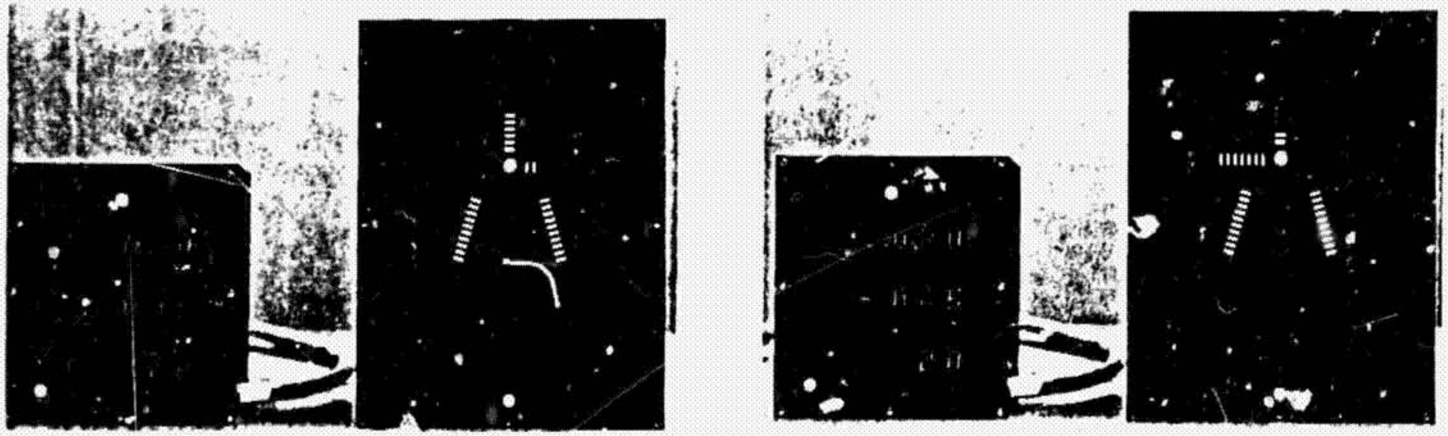

c) 180 deg ROTATION

d) 270 deg ROTATION

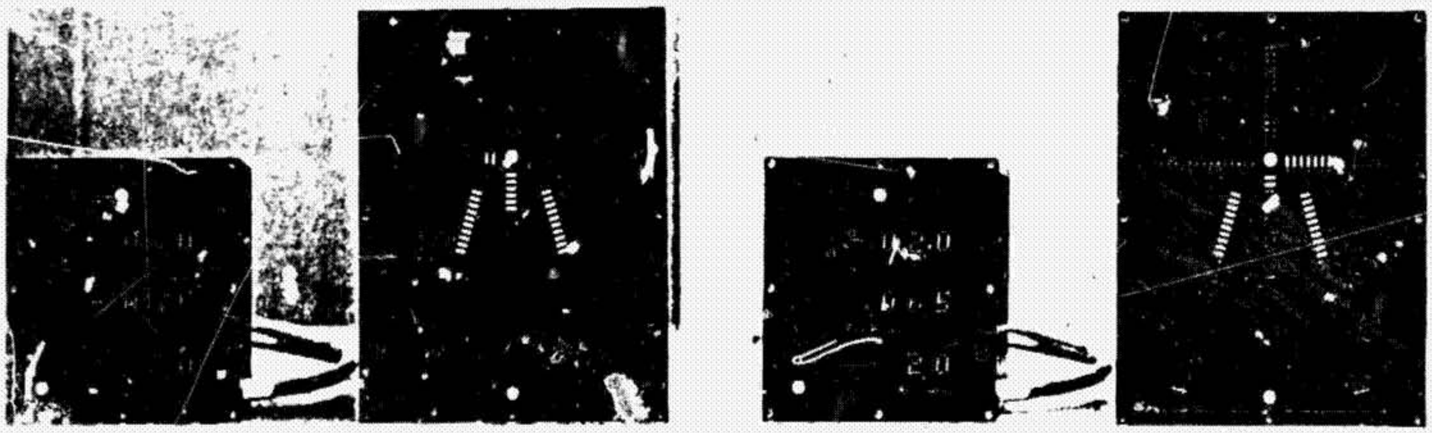

Figure 4. Algorithmic rotation of pitch and yaw error axes in the displays

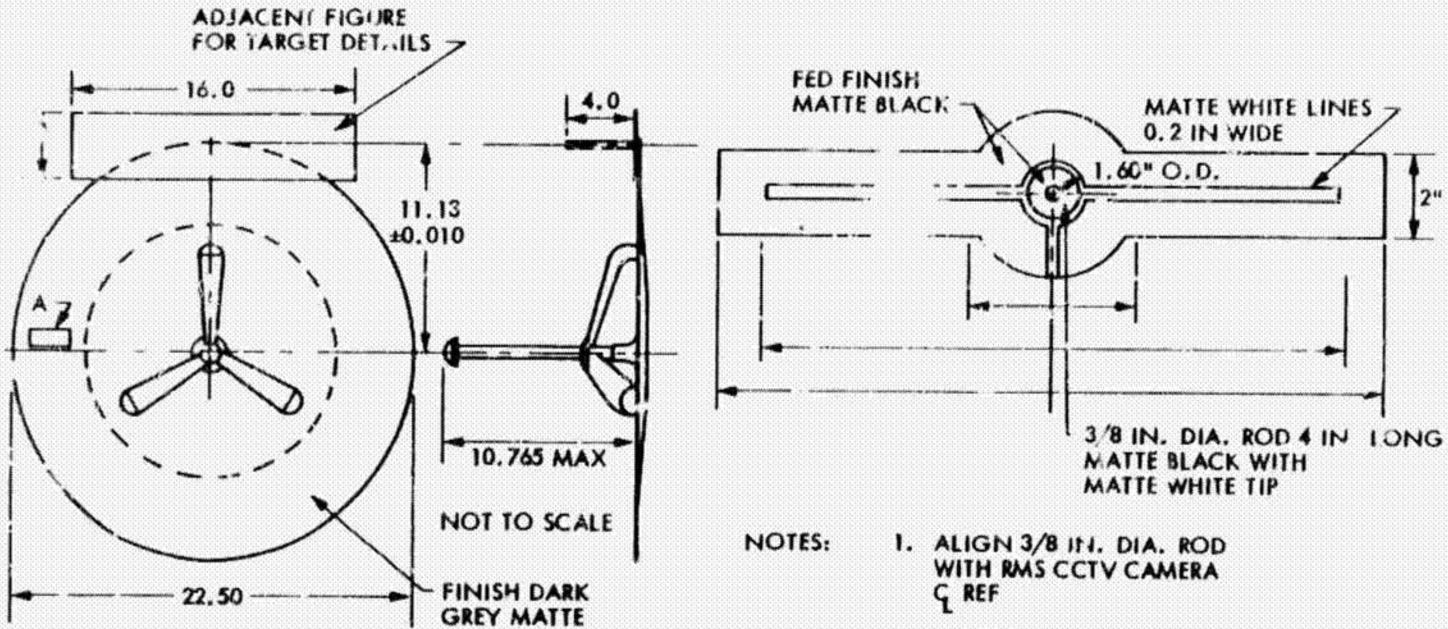
ADJACENT FIGURE
FOR TARGET DETAILS
16.0
4.0
11.13
±0.010
A
10.765 MAX
NOT TO SCALE
22.50
FINISH DARK
GREY MATTE
FED FINISH
MATTE BLACK
MATTE WHITE LINES
0.2 IN WIDE
1.60" O.D.
2"
3/8 IN. DIA. ROD 4 IN LONG
MATTE BLACK WITH
MATTE WHITE TIP

NOTES:
1. ALIGN 3/8 IN. DIA. ROD WITH RMS CCTV CAMERA ℄ REF
2. TARGET PLATE CUTOUT AND PAINT MASK (LINE WIDTH AND LOCATION) ACCURACY IS ±0.02 IN.

Figure 5. Standard visual target with standard grapple fixture

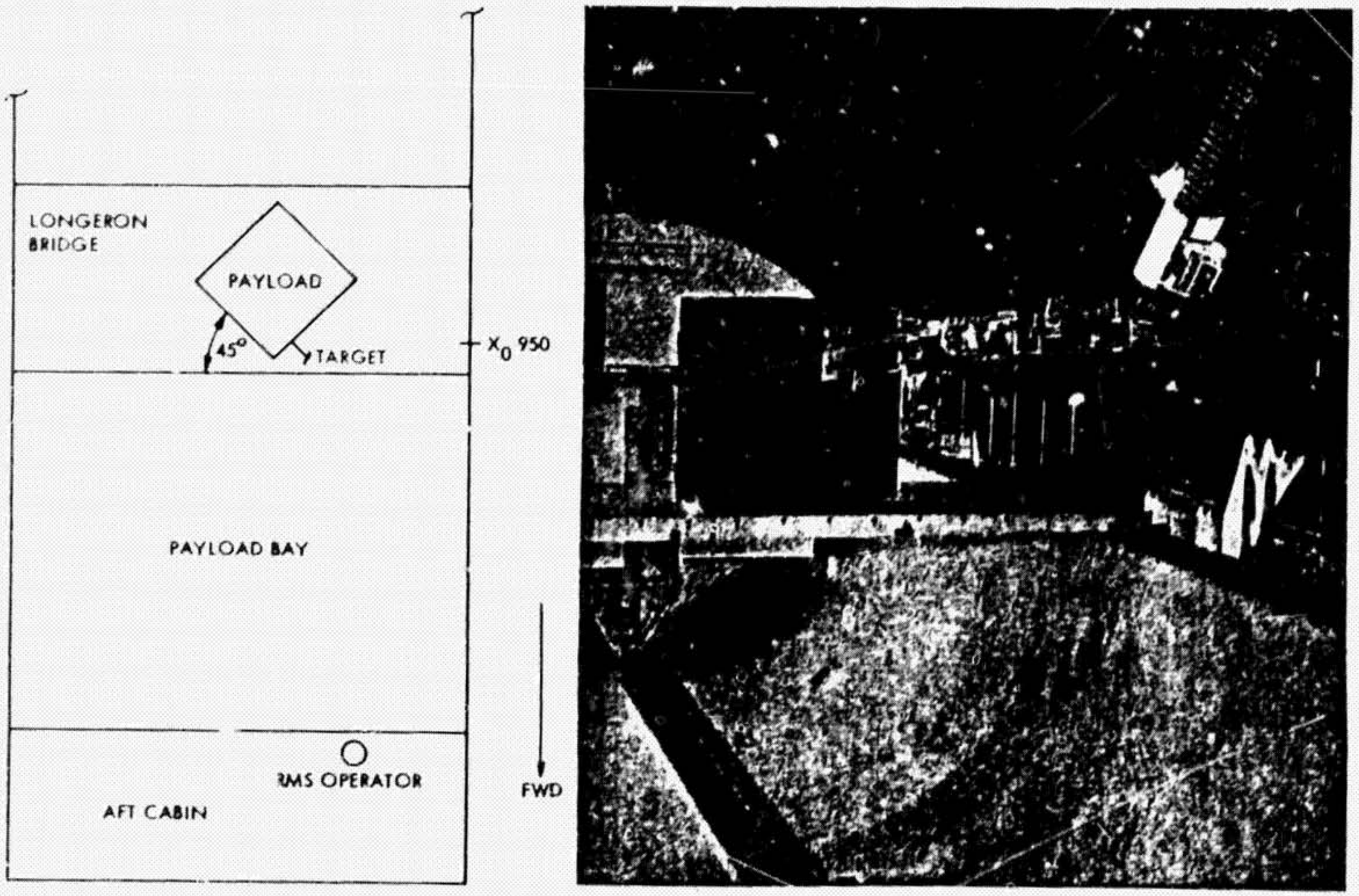
LONGERON
BRIDGE
PAYLOAD
45°
TARGET
X_0 950
PAYLOAD BAY
FWD
RMS OPERATOR
AFT CABIN

Figure 6. Static test scene in Shuttle payload bay

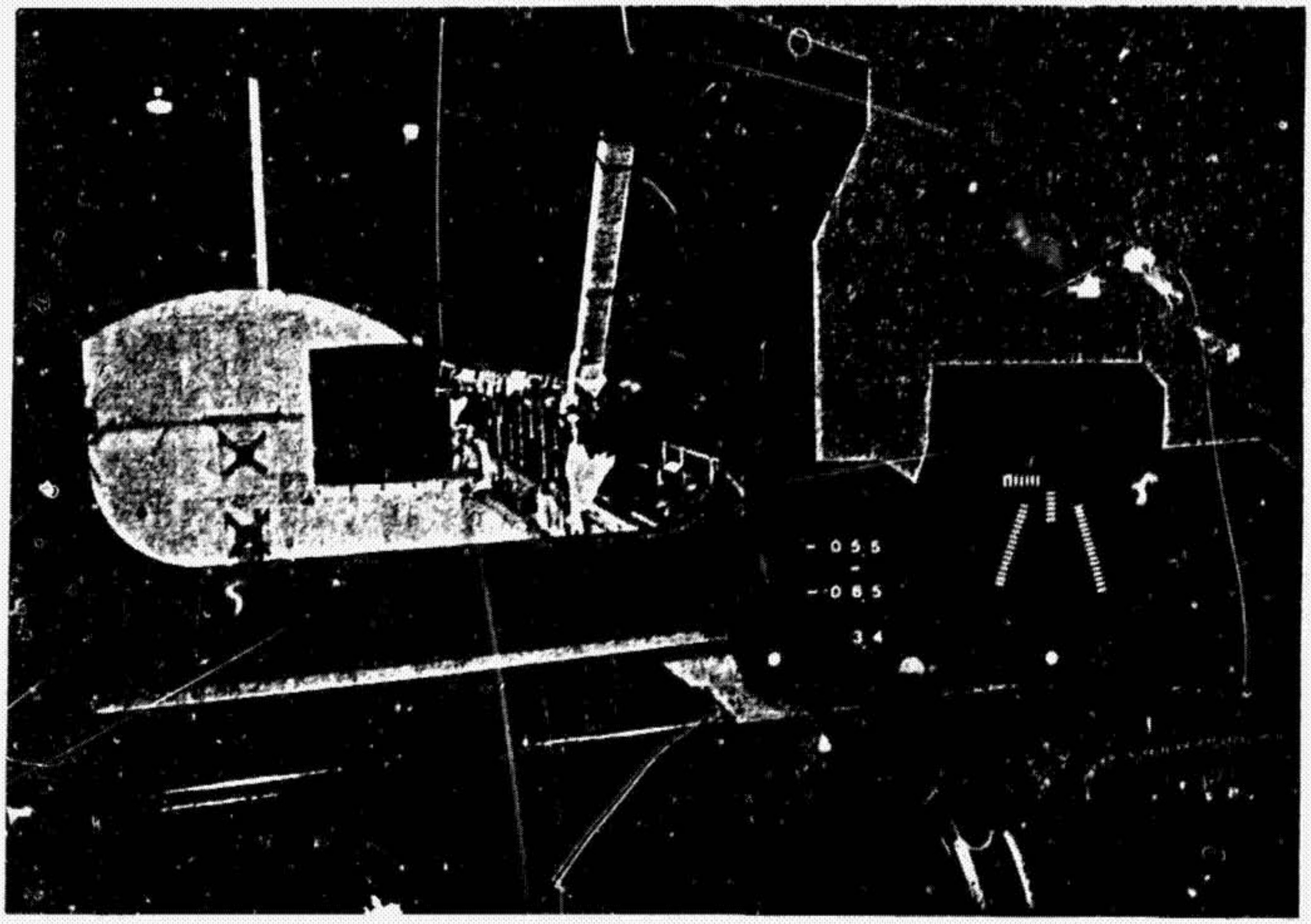

Figure 7. Proximity sensor displays in Space Shuttle cabin

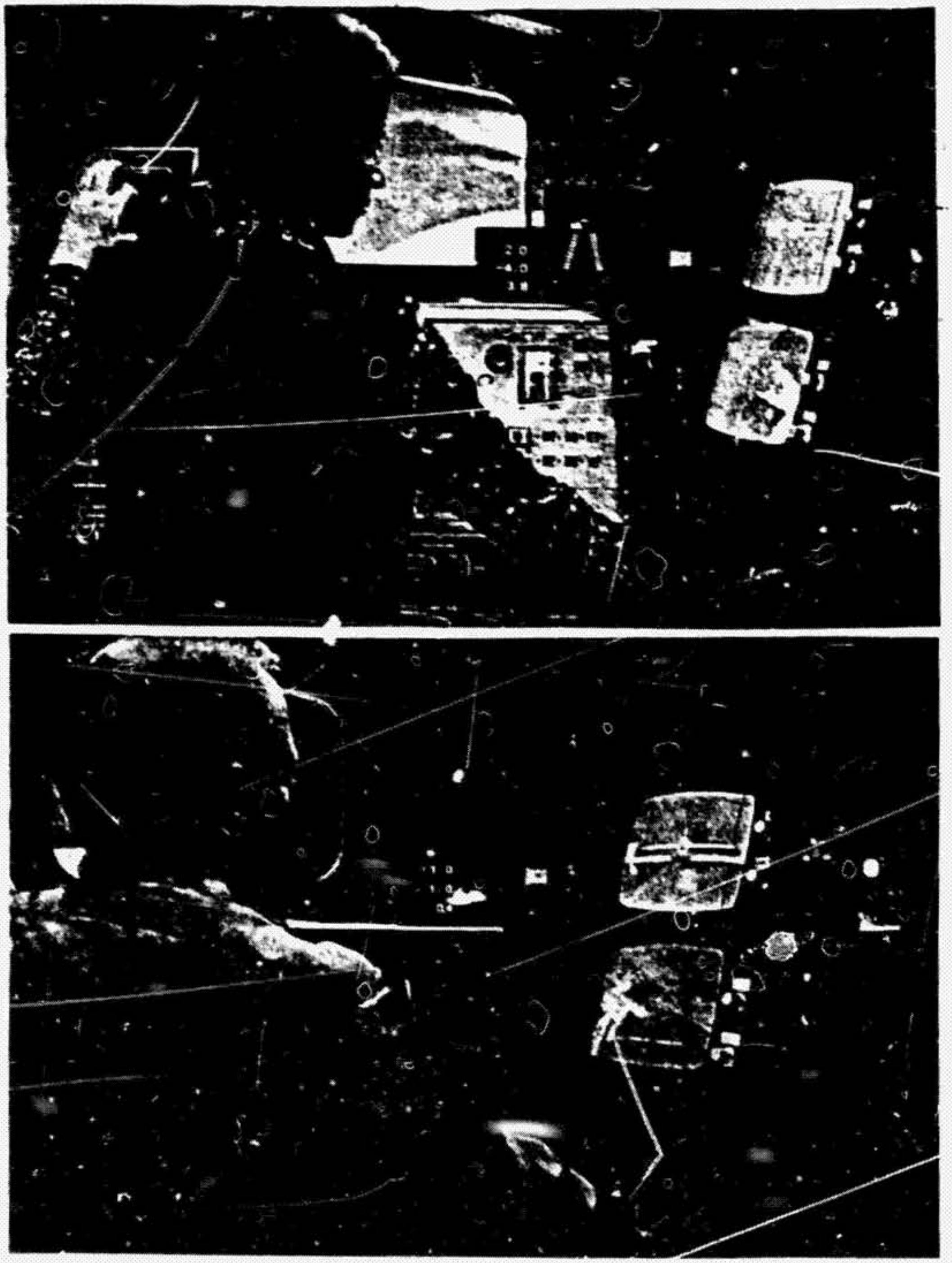

Figure 8. Operators using proximity sensor displays in Shuttle cab during static test (top picture) and dynamic test (lower picture)

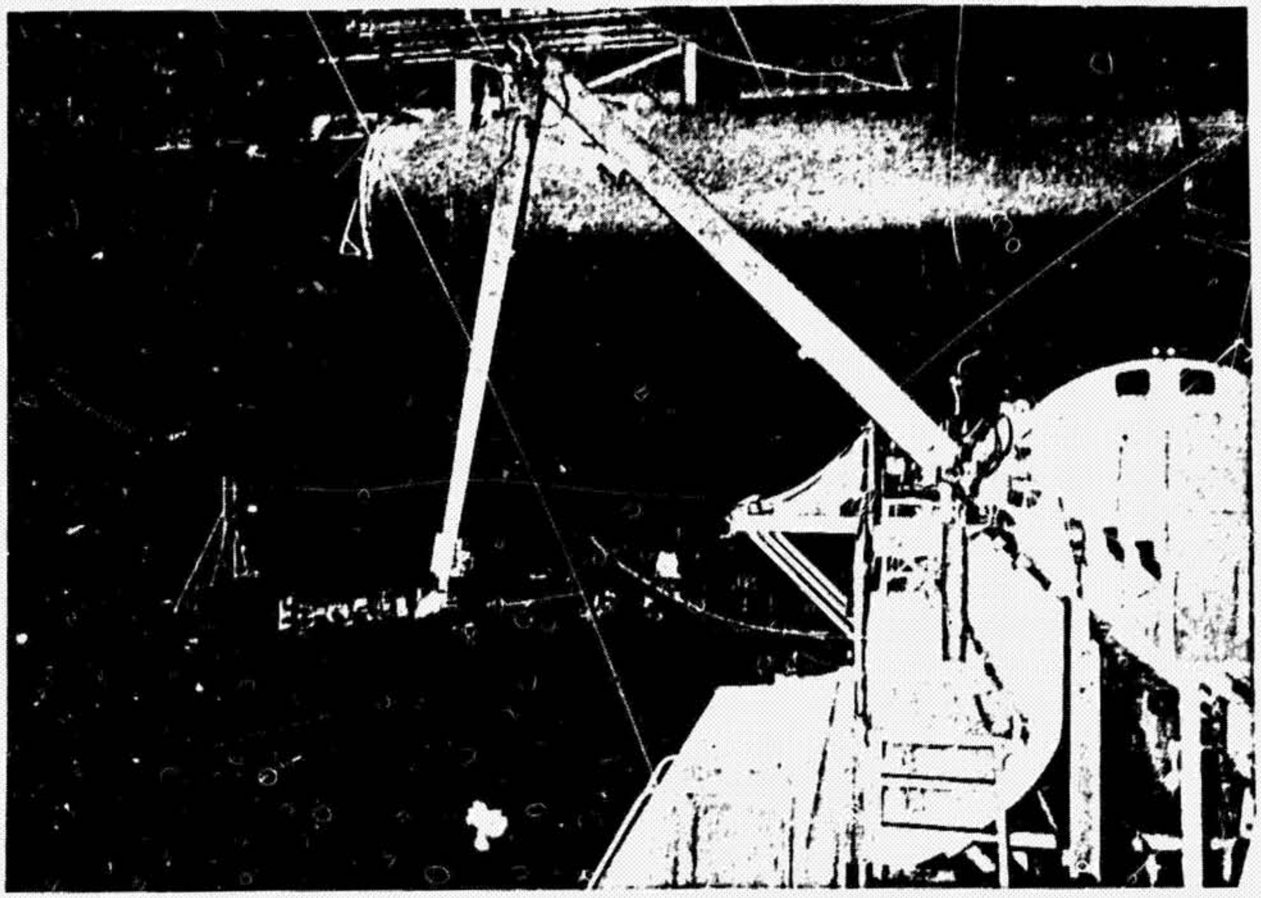

Figure 9. Dynamic test scene

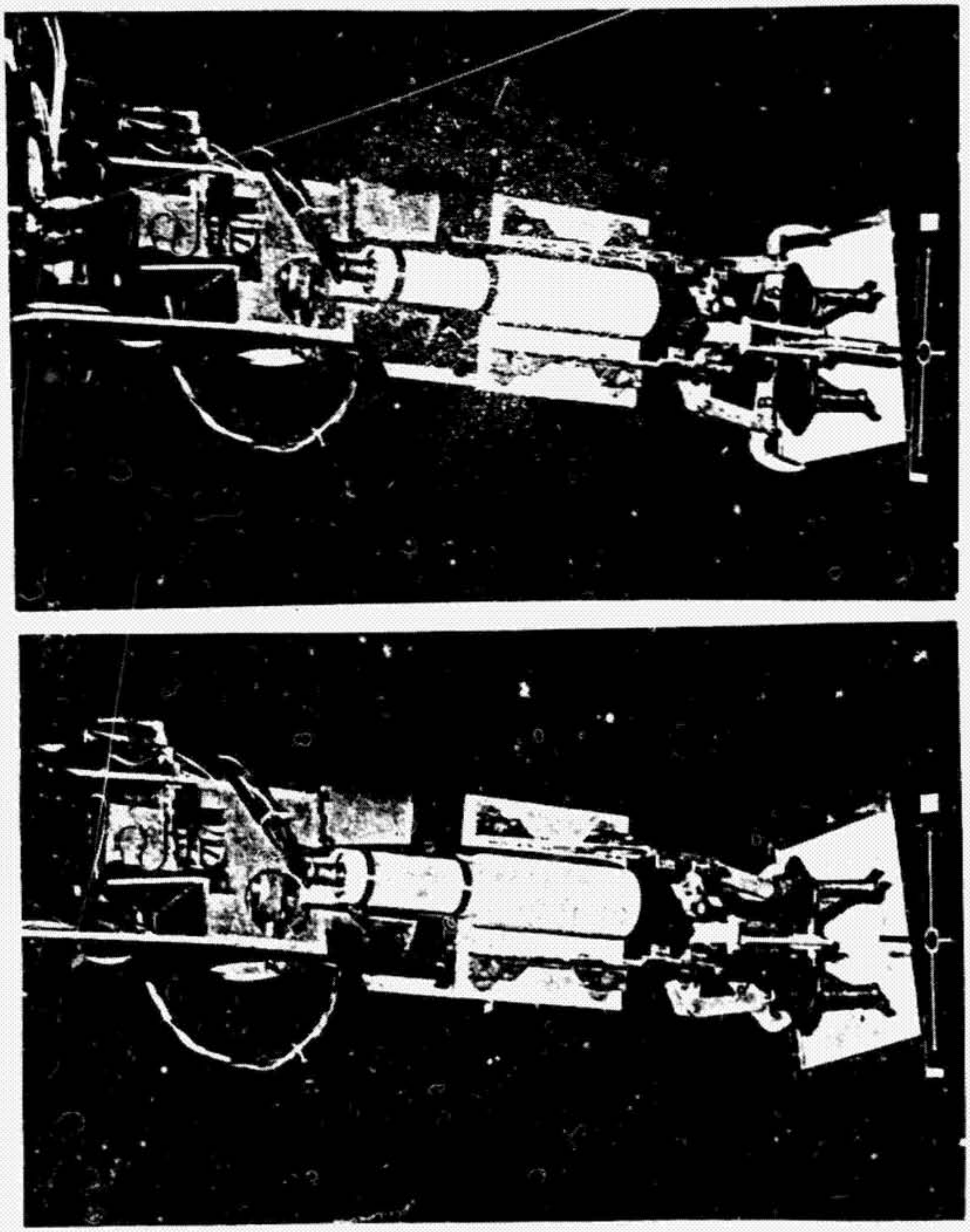

Figure 10. Precision controlled grasp

A NEW FEEDBACK INSTRUMENT FOR ROBOTS AND MANIPULATORS, AND ITS USE IN ROBOT TEACHING, SELF CORRECTION AND LEARNING

By

D. S. Seltzer and

D. E. Whitney

The Charles Stark Draper Laboratory, Inc.

Cambridge, MA 02138

Abstract

A new type of tactile sensing device, the Instrumented Remote Center Compliance (IRCC) has been developed for use with industrial robots and manipulators. The IRCC combines a passive mechanical error-absorbing structure with instrumentation capable of measuring position errors to a resolution of 0.1 mm and angular errors to a resolution of 10^{-3} radians. The IRCC can aid a robot operator during teaching by providing tactile information. Current experiments indicate that this information can be utilized by either displaying it to the operator, or incorporating it directly in a computer-controlled feedback loop. Future research efforts will examine the use of the IRCC for performance monitoring and correction for long term effects such as tool wear, part variation, and robot drift. The approach is based on Kalman Filter models of the robot, the sensor, and an ensemble of repeated operations such as part transfers or assemblies. Applications include searching a visually occluded environment, tracking drift, correcting initial condition errors or detecting malfunctions.

JMIT

ABSTRACT

THE NOSC/MIT SUBMERSIBLE-MANIPULATOR: AN EXPERIMENT IN REMOTE SUPERVISORY CONTROL OF A MICROPROCESSOR BASED ROBOT

Dana Yoerger
Thomas Sheridan
Massachusetts Institute of Technology

This paper is a progress report on the development of an experimental free-swimming submersible with a manipulator arm. The system will function in the undersea environment while being controlled remotely in a supervisory mode by a human operator. The electrically powered arm is controlled by the human operator with the aid of microcomputers both on the submersible and on the surface.

Development will begin with a manual control system and a tether for communication to and from the vehicle. After supervisory concepts such as preprogrammed tasks, motion compensation, and active accomodation have been implemented, the vehicle will be made free swimming. Communication will then be accomplished through an acoustic data link.

Due to the limited bandwidth and delays imposed by the acoustic data link, continuous manual control via the human operator is not possible. Therefore, the manipulator must be able to complete tasks with only high level commands from the surface. Vehicle motion, unexpected collisions, as well as substantial position errors must be dealt with by the relatively modest microcomputer. The microcomputer on the surface will be used to provide the operator with computer aided displays to further reduce the effects of the acoustic link.

N82 34075

D38

ANALYSIS OF DRIVER PERFORMANCE UNDER REDUCED VISIBILITY

Wolf-Dieter Kaeppler
Forschungsinstitut fuer Anthropotechnik (FAT)
D-5307 Wachtberg, F.R. Germany

ABSTRACT

Mathematical models describing vehicle dynamics as well as human behavior may be useful in evaluating driver performance and in establishing design criteria for vehicles more compatible with man. In 1977, a two-level model of driver steering behavior was developed, but its parameters were identified for clear visibility conditions only. Since driver performance degrades under conditions of reduced visibility, e.g. fog, the two-level model should be investigated to determine its applicability to such conditions.

The data analysis of a recently performed driving simulation experiment showed that the model still performed reasonably well under fog conditions, although there was a degradation in its predictive capacity during fog. Some additional parameters affecting anticipation and lag time may improve the model's performance for reduced visibility conditions.

1. INTRODUCTION AND TWO-LEVEL MODEL

Mathematical models may be useful in evaluating driver performance and in establishing design criteria for vehicles more compatible with man. The state of the art of mathematical description of car dynamics is rather high. However, there is still a lack of information about the dynamic behavior of car drivers.

Based on the idea that human behavior in lateral vehicle control can be described in terms of a multi-level control task, Donges [1] has developed a two-level model of driver steering behavior. The model is split into anticipatory and compensatory task levels (Fig. 1) which are working in parallel.

At the anticipatory level, the driver is presented with an outside forward view of the required path curvature K_S which serves as the forcing function. Perceiving the future course of the road, he is able to react with a steering angle λ_S in advance to turns and obstacles.

At the compensatory level, the driver compares actual and required paths by observing, e.g., heading angle error ψ_Δ and lateral deviation y_Δ of the vehicle. From this information, a compensatory steering angle λ_R is deduced to correct the course of the car.

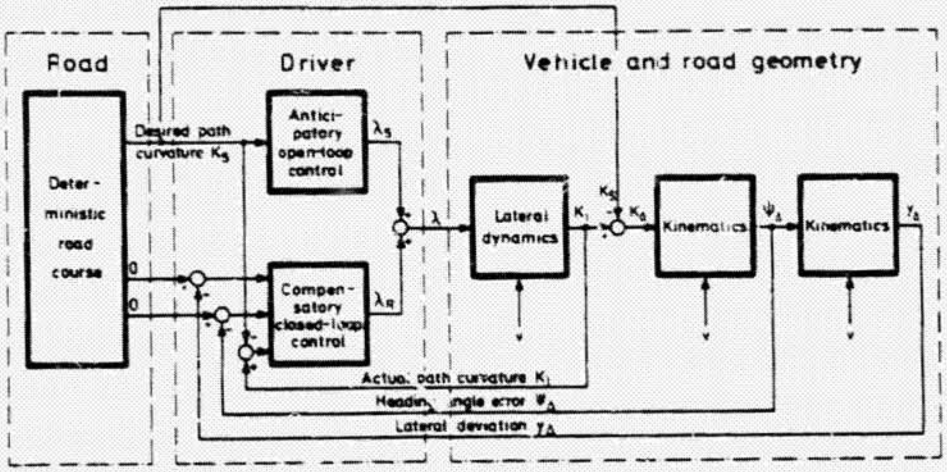
Road
Driver
Vehicle and road geometry
Deter-ministic road course
Desired path curvature K_S
Antici-patory open-loop control
λ_S
0
0
Compen-satory closed-loop control
λ_R
λ
Lateral dynamics
K_1
K_S
K_Δ
Kinematics
ψ_Δ
Kinematics
y_Δ
Actual path curvature K_1
Heading angle error ψ_Δ
Lateral deviation y_Δ

Fig. 1 : A schematic diagram of the two-level model of driver steering behavior in the driver-vehicle-road system (from Donges [1])

So far, parameters for this model have only been identified for clear visibility conditions. Driver performance, however, degrades under conditions of reduced visibility (McLean [2], and others [3;4;5;6]). The two-level model should be able to predict this degradation since reduced visibility, e.g., fog will mainly affect the anticipatory level (Fig. 2).

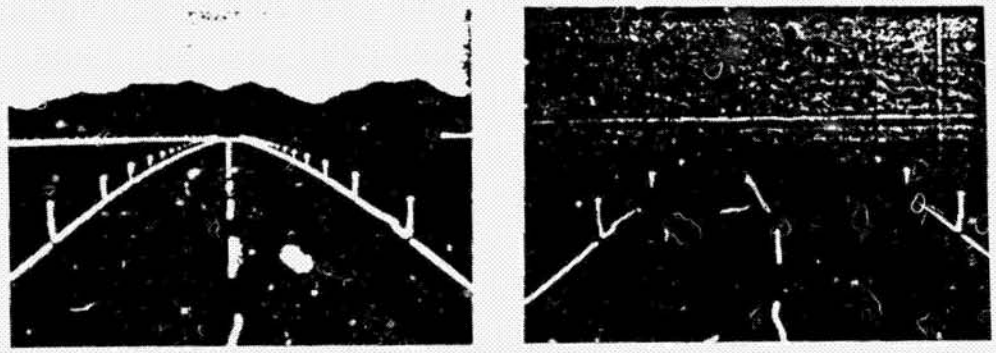

Fig. 2 : Visual simulation with a stylized two lane road
a) when clear b) during fog

With clear visibility, the apparent movement of the mountain scenery provides cues about the heading behavior of the car. The direction of an approaching turn as well as how sharp the turn is can also be determined. With this information and based on perhaps his velocity or distance judgment to the curve, the driver is able to make a suitable steering movement. In fog, he gets less information on approaching turns. In consequence, parameters of the two-level model may change.

To examine this supposition and to find out if this model in general is able to predict the degraded performance reasonably well, a driving simulation experiment has been set up and performed [7].

2. DRIVING SIMULATOR AND EXPERIMENTAL PROCEDURE

The simulator used (Fig. 3) includes a real car cabin converted to simulation purposes, longitudinal and lateral vehicle dynamics, driving noise, rolling motion and the outside forward view. The stylized image of the road can be presented to the driver under several visibility conditions (see again Fig. 2) [8].

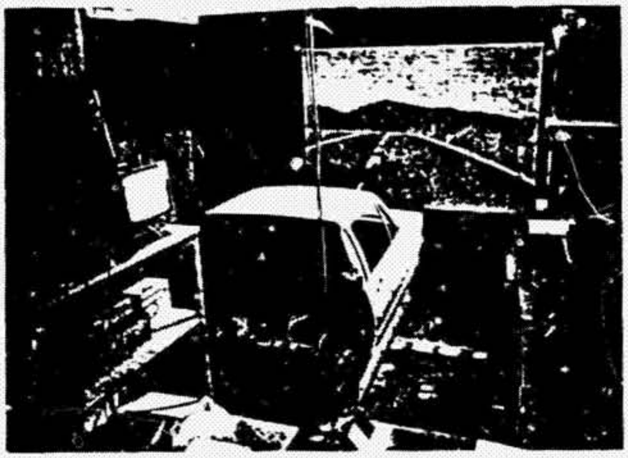

Fig. 3 : The Driving Simulator of the FAT

In the experiment, visibility condition, i.e., clear and fog (visibility ranges of 400 m and 33 m respectively) was the independent variable. The dependent variables of interest here included the measures :

velocity	v
steering angle	λ
heading angle error	ψ_Δ
lateral deviation	y_Δ

and the model parameters for the anticipatory and compensatory levels :

anticipation time	T_A	time delay	τ_H
lag time	T_1	heading gain	h_ψ
steering gain	h_S	deviation gain	h_y .

Six experienced male drivers took part in the experiment. They were instructed to drive safely but as quickly as conditions permit. The driving task consisted of six laps on a closed road circuit. After two training sessions of 20 minutes each under clear conditions, the experiments were run at intervals of one day.

3. RESULTS AND DISCUSSION

As one might expect, mean lap speeds for each person and for the group were lower for fog conditions with $17\,m \cdot s^{-1}$ (meters per second) than when clear which was $27\,m \cdot s^{-1}$ (Fig. 4).

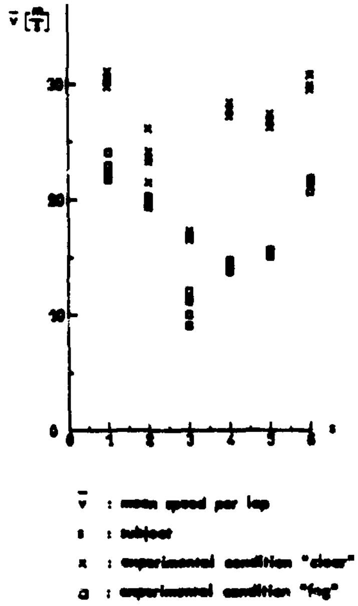

Fig. 4 : Mean lap speeds for different subjects and visibility conditions

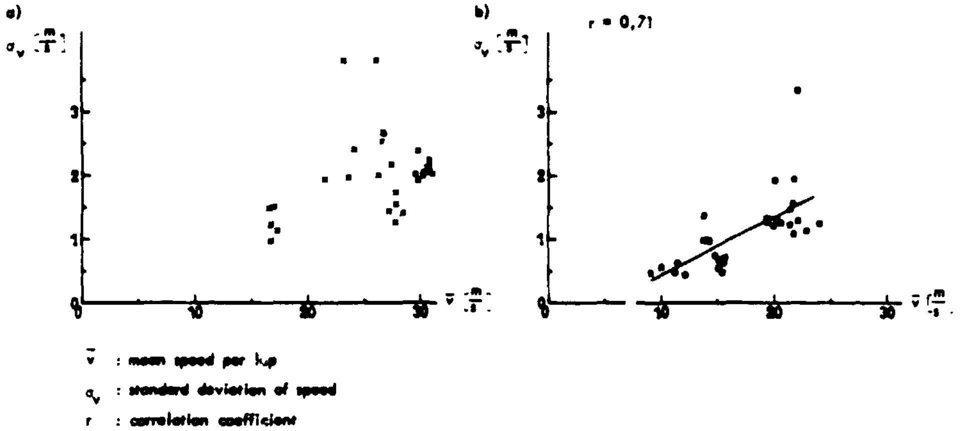

Fig. 5 : Speed variability as a function of speed
a) when clear b) during fog

In addition, lap speeds were less variable under the fog condition with a standard deviation of 1.3 compared with 2.1 for the clear condition (see Fig. 5), probably due to the more restricted speed range available to the subjects.

Also, during fog conditions driving behavior is more conservative [3] leading subjects to refrain from increasing their speeds between curves (see also FG in Fig. 8a).

In both experimental conditions, lane deviations increased with driving speed and the absolute values of lane deviations were approximately the same below 18 m · s^{-1}. Above this speed, absolute lane deviations increased more under the fog condition (Fig. 6).

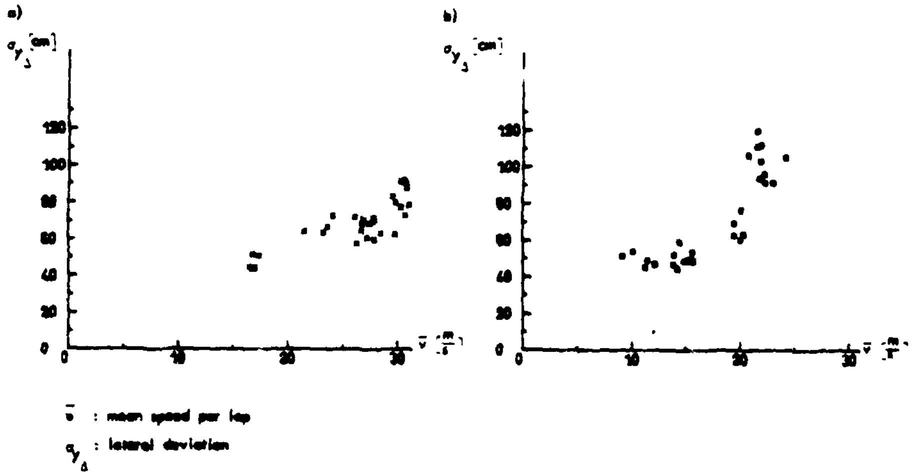

Fig. 6 : Lane deviation as a function of speed
a) when clear b) during fog

The test course consists of 24 segments of constant curvature. A step in road curvature occurs where two of these segments join together. When clear, this is seen long before it is reached by the driver so that he is able to react in advance. Time histories (means and standard deviations averaged over 30 individual time histories) of the dependent variables under clear and fog conditions are shown in Figure 7 for a left hand turn.

The speed variation is quite small though six subjects are involved (see Fig. 7c). When it is clear, the steering reaction shown in the left part of Fig. 7d is starting at a certain time prior to the step change. The steering angle shows a lagged transient with a small overshoot. The success of this reaction is illustrated by the fact that the lateral deviation (Fig. 7f) tends to be evenly distributed around the center-line with a bias in the direction of the curve, i.e., more left deviations in left hand turns.

In the right part of Fig. 7, the time histories under fog conditions are shown. The steering reaction (Fig. 7d) starts late in response to the step change resulting in a large lane deviation to the right of the center-line in a left turn (Fig. 7f). This graph also shows a steep transient with a large overshoot. Clearly, the reduced information in the fog condition does not permit the driver to perform properly.

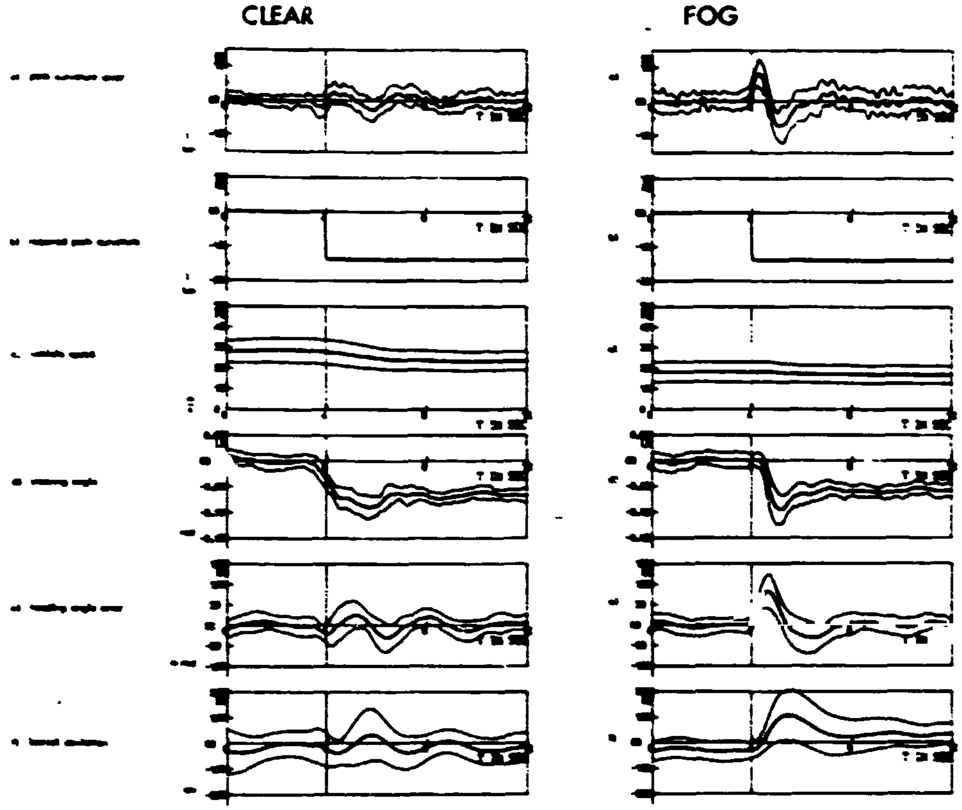

Fig. 7 : Time histories of system variables in a left curve for clear and fog conditions

In course segments similar to the above-mentioned, the six parameters of the two-level model have been identified. At this time, the identification is completed for two representative course segments, a right and a left hand turn. The parameters of the two-level model did in fact change to a certain extent under the fog condition especially anticipation time as can be seen in the following Table 1.

Table 1 : Parameter means of the two-level model for clear and fog conditions

Model Level	Parameter	Clear	Fog
Anticipatory Level	anticipation time (sec.) lag time (sec.) steering gain (deg.x km)	0.40 0.41 0.31	- 0.14 0.54 0.26
Compensatory Level	time delay (sec.) heading gain(deg./deg.) deviation gain (deg./cm)	0.34 0.33 0.0039	0.63 0.39 0.0043
steering sensitivity	(deg.$^{-1}$ x km^{-1})	0.16	0.17
steering ratio		23.2	

C - 8

To give an impression of the efficiency of the two-level model, combined time histories of one driver, the driver model and its components are shown in Fig. 8 for an arbitrarily chosen example for each of the visibility conditions.

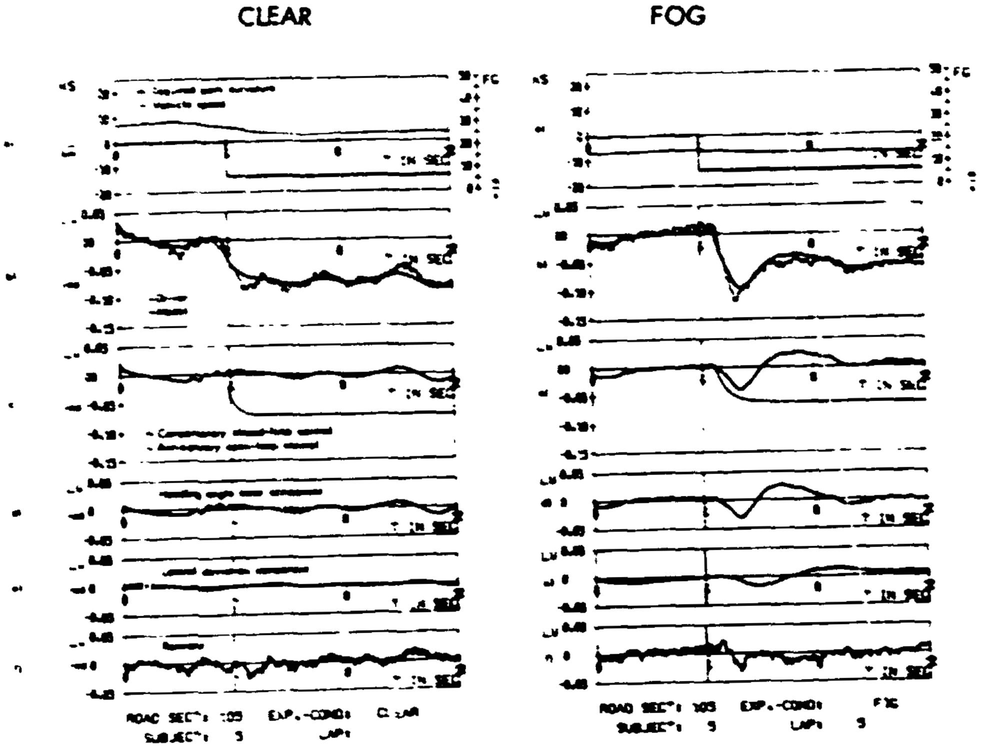

Fig. 8 : Time histories of steering angles (LW) of one driver, driver model and driver model components

Required path curvature (KS) and vehicle speed (FG) are shown in Fig. 8a to describe the experimental situation. As one can see in Fig. 8b, the two-level model predicts driver steering reaction reasonably well in clear and fog conditions although better so under clear conditions which follows from the detailed data analysis. It turns out that for both conditions heading angle inputs account for the largest part (see Fig. 8d) of the compensatory level response shown in Figure 8c.

In fog, the model accounts for a smaller portion of the steering reaction at the anticipatory level. One reason is that the chosen first order lag is not able to reproduce the overshoot which occured in the fog (see Fig. 8b). Besides, the transient of the model is not as steep as the experimental data show (Fig. 8b and c). This is because the anticipation time T_A could not always be identified correctly by the least mean square method used here. During fog, the driver makes steering movements to the left or right, not really knowing when a turn will appear and what kind of turn this will be. These early steering movements may be interpreted by the model as early reactions to the curve.

Some modified least mean square methods will be evaluated in the future to clear away this defect. It also appears that the two-level model could, perhaps, be improved for limited visibility conditions by including additional parameters affecting anticipation and lag time.

REFERENCES

[1] Donges, E., Ein Zwei-Ebenen-Modell des menschlichen Lenkverhaltens. Forschungsinstitut für Anthropotechnik, Report No. 27, Wachtberg, 1977.

[2] McLean, J.R., Hoffmann, E.R., The Effects of Restricted Preview on Driver Steering Control and Performance. Human Factors, 15(1973)4, p. 421-430.

[3] Kochmond, W.C., Perchonok, K., Highway Fog. Highway Research Board, Report No. 95, Buffalo, NY, 1970.

[4] Heiss, W.H., Highway Fog. Transportation Research Board, Report No. 171, Wash., D.C., 1976.

[5] Lane, F.D., Speed Advisory Information for Reduced Visibility Conditions. NTIS, Salem, Oreg., 1975.

[6] Allen, R.W., McRuer, D.T., Driver Steering Dynamics Measured in a Car Simulator under a Range of Visibility and Road-marking Conditions. Proceedings 13th Annual Conference on Manual Control, MIT, Cambridge, Mass., 1977, p. 180-196.

[7] Koeppler, W.-D., Fahrverhalten bei Freier Sicht und bei Sichtbehinderung durch Nebel. Forschungsinstitut für Anthropotechnik, Wachtberg (Report will be published).

[8] Donges, E., Der Fahrsimulator des Forschungsinstitutes für Anthropotechnik. Report No. 41, Wachtberg, 1978.

1. Report No. NASA TM-84273	2. Government Accession No.	3. Recipient's Catalog No.
4. Title and Subtitle SIXTEENTH ANNUAL CONFERENCE ON MANUAL CONTROL*		5. Report Date July 1982 6. Performing Organization Code
7. Author(s)		8. Performing Organization Report No. A-9000
9. Performing Organization Name and Address Massachusetts Institute of Technology, Cambridge, Mass. 02139 and NASA Ames Research Center, Moffett Field, CA 94035		10. Work Unit No. 11. Contract or Grant No.
12. Sponsoring Agency Name and Address National Aeronautics and Space Administration, Washington, D.C. 20546		13. Type of Report and Period Covered Technical Memorandum 14. Sponsoring Agency Code

15. Supplementary Notes

*Proceedings of a meeting held at Massachusetts Institute of Technology, Cambridge, Massachusetts, May 5-7, 1980

16. Abstract

This volume contains a compilation of written versions of papers presented at the Sixteenth Annual Conference on Manual Control in a meeting held at the Massachusetts Institute of Technology, Cambridge, July 5-7, 1980. Nine main topics were covered in this three-day conference in sessions titled: Operator Modeling, Measurement of Human Response, Mental Workload, Pilot/Operator Opinion, Effects of Motion, Aircraft Displays, Supervisory Control, Automobile Driving, and Remote Manipulation.

17. Key Words (Suggested by Author(s)) Manual Control, Physiological Control, Displays, Vehicle handling qualities, Operator performance, Simulation		18. Distribution Statement Unlimited Subject Category - 54	
19. Security Classif. (of this report) Unclassified	20. Security Classif. (of this page) Unclassified	21. No. of Pages 647	22. Price* A26

*For sale by the National Technical Information Service, Springfield, Virginia 22161